REPOSITIONING OF ASTEMIZOLE FOR MALARIA

Dickson Mambwe

Supervisor:

Prof. Kelly Chibale

Department of Chemistry, University of Cape Town

Thesis Presented for the Degree of

DOCTOR OF PHILOSOPHY

In the Department of Chemistry, Faculty of Science

UNIVERSITY OF CAPE TOWN

March 2021

TABLE OF CONTENTS

Contents Page

LIST OF FIGURES

LIST OF SCHEMES

LIST OF TABLES

DECLARATION

I, **Dickson Mambwe**, hereby declare the following:

1. That this thesis is my own original work, both in concept and execution, apart from the normal guidance of my supervisor.
2. That in instances where: (i) others' work has been cited, and (ii) biological or physicochemical assays where not performed by myself; this has been fully referenced and/or acknowledged.
3. That neither the substance or any part of this work has been, is being, or is intended to be submitted for another degree at this University or any other University.
4. That I grant the University of Cape Town free license to reproduce this work, in whole or in part, for the purpose of research.

I hereby present this thesis in fulfilment of the requirements for the degree of Doctor of Philosophy (Ph.D.) in the Department of Chemistry, Faculty of Science at the University of Cape Town.

Signed: _____ Date: 19th March 2021

DEDICATION

To my beloved wife, Muma Mulenga Mambwe, as a sign of my gratitude and appreciation for your love, enduring patience, support, understanding, prayers, and encouragements throughout this journey. You truly are my blessing, a rock, and a woman amongst women. Natotela mukashi wandi.

To my parents, Mr. Aston Kaunda Mambwe (AKM) & Mrs. Given Kalobwe Mulenga Mambwe (GKM). Thank you for the enduring support, your constant prayers to Jehovah in my favour, and the faith in me that you have constantly demonstrated not only through my Ph.D journey, but throughout my life. I appreciate you and may Jehovah God the almighty keep you in his blessing. Natotela mwebafyashi.

To my siblings: Given, Aston, Mathias 'suepey', Alice and Paul. For your brotherly love, care and understanding. There is never a dull moment with you, the laughter we shared was like medicine to an otherwise challenging journey.

ACKNOWLEDGEMENT

First and foremost, I would like to thank the Almighty God, Jehovah, for my life, for seeing me through this journey in good health, and providing for me in ways I cannot comprehend. May your name be exalted.

May I express my most sincere gratitude to my supervisor, Prof. Kelly Chibale, for giving me an opportunity to work with you in your laboratory and be a part of your research group. Your endless support, patience, steady guidance, and constant encouragement truly made this journey a lot easier to bear. Thank you for always being there, for being my inspiration and an extraordinary role model. I cannot thank you enough nor even find the words that befit how thankful I am, but allow me to simply say; *ndi panshi*, *natotela sana mukwai*. May Jehovah bless you.

A huge thank you to my mentors, Dr. Malkeet Kumar, Dr. Peter Mubanga Cheuka and Dr. Preshendren '*Preshen*' Govender for the role that they played from the time I started this journey (settling into the lab), up until now. Special thanks go to Mrs. Elaine Rutherfoord-Jones, Ms. Saroja Naicker and Mrs. Deidre Van Rooyen for the amazing administrative work and support you provide to the research group. I owe it to you for all the logistical arrangements and admin work you assisted with, which without you would have been a complete nightmare to make. Your support is greatly appreciated. Many thanks to the former and current members of the Kelly Chibale (KC) academic group as well as Research Scientists and post-docs at the Drug Discovery and Development Centre (H3D). Thank you for your friendship, comradery, and your assistance in many aspects. Your positive and constructive feedback in group meetings encouraged and inspired me. I learned a great deal while you shared your work. Special thanks go to Dr. Aloysius N. Nchinda, Dr. Vir Reddy, Dr. Rudolf Muller, Dr. Dominic Castell, Dr. Donald Seanego, Dr. Shepherd S. Siangwata and Dr. Godwin A. Dziwornu, for your constant check-ups on me, for sharing effective tips in synthetic chemistry, and useful literature along the way.

May I also extend my thanks to Dr. Dale Taylor (H3D Pharmacology), Mrs. Nina Lawrence, Dr. Mathew Njoroge, Mr. Cleavon Cloete (H3D DMPK), and rest of the team for carrying out the different assays that were crucial for this project. In the same vein, I would like to thank Mr. Pete Roberts and Dr. Marwaan Rylands for their assistance in running the NMR spectroscopy experiments.

I would like to thank our collaborators on proof-of-concept experiments, malaria life-cycle stage activity assessment, mode of action and other assays. These include Dr. Sergio Wittlin and his team at the Swiss Tropical Institute for Public Health, Basel (Switzerland), Prof. Lyn-Marie Birkholtz and her team at the Institute for Sustainable Malaria Control,

University of Pretoria, Pretoria (South Africa), and Prof. Tim Egan and his research group (UCT Chemistry).

I am grateful to Novartis Pharma AG and University of Basel (UniBas) for the opportunity to participate in the 2018 Next Generation Scientist Program. A huge thank you to Ms. Akiko Keller, Dr. Fareed Mirza, Dr. Ulrich Hassiepen, and the rest of the core team for their hard work in making the program a success. Special thanks also go to my mentors, Dr. Cara Brocklehurst, and Dr. Nikolaus Stiefl, as well as other members of both the Novartis Pharma AG Genesis Microcycle (Basel, Switzerland & Boston, United States) and Synthesis and Technologies (S&T) teams. Thank you for the knowledge you imparted on synthetic miniaturization using photo-redox chemistry for new chemistry modalities during my internship, and the mentorship you continue to provide to this day. In the same vein, many thanks go to the Chemical Abstract Service (CAS) and the American Chemical Society (ACS) for the opportunity to participate in the 2019 CAS Future Leaders Program. To Ms. Mindy Pozenel, Dr. Peter Carlton, and the organizing team, thank you for a life-changing opportunity and a fantastic program.

To my family, and my wife (Dr. Muma M. Mulenga, MD), and dear friend Dr. Hanson K. Chishimba, thank you for your constant support and encouragements throughout this journey. I honestly could never have done it without a strong support system.

I would like to extend my thanks to the South African Medical Research Council, South African National Research Foundation (NRF), Novartis Research Foundation and the UCT Post-graduate Funding Office (PGFO) for their generous financial assistance, without which this work would not have been possible.

Lastly but not the least. I thank myself for working hard, staying focused and not losing sight of what I was fighting for.

PUBLICATIONS, CONFERENCES & TRAINING PROGRAMS

PUBLICATIONS

1. **Dickson Mambwe**, Malkeet Kumar, Richard Ferger *et al.* Structure–Activity Relationship Studies Reveal New Astemizole Analogues Active against Plasmodium falciparum In Vitro. *ACS Medicinal Chemistry Letters* 2021 12 (8), 1333-1341.
2. Malkeet Kumar; John Okombo; **Dickson Mambwe**; Dale Taylor; *et al.* Multistage Antiplasmodium Activity of Astemizole Analogues and Inhibition of Hemozoin Formation as a Contributor to Their Mode of Action. *ACS Infect. Dis*. 2019, 5 (2), 303–315.
3. Jovana V Milić, Andreas Ehnbom, Mahlet Garedew, Paulette Vincent-Ruz, Tracy H Schloemer…, **Dickson Mambwe**, et al. The Future of Scientific Leadership Is Interdisciplinary: The 2019 CAS Future Leaders Share Their Vision. *iScience* **2020**, *23* (9), 101442.
4. César A. Urbina-Blanco, Safia Z. Jilani, Isaiah R. Speight, Michael J. Bojdys, Tomislav Friščić, J. Fraser Stoddart, Toby L. Nelson…, **Dickson Mambwe** et al. A Diverse View of Science to Catalyse Change. *Nat. Chem.* **2020**, *12* (9), 773–776.

CONFERENCES & TRAINING PROGRAMS

1. Novartis Next Generation Scientist (NGS) Program. Novartis Pharma AG – Basel, Switzerland. 16 Fabrikstrasse, Global Discovery Chemistry, GDC (1st June – 30th August 2018). **Poster** presentation on Research Day (29th August 2018) Title: *State-of-the-art Catalytic Transformations on Microscale.*
2. Keystone Symposium, G1 The Makaria Endgame. Innovation in Therapeutics, Vector Control & Public Health Tools – Addis Ababa, Ethiopia (30th October – 2nd November 2019). **Poster** presentation Title: *Ester Bioisostere analogues of Astemizole as potential antimalarial agents.*
3. ITRG 2290 Malaria Research Symposium. Crossing Boundaries – Wallenberg Research Centre, STIAs, Stellenbosch, South Africa (30th September – 1st October 2019). **Oral** Presentation Title: *Ester Bioisostere analogues of Astemizole as potential antimalarial agents.*
4. ACS Fall National Meeting 2019. Chemistry & Water – San Diego, California, USA (26th – 30th August 2019). **Poster** Presentation Title: *Ester Bioisostere analogues of Astemizole as potential antimalarial agents.*
5. The Chemical Society of Zambia, 5th National Symposium on Chemistry, Materials & Energy (7 – 8th November 2019). **Oral** Presentation Title: *Towards leveraging the potential of the antihistamine drug Astemizole. A repositioning approach for its development as an antimalarial*

ABSTRACT

Malaria remains one of the most important parasitic infectious diseases as far as human suffering is concerned. With almost half of the world's population at risk, its burden is felt worldwide as seen by the high number of deaths recorded each year (405,000 in 2018: WHO World Malaria Report 2019). Unfortunately, over 90% of this mortality rate is recorded in Africa alone, with the highest risk being in children under the age of five (5) and pregnant women. Partly, this is due to the unfortunate spread of resistance to most drugs that were once effective and safe, including Artemisinins which form the basis of the current first-line regimen in the treatment of malaria. For this reason, it is crucial to invest research efforts using various approaches in the drug discovery arsenal to develop novel, and structurally diverse antimalarials with different modes of action. These new antimalarials should not only be able to circumvent resistance but need to be efficacious at different life cycle stages of the parasite (multi-stage activity).

This Ph.D. project pursued a drug repositioning approach on Astemizole (AST, Figure 1), a second-generation antihistamine drug which was previously identified as an antimalarial agent by Chong *et al.*, at the Johns Hopkins University School of Medicine through *via* a high-throughput screening (HTS) of diverse marketed drugs. AST was active against chloroquine-sensitive (CQ-S) and multi-drug resistant (MDR) laboratory strains of the human malaria parasite *Plasmodium falciparum* (*P. falciparum*) and demonstrated *in vivo* efficacy in two mouse infection models of malaria namely, *P. Vinckei* and *P. Yoelii*. However, in addition to its low solubility, AST possesses a serious and fatal cardiotoxicity risk, evidenced by its ability to potently inhibit the human *ether-á-go-go*-related gene (hERG) encoded potassium (K+) channels. This liability led to the withdrawal of AST in most countries during the late 1970's and it is still being discontinued for use in some countries to date.

Towards repositioning of AST, structure-activity relationship (SAR) studies were carried out in two sequential optimization stages (phase I and II, Figure 1), with phase I iteratively leading into phase II (Figure 1). Across the two phases, medicinal chemistry strategies aimed at improving solubility and reducing hERG inhibition were employed. Exploratory phase I adopted strategies such as reduction of lipophilicity (clog*P*, SAR's 1 – 3, Figure 1), introduction of water solubilizing groups (SAR's 1 – 3), disruption of molecular planarity *via* aromatic ring saturation and/or truncation (SAR's 1 & 3), replacement of piperidine with other rings (i.e., piperazine etc. SAR 4), formation zwitterionic molecules (SAR's 1 & 2) and bioisosterism (SAR 2). Front-runner compounds **67**/DM-253 and **68**/DM-147

(Figure 1) from exploratory phase I, were used as templates in advanced phase II, where some of the previously used strategies were also applied (SAR 6), including other strategies such as making subtle modifications (SAR's 7 & 8), incorporation of amides (SAR 5) and reduction the basicity (p*K*a) of the piperidine nitrogen (SAR 8). The progression of compounds for various assays was conducted using a screening cascade in which well-defined cut-offs were set. Based on *in vitro* antiplasmodium potency and solubility, compounds were progressed for *in vitro* cytotoxicity assessment in the Chinese hamster ovary cell-line (CHO) and human epithelial cell-line (HepG2) followed by hepatic microsomal metabolic stability evaluation. Representative compounds were evaluated for their inhibition of hERG K+ channels based on antiplasmodium potency, physicochemical properties and to represent hERG affinity reducing strategies utilized. Frontrunner compounds with favourable *in vitro* potency, cytotoxicity and microsomal metabolic stability were further progressed for *in vivo* proof-of-concept (PoC) and pharmacokinetic studies in mice.

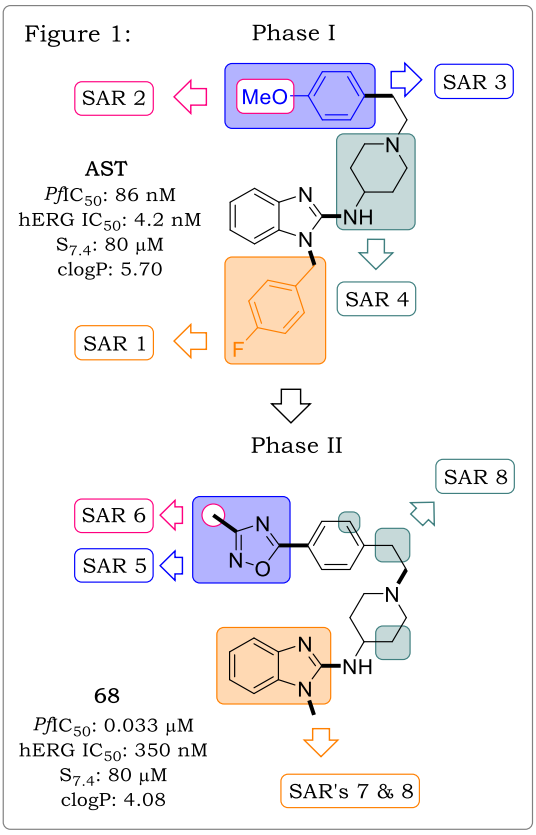

A series of highly potent (*Pf*IC$_{50}$ = 0.012 – 0.100 µM) and soluble (S$_{7.4}$ >100 µM) compounds with low hERG affinity (selectivity indices, SI = 10 – 298) compared to AST (SI = 0.05) have been identified. The analogues possess no significant cytotoxicity, as observed in the relatively high selectivity's (SI = 65 – >2000). In order to assess the potential for multi-stage activity, a diverse set of analogues across the SARs were tested for their gametocytocidal properties. This assessment not only revealed the potential for transmission blocking in some of the analogues, but also identified analogues with dual and/or stage-specificity (>75% inhibition at 5 µM). On precedent that AST had initially been implicated to act *via* inhibition of parasitic hemozoin biosynthesis, selected analogues were assessed for their ability to inhibit this process *via* a surrogate β-hematin inhibition assay (βHIA) to shed light on the potential mode of action. Strong inhibitors of β-hematin formation (IC$_{50}$ < 100 µM) have been identified, corroborating previous findings which suggest that hemozoin formation inhibition is a contributing mode of action for the observed antimalarial properties of AST and related analogues. Compound **67**/DM-253 displays >1000-fold higher selectivity over hERG compared to AST and has been identified as the first AST analogue to demonstrate high efficacy (99%) in *P. Berghei*-infected mice

when dosed orally (*p.o.*) at 50 mg.kg^{-1} once daily for four days, with a mice survival rate of 14 days. On the other hand, its closely related and discreetly modified derivative (**149**/DM-20-030) retains high *in vitro* potency (*Pf*NF54 IC_{50} = 0.017 µM) while demonstrating higher solubility, significantly lower hERG selectivity and no cytotoxicity in CHO cells compared to both AST and **67**/DM-253. The low hERG affinity of compound **149**/DM-20-030 represents a selectivity improvement of >5000-fold compared to hit compound AST.

The second component of this project was aimed at expanding the SAR of antimalarial chloroquine (CQ)-astemizole hybrid molecule **H-2** (Figure 2), which was reported in 2009 by Musonda *et al.* In their work, they showed that hybridization of AST and CQ is a viable strategy to overcome CQ resistance in *P. falciparum*. However, low solubility and suboptimal physicochemical and drug-like properties (i.e., clog*P*) would prevent the progression of the hybrids from further development. Therefore, a preliminary SAR study was carried out to improve physicochemical properties. As shown in Figure 2, three modification sites were identified based on the SAR of both AST and CQ. SAR 1 sought to remove and/or replace the 4-benzyl moiety with both aliphatic and heterocyclic moieties, and to replace the 4-Fluoro group (or 7-Cl group in CQ, SAR 3) with water solubilizing groups. On the other hand, SAR 2 was designed to incorporate water soluble groups at the 5-benzimidazole position. Compared to **H-2**, structural modifications in SAR 3 reduced the antiplasmodium activity of the hybrids, albeit solubility was improved. However, modifications involving SAR 2 and that of the benzyl sidechain on the AST portion (SAR 1) led to the identification of analogues with better or comparable potency (*Pf*IC_{50} = 0.016 – 0.053 µM) to **H-2**, with better solubility ($S_{7.4}$ < 80 µM) and physicochemical properties (i.e., clogP < 4.6).

Figure 2:

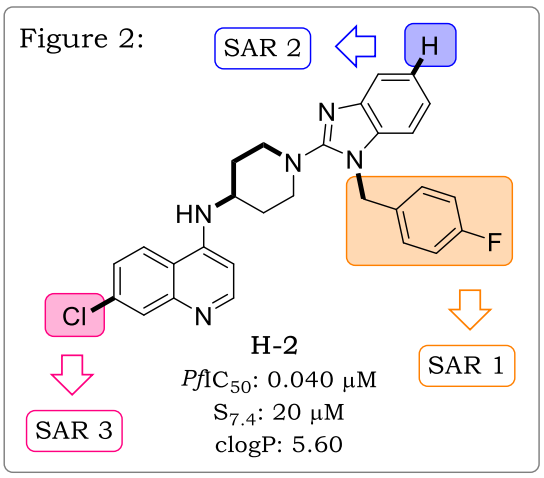

The work presented in this Ph.D thesis has provided an opportunity for further development of the AST scaffold for malaria by revealing critical antimalarial activity, hERG and cytotoxicity SARs, including structural-property relationships (SPRs) and DMPK profiles.

DEFINITIONS OF ABBREVIATIONS AND SYMBOLS USED

Å	Angstrom
α	Alpha
λ	Wavelength
a	Axial
ACTs	Artemisinin combination therapies
ADME	Absorption, distribution, metabolism, and excretion
ADME/tox	Absorption, distribution, metabolism, and excretion/toxicity
AIDS	Acquired immunodeficiency syndrome
APCI	Atmospheric pressure chemical ionization
AST	Astemizole
AST-CQ	Astemizole-Chloroquine
AR	Analytical reagent
β-HIA	β-Hematin inhibition assay
Boc	*tert*-Butyloxycarbonyl
br-s	Broad singlet
CHO	Chinese Hamster Ovarian
°C	Degrees Celsius
CDI	1,1-Carbonyldiimidazole
CF_3	Trifluoromethyl
CL_{int}	Predicted intrinsic clearance
clog*P*	Calculated log in base 10 of lipophilicity
^{13}C-NMR	Carbon-13 nuclear magnetic resonance
COSY	Correlation spectroscopy
CQ	Chloroquine
CRISPR-Cas9	Clustered Regularly Interspaced Short Palindromic Repeats-associated protein 9
Cryo-EM	Single-particle cryo-electron microscopy
CYPs	Cytochrome P450 enzymes
d	Doublet
Da	Daltons
DAD	Diode array detector
DAST	Diethylaminosulfur trifluoride
DBS	Dried-blood spot
DCC	N,N'-Dicyclohexylcarbodiimide
DCM	Dichloromethane
dd	Doublet of doublets
ddd	Doublet of doublets of doublets
ddq	Doublet of doublets of quartets
ddt	Doublet of doublets of triplets
DDT	Dichlorodiphenyltrichloroethane
DHA-P	Dihydroartemisinin–piperaquine
DHFR	Dihydrofolate reductase
DIPEA	*N*,*N*-diisopropylethylamine
DMAP	4-Dimethylaminopyridine
DMAST	Desmethylastemizole
DMF	*N*,*N*-Dimethylformamide
DMPK	Drug metabolism and pharmacokinetics
DMSO-d_6	Deuterated dimethyl sulfoxide
DNA	Deoxyribonucleic acid
dtd	Doublet of triplets of doublets
dq	Doublet of a quartet
DV	Digestive vacuole
e	Equatorial
EC_{50}	Concentration of a drug that is required for 50% inhibition *in vitro*
ECG	Electrocardiogram

EDCI	1-Ethyl-3-(3-dimethylaminopropyl)carbodiimide
EG	Early-stage gametocytes
E_H	Hepatic extraction ratio
EMA	European Medicines Agency
ESI	Electrospray ionization
EtOAc	Ethyl acetate
EtOH	Ethanol
EWGs	Electron withdrawing groups
F	Phenylalanine
FDA	Food and Drug Administration
GSK	GlaxoSmithKline
HOAc	Acetic acid
^3H	Tritium
H_2	Hydrogen
HBA	Hydrogen bond acceptors
HBD	Hydrogen bond donors
H2L	Hit-to-lead
^{1}H-NMR	Proton nuclear magnetic resonance
HEPES	4-(2-Hydroxyethyl)-1-piperazine-ethanesulphonic acid
hERG	Human *ether-á-go-go*-related gene
HepG2	Human hepatocellular liver carcinoma
HIV	Human immunodeficiency virus
HLMs	Human liver microsomes
HPLC-MS	High pressure liquid chromatography mass spectrometry
HSQC	Heteronuclear Single Quantum Coherence
HTS	High throughput screening
Hz	Hertz
IC_{50}	Concentration of a drug that is required for 50% inhibition *in vitro*
I_{Kr}	Rapid delayed rectifier current
IPTp	Intermittent preventive treatment in pregnancy
IRS	Indoor residual spraying
ITN	Insecticide-treated net
iv	Intravenous
J	Coupling constant
JTEG	Joint Technical Expert Group on Malaria Vaccines
K	Lysine
K1	Drug resistant strain of *Plasmodium falciparum*
µl	Microliter
LCMS	Liquid chromatography mass spectrometry
LG	Late-stage gametocytes
LipE	Lipophilic efficiency
LipMetE	Lipophilic metabolism efficiency
LHS	Left hand side
LLE	Lipophilic efficiency
LL-ITN	Long-lasting insecticide treated bed nets
LO	Lead optimization
logD	Logarithm of partitioning coefficient of a compound between *n*-octanol and water
LQTS	Long-QT syndrome
Lys	Lysine
m	Multiplet
M	Molar concentration
mAU	Milliabsorbance units
MDA	Mass drug administration
MDR	Multi-drug resistant
MeCN	Acetonitrile
MeOH	Methanol
MLMs	Mouse liver microsomes

MsCl	Methanesulfonyl chloride
MSD	Mean survival days
MHz	Megahertz
MMV	Medicines for Malaria Venture
MoA	Mode of Action or Mechanism of Action
MoR	Mechanism of Resistance
m.p.	Melting point
MTT	3-(4,5-Dimethylthiazol-2-yl)-2,5-diphenyltetrazolium bromide
MW	Molecular weight
mV	Millivolts
m/z	Mass to charge ratio
N-1	Nitrogen 1
NADPH	Nicotinamide adenine dinucleotide phosphate
$Na(OAc)_3BH$	Sodium triacetoxy borohydride
NaO*t*-Bu	Sodium *tert*-butoxide
NBD	7-nitrobenz-2-oxa-1,3-diazole
NBD-Cl	4-chloro-7-nitrobenzofurazan
NCEs	New chemical entities
ND	Not determined
NH_4OAc	Ammonium acetate
NH_4Cl	Ammonium chloride
Nor-AST	Nor-Astemizole
nM	Nanomolar
nm	Nanometre
µM	Micromolar
NF54	Drug sensitive strain of *Plasmodium falciparum*
pLDH	Parasite lactate dehydrogenase
P. berghei	*Plasmodium berghei*
PBS	Phosphate buffered saline
P. cynomolgi	*Plasmodium cynomolgi*
Pd	Palladium
PD	Pharmacodynamics
$Pd(OAc)_2$	Palladium(II) acetate
Pd/C	Palladium on carbon
$Pd(dppf)_2Cl_2$	(1,1'-Bis(diphenylphosphino)ferrocene)palladium(II) dichloride
P. f	*Plasmodium falciparum*
P. falciparum	*Plasmodium falciparum*
pH	negative log to base 10 of H+ concentration
pIC_{50}	negative log to base 10 of IC_{50} in Molar concentration
PK	Pharmacokinetics
p*K*a	Negative log to base 10 of the acid dissociation constant
***Pf*PI4K**	*Plasmodium falciparum* phosphatidylinositol 4-OH kinase
P. knowlesi	*Plasmodium knowlesi*
P. malariae	*Plasmodium malariae*
p.o.	*Per os* (orally administered *via* an oral gavage)
PoC	Proof-of-concept
P. ovale	*Plasmodium ovale*
PPh_3	Triphenylphosphine
ppm	Parts per million
P. vinckei	*Plasmodium vinckei*
P. vivax	*Plasmodium vivax*
P. yoelii	*Plasmodium yoelii*
q	Quartet
QSAR	Quantitative structure-activity relationship
QT_c	Corrected QT interval
RBCs	Red blood cells
RDT	Rapid diagnostic test
R_f	Retardation factor on thin layer chromatography

RHS	Right hand side
RLMs	Rat liver microsomes
Ro5	Rule of Five
rpm	Revolutions per minute
RT	Reverse transcriptase
rt	Room temperature
RuPhos	2-Dicyclohexylphosphino-2',6'-diisopropoxybiphenyl
s	Singlet
SAR	Structure-activity relationship
SCID	Severe combined immunodeficient
SD	Standard deviation
SERCaP	Single exposure radical cure and prophylaxis
SI	Selectivity index
SIT	Sterile Insect Technique
SMILES	Simplified Molecular Input Line Entry Specification
S_NAr	Nucleophilic aromatic substitution
S_N2	Nucleophilic substitution bimolecular
SO_2Me	Sulfonylmethyl
SPR	Structure-property relationship
t	Triplet
$t_{1/2}$	Half-life
TB	Tuberculosis
TCDI	1,1-thiocarbonyldiimidazole
TCP	Target candidate profile
td	Triplet of doublets
TdP	Torsades de pointes
TEA	Triethylamine
tert	Tertiary
THF	Tetrahydrofuran
TFA	Trifluoroacetic acid
TFAA	Trifluoroacetic acid anhydride
$Ti(OiPr)_4$	Titanium (IV) isopropoxide
TMS	Trimethyl silyl
TLC	Thin layer chromatography
TPP	Target product profile
TPSA	Topological polar surface area
TsCl	Tosyl chloride
t_R	HPLC-MS retention time
tt	Triplet of triplets
UV	Ultraviolet
UV-vis	Ultraviolet-visible
WHO	World Health Organization

CHAPTER 1

INTRODUCTION & LITERATURE REVIEW

1.1 Chapter Overview

This chapter provides a brief overview of malaria as a disease. Malaria is described in the context of epidemiology and etiology, extending to prevention, control, and treatment, as well as the challenges faced with current treatments. Research for new antimalarials, the current drug development pipeline in line with the malaria eradication agenda as defined by the World Health Organization (WHO) is presented. As one of the leading causes of drug toxicity and reason for drug withdrawal, drug induced cardiotoxicity by inhibition or blockade of the human-ether-*a-go-go*-related gene (hERG) potassium ion (K+) channel is described, including known strategies of attenuating drug affinity. The chapter then highlights the importance of optimizing solubility in early-stage drug discovery and describes the various strategies to optimize this property. Drug discovery approaches such as bioisosterism and molecular hybridization are described, leading up to the concept of drug repurposing and repositioning. In epilogue, the chapter introduces the benzimidazole scaffold, highlighting its significance and broad pharmacological properties, including its relevance in malaria drug discovery. Concluding subsections describe the discovery of antimalarial properties of the benzimidazole-based antihistamine drug astemizole and current progress in its repositioning as an antimalarial agent, which forms the basis of this thesis work. Finally, the chapter lays out the research program providing justification for the study and stating the research question and specific aims/objectives.

1.2 Malaria – A Global Scourge Spanning for Centuries

1.2.1 Introduction

The chronicle of malaria parasites has been known to precede human history. It had appeared in Greek writings from around 500 BC, with Hippocrates (460 – 377 BC) having been the first physician to make a description of malarial symptoms such as chills, fever, sweats, exacerbations, as wells the different clinical forms of the condition.[1] There are contradictory reports with respect to the origin of *P. falciparum*, the most virulent form of the parasite known to infect humans. Although the *P. falciparum* DNA has been detected in Egyptian mummies and skeletons (500 – 3500 BC),[2] other evidence points to Ape species (chimpanzees and gorillas) as the apparent origin.[3] Likewise, controversy also extends to an avian (bird) parasite as a source of *falciparum* malaria for both humans and chimpanzees.[4]

For centuries, malaria was one of the determining factors of socioeconomic and demographic evolution in the Italian peninsula, attracting the attention of scientists,

historians and even politicians.[5] Pope St. Gregory I, also known as Gregory the great (540 – 605) suffered from malaria himself, this was during the fall of the agricultural and economic prosperity of the roman empire, facilitating the spread of malaria to the region.[6,7]

Over 125 different species of malaria are known to infect mammals, birds and reptiles, with virulence varying in host species.[8] Scientific evidence has pinned down the emergence of malaria in the Ethiopian region of Africa[9] and developing by way of the Nile river, to the Mediterranean region, Asia, then Europe. The disease developed over time with humans due to increased mobility, becoming a worldwide disease by the 1800's.[7,9] The supposition of the nature of the illness became widely spread leading up to the first evidence of the causative parasite in humans. The word "malaria" was coined and used for the first time to describe the disease, in Italy by Francesco Puccinotti in his 1838 book. The word was derived from Italian words "mal'aria", meaning "bad air" or "evil air" or "corrupted air", and this had been the description since the 1400s.[7,10] The spread of malaria to the new worlds (the Americas) is thought to have been necessitated by Christopher Columbus and the Spanish conquistadors (colonists) during the slave trade in the 1500s. The trade lasted over 400 years, resulting in the death of millions of Africans (in-transit) from malaria.[9]

Travelling propagated the spread of malaria, but so did it inspire prevention and treatment methods. Prior to the 17th century, treatment was based on purging and bleeding, a practice which killed more than it cured. Other remedies would, though bizarre include; wearing of the largest tooth of a fish as an amulet, consumption of cold drinks containing cucumber, camphor or garlic and eating of spiders in whole.[9,11] Other used practices included slow skin cauterization by burning specific grasses.[9]

The efforts of individual scientist have contributed greatly to the advancement in understanding of the disease and discovery of medicines for malaria. During the late 19th century (1807), John Crawford, an Irish ship surgeon asserted the mode of transmission to human, stating that "–by eggs insinuated without our knowledge, into our bodies, through bites of animalcules and insect-like fleas– ".[9] By 1880, evidence of parasites in blood was confirmed by Alphonse Laveran, a French military surgeon.[12] Through the work of Patrick Manson and Ronald Ross (1897), elements of what would be known as oocytes of *P. falciparum* in *anopheles'* mosquitos after a blood meal where noticed.[13] In the same year, Giovanni Battista Grassi, Amico Bignami and Giuseppe Bastianelli, all Italian researchers, showed that the female *anopheles'* mosquito was the vector and responsible for human-to-human transmissions. They also detailed the life cycles of 3 malaria species (*P. falciparum, P. vivax* and *P. malariae*).[14]

The revolution of malaria treatment is known to have begun with the arrival of the Jesuits missionary travelers, and the discovery of the properties of cinchona bark towards malaria.[15] During the 1st world war (WWI), malaria was responsible for a high rate of death

on the Macedonian front, and it was at this point that quinine, spiked with wine or spirits (i.e., gin, given as gin-and-tonic beverage) was used as prophylaxis.[16] The development of synthetic antimalarials was equally spurred by war, after most cinchona plantations had been destroyed because of it, and quinine supply became uncertain. Countries such as Germany, Britain and America[17] took a lead into carrying out research and preparation of the first series of synthetic antimalarials such as pamaquine, proguanil, mepacrine, and chloroquine, leading up to the second generation sulfones and sulfonamides, and later on; mefloquine, 8-aminoquinolines and peroxides derived from *Artemisia annua.*[17]

The demystification of malaria took more than 4 millennia. This disease continues to be one of the most debilitating diseases of humanity, affecting social, economic and health problems especially in tropical, low- and middle-income countries. The fight against it has never been more heightened than now.

1.2.2 Epidemiology

According to the latest (2019) World Malaria Report, nearly half of the world's population was at risk of malaria in 2018. In that year, an estimated 228 million cases occurred worldwide with the African region continuing to bear the largest burden, accounting for 93% of the global incidence rate. *P. falciparum* is the most prevalent in the African region while *P. vivax* has been known to be prevalent in the WHO South-East Asia region as well as the America, and this strain was responsible for 53% and 75% of cases in those two regions respectively.[19] During the year 2018, 405,000 deaths were recorded, the WHO African region accounted for 94% of total deaths. About 24 million children are estimated to have been infected with *P. falciparum*, in sub-Saharan Africa and an estimated 1.8 million of them were likely to develop severe anemia. Of the total global death toll, 67% were children under the age of five (5),[19] maintaining the unfortunate death of "one child every two (2) minutes" statistic.

It has been reported that nearly 85% of all malaria cases in 2018 occurred in only 19 countries, and 18 of which are African countries and India (Figure 1.1), with Nigeria topping the least with 25% incidence, followed by the Democratic Republic of the Congo (12%). Although, the reduction in incidence of malaria has seemingly been stagnant since 2014, a gratifyingly steady reduction has been recorded from 2010, this is evident in the number of cases recorded per 1000 population (71 in 2010 to 57; 2014 – 2018) as well as mortality rate (23.3% in 2010 to 17.7% in 2018) in the last decade.

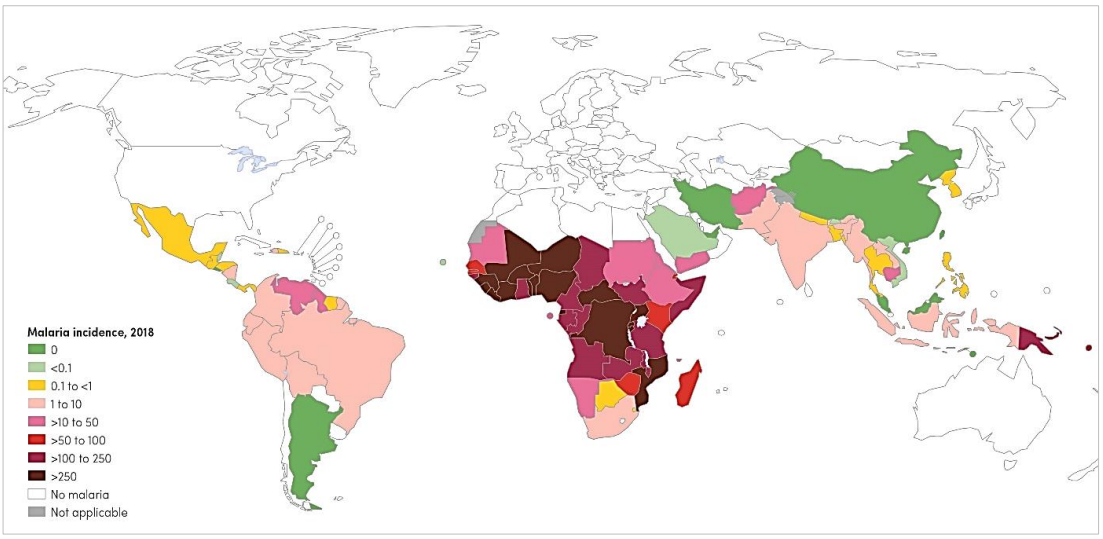

Figure 1.1: Map of malaria case incidence rate (cases per 1000 population) by country in 2018[1]

The global malaria elimination net is widening. For instance, in the year 2000, there were 108 malaria endemic countries, compared to only 91 in 2018 (Figure 1.2). This represents sixteen 16 countries in which malaria has been eliminated, that is; countries with zero indigenous cases for over 3 consecutive years.[19] This can, in part be attributed to the various malaria elimination and prevention strategies that have been established as well as heightened investments in malaria research over the last decade. Cambodia, at the heart of the Greater Mekong Sub-region (GMS) reported for the first time in the country's history, no malaria related deaths in 2018, additionally the region recorded a 76% drop in malaria cases between 2010 and 2018, with a 95% drop in deaths.[19]

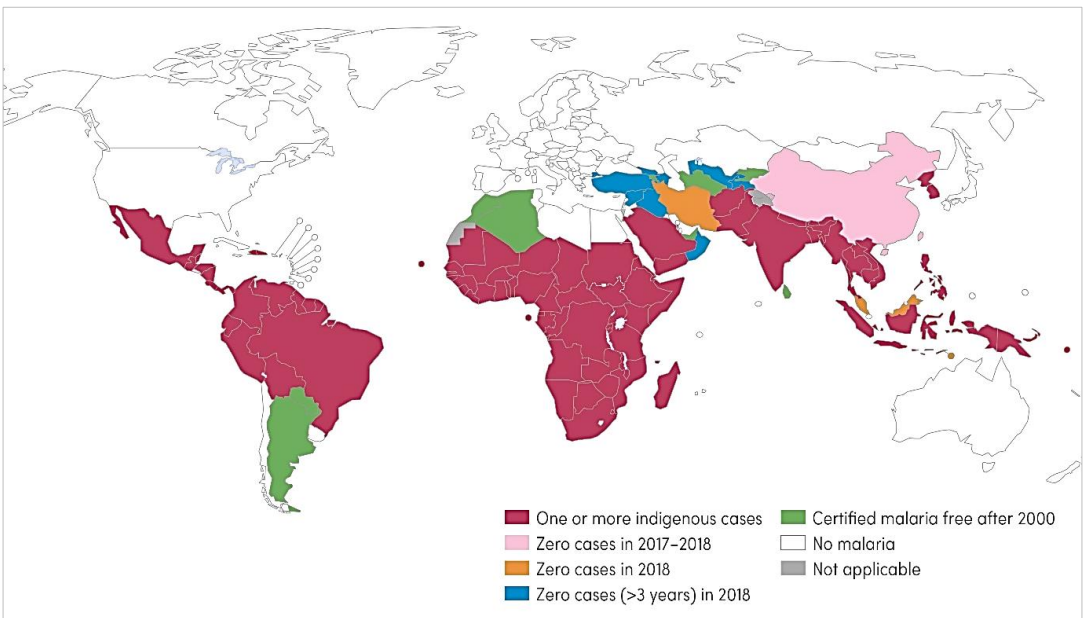

Figure 1.2: Countries with indigenous cases in 2000 and their status by 2018[1]

While countries in the Asia and South America continue to report zero indigenous cases, this has not been the case in Africa, except for Algeria, which was certified malaria-free in early 2019. Sub-Saharan Africa (SSA) is known to sit at the center of the global HIV epidemic with the highest prevalence and incidence globally. In this region, women account for about 57% of all people living with HIV.[20] Coupled with the malaria burden in this region, pregnant women are particularly at risk and vulnerable. The region has over 12 million women in their reproductive age, and over 1 million pregnancies each year are complicated by the deleterious malaria and HIV coinfection, increasing the risk of miscarriages, stillbirth and other birth complications.[20,21] Other risk groups include, children under the age of 5 years, non-immune individuals (mostly travelers and immigrants)[19] and sadly, the huge population of the poor and vulnerable living on an economic knife-edge, whose illness from malaria continues to push them into a downward spiral of poverty and vulnerability.[22]

1.2.3 Etiology, Life Cycle and Pathogenesis

Parasites of protozoan species and *Plasmodium* genus are known to cause malaria in humans. There are primarily 4 species namely, *P. falciparum*, *P. malariae*, *P. vivax* and *P. ovale*. Among these, *P. falciparum* is the most virulent and most prevalent, accounting for the largest burden, especially in Sub-Saharan Africa, followed by *P. vivax*, which is predominantly found in Asia, West Pacific and the Americas.[19,23] In recent years, *P. knowlesi*, a species known to cause severe malaria in monkeys in South-East Asia and closely related to *P. malariae*, has been reported to infect humans, regrettably making it the 5th human malaria parasite.[24] Infections resulting from *P. malariae* and *P. ovale* are rare (<1%), especially in the African context. However, Asia, and particularly the Philippines, Malaysia and Thailand have a high parasite load with *P. malariae*, which is often regarded as potentially lethal *P. knowlesi*.[19,24]

In order to develop strategies for the control and/or prevention of malaria, the life cycle and pathogenesis of the disease must be well understood. This is particularly important if stage specific or multistage antimalarials are to be developed.[26] Pathogenesis is defined as the biological mechanism involved in causing a disease state, this involves various host and parasite factors responsible for the manifestation of the disease.[27] On the other hand, the life cycle is a repetitive and cyclical sequence of changes through which a pathogen goes before returning to some initial state, this may involve both asexual and sexual stages.[28]

The life cycle of the malaria parasite (Figure 1.3) involves two hosts: the female *Anopheles* mosquito and a human being. However, pathogenesis is only manifested in humans, while the mosquito functions as a vector.[29]

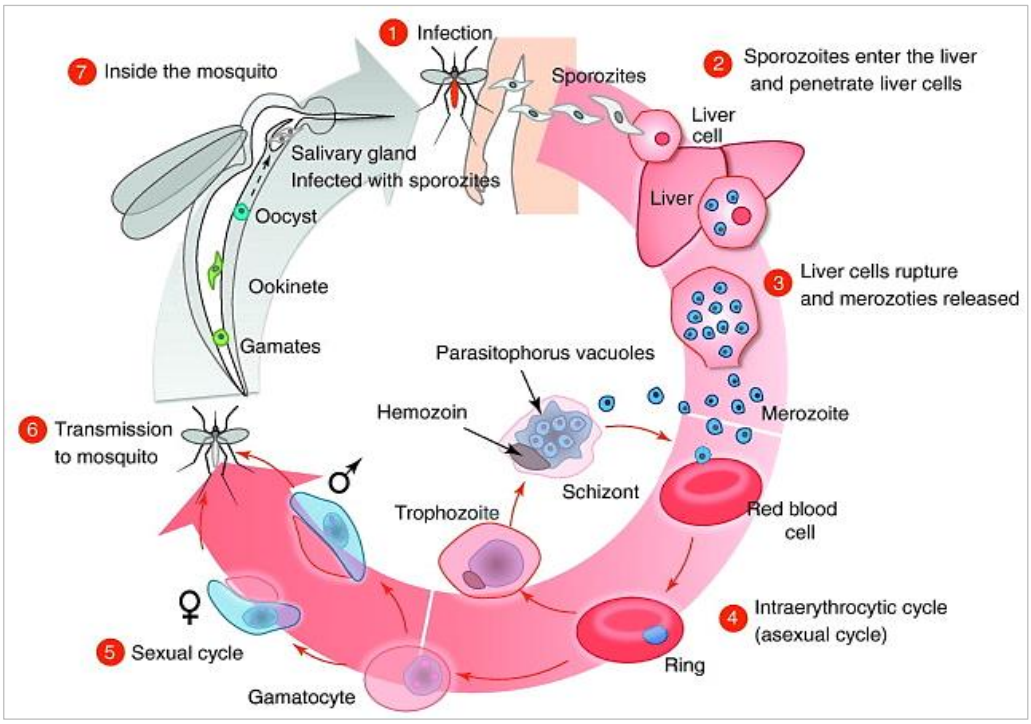

Figure 1.3: Malaria Parasite Life Cycle.[30]

During a blood meal, the mosquito injects the parasites in the form of sporozoites into the subcutaneous tissue and bloodstream of the human host, which then travel to the liver (Figure 1.3). In the liver, sporozoites invade liver cells (hepatocytes) where they develop into schizonts, a process called exo-erythrocytic schizogony, which takes about six (6) days. The schizonts then rapture, each releasing tens of thousands of merozoites. In *P. vivax* and *P. ovale*, it is during the liver stage at which, if untreated, dormant hypnozoites can develop and persist for up to years in the liver and cause relapse at any point.[27,31] Upon release, the merozoites enter the bloodstream, where they invade red blood cells (RBCs) and initiate the intraerythrocytic cycle or erythrocytic schizogony. It is during this blood stage when disease manifests clinically (symptomatic). Merozoites grow and multiply inside the RBCs to become trophozoites. Trophozoites have a uni-nucleate (ring stage) immature stage which is followed by a maturity stage leading to the formation of schizonts (multi-nuclei cells). Schizonts divide and rapture, producing more merozoites causing secondary infection of RBCs, thereby setting the cycle of rapture and re-infection.[27,30] During this stage, toxic materials also spread to cause numerous malaria symptoms including fever, shivering and in some cases, vomiting.[30]

Not all trophozoites (ring-stage) mature into schizonts, some of them develop into gametocytes, which are sexual forms (male and female gametes) of the parasite. However, gametocytes cannot develop further in the human host, hence they would have to be extracted by a mosquito again.[30] Parasite development in the mosquito is called the sporogonic cycle, and it begins with the uptake of gametocytes during a blood meal (Figure 1.3). Male and female gametes fuse together in the mosquito's intestines and differentiate

into oocytes, which undergo a series of mitotic divisions to become sporozoites. These newborn sporozoites move to the salivary glands of the mosquito, ready for infection during the next blood meal.[30]

The parasite manipulates the mosquitoes' feeding behavior to facilitate its development and survival. The production of oocytes has been shown to decrease the biting ability and fecundity of the *anopheles* mosquito, and upon production of sporozoites, the probing (biting) period and frequency of the mosquito is heightened.[29]

1.3 Prevention, Control & Treatment of Malaria

Malaria prevention, control and treatment depends on the relationships of human, parasite, and mosquito (intrinsic factors), with respect to environmental and socio-economic (extrinsic factors). Interventions rely on vector control, antimalarial drugs, personal protection, and research.[32]

1.3.1 Prevention and Control – Strategies and Methods

Malaria prevention and control are aimed at reducing the transmission of disease to a level that is no longer a public health problem, or acceptable to the community.

1.3.1.1 Vector Control

Vector control measures are aimed at reducing the adult mosquito population, reduce their lifespan of the anopheles (adult female) and prevent contact with humans. Most measures take advantage of the characteristics and survival requirements of mosquitoes, with many of the methods targeting the larval development and resting or feeding behavior of adult mosquitoes.[33] These strategies include; indoor residual spraying (IRS), personal protection measures (i.e. insecticide-treated nets (ITNs) and repellents/insecticides) and genetic control.

1.3.1.1.1 Indoor Residual Spraying and Insecticide Treated Nets

IRS involves the spraying of an insecticide inside residential walls and ceilings. It is performed with a wearable hand-operated compression sprayer containing a suspension of the insecticide active ingredient. Depending on the surface and insecticide used, the effect can last for extended periods.[34] Various considerations are taken into account in selecting the insecticides, such as residual effectiveness, safety, environmental impact and cost. Examples of WHO recommended insecticides include the organochloride derivative dichlorodiphenyltrichloroethane (DDT) and organophosphates (malathion, fenitrothion and pirimiphosmethyl) which requires once to twice (1 – 2) and three or more (≥ 3) applications per year, respectively. DDT was particularly the major reason for the success of malaria control in the 1950's and 1960's in southern United States, Caribbean islands, south Europe and former USSR.[33,34] Due to its efficacy, low cost and low toxicity, DDT is

still in limited use in areas with a high malaria burden, although with rigorous control, following a phase out recommendation by WHO in the mid-1990's due to its harmful effects to the environment and wildlife. Many regions have switched to pyrethroids such as alpha-cypermethrin, cyfluthrin and etofenprox, although mosquito resistance to these has been observed in areas like Kwazulu-Natal (KZN), in South Africa.[34]

The use of long-lasting insecticide treated bed nets (LL-ITN) has been an effective method for vector control, saving lives of many children and pregnant women. A study (2014 – 2016) in Uganda involving 400 individuals showed that parasitemia prevalence remained at 11.3% in children of less than 5 years old and >15% in order groups, even after the combined use of LL-ITN and IRS (three rounds).[34,35] This study shows that there is no guarantee these strategies, even when used together, can effectively eliminate parasitemia and transmission.

1.3.1.1.2 Larval Control

Larval control using larvicides plays a useful role in vector control. This strategy requires identification of potential breeding sites or places in communities. Intervention at this stage guarantees the potential of larva not to develop into an adult mosquito. Insect group regulators such as pyriproxyfen (granular form) can be used in water filled pits and ponds to prevent larva metamorphosis.[34] This strategy was particularly used in Sri Lanka , where malaria eradication was nearly achieved in the 1960's.[36] In Kenya, the use of the highly specific bacterial toxin *Bacillus thuringiensis israelensis* (*Bti*) led to a reduction in the density of *Anopheles gambiae* (*An. Gambiae*), when it was used in aquatic habitats.[37]

Other larval control strategies include the use of larvivorous fish species (e.g. *Gambusia* and *Poecilia*), which are ardent feeders on mosquito larvae.[38] This strategy was particularly used in several villages in India, where the fish was stocked in village wells and ponds (1998 – 2002). During this period, no malaria cases were detected. Additionally, it allowed the villagers to continue their livelihoods without the threat of insecticide damage.[34] The challenge of larvicide usage is scaling to large scale coverage or national public usefulness.[34]

1.3.1.1.4 Genetic Approach (The Gene Drive)

There are various genetic control strategies for malaria. However, the most common ones involve the use of male mosquitoes to introduce genetic factors that prevent eggs from hatching, prevent larvae survival or production of adult *anopheles* that are incapable of transmitting the disease.[34] In a technique called the Sterile Insect Technique (SIT), males carrying sterilizing factors with lethal mutations (introduced *via* irradiation) are targeted at population of females (*An. arabiensis*) that have not mated.[34,40]

Genetic engineering has led to the development of population-suppression mosquito strains such as the 'flightless female' *Ae aegypti*. This strain has a genetic element encoding for a toxin that destroys the wing muscles of females, this way, they are not able to fly and search for food or oviposition sites. This gene is spread into the population by male-carriers, which themselves are not affected by the transgene.[41] Large cage trials for population suppression using male carriers in Brazil and Florida (US) have been used.[42] The introduction of CRISPR-Cas9-mediated gene-editing in 2012 opened a new paradigm into vector control in malaria research with the first specific gene-mutants created by 2015 using *Ae. aegypti*, *An. gambiae* and *An. stephensi*.[43] This genetic tool enables the suppression of the reproductive capabilities of the mosquito population by targeting female fertility genes or by introducing a sex distorter on the Y-chromosome in the form of a nuclease designed to shred the X-chromosome during the meiotic stage. Both of these strategies have the potential to cause a significant reduction in the number of fertile females which would eventually collapse the population.[45] Another strategy is modification of females so that they could no longer support parasite development, either by knocking out a mosquito gene needed for parasite transmission (e.g., a receptor recognized by the parasite as it moves through the mosquito), or by introducing ('knocking in') a gene that interferes with parasite development.[46] Other genetic strategies include the change of the anopheles' host preference so that they feed on non-humans.

1.3.1.2 Chemoprophylaxis, Vaccines and Mass Drug Administration (MDA)

1.3.1.2.1 Chemoprophylaxis

Chemoprophylaxis is the administration of a drug to prevent the development of a disease. The use of a chemoprophylactic agent is based on the knowledge of the epidemiology and clinical implications of the disease for which the protection is being sought. The drug is taken pre-exposure or after potential exposure to malaria.[47] This strategy is highly recommended for people traveling to malaria endemic regions. However, this strategy is not prescribed as a remedy to the residents of malaria endemic countries.

Chemoprophylaxis is categorized as either primary or terminal. Primary chemoprophylaxis refers to the use of an antimalarial drug 2 – 20 days before travelling to a malaria region, continuation for the duration of the stay and for 1 – 4 weeks after return. To prevent the establishment of infection in the liver by inhibiting the pre-erythrocytic schizogony, primaquine and proguanil are administered as prophylactic agents. On the other hand, the use of blood schizonticides like clindamycin and primaquine would suppress the blood forms of the parasite and thereby protect against clinical illness. This is known as suppressive chemoprophylaxis. Terminal chemoprophylaxis on the other hand, is the administration of primaquine (usually with chloroquine) for two-weeks after return, to clear the hypnozoites that may have developed from a *P. vivax* or *P. ovale* infection that can

cause relapse. This is only prescribed for individuals who have had prolonged exposure in malaria endemic regions.[48]

Although travel during pregnancy is discouraged, in an unavoidable circumstance, the benefits of prophylaxis must balance against the risk of infection and the drug side effects. Usually, combinations are used for pregnant women and these include; chloroquine-proguanil, artesunate-mefloquine (second and third trimester only), atovaquone-proguanil and sulfadoxine-pyrimethamine (SP).[50]

1.3.1.2.2 Malaria Vaccines

Malaria vaccine development began with seminal studies using irradiated sporozoites in the 1960's. There has been steady progress ever since although even after 50 years, there is still no licensed product.[51] Noteworthy, there are almost 20 candidates in development at different stages, and RTS,S/AS01 is invaluably the most extensively tested vaccine candidate for the prevention of *P. falciparum*. The GlaxoSmithKline (GSK) vaccine candidate has been in development for over 3 decades and is up to now the only vaccine that shows protection against malaria in young children in a phase III trial.[51,52] Following a rigorous quality, safety and efficacy assessment by the European Medicines Authority (EMA) and issuance of a positive scientific opinion in 2015, as well as that of the Joint Technical Expert Group on Malaria Vaccines (JTEG) in early 2016, WHO recommended pilot implementation of the RTS,S/AS01 vaccine in distinct settings three (3) in sub-Saharan African countries namely; Ghana, Kenya and Malawi, to generate critical evidence that would enable decision making about potential for wider use.[52,53] This pilot program was rolled out in April of 2019 targeting children from 5 – 24 months and is expected to be completed by 2023.[52] The WHO recommends the use of a 4 dose schedule, done under the context of ongoing proven malaria control measures, particularly, the use of LL-ITNs, access to rapid diagnostic testing (RDTs) and artemisinin-based combination therapies (ACTs). If successful, RTS,S/AS01 will make a major milestone in the malaria field.[51,52]

1.3.1.2.3 Mass Drug Administration (MDA)

Another strategy that accelerate progress in malaria management is mass drug administration (MDA).[54] MDA is defined by the WHO as administering of a full therapeutic course of antimalarial medicines, irrespective of the presence of symptoms or infection, to a defined population living in a defined geographical area.[55] The first objective is reduction of transmission intensity and multi-drug resistance. This objective is envisaged to reduce the parasite biomass in a community in order to prevent new infections for a certain period. The second objective is the reduction of morbidity and mortality, especially during epidemics when the health systems are overwhelmed and unable to provide core malaria preventive and curative services. However, the logistical complexity of MDA requires a high level of community participation for the strategy to be successful. This strategy has been

particularly utilized in Cambodia, where 4 endemic villages randomized with 3 rounds of MDA using a 3-day course of dihydroartemisinin–piperaquine (DHA-P). High coverage was achieved and there were no clinical falciparum cases for at least 1 year.[56] A similar study has been conducted in Gambia in a low-transmission area with satisfactory results of reduced malaria infection and clinical disease during the first 3 months.[57]

MDA has challenges relating to compliance especially if multiple dose regimens are used, which is why a single-dose regimen would be very beneficial.[58] Second, MDA can be expected to select for drug resistance, especially when using an ACT with mixed pharmacokinetics such as DHA-P.[59] *P. falciparum* resistance to both artemisinins and piperaquine has emerged in Southeast Asia, accompanied by unacceptable failure rates for treatment with DHA-P.[59] Thirdly, the potential for cardiotoxicity as a result of DHA-P use has been a concern, even though there has not been any clinical manifestation of this risk.[58]

1.3.2 Malaria Chemotherapy – Current Status and Challenges

Effective as malaria control and preventive measures may be, malaria infections do happen, and these are treated by use of antimalaria drugs. Since the isolation of the first chemically pure and effective antimalarial, quinine (Figure 1.4) in 1820, there have been other synthetic and natural compounds developed.[61] Additionally, the complexity of the parasite life cycle renders it druggable at different stages, either with mono or combination therapies.[62] However, most of these drugs have been rendered less active over time due to the emergence of resistant parasites.

Chloroquine (CQ, Figure 1.4) was the first synthetic antimalarial to be produced on a large scale. It's usage dates back to the 1940s. It was used for the treatment of virulent *P. falciparum* and the so-called benign malarias *P. malariae*, *P. vivax* and *P. ovale*, targeting the blood stage of these parasites.[63] Although it remains effective against the benign malaria, *P. falciparum* resistance to CQ was first reported as early as 1950, and over the years, leading to the development of laboratory strains such as K1, W2, 7GB, Dd2 etc. which are used in potency assays as a way of showing efficacy and stratifying molecules with cross-resistance. CQ remains in use for *P. vivax* in endemic regions where resistance has not developed.[61] Mefloquine was originally developed and introduced for the treatment of CQ-resistance malaria in the 1970's by the United States (US) army. It has been used both as a prophylactic and curative drug. It is still sold in racemic form as lariam. Halofantrine, which is more active against *P. vivax* than mefloquine, was another drug developed by the Walter Reed Army Institute of Research for the treatment of all forms of human malaria. Unfortunately, the use of halofantrine diminished due to undesirable side effects relating to cardiotoxicity.[61,64]

Currently, the WHO recommends the use of artemisinin-based combination therapy (ACTs) which use a highly efficacious, fast- and short-acting artemisinin derivative, in combination with 1 or more complementary compounds which are long acting and possessing a different mechanism of action.[61] This way, there is complete protection to resistance towards artemisinins. Additionally, dosing convenience is facilitated.[65] Artemisinin was first isolated in 1971 from the *Artemisia annua* plant, a herb commonly used in Chinese medicine and has been shown to be efficacious against all multi-drug resistance (MDR) forms of *P. falciparum*. The most common derivatives of artemisinin include artemether, artesunate, dihydroartemisinin (DHA) and arteether (Figure 1.4). Some of the common ACTs include; artesunate-sulfadoxine-pyrimethamine, artesunate-amodiaquine, artemether-lumefantrine, artesunate-mefloquine, artesunate-pyronaridine, dihydroartemisinin-piperaquine and artesunate-atovaquone-proguanil.[61,65]

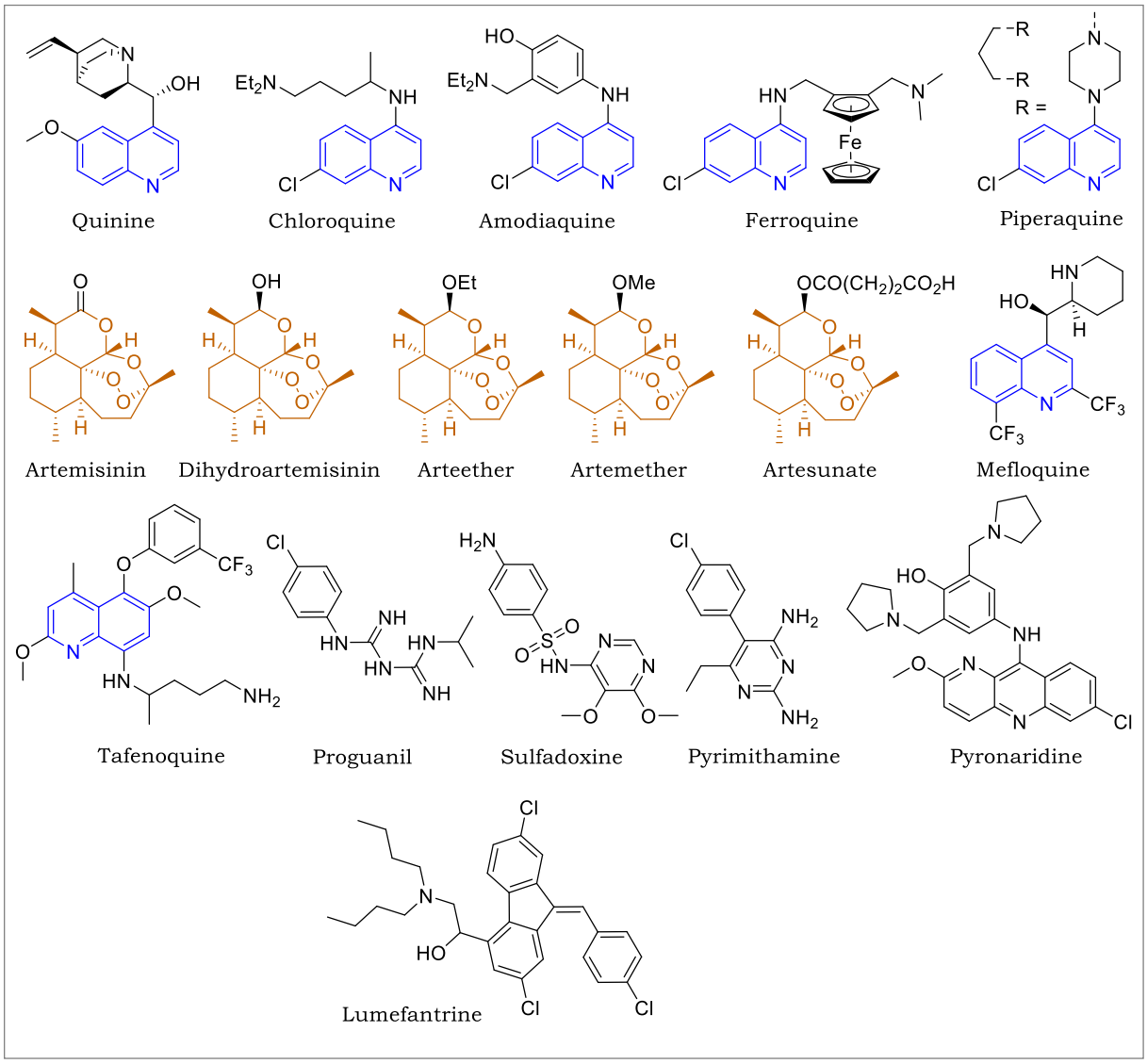

Figure 1.4: Chemical structures of some antimalarials in clinical use

The mechanism of action of artemisinins has been a subject of debate. The most accepted theory is that the molecule is activated by haem to generate free radicals which have a

deleterious towards proteins essential for parasite survival.[61] Although slow to develop, resistance towards artemisinins was reported in western Cambodia in 2008,[66] ten (10) years down the line, 30 independent cases or artemisinin resistance were reported in Southeast Asia, especially with the DHA-piperaquine ACT.[67]

Amodiaquine (AQ) has a similar mode of action (MoA) to CQ and is mainly used to treat uncomplicated *P. falciparum* malaria, usually in combination with artesunate (as camoquine® or coarsucam™).[61] Lumefantrine is thought to act by inhibition of nucleic acid and protein synthesis through the inhibition of hemozoin formation *via* complexation with haematin. It is currently used in combination with artemether under the coartem® trade name.[61,68] Atovaquone-proguanil has been an effective combination for CQ-resistance malaria with synergistic effects. These two drugs have different mechanisms, with atovaquone being a cytochrome bc_1 complex inhibitor which blocks mitochondrial electron transport,[69] while proguanil is a potent inhibitor of dihydrofolate reductase (DHFR) resulting in disruption of deoxythymidylate synthesis.[69] Antifolates pyrimethamine and sulfadoxine (Figure 1.4) are both parasite folate biosynthesis pathway disruptors, and are used in combination as SP under the trade name Fansidar® and constitute a WHO-recommendation for pregnant women as an intermittent preventive treatment in pregnancy (IPTp) course. It is administered at each of the three antenatal care visits in the third trimester. In addition to its suppression and clearance of asymptomatic infections from the placenta, SP provides prophylaxis for up to 6 weeks post-treatment.[61,62] Pyronaridine, another hemozoin formation inhibitor is used in combination with artesunate (as Pyramax®) against CQ-resistance strains.[61] More recently, tafenoquine (TQ), sold under the brand name krintafel, has been approved as the first new single-dose treatment for radical treatment of *P. vivax*. It is thought to be a pro-drug which is metabolized to active quinine-TQ.[61,72]

The continuous emergence of resistance towards artemisinins in countries in the GMS pauses a threat to the current effective regimen for malarial treatment. Additionally, the current antimalarial drug portfolio has several shortcomings that need immediate attention. Therefore, the need for development of affordable and structurally diverse antimalarials that not only offer chemoprotection, but also prevent re-infection by having multi-stage activity and potential for single dose curative properties is required.

1.4 Antimalarial Drug Development Pipeline

The Medicines for Malaria Venture (MMV) is a non-governmental public-private partnership whose mandate is to lead an effort to develop new antimalarial treatments by collaborating with various partners along the drug development (academia and big pharma) value chain, from the very early stage of drug development and lead optimization (LO) to the progression of preclinical candidates through to clinical trials and ultimately,

introduction of a new drug to the market.[61] Since its establishment in 1999, it has front-lined efforts to introduce new antimalarial drugs using a robust and strict progression criteria which demands: novel modes of action without cross-resistance to current antimalarials, single-dose curative properties, activity against both asexual blood (disease causing) and gametocytes (transmission blockers), compounds that prevent infection (chemoprotectives) and those that target the liver stage in *P. vivax* (anti-relapse agents). Figure 1.5 shows the various MMV supported projects at various developmental stages in the current antimalarial drug pipeline.[26,61]

In addition to identification of new antimalarials, another way of discovering new antimalarials is the exploration of new combination partners and repurposing of old drugs. The former is now a strict routine requirement aimed at combating resistance for newly discovered molecules or assist in the delivery of a drug thereby allowing it to be effective, and the latter is advantageous since the compound(s) would have already shown efficacy and safety profiles during development for the initial disease indication.[61]

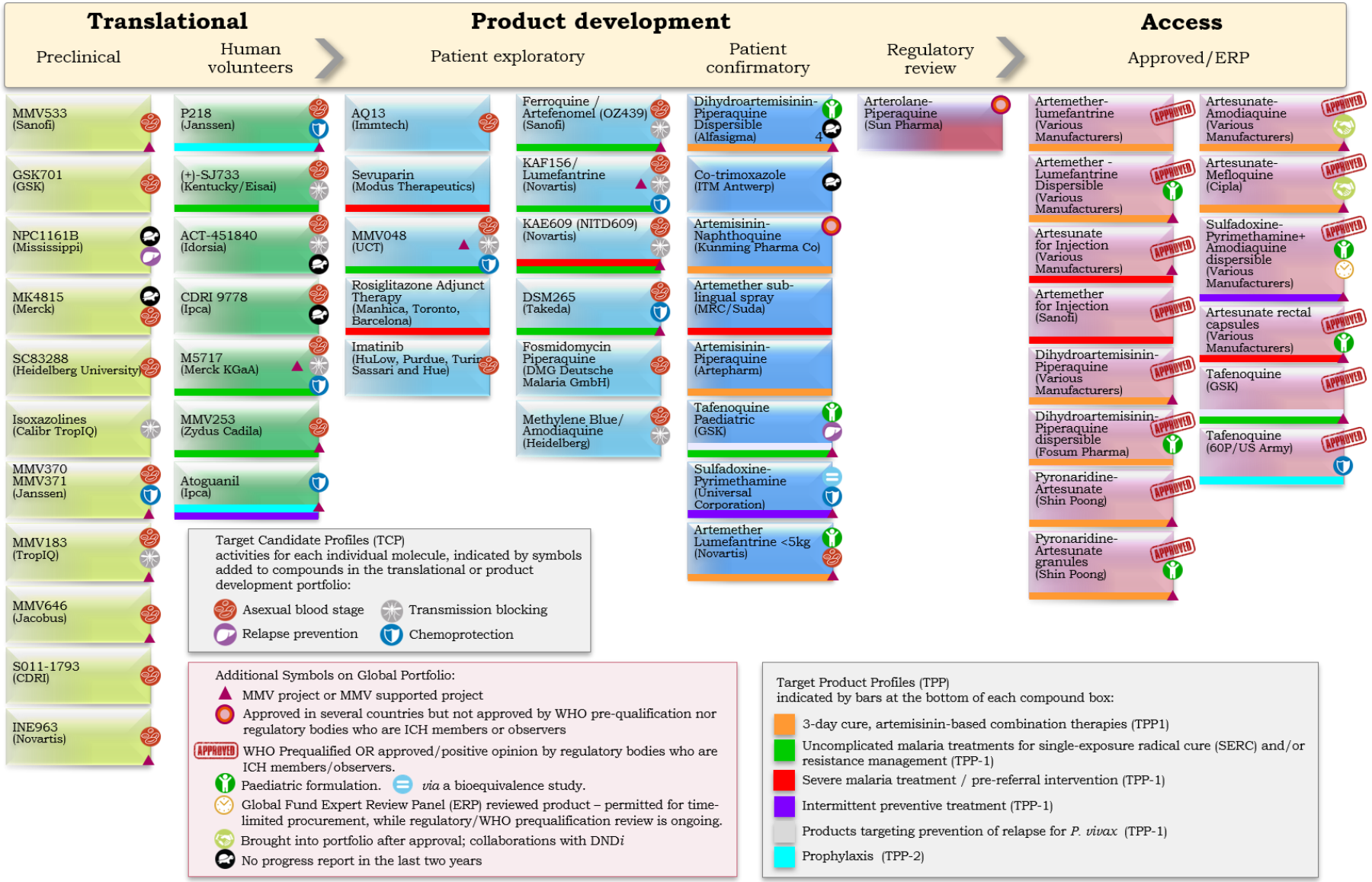

Figure 1.5: MMV supported projects at different stages of the development pipeline (A redraw adapted from the MMV-supported projects webpage).[73]

Examples of repurposed drugs currently in development include methylene blue, which is also a synthetic dye, used to treat methemoglobinemia, it is in development as an antimalarial in combination with primaquine having completed phase II trials in 2017. Fosmidomycin, an antibiotic completed phase II trials in 2015 in combination with piperaquine. Imatinib is a cancer drug currently in phase II trials as a triple combination with DHA and piperaquine. Sevuparin is a sickle cell therapeutic currently in phase I/II clinical study in combination with atovaquone-proguanil (Figure 1.5).[61]

The chemical structures of some of the novel antimalarial drugs in development are shown in Figure 1.6 below.

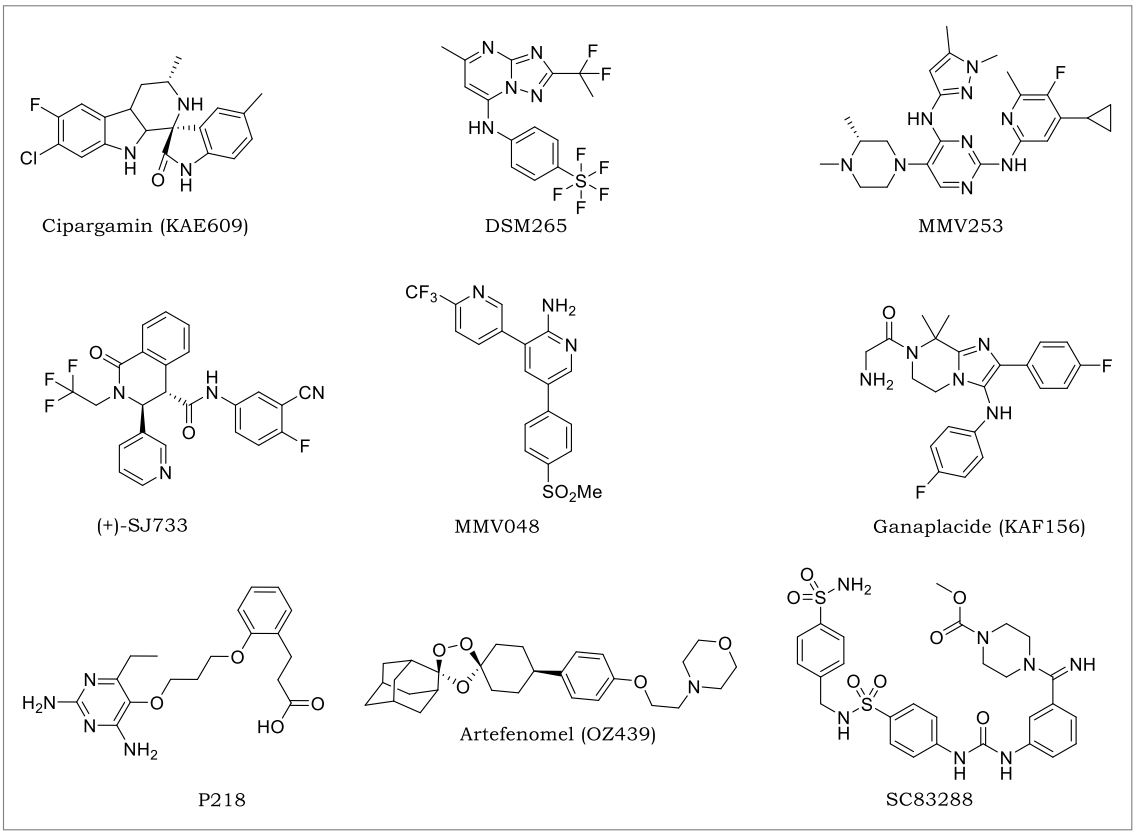

Figure 1.6: Chemical structures of some novel antimalarials in development

A number of review articles have been published in the recent years giving full details of the discovery and development of drugs which are currently in preclinical, translational, patient exploratory and product development phases of the malaria pipeline.[61,62]

1.5 The Malaria Endgame & Global Technical Strategies

There has been progress in the malaria armamentarium over the last decade, which has translated to a dramatic increase in the diversity of new molecules present in the pre-clinical and early development pipeline. To say the least, the development of resistance to the first-line effective artemisinins in the GMS and the need to provide simplified medicines has driven this paradigm shift. In 2007, the WHO in partnership with the Bill and Melinda

Gates foundation announced their strategic long-term goals for the eradication of malaria.[26]

This has shifted the focus on malaria eradication rather than control and requires different types of profiles for antimalarial medication. Using what has been learned about new medicines in the pipeline, and the challenges of elimination, a clear road maps on profiles of new therapy have been discussed and formulated by the global malaria community leading up to the proposal of target candidate profiles (TCP) and target product profiles (TPP).[26,74] In TCP, the 'candidate' refers to an individual molecule, and global MMV portfolio, these molecules are in either formal regulatory preclinical safety assessment or in human volunteer studies. In TTP, the 'product' refers to a final access-ready product, which may contain two (2) or more active candidates in the appropriate formulation.[26] TPP guidelines have been adopted by the regulatory agencies as a minimum requirement and provides a platform for shared agreement of what constitutes a successful drug. These guidelines are discussed in this subsection.

1.5.1 Single-Dose Cure (TCP_1 & TCP_2)

This profile has also been termed as the single encounter radical cure and post-treatment prophylaxis (SERCaP). To achieve this, there would ideally be needed to combine two or more molecules, a fast-acting molecule which rapidly clears parasite load, with a long-acting partner capable of killing off the residual parasites and offer longer protection.[74] TTP_1 & TTP_2 would ensure transmission prevention, and foster compliance through simplification of the therapeutic regimen from three (3) to six (6) doses, to only one (1), that which can be given after a single encounter with a health worker.[26] According to the MMV experience, successful compounds should typically have *in vitro* activities with an IC_{50} or $EC_{50} < 10$ nM against laboratory-adapted strains and clinical isolates, and a single-digit ED_{90} ($mg.kg^{-1}$) *in vivo* efficacy in a relevant humanized mouse model of *P. falciparum* i.e. the human erythrocyte-engrafted severe combined immunodeficient (SCID) mouse model.[74,75] It should, however, be noted that the goal-post is not fixed, and the priority would change especially in regions where current therapy is incapable of producing adequate clinical and parasitological response (ACPR). The focus in that case would be an active molecule on existing resistant strains, rather than simplification of cure.

1.5.2 Multi-Stage Antimalarial Activity

In addition to erythrocytic-stage killing, TCP_3 requires that an ideal combination be also able to prevent relapse resulting from hypnozoites of dormant liver stages (*P. vivax*) and the sexual stages of the parasite either in the human or the mosquito. While primaquine has this activity profile for preventing *P. vivax* it needs to be given for up to 14-days to reliably clear the *P. vivax* hypnozoites, which brings about compliance issues, additionally it causes hemolysis in glucose-6-phosphate dehydrogenase (G6PD)-deficient patients and

has gastrointestinal adverse effects.[26] The *P. cynomolgi* infected primary rhesus hepatocytes are now the only available system for testing for this profile.[76]

New molecules would require possessing anti-gametocyte activity in combination to long-acting pharmacokinetics, this is particularly a challenge for artemisinin derivates, which are active against late-stage gametocytes (LG IV/V), but do not prevent malarial clinically on their own due to their short half-lives. Respectively, the standard membrane feeding assay (SMFA) or mouse-mouse transmission models are used to assess formal transmission to the mosquito vector and in the mammalian host.[26,74]

TCP_4 stipulates drugs that offer chemoprotection by targeting pre-erythrocytic stages, which would prevent manifestation of malaria. With the challenges associated with the discovery of a vaccine for a protozoan parasite like *Plasmodium*, chemoprophylactic drugs offer the best option since quinine.[74] This can be achieved by killing sporozoites, schizonts or the parasites at the point where they emerge from the liver stages before they infect the RBCs. The current gold-standards atovaquone/proguanil and mefloquine are far from ideal due to the daily to weekly frequency of administration, although cost factors will be an important consideration for such a drug. An alternative would be a slow-release formulation of a potent and efficacious chemoprophylactic agent.[74]

1.5.3 Resistance Armored Novel Chemotypes

As covered in TCP_1, resistance can also be avoided by development of new and novel chemotypes that do not share a similar mechanism of action or resistance with an already existing drug. The open-access Malaria Box offers several different chemotypes for which resistance cannot be generated using the current laboratory strains and clinical isolates from geographical regions of established antimalarial drug resistance. Priority to pan-active molecules from the scaffolds in this box would be prioritized for optimization alongside target identification.[26,78]

1.6 Cardiotoxicity in Drug Discovery & Development

Cardiovascular diseases are among the causes of death globally, and drug-induced cardiotoxicity is one of the leading causes of drug withdrawals. The risk of cardiotoxicity for a drug is typically tested by an *in vitro* inhibition of the human-ether-*a-go-go*-related gene (hERG), which encodes K+ channels. The hERG K+ channels are expressed in a range of tissues including neurons, smooth muscles, and neuroendocrine glands but primarily, they are best characterized in cardiac cells (myocytes). The hERG channel current has been shown to have properties similar to the rapidly activating delayed rectifier K+ current (I_{Kr}), and plays a crucial role in the normal cardiac action potential repolarization in the mammalian heart.[80,81] The hERG K+ channel is one of great medical relevance, such that inherited mutations on the encoding genes (hERG, $KCNQ_1$ etc.) or drug-induced blockade there-of, results in rare congenital long-QT syndrome (LQTS) which increases the risk of

developing fatal cardiac arrhythmias such as torsades de pointes (TdP).[80,82] Young and otherwise healthy individuals manifest LQTS on an electrocardiogram (ECG) as shown in Figure 1.7, as sign of either inherited or drug induced abnormal cardiac repolarization.[84,85]

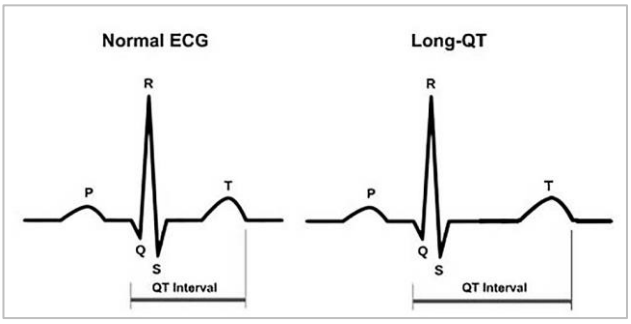

Figure 1.7: Schematic showing an ECG with a normal (left) and prolonged (right) QT intervals (Image obtained from Labmedica.com).[86]

Since the withdrawal of most approved drugs due to this liability, it has become common practice to screen compounds for hERG channel inhibition activity early during the drug discovery process, additionally, understanding the molecular basis of drug binding to hERG is crucial for the rational design of drugs that would be devoid of this risk.[87]

1.6.1 Inhibition of the human-*ether-a-go-go*-related gene (hERG) Potassium Channels: Structural Basis for Drug-Induced Cardiac Arrhythmias

The biophysics of the cardiac action potential in relation to the electrocardiogram (ECG) has been extensively studied and discussed, establishing that nanomolar blockade or inhibition of the hERG channel by certain drugs can result into action potential duration prolongation and consequently increase the QT interval.[88] To date, the crystal structure of the hERG channel has not been solved. However, the recent determination of the hERG channel structure using single-particle cryo-electron microscopy (cryo-EM) provides useful insights into how these channels work. It also suggests a way forward in the quest to understand why these channels are so promiscuous to drug binding.[82] Currently, *in silico* and ligand-based models have presented a useful starting point and strategy to develop new hits or drug leads with a good balance between potency and cardiac toxicity. These methods have furnished the understanding of how the hERG channel fits with a molecule giving a clue to better understand and inform drug design.[89]

Briefly, hERG is a member of the family of voltage gated K^+ channels (Figure 1.8), it is composed of four (4) identical subunits that each contain six transmembrane-spanning domains ($S_1 - S_6$).

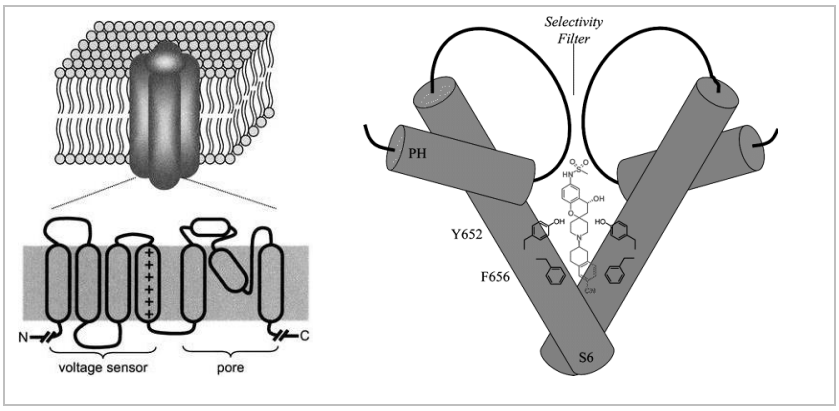

Figure 1.8: *Left:* Voltage gated K^+ channels exist as homotetramers with each subunit containing six transmembrane domains, and a pore helix interposed between the fifth and sixth TM domains.[80] *Right:* Schematic depiction of the putative interactions between a spiropiperidine-based antiarrhythmic agent MK-499 and the hERG channel.[88]

The S4 domain contains six (6) positive charges, while the amino acid sequence that extends from the beginning of the S_5 to the end of the S_6, in each of the subunits, form the pore and the selectivity filter of the channel.[88] Mutations and homology modelling studies derived from *Streptomyces lividans* KcsA K+ channel crystal structure show that aromatic residues phenylalanine-656 (F^{656}) and tyrosine-652 (Y^{652}) on the S_6 domain are important for interactions with the potent hERG blocker MK-499 (Figure 1.8).[82,88]

Ekins and co-workers used the Catalyst® software to generate a pharmacophore based on fifteen (15) molecules from the literature. In their analysis, they depict a pharmacophore (Figure 1.9) with four hydrophobic features (which are not necessarily simultaneous and present in all the considered molecules) and one positively ionizable group, exemplified by hERG blocker terfanidine.[89,90] Cavalli and co-workers adopted a "constructionist" approach to generate a pharmacophore construct, consisting of a crystal structure of antihistamine drug astemizole, a potent hERG blocker (IC_{50}: 0.9 nM), onto which they overlapped 30 other molecules starting from those with similar geometric and spatial characteristics.[91] The superimposition led to the identification of further pharmacophoric features which were used to develop a CoMFA® model correlating the 3D stereo-electronic characteristics of the molecules with their hERG blocking potency. This model consists of one protonated nitrogen function and three aromatic rings (Figure 1.9).[88,89]

The similarity of the two models is the presence of an ionizable function (basic protonatable nitrogen) bearing hydrophobic groups located at similar distances. It is evident that most hERG channel blockers have a tertiary amine group, which gets protonated at physiological pH and plays an important role for the binding of the molecule and hERG channel, this happens *via* hERG S_6 Y^{652} participation in π−cation type interactions with the protonated nitrogen.[89,92] Additionally, molecular aromatic rings (hydrophobic moieties) are associated

with π-stacking or hydrophobic interactions with aromatic rings of amino acid residue F^{656} within the hERG channel cavity (Figure 1.8).[88,89]

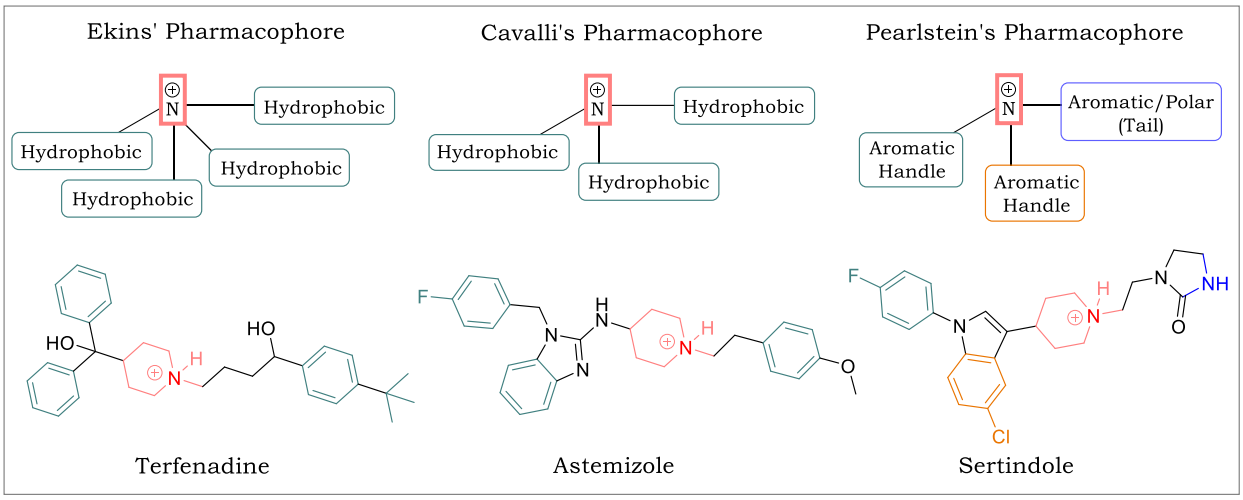

Figure 1.9: Schematic representation of Ekins', Cavalli's and Pearlstein's hERG pharmacophores. A redraw adopted from Amanda et al.[89]

Pearlstein et al. used a CoMSiA® 3D QSAR approach to analyze hERG inhibitors to derive a pharmacophore which confirmed Ekins and Cavalli models. This model highlights that molecules which penetrates the hERG channel pore from the intracellular side might orientate themselves with the long 'tail' pointing towards the selectivity filter of the channel and the hydrophobic head or 'handle', which blocks the intracellular entrance (Figures 1.8 and 1.9).[89,93]

Chloe's model arising from molecular docking of 69 known hERG blockers and IC_{50} distribution suggests a three key interaction model, in which the hydrogen bond between the protonated nitrogen of the channel blocker and the carbonyl oxygen of hERG residue threonine-623 (T^{623}) below the selective filter in the S_6 domain plays a key role, in addition to the π−cation and π−stacking interactions present in the standard model.[89,94]

1.6.2 Strategies to Reduce hERG affinity

The hERG challenge lies on balancing its affinity without altering the preferred biological effect, therefore in lead optimization, the objective would be to identify which parameter(s) influences ion channel inhibition without disrupting the desired pharmacological effect and other drug-like properties.

Some of the strategies that are used, from the understanding of the underlying mechanism of ligand-hERG channel binding include: formation of zwitterions, control of clogP, p*K*a lowering, π-π stacking altering, equatorial axis modification, chain rigidification and subtle modifications.[89] A description of each of these strategy is hereby given and where necessary, examples are provided.

1.6.2.1 Formation of Zwitterionic Species

This approach physically limits the membrane permeability of a compound through formation of a zwitterionic species. This can be achieved by introducing a carboxylic acid moiety into a compound containing a basic tertiary nitrogen. This consequently prevents access of a drug molecule to the transmembrane binding site and thereby minimizing any potential interaction with hERG. The shortcoming of this strategy is that by virtue of being a zwitterion, the molecule would have poor cell membrane permeability and consequently, suboptimal oral bioavailability attributed to poor absorption.[88]

This approach has been widely employed especially after the discovery of fexofenadine (**2**, Figure 1.10), a primary in vivo metabolite of antihistamine drug terfenadine (**1**). Terfenadine was initially discontinued after indications of TdP was associated with its use. It was later discovered that the primary metabolite is a carboxylate, which was also responsible for the observed therapeutic effects of the parent. Additionally, the active metabolite exhibits significantly low affinity for hERG and no effects on the QT interval.[88,95]

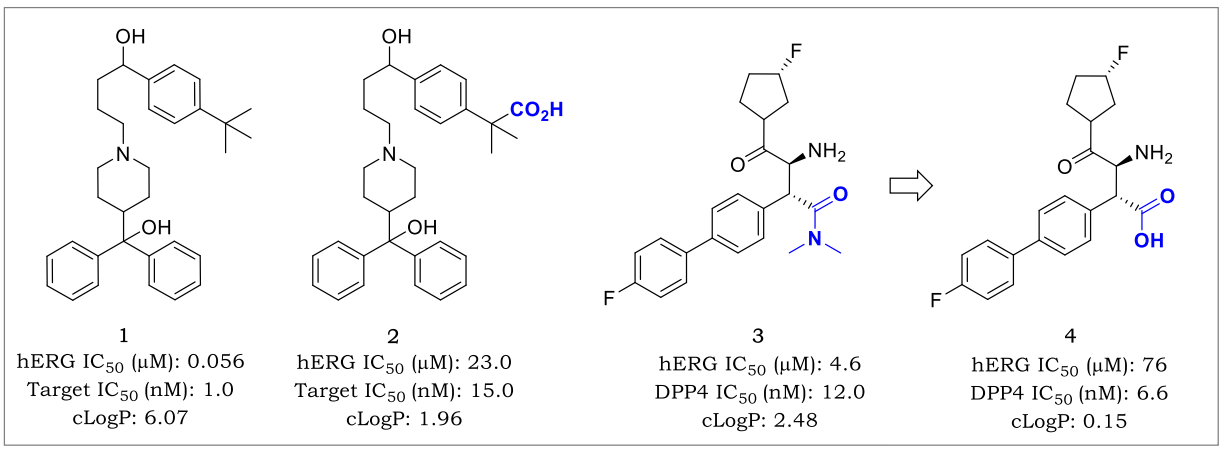

1
hERG IC_{50} (μM): 0.056
Target IC_{50} (nM): 1.0
cLogP: 6.07

2
hERG IC_{50} (μM): 23.0
Target IC_{50} (nM): 15.0
cLogP: 1.96

3
hERG IC_{50} (μM): 4.6
DPP4 IC_{50} (nM): 12.0
cLogP: 2.48

4
hERG IC_{50} (μM): 76
DPP4 IC_{50} (nM): 6.6
cLogP: 0.15

Figure 1.10: Structures of Terfenadine (**1**), its metabolite Fexofenadine (**2**) and hERG optimization of DPP4 Inhibitor **3** using the zwitterion approach.

There are several literature examples of the use of the zwitterion approach to counter hERG, either by introduction of the carboxylic acid moiety or its bioisosteres,[96–98] for instance, conversion of biaryl-β-methylphenylalanine carboxamide **3**, a dipeptidyl peptidase-4 (DPP4) inhibitor to the carboxylic acid analogue **4** gave a 16-fold reduction in hERG activity, while retaining potency against the DPP4 target. However, as previously mentioned at the beginning of this subsection (**1.6.2.1**), there is often tradeoff between selectivity over hERG and oral bioavailability of carboxylates. Therefore, in this particular case, a concomitant reduction in oral bioavailability was observed between the two compounds (**3**, F = 67% → **4**, F = 16%; Figure 1.10). This emphasizes, under certain circumstances a limitation for the utilization of this approach.

1.6.2.2 Control of Lipophilicity (clogP)

High lipophilicity (clog*P*) has been shown to be one of the key determinants of hERG selectivity. Therefore, lipophilicity-lowering strategies, for instance, incorporating groups with hydrogen-bonding potential and the replacement of high lipophilic groups with less lipophilic ones have proved to be useful in controlling the selectivity over hERG.[88,99] Other clogP lowering strategies include; exploration of polar bulky substitutions,[100] deletion or saturation of an aromatic group thus removing an important pharmacophoric element for hERG binding,[101] or replacement of said aromatic moiety with other groups like the nitrile, amide or urea have all shown significant reduction in lipophilicity, improving the pharmacokinetics and selectivity over hERG.[88,102]

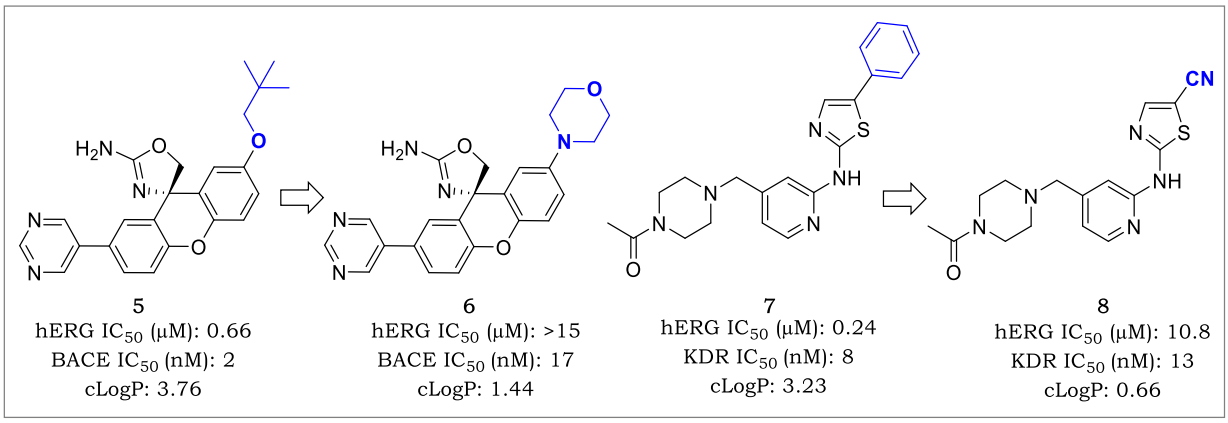

Figure 1.11: The use of lipophilicity lowering strategy to reduce hERG affinity. Structures of BACE-1 Inhibitors **5**, **6** and KDR Kinase Inhibitors **7** and **8**

In an SAR study of aminoxazoline xanthene **5** (Figure 1.11) an inhibitor of *β*-site amyloid precursor protein cleaving enzyme 1 (BACE-1), introduction of hydrophilic groups on such as morpholine (**6**) or other polar hydroxyl groups resulted in compounds with up to >22-fold lower hERG activity.[103] Likewise, reduction of cLogP from 3.23 to 0.66 by replacement of phenyl group in transmembrane receptor tyrosine kinase (KDR) inhibitor **7** with nitrile **8** resulted in a 45-fold reduction of hERG potency. Within the series, the polar N-substituted piperazine substitution was also found to be crucial in maintaining an overall optimal PK and hERG profile.[88,101]

1.6.2.3 Attenuation of pKa (Reduce Basicity of Nitrogen)

Tertiary amines are more basic than secondary and primary amines. Therefore, the presence of a tertiary amino (protonatable) group increases the likelihood of the compound to block the hERG channel.[93] Conversely, decreasing the p*K*a of the amine has the potential to decrease hERG potency by destabilizing the protonated (ammonium ion) species and preventing their interaction (π−cation) with aromatic residues lining the pocket of the hERG channel.[88] Notable success has been achieved through introduction of fluorine, a hydrogen bioisostere, at the *β*-position to the amine, the F-inductive effect allows for the

decrease in basicity commiserating less activity at I_{Kr}, while having a negligible effect on the ligand size and lipophilicity.[89] Larger pKa reduction can be accomplished with introduction of a hydroxy, alkoxy or keto group at the *β*-position to the amine, although this maintains lipophilicity to a lesser extent than fluorination.[88,89,104] Other basicity reducing strategies include replacement of piperidine with piperazine, pyrrolidine or morpholine, which additively reduces cLogP.[101,105,106] This strategy is, however, less effective for less tractable classes of compounds where the basicity of the nitrogen is critical for potency.

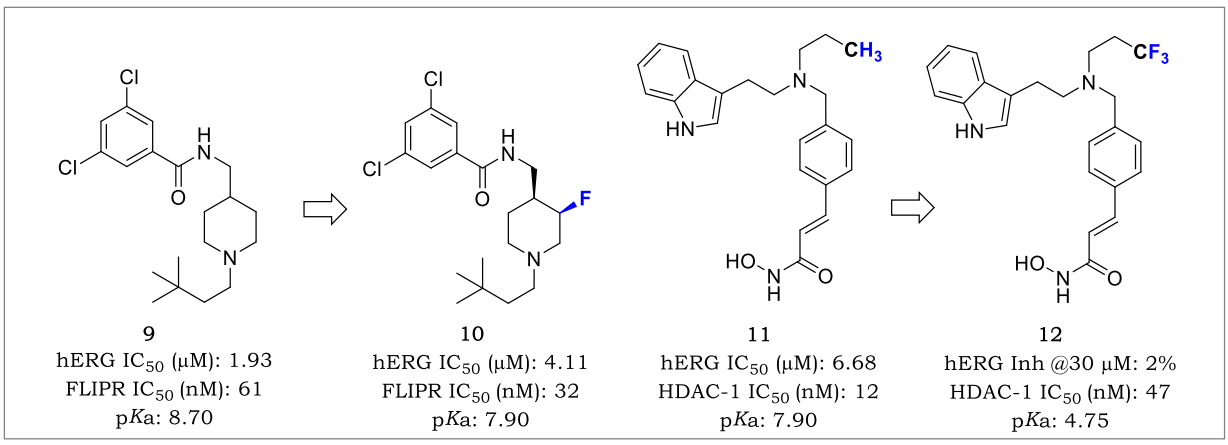

Figure 1.12: The use of basicity (p*K*a) lowering strategy to reduce hERG affinity. Structures of T-type calcium channels antagonists **9**, **10** and HDAC Inhibitors **11** and **12**

Beta (β) mono fluorination has particularly been utilized in the discovery of selective T-type calcium channel antagonists as antihypertensive agents. Fluorine incorporation in **9** (Figure 1.12), as a p*K*a reducing strategy shows a reduction in hERG activity, while improving potency in the high-throughput cell-based calcium flux (FLIPR) assay, as observed in β-fluoro analogue **10**.[107] In another instance, introduction of a trifluoromethyl (CF_3-) group in hydroxamate-based histone deacetylase (HDAC) inhibitor **11** abolished hERG affinity (**12**). In this case, the amine basicity was modulated at an 'insulated' position from the other variables and consequently, HDAC activity was not obfuscated significantly.[88,89,108]

1.6.2.4 Altering pi-pi (π−π) Stacking

As described previously in section **1.6.1**, π-π interactions between aromatic moieties in a drug molecule and those of the residues of amino acids F_{656} and Y_{652} on the S6 domain of the hERG channel, are important components to hERG affinity. Thus, strategies that impair such interactions may help in minimizing hERG channel affinity. Such strategies include; aromatic moiety saturation, deletion, replacement with smaller aliphatic moieties, or ring substitution with polar deactivating/electron withdrawing groups such as amide, nitro, or sulfone/sulfoxide moieties, or removal of an electron-donating group.[88,109–111] These ring substitutions significantly reduce *p*-electronic density thereby altering π−π

interactions between phenyl ring and aromatic residues.[109] *Ortho*-substitution (e.g. methylation) in bi-aryl systems also disrupt π−π stacking by forcing the molecule out of plane. Other strategies include, introducing a nitrogen heteroatom in a phenyl moiety to yield a pyridine, pyrimidine, pyrazine or pyridazine.[112]

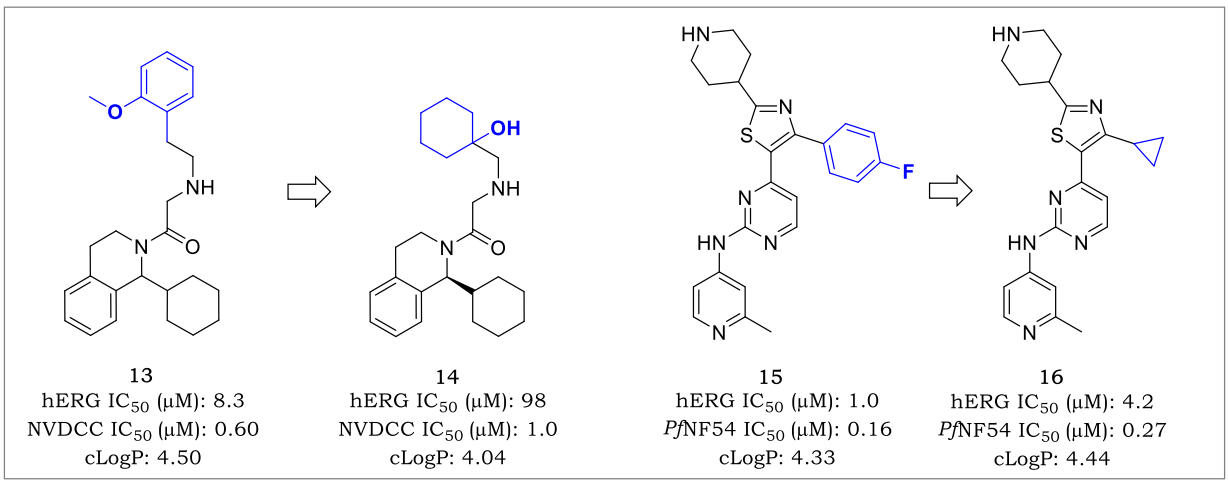

Figure 1.13: The use pi-pi (π-π) stacking disrupting strategies to reduce hERG affinity. Structures of NVDCC **13**, **14** and PKG Inhibitors **15** and **16**

For instance, disruption of π−π interactions was successfully utilized to minimize hERG inhibition of tetrahydro-isoquinolone **13** (Figure 1.13), an N-type calcium channel blocker (NVDCC) used for the treatment of neuropathic pain. The bioisosteric substitution of the phenyl group to an aliphatic ring in **14** improved selectivity over hERG channel inhibition by 6-fold.[89,113] In the same way, replacement of the *p*-fluorophenyl group of antiplasmodium cGMP-dependent protein kinase (PKG) inhibitor **15** by a cyclopropyl moiety in **16** attenuates hERG inhibitory by 4-fold while maintaining the biological activity of the derivative.[89,114]

1.6.2.5 Subtle Modifications

For certain chemical families, the strategies described above may not be successful. Subtle or discrete changes in the molecular architecture of a hERG inhibitor which results in minimal overall impact on molecular properties, can play a significant role in disrupting putative interactions and affect affinity for the hERG channel.[88] For instance, the replacement of the central spiro piperidine-pyrrolidine linker in antitubercular benzothiazinone **17** (Figure 1.11) by an azabicyclo[2.2.2]octane ring in **18** showed a significant decrease in hERG affinity while maintaining potency.

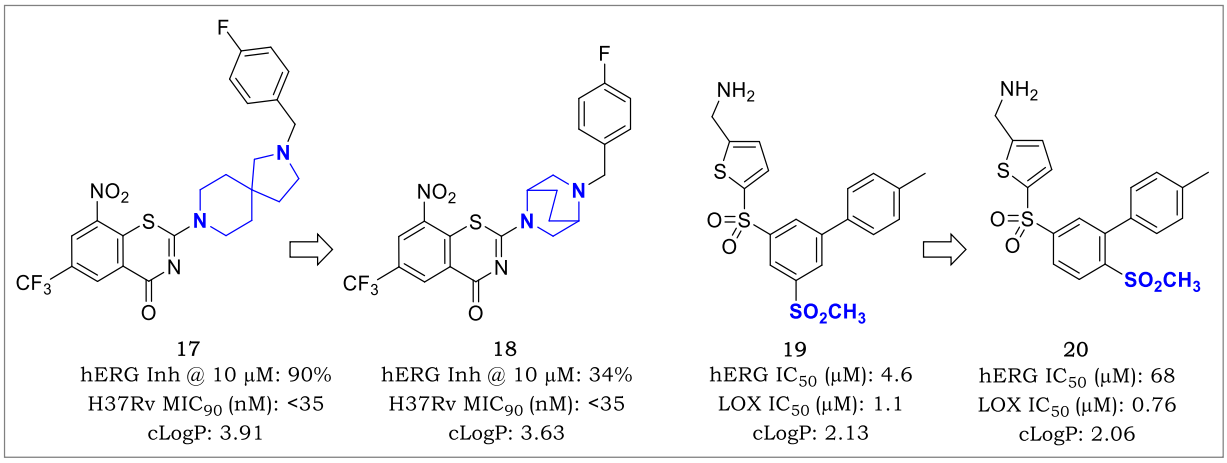

Figure 1.14: Subtle modifications as a strategy to reduce hERG affinity. Structures of antitubercular agents **17**, **18** and anti-metastatic agents (LOX Inhibitors) **19** and **20**

In the same SAR study, replacement of the *p*-fluoro-benzyl moiety in **17** with *p*-fluoro-phenyl (-CH_2- deletion) brought about even lower hERG potency (23% Inhibition at 10 µM) with retained antimycobacterial activity.[115] In the development of a series of 2-aminomethylene-5-sulfonyl-thiophenes as lysyl oxidase (LOX) inhibitors for cancer therapy, introduction of a methyl sulfone substitution greatly increases the biological activity but also influenced hERG affinity. Interestingly, the regio-position of the sulfone moiety played a critical role in controlling hERG binding with up to ~15-fold improvement between the meta-(**19**) and the para-sulfonyl (**20**) derivatives (Figure 1.14).[116]

1.6.2.6 Stereoselective & Combination Effects

Several studies have shown and emphasized the potential of stereoselectivity between distinct enantiomers towards hERG channel blockade.[117] One of the first demonstration of this effect was by Kanai et al when they disclosed that anesthetic *(S)*-bupivacaine was a more potent hERG inhibitor than *(R)*-bupivacaine.[89,118]

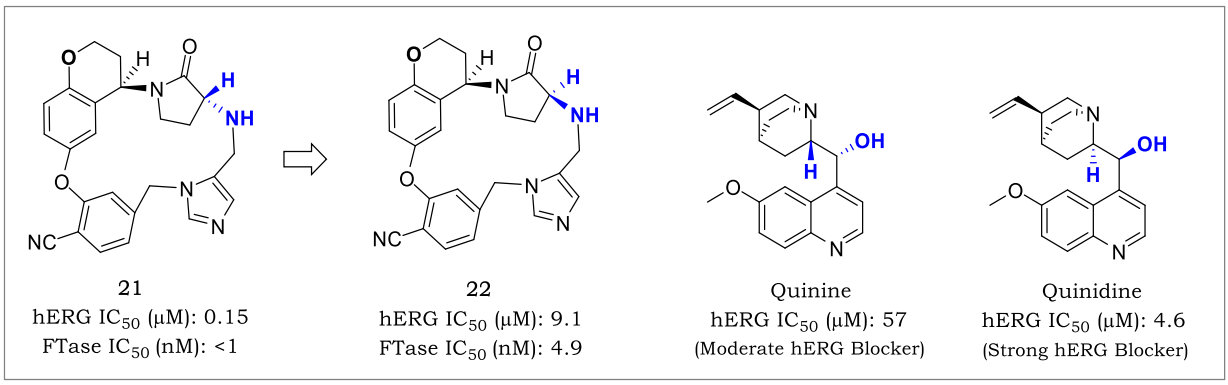

Figure 1.15: Stereoselective and Combinations in attenuating hERG affinity. Structures of anticancer agents **21**, **22** and diastereomers Quinine and Quinidine

In the same context, quinidine (antiarrhythmic) and its dextrorotatory diastereomer quinine (antimalarial), do not only have different pharmacological profiles, but also differ in their level of interaction with hERG K^+ channels (Figure 1.15) . Both quinidine and quinine show prolongation of the QTc interval, but the maximum change after quinine infusion has been shown to be approximately half of that observed after quinidine infusion. However, no significant cardiotoxicity has been reported in large prospective studies of quinine in both uncomplicated and severe falciparum malaria, with total plasma concentrations up to 20 μg/mL *in vivo*. By contrast, at comparable concentrations of free drug quinidine is hypotensive and causes marked QT prolongation.[119] In another example involving novel anti-cancer pyrrolidinone-based farnesyltransferase (FTI) inhibitors, the *(S)*-analogue **21** (Figure 1.15) showed a significant 60-fold drop in hERG affinity achieved by preparation of a diastereomerically related *(R)*-analogue **22**.[120,121]

Evidently, there are no absolute rules which can be used in early stages of drug development for the detection of an effect on cardiac repolarization, but several principles can be emphasized as highlighted in this concise review. Some of these strategies will be used in this project.

1.7 Solubility in Drug Discovery & Development

Poorly soluble compounds not only create issues for *in vitro* and *in vivo* assays in early drug discovery, but also place a significant burden on clinical drug development. Typically, compounds with insufficient solubility have a higher risk of attrition and associated higher costs in development.[122] Drug absorption, sufficient bioavailability and a favorable pharmacokinetic profile in humans are among the major challenges in oral delivery of new drug substances.[123] The oral bioavailability of a drug is dependent on the degree of intestinal absorption which is in turn affected by solubility, permeability and the pre-systemic metabolism. Therefore, low solubility will limit absorption and cause low oral bioavailability of a drug. Additionally, poorly soluble compounds are more susceptible to food effects and often exhibit large individual variability for in vivo exposure.[122–124] It is, therefore, important that drug discovery programs (during compound design and optimization) as well as pharmaceutical development programs (early and late stages) generate drug candidates with sufficient aqueous solubility.[124]

Medicinal chemists have a huge challenge to design small molecular entities (NCE's) with balanced multiple crucial parameters. This balance must be established between target potency, minimal off-target activity, absorption, distribution, metabolism and excretion properties (ADME), safety properties, efficacy in preclinical models and patentability.[122] Ideally NCEs should have sufficient solubility to ensure adequate drug exposures in preclinical pharmacokinetic, efficacy and toxicology studies to ultimately underwrite clinical candidate selection.[125] Several approaches have been developed to improve solubility of initial screening hits and during the lead optimization (LO). Some successful

strategies are discussed in this section and where necessary, examples are cited from literature.

1.7.1 Chemical Strategies to Improve Solubility

1.7.1.1 Reduction of Lipophilicity

Lipophilicity lowering strategies often translate to improved aqueous solubility. Some of these are similar to those already outlined in Section **1.6.2.2** for the control of clogP in hERG attenuation. These include: replacement of or substitution aromatic moieties with groups that have hydrogen bonding capability, removal or replacement of halogen atoms and methylation of amides.[126] Removal of or reduction of alkyl chain length allows for the freedom of movement into different orientations and conformations which influences the crystal packing and consequently reducing solubility.[127]

1.7.1.2 Introduction of Ionizable Groups and Salt Formation

Incorporation of water solubilizing groups is a widely used strategy to improve solubility. This strategy is most effective if used at positions that do not alter other important properties like potency. Such groups include amino, tetrazoles, hydroxyl-cyclo-alkyl, sulfoxide, sulfone, hydroxyl, amide, carboxyl, and phosphate.[128] For instance, the use of alkoxy amines tethered to the core pharmacophore has been successfully applied in the discovery of calcium channel blocker amlodipine,[129] estrogen receptor modulator tamoxifen[130] and farnesoid X receptor (FXR) agonists[131] with a significant increase in solubility compared to the original lead molecules.

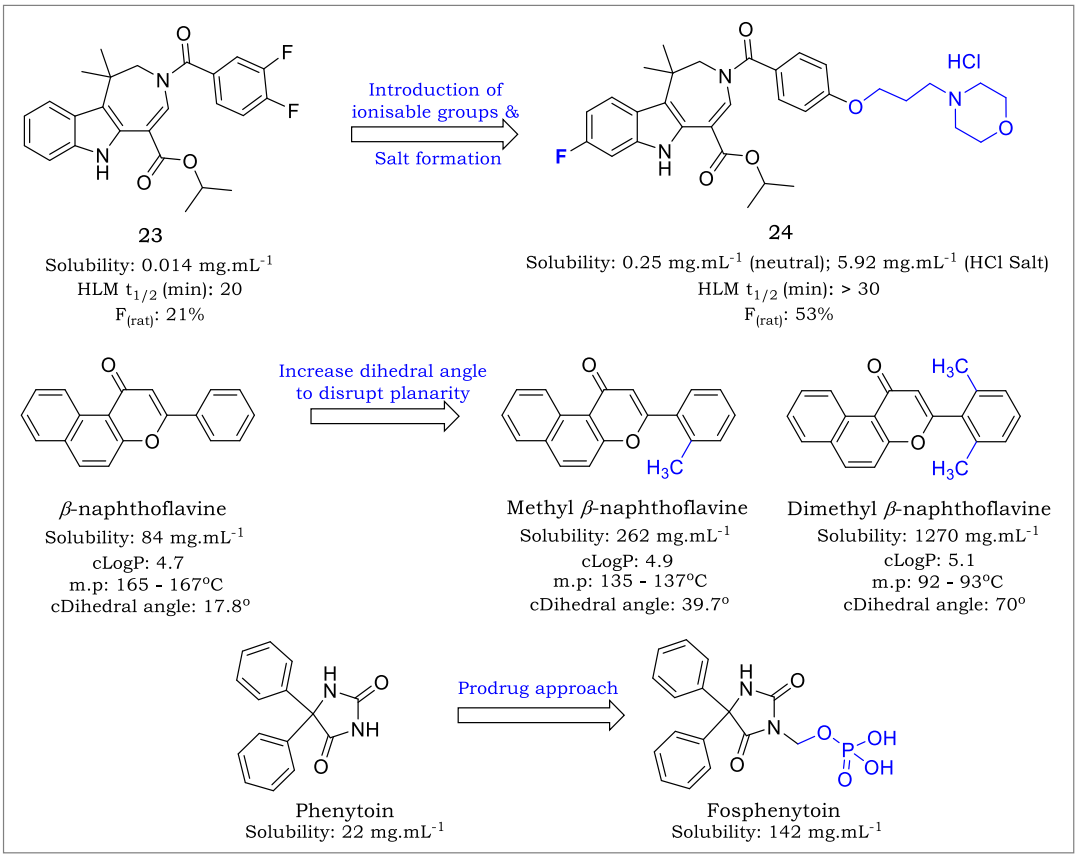

Figure 1.16: Examples of chemical modification approaches to improve solubility

As shown in Figure 1.16, introducing a basic amine as an ionizable center in lead compound **23** (an FXR agonists), and a floppy tail to disrupt the crystal packing led to improved solubility and metabolic stability, translating to high oral bioavailability of drug candidate **24**. This example also shows the opportunity that lies in ionizable groups to form salts which generate superior biopharmaceutical properties.[122,131] An appropriate salt form can increase dissolution rate and lead to faster and more complete oral absorption [that is: shorter T_{max}, higher C_{max} and area under the curve (AUC)].[122] An additional example is that of anti-inflammatory drug Piroxicam, the salt form show significant increase in dissolution rate and oral bioavailability compared with the neutral molecule.[132]

1.7.1.3 Disruption of Molecular Planarity

Under certain circumstances, classical approaches described above do not bring about improved solubility without interfering with biological properties by disrupting the ligand-target interactions.[133] One other approach that has been utilized to avoid drastic structural changes is the disruption of molecular planarity and symmetry. The relationship between solubility, lipophilicity and melting point can be summarized in the equation below, derived by Yalkowski.[133] It shows that melting point is related to crystallinity and crystal packing energies while log P is a measure of the interaction of the solute with water. Since crystal packing (π-π) stacking) of a molecule is influenced by both molecular planarity and symmetry, it can be expected that disruption of planarity would result in a decrease in the

crystal packing efficiency and melting point thereby improving solubility.[133] Additionally, reduction in the melting point has been correlated to increase in molecular sp^3 character, defining molecular complexity (presence of chiral centers), which leads to soluble molecules with a high propensity of clinical success.[134]

$$\text{Log (solubility, M)} = 0.5 - (\log P) - 0.01([\text{melting Point, }^{o}C] - 25)$$

Crystal packing reduction strategies such as, partial, or complete ring saturation (increase sp^3 character), removal of aromaticity, introduction of substituents (i.e., methyl group in a bicyclic structure in such a way that increases the dihedral angle and twisting of fused rings have all been proved to be useful in improving solubility.

In one example, Ishikawa and co-workers successfully improved solubility of β-naphthoflavone (Figure 1.16) an a biaryl hydrocarbon receptor (AhR) agonist, an inducer of detoxification enzymes such as CYPs.[133] Subtle introduction of a one or two methyl group(s) at the *ortho*-position in the biaryl system increased the solubility by 4-fold and 15-fold respectively. Using density function theory calculations, they showed substantial increase in the dihedral angle in both the mono-methylated (37.9°) and di-methylated (70.0°) analogues compared to the unsubstituted parent molecule (17.8°) which shows a complete twisting of the molecule out of plane reducing crystal packing. Fluorination also brings about a similar observation.[133]

1.7.1.4 Prodrug Approach

A Prodrug is a bio-reversible derivative of a drug molecule that must undergo an enzymatic and/or chemical transformation *in vivo* to release the active parent drug, which can then exert its desired pharmacological effect.[135] Prodrug approaches are frequently applied to improve solubility of insoluble compounds, enhance oral absorption and enable safe and effective intravenous formulations. However, it is crucial to exercise caution when considering a prodrug strategy as there is a potential toxicity risk associated by the release of the prodrug-solubilizing auxiliary from the prodrug.[137] The use of water-soluble prodrugs include amino esters, alkyl esters and polyethylene glycol (PEG), however phosphate esters ($R–OPO_3H_2$ or $R–OPO_3Na_2$) have had a clinical precedence whenever solubility has been increased by orders of magnitude over the parent drugs. Phosphate esters rely on alkaline phosphatase enzymatic cleavage in the gut lumen or blood to release the parent drug.[122] One example is that of fosphenytoin (Figure 1.16), a water-soluble phenytoin prodrug used only in hospitals for the treatment of epileptic seizures.[138]

Other strategies include physical modifications which address solubility without modifying the chemical structure of the compound, these include: use of co-solvents,[140] surfactants and cyclodextrins,[141] particle size reduction, co-crystals and polymorphs[142] as well as amorphous solid dispersion.[143]

Some of these approaches will be utilized to improve the aqueous solubility of astemizole in this project.

1.8 Bioisosterism in Drug Discovery & Development

In drug development, a lead compound (LC) can be associated with undesirable characteristics. Therefore, during lead optimization (LO), there may be need to improve potency further, enhance selectivity, alter physical properties, reduce or redirect metabolism, eliminate or modify toxicophores and optimize pharmacokinetics (PK).[144] In contemporary medicinal chemistry, bioisosterism has been adopted as one of the fundamental tactical approaches used to address specific problems associated with a compound and impinge the long-term success of a drug candidate. It presents both a qualitative and intuitive approach for the rational molecular modification of LC's into a more clinically effective, safer and ideal drug candidate.[145,146]

The concept of a isosterism was first created in 1919 by Irving Langmuir, who defined an 'isostere' as atoms or molecules which possess the same number and/or arrangement of electrons.[144] However, bioisosteres relate to structurally distinct 'atoms or groups of atoms' recognized similarly by biological systems, and the term bioisostere has its origins in Erlenmeyer's work in the 1930s, although the term wasn't introduced until 1950 by Harris Friedman, who defined it as 'compounds eliciting a similar biological effect' while recognizing that compounds may be isosteric but not necessarily bioisosteric.[145,147] In modern medicinal chemistry, a bioisostere is defined as a chemical substituent, atom, or group of atoms, or even an entire scaffold with similar physical and/or chemical properties, which produce broadly similar biological properties to another chemical compound.[148] Therefore, the objective of a bioisosteric replacement would be with a surrogate structure that not only elicits functional mimicry but solves a specific liability associated with the lead compound.

The design of bioisosteres introduces structural changes which can either be beneficial or deleterious depending on the context, with size, shape, electronic distribution, polarizability, dipole, polarity, lipophilicity, and pKa potentially playing key contributing roles in molecular recognition and mimicry. Therefore, careful analysis of such parameters and understanding of a particular molecular environment of the biological target is of great importance in the design and choice of bioisosteres.[144,148] Bioisostere are classified in two broad categories; classical and non-classical

1.8.1 Classical Bioisosteres

Classical bioisosteres represent the early appreciation of the concept which encompass structurally simple, mono-, di-, and trivalent atoms or groups and ring equivalents summarized in Figure 1.17.[145] This class of bioisosteric replacements have been utilized to mitigate various liabilities in drug discovery.

For instance, by H (**25**) → F (**26**) interchange in a lead optimization (Figure 1.17) of a series of receptor tyrosine kinase (RTK) inhibitors as potential anticancer agents, a team at Global Pharma R&D, successfully improved oral exposure and achieved good PK profiles in different species while significantly inhibited tumor growth in several preclinical animal models. Based on its overall *in vitro* and *in vivo* profile, **26** was progressed for clinical evaluation.[145,149] In another example, fluorinated cyclooxygenase inhibitor **27** exhibited an undesirably *in vivo* (rat) long half-life of 221 h, this precipitated the examination of the CH_3 and NH_2 moieties as a replacement for the F-atom and methyl group respectively. This way a vulnerable metabolic soft spot was introduced, taking advantage of the effect of phase-I cytochrome-P450 (CYP)-mediated benzylic hydroxylation and phase-II conjugation with glucuronic acid, respectively.

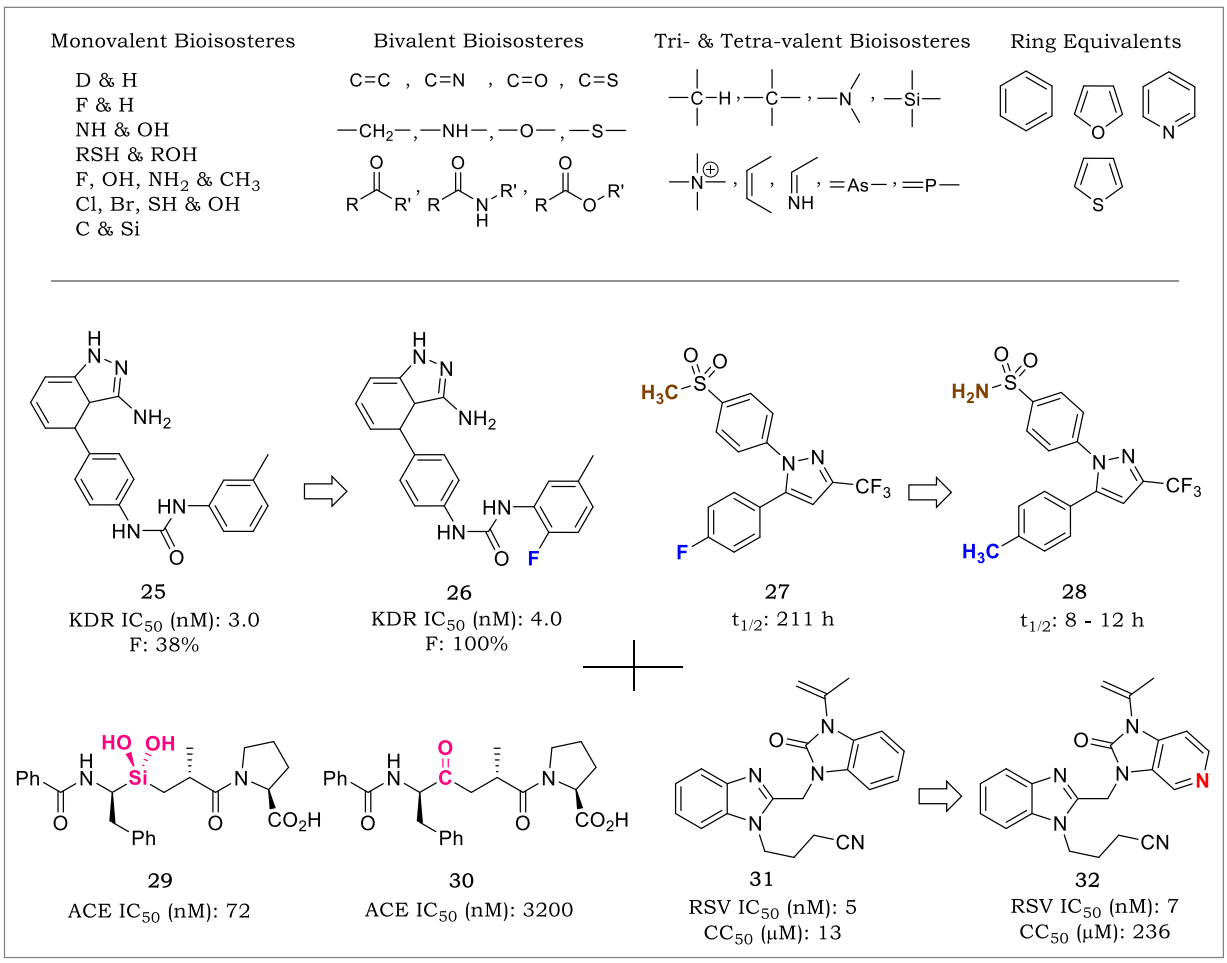

Figure 1.17: Examples of classical bioisosteres and their successful utilization in lead optimization

This led to the identification of celecoxib (**28**) with a half-life of 8-12 h. Celecoxib was introduced on the Brazilian market in 1999 by Pfizer/Searle Laboratories to treat rheumatoid arthritis and other inflammatory conditions.[144,145]

The utilization of silicon as an isostere of carbon has been reported in several bioactive molecules, some of which have been advanced into clinical studies.[145] Sila-substitution (C/Si exchange) have not been exploited to a significant extent due to concerns over the

potential toxicity. However, it presents a unique opportunity to search for new drug-like candidates with superior properties and a clear intellectual property (IP) position.[150] One example is that of Si-based angiotensin converting enzyme (ACE) inhibitor **29** (ACE IC_{50}: 72 nM), which is more potent (~45-fold) than the C-based homologue **30** (ACE IC_{50}: 3200 nM) (Figure 1.17). This has been hypothesized to be as a function of conformational differences imparted by silicon.[145,151]

As a final example, N/CH bioisosteric exchange has been utilized in the development of respiratory syncytial virus (RSV) inhibitors for antiviral potency, cytotoxicity, and metabolic stability. The pyridine ring was pursued systematically with the objective of reducing the hydroxylation of the phenyl ring seen in the parent benzimidazol-2-one **31**. The topological location of the N-atom played a critical role, and preferred compounds demonstrated improved metabolic stability and increased solubility without introducing the burden of CYP-inhibition, a potential problem with pyridine derivatives. The 6-aza-benzimidazol-2-one discovered with **32** was ultimately incorporated into the clinical candidate that emerged from these studies.[145,152]

1.8.2 Non-Classical Bioisosteres

In contrast to classical bioisosteres, nonclassical bioisosteres extend the concept to structural elements that offer a more sophisticated form of biochemical mimicry which relies upon functionality that can differ substantially in electronic, physicochemical, steric, and topological representation from that being emulated. It includes replacements wherein a noncyclic functional moiety mimics a cyclic group sterically or electronically resulting in retention of biological activity.[145,146,153] Examples of non-classical bioisosteres for functional groups commonly found in drugs are presented in Figure 1.18.

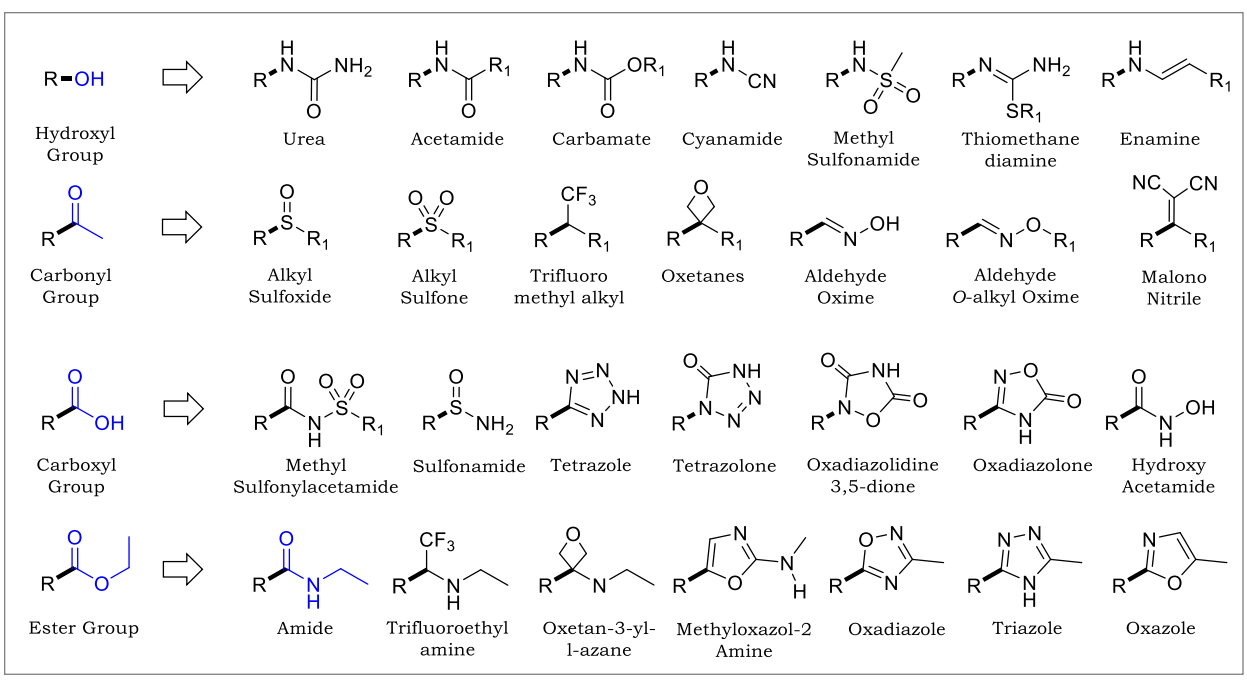

Figure 1. 18: Examples of some non-classical bioisosteres of Hydroxyl, Carbonyl, Carboxyl, Ester and Amide functional groups

In early hit-to-lead progression of antimycobacterial agents targeting the promiscuous cytochrome bc_1 in *mycobacterium tuberculosis* (*Mtb*), a team at the University of Cape Town, H3D, developed an initial ester hit **34** (Figure 1.19) compound into an early lead molecule **35** by bioisosteric replacement of the metabolic labile ester moiety with a methyl oxadiazole bioisostere. This resulted in good *in vitro* metabolic stability (97% compound retention after incubation in Human S9 fraction for 40 minutes) and improved potency (2-fold). Although this stability did not translate to good exposure and in vivo efficacy, it demonstrates the successful utilization of bioisosterism to improve metabolic stability.[154]

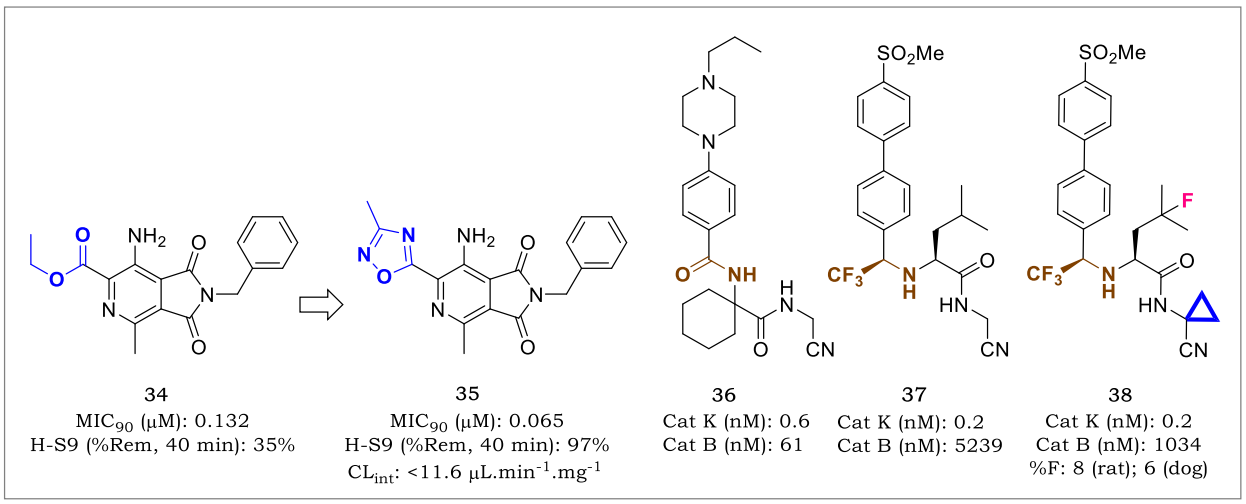

Figure 1.19: Examples of successful utilization of non-classical bioisosterism in lead optimization

More effectively, the application of both classical and non-classical bioisosterism has been found in the design of cathepsin K (Cat K) inhibitor odanacatib (**38**) (Figure 1.19), a Merck compound which advanced into phase-III clinical evaluation as a potential treatment of osteoporosis in patients, before termination due to risks associated with atrial fibrillation and stroke.[155,156] Optimization of **36** led to the identification **37**, a compound in which the amide moiety was replaced by a trifluoroethylamine element, resulting in improved potency and selectivity but poorer pharmacokinetic properties. Odanacatib (**38**) was the product of further refinement that solved both problems, with the fluorinated valine blocking hydroxylation and the quaternary cyclopropyl moiety at position 1 reducing the propensity for amide hydrolysis.[145,156]

1.9 Hybridization in Drug Discovery & Development

The registration of new drugs to treat various pathologies with a high social-economic impact such as malaria has suffered a continuous decrease over the past two decades. This particularly presents a big challenge for the pharmaceutical industry and demands a continuous effort to the development of new, efficient, selective and

economically accessible therapeutic tools.[157] To that effect, the rational planning of new synthetic prototypes has utilized a series of methods of structural modification to generate new compounds endowed with superior bioactivities and optimized PK and PD properties. Such compounds can result from exploring bioactive substances' fragments (Fragment-Based Drug Design, FBDD), active metabolites of drugs, bioisosterism, molecular hybridization and selective optimization of side effects of drugs.[157] Molecular hybridization will be one of particular consideration in the context of malaria drug discovery in this body of work.

Molecular hybridization is a strategy of rational design of new ligands or prototypes which involves the covalent combination of two or more pharmacophores of different bioactive substances of natural or synthetic origin to produce a hybrid compound with improved affinity and efficacy compared to the parent drugs.[157,158] The merged pharmacophores address the active site of different target and may offer the possibility of circumventing resistance. The concept is closely related to the pro-drug and combination therapy, with the main difference being that the action of a prodrug depends on its *in vivo* metabolism (cleavage) and combination therapy involves the administration of two separate drugs or active pharmaceutical ingredients in one single dose formulation respectively.[158] Hybrid molecules potentially offer several advantages including (i) cost-effective/affordability – the full cost of developing one hybrid molecule outweighs that which is associated with the development of two or more drugs individually followed by an additional assessment of the combination therapy of those two (or more) drugs. Secondly (ii), hybrids reduce the risk of drug-drug interactions – this can occur when two or more drugs are co-administered (i.e., combination therapy) leading to changes in systemic exposure as a result of one drug up- or down-regulating the metabolizing enzymes of the other drug. This may lead to adverse reactions, increased toxicity, or rapid clearance of one of the drugs. Thirdly (iii), hybrids may offer improved pharmacokinetic (PK)/pharmacodynamics (PD), physicochemical properties and reduce toxicity over combinations. This is because PK/PD properties of one molecule are easier to manipulate, compared to those of two individual drugs that have to be co-administered. Additionally, if the toxicophore of one fragment in a hybrid does not overlap the pharmacophore, it is possible to redesign the molecule and obliterate the toxicity.[159] Lastly (iv), hybrids may offer the possibility to reduce the potential for the emergence of drug resistance to one pharmacophore, if the covalently linked pharmacophores target dissimilar targets, and employ multiple mechanisms of action (MoAs).[160,161] However, the hybridization does also come with a down side, for instance by virtue of being a hybrid, these molecules are usually large, and this may reduce bioavailability and reduce or lose the ability to cross the blood-brain barrier (BBB).[158,162]

A generalization of the method of molecular hybridization, regardless of the produced type of homology, was proposed by Holland by using the concepts of biological evolution

to explain the chemical evolution. He employed genetic algorithms (GAs) that are evolutionary and strategic searches of optimization based on the Darwinian model of natural and evolutionary selection. In this context, relating to hybridization, a population of parent molecules (privileged pharmacophores) evolve dynamically by genetic crossing and optimization to produce subsequent generations of hybrid daughter molecules by recombination of structural sub-unities.[157]

1.9.1 Hybrid Compounds in Malaria Drug Discovery

Malaria has attracted drug discovery research efforts through molecular hybridization, especially involving quinoline and 1,2,4-trioxane molecular motifs (Figure 1.20).[163] The quinoline pharmacophore was the first to enter human medicine for the treatment of malaria through quinine, a cinchona alkaloid, which then inspired the design and introduction of many marketed antimalarial drug classes the likes of which chloroquine, amodiaquine, mefloquine etc. belong.[16]

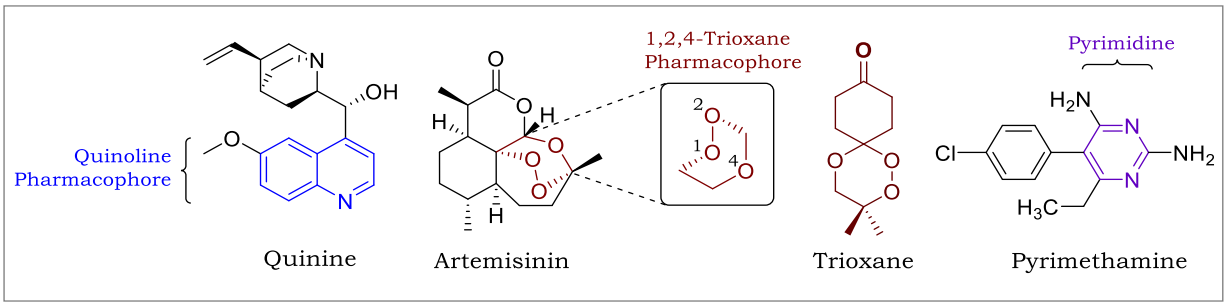

Figure 1.20: Chemical structures of quinine, artemisinin and pyrimethamine illustrating the quinoline,1,2,4-trioxane (trioxane) and pyrimidine pharmacophores

The inhibition of hemozoin formation during the erythrocytic schizogony (blood-stage) has been the widely accepted mode of action for quinoline-based antimalarials. Briefly, during this stage plasmodia generates amino acids needed for its biosynthetic and metabolic processes by ingesting and degrading large amounts of hemoglobin. This consequently also generates toxic redox-active heme (ferriprotoporphyrin IX), which the parasite detoxifies by biomineralization into crystalline hemozoin within the digestive vacuo (DV), where the drugs accumulate by pH trapping. Complexation of quinolines with heme via π-π stacking inhibits the detoxification process, allowing the accumulation of heme which induces oxidative stress and kills the parasite.[163–166]

1,2,4-trioxane motifs on the other hand are principally the main pharmacophore in artemisinins, which as previously described, forms the basis of the current WHO-recommended treatment regimen for malaria. Although the biochemical targets for artemisinins have not be deconvoluted, research has indicated that the endoperoxide present in this pharmacophore acts as a warhead which undergoes reductive cleavage to generate oxyradicals. These radicals are thought to effectively produce antimalarial effects

by alkylation with essential plasmodium proteins including tumor and heme-binding proteins, as well as proteases involved in hemoglobin degradation and interference with the mitochondrial electron transport system of *P. falciparum*.[167]

1.9.2 Artemisinin & Aminoquinoline-Based Hybrids

Examples of pharmacophore partners in artemisinin and aminoquinoline-based hybrids include trioxaquines and trioxolaquines. These contain a synthetic trioxane or trioxolane motif linked to artemisinin or aminoquinoline (usually CQ) *via* a diamino alkyl chain of two to four methylene groups or a cyclohexyl ring. This subsection will offer only a few examples of hybrids from this class.

The Palumed-Sanofi collaboration drug candidate **PA1103** (Figure 1.21) is one of the most attractive hybrids in this class due to its good potency (*Pf*W2 IC_{50}: 15 nM, *Pf*D6 IC_{50}: 7 nM, Gabon *Pf*-Clinical Isolates IC_{50}: 14.0 – 28.1 nM) for both diastereomers, its demonstrated efficacy in the *P. falciparum* humanized mouse model (*Pf*NOD/LtSz-SCID: 96% parasitemia reduction at 63 $mg.kg^{-1}$) and favorable ADMET properties both diastereomers.

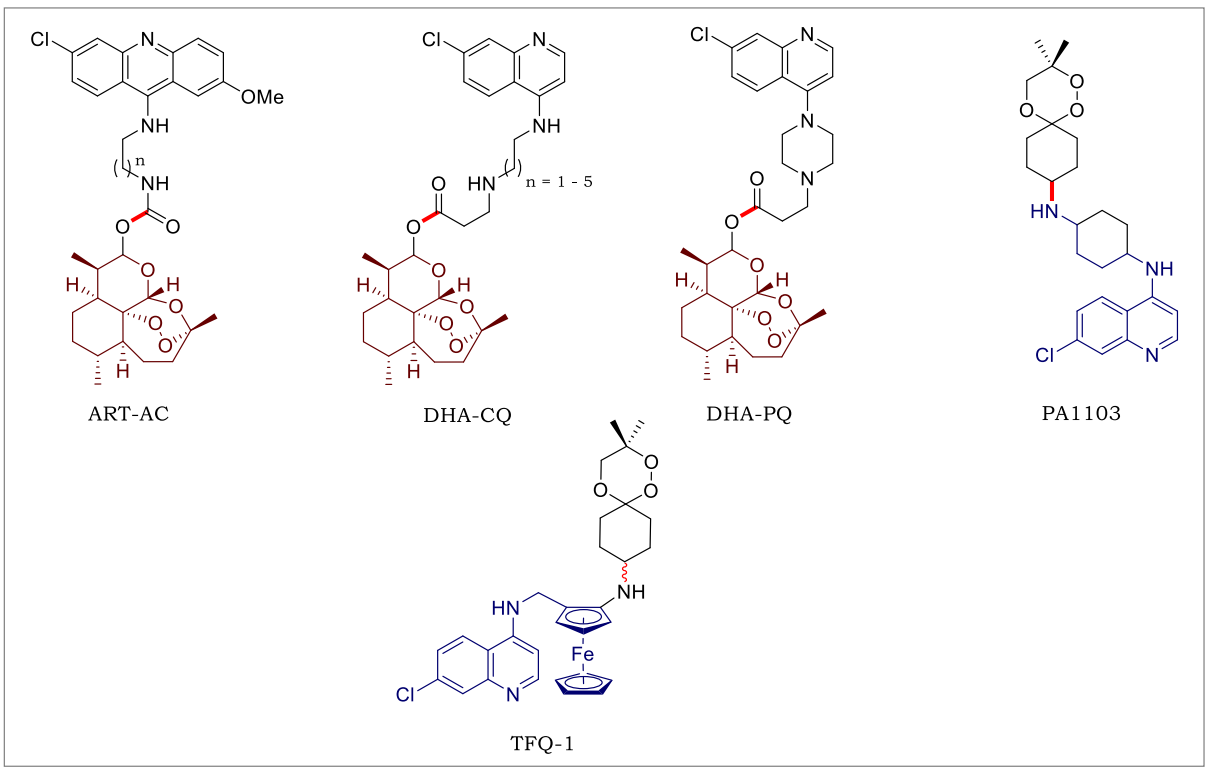

Figure 1.21: Examples of some antimalarial hybrid molecules. The red bond (—) shows point of attachment between two pharmacophores

The compound exhibits artemisinin and chloroquine-like dual action and was selected at the beginning of 2007 for regulatory drug development as a promising covalent bi-therapy strategy.[163,168] Trioxaferroquines, TFQs (Figure 1.21) are hybrid molecules in which a 1,2,4-trioxane motif if covalently linked to a ferroquine-like moiety. François and colleagues covalently linked ferroquine and related trioxanes to develop trioxaferroquines

which showed in vitro activities comparable to that of FQ (*Pf*FcB1 and *Pf*FcM29 IC_{50}'s: 10 – 20 nM).

To test the hypothesis, they also developed hybrids devoid of the quinoline fragment, which showed weaker activities (IC_{50}'s: >150nM). **TFQ-1** (Figure 1.21) was progressed for in vivo antimalarial evaluation in *P. vinckei* where it showed rapid parasitemia clearance to below detectable levels in mice orally dosed at 10 $mg.kg^{-1}$, however a curative effect was not obtained at doses below 25 $mg.kg^{-1}$.[169]

In 2009, O'Neill and co-workers reported a series of artemisinin-acridine hybrids (**ART-AC**, Figure 1.21) with antiplasmodium and antitumoral activity. Acridines are a widely used 4-aminoquinoline embedded molecular scaffold. The team hypothesized that incorporation of slow acting polar and acridines could improve the pharmacokinetic profile of artemisinins and act as a targeting moiety into the DV of the intraerythrocytic plasmodia.[163,170] Amide coupling of allyldeoxoartemisinin to 9-diami-noalkyl-6-chloro-2-methoxyacridines afforded four hybrid compounds which showed moderate activity compared to DHA in the multi-drug resistance strain (*Pf*3D7 IC_{50}: 5.96 – 20.34 nM).[171] This rationale provided scientific proof of concept for future discovery of more active artemisinin-acridine hybrid molecules.[163]

In another effort to improve PK properties and mitigate provide proof-of-concept of reducing the potential of resistance of both 4-aminoquinolies and artemisinins, Feng and co-workers reported the design and synthesis of DHA-aminoquinoline analogies based on CQ and piperaquine (PQ). By maintaining the number of carbons in the 4-diaminoalkyl linker between 2 and 6, optimal biological activity was achieved. These analogues **DHA-CQ** and **DHA-PQ** showed relatively comparable activities (*Pf*Dd2 IC_{50}: 10.0 – 54 nM; *Pf*D10 IC_{50}: 10.7 – 56 nM) to their parent compounds (CQ *Pf*Dd2/*Pf*D10 IC_{50}: 145.4/30.6 nM and DHA *Pf*Dd2/*Pf*D10 IC_{50}: 3.0/4.1 nM). The activities antiplasmodium of the quinoline amine precursors against the CQ-resistant *Pf*Dd2 strain were much lower than against the CQ-sensitive *Pf*D10 strain (RI > 4.0), which indicates a possible cross-resistance with CQ.[163,172]

1.10 Repurposing and Repositioning in Antimalarial Drug Discovery

The bench to market drug discovery process is an immensely expensive and lengthy process, typically taking at least 12 years.[173] In their 2007 *Nature* commentary entitled '*New uses for old drugs'*, Chong and Sullivan Jr argued this fact, challenging the scientific community to create a comprehensive drug library which would be screened for every neglected disease by 2011.[174]

Drug repurposing, repositioning, and rescue (DRPx) allow pre-existing drugs to be used for indications that were not their initial target. Although in some cases drug 'repositioning' and 'repurposing' are used interchangeably, they are quite different. Drug repurposing refers to a situation in which an existing approved drug for a specific disease is found to

have activity against another disease and is used as such, by optimizing the doses in preclinical and clinical stages. Drug repositioning on the other hand, describes a scenario where an active drug in one disease area, serves as a template for structural modification to yield derivatives or analogues that are active in a different disease.[175]

As the pharmacologist and Nobel laureate James Black said, '*the most fruitful basis for the discovery of a new drug is to start with an old drug*'.[174] It is no surprise that in times of a devastating global pandemic like the current Coronavirus disease 2019 (COVID-19), caused by the novel severe acute respiratory syndrome Coronavirus (SARS-CoV-2), it was old drugs such as antimalarial Chloroquine (CQ) and its derivative Hydroxychloroquine (HCQ), antiviral Remdesivir and antibiotic Azithromycin, which were at the initial frontline as potential treatments.[176,177] Repurposing and repositioning reduce both the cost (~40%) and timeline for drug discovery and development. This is because the drug(s) would have known pharmacokinetics and safety profiles and are often approved by regulatory agencies for human use, any newly identified use can be rapidly evaluated in Phase II clinical trials, which typically last two years.[173]

There are several considerations that can help researchers identify potential drug candidates for repositioning or repurposing. For instance, knowledge of additional targets of a drug, their role(s) in other different biological pathways, as well as the similarities and/or differences in cell biology and pathogenesis of other diseases. Examples in which these approaches have been successfully used to deliver drugs and treatment for different diseases are many. In this body of work, the examples cited are in the context of malaria. Figure 1.22 shows examples of drugs with their original indications in which they are/were used, that have now been repurposed for malaria and some of which possess antimalarial properties and would serve as potential starting points for repositioning.

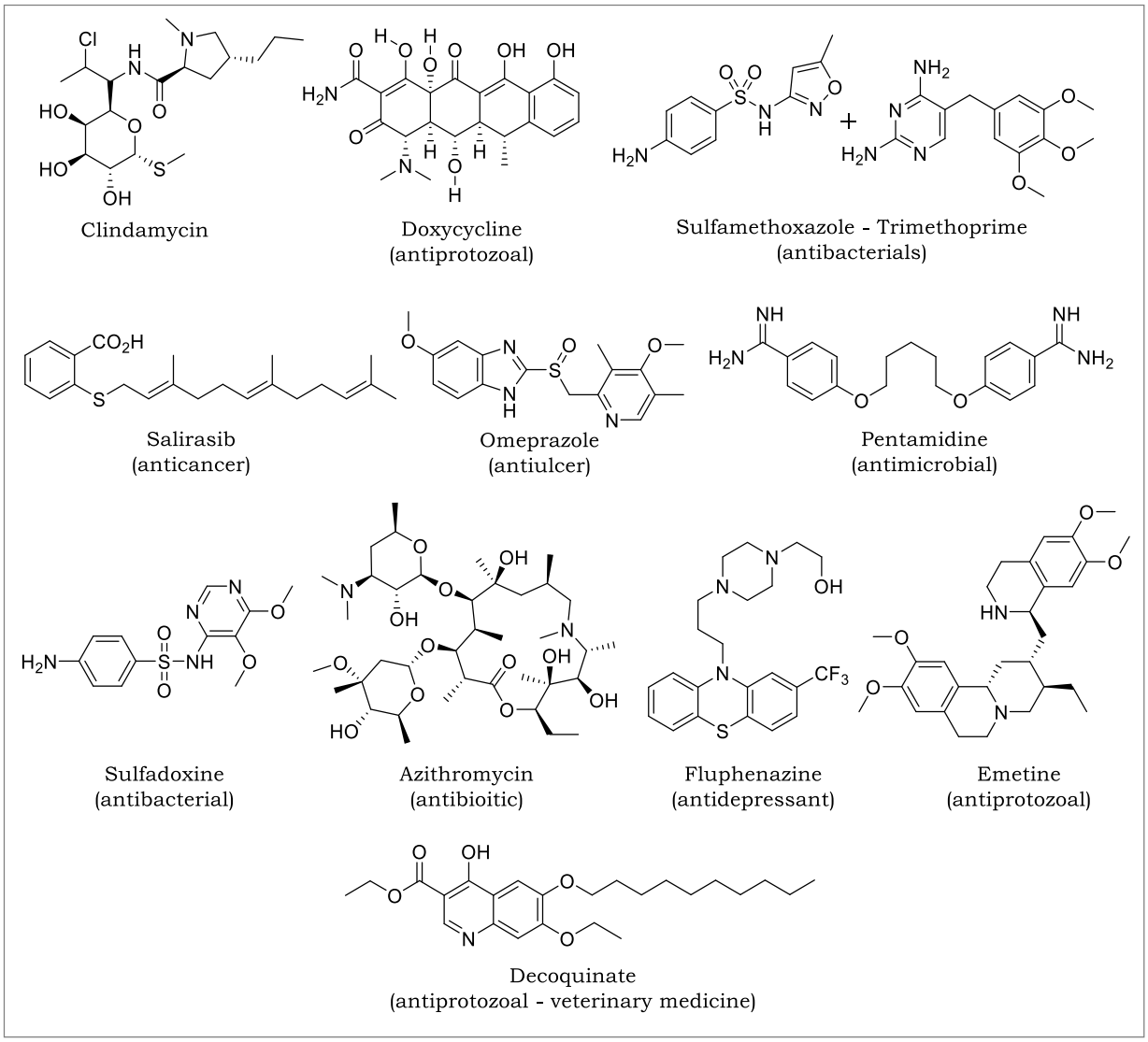

Figure 1.22: Chemical structures of some repurposed antimalarial drugs and potential drugs for repositioning with potent antiplasmodium activity

1.11 Pharmacological Properties of Benzimidazole Chemotypes

Benzimidazole is a bicyclic heterocyclic compound of fused of benzene and imidazole rings (Figure 1.23). Benzimidazole derivatives are structural isosteres of naturally occurring purine nucleotides, which allows them to interact easily with the biopolymers of the living system such as proteins, enzymes, and receptors. It has been comprehensively used in medicinal chemistry and found applications in diverse therapeutic and clinical areas including anticancer, hormone antagonists, antiviral, anti-HIV, anthelmintic, antiprotozoal, antimycobacterial, antihypertensive, anti-inflammatory, analgesic, anxiolytic, antiallergic, coagulant, anticoagulant, antioxidant, antidiabetic etc. as shown in Figure 1.23.[178]

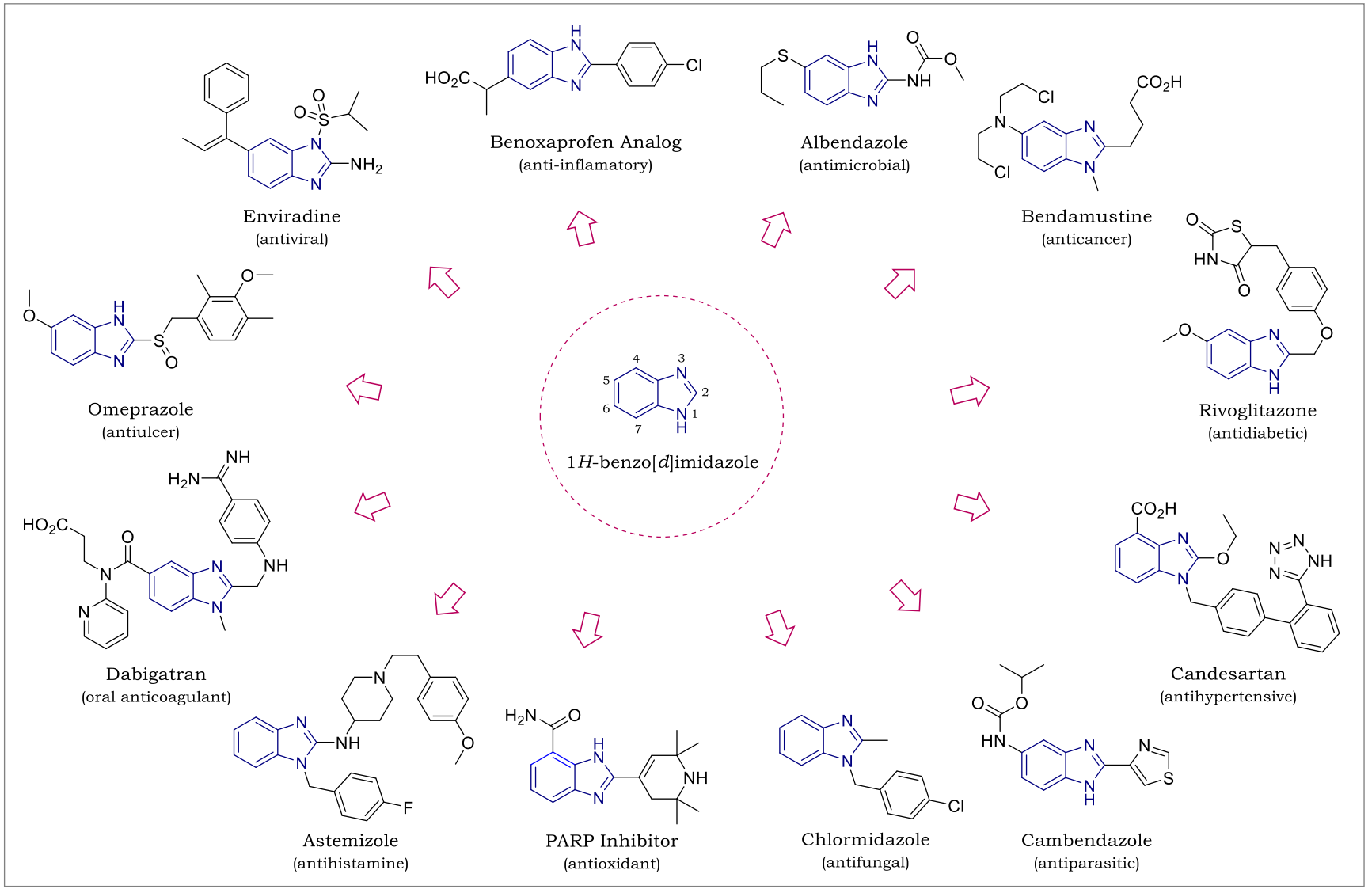

Figure 1.23: Structures of some drugs from various diseases incorporating the benzimidazole nucleus.

1.12 Antimalarial Properties of Benzimidazoles

There has been a heightened interest in the development of benzimidazoles as antimalarials in the last decade, and new opportunities for drug discovery are opening up. This is in part due to increased screening of diverse libraries and the public release of novel antiplasmodium data sets within the disease area. Some examples of benzimidazole based antiplasmodium and antimalarial agents are discussed in this subsection and described in Figure 1.24.

A series of *N*-aryl-2-aminobenzimidazoles emerged as novel hits in an HTS of an AstraZeneca corporate compound collection against the asexual blood stage of *P. falciparum*. Through a hit-to-lead, compound **39** (Figure 1.24) was one of the analogues identified as a potent lead (*Pf* NF54 IC_{50}: 0.053 μM) demonstrating efficacy in both murine and humanized mouse models (*Pb* ED_{90}: <30 $mg.kg^{-1}$; *Pf* SCID ED_{90}: 12.8 $mg.kg^{-1}$) and excellent rat PK (F: 100%, $t_{1/2}$: 5.1 h) which translated in curative effects of the compound in *P. berghei*-infected mice at 50 $mg.kg^{-1}$.[179] Compound **39** retained its potency when tested against a panel of *Pf* transgenic lines carrying resistance mutations (*Pf*ATP4 ad *Pf*PI4K) indicating a different mode of action. Additionally, it exhibited rapid killing properties highlighting the promise of the benzimidazole class for malarial treatment.[179]

Through an in-depth analysis of the GlaxoSmithKline (GSK; Tres Cantos Antimalarial Set, TCAMS) corporate collection, a series of benzimidazole-based compounds were found to poses antiplasmodium properties.[180,181] From this set, Keurulainen and co-workers conducted a hit-to-lead developability-focused study in which compound **40** emerged as a potent (*Pf* 3D7 IC_{50}: 0.094 μM; Figure 1.24) derivative. It reduced parasitemia below detectable limits in the *Pf*SCID humanized mouse model of malaria (*Pf*$3D^{70087/N9}$) within two (2) doses, showing a parasite clearance rate consistent with fast-acting antimalarials like dihydroartemisinin (DHA) and piperaquine. Some of the challenges that would need to be addressed in this series include mitigation of potential toxicity observed on the basis of hERG ion works assay and the cross-resistance with *Pf*W2 strain.[182]

In another effort, a team at Genzyme Corporation collaborated with MMV to find small molecule inhibitors of *Pf*DHODH, through this, a HTS was conducted in which a benzimidazole small molecule was identified.[183]

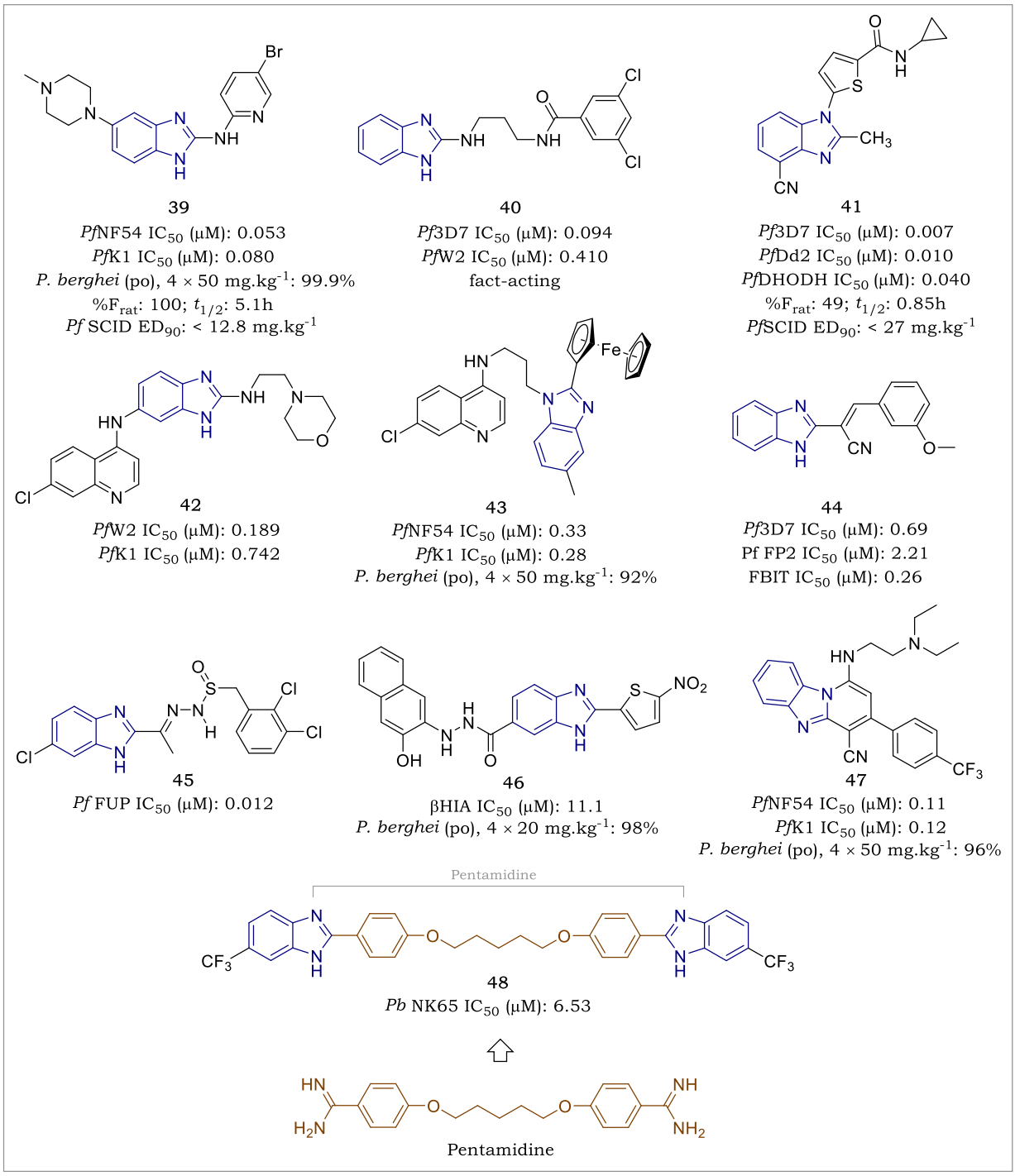

Figure 1.24: Examples of some antimalarial and antiplasmodium agents based on benzimidazole

Hit-to-lead on this hit generated advanced analogues which had CYP-mediated metabolism and hERG inhibition liabilities. In their recent work, they show the optimized lead compound **41** as a potential drug candidate.[184,185] Compound **41** has single digit nanomolar potency (*Pf* 3D7 IC_{50}: 7 nM), marginal hERG affinity (hERG IC_{50}: 53 μM; SI: >7500) with no signs of cross resistance with existing antimalarials (*Pf* Dd2 IC_{50}: 10 nM). Its good rat PK (F: 49%) translates to *in vivo* efficacy (*P. berghei*, ED_{90}: 28 mg.kg^{-1}; *Pf*SCID, ED_{90}: 27 mg.kg^{-1}). No off-target activities in a 54-receptor pharmacology panel at 10 μM were observed, corroborating on target activity against *Pf*DHODH (IC_{50}: 40 nM). The

compound has a good ADME profile with <0.7 and <0.6 mL.min^{-1}.kg^{-1} in human microsomes and hepatocytes, respectively. In a repeat dose toxicology study in rat at 0, 50, 150, 450, and 600 mg.kg^{-1} PO QD for 7 days followed by a 7-day washout period, the NOAEL was >600mg.kg^{-1} (C_{max}, 29 µg.mL^{-1}; AUC, 328 µg*h.mL^{-1}), and the predicted human therapeutic margin was >5.5. Based on this data, **41** was selected as a small molecule potential drug development candidate.[185]

In their quest to identify analogues of amodiaquine (AQ) devoid of the toxicity associated with its reactive metabolites, Chibale and co-workers identified a series of benzothiazole-, benzoxazole- and benzimidazole-amodiaquine analogues retaining AQ-potency. Among the benzimidazole series was compound **42** (Figure 1.24) showing moderate activity (*Pf* NF54 IC_{50}: 0.189 µM, *Pf* K1 IC_{50}: 0.742 µM).[186] Although the benzimidazole series was not progress to streamlined assays due to lower potency and higher potential for *in vivo* bioactivation compared to their benzoxazole counterparts, they set a basis for further utilization as optimization starting points.

Baartzes and colleagues took a molecular hybridization approach to combine the 4-aminoquinoline (CQ) and benzimidazole moieties and their ferrocenyl analogues to leverage the privileged nature of the two scaffolds as antimalarial and antimycobacterial (TB) agents and as a strategy to overcome *P. falciparum* resistance to CQ. Ferrocenyl-hybrid **43** (Figure 1.24) showed superior activity (*Pf* NF54 IC_{50}: 0.33 µM) to its Phenyl derivative (*Pf* NF54 IC_{50}: 0.784 µM). This potency translated to in vivo efficacy of **41**, showing a 92% parasitemia reduction in mice infected with *P. berghe*i at 50 mg.mg^{-1}. In addition to the potent hemozoin formation inhibition properties (βHIA IC_{50}: 16 µM), hybrid **43** demonstrated dose-dependent cleavage of pIC57 in a ROS study. Suggesting that the presence of the redox-active ferrocenyl moiety adds an additional mechanism that contributes to its efficacy by generation of reactive oxygen species (ROS) which cause parasite damage by cleavage of parasitic circular plasmid DNA.[187]

In their quest to identify novel dual receptor antimalarial leads, Sharma *et al* synthesized a series of benzimidazole acetonitrile analogues. When tested in the CQ-sensitive strain *Pf*3D7, Compound **44** (Figure 1.24) emerged as the most active analogue (IC_{50}: 0.69 µM), showing dual activity by inhibition of both Falcipains-2 (FP2 IC_{50}: 2.21 µM) and β-hematin formation through heme binding studies in a ferriprotoporphyrin IX biomineralization inhibition test (FBIT). This study set this series as a potential starting point for further SAR derivation.[188]

Gaining inspiration from the iron-chelating properties of thiosemicarbazones and their broad activities in protozoan parasites including *P. falciparum*,[189] Divatia and co-workers prepared a series of benzimidazole-thiosemicarbazone derivatives as potential antiplasmodium agents. From this series, Compound **45** (Figure 1.24) was among the most

active analogues (IC_{50}: 0.012 μM).[190] Combining benzimidazole as a privileged scaffold and nitroaromatic character which has been extensively used in anaerobic infections and have a direct proof that free-radical metabolites are involved in applications to antiparasitic and antibacterial pharmacology,[191] Camacho *et al* synthesized a series of nitro-furan and nitro-thiophene tethered benzimidazole-5-carbohydrazides as potential antiplasmodium and antimycobacterial agents. From this work, Compound **46** (Figure 1.24) emerged as one of the most active inhibitors of the hemozoin formation pathway (βHIA IC_{50}: 11.1 μM; CQ-βHIA IC_{50}: 22 ± 2 μM) translating to good in vivo efficacy in the *P. berghei* mouse (98% Parasitemia reduction at 20 mg.kg-1 on day four post dosing). The authors indicated to have a follow-up PK evaluation of this series of analogues.[192]

As a matter of consideration, benzimidazole structurally related pyrido[1,2-*a*]benzimidazoles (PBI) have in the last decade been of focus in malaria and schistosomiasis research. Within our research group, this was precipitated by work carried out by Ndakala and co-workers.[193] In this initial work, Compound **47** was identified as a potent (*Pf* NF54 IC_{50}: 0.11 μM, *Pf* K1 IC_{50}: 0.047 μM), selective (CHO IC_{50}: 28.8 μM, SI: 612) and efficacious lead (96% parasitemia reduction at 50 $mg.kg^{-1}$).[193] This study initiated a series of optimizations within the PBI class, which has led to the identification of pan-active antimalarial analogues with favorable PK profiles.[194]

As a part of their search for basic structural requirements for antiprotozoal activity, including *Plasmodium*, Torres-Gómez and co-workers synthesized a series of hybrids between benzimidazole and the drug pentamidine.[195] Pentamidine is an aromatic diamidine used at primary stage in African trypanosomiasis, antimony-resistant leishmaniasis, and AIDS associated *Pneumocystis jirovecii* pneumonia, however, its ineffective orally and presents several toxic effects.[196] Compound **48** (Figure 1.24) emerged as the most active hybrid when tested *in vitro* against the CQ-sensitive *P. berghei* strain NK65 (IC_{50}: 6.53 μM).[195]

1.12.1 Astemizole: Benzimidazole Template for Antimalarial Repositioning

1.12.1.1 A Short-lived Clinical Use

Astemizole, AST (Figure 1.25) is a synthetic piperidinyl-benzimidazole derivative, a second generation long-acting, non-sedating and selective histamine H_1-receptor antagonist (H_1 IC_{50}: 4.0 nM). It was discovered by Janssen Pharmaceutica in 1977 and marketed under the brand name Hismanal after approval by the FDA in 1988.[197]

The pharmacokinetics of AST is similar in both adults and children. In humans, it is quickly absorbed, reaching plasma concentration within 1–4h after single oral doses (10–40 mg). It undergoes rapid CYP-mediated metabolism, by primarily CYP2D6 and CYP3A4[198] leading to the generation of its principle and active metabolite desmethylastemizole, DMAST (Figure 1.27) resulting from oxidative *O*-demethylation.[199]

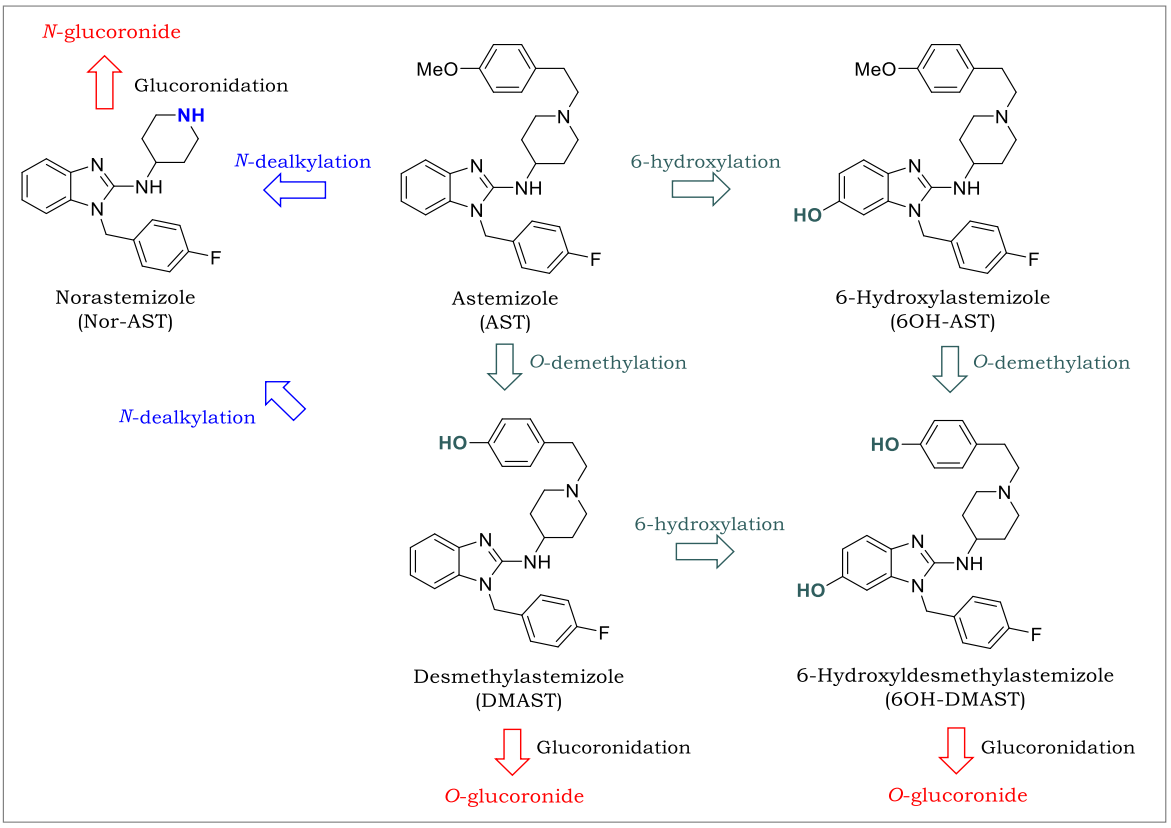

Figure 1.25: A proposed metabolic pathway of Astemizole in man and structures its metabolites, desmethylastemizole (DMAST), norastemizole (Nor-AST), 6-hydroxylastemizole (6OH-AST) and 6-hydroxyldesmethylastemizole (6OH-DMAST).[198]

DMAST retains antihistaminic activity and contributes significantly to AST's efficacy. It is highly bound to plasma proteins (~97%) and maintains a steady-state serum concentration which exceeds that of AST by more than 30-fold.[199,200] It has a half-life ($t_{1/2}$) of 9–11 days and is eliminated mainly *via* hepatic biotransformation. The second metabolite is Norastemizole (Figure 1.25), generated from oxidative *N*-dealkylation of the parent drug. It appears in low concentrations following AST administration and reported to possess more potent H_1-receptor activity than AST and DMAST.[200,201] The third metabolite is 6-hydroxyldesmethylastemizole, 6OH-DMAST (Figure 1.25) which is generated either from aromatic hydroxylation DMAST or *via* *O*-demethylation of 6-hydroxylastemizole (6OH-AST). When studied in human volunteers following oral administration of 30 mg labeled ^{14}C-AST, excretion amounting to only 40–54% of the dose at 4 days and 61–79% of the dose at 14 days was observed. Radioactivity was excreted mainly in the faeces: 54–73% of the dose within 14 days and only 5.4–6.3% was excreted in the urine. The 3 major metabolites each accounted for 17–30% of the radioactivity excreted in the faeces, whereas the major metabolites detected in the urine were the glucuronides of desmethylastemizole and norastemizole. Unchanged astemizole was not recovered in the urine or faeces.[202]

Leading up to its withdrawal, a 1999 study of Astemizole and its metabolites by Zhou *et al* found that AST and DMAST truly cause acquired long QT syndrome, by equipotently

blocking (AST-hERG IC_{50}: 0.9 nM; DMAST-hERG IC_{50}: 1.0 nM) the rapidly activating delayed rectifier K+ current I_{Kr} and the human ether-a-*go-go*-related gene (hERG) that underly it. These findings, combined with the ADME data of AST mentioned earlier, support the postulate that DMAST plays a major role in the side effects associated with astemizole intake. They concluded that AST and DMAST are among the most potent hERG channel-blocking drugs yet studied. On the other hand, Norastemizole blocks hERG K+ current weaker (Nor-AST-hERG IC_{50}: 27.7 nM) and has not been associated with any of the side effects, hence has been continued as a developmental antihistamine drug.[198,200] As described earlier in this chapter, Zhou *et al* also confirmed the chemical structure-activity requirements important for block of I_{Kr}, that is; presence of a tertiary amine, flanked by three aromatic moieties which are linked by bulky aliphatic chains.[88,89]

1.12.1.2 Discovery of the Antimalarial Properties of Astemizole

Preceding their *Nature* commentary on drug repurposing and repositioning in 2007, Chong *et al* assembled a library of 1,937 FDA-approved drugs and 750 drugs that were either approved for use or undergoing phase II clinical trials. This collection, called the Johns Hopkins Clinical Compound Library (JHCCL), was subjected to a medium throughput screen (MTS) at 10 μM for inhibition of *P. falciparum* growth. Using a discriminatory Inhibition of >50%, 189 compounds across many classes were identified. Following the elimination of topical drugs, already known antimalarials, cytotoxic drugs and compounds previously reported to inhibit the malaria parasite, they determined the IC_{50} values for the 87 remaining drugs. Among these, astemizole and desmethylastemizole were identified as sub-micromolar *in vitro* inhibitors of 3 different multi-drug resistance (3D7) and sensitive strains (Dd2 and ItG) of *P. falciparum* (Table 1.1).[203]

Table 1.1: Astemizole *in vitro* inhibition of three *P. falciparum* strains of different chloroquine sensitivity.[203]

Pf Strain	IC_{50} (μM)			
	AST	DMAST	Nor-AST	CQ
3D7	0.227	0.117	4.477	0.032
Dd2	0.457	0.106	3.590	0.079
ItG	0.734	0.057	2.230	0.107

Notably, DMAST had better activity than AST ranging from 2- to 12-fold in the panel of the 3 *in vitro* laboratory strains. Conversely, norastemizole showed weaker inhibition. Additionally, using *Pf*3D7 and *Pf*Dd2, both AST and CQ showed synergistic effects when administered in combination with current antimalarials such as chloroquine, artemisinin and quinidine.[203] Further, they showed *in vivo* efficacy of AST and DMAST in the standard 4-day parasite suppression test using two different malarial mouse models, CQ-sensitive *P. vinckei* and CQ-resistance *P. yoelii* as shown in Table 1.2 below.[203]

Table 1.2: Astemizole *in vivo* parasitemia reduction in *P. vinckei* and *P. yoelii* mouse infection models.[203]

Mouse Infection Model	Parasitemia Reduction (oral dose)	
	AST	DMAST
P. vinckei	80% (15 mg.kg^{-1}.day^{-1})	81% (30 mg.kg^{-1}.day^{-1})
P. yoelii	44% (15 mg.kg^{-1}.day^{-1})	40% (15 mg.kg^{-1}.day^{-1})

Up to 80% parasitemia reduction was observed in the sensitive strain for both AST and DMAST at 15 and 30 mg.kg^{-1}.day^{-1}, with recrudescence occurring when treatment was stopped after 4 days. However, curative effects were only achieved after dosing up to 300 mg.kg^{-1}.day^{-1}.[203]

Having identified the AST pharmacophore a starting point for further development, many researchers have made analogues to mitigate hERG and improve antimalarial activity. Musonda and co-workers at Pfizer took a molecular hybridization approach by designing and synthesizing chloroquine and astemizole hybrids to achieve dual activity and as a strategy overcome *P. falciparum* resistance to CQ (Figure 1.26). Their frontrunner analogues showed up to 10-fold better activity than CQ in the drug-resistant *Pf*K1 strain. Additionally, when tested *in vivo*, using *P. berghei*-infected mice, two analogues demonstrated efficacy, with 99% parasitemia reduction at 50 mg.kg^{-1}.[204]

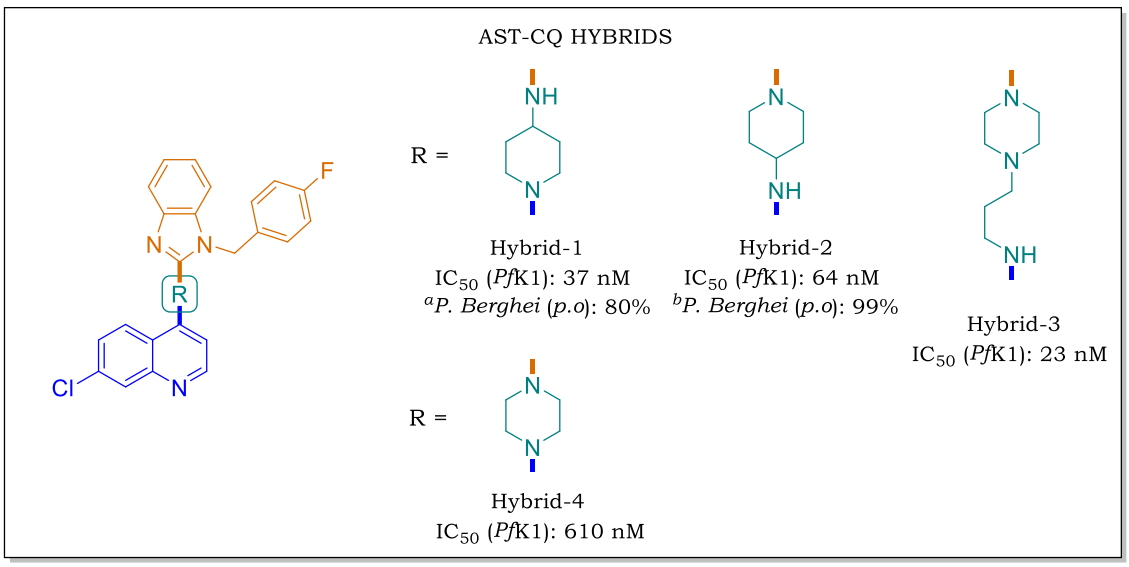

Figure 1.26: Pharmacophore details of chloroquine (CQ) and astemizole (AST), and hybridization SAR exploration carried out by Musonda *et al.*[204] [a]Dose = 4 × 20 mg.kg^{-1} for 4 days; [b]Dose = 4 × 25 mg.kg^{-1} for 4 days

Roman *et al* designed and synthesized analogues of astemizole with the goal determining the SAR required for activity and cytotoxicity. Of the 28 analogues synthesized, 9 had IC_{50} values in the nanomolar range (*Pf*ItG IC_{50}: 0.070 – 0.50 µM) and showed varied cytotoxicity

in the Chinese hamster ovary cell line (CHO SI: 4 – 50). While all the analogues had the benzimidazole core, the authors speculated its importance for antiplasmodium activity. They showed that the presence of appropriate appendages at positions 1 and 2 was critical for fine tuning toxicity, and that the presence of a secondary (2 °) cyclic amine at position 2, substitution of benzene in the benzimidazole core and replacement of fluorine with trifluoromethyl (CF_3) in the *p*-fluorobenzyl moiety of astemizole can be used to disconnect the antihistaminic and the antimalarial activity (Figure 1.27). Their study laid a foundation for further investigation of structural features that required for activity and cytotoxicity.[205]

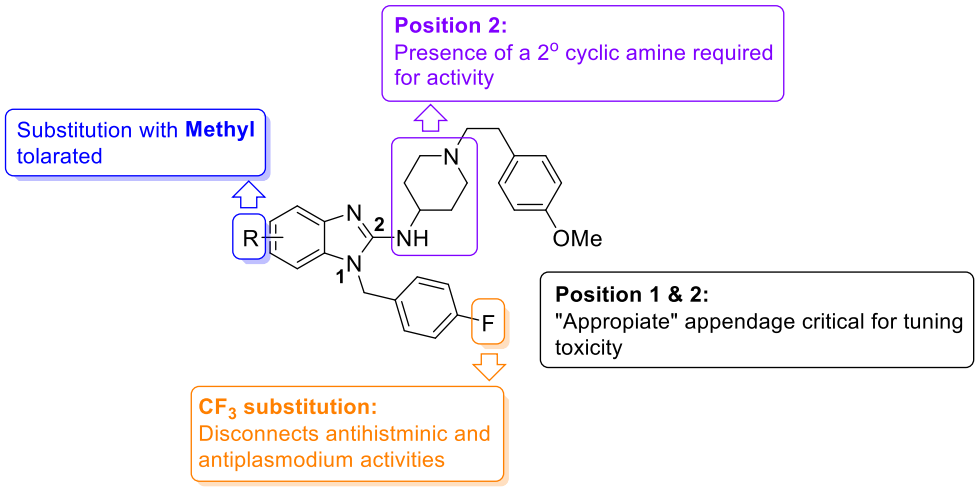

Figure 1.27: Representation of astemizole antiplasmodium activity and CHO cytotoxicity SAR according to Roman *et al.*

More recently, Tian and colleagues conducted a systematic structural variation of AST, which led to the discovery of novel derivatives with potent antiplasmodium activities. The most potent congeners, **49** and **50** (Table 1.3) displayed IC_{50} values of 30 nM against *Pf*3D7. Importantly, one of these analogues also showed a reduced hERG inhibition of up to 3200-fold improvement, when compared to AST. Unfortunately, the most promising analogue (potent antiparasitic activity, while having a reduced hERG affinity) is a very lipophilic compound (clogP: 7.7). Therefore, the authors suggested further research to focus on improving the drug-like properties of the compounds by reducing lipophilicity and improving aqueous solubility. With respect to SAR, they showed that structural variety is tolerated at the imidazole nitrogen of AST (Position 1). They claimed that modifications at this position allows also to tune hERG inhibition.[206]

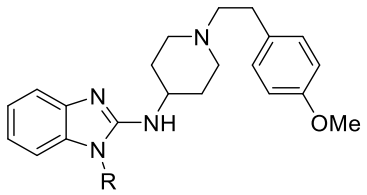

	R	*Pf*3D7 IC_{50} (μM)	hERG IC_{50} (μM)	hERG SI	clogP
49	C_6H_{13}	0.030	0.029	1.0	6.65
50	C_8H_{17}	0.029	3.270	110.4	7.70
51	$C_{10}H_{21}$	0.112	2.069	18.4	8.77
AST	4-F-Bn	0.171	0.304	1.8	5.82

Table 1.3: Examples of 1-alkyl substituted analogues of astemizole with potent antiplasmodium activity by Tian *et al.*[206]

1.13 Research Program

1.13.1 Justification of the Study

As described in this chapter, drugs that were once effective and saved millions of lives, drugs such as chloroquine (CQ) have suffered resistance, what is more worrying is that this resistance keeps spreading to the current first-line treatment, the ACTs.[19] Although this resistance has of yet only been observed in the Greater Mekong Sub-region (GMS), it is not a matter of 'if', but 'when', that resistance will surface in endemic countries in Africa and the world over, if something is not done about it quickly. For this reason, collaborative efforts from industry (Pharma) and academia is required, in order to deliver ideal candidates which would contribute to replenishing the antimalarial drug development pipeline with novel, structurally diverse and pan-active chemical scaffolds with potential to be ideal TPP criteria for new therapies.[26]

Benzimidazole is a broadly used scaffold,[178] which has in recent years found heightened applications to malaria than in previous years. As described earlier, it offers opportunities to target the malaria parasite at multiple stages and with novel mechanisms of action,[185] a characteristic that would potentially make benzimidazole-based drug leads less prone to cross resistance with existing antimalarials.

The discovery of the antimalarial properties of astemizole warrants its utilization for development as an antimalarial drug through repositioning. This research will attempt to use medicinal chemistry approaches to de-risk the hERG liability of astemizole, improve solubility and leverage its potential as an antimalarial drug. The research will embody aspects described in this chapter, including molecular hybridization with other antimalarials and target identification approaches to contribute towards understanding of the underlying mode of action and/or resistance for this class of compounds.

1.13.2 Research Question

The research question is whether it will be possible to identify astemizole-based antimalarial drug leads with favorable solubility, hERG, physicochemical and drug metabolism and pharmacokinetics (DMPK) properties.

1.13.3 Study Objectives

1. To utilize astemizole as a template for the design and synthesize novel potential antimalarial agents.
2. To evaluate the solubility and cardiotoxicity (hERG) risk profile of synthesized astemizole analogues.

1.13.4 Specific Aims

1. To synthesize and characterize antimalarial astemizole analogues designed to improve solubility and hERG inhibition profiles.
2. To profile the synthesized analogues (compounds) with respect to *in vitro* antiplasmodium activity, cytotoxicity, solubility and hERG.
3. To investigate and derive antiplasmodium structure-activity relationship (SAR) as well as solubility structure-property relationship (SPR) profiles.
4. To investigate of the factors affecting solubility and deduce relationships.
5. To evaluate potent, soluble, non-cytotoxic and metabolically stable compounds for *in vivo* proof of concept (PoC) and pharmacokinetics (PK).

1.14 References

(1) Cunha, C. B.; Cunha, B. A. Brief History of the Clinical Diagnosis of Malaria: From Hippocrates to Osler. *J. Vector Borne Dis.* **2008**, *45* (3), 194–199.

(2) Nerlich, A. G.; Schraut, B.; Dittrich, S.; Jelinek, T.; Zink, A. R. Plasmodium Falciparum in Ancient Egypt. *Emerg. Infect. Dis.* **2008**, *14* (8), 1317–1319.

(3) Liu, W.; Li, Y.; Learn, G. H.; Rudicell, R. S.; Robertson, J. D.; Keele, B. F.; Ndjango, J.-B. N.; Sanz, C. M.; Morgan, D. B.; Locatelli, S.; et al. Origin of the Human Malaria Parasite Plasmodium Falciparum in Gorillas. *Nature* **2010**, *467* (7314), 420–425.

(4) Wolfe, N. D.; Dunavan, C. P.; Diamond, J. Origins of Major Human Infectious Diseases. *Nature* **2007**, *447* (7142), 279–283.

(5) Bonelli, F. La Malaria Nella Storia Demografica Ed Economica D'Italia: Primi Lineamenti Di Una Ricerca. *Stud. Stor.* **1996**, *7* (4), 659–687.

(6) Celli-Fraentzel, A. The History of Malaria in the Roman Campagna from Ancient Times. *John Bale, Sons Danielsson, Ltd.* **1933**, *8*, 226.

(7) Neghina, R.; Iacobiciu, I.; Neghina, A. M.; Marincu, I. Malaria, a Journey in Time: In Search of the Lost Myths and Forgotten Stories. *Am. J. Med. Sci.* **2010**, *340* (6), 492–498.

(8) When was malaria first discovered and by whom? How is the disease transmitted? What are its effects? https://www.scientificamerican.com/article/when-was-malaria-first-di/. Date Accessed: 15th July, 2020.

(9) Schlagenhauf, P. Malaria: From Prehistory to Present. *Infect. Dis. Clin. North Am.* **2004**, *18* (2), 189–205.

(10) Snowden, F. *The Conquest of Malaria: Italy, 1900-1962*; New Haven (CT)/London: Yale University Press, 2006.

(11) Keeble, T. W. A Cure for the Ague: The Contribution of Robert Talbor (1642-81). *J. R. Soc. Med.* **1997**, *90* (5), 285–290.

(12) Cox, F. E. . History of Human Parasitic Diseases. *Infect. Dis. Clin. North Am.* **2004**, *18* (2), 171–188.

(13) Yoeli, M. Sir Ronald Ross and the Evolution of Malaria Research. *Bull. N. Y. Acad. Med.* **1973**, *49* (8), 722–735.

(14) Capanna, E. Grassi versus Ross: Who Solved the Riddle of Malaria? *Int. Microbiol.* **2006**, *9* (1), 69–74.

(15) Gray, John; William, Arrot; Phill, M. An Account of the Peruvian or Jesuits Bark, by Mr. John Gray, F. R. S. Now at Cartagena in the Spanish West-Indies; Extracted from Some Papers Given Him by Mr. William Arrot, a Scotch Surgeon, Who Had Gather'd It at the Place Where It Grows in Peru. Commu. *Philos. Trans.* **1737**, *40*, 81–86.

(16) Greenwood, D. The Quinine Connection. *J. Antimicrob. Chemother.* **1992**, *30* (4),

417–427.

(17) Greenwood, D. Conflicts of Interest: The Genesis of Synthetic Antimalarial Agents in Peace and War. *J. Antimicrob. Chemother.* **1995**, *36* (5), 857–872.

(18) Schlagenhauf, P. In Pursuit of the Persistent Plasmodium. *J. Travel Med.* **1998**, *5* (3), 113–115.

(19) World Health Organization. *World Malaria Report 2019. Geneva.*; 2019.

(20) González, R.; Sevene, E.; Jagoe, G.; Slutsker, L.; Menéndez, C. A Public Health Paradox: The Women Most Vulnerable to Malaria Are the Least Protected. *PLOS Med.* **2016**, *13* (5), e1002014.

(21) UNAIDS/WHO. *UNAIDS/WHO. Global Report: UNAIDS Report on the Global AIDS Epidemic 2013*; 2013.

(22) Asenso-Okyere, W. K. Socioeconomic Factors in Malaria Control. *World Health Forum* **1994**, *15* (3), 265–268.

(23) Guerra, C. A.; Gikandi, P. W.; Tatem, A. J.; Noor, A. M.; Smith, D. L.; Hay, S. I.; Snow, R. W. The Limits and Intensity of Plasmodium Falciparum Transmission: Implications for Malaria Control and Elimination Worldwide. *PLoS Med.* **2008**, *5* (2), e38.

(24) White, N. J. Plasmodium Knowlesi: The Fifth Human Malaria Parasite. *Clin. Infect. Dis.* **2008**, *46* (2), 172–173.

(25) Cox-Singh, J.; Davis, T. M. E.; Lee, K.-S.; Shamsul, S. S. G.; Matusop, A.; Ratnam, S.; Rahman, H. A.; Conway, D. J.; Singh, B. Plasmodium Knowlesi Malaria in Humans Is Widely Distributed and Potentially Life Threatening. *Clin. Infect. Dis.* **2008**, *46* (2), 165–171.

(26) Burrows, J. N.; Duparc, S.; Gutteridge, W. E.; Hooft van Huijsduijnen, R.; Kaszubska, W.; Macintyre, F.; Mazzuri, S.; Möhrle, J. J.; Wells, T. N. C. New Developments in Anti-Malarial Target Candidate and Product Profiles. *Malar. J.* **2017**, *16* (1), 26.

(27) Miller, L.; Good, M.; Milon, G. Malaria Pathogenesis. *Science (80-.).* **1994**, *264* (5167), 1878–1883.

(28) Bell, G.; Koufopanou, V. The Architecture of the Life Cycle in Small Organisms. *Philos. Trans. - R. Soc. London, B* **1991**, *332* (1262), 81–89.

(29) Schwartz, A.; Koella, J. C. Trade-Offs, Conflicts of Interest and Manipulation in Plasmodium–Mosquito Interactions. *Trends Parasitol.* **2001**, *17* (4), 189–194.

(30) Cho, S.; Kim, S.; Kim, Y.; Park, Y. Optical Imaging Techniques for the Study of Malaria. *Trends Biotechnol.* **2012**, *30* (2), 71–79.

(31) Miller, L. H.; Baruch, D. I.; Marsh, K.; Doumbo, O. K. The Pathogenic Basis of Malaria. *Nature* **2002**, *415* (6872), 673–679.

(32) Breman, J. G. Eradicating Malaria. *Sci. Prog.* **2009**, *92* (1), 1–38.

(33) WHO, W. H. O. *Vector Control for Malaria and Other Mosquito-Borne Diseases: Report*

of a WHO Study Group; Geneva, 1995.

(34) Breman, J. G. Malaria: Epidemiology, Prevention and Control. https://www.uptodate.com/contents/malaria-epidemiology-prevention-and-control. Date Accessed: 20th July, 2020.

(35) Nankabirwa, J. I.; Briggs, J.; Rek, J.; Arinaitwe, E.; Nayebare, P.; Katrak, S.; Staedke, S. G.; Rosenthal, P. J.; Rodriguez-Barraquer, I.; Kamya, M. R.; et al. Persistent Parasitemia Despite Dramatic Reduction in Malaria Incidence After 3 Rounds of Indoor Residual Spraying in Tororo, Uganda. *J. Infect. Dis.* **2019**, *219* (7), 1104–1111.

(36) Yapabandara, A. M.; Curtis, C. F.; Wickramasinghe, M. B.; Fernando, W. P. Control of Malaria Vectors with the Insect Growth Regulator Pyriproxyfen in a Gem-Mining Area in Sri Lanka. *Acta Trop.* **2001**, *80* (3), 265–276.

(37) Fillinger, U.; Lindsay, S. W. Suppression of Exposure to Malaria Vectors by an Order of Magnitude Using Microbial Larvicides in Rural Kenya. *Trop. Med. Int. Heal.* **2006**, *11* (11), 1629–1642.

(38) Walshe, D. P.; Garner, P.; Adeel, A. A.; Pyke, G. H.; Burkot, T. R. Larvivorous Fish for Preventing Malaria Transmission. *Cochrane Database Syst. Rev.* **2017**.

(39) Ghosh, S. K.; Tiwari, S. N.; Sathyanarayan, T. S.; Sampath, T. R. R.; Sharma, V. P.; Nanda, N.; Joshi, H.; Adak, T.; Subbarao, S. K. Larvivorous Fish in Wells Target the Malaria Vector Sibling Species of the Anopheles Culicifacies Complex in Villages in Karnataka, India. *Trans. R. Soc. Trop. Med. Hyg.* **2005**, *99* (2), 101–105.

(40) Andreasen, M. H.; Curtis, C. F. Optimal Life Stage for Radiation Sterilization of Anopheles Males and Their Fitness for Release. *Med. Vet. Entomol.* **2005**, *19* (3), 238–244.

(41) Macias, V.; Ohm, J.; Rasgon, J. Gene Drive for Mosquito Control: Where Did It Come from and Where Are We Headed? *Int. J. Environ. Res. Public Health* **2017**, *14* (9), 1006.

(42) Carvalho, D. O.; McKemey, A. R.; Garziera, L.; Lacroix, R.; Donnelly, C. A.; Alphey, L.; Malavasi, A.; Capurro, M. L. Suppression of a Field Population of Aedes Aegypti in Brazil by Sustained Release of Transgenic Male Mosquitoes. *PLoS Negl. Trop. Dis.* **2015**, *9* (7), e0003864.

(43) Basu, S.; Aryan, A.; Overcash, J. M.; Samuel, G. H.; Anderson, M. A. E.; Dahlem, T. J.; Myles, K. M.; Adelman, Z. N. Silencing of End-Joining Repair for Efficient Site-Specific Gene Insertion after TALEN/CRISPR Mutagenesis in Aedes Aegypti. *Proc. Natl. Acad. Sci.* **2015**, *112* (13), 4038–4043.

(44) Hammond, A.; Galizi, R.; Kyrou, K.; Simoni, A.; Siniscalchi, C.; Katsanos, D.; Gribble, M.; Baker, D.; Marois, E.; Russell, S.; et al. A CRISPR-Cas9 Gene Drive System Targeting Female Reproduction in the Malaria Mosquito Vector Anopheles Gambiae. *Nat. Biotechnol.* **2016**, *34* (1), 78–83.

(45) Kyrou, K.; Hammond, A. M.; Galizi, R.; Kranjc, N.; Burt, A.; Beaghton, A. K.; Nolan, T.; Crisanti, A. A CRISPR–Cas9 Gene Drive Targeting Doublesex Causes Complete Population Suppression in Caged Anopheles Gambiae Mosquitoes. *Nat. Biotechnol.* **2018**, *36* (11), 1062–1066.

(46) Burt, A.; Coulibaly, M.; Crisanti, A.; Diabate, A.; Kayondo, J. K. Gene Drive to Reduce Malaria Transmission in Sub-Saharan Africa. *J. Responsible Innov.* **2018**, *5* (sup1), S66–S80.

(47) McBride, W. J. H. Chemoprophylaxis of Tropical Infectious Diseases. *Pharmaceuticals* **2010**, *3* (5), 1561–1575.

(48) Juckett, G. Malaria Prevention in Travelers. *Am. Fam. Physician* **1999**, *59* (9), 2523–2530, 2535–2536.

(49) Malaria Prophylaxis https://www.malariasite.com/prophylaxis/.

(50) Fernando, S. D.; Rodrigo, C.; Rajapakse, S. Chemoprophylaxis in Malaria: Drugs, Evidence of Efficacy and Costs. *Asian Pac. J. Trop. Med.* **2011**, *4* (4), 330–336.

(51) Draper, S. J.; Sack, B. K.; King, C. R.; Nielsen, C. M.; Rayner, J. C.; Higgins, M. K.; Long, C. A.; Seder, R. A. Malaria Vaccines: Recent Advances and New Horizons. *Cell Host Microbe* **2018**, *24* (1), 43–56.

(52) Framework for Policy Decision on RTS, S. W. G. W. S. *Proposed Framework for Policy Decision on RTS,S/AS01 Malaria Vaccine*; 2019.

(53) WHO, W. H. O. Malaria Vaccine: WHO Position Paper, January 2016 – Recommendations. *Vaccine* **2018**, *36* (25), 3576–3577.

(54) Brady, O. J.; Slater, H. C.; Pemberton-Ross, P.; Wenger, E.; Maude, R. J.; Ghani, A. C.; Penny, M. A.; Gerardin, J.; White, L. J.; Chitnis, N.; et al. Role of Mass Drug Administration in Elimination of Plasmodium Falciparum Malaria: A Consensus Modelling Study. *Lancet Glob. Heal.* **2017**, *5* (7), e680–e687.

(55) WHO, W. H. O. *Mass Drug Administration for Falciparum Malaria*; 2017.

(56) Tripura, R.; Peto, T. J.; Chea, N.; Chan, D.; Mukaka, M.; Sirithiranont, P.; Dhorda, M.; Promnarate, C.; Imwong, M.; von Seidlein, L.; et al. A Controlled Trial of Mass Drug Administration to Interrupt Transmission of Multidrug-Resistant Falciparum Malaria in Cambodian Villages. *Clin. Infect. Dis.* **2018**, *67* (6), 817–826.

(57) Mwesigwa, J.; Achan, J.; Affara, M.; Wathuo, M.; Worwui, A.; Mohammed, N. I.; Kanuteh, F.; Prom, A.; Dierickx, S.; di Tanna, G. L.; et al. Mass Drug Administration With Dihydroartemisinin-Piperaquine and Malaria Transmission Dynamics in The Gambia: A Prospective Cohort Study. *Clin. Infect. Dis.* **2019**, *69* (2), 278–286.

(58) Guler, J. L.; Rosenthal, P. J. Mass Drug Administration to Control and Eliminate Malaria in Africa: How Do We Best Utilize the Tools at Hand? *Clin. Infect. Dis.* **2019**, *69* (2), 287–289.

(59) Amaratunga, C.; Lim, P.; Suon, S.; Sreng, S.; Mao, S.; Sopha, C.; Sam, B.; Dek, D.; Try, V.; Amato, R.; et al. Dihydroartemisinin–Piperaquine Resistance in Plasmodium

Falciparum Malaria in Cambodia: A Multisite Prospective Cohort Study. *Lancet Infect. Dis.* **2016**, *16* (3), 357–365.

(60) Amato, R.; Lim, P.; Miotto, O.; Amaratunga, C.; Dek, D.; Pearson, R. D.; Almagro-Garcia, J.; Neal, A. T.; Sreng, S.; Suon, S.; et al. Genetic Markers Associated with Dihydroartemisinin–Piperaquine Failure in Plasmodium Falciparum Malaria in Cambodia: A Genotype–Phenotype Association Study. *Lancet Infect. Dis.* **2017**, *17* (2), 164–173.

(61) Tse, E. G.; Korsik, M.; Todd, M. H. The Past, Present and Future of Anti-Malarial Medicines. *Malar. J.* **2019**, *18* (1), 93.

(62) Okombo, J.; Chibale, K. Recent Updates in the Discovery and Development of Novel Antimalarial Drug Candidates. *Medchemcomm* **2018**, *9* (3), 437–453.

(63) White, N. J. The Treatment of Malaria. *N. Engl. J. Med.* **1996**, *335* (11), 800–806.

(64) White, N. J. The Treatment of Malaria. *N. Engl. J. Med.* **1996**, *335*, 800–806.

(65) White, N. J.; Nosten, F. Artemisinin-Based Combination Treatment of Falciparum Malaria. *Am. J. Trop. Med. Hyg.* **2007**, *77* (6_Suppl), 181–192.

(66) Noedl, H.; Se, Y.; Schaecher, K.; Smith, B. L.; Socheat, D.; Fukuda, M. M. Evidence of Artemisinin-Resistant Malaria in Western Cambodia. *N. Engl. J. Med.* **2008**, *359* (24), 2619–2620.

(67) Amato, R.; Pearson, R. D.; Almagro-Garcia, J.; Amaratunga, C.; Lim, P.; Suon, S.; Sreng, S.; Drury, E.; Stalker, J.; Miotto, O.; et al. Origins of the Current Outbreak of Multidrug-Resistant Malaria in Southeast Asia: A Retrospective Genetic Study. *Lancet Infect. Dis.* **2018**, *18* (3), 337–345.

(68) Combrinck, J. M.; Mabotha, T. E.; Ncokazi, K. K.; Ambele, M. A.; Taylor, D.; Smith, P. J.; Hoppe, H. C.; Egan, T. J. Insights into the Role of Heme in the Mechanism of Action of Antimalarials. *ACS Chem. Biol.* **2013**, *8* (1), 133–137.

(69) Fry, M.; Pudney, M. Site of Action of the Antimalarial Hydroxynaphthoquinone, 2-[Trans-4-(4'-Chlorophenyl) Cyclohexyl]-3- Hydroxy-1,4-Naphthoquinone (566C80). *Biochem. Pharmacol.* **1992**, *43* (7), 1545–1553.

(70) Srivastava, I. K.; Vaidya, A. B. A Mechanism for the Synergistic Antimalarial Action of Atovaquone and Proguanil. *Antimicrob. Agents Chemother.* **1999**, *43* (6), 1334–1339.

(71) Chico, R. M.; Chaponda, E. B.; Ariti, C.; Chandramohan, D. Sulfadoxine-Pyrimethamine Exhibits Dose-Response Protection Against Adverse Birth Outcomes Related to Malaria and Sexually Transmitted and Reproductive Tract Infections. *Clin. Infect. Dis.* **2017**, *64* (8), 1043–1051.

(72) Medicines for Malaria Venture. US FDA approves Krintafel (tafenoquine) for the radical cure of P. vivax malaria https://www.mmv.org/newsroom/press-releases/us-fda-approves-krintafel-tafenoquine-radical-cure-p-vivax-malaria.

(73) Medicines for Malaria Venture. MMV-supported projects

https://www.mmv.org/research-development/mmv-supported-projects.

(74) Burrows, J. N.; Hooft van Huijsduijnen, R.; Möhrle, J. J.; Oeuvray, C.; Wells, T. N. Designing the next Generation of Medicines for Malaria Control and Eradication. *Malar. J.* **2013**, *12* (1), 187.

(75) Angulo-Barturen, I.; Jiménez-Díaz, M. B.; Mulet, T.; Rullas, J.; Herreros, E.; Ferrer, S.; Jiménez, E.; Mendoza, A.; Regadera, J.; Rosenthal, P. J.; et al. A Murine Model of Falciparum-Malaria by In Vivo Selection of Competent Strains in Non-Myelodepleted Mice Engrafted with Human Erythrocytes. *PLoS One* **2008**, *3* (5), e2252.

(76) Dembele, L.; Gego, A.; Zeeman, A.-M.; Franetich, J.-F.; Silvie, O.; Rametti, A.; Le Grand, R.; Dereuddre-Bosquet, N.; Sauerwein, R.; van Gemert, G.-J.; et al. Towards an In Vitro Model of Plasmodium Hypnozoites Suitable for Drug Discovery. *PLoS One* **2011**, *6* (3), e18162.

(77) Bousema, T.; Dinglasan, R. R.; Morlais, I.; Gouagna, L. C.; van Warmerdam, T.; Awono-Ambene, P. H.; Bonnet, S.; Diallo, M.; Coulibaly, M.; Tchuinkam, T.; et al. Mosquito Feeding Assays to Determine the Infectiousness of Naturally Infected Plasmodium Falciparum Gametocyte Carriers. *PLoS One* **2012**, *7* (8), e42821.

(78) Corey, V. C.; Lukens, A. K.; Istvan, E. S.; Lee, M. C. S.; Franco, V.; Magistrado, P.; Coburn-Flynn, O.; Sakata-Kato, T.; Fuchs, O.; Gnädig, N. F.; et al. A Broad Analysis of Resistance Development in the Malaria Parasite. *Nat. Commun.* **2016**, *7* (1), 11901.

(79) Spangenberg, T.; Burrows, J. N.; Kowalczyk, P.; McDonald, S.; Wells, T. N. C.; Willis, P. The Open Access Malaria Box: A Drug Discovery Catalyst for Neglected Diseases. *PLoS One* **2013**, *8* (6), e62906.

(80) Kuchel, P. W.; Torres, A. M.; Campbell, T. J.; Vandenberg, J. I. The HERG K + Channel: Progress in Understanding the Molecular Basis of Its Unusual Gating Kinetics. *Eur. Biophys. J.* **2004**, *33* (2), 89–97.

(81) Zhou, Z.; Gong, Q.; Epstein, M. L.; January, C. T. HERG Channel Dysfunction in Human Long QT Syndrome: Intracellular Transport and Functional Defects. *J. Biol. Chem.* **1998**, *273*, 21061–21066.

(82) Vandenberg, J. I.; Perozo, E.; Allen, T. W. Towards a Structural View of Drug Binding to HERG K + Channels. *Trends Pharmacol. Sci.* **2017**, *38* (10), 899–907.

(83) Li, M.; Ramos, L. G. Drug-Induced QT Prolongation And Torsades de Pointes. *P T* **2017**, *42* (7), 473–477.

(84) Curran, M. E.; Splawski, I.; Timothy, K. W.; Vincen, G. M.; Green, E. D.; Keating, M. T. A Molecular Basis for Cardiac Arrhythmia: HERG Mutations Cause Long QT Syndrome. *Cell* **1995**, *80*, 795–803.

(85) Drici, M. D.; Barhanin, J. Cardiac K+ Channels and Drug-Acquired Long QT Syndrome. *Therapie 55*, 185–193.

(86) LabMedica International. Several Genes Linked to Long QT Syndrome Reappraised https://www.labmedica.com/molecular-diagnostics/articles/294780919/several-genes-linked-to-long-qt-syndrome-reappraised.html (accessed May 4, 2020).

(87) Fernandez, D.; Ghanta, A.; Kauffman, G. W.; Sanguinetti, M. C. Physicochemical Features of the HERG Channel Drug Binding Site. *J. Biol. Chem.* **2004**, *279* (11), 10120–10127.

(88) Jamieson, C.; Moir, E. M.; Rankovic, Z.; Wishart, G. Medicinal Chemistry of HERG Optimizations: Highlights and Hang-Ups. *J. Med. Chem.* **2006**, *49* (17), 5029–5046.

(89) Garrido, A.; Lepailleur, A.; Mignani, S. M.; Dallemagne, P.; Rochais, C. HERG Toxicity Assessment: Useful Guidelines for Drug Design. *Eur. J. Med. Chem.* **2020**, *195*, 112290.

(90) Ekins, S.; Crumb, W. J.; Sarazan, R. D.; Wikel, J. H.; Wrighton, S. A. Three-Dimensional Quantitative Structure-Activity Relationship for Inhibition of Human Ether-a-Go-Go -Related Gene Potassium Channel. *J. Pharmacol. Exp. Ther.* **2002**, *301* (2), 427–434. https://doi.org/10.1124/jpet.301.2.427.

(91) Cavalli, A.; Poluzzi, E.; De Ponti, F.; Recanatini, M. Toward a Pharmacophore for Drugs Inducing the Long QT Syndrome: Insights from a CoMFA Study of HERG K + Channel Blockers. *J. Med. Chem.* **2002**, *45* (18), 3844–3853.

(92) Saxena, P.; Zangerl-Plessl, E.-M.; Linder, T.; Windisch, A.; Hohaus, A.; Timin, E.; Hering, S.; Stary-Weinzinger, A. New Potential Binding Determinant for HERG Channel Inhibitors. *Sci. Rep.* **2016**, *6* (1), 24182.

(93) Pearlstein, R. A.; Vaz, R. J.; Kang, J.; Chen, X.-L.; Preobrazhenskaya, M.; Shchekotikhin, A. E.; Korolev, A. M.; Lysenkova, L. N.; Miroshnikova, O. V; Hendrix, J.; et al. Characterization of HERG Potassium Channel Inhibition Using CoMSiA 3D QSAR and Homology Modeling Approaches. *Bioorg. Med. Chem. Lett.* **2003**, *13* (10), 1829–1835.

(94) Choe, H.; Nah, K. H.; Lee, S. N.; Lee, H. S.; Lee, H. S.; Jo, S. H.; Leem, C. H.; Jang, Y. J. A Novel Hypothesis for the Binding Mode of HERG Channel Blockers. *Biochem. Biophys. Res. Commun.* **2006**, *344* (1), 72–78.

(95) Rampe, D.; Wible, B.; Brown, A. M.; Dage, R. C. Effects of Terfenadine and Its Metabolites on a Delayed Rectifier K+ Channel Cloned from Human Heart. *Mol. Pharmacol.* **1993**, *44* (6), 1240–1245.

(96) Edmondson, S. D.; Mastracchio, A.; Duffy, J. L.; Eiermann, G. J.; He, H.; Ita, I.; Leiting, B.; Leone, J. F.; Lyons, K. A.; Makarewicz, A. M.; et al. Discovery of Potent and Selective Orally Bioavailable β-Substituted Phenylalanine Derived Dipeptidyl Peptidase IV Inhibitors. *Bioorg. Med. Chem. Lett.* **2005**, *15* (12), 3048–3052.

(97) Vaz, R. J.; Gao, Z.; Pribish, J.; Chen, X.; Levell, J.; Davis, L.; Albert, E.; Brollo, M.; Ugolini, A.; Cramer, D. M.; et al. Design of Bivalent Ligands Using Hydrogen Bond Linkers: Synthesis and Evaluation of Inhibitors for Human β-Tryptase. *Bioorg. Med.*

Chem. Lett. **2004**, *14* (24), 6053–6056.

(98) Xu, J.; Wei, L.; Mathvink, R.; He, J.; Park, Y.-J.; He, H.; Leiting, B.; Lyons, K. A.; Marsilio, F.; Patel, R. A.; et al. Discovery of Potent and Selective Phenylalanine Based Dipeptidyl Peptidase IV Inhibitors. *Bioorg. Med. Chem. Lett.* **2005**, *15* (10), 2533–2536.

(99) Fraley, M. E.; Arrington, K. L.; Buser, C. A.; Ciecko, P. A.; Coll, K. E.; Fernandes, C.; Hartman, G. D.; Hoffman, W. F.; Lynch, J. J.; McFall, R. C.; et al. Optimization of the Indolyl Quinolinone Class of KDR (VEGFR-2) Kinase Inhibitors. *Bioorg. Med. Chem. Lett.* **2004**, *14*, 351–355.

(100) Hameed P, S.; Manjrekar, P.; Raichurkar, A.; Shinde, V.; Puttur, J.; Shanbhag, G.; Chinnapattu, M.; Patil, V.; Rudrapatana, S.; Sharma, S.; et al. Left-Hand Side Exploration of Novel Bacterial Topoisomerase Inhibitors to Improve Selectivity against HERG Binding. *ACS Med. Chem. Lett.* **2015**, *6*, 741–746.

(101) Bilodeau, M. T.; Balitza, A. E.; Koester, T. J.; Manley, P. J.; Rodman, L. D.; Buser-Doepner, C.; Coll, K. E.; Fernandes, C.; Gibbs, J. B.; Heimbrook, D. C.; et al. Potent N -(1,3-Thiazol-2-Yl)Pyridin-2-Amine Vascular Endothelial Growth Factor Receptor Tyrosine Kinase Inhibitors with Excellent Pharmacokinetics and Low Affinity for the HERG Ion Channel. *J. Med. Chem.* **2004**, *47*, 6363–6372.

(102) Skerlj, R.; Bridger, G.; Zhou, Y.; Bourque, E.; McEachern, E.; Danthi, S.; Langille, J.; Harwig, C.; Veale, D.; Carpenter, B.; et al. Mitigating HERG Inhibition: Design of Orally Bioavailable CCR5 Antagonists as Potent Inhibitors of R5 HIV-1 Replication. *ACS Med. Chem. Lett.* **2012**, *3*, 216–221.

(103) Epstein, O.; Bryan, M. C.; Cheng, A. C.; Derakhchan, K.; Dineen, T. A.; Hickman, D.; Hua, Z.; Human, J. B.; Kreiman, C.; Marx, I. E.; et al. Lead Optimization and Modulation of HERG Activity in a Series of Aminooxazoline Xanthene β-Site Amyloid Precursor Protein Cleaving Enzyme (BACE1) Inhibitors. *J. Med. Chem.* **2014**, *57* (23), 9796–9810.

(104) Fish, L. R.; Gilligan, M. T.; Humphries, A. C.; Ivarsson, M.; Ladduwahetty, T.; Merchant, K. J.; O'Connor, D.; Patel, S.; Philipps, E.; Vargas, H. M.; et al. 4-Fluorosulfonylpiperidines: Selective 5-HT2A Ligands for the Treatment of Insomnia. *Bioorg. Med. Chem. Lett.* **2005**, *15* (16), 3665–3669.

(105) Zhang, H.-C.; Derian, C. K.; McComsey, D. F.; White, K. B.; Ye, H.; Hecker, L. R.; Li, J.; Addo, M. F.; Croll, D.; Eckardt, A. J.; et al. Novel Indolylindazolylmaleimides as Inhibitors of Protein Kinase C-β: Synthesis, Biological Activity, and Cardiovascular Safety †. *J. Med. Chem.* **2005**, *48* (6), 1725–1728.

(106) Bourrain, S.; Collins, I.; Neduvelil, J. G.; Rowley, M.; Leeson, P. D.; Patel, S.; Patel, S.; Emms, F.; Marwood, R.; Chapman, K. L.; et al. Substituted Pyrazoles as Novel Selective Ligands for the Human Dopamine D 4 Receptor. *Bioorg. Med. Chem.* **1998**, *6* (10), 1731–1743.

(107) Yang, Z.-Q.; Barrow, J. C.; Shipe, W. D.; Schlegel, K.-A. S.; Shu, Y.; Yang, F. V.; Lindsley, C. W.; Rittle, K. E.; Bock, M. G.; Hartman, G. D.; et al. Discovery of 1,4-Substituted Piperidines as Potent and Selective Inhibitors of T-Type Calcium Channels. *J. Med. Chem.* **2008**, *51* (20), 6471–6477.

(108) Shultz, M. D.; Cao, X.; Chen, C. H.; Cho, Y. S.; Davis, N. R.; Eckman, J.; Fan, J.; Fekete, A.; Firestone, B.; Flynn, J.; et al. Optimization of the in Vitro Cardiac Safety of Hydroxamate-Based Histone Deacetylase Inhibitors. *J. Med. Chem.* **2011**, *54* (13), 4752–4772.

(109) Sakauchi, N.; Kohara, Y.; Sato, A.; Suzaki, T.; Imai, Y.; Okabe, Y.; Imai, S.; Saikawa, R.; Nagabukuro, H.; Kuno, H.; et al. Discovery of 5-Chloro-1-(5-Chloro-2-(Methylsulfonyl)Benzyl)-2-Imino-1,2-Dihydropyridine-3-Carboxamide (TAK-259) as a Novel, Selective, and Orally Active α 1D Adrenoceptor Antagonist with Antiurinary Frequency Effects: Reducing Human Ether-a-Go-Go-Related. *J. Med. Chem.* **2016**, *59* (7), 2989–3002.

(110) Berglund, S.; Egner, B. J.; Gradén, H.; Gradén, J.; Morgan, D. G. A.; Inghardt, T.; Giordanetto, F. Optimization of Piperidin-4-Yl-Urea-Containing Melanin-Concentrating Hormone Receptor 1 (MCH-R1) Antagonists: Reducing HERG-Associated Liabilities. *Bioorg. Med. Chem. Lett.* **2009**, *19* (15), 4274–4279.

(111) Hirose, H.; Yamasaki, T.; Ogino, M.; Mizojiri, R.; Tamura-Okano, Y.; Yashiro, H.; Muraki, Y.; Nakano, Y.; Sugama, J.; Hata, A.; et al. Discovery of Novel 5-Oxa-2,6-Diazaspiro[3.4]Oct-6-Ene Derivatives as Potent, Selective, and Orally Available Somatostatin Receptor Subtype 5 (SSTR5) Antagonists for Treatment of Type 2 Diabetes Mellitus. *Bioorg. Med. Chem.* **2017**, *25* (15), 4175–4193.

(112) Wrobleski, S. T.; Moslin, R.; Lin, S.; Zhang, Y.; Spergel, S.; Kempson, J.; Tokarski, J. S.; Strnad, J.; Zupa-Fernandez, A.; Cheng, L.; et al. Highly Selective Inhibition of Tyrosine Kinase 2 (TYK2) for the Treatment of Autoimmune Diseases: Discovery of the Allosteric Inhibitor BMS-986165. *J. Med. Chem.* **2019**, *62* (20), 8973–8995.

(113) Ogiyama, T.; Inoue, M.; Honda, S.; Yamada, H.; Watanabe, T.; Gotoh, T.; Kiso, T.; Koakutsu, A.; Kakimoto, S.; Shishikura, J. Discovery of Novel Tetrahydroisoquinoline Derivatives as Orally Active N-Type Calcium Channel Blockers with High Selectivity for HERG Potassium Channels. *Bioorg. Med. Chem.* **2014**, *22* (24), 6899–6907.

(114) Matralis, A. N.; Malik, A.; Penzo, M.; Moreno, I.; Almela, M. J.; Camino, I.; Crespo, B.; Saadeddin, A.; Ghidelli-Disse, S.; Rueda, L.; et al. Development of Chemical Entities Endowed with Potent Fast-Killing Properties against Plasmodium Falciparum Malaria Parasites. *J. Med. Chem.* **2019**, *62* (20), 9217–9235.

(115) Lv, K.; Wang, A.; Tao, Z.; Fu, L.; Liu, H.; Wang, B.; Ma, C.; Wang, H.; Ma, X.; Han, B.; et al. HERG Optimizations of IMB1603, Discovery of Alternative Benzothiazinones as New Antitubercular Agents. *Eur. J. Med. Chem.* **2019**, *179*,

208–217.

(116) Leung, L.; Niculescu-Duvaz, D.; Smithen, D.; Lopes, F.; Callens, C.; McLeary, R.; Saturno, G.; Davies, L.; Aljarah, M.; Brown, M.; et al. Anti-Metastatic Inhibitors of Lysyl Oxidase (LOX): Design and Structure–Activity Relationships. *J. Med. Chem.* **2019**, *62* (12), 5863–5884.

(117) Grilo, L. S.; Carrupt, P.-A.; Abriel, H. Stereoselective Inhibition of the HERG1 Potassium Channel. *Front. Pharmacol.* **2010**, *1*.

(118) Kanai, Y.; Tateyama, S.; Nakamura, T.; Kasaba, T.; Takasaki, M. Effects of Levobupivacaine, Bupivacaine, and Ropivacaine on Tail-Flick Response and Motor Function in Rats Following Epidural or Intrathecal Administration1. *Reg. Anesth. Pain Med.* **1999**, *24* (5), 444–452.

(119) White, N. J. Cardiotoxicity of Antimalarial Drugs. *Lancet Infect. Dis.* **2007**, *7* (8), 549–558.

(120) Bell, I. M.; Gallicchio, S. N.; Abrams, M.; Beshore, D. C.; Buser, C. A.; Culberson, J. C.; Davide, J.; Ellis-Hutchings, M.; Fernandes, C.; Gibbs, J. B.; et al. Design and Biological Activity of (S)-4-(5-{[1-(3-Chlorobenzyl)-2- Oxopyrrolidin-3-Ylamino]Methyl}imidazol-1-Ylmethyl)Benzonitrile, a 3-Aminopyrrolidinone Farnesyltransferase Inhibitor with Excellent Cell Potency. *J. Med. Chem.* **2001**, *44* (18), 2933–2949.

(121) Bell, I. M.; Gallicchio, S. N.; Abrams, M.; Beese, L. S.; Beshore, D. C.; Bhimnathwala, H.; Bogusky, M. J.; Buser, C. A.; Culberson, J. C.; Davide, J.; et al. 3-Aminopyrrolidinone Farnesyltransferase Inhibitors: Design of Macrocyclic Compounds with Improved Pharmacokinetics and Excellent Cell Potency. *J. Med. Chem.* **2002**, *45* (12), 2388–2409.

(122) Di, L.; Fish, P. V.; Mano, T. Bridging Solubility between Drug Discovery and Development. *Drug Discov. Today* **2012**, *17* (9–10), 486–495.

(123) Stegemann, S.; Leveiller, F.; Franchi, D.; de Jong, H.; Lindén, H. When Poor Solubility Becomes an Issue: From Early Stage to Proof of Concept. *Eur. J. Pharm. Sci.* **2007**, *31*, 249–261.

(124) Kerns, E. H.; Di, L. Solubility. In *Drug-like Properties: Concepts, Structure Design and Methods*; Elsevier, 2008; pp 56–85.

(125) Sugano, K.; Okazaki, A.; Sugimoto, S.; Tavornvipas, S.; Omura, A.; Mano, T. Solubility and Dissolution Profile Assessment in Drug Discovery. *Drug Metab. Pharmacokinet.* **2007**, *22* (4), 225–254.

(126) Leach, A. G.; Jones, H. D.; Cosgrove, D. A.; Kenny, P. W.; Ruston, L.; MacFaul, P.; Wood, J. M.; Colclough, N.; Law, B. Matched Molecular Pairs as a Guide in the Optimization of Pharmaceutical Properties; a Study of Aqueous Solubility, Plasma Protein Binding and Oral Exposure. *J. Med. Chem.* **2006**, *49*, 6672–6682.

(127) Forster, S.; Buckton, G.; Beezer, A. E. The Importance of Chain Length on the

Wettability and Solubility of Organic Homologs. *Int. J. Pharm.* **1991**, *72*, 29–34.

(128) Le Manach, C.; Paquet, T.; Gonzàlez Cabrera, D.; Younis, Y.; Taylor, D.; Wiesner, L.; Lawrence, N.; Schwager, S.; Waterson, D.; Witty, M. J.; et al. Medicinal Chemistry Optimization of Antiplasmodial Imidazopyridazine Hits from High Throughput Screening of a SoftFocus Kinase Library: Part 2. *J. Med. Chem.* **2014**, *57*, 8839–8848.

(129) Arrowsmith, J. E.; Campbell, S. F.; Cross, P. E.; Stubbs, J. K.; Burges, R. A.; Gardiner, D. G.; Blackburn, K. J. Long-Acting Dihydropyridine Calcium Antagonists. 1. 2-Alkoxymethyl Derivatives Incorporating Basic Substituents. *J. Med. Chem.* **1986**, *29* (9), 1696–1702.

(130) Jordan, V. C. Tamoxifen: A Most Unlikely Pioneering Medicine. *Nat. Rev. Drug Discov.* **2003**, *2* (3), 205–213.

(131) Lundquist, J. T.; Harnish, D. C.; Kim, C. Y.; Mehlmann, J. F.; Unwalla, R. J.; Phipps, K. M.; Crawley, M. L.; Commons, T.; Green, D. M.; Xu, W.; et al. Improvement of Physiochemical Properties of the Tetrahydroazepinoindole Series of Farnesoid X Receptor (FXR) Agonists: Beneficial Modulation of Lipids in Primates. *J. Med. Chem.* **2010**, *53* (4), 1774–1787.

(132) GWAK, H.; CHOI, J.; CHOI, H. Enhanced Bioavailability of Piroxicam via Salt Formation with Ethanolamines. *Int. J. Pharm.* **2005**.

(133) Ishikawa, M.; Hashimoto, Y. Improvement in Aqueous Solubility in Small Molecule Drug Discovery Programs by Disruption of Molecular Planarity and Symmetry. *J. Med. Chem.* **2011**, *54*, 1539–1554.

(134) Lovering, F.; Bikker, J.; Humblet, C. Escape from Flatland: Increasing Saturation as an Approach to Improving Clinical Success. *J. Med. Chem.* **2009**, *52* (21), 6752–6756.

(135) Han, H.-K.; Amidon, G. L. Targeted Prodrug Design to Optimize Drug Delivery. *AAPS PharmSci* **2000**, *2* (1), 48–58.

(136) Rautio, J.; Kumpulainen, H.; Heimbach, T.; Oliyai, R.; Oh, D.; Järvinen, T.; Savolainen, J. Prodrugs: Design and Clinical Applications. *Nat. Rev. Drug Discov.* **2008**, *7* (3), 255–270.

(137) Ettmayer, P.; Amidon, G. L.; Clement, B.; Testa, B. Lessons Learned from Marketed and Investigational Prodrugs. *J. Med. Chem.* **2004**, *47* (10), 2393–2404.

(138) Stella, V. J. A Case for Prodrugs: Fosphenytoin. *Adv. Drug Deliv. Rev.* **1996**, *19* (2), 311–330.

(139) Stella, V. J.; Nti-Addae, K. W. Prodrug Strategies to Overcome Poor Water Solubility. *Adv. Drug Deliv. Rev.* **2007**, *59* (7), 677–694.

(140) Williams, H. D.; Trevaskis, N. L.; Charman, S. A.; Shanker, R. M.; Charman, W. N.; Pouton, C. W.; Porter, C. J. H. Strategies to Address Low Drug Solubility in Discovery and Development. *Pharmacol. Rev.* **2013**, *65* (1), 315–499.

(141) Pouton, C. W. Formulation of Poorly Water-Soluble Drugs for Oral Administration: Physicochemical and Physiological Issues and the Lipid Formulation Classification System. *Eur. J. Pharm. Sci.* **2006**, *29* (3–4), 278–287.

(142) Van Eerdenbrugh, B.; Van den Mooter, G.; Augustijns, P. Top-down Production of Drug Nanocrystals: Nanosuspension Stabilization, Miniaturization and Transformation into Solid Products. *Int. J. Pharm.* **2008**, *364* (1), 64–75.

(143) Vasconcelos, T.; Sarmento, B.; Costa, P. Solid Dispersions as Strategy to Improve Oral Bioavailability of Poor Water Soluble Drugs. *Drug Discov. Today* **2007**, *12* (23–24), 1068–1075.

(144) Lima, L.; Barreiro, E. Bioisosterism: A Useful Strategy for Molecular Modification and Drug Design. *Curr. Med. Chem.* **2005**, *12* (1), 23–49.

(145) Meanwell, N. A. Synopsis of Some Recent Tactical Application of Bioisosteres in Drug Design. *J. Med. Chem.* **2011**, *54* (8), 2529–2591.

(146) Patani, G. A.; LaVoie, E. J. Bioisosterism: A Rational Approach in Drug Design. *Chem. Rev.* **1996**, *96* (8), 3147–3176.

(147) Wang, R.; Ding, T.; Jiang, L.; He, W.; Yi, W. Fluoromethoxymethylation of Nitrogen Heterocyclic Compounds with Fluoromethyl Iodide. *J. Org. Chem.* **2020**, *85* (6), 3993–4001.

(148) Lassalas, P.; Gay, B.; Lasfargeas, C.; James, M. J.; Tran, V.; Vijayendran, K. G.; Brunden, K. R.; Kozlowski, M. C.; Thomas, C. J.; Smith, A. B.; et al. Structure Property Relationships of Carboxylic Acid Isosteres. *J. Med. Chem.* **2016**, *59* (7), 3183–3203.

(149) Dai, Y.; Hartandi, K.; Ji, Z.; Ahmed, A. A.; Albert, D. H.; Bauch, J. L.; Bouska, J. J.; Bousquet, P. F.; Cunha, G. A.; Glaser, K. B.; et al. Discovery of N -(4-(3-Amino-1 H -Indazol-4-Yl)Phenyl)- N '-(2-Fluoro-5-Methylphenyl)Urea (ABT-869), a 3-Aminoindazole-Based Orally Active Multitargeted Receptor Tyrosine Kinase Inhibitor. *J. Med. Chem.* **2007**, *50* (7), 1584–1597.

(150) Showell, G. A.; Mills, J. S. Chemistry Challenges in Lead Optimization: Silicon Isosteres in Drug Discovery. *Drug Discov. Today* **2003**, *8* (12), 551–556.

(151) Kim, J.; Sieburth, S. M. Silanediol Peptidomimetics. Evaluation of Four Diastereomeric ACE Inhibitors. *Bioorg. Med. Chem. Lett.* **2004**, *14* (11), 2853–2856.

(152) Yu, K.-L.; Sin, N.; Civiello, R. L.; Wang, X. A.; Combrink, K. D.; Gulgeze, H. B.; Venables, B. L.; Wright, J. J. K.; Dalterio, R. A.; Zadjura, L.; et al. Respiratory Syncytial Virus Fusion Inhibitors. Part 4: Optimization for Oral Bioavailability. *Bioorg. Med. Chem. Lett.* **2007**, *17* (4), 895–901.

(153) Brown, N. Bioisosterism in Medicinal Chemistry. In *Bioisosteres in Medicinal Chemistry*; Wiley-VCH Verlag GmbH & Co. KGaA: Weinheim, Germany, 2012; pp 1–14.

(154) van der Westhuyzen, R.; Winks, S.; Wilson, C. R.; Boyle, G. A.; Gessner, R. K.; Soares

de Melo, C.; Taylor, D.; de Kock, C.; Njoroge, M.; Brunschwig, C.; et al. Pyrrolo[3,4-c]Pyridine-1,3(2 H)-Diones: A Novel Antimycobacterial Class Targeting Mycobacterial Respiration. *J. Med. Chem.* **2015**, *58* (23), 9371–9381.

(155) Cabal, A.; Williams, D. S.; Jayakar, R. Y.; Zhang, J.; Sardesai, S.; Duong, L. T. Long-Term Treatment with Odanacatib Maintains Normal Trabecular Biomechanical Properties in Ovariectomized Adult Monkeys as Demonstrated by Micro-CT-Based Finite Element Analysis. *Bone Reports* **2017**, *6*, 26–33.

(156) Sun, S.; Jia, Q.; Zhang, Z. Applications of Amide Isosteres in Medicinal Chemistry. *Bioorg. Med. Chem. Lett.* **2019**, *29* (18), 2535–2550.

(157) Claudio Viegas-Junior; Eliezer J. Barreiro; Carlos Alberto Manssour Fraga. Molecular Hybridization: A Useful Tool in the Design of New Drug Prototypes. *Curr. Med. Chem.* **2007**, *14* (17), 1829–1852.

(158) Sunil, R. J. S. P. A. J. Molecular Hybridization-An Emanating Tool in Drug Design. *Med Chem (Los Angeles)* **2019**, *9*, 91–95.

(159) Agarwal, D.; Gupta, R. D.; Awasthi, S. K. Are Antimalarial Hybrid Molecules a Close Reality or a Distant Dream? *Antimicrob. Agents Chemother.* **2017**, *61* (5).

(160) Pokrovskaya, V.; Baasov, T. Dual-Acting Hybrid Antibiotics: A Promising Strategy to Combat Bacterial Resistance. *Expert Opin. Drug Discov.* **2010**, *5* (9), 883–902.

(161) Feng, L.; Xu, Z.; Chang, L.; Li, C.; Yan, X.; Gao, C.; Ding, C.; Zhao, F.; Shi, F.; Wu, X. Hybrid Molecules with Potential in Vitro Antiplasmodial and in Vivo Antimalarial Activity against Drug-resistant Plasmodium Falciparum. *Med. Res. Rev.* **2020**, *40* (3), 931–971.

(162) Decker, M. Introduction. In *Design of Hybrid Molecules for Drug Development*; Elsevier, 2017; pp 1–3.

(163) Njogu, P. M.; Okombo, J.; Chibale, K. Designed Hybrid Compounds for Tropical Parasitic Diseases. In *Design of Hybrid Molecules for Drug Development*; Elsevier, 2017; pp 83–135.

(164) Egan, T. J.; Hunter, R.; Kaschula, C. H.; Marques, H. M.; Misplon, A.; Walden, J. Structure−Function Relationships in Aminoquinolines: Effect of Amino and Chloro Groups on Quinoline−Hematin Complex Formation, Inhibition of β-Hematin Formation, and Antiplasmodial Activity. *J. Med. Chem.* **2000**, *43* (2), 283–291.

(165) Egan, T. J. Recent Advances in Understanding the Mechanism of Hemozoin (Malaria Pigment) Formation. *J. Inorg. Biochem.* **2008**, *102* (5–6), 1288–1299.

(166) Krugliak, M.; Zhang, J.; Ginsburg, H. Intraerythrocytic Plasmodium Falciparum Utilizes Only a Fraction of the Amino Acids Derived from the Digestion of Host Cell Cytosol for the Biosynthesis of Its Proteins. *Mol. Biochem. Parasitol.* **2002**, *119* (2), 249–256.

(167) O'Neill, P. M.; Barton, V. E.; Ward, S. A. The Molecular Mechanism of Action of Artemisinin—The Debate Continues. *Molecules* **2010**, *15* (3), 1705–1721.

(168) Cosledan, F.; Fraisse, L.; Pellet, A.; Guillou, F.; Mordmuller, B.; Kremsner, P. G.; Moreno, A.; Mazier, D.; Maffrand, J.-P.; Meunier, B. Selection of a Trioxaquine as an Antimalarial Drug Candidate. *Proc. Natl. Acad. Sci.* **2008**, *105* (45), 17579–17584.

(169) Bellot, F.; Coslédan, F.; Vendier, L.; Brocard, J.; Meunier, B.; Robert, A. Trioxaferroquines as New Hybrid Antimalarial Drugs. *J. Med. Chem.* **2010**, *53* (10), 4103–4109.

(170) Walsh, J.; Bell, A. Hybrid Drugs for Malaria. *Curr. Pharm. Des.* **2009**, *15* (25), 2970–2985.

(171) Jones, M.; Mercer, A. E.; Stocks, P. A.; La Pensée, L. J. I.; Cosstick, R.; Park, B. K.; Kennedy, M. E.; Piantanida, I.; Ward, S. A.; Davies, J.; et al. Antitumour and Antimalarial Activity of Artemisinin–Acridine Hybrids. *Bioorg. Med. Chem. Lett.* **2009**, *19* (7), 2033–2037.

(172) Feng, T.-S.; Guantai, E. M.; Nell, M. J.; van Rensburg, C. E. J.; Hoppe, H. C.; Chibale, K. Antiplasmodial and Antitumor Activity of Dihydroartemisinin Analogs Derived via the Aza-Michael Addition Reaction. *Bioorg. Med. Chem. Lett.* **2011**, *21* (10), 2882–2886.

(173) DiMasi, J. A.; Hansen, R. W.; Grabowski, H. G. The Price of Innovation: New Estimates of Drug Development Costs. *J. Health Econ.* **2003**, *22* (2), 151–185.

(174) Chong, C. R.; Sullivan, D. J. New Uses for Old Drugs. *Nature* **2007**, *448*, 645–646.

(175) Njoroge, M.; Njuguna, N. M.; Mutai, P.; Ongarora, D. S. B.; Smith, P. W.; Chibale, K. Recent Approaches to Chemical Discovery and Development Against Malaria and the Neglected Tropical Diseases Human African Trypanosomiasis and Schistosomiasis. *Chem. Rev.* **2014**, *114* (22), 11138–11163.

(176) Gautret, P.; Lagier, J.-C.; Parola, P.; Hoang, V. T.; Meddeb, L.; Mailhe, M.; Doudier, B.; Courjon, J.; Giordanengo, V.; Vieira, V. E.; et al. Hydroxychloroquine and Azithromycin as a Treatment of COVID-19: Results of an Open-Label Non-Randomized Clinical Trial. *Int. J. Antimicrob. Agents* **2020**, 105949.

(177) Al-Tawfiq, J. A.; Al-Homoud, A. H.; Memish, Z. A. Remdesivir as a Possible Therapeutic Option for the COVID-19. *Travel Med. Infect. Dis.* **2020**, 101615.

(178) Narasimhan, B.; Sharma, D.; Kumar, P. Benzimidazole: A Medicinally Important Heterocyclic Moiety. *Med. Chem. Res.* **2012**, *21* (3), 269–283.

(179) Ramachandran, S.; Hameed P., S.; Srivastava, A.; Shanbhag, G.; Morayya, S.; Rautela, N.; Awasthy, D.; Kavanagh, S.; Bharath, S.; Reddy, J.; et al. N -Aryl-2-Aminobenzimidazoles: Novel, Efficacious, Antimalarial Lead Compounds. *J. Med. Chem.* **2014**, *57* (15), 6642–6652.

(180) Calderón, F.; Barros, D.; Bueno, J. M.; Coterón, J. M.; Fernández, E.; Gamo, F. J.; Lavandera, J. L.; León, M. L.; Macdonald, S. J. F.; Mallo, A.; et al. An Invitation to Open Innovation in Malaria Drug Discovery: 47 Quality Starting Points from the TCAMS. *ACS Med. Chem. Lett.* **2011**, *2* (10), 741–746.

(181) Rueda, L.; Castellote, I.; Castro-Pichel, J.; Chaparro, M. J.; de la Rosa, J. C.; Garcia-Perez, A.; Gordo, M.; Jimenez-Diaz, M. B.; Kessler, A.; Macdonald, S. J. F.; et al. Cyclopropyl Carboxamides: A New Oral Antimalarial Series Derived from the Tres Cantos Anti-Malarial Set (TCAMS). *ACS Med. Chem. Lett.* **2011**, *2* (11), 840–844.

(182) Keurulainen, L.; Vahermo, M.; Puente-Felipe, M.; Sandoval-Izquierdo, E.; Crespo-Fernández, B.; Guijarro-López, L.; Huertas-Valentín, L.; de las Heras-Dueña, L.; Leino, T. O.; Siiskonen, A.; et al. A Developability-Focused Optimization Approach Allows Identification of in Vivo Fast-Acting Antimalarials: N -[3-[(Benzimidazol-2-Yl)Amino]Propyl]Amides. *J. Med. Chem.* **2015**, *58* (11), 4573–4580.

(183) Patel, V.; Booker, M.; Kramer, M.; Ross, L.; Celatka, C. A.; Kennedy, L. M.; Dvorin, J. D.; Duraisingh, M. T.; Sliz, P.; Wirth, D. F.; et al. Identification and Characterization of Small Molecule Inhibitors of Plasmodium Falciparum Dihydroorotate Dehydrogenase. *J. Biol. Chem.* **2008**, *283* (50), 35078–35085.

(184) Booker, M. L.; Bastos, C. M.; Kramer, M. L.; Barker, R. H.; Skerlj, R.; Sidhu, A. B.; Deng, X.; Celatka, C.; Cortese, J. F.; Guerrero Bravo, J. E.; et al. Novel Inhibitors of Plasmodium Falciparum Dihydroorotate Dehydrogenase with Anti-Malarial Activity in the Mouse Model. *J. Biol. Chem.* **2010**, *285* (43), 33054–33064.

(185) Skerlj, R. T.; Bastos, C. M.; Booker, M. L.; Kramer, M. L.; Barker, R. H.; Celatka, C. A.; O'Shea, T. J.; Munoz, B.; Sidhu, A. B.; Cortese, J. F.; et al. Optimization of Potent Inhibitors of P. Falciparum Dihydroorotate Dehydrogenase for the Treatment of Malaria. *ACS Med. Chem. Lett.* **2011**, *2* (9), 708–713.

(186) Ongarora, D. S. B.; Strydom, N.; Wicht, K.; Njoroge, M.; Wiesner, L.; Egan, T. J.; Wittlin, S.; Jurva, U.; Masimirembwa, C. M.; Chibale, K. Antimalarial Benzoheterocyclic 4-Aminoquinolines: Structure–Activity Relationship, in Vivo Evaluation, Mechanistic and Bioactivation Studies. *Bioorg. Med. Chem.* **2015**, *23* (17), 5419–5432.

(187) Baartzes, N.; Stringer, T.; Seldon, R.; Warner, D. F.; Taylor, D.; Wittlin, S.; Chibale, K.; Smith, G. S. Bioisosteric Ferrocenyl Aminoquinoline-Benzimidazole Hybrids: Antimicrobial Evaluation and Mechanistic Insights. *Eur. J. Med. Chem.* **2019**, *180*, 121–133.

(188) Sharma, K.; Shrivastava, A.; Mehra, R. N.; Deora, G. S.; Alam, M. M.; Zaman, M. S.; Akhter, M. Synthesis of Novel Benzimidazole Acrylonitriles for Inhibition of Plasmodium Falciparum Growth by Dual Target Inhibition. *Arch. Pharm. (Weinheim).* **2018**, *351* (1), 1700251.

(189) Cabantchik, Z. I. Iron Chelators as Antimalarials: The Biochemical Basis of Selective Cytotoxicity. *Parasitol. Today* **1995**, *11* (2), 74–78.

(190) Divatia, S. M.; Rajani, D. P.; Rajani, S. D.; Patel, H. D. Novel Thiosemicarbazone Derivatives Containing Benzimidazole Moiety: Green Synthesis and Anti-Malarial Activity. *Arab. J. Chem.* **2019**, *12* (7), 1641–1651.

(191) Kim, P.; Kang, S.; Boshoff, H. I.; Jiricek, J.; Collins, M.; Singh, R.; Manjunatha, U. H.; Niyomrattanakit, P.; Zhang, L.; Goodwin, M.; et al. Structure−Activity Relationships of Antitubercular Nitroimidazoles. 2. Determinants of Aerobic Activity and Quantitative Structure−Activity Relationships. *J. Med. Chem.* **2009**, *52* (5), 1329–1344.

(192) Camacho, J.; Barazarte, A.; Gamboa, N.; Rodrigues, J.; Rojas, R.; Vaisberg, A.; Gilman, R.; Charris, J. Synthesis and Biological Evaluation of Benzimidazole-5-Carbohydrazide Derivatives as Antimalarial, Cytotoxic and Antitubercular Agents. *Bioorg. Med. Chem.* **2011**, *19* (6), 2023–2029.

(193) Ndakala, A. J.; Gessner, R. K.; Gitari, P. W.; October, N.; White, K. L.; Hudson, A.; Fakorede, F.; Shackleford, D. M.; Kaiser, M.; Yeates, C.; et al. Antimalarial Pyrido[1,2- a]Benzimidazoles. *J. Med. Chem.* **2011**, *54* (13), 4581–4589.

(194) Mayoka, G.; Njoroge, M.; Okombo, J.; Gibhard, L.; Sanches-Vaz, M.; Fontinha, D.; Birkholtz, L.-M.; Reader, J.; van der Watt, M.; Coetzer, T. L.; et al. Structure–Activity Relationship Studies and Plasmodium Life Cycle Profiling Identifies Pan-Active N -Aryl-3-Trifluoromethyl Pyrido[1,2- a]Benzimidazoles Which Are Efficacious in an in Vivo Mouse Model of Malaria. *J. Med. Chem.* **2019**, *62* (2), 1022–1035.

(195) Torres-Gómez, H.; Hernández-Núñez, E.; León-Rivera, I.; Guerrero-Alvarez, J.; Cedillo-Rivera, R.; Moo-Puc, R.; Argotte-Ramos, R.; Carmen Rodríguez-Gutiérrez, M. del; Chan-Bacab, M. J.; Navarrete-Vázquez, G. Design, Synthesis and in Vitro Antiprotozoal Activity of Benzimidazole-Pentamidine Hybrids. *Bioorg. Med. Chem. Lett.* **2008**, *18* (11), 3147–3151.

(196) Balaña-Fouce, R.; Redondo, C. M.; Pérez-Pertejo, Y.; Díaz-González, R.; Reguera, R. M. Targeting Atypical Trypanosomatid DNA Topoisomerase I. *Drug Discov. Today* **2006**, *11* (15–16), 733–740.

(197) Janssens, M. M.-. L. Astemizole. *Clin. Rev. Allergy* **1993**, *11* (1), 35–63.

(198) Matsumoto, S.; Yamazoe, Y. Involvement of Multiple Human Cytochromes P450 in the Liver Microsomal Metabolism of Astemizole and a Comparison with Terfenadine. *Br. J. Clin. Pharmacol.* **2001**, *51* (2), 133–142.

(199) Heykants, J.; van Peer, A.; Woestenborghs, R.; Jageneau, A.; Vanden Bussche, G. Dose-Proportionality, Bioavailability, and Steady-State Kinetics of Astemizole in Man. *Drug Dev. Res.* **1986**, *8* (1–4), 71–78.

(200) Zhou, Z.; Vorperian, V. R.; Gong, Q.; Zhang, S.; January, C. T. Block of HERG Potassium Channels by the Antihistamine Astemizole and Its Metabolites Desmethylastemizole and Norastemizole. *J. Cardiovasc. Electrophysiol.* **1999**, *10*, 836–843.

(201) Kamei, C.; Mio, M.; Izushi, K.; Kitazumi, K.; Tsujimoto, S.; Fujisawa, K.; Adachi, Y.; Tasaka, K. Antiallergic Effects of Major Metabolites of Astemizole in Rats and Guinea Pigs. *Arzneimittelforschung.* **1991**, *41*, 932–936.

(202) Richards, D. M.; Brogden, R. N.; Heel, R. C.; Speight, T. M.; Avery, G. S. Astemizole. *Drugs* **1984**, *28* (1), 38–61.

(203) Chong, C. R.; Chen, X.; Shi, L.; Liu, J. O.; Sullivan, D. J. A Clinical Drug Library Screen Identifies Astemizole as an Antimalarial Agent. *Nat. Chem. Biol.* **2006**, *2*, 415–416.

(204) Musonda, C. C.; Whitlock, G. A.; Witty, M. J.; Brun, R.; Kaiser, M. Chloroquine–Astemizole Hybrids with Potent in Vitro and in Vivo Antiplasmodial Activity. *Bioorg. Med. Chem. Lett.* **2009**, *19*, 481–484.

(205) Roman, G.; Crandall, I. E.; Szarek, W. A. Synthesis and Anti- Plasmodium Activity of Benzimidazole Analogues Structurally Related to Astemizole. *ChemMedChem* **2013**, *8*, 1795–1804.

(206) Tian, J.; Vandermosten, L.; Peigneur, S.; Moreels, L.; Rozenski, J.; Tytgat, J.; Herdewijn, P.; Van den Steen, P. E.; De Jonghe, S. Astemizole Analogues with Reduced HERG Inhibition as Potent Antimalarial Compounds. *Bioorg. Med. Chem.* **2017**, *25* (24), 6332–6344.

CHAPTER 2

DESIGN, SYNTHESIS, AND CHARACTERIZATION

2.1 Chapter Overview

In this chapter, the rationale, design, chemical synthesis, and characterization of targeted astemizole (AST) and astemizole-chloroquine (AST-CQ) analogues are described. Two design phases (phases I and II) based on AST as a molecular template are conducted. Frontrunner analogues **67** and **68** from exploratory phase I studies were iteratively used as templates for the design of phase II analogues. The chemistry employed to achieve the target analogues is described and selected non-trivial reaction mechanisms shown. Each section concludes with a representative description of relevant intermediates and target compounds as examples of the characterization of molecules in each compound class.

2.2 Phase I Exploratory AST Analogues: Rationale and Design

Following identification of the antimalarial properties of AST by Chong *et al*,[1] various teams have worked towards setting the structure-activity relationship (SAR) baseline which forms the basis of this work. Roman and co-workers showed that: (i) the presence of a secondary (2°) amine at benzimidazole position 2 (Figures 2.1–2.2) is crucial for activity, and (ii) substitution of the phenyl moiety in the benzimidazole core and replacement of fluorine with trifluoromethyl (CF_3) in the 4-fluorobenzyl substituent of AST may be used to uncouple antihistaminic and antimalarial activities.[2]

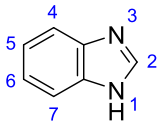

Figure 2.1: Structure and numbering of the benzimidazole ring

Furthermore, De Jonghe *et al* highlighted the tolerance of structural variety at the benzimidazole N-1 position in AST, showed that modifications at this position allowed for the tuning of human ether-*à-go-go*-related gene (hERG) inhibition. The authors showed that N-1 substitution with aliphatic cyclic, branched, or straight chains of up to ten (10) carbons was tolerated (*Pf*IC_{50}: < 0.416 μM).

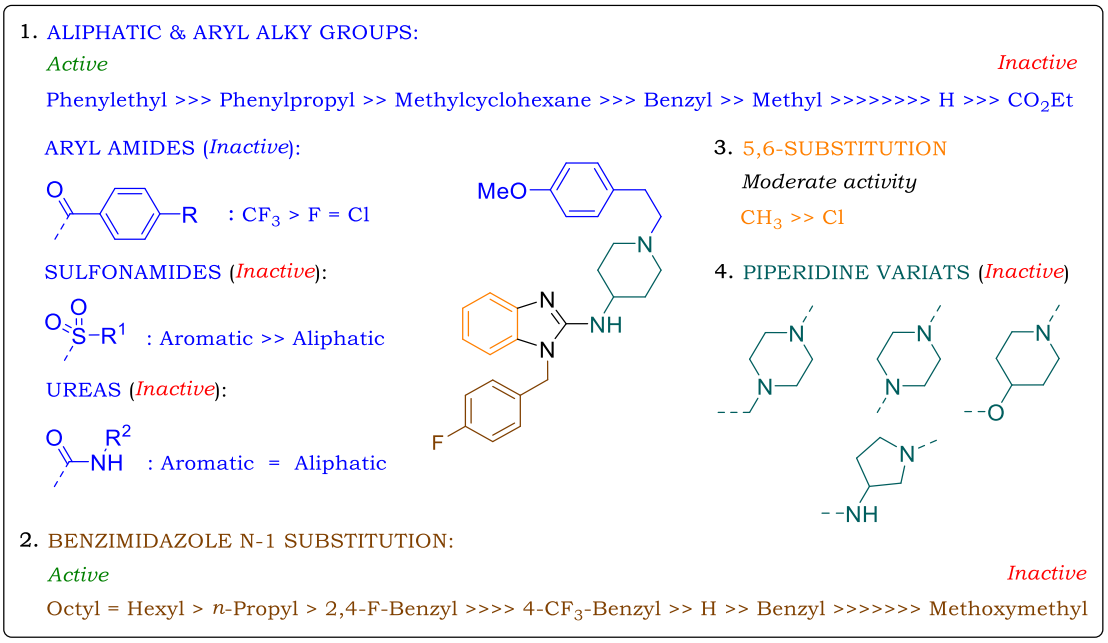

Figure 2.2: Summary of the structure-activity relationship (SAR) of astemizole (AST) as reported by Roman and colleagues,[2] and De Jonghe and co-workers.[3]

However, incorporation of an electronegative atom in the chain led to a loss of activity, as exemplified by the propyl (*Pf*IC_{50}: 0.416 µM) and methoxymethyl (*Pf*IC_{50}: 6.740 µM) match pair. The one analogue in which hERG was significantly diminished (1-octyl, *Pf*IC_{50}: 0.029 µM; hERG IC_{50}: 3.27 µM; clogP: 7.70) was highly lipophilic and less drug-like (highly susceptible to metabolism).[3] Regrettably, the cytotoxicity of these analogues was not reported, and it is therefore unclear whether the activity observed was a result of qualitative intrinsic antiplasmodium potency or indiscriminate cell-killing arising from cytotoxicity, a promiscuous property which may be expected in highly lipophilic compounds (toxic polypharmacology).

The work described above also revealed other key noteworthy structural features. Briefly, replacement of the 4-methoxy-phenylethyl moiety with sulfonamide, amide and urea functionalities led to a complete loss of activity (Figure 2.2), a trend that is consistent with the work reported by Roman *et al* with regard to the *N*-ethyl carboxylate (*N*-CO_2Et) synthetic intermediates. This observation may be explained on the basis of the importance of sufficient basicity (p*K*a) of the piperidine nitrogen for the accumulation of AST at the putative site of action. Chong *et al.* showed that, like quinoline antimalarials, AST and desmethylastemizole (DMAST) both accumulate within the *P. falciparum* digestive food vacuole (FV) and co-purify with hemozoin. This was later confirmed by work conducted in our research group, suggesting that inhibition of hemozoin formation is a contributing mechanism for the mode of action of AST and its analogues.[1,4]

For the above-mentioned reason, drastic reduction or a complete loss of activity may be expected when the piperidine nitrogen is in close proximity with electron-withdrawing

groups, as is the case in sulfonamides, amides, ureas (De Jonghe *et al.*), and carboxylate derivatives (Roman *et al.*). Hypothetically, in such analogues, the basicity of the nitrogen may be too low, leading to low drug accumulation in the FV at physiological pH. However, *N*-alkylation of the piperidine nitrogen is essential for antiplasmodium activity. This is exemplified by the low activity of norastemizole (IC_{50}: 2.304 μM), which lacks *N*-substitution, compared to alkyl derivatives with *N*-phenylethyl (IC_{50}: 0.125 μM) and *N*-(3-phenyl)propyl (IC_{50}: 0.196 μM), whose activities are comparable to that of AST (IC_{50}: 0.162 μM; Figure 2.2).

In addition to this SAR, previous work on the SAR of AST performed in our research group revealed that separately, the substitution of the lateral 4-methoxy and 4-fluoro groups with either cyano (CN) or amide groups produced analogues with increased or equipotent antiplasmodium activity and lower lipophilicity (clogP), thus resulting in improved solubility (Figure 2.3).

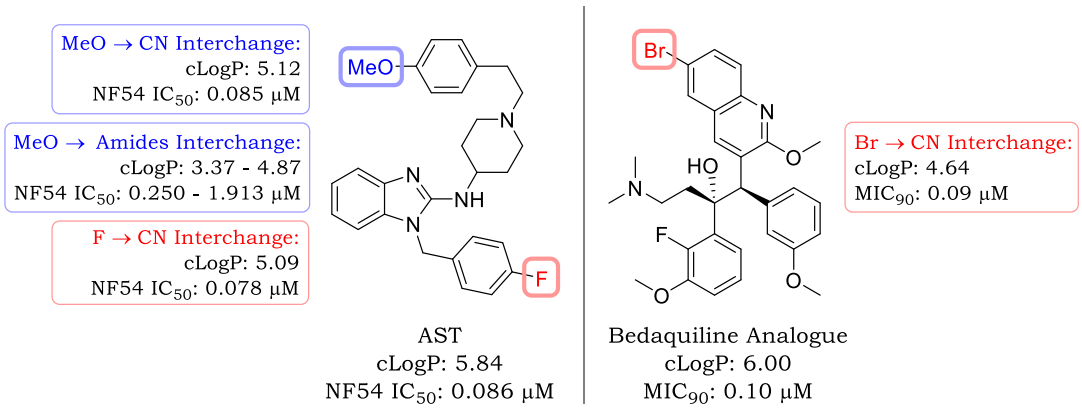

Figure 2.3: Effect of cyanation on the activity and lipophilicity (cLogP) of astemizole and bedaquiline analogues[5]

In the work of Conole *et al.*,[5] the CN group was identified as an effective substituent for aromatic halogens (Br, Cl, I or F), showing that cyanated analogues of the antitubercular drug bedaquiline had lower lipophilicity and only modest effects on antimycobacterial activity (MIC_{90}) compared to bromo analogues over a diverse SAR. This observation suggested that the CN group could be a useful halogen substitution for potentially effective, more soluble and safer (hERG) analogues (Figure 2.3).[5] Based on this and other examples from literature, it was hypothesized that the AST analogue with the 4-cyano group replacing both the 4-fluoro group on the benzyl portion and the 4-methoxy group on the lateral phenyl moiety of AST (Figure 2.5), would be the best starting point from which analogues with potentially improved activity, metabolic stability, solubility, and hERG profiles could be designed.

Rational design was employed using the Craig plot to navigate different substituents and identify groups with similar physicochemical properties. The Craig plot (Figure 2.4) is a

two-dimensional (2D) plot in which Hammet [σ] and Hansch [π] substituent constants are displayed for a set of isosteric substituents.[6] The σ constant characterizes the electronic nature/effects (withdrawing or donating) of substituents while the π parameter describes their hydrophobicity.[6,7]

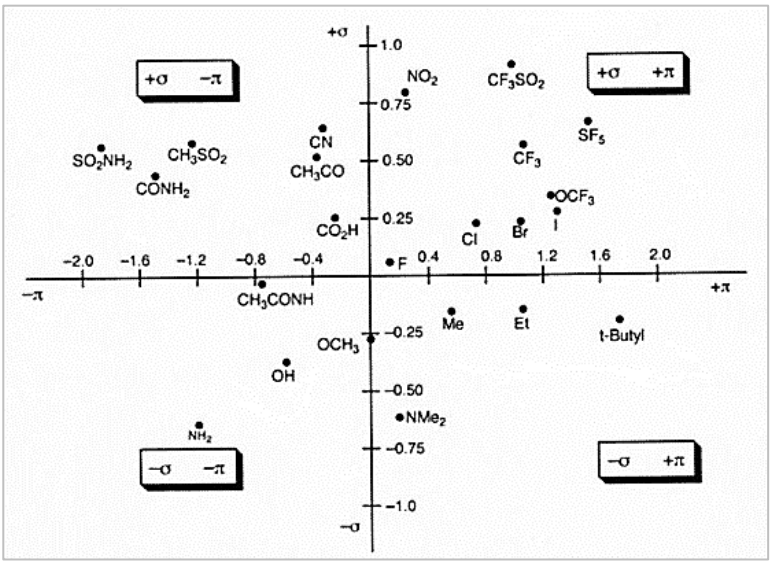

Figure 2.4: Craig Plot of Hammett constants (σ) against hydrophobicity (π).[6]

Thus, in **SAR 1**, the fluoro group in the *p*-F-benzyl moiety (Figure 2.5) was replaced with substituents to best represent each quadrant and bring about variety in terms of electronic, steric, and hydrophobicity effects on the target compounds. Furthermore, **SAR 1** explorations included 1,2 and 1,3-disubstitution (F/CN) on the benzyl moiety, and introduction of three-dimensional (3D) character *via* the methylation of the methylene linker (CH_2) as a strategy to disrupt molecular planarity.

In **SAR 2**, the significance of the phenyl moiety was investigated, while utilizing hERG mitigation strategies discussed in section 1.6.2. Among the strategies employed were: (i) introduction of water solubilizing groups at the 4-position and (i) replacement of the phenyl moiety with both heterocyclic (Figure 2.5) and hetero-aliphatic rings, both of which were envisaged to reduce lipophilicity (clogP). In the case of hetero-aliphatic replacements, the goal was to disrupt aromaticity and increase molecular complexity.

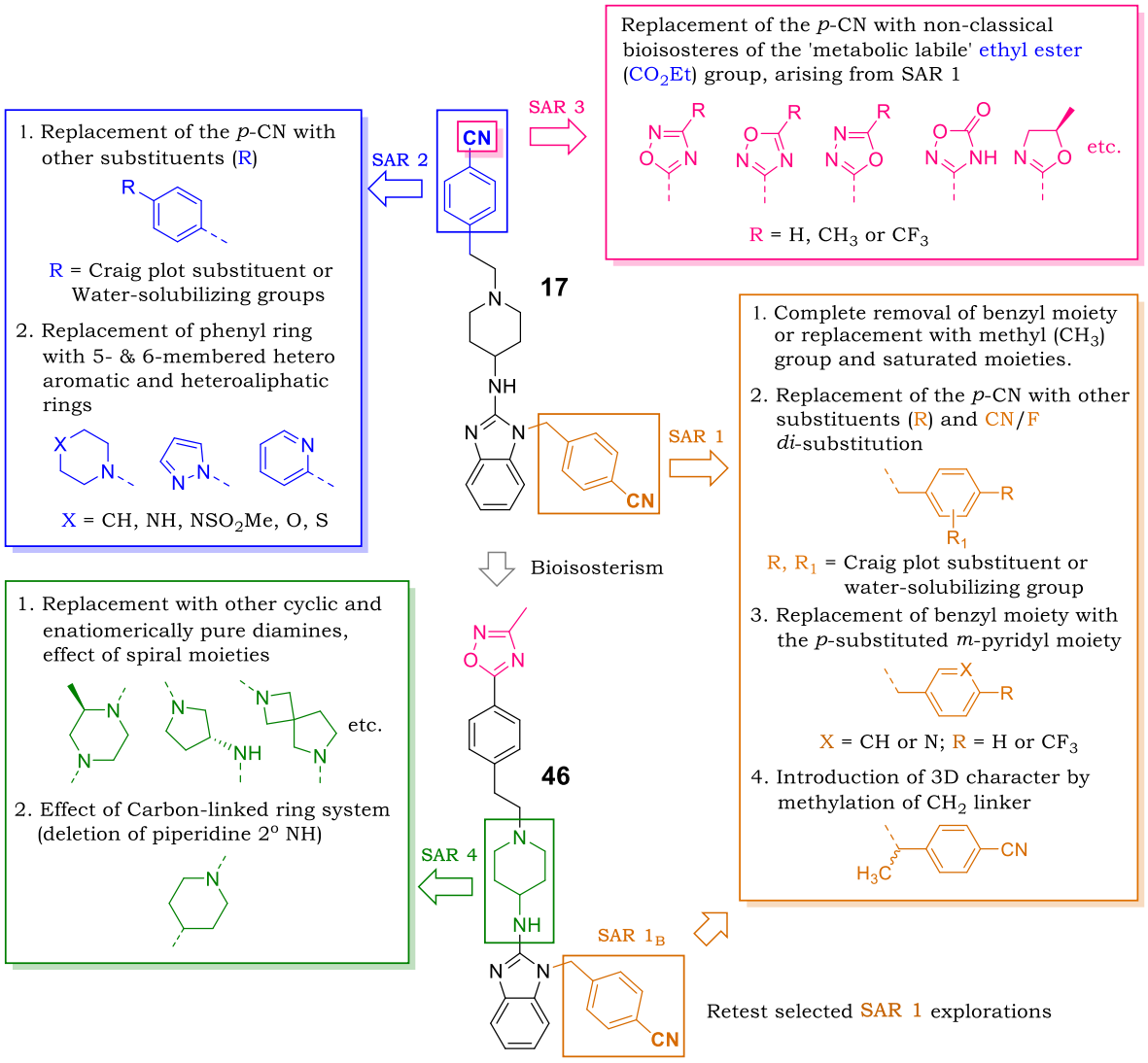

Figure 2.5: SAR-guided design of phase I AST analogues based on compound **17** and **46**

Both SARs 1 and 2 incorporated an analogue containing a carboxylic acid moiety (CO_2H) which, due to the presence of the basic tertiary (3°) piperidine nitrogen in the molecule was anticipated to furnish zwitterionic character, as a strategy towards potentially reducing the affinity for hERG K+ channels.

Following the identification of the ethyl ester (4-CO_2Et, compound **38**) from SAR 1 as a favorable substituent on the lateral phenyl ring, **SAR 3** was designed to explore various non-classical ester bioisosteres as potential replacements, in order to mitigate the underlying metabolic liability (*via* CYP-mediated hydrolysis) associated with esters. As described in section 1.8, there are several examples of ester bioisosteres, including amides. However, the initial focus of this Ph.D thesis work was on ring replacements, particularly small five-membered heterocycles such as oxadiazoles and oxazolines (Figure 2.5) to maintain molecular (spatial) geometry, increase structural rigidity and enhance hydrogen bonding capacity.[8,9]

Compound **46** (Figure 2.5) bearing the 1,2,4-oxadiazole moiety was identified as the front-runner with the best balance of potency, cytotoxicity, solubility, and metabolic stability profiles compared to both AST and its ethyl ester match pair **38**. Therefore, it was used as a template to derivatize further SAR.

Work by both Roman *et al* [2] and De Jonghe *et al.*,[3] established the 4-amino piperidine linkage as the optimum diaminoalkyl moiety for antiplasmodium activity. Roman *et al.* further showed the importance of the 2° amino (RR'NH) group as opposed to the ether group (ROR') at the 2-benzimidazole position. However, this observation had to be validated in the context of this work following the identification **46**. Therefore, **SAR 4** (Figure 2.5) included the exploration of piperidine replacements such as piperazine and its substituted forms, a strategy which is known to reduce affinity for hERG.[10] Additionally, the preparation of enantiomerically pure forms of pyrrolidine (R/S) analogues as opposed to the previously reported racemic mixture, takes into account that activity and toxicity or lack thereof, including hERG affinity [11] may be observed in one enantiomer and not the other. A spiro diaminoalkyl substituent and a C-linked piperidine were also conceptually tested for SAR diversity and molecular complexity in the linker.

SAR 1_B was designed to retest some of the benzimidazole *N*-1 substituents that had shown potency in phase I, such as 4-CF_3-benzyl, pyridyl moieties and disubstituted benzyl moieties. As a strategy to reduce hERG, ring saturation was utilized by replacement of the benzyl moiety with cyclic aliphatic rings.[12] Additionally, aromaticity was removed by complete removal/truncation of the benzyl moiety or replacement with a methyl group (Figure 2.5).

2.3 Chemistry: Phase I

2.3.1 Retrosynthesis (Disconnection Approach)

Following the design of target analogues, a retrosynthetic analysis was conducted to determine the best synthetic route for efficient preparation of designed analogues in a tractable manner (Figure 2.6).

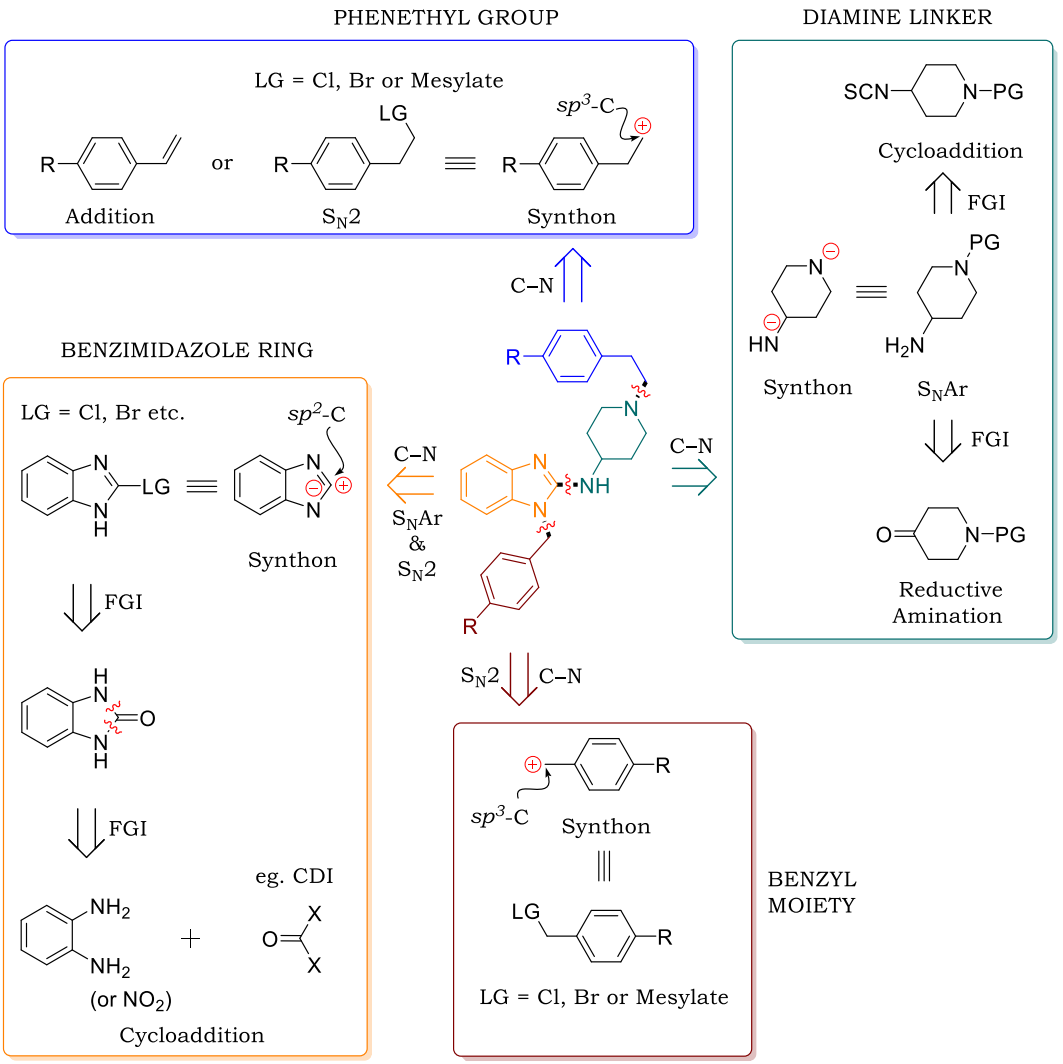

LG: leaving group
S_N2: bimolecular nucleophilic substitution
PG: protecting group

FGI: functional group interchange
S_NAr: nucleophilic aromatic substitution
C-N: carbon-nitrogen bond break

Figure 2.6: Retrosynthetic analysis map for the preparation of astemizole analogues

Disconnection of the C-N bonds around the benzimidazole core and the piperidine ring using known synthetic chemistry approaches led to the identification of various precursors that would be either synthetically prepared or commercially sourced.

On the other hand (phase I **SAR 3**), the synthetic methodology of oxadiazoles and oxazolines continues to evolve towards methods that render their access highly amenable for miniaturization and automation. Various procedures to access 1,2,4- and 1,3,4-oxadiazoles as effective ester bioisosteres are widely described in the literature. These methods vary in reaction times, product purities and yields, as well as ease of control of reaction parameters.[13] As shown in the retrosynthesis analysis in Figure 2.7, 1,2,4-oxadiazoles are most commonly prepared from amidoximes and acetylating agents such as acid chlorides, carboxylic acids or anhydrides as shown in Figure 2.4.[14] Amidoximes are often either commercially available or easily accessible by reaction of nitriles with hydroxylamines.

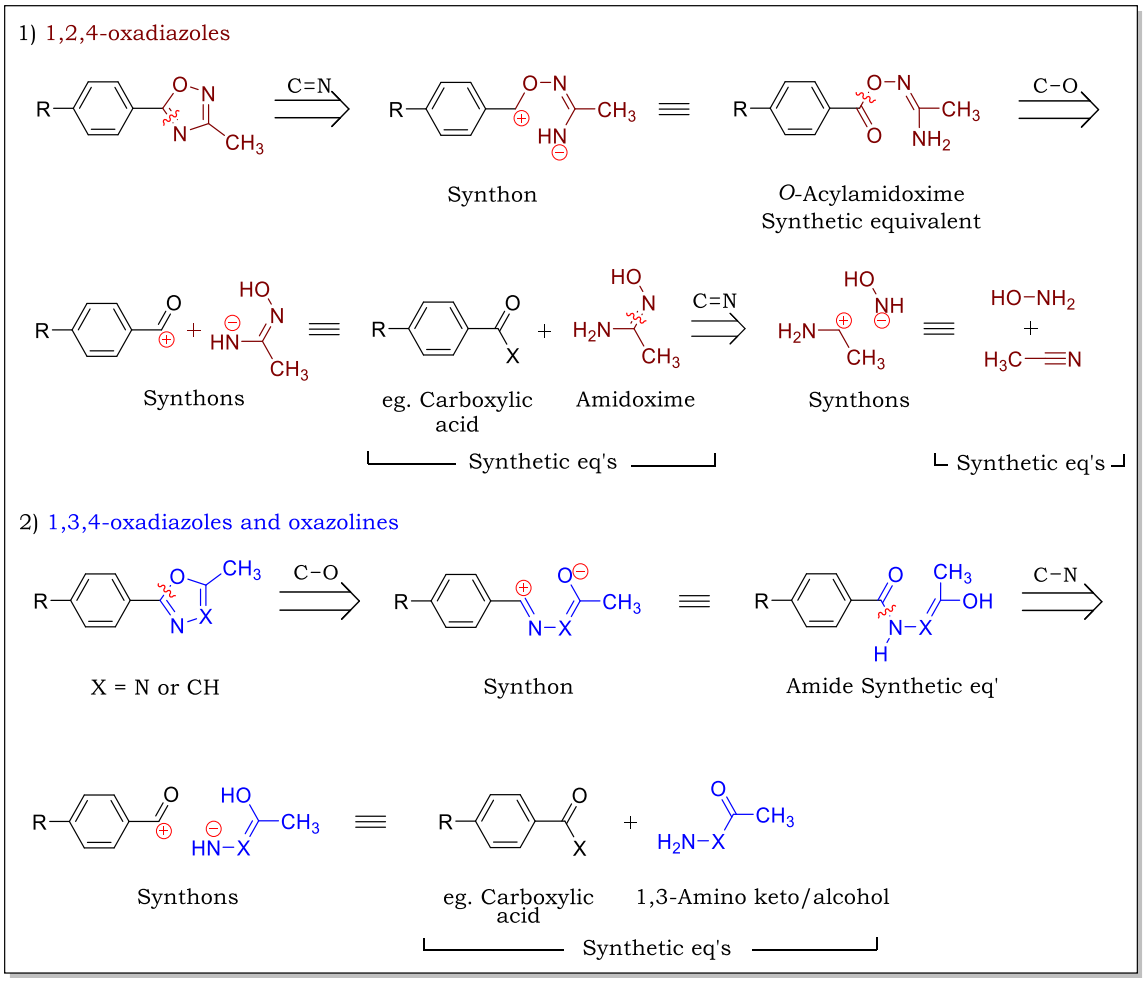

Figure 2.7: Retrosynthetic analysis for the preparation of oxadiazoles and oxazolines

Cyclization of the resulting *O*-acylamidoxime can be achieved by a variety of procedures including microwave-assisted methods,[15,16] heating or the use of a catalyst i.e. *p*-toluene sulfonic acid (*p*-TSA) and/or a dehydrating agents.[14] Recently, a combination of polymer-assisted solution phase (PASP) and high-speed microwave synthesis was reported to efficiently convert carboxylic acids and amidoximes to 1,2,3-oxadiazoles directly.[15] Additionally, single continuous microreactor sequence techniques have been described to prepare 1,2,4-oxadiazoles from nitriles.[17] As for 1,3,4-oxadiazoles and oxazolines, the most commonly adopted approach involves the cyclization of diacylhydrazines and 3-hydroxylamides respectively, using heat and reagents such as $SOCl_2$, $POCl_3$ and P_4O_{10}. These conditions influence the efficiency and stereospecificity of the cyclization reaction.[18–21]

Modifications were made to the methods previously reported to achieve compatibility with sensitive functionalities present in the starting materials used, to enable the efficient formation of target molecules. Various small molecule starting points (precursors) were synthesized and used in various schemes to prepare both phases I and II target molecules (Scheme 2.1) to minimize the number of steps and intermediates as much as possible.

2.3.2 Synthesis of Precursor Intermediates (1 – 11) Required for Preparation of AST Analogues

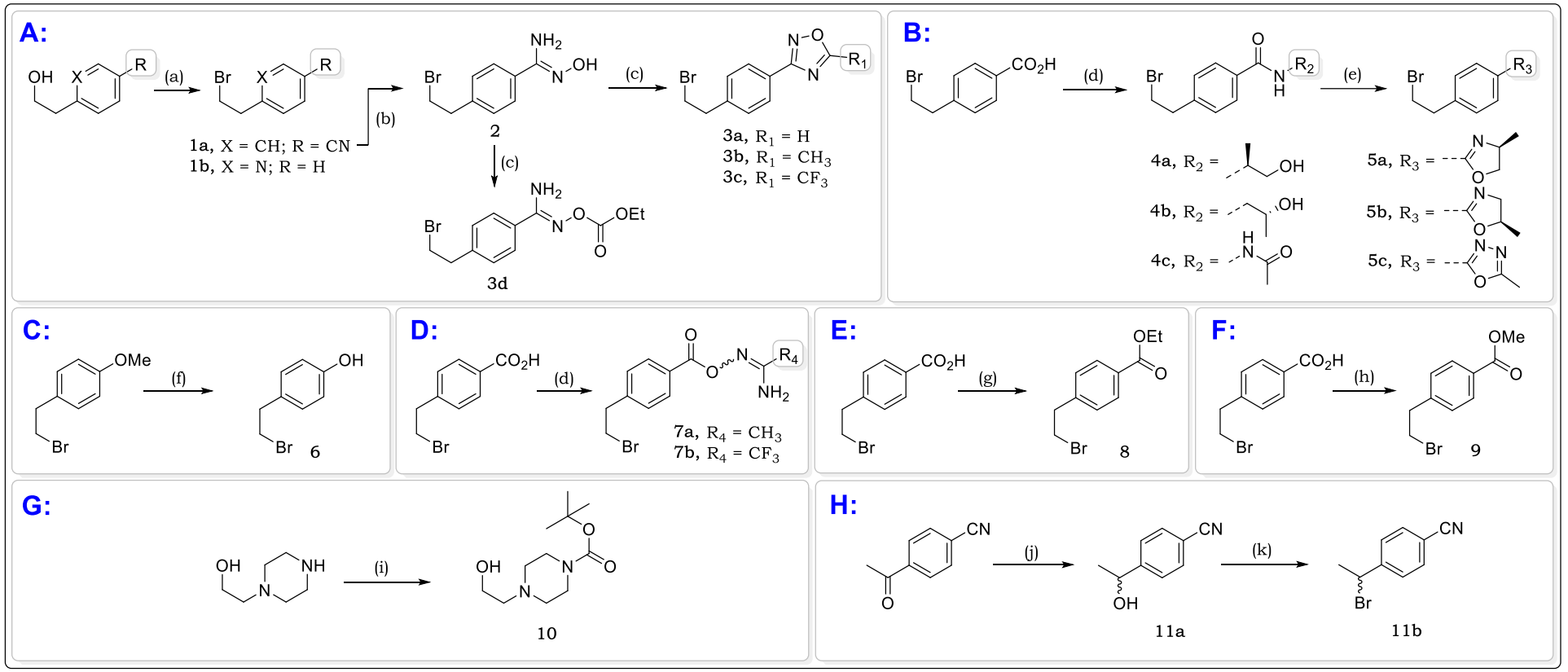

Scheme 2.1: Synthetic protocol towards precursors intermediates **1 – 11**

Reagents and conditions: (a) PPh_3, CBr_4, DCM, 0 – 18 °C, 2 h (**1a**, 81%; **1b**, 70%); (b) *(i)* $NH_2OH{\cdot}HCl$, 8-hydroxyquinolone, TEA, ethanol, 79 °C reflux, 1.5 h, *(ii)* 21 °C, 10% HCl, pH 3 (**2**, 82%); (c) for **3a**: $CH(EtO)_3$, $BF_3.OEt_2$, Pyridine, 80 °C reflux, 1 h (51%); for **3b**: Acetyl chloride, 70 °C, 0.5 h (80%); for **3c**: $(CF_3CO)_2O$, DCM, Pyridine, 22 °C, 20 min (76%); for **3d**: $ClCO_2Et$, K_2CO_3, Acetone, 0 – 4 °C, 3 h (98%); (d) EDCI/DMAP, DCM, 18 °C, 2 h; using (S)-2-aminopropan-1-ol (**4a**, 80%), and (R)-1-aminopropan-2-ol (**4b**, 91%), using Acetylhydrazine (**4c**, 65%), using N-hydroxyacetimidamide (**7a**, 90%); using (E)-2,2,2-trifluoro-N'-hydroxyacetimidamide (**7b**, 78%); (e) TsCl, TEA, DCM, 30 °C, 0.5 h [**5a**, 70%; **5b**, 85%; **5c**, (88%)]; (f) BBr_3, DCM, –78 °C – 0 °C, 24 h (**6**, 46%); (g) 9.5N HCl in ethanol, 80 °C, 12 h (**8**, 85%); (h) TMS-CHN_2, MeOH, Toluene, 21 °C, 0.5 h (**9**, 97%); (i) Boc_2O, DMAP, THF, 21 °C, 2 h (**10**, 98%); (j) *(i)* $NaBH_4$, MeOH, 18 °C, 2 h, *(ii)* H_2O (**11a**, 83%); (k) TMS-Br, 20 °C, 2 h (**11b**, 72%).

Synthetic precursors required for the preparation of target compounds were synthesized following the approaches outlined in Scheme 2.1. *Appel* reaction using triphenyl phosphine (PPh_3)/tetrabromomethane (CBr_4) enabled efficient preparation of alkyl bromide precursor intermediates **1a** and **1b** from alcohols 4-(2-hydroxyethyl) benzonitrile and 2-pyridinethanol, respectively.[22] Treatment of nitrile **1a** with hydroxylamine hydrochloride ($NH_2OH{\cdot}HCl$) in ethanol afforded amidoxime intermediate **2** in excellent yield (93%), from which subsequent 1,2,4-oxadiazoles (**3a** – **c**) and oxadiazolone (**3d**) intermediates were prepared.

5-H-1,2,4-oxadiazole **3a** (Scheme 2.1A) was synthesized from amidoxime **2**, through a boron trifluoride etherate ($BF_3{\cdot}OEt_2$)-catalyzed ring closure using triethoxymethane [$CH(EtO)_3$] as the carbon source,[23] while 5-methyl-1,2,4-oxadiazole **3b** was synthesized in high yield (80%) by heating amidoxime **2** in acetyl chloride. In a similar manner and at low temperatures, treatment of amidoxime **2** with trifluoroacetic anhydride $(CF_3CO)_2O$ and ethyl carbonochloridate $ClCO_2Et$ afforded 5-trifluoromethy-1,2,4-oxadiazole (**3c**) and oxadiazolone ester precursor (**3d**), respectively.

Coupling of 4-(2-bromoethyl) benzoic acid with respective amines (or acetohydrazide) and amidoximes using 1-ethyl-3-(3-dimethylaminopropyl)carbodiimide/4-dimethylaminopyridine (EDCI/DMAP) as the coupling agents afforded amides **4a**–**4c** and *O*-acylamidoximes **7a**–**7b** in relatively high yields (65–91%), respectively. Oxazolines (**5a** and **5b**) and 1,3,4-oxadiazole **5c** were synthesized from their respective amides **4a**–**4c**, *via* tosyl chloride (TsCl)-mediated ring closure in DCM at 30 °C.[8] The use of catalytic TsCl at low temperature in this method proved to be more efficient than thermal cyclization or the use of Lewis base catalysts (i.e. $POCl_3$), both of which would have led to the loss of the bromide functionality *via* dehydrohalogenation.

Phenol intermediate **6** was prepared in moderate yield (46%) *via* boron tribromide (BBr_3)-assisted ether cleavage (*O*-demethylation) of commercially available 4-methoxyphenethyl bromide at very low temperatures (-78 °C).[24] Ethyl and methyl esters **8** and **9** where synthesized from 4-(2-bromoethyl) benzoic acid through acid-catalyzed and trimethylsilyl diazomethane ($TMS\text{-}CHN_2$)-mediated esterification, respectively.[25]

N-*tert*-butyloxycarbonyl (*N*-Boc) protection of 1-(2-hydroxyethyl) piperazine was performed using di-*tert*-butyl dicarbonate (Boc_2O) with catalytic DMAP in THF **10**.[26] Bromide **11b** was synthesized from commercially available 4-cyanoacetophenone by keto reduction to 2° alcohol (**11a**) using sodium borohydride ($NaBH_4$),[27] followed by bromination using bromotrimethylsilane (TMS-Br).[28]

2.3.3 Proposed Reaction Mechanisms and Characterization of Precursors

Here, attempts are made to describe the mechanistic details through which the chemical transformations in each synthetic scheme are achieved. All reactions were monitored *via* thin layer chromatography (TLC) and characterization was conducted primarily *via*: (i) high pressure liquid chromatography coupled to a mass spectrometer (HPLC-MS) and (ii) proton nuclear magnetic resonance spectroscopy (^{1}H-NMR). In addition, ^{13}C-NMR was used for full characterization of all final compounds. Characterization data (^{1}H-NMR, ^{13}C-NMR, and HPLC-MS) for representative final compounds are shown for each series.

2.3.3.1 *Appel* Reaction (step A, Scheme 2.1A) and TMSBr Bromination (Step K, Scheme 2.1H)

The conversion of alcohols to alkyl halides in the *Appel* reaction begins with the generation of reactive species from triphenyl phosphine (PPh_3) and *tetra*-bromomethane (CBr_4) as shown in Scheme 2.2A.

Mechanistically, abstraction of an alcoholic proton (acidic) by the tribromomethane carbanion generates a negative charge at oxygen which then nucleophilically attacks at phosphorus in the reactive species (BrPPh3)+ to generate a resonance stabilized oxyphosphonium intermediate (Scheme 2.2A). The oxygen is transformed into a good leaving group, and a bimolecular nucleophilic substitution (S_N2) by the *in situ* generated bromide ion occurs to produce the alkyl bromide and triphenylphosphine oxide (Ph_3PO) as a by-product.[29] Formation of the alkyl bromide was confirmed by the change in the retardation factor (R_f on TLC), and the presence of the characteristic bromo-pattern (*m/z* = M+, M+2; HPLC-MS). Additionally, ^{1}H-NMR confirmed the disappearance of the hydroxy proton triplet signal at 5.16 ppm (Figure 2.8, **1a**).

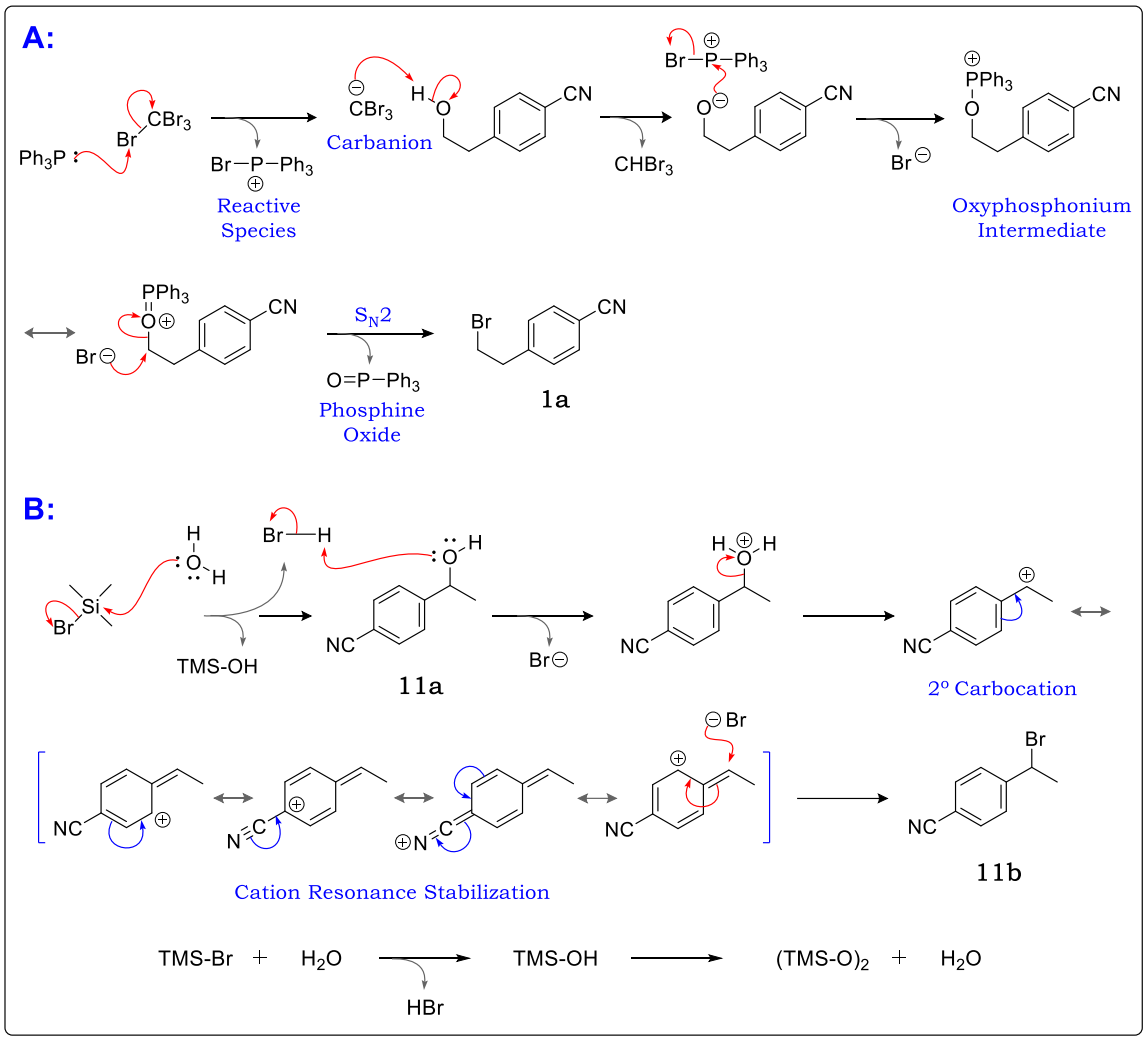

Scheme 2.2: Proposed reaction mechanisms for (A) *Appel* bromination and (B) TMS-Br bromination of 2° alcohols

Following the reduction of 4-acetylbenzonitrile to 2° alcohol (**11a**) using $NaBH_4$, bromination was performed using TMS-Br (Scheme 2.1H). In this reaction, initial hydrolysis of TMS-Br by a small amount of water included in the reaction system produces *in situ* acidic HBr. As a result, the alcohol undergoes protonation and subsequent dehydration to generate a 2° carbocation which is highly stabilized by resonance through the aromatic system extending to the nitrile in the *para* position. The carbocation then reacts with the liberated bromide (*via* unimolecular nucleophilic substitution, S_N1) to produce the brominated product **11b**. The water expelled by the dehydration step reacts with excess TMS-Br to generate TMSOH molecules, which are easily condensed into more stable $(TMS)_2O$ and water.[28,30] TLC, HPLC-MS and ^{1}H-NMR confirmed this conversion.

2.3.3.2 $BF_3(OEt)_3$–mediated Ring Closure: Preparation of 1,2,4-Oxadiazole (Step C, Scheme 2.1A)

The preparation of amidoxime **2** provided access to various precursors as shown previously. For 5-H-1,2,4-oxadiazole (**3a**), the first step is nucleophilic attack by amidoxime oxygen at the central carbon in triethyl orthoformate ($CH(EtO)_3$) to eliminate the first molecule of ethanol and regeneration of the BF_3OEt_3 catalyst (Scheme 2.3). This step is followed by an intramolecular S_N2 displacement step by the amidine nitrogen onto the central carbon of R-$CH(EtO)_2$ resulting in the generation of another molecule of ethanol. The final ethanol molecule is eliminated through an aromatization-driven step to produce the desired precursor.

The loss of amidoxime amino (NH_2) and hydroxy (OH) proton signals, alongside the appearance of a sharp singlet downfield (δ = 9.24 ppm) integrating for one proton confirmed the formation of this intermediate via ^{1}H NMR (Figure 2.8).

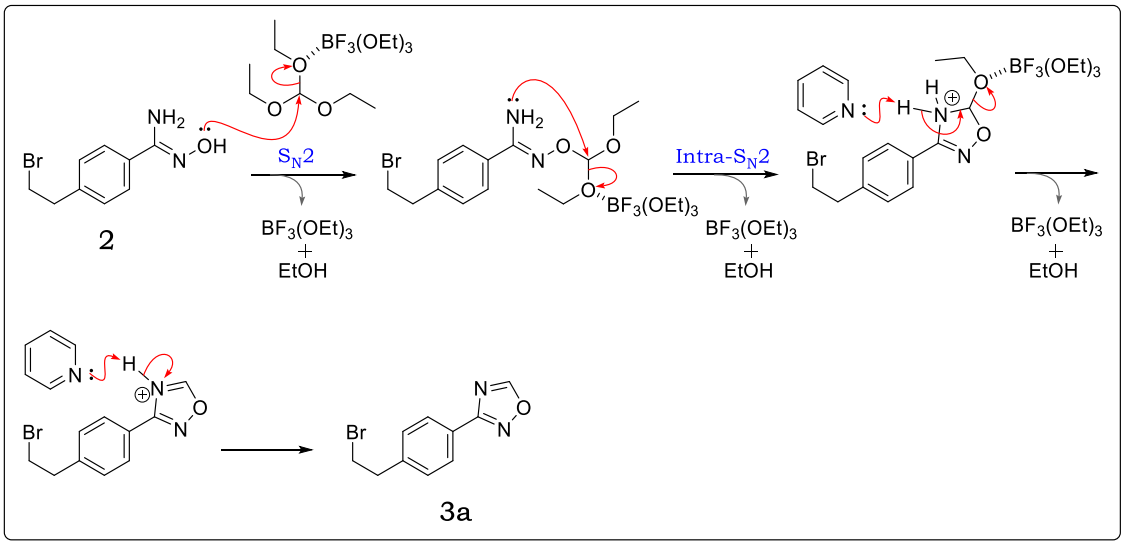

Scheme 2.3: Proposed reaction mechanisms for $BF_3(OEt)_3$-catalysed 1,2,4-oxadiazole formation from *N*-hydroxyamidines

Formation of **3b**, **3c** and **3d** proceeds *via* an initial nucleophilic attack at the carbon centre of the appropriate precursor (mechanisms not shown). This step is followed by elimination of chloride (for **3b** and **3d**) or trifluoro acetate (for **3c**) leaving groups to produce an ester-like intermediates. Ester intermediates of **3b** and **3c** undergo a further intramolecular cyclization/condensation to form 3-methyl-1,2,4-oxadiazole and 3-trifluoromethyl-1,2,4-oxadiazole, respectively. In addition, **3d** was used in ester form in the next steps. Conversion of these intermediates was confirmed *via* ^{1}H-NMR (Figure 2.8).

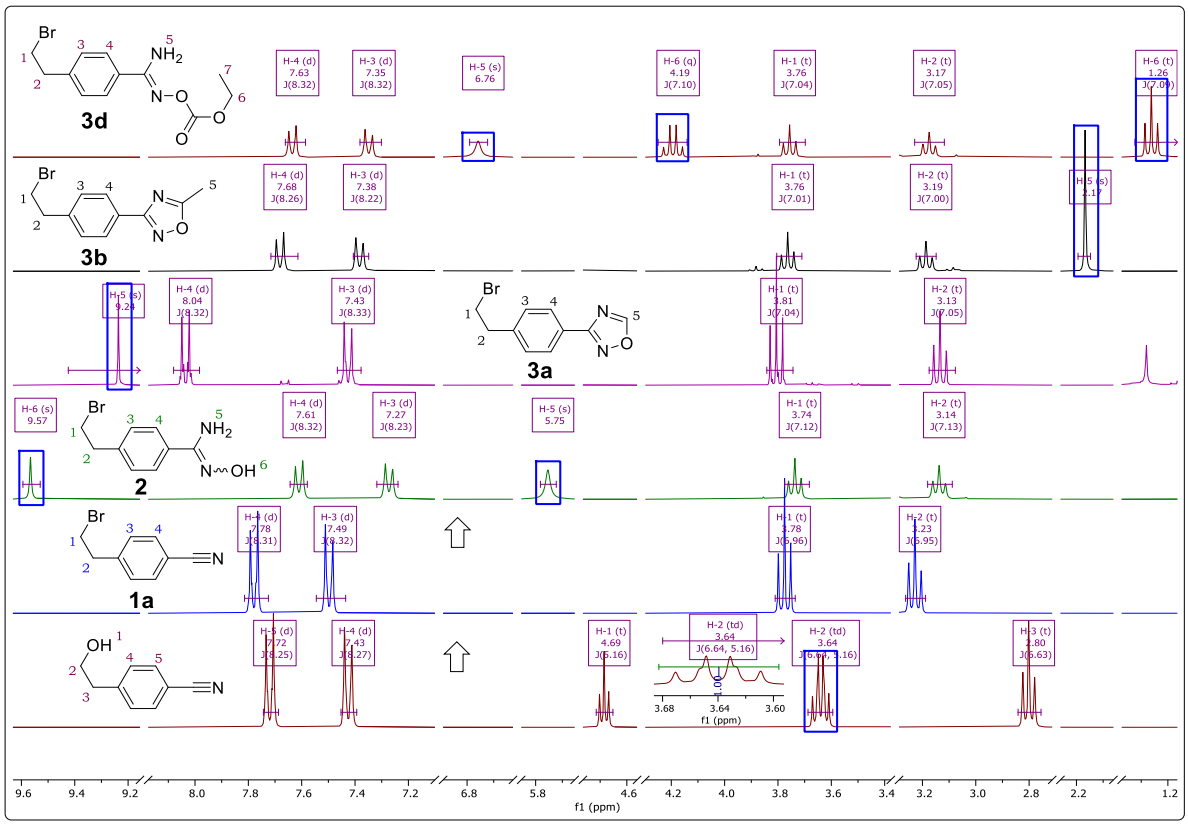

Figure 2.8: Stacked ^{1}H-NMR spectra *(bottom to top)* showing formation of **1a**, **2**, and other representative alkyl bromide precursors (**3a**, **3b** and **3d**)

2.3.3.4 Amide Bond Formation using EDCI/DMAP Coupling Agents (Step D, Scheme 2.1)

The formation of the amide bond to yield amides **4a** – **4c** and *O*-acylamidoximes **7a** – **b** was achieved *via* the use of EDCI/DMAP as coupling reagents. The mechanism for this reaction, and others which utilize carbodiimides such as EDCI is well documented in literature.[31,32] The reaction is initiated by the deprotonation of the carboxylic acid to a strongly nucleophilic carboxylate (Scheme 2.4). The carboxylate oxygen then attacks the carbodiimide carbon of EDCI followed by proton exchange/transfer (PT) to generate the highly unstable *O*-acylisourea. The carbonyl carbon in the *O*-acylisourea is flanked by strong electron-withdrawing groups of atoms and is therefore highly electrophilic and susceptible to nucleophilic attack.

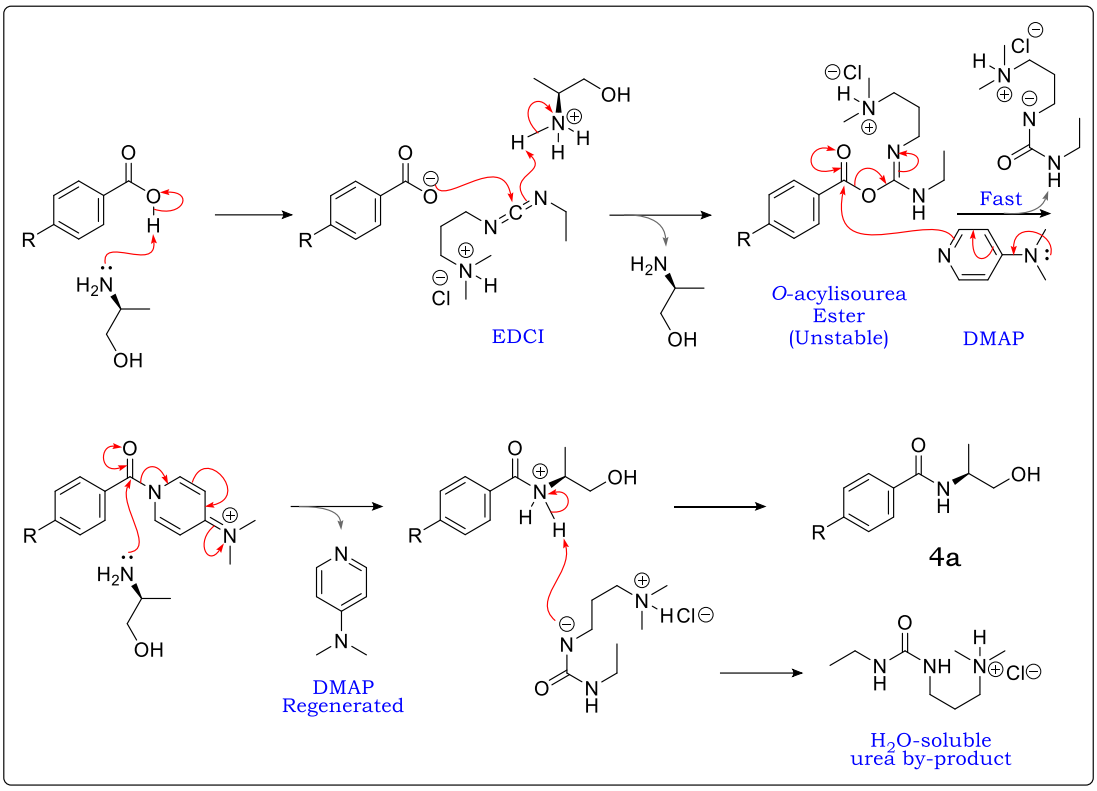

Scheme 2.4: Reaction mechanism for EDCI/DMAP amide bond formation

In order to achieve stability, the *O*-acylisourea could rearrange *via* an acetyl transfer to form *N*-acylurea. However, the DMAP which is added to the reaction prior circumvents the occurrence of this undesirable rearrangement by reacting with the *O*-acylisourea ester at a much faster rate, while still generating a reactive DMAP-intermediate susceptible to nucleophilic attack by the amine nitrogen to form the desired amide, and regeneration of DMAP. A water-soluble urea analogue of EDCI is produced as a by-product.[31] Formation was confirmed by HPLC-MS *via* positive mode electrospray ionization/atmospheric pressure chemical ionization (ESI/APCI+): m/z [M+1] = **4a** and **4b**; 286.0, 288.0 (calculated: 285.04, 287.03). ^{1}H-NMR showed the appearance of additional aliphatic protons including a highly pronounced methyl proton doublet up-field as expected (Figure 2.9). In hydrazide **4c**, the methyl protons resonated at δ = 2.05 ppm, splitting as a singlet.

2.3.3.5 Oxazoline and 1,3,4-oxadiazole Formation (Step E, Scheme 2.1B)

Following amide bond formation to generate 3-hydroxylamides **4a** – **b** and *N,N*-diacetylhydrazine **4c**, a cyclisation reaction to form the corresponding oxazolines and 1,3,4-oxadiazole respectively was facilitated by TsCl and triethylamine (TEA) in DCM. Mechanistically (Scheme 2.5), tosylation of the hydroxyl group is followed by the intramolecular nucleophilic substitution (S_N2) by amide oxygen.

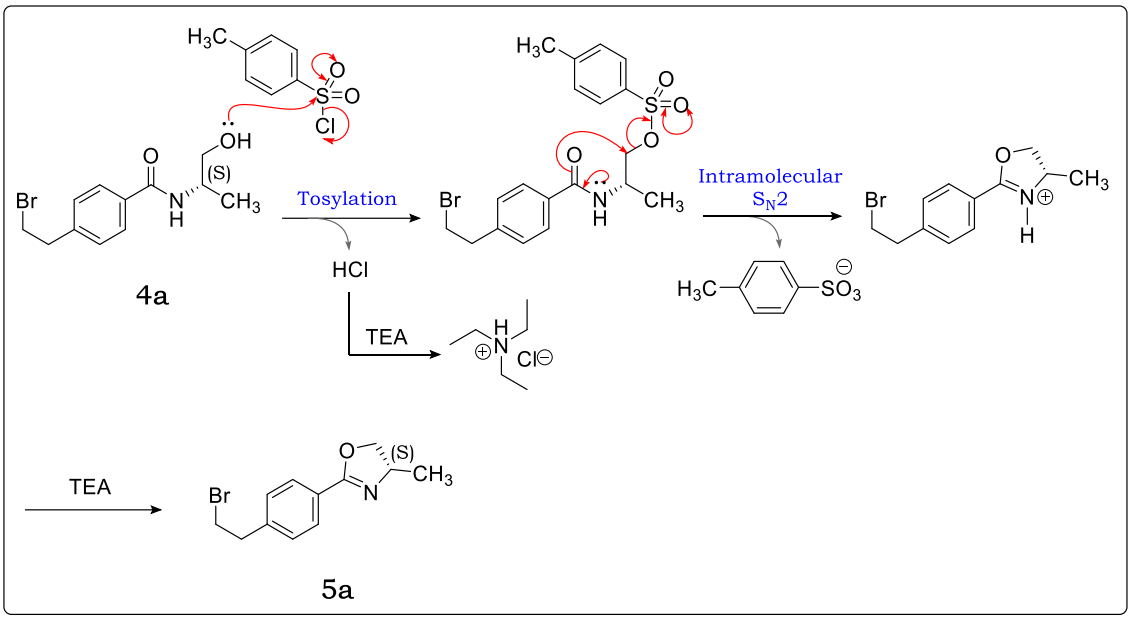

Scheme 2.5: Proposed reaction mechanisms for the formation of oxazolines (**5a**, **5b**) and 1,3,4-oxadiazole (**5c**)

This step leads to the displacement of the benzenesulfonate as a good leaving group. TEA mops up the protons on the charged imine species forming neutral oxazoline/oxadiazole ring, and maintaining the configuration (S, for **5a**) of the chiral centre.

Mass spectrum (HPLC-MS) analysis revealed loss of m/z – 18.0 amu (water), from the amide molecular weight (MW), which confirmed successful condensation by cyclization in this series. As an example, the ^{1}H-NMR experiment of oxazoline **5a** revealed a change in the splitting pattern of the chiral centre proton (**H-5**) compared to that in precursor amide **4a** (Figure 2.9). In **5a**, proton **H-5** splits as a doublet of doublet of quartets (*ddq*) with coupling constants (*J*) of 9.34, 7.68 and 6.58 hertz (Hz), arising from its relationship with two ring protons at **H-7** (two doublets, large *J*'s) and the methyl group **H-6** (quartet, small *J*). Specific rotation was determined *via* polarimetry and found to be $[a]^{25}_{D}$ = +2.80°.

In precursor amide **4a**, the same proton **H-5** appears as a triplet of quartets (*tq*, J = 6.80, 6.10 Hz), which in this case spectrally appears as a sextet at δ = 4.18 ppm (Figure 2.9) due to overlapping subpeaks.[33] This is because open chain methylene protons **H-7** are chemically equivalent and therefore split **H-5** as a triplet. These relationships are shown in Scheme 2.6.

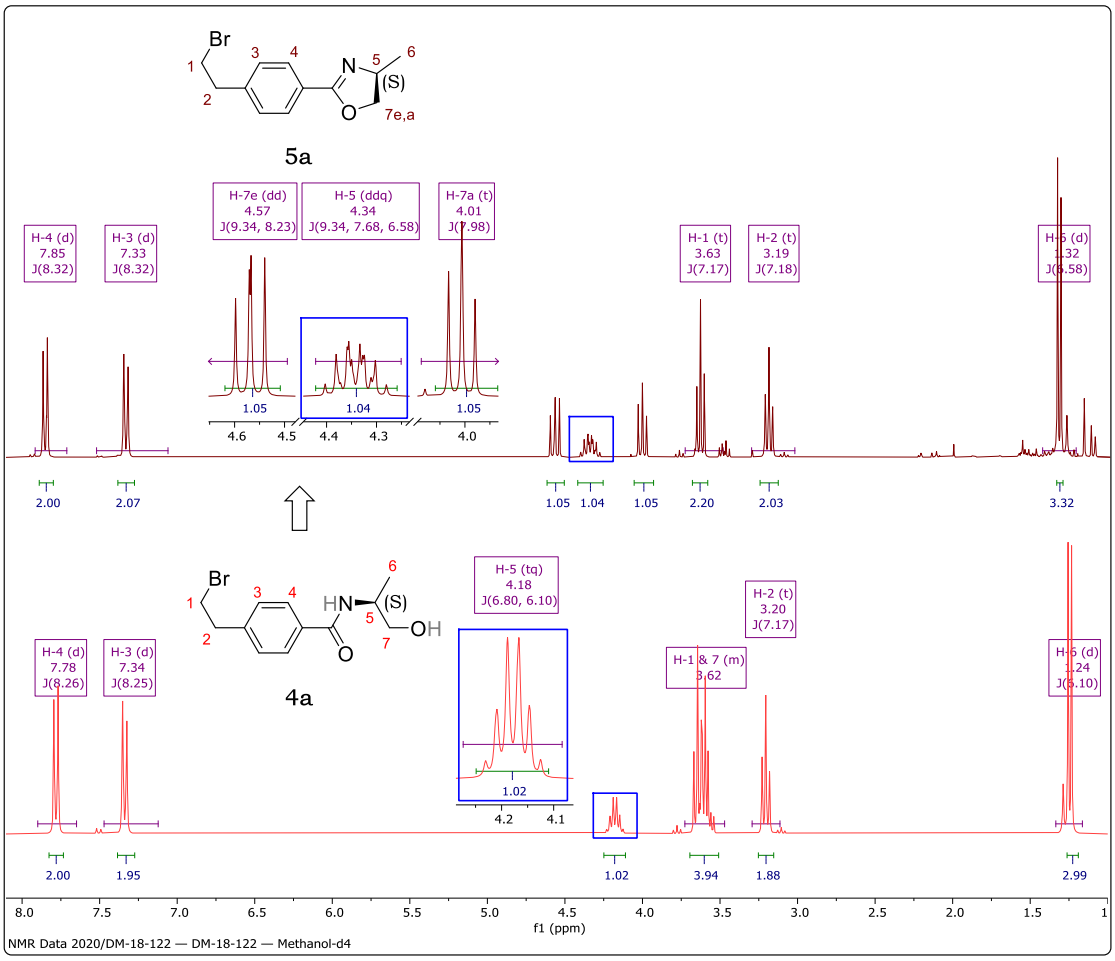

Figure 2.9: Stacked ^{1}H-NMR spectra *(from bottom to top)* showing formation of **5a**, from **4a**

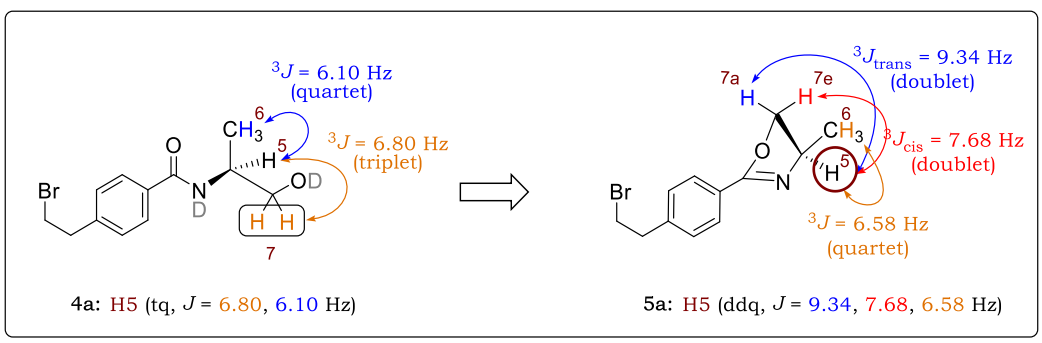

Scheme 2.6: Representation of the splitting patterns observed for proton H-5 in amide **4a** and oxazole **5a**

2.3.3.6 BBr_3 aryl O-demethylation (Step F, Scheme 2.1C)

Phenols can be readily obtained from aryl methyl ethers *via* a variety of methods. One of these utilizes boron tribromide, a strong Lewis acid, which also offers an advantage due to its tolerance of several other functional groups in the target molecules, including aliphatic halides. BBr_3-asssited *O*-demethylation occurs *via* an S_N2 mechanism initiated by nucleophilic attack of methyl ether oxygen onto the boron centre in BBr_3 leading to the formation of the ether-BBr_3 adducts (Scheme 2.7). Thereafter, an S_N2 involving two ether–

BBr_3 adducts follows, each acting as a reaction substrate, and as a bromide ion donor. During this step, bromide from one ether–BBr_3 molecule abstracts the methyl group of another ether–BBr_3 substrate, cleaving the C–O bond to produce CH_3Br and ethoxy-BBr_2. The ethoxy-BBr_2 species undergoes hydrolysis upon quenching and work-up with water to afford the phenol product **6**.[34,35]

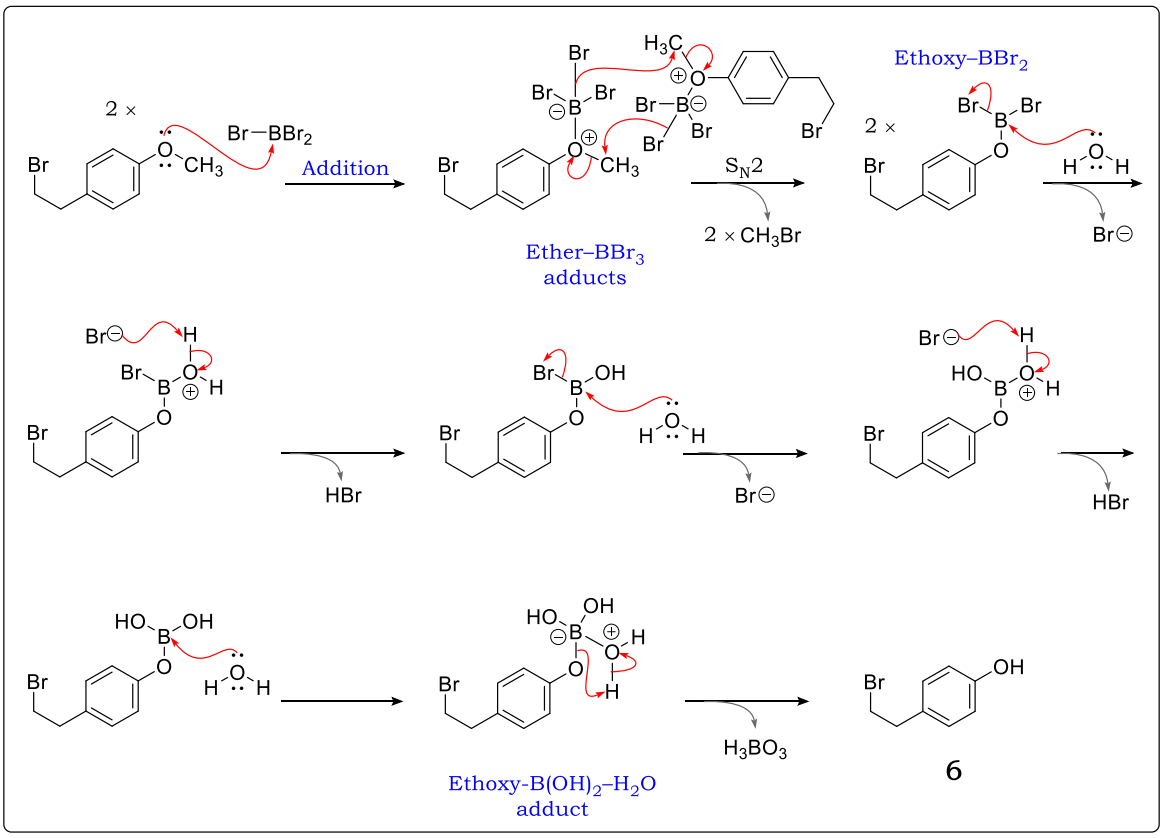

Scheme 2.7: Proposed reaction mechanisms for catalytic *O*-demethylation

During the hydrolysis cycle, each water molecule displaces a bromide ion in ethoxy-BBr_2 to produce *in situ* HBr. In the final step, an intramolecular rearrangement of the ethoxy-$B(OH)_2$–H_2O adduct leads to the formation of boric acid (H_3BO_3) and the phenol product **6**. Two molecules of HBr are produced for every boric acid molecule.

Upon work-up, the change in polarity (R_f, 0.68 to 0.50) on TLC indicated successful transformation. ^{1}H-NMR analysis of the pure isolated product revealed no signs of the methyl singlet up-field, but the appearance of a phenolic proton singlet down-field at δ = 9.23 ppm. Additionally, two (2) pairs of methylene protons were observed *via* ^{1}HNMR, each splitting as a triplet with a coupling constant (*J*) of 7.4 Hz, indicating that the alkyl bromide moiety was unaltered.

2.3.3.7 Methyl Esterification using TMS-Diazomethane (Step H, Scheme 2.1F)

Diazomethane (CH_2N_2) offers a quick and efficient means of preparing methyl esters from carboxylic acids (*O*-methylation). However, CH_2N_2 is highly flammable and toxic among

other hazards.[36] Therefore, to avoid exposure to these hazards, a safer method that utilizes trimethylsilyldiazomethane (TMS-CHN_2) as a precursor to produce CH_2N_2 *in situ* was employed.

The reaction is carried out in a 1:1 toluene-methanol solvent matrix. The first step is formation of the TMS-$CH_2N_2^+$ cationic moiety (Scheme 2.8) after abstraction of the carboxylic acid proton by the TMS-CHN_2 carbon. The cationic moiety coordinates with methanol *via* silicon (Si) to form a methoxonium complex. This renders the methanolic proton highly acidic and is then quickly abstracted by the carboxylate to regenerate the carboxylic acid. The carboxylic acid thus acts as a catalyst, first as an acid, then as a base, for the methanolysis of TMS-CHN_2 to generate free CH_2N_2 *in situ*.[25] The methyl ester is generated in a subsequent standard reaction of carboxylic acids with the diazomethane (Scheme 2.8).

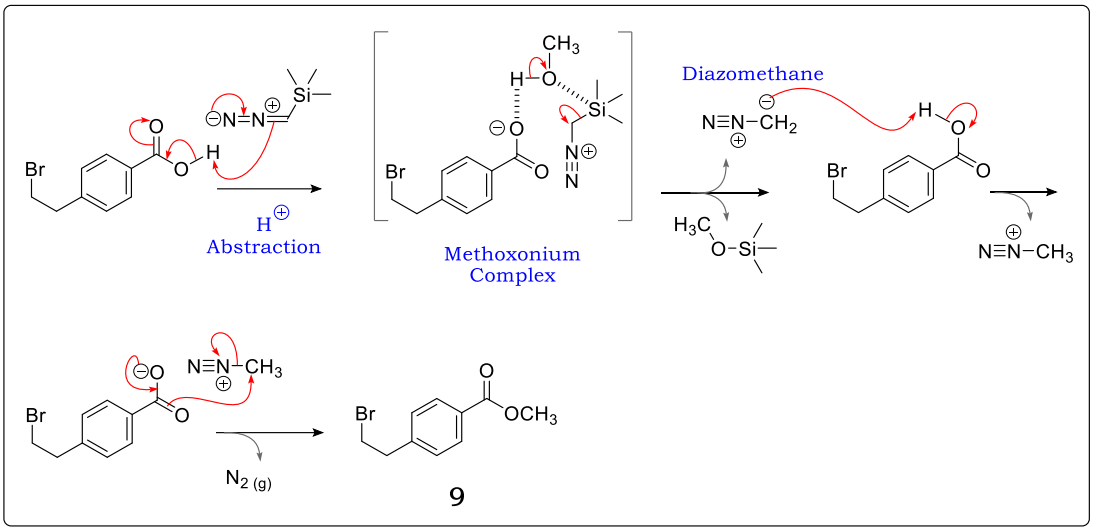

Scheme 2.8: Proposed reaction mechanisms for methyl esterification using diazomethane

The transformation was monitored *via* TLC and confirmed by the appearance of a methyl proton singlet up-field (δ = 3.85 ppm) in the ^{1}H-NMR spectrum. The presence of the bromo-pattern (*m/z* = M+, M+2) in the HPLC-MS spectrum and two pairs of methylene protons in the ^{1}H-NMR spectrum confirmed retention of the alkyl bromide functionality.

2.3.4 Synthesis of Phase I, SARs 1 – 3 Target Compounds (15 – 54)

As shown in Scheme 2.9, synthesis was initiated *via* *N*-alkylation of 2-chloro-1*H*-benzimidazole using commercially available alky halides in the presence of K_2CO_3 to afford 2-chloro-1-alkyl-benzimidazoles **12** in high yields (85 – 98%).

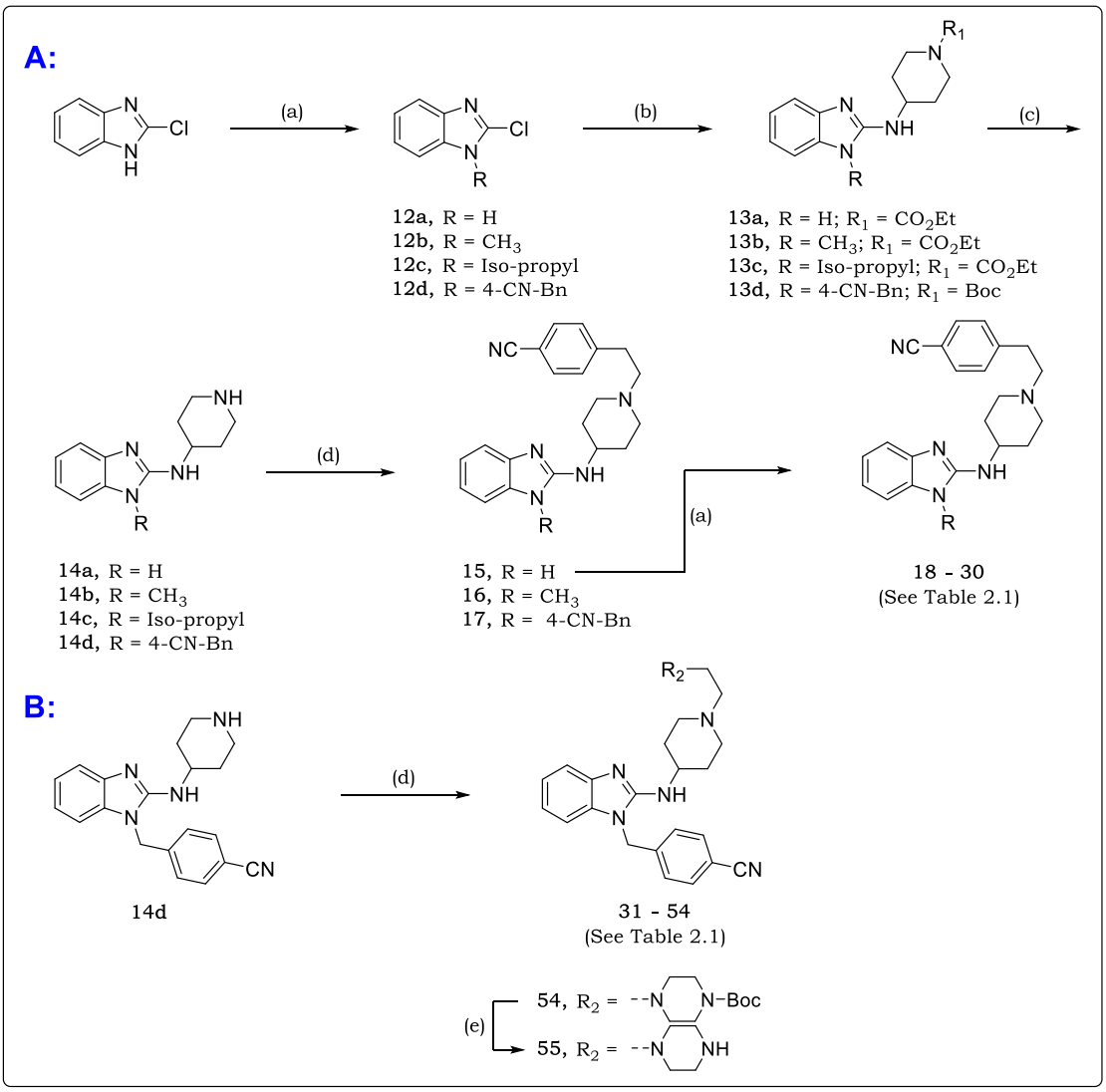

Scheme 2.9: Synthetic protocol towards the formation of target compounds **15 – 55**

Reagents and conditions: (a) alkyl halide, acetone, K_2CO_3, 23 °C, 2 – 12 h (85 – 98%) or alkyl halide, DMF, K_2CO_3, 70 °C, 12 h (58 – 80%); (b) ethyl 4-aminopiperidine-1-carboxylate or *tert*-butyl 4-aminopiperidine-1-carboxylate, TEA, 150 °C, 2 – 12 h (60 – 85%); (c) 48% HBr, 120 °C, 2 h or TFA, DCM, 20 °C, 3 h (71 – 98%); (d) Phenethyl bromides (**1** – **8** or **11b**) or *O*-Mesylates (**10**), K_2CO_3, MeCN, 80 °C, 5 – 12 h (48 – 91%); (e) TFA, DCM, 21 °C, 2h, then amberlyst-A21, DCM, 3 h (**55**, 95%).

Subsequent nucleophilic aromatic substitution (S_NAr) at 150 °C using either ethyl 4-aminopiperidine-1-carboxylate or *tert*-butyl 4-aminopiperidine-1-carboxylate in the presence of TEA, furnished *N*-ethyl carboxylate, and *N*-Boc-protected intermediates **13**, respectively.

The *N*-Boc-protected amine was used to prepare **13d** considering the presence of a nitrile in the precursor (**12d**), whose labile nature towards hydrolysis would not withstand the harsh deprotection conditions employed for ethyl carboxylates involving a reflux at 120 °C in highly acidic aqueous medium (48% HBr).[3] Deprotection of intermediates **13** in acidic media afforded the free amines **14** in high yields (71 – 98%). Treatment of free amines with appropriately commercially available or previously prepared phenethyl halides (**1** – **8** or **11b**) and *O*-mesylates (**10a** or **10b**) in a potassium carbonate (K_2CO_3)-mediated S_N2

reaction afforded target compounds **15** – **17** and **31** – **55**. Target compounds **18** – **30** were prepared *via* direct *N*-alkylation of commercially available alkyl bromides with 1H-benzimidazole **15** using K_2CO_3 in DMF.[2,3] Synthesized analogues and isolated yields are summarized in Table 2.1.

Table 2.1: Isolated yields for phase I target analogues (**SARs 1 – 3**)

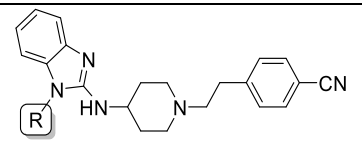

Code	R	R_1	Yield (%)
15	H	-	85
16	Me	-	84
17	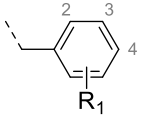	4-CN	86
18		3-F,4-CN	81
19		2-CN,4-F	79
20		2-F,4-CN	73
21		4-OMe	88
22		4-SO_2Me	93
23		4-NO_2	96
24		4-CO_2Me	93
25		4-CO_2H	90
26		4-CF_3	90
27		4-CH_3	88
28	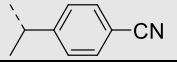	-	78
29	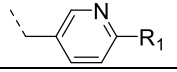	CF_3	74
30		CH_3	92

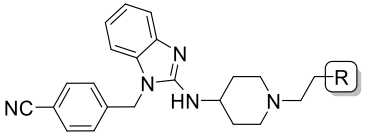

Code	R	R_1	Yield (%)
31	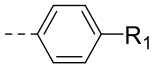	H	75
32		OH	63
33		SO_2Me	88
34		CH_3	76
35		CF_3	79
36		NO_2	77
37		CO_2Me	89
38		CO_2Et	55
39		CO_2H	96
40			72
41		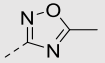	61
42		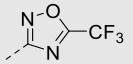	78
43		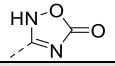	68

Code	R	R_1	Yield (%)
44			58
45			81
46	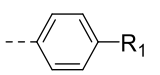		65
47		CF_3	75
48			48
49			53
50			75
51			45
52	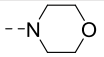		42
53	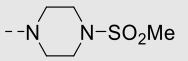		65
54	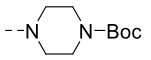		46
55	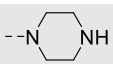		95

2.3.5 Proposed Reaction Mechanisms and Characterization, Phase I SARs 1-3

2.3.5.1 N-alkylation and Nucleophilic Aromatic Substitution, S_NAr (steps A and B, Scheme 2.9)

Synthesis of intermediates **12** proceeded *via* S_N2 initiated by the abstraction of the imidazole N-H hydrogen by K_2CO_3 (Scheme 2.10). The electron-push from the resulting lone pair at position 1 (N-1) leads to nucleophilic attack by the π-bond electrons on nucleophilic nitrogen at position 3 (N-3) to the electron deficient C–X sp^3 carbon in the alkyl halide. This concertedly leads to the substitution of halide, which results in the formation of intermediates **12**.

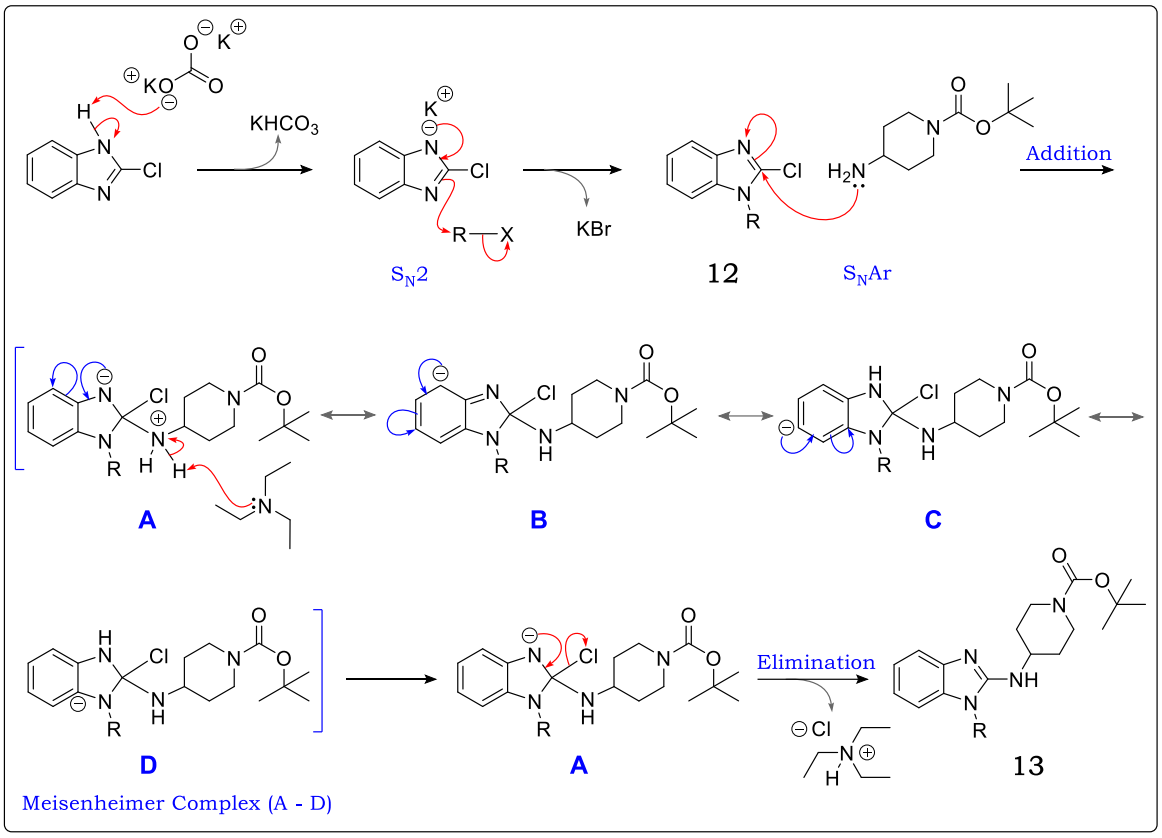

Scheme 2.10: Proposed reaction mechanisms *N*-alkylation S_N2 and S_NAr

Nucleophilic aromatic substitution (S_NAr) takes place *via* a two-step process involving an addition-elimination sequence. In this case, nucleophilic addition of the primary nitrogen from 4-amino-*N*-Boc-piperidine at the benzimidazole aromatic carbon bearing the chloro leaving group leads to the formation of an anionic intermediate with a highly delocalized charge, otherwise called a Meisenheimer complex (**A** – **D**, Scheme 2.10).[37] In the second step, the chloride leaving group is eliminated to restore aromaticity, thus furnishing the C–N bond in **13**. TEA mops up the generated protons preventing the protonation of the amine nucleophile and *in situ* deprotection of the Boc group.

The observed ^{1}H-NMR spectrum of **12b** (Figure 2.10), shows that proton **H-1** is the most de-shielded proton, followed by **H-4**. Consistently, both are closer to the electron-rich

benzimidazole nitrogen atoms and resonate as doublet of doublets (*dd*, J = 8.50, 1.10 Hz and J = 8.10, 1.13 Hz, respectively).

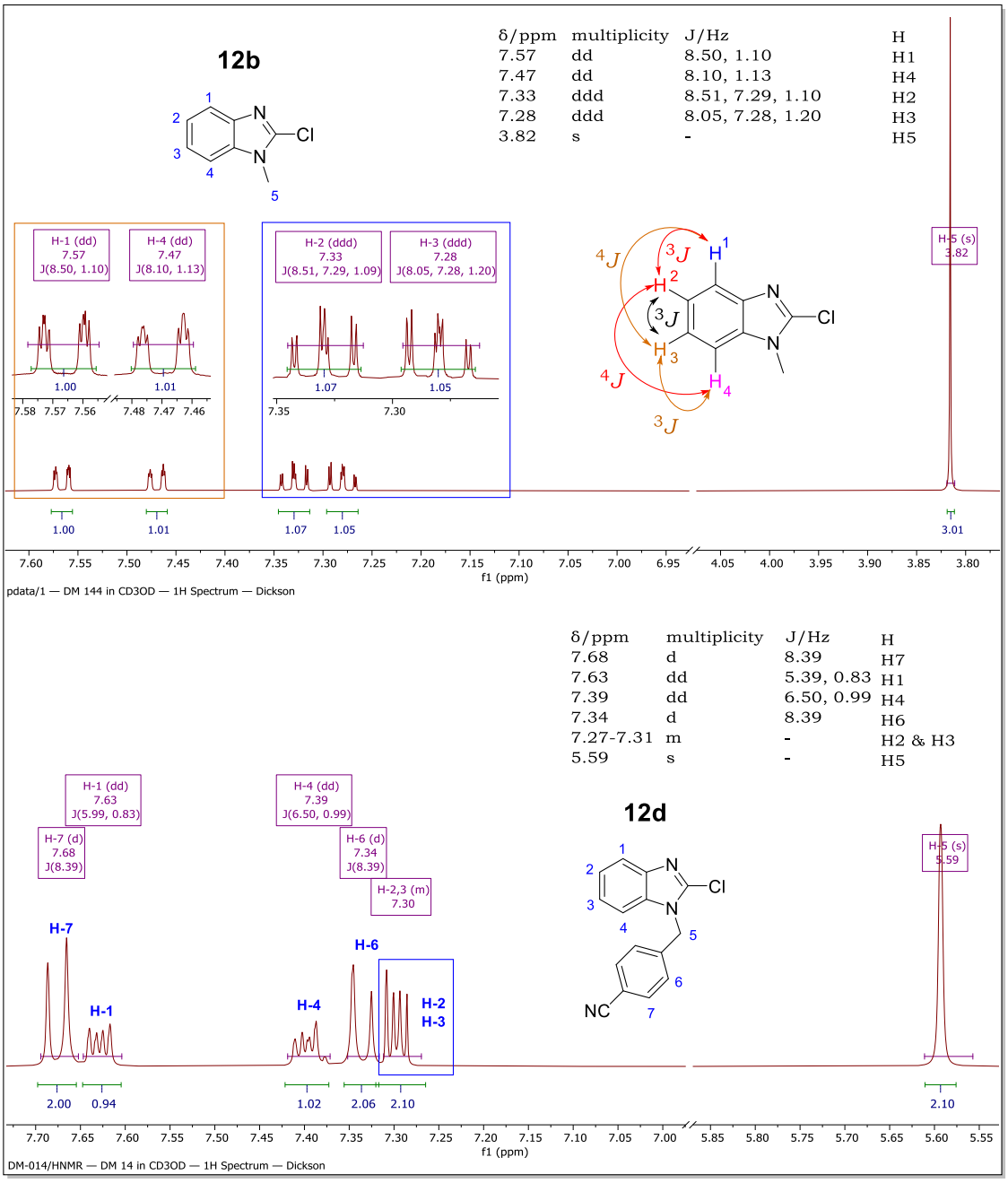

Figure 2.10: ^{1}H-NMR spectrum of **12b** (top) and **12d** (bottom) in methanol-d_4 at 600 MHz

This splitting pattern is due to separate short range (large ^3J) and long range (small ^4J) interactions with **H-2** and **H-3** respectively. However, protons **H-2** and **H-3** each resonates as doublet of doublets of doublets (*ddd*, J = 8.51, 7.29, 1.10 Hz and J = 8.05, 7.28, 1.20 Hz respectively). Judging from the coupling constants, they are each split first by their immediate de-shielded neighbour (largest ^3J), then by each other (large ^3J) and last through long-range (smallest ^4J) coupling, to the other de-shielded proton (Figure 2.10). The same benzimidazole proton splitting pattern was observed for aromatic substituted analogue

12d, in addition to the two doublets (**H6** and **H-7**) attributable to the benzyl group (Figure 2.10).

Successful synthesis of these intermediates was additionally confirmed *via* HPLC-MS analysis. For instance, **12b** and **12d** exhibited pseudo-molecular ions of 167.0, 169.1 [M–H] and 267.9, 269.9 [M+H] respectively, consistent with the calculated exact masses of the molecular formula ($C_8H_7ClN_2$ and $C_{15}H_{10}ClN_3$).

Following aromatic nucleophilic substitution (S_NAr), the most striking feature confirming successful C–N bond formation was the appearance of aliphatic signals associated with the piperidine ring and the protecting group (Figure 2.11). Citing intermediate **13d** as an example, proton **H-8** resonates as a triplet of triplets (*tt*) appearing up-field at δ = 3.94 ppm. As illustrated in Figure 2.11, this pattern is due to ^3J splitting by two symmetrically identical pairs of axial (**H-9a**, large $^3J_{trans}$) and equatorial (**H-9e**, small $^3J_{cis}$) protons on the piperidine ring. Being in the shielded region of the chair conformation, the equatorial protons **H-10e** resonate downfield as a multiplet (*m*) at δ = 4.05 ppm while the less shielded axial **H-10a** protons (deshielding region)[38] resonated further up-field at δ 2.93 ppm. The signals of **H-9** protons were equally resolved into **H-9e** and **H-9a** signals, both resonating as multiplets at δ = 2.03 and 1.44 ppm respectively, each integrating for two (2) protons. As expected, the CH_3 protons of the *tert*-butyl carboxylate were the most shielded appearing as a singlet overlapping with **H-9a** protons at δ = 1.44 ppm.

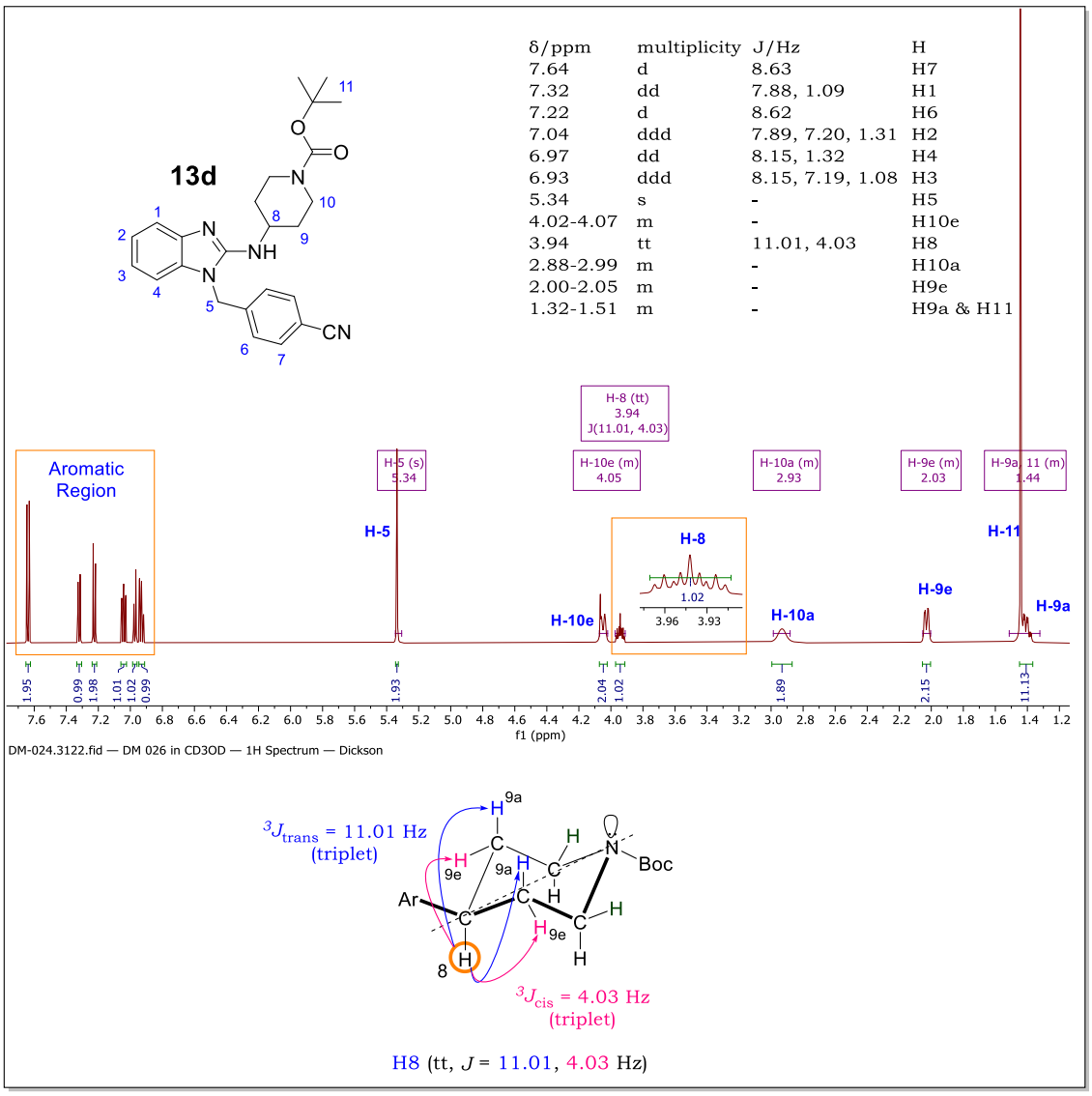

Figure 2. 11: ^{1}H-NMR spectrum of **13d** in methanol-d_4 at 600 MHz

2.3.5.2 N-Boc deprotection (step C, Scheme 2.9)

Deprotection in acidic medium, a step leading to the formation of free amines **14a** – **14d** takes place *via* a well-established mechanism as shown below for *N*-Boc deprotection using trifluoroacetic acid (TFA). As shown in Scheme 2.11, the electron-rich carbonyl oxygen in the carbamate is initially protonated by TFA, leading to an electron rearrangement that stabilizes the formal charge and consequently eliminates the *tert*-butyl tertiary (3°) carbocation. This generates a carbamic acid intermediate that quickly undergoes decarboxylation to give a deprotected amine. As soon as the amine is formed, protonation occurs because of the presence of excess acid to produce a TFA salt. Treatment of the salt with amberlyst-A21 free base resin liberates the free amines **14**. The generated carbocation undergoes deprotonation by TFA to form isobutylene gas which escapes from the reaction alongside CO_2. Alternatively, it has been hypothesized that the carbocation may also be quenched by nucleophilic attack to form *tert*-butyl trifluoroacetate or oligomers *via* polymerization (not shown).

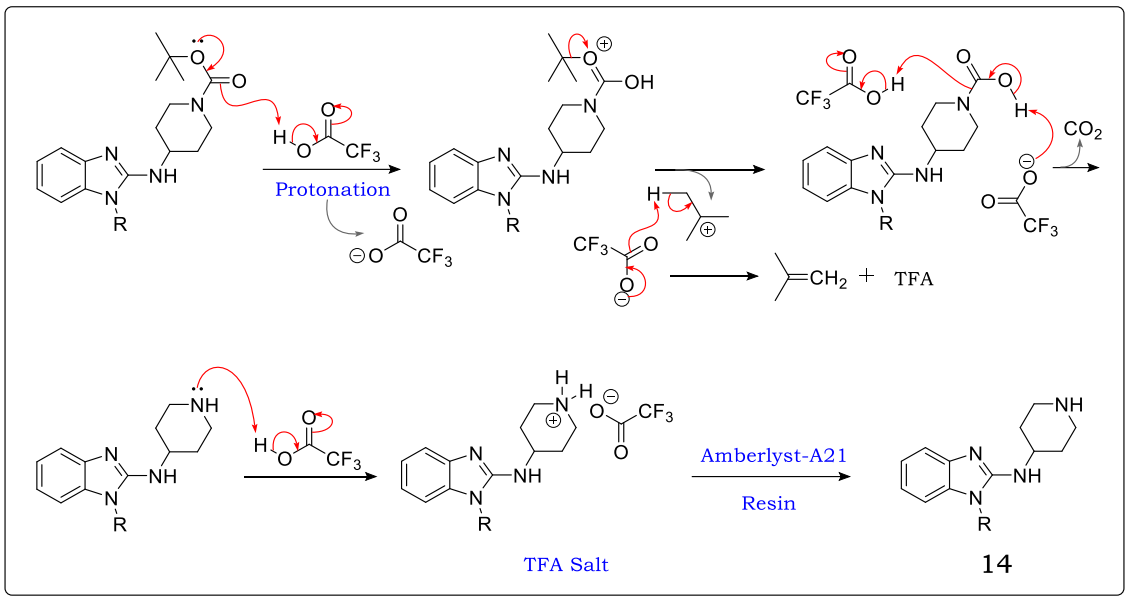

Scheme 2. 11: Proposed reaction mechanisms for *N*-Boc deprotection using TFA

The loss of the 9-proton singlet signal upfield in the ^{1}H-NMR spectra of these intermediates confirmed successful *N*-Boc deprotection while the disappearance of the ethyl CH_2-proton quartet and CH_3-proton triplet upfield confirmed ethyl carbamate removal.

Following deprotection, the splitting pattern for some of the piperidine protons could be properly resolved. For instance, in intermediate **14d** (Figure 2.12), deshielded equatorial pairs **H-10e** protons at δ = 3.07 ppm split as a doublet of triplets (dt) while the shielded axial protons **H-10a** and **H-9a** split as triplet of doublets (*td*) and doublet of triplets of doublets (*dtd*), resonating at δ = 2.74 and 1.46 ppm, respectively. The triplet of doublets splitting pattern of **H-10a** is attributed to an initial equal splitting by germinal **H-10e** and vicinal **H-9a** ($^{2,3}J$ = 12.54 Hz) giving a triplet, and secondly by a weak coupling to vicinal **H-9e** ($^{3}J_{ax\text{-}eq}$ = 2.62 Hz; Figure 2.13). The phenomena of equal splitting of an axial proton in cyclohexanes by its germinal neighbor ($^{2}J_{eq\text{-}ax}$) and that of the adjacent vicinal axial proton ($^{3}J_{ax\text{-}ax}$) is well documented.[39]

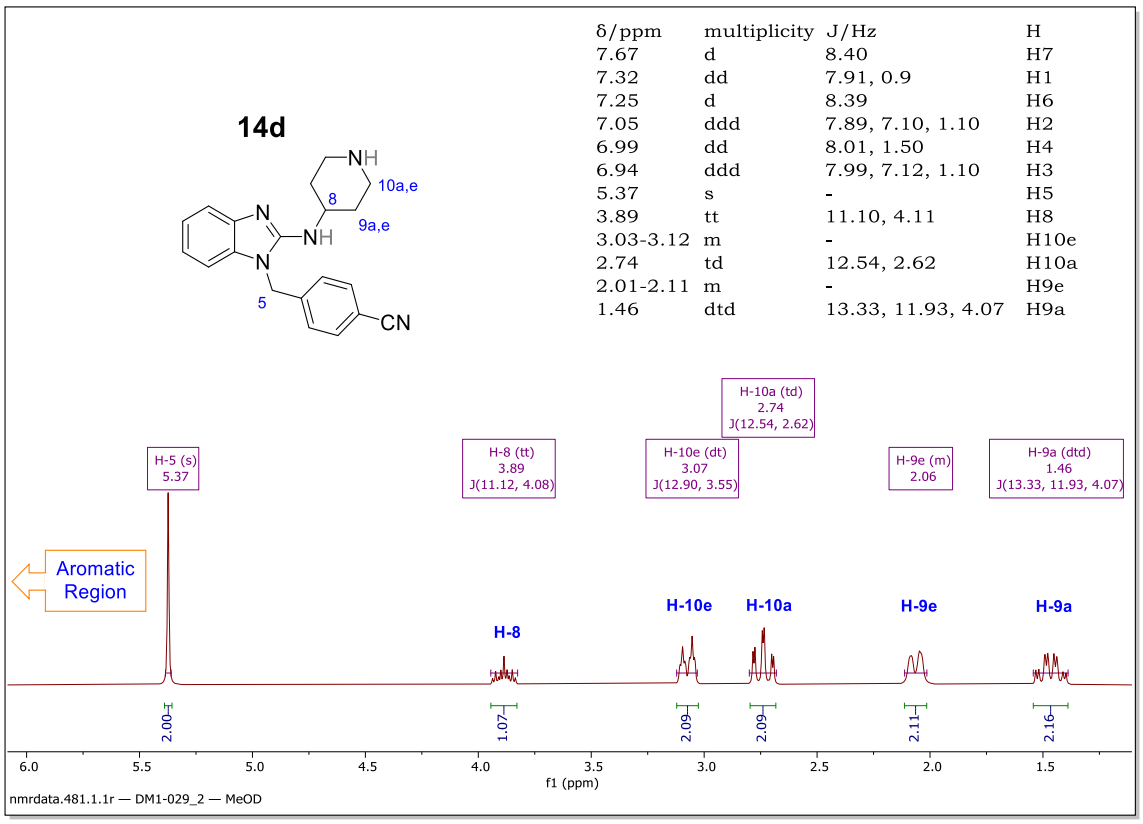

Figure 2. 12: ^{1}H-NMR spectrum of **14d** in methanol-d_4 at 400 MHz

In a similar way, the doublet of triplets of doublets observed for **H-9a** arises from coupling to vicinal axial proton **H-8** ($^{3}J_{trans}$ = 13.33 Hz), followed by equal coupling to germinal **H-9e** and vicinal **H-10a** (^{3}J = 11.93 Hz) and finally, weak coupling to vicinal **H-10e** ($^{3}J_{cis}$ = 4.07 Hz) as shown below.

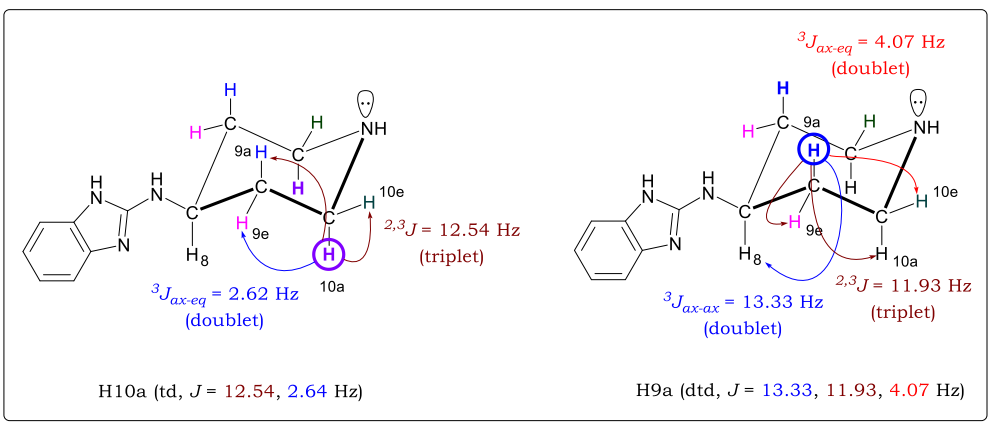

Figure 2. 13: Description of the observed triplet of doublets (td) and doublet of triplet of a doublet (dtd) splitting patterns for piperidine protons H10a (*left*) and H9a (*right*), respectively

In addition to the triplet of triplet signal observed for **H-8**, the splitting pattern of **H-9a** further confirms that the bulky amino benzimidazole group is in the equatorial position while **H-8** is in the axial position. This is because vicinal *trans* (axial-axial) couplings are stronger (large *J*) than *cis* (axial-equatorial) couplings (smaller *J*).[39] Notably, the removal of the protecting group caused significant perturbation in the extent of shielding for the

adjacent piperidine protons. For instance, the equatorial protons **H-10e** in **14d** are less de-shielded than the **H-8** proton, resonating at δ = 3.07 ppm compared to 4.05 ppm in the precursor **13d**.

Consistently, *N*-ethyl carboxylate and *N*-Boc deprotection was accompanied by loss of 72.0 and 100.00 *m/z* units respectively, corresponding to the mass of the removed carbamate. For **14d**, a pseudo-molecular ion observed at 332.2 [M+H] consistent with the calculated mass for the formula $C_{20}H_{25}N_5O$.

2.3.5.3 Piperidinyl N-alkylation and 1,2,4-Oxadiazole formation (step D, Scheme 2.9)

The final step leading to the formation of target compounds is an S_N2 in the presence of K_2CO_3 (Scheme 2.12A).

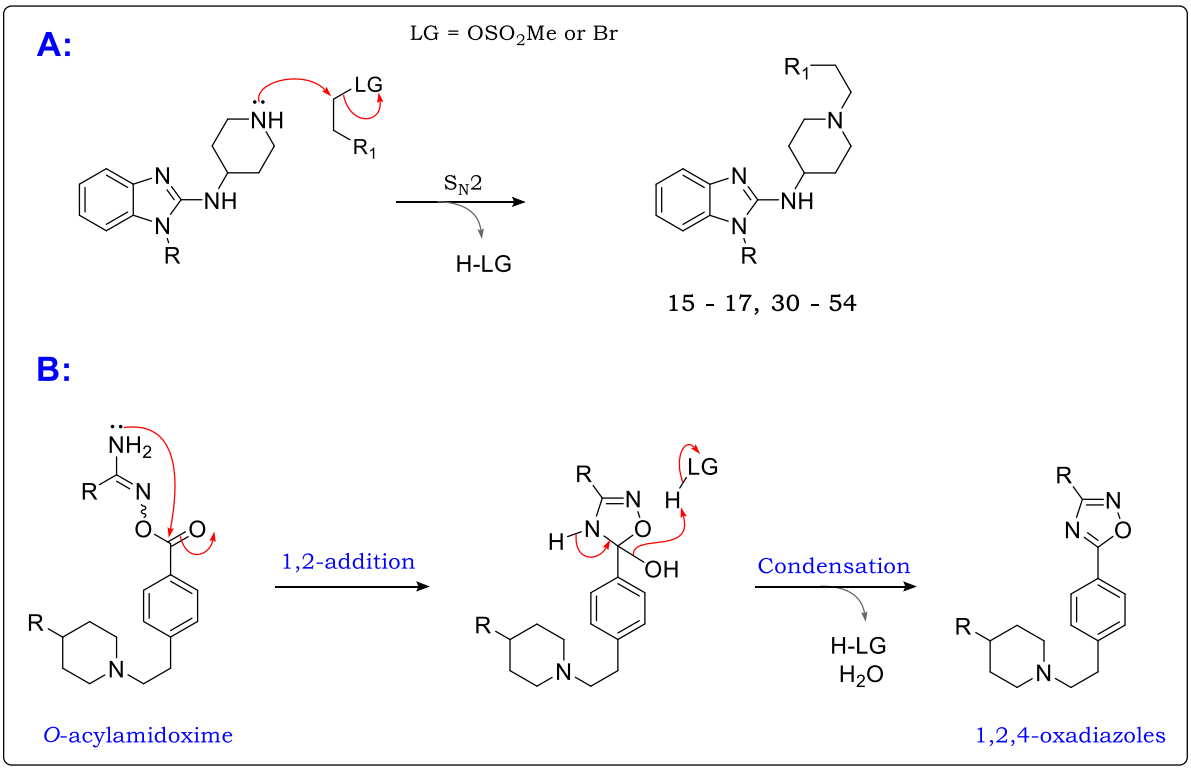

Scheme 2.12: Proposed reaction mechanisms for [A] final step nucleophilic substitution and [B] formation of the 1,2,4-oxadiazole heterocycle

Mechanistically, nucleophilic attack by the piperidine lone pair of electrons onto the electron deficient alkyl bromide or mesylate carbon leads to the displacement of the leaving group to form the products (Scheme 2.12A). Following nucleophilic substitution, *O*-acylamidoximes undergo cyclodehydration to form 1,2,4-oxadiazoles under the same reaction conditions. This is initiated by intramolecular nucleophilic attack by the amidoxime nitrogen onto the electrophilic *O*-acyl carbonyl carbon (1,2-addition) leading to the generation of a cyclic hemiketal-like intermediate, which undergoes proton transfer and subsequent elimination of water, driven by aromatization to form the 1,2,4-oxadiazole heterocycle (Scheme 2.12B)

Successful nucleophilic substitution was generally confirmed by the presence of two pairs of diagnostic methylene protons and contextualized by the appearance of other diagnostic signals in the ^{1}H-NMR spectra. Examples of respective spectroscopic characterization of target compounds from each SAR are described.

The ^{1}H-NMR spectrum for target compound **15** as shown in Figure 2.14. The two pairs of methylene protons (**H-7** and **H-8**) resonate as coalesced multiplets because of their continuous change of magnetic environment, consequently undergoing both geminal (^{2}J) and vicinal (^{3}J) coupling with each other. Attempts to separate these multiples into the expected pair of triplets by using variable-temperature ^{1}H-NMR (VT-NMR) at 30, 50, 75 and 90 °C proved unsuccessful. Solid state ^{1}H-NMR at very low temperature may be one way to capture a single timescale and resolve these. Compared to **H-8** (δ = 2.70 ppm), the **H-7** protons are relatively more de-shielded, as expected due to significant electron withdrawing by the piperidine nitrogen (Figure 2.14).

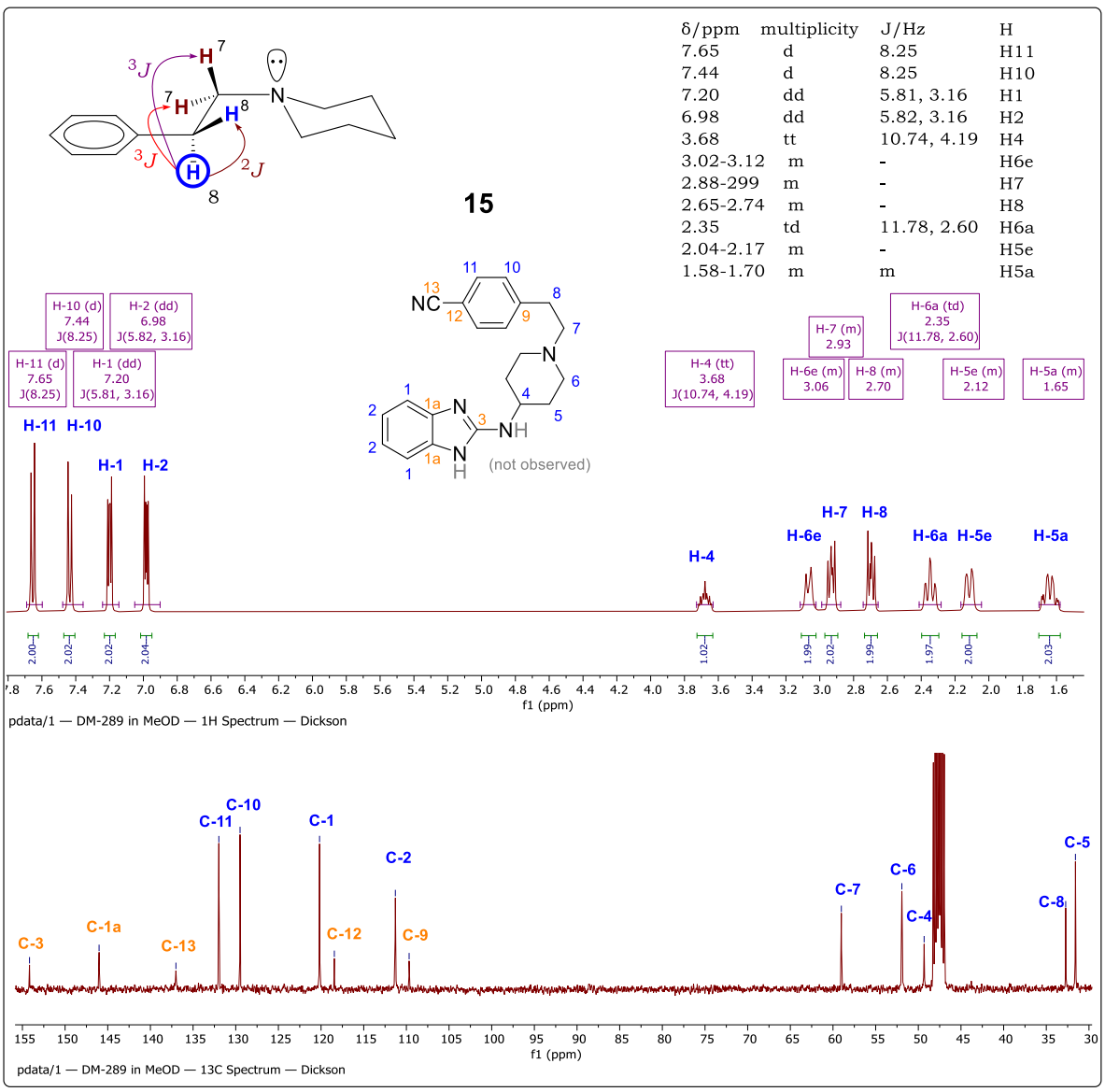

Figure 2. 14: ^{1}H-NMR (*top*) & ^{13}C-NMR (*bottom*) spectra of **15** in Methanol-d_4 at 400 MHz

Additionally, a finely resolved pair of doublets integrating for two protons each, appears in the aromatic region (δ = 7.65 and 7.44 ppm). These protons are attributable to symmetrical **H-10** (×2) and **H-11** (×2) in the phenyl group coupling with each (J = 8.25 Hz). Benzimidazole protons **H-1** and **H-2** share a chemical environment due to the symmetry that runs in the molecule in the most stable resonance form. Each proton in the pair couples with its immediate neighbour (^3J) and further with a ^4J partner. Consequently, each pair splits as a doublet of doublets ($^{3,4}J$ = 5.81, 3.16 Hz).

^{13}C-NMR spectroscopy confirmed the chemical structures of some intermediates and final compounds. For instance, the ^{13}C-NMR spectrum of **15** (Figure 2.14) revealed fourteen (14) distinct carbon signals, attributable to the twenty-one (21) carbons present in the molecule. As expected, aromatic phenyl (four carbons) and benzimidazole (seven carbons) resonated downfield, alongside other de-shielded carbons attached to electronegative atoms (i.e., the nitrile carbon **C-13**). The most deshielded carbon is **C-3** (δ = 154.17 ppm) due to is precise three-way flanked position between nitrogen atoms. Two benzimidazole and two phenylic signals had greater intensity, each arising from two carbons in the same chemical environment. These are carbons **C-1** and **C-2** in benzimidazole, as well as carbons **C-10** and **C-11** in the phenyl ring.

A similar trend was observed for piperidine protons in which only two signals where recorded attributable to two pairs of **C-5** and **C-6** carbons in a chemically equivalent environment. Additionally, carbons **C-6** (δ = 51.93 ppm) were the most de-shielded piperidine carbons by virtue of their proximity to electronegative nitrogen atoms in comparison with **C-5** carbons (δ = 31.58 ppm). The rest of the signals where successfully assigned to their carbons relative to the electronic environments and carbon type (Figure 2.14). HPLC-MS analysis revealed 99% purity of **15** based on the peak area. The mass spectrum revealed a pseudo-molecular ion (M+H)+ in the positive ionization mode at 364.20 (100%) which correlates to the calculated molecular weight for $C_{21}H_{23}N_5$.

Following the synthesis and full characterization of **15** and **14d**, these were used as crucial intermediates for the preparation of final compounds **18 – 30** (**SAR 1**) and **31** – **55** (**SAR 2** and **3**). As shown in Scheme 2.9, these reactions were carried out by stirring either **15** or **14d** with an appropriate alkyl halide and K_2CO_3 in DMF at 70 °C or refluxing in MeCN. Examples of full characterization of compounds in each SAR and compound class are presented here.

Following benzimidazole N-alkylation of **15**, the ^{1}H-NMR spectrum of **28** (Figure 2.15), was consistent with the structure of the compound. As such, the diagnostic methyl group protons (**H-6**) resonated upfield at δ = 1.93 ppm as a doublet, due to splitting by **H-5** (^3J = 7.07 Hz). **H-5** resonates as a quartet further downfield (δ = 5.85 ppm) due to its precise position next to the electronegative benzimidazole nitrogen atom. Additionally, the new

benzyl aromatic protons **H-8** and **H-9** were accounted for and represented by a doublet (^3J = 8.29 Hz) belonging to the two de-shielded **H-9** protons, while the two less de-shielded **H-8** protons overlapped with phenylic **H-19** protons resonating at δ 7.42 – 7.44 ppm as a multiplet and integrating for four (4) protons.

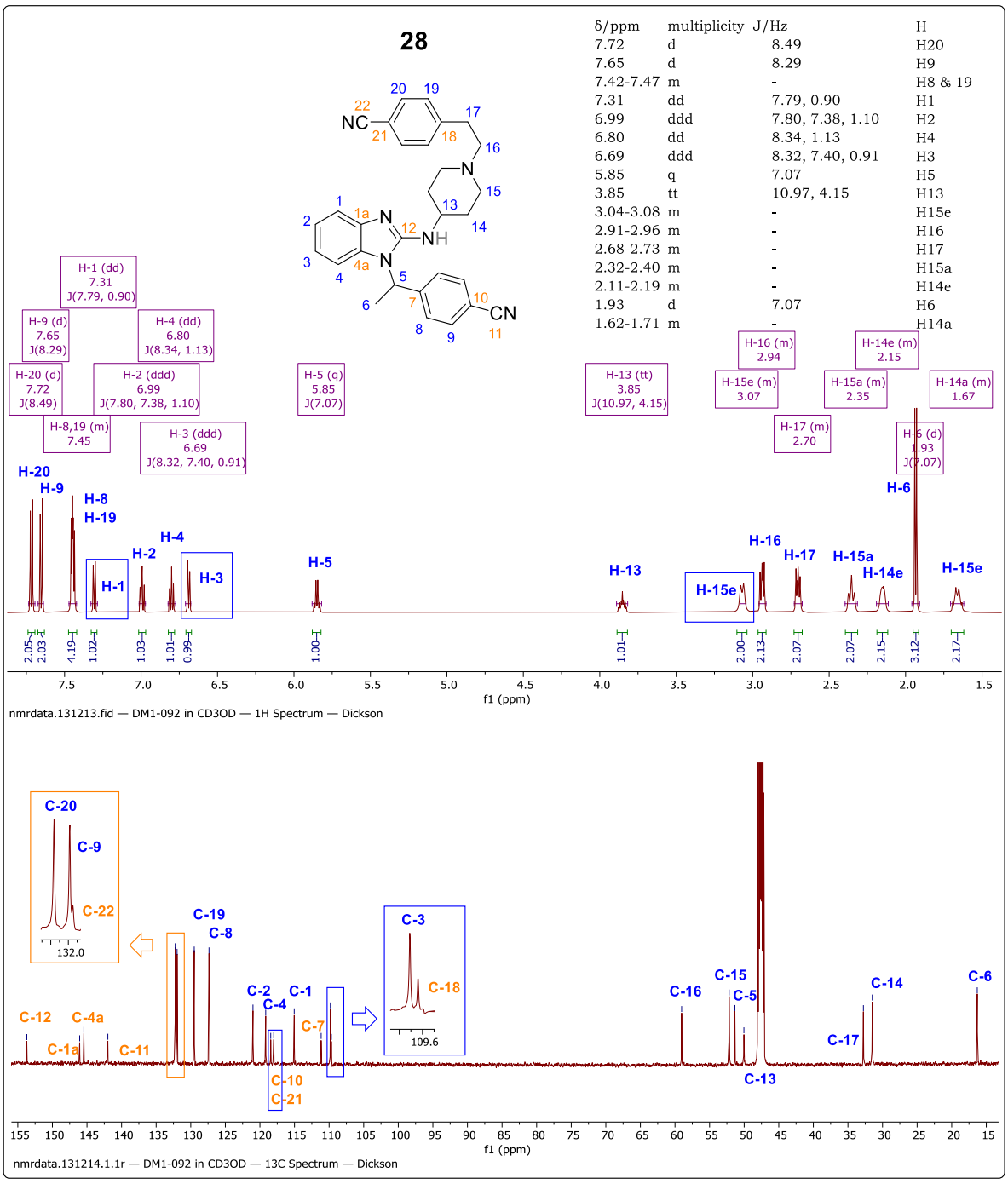

Figure 2.15: ^{1}H-NMR (*top*) and ^{13}C-NMR (*bottom*) spectra of **28** in methanol-d_4 at 400 and 101 MHz respectively

All the analogues in **SAR 1** showed similar ^{1}H-NMR spectra with variations in the resonance and splitting patterns in the aromatic region.

^{13}C-NMR provided further evidence of the structure of **28**. As shown in Figure 2.15, all the twenty-four (24) expected signals were accounted for, representing thirty (30) carbon atoms. The diagnostic signals where due to the 4-cyano benzyl moiety. Aliphatic methyl carbon **C-6** was the most shielded, resonating at δ = 16.30 ppm followed by **C-14** (δ = 31.48 ppm). As expected, **C-8** and **C-9** carbon signals each represent two carbons in the same chemical environment and resonate with high intensity at δ = 127.36 and δ = 131.88 ppm, respectively. The rest of the carbons in this moiety were assigned based on their electronic environment.

The ^{1}H-NMR for pyridyl analogue **50**, which represents compounds in **SAR 2** in which the phenyl moiety is replaced by other heterocycles, is shown in Figure 2.16.

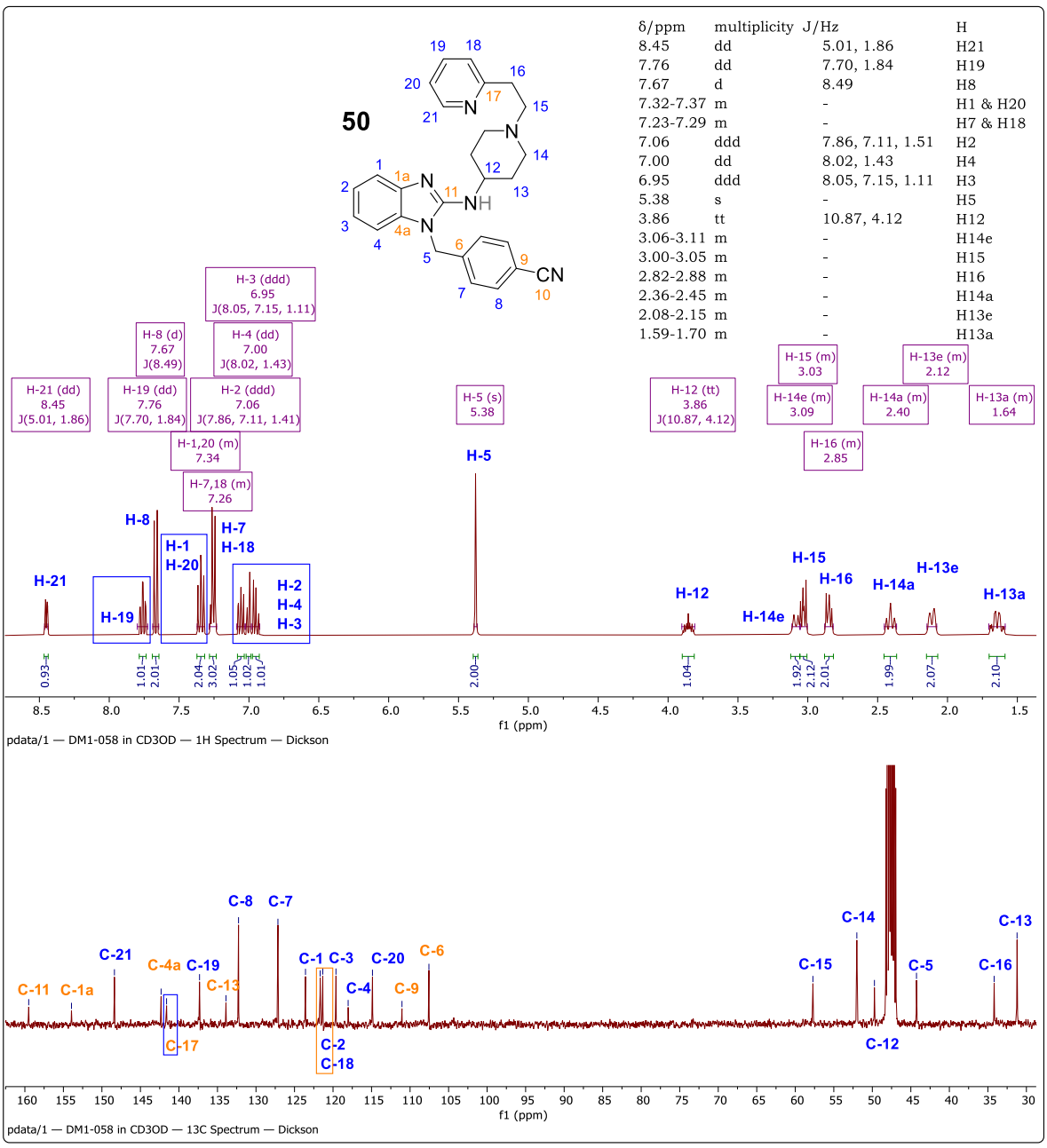

Figure 2.16: ^{1}H-NMR (*top*) and ^{13}C-NMR (*bottom*) spectra of **50** in methanol-d_4 at 400 and 101 MHz respectively

The pyridyl protons are accounted for in the aromatic region with **H-21** as the most de-shielded proton resonating furthest downfield at δ = 8.45 ppm as a doublet of doublets (*J* = 5.01, 1.86 Hz) due to vicinal (^{3}J) and long-range (^{4}J) coupling with **H-20** and **H-19**, respectively. Judging from the coupling constants, **H-19** is the second most de-shielded proton, resonating as a triplet of doublets (*J* = 7.70, 1.86 Hz) at δ = 7.76 ppm due to equal splitting by vicinal **H-20** and **H-18** and a long-range **H-21**. Protons **H-18** and **H-20** were accounted for in the multiplet overlaps with **H-7** and **H-1** at δ = 7.32–7.37 ppm and δ = 7.23–7.29 ppm, respectively. There were twenty-three (23) distinct ^{13}C-NMR signals accounting for all 27 carbon atoms present in **50** (Figure 2.16).

The last class of compounds in phase I was represented by **SAR 3** non-classical ethyl ester bioisosteres such as **45**, a 4-methyl oxazoline derivative. As shown in the ^{1}H-NMR spectra (Figure 2.17), all protons were accounted for and are consistent with the structure of **45**. Consistently, methyl protons **H-24** were the most shielded resonating at δ = 1.33 ppm as a doublet (*J* = 6.64 Hz). Protons **H-22** were represented by two distinct doublet of doublets (*dd*) at δ = 4.01 and 4.57 ppm based on their interaction with proton **H-23**. Judging from the coupling constants, proton **H-22e** at δ = 4.57 ppm is trans to **H-23**, with a large coupling constant (^{3}J = 9.32 Hz) whereas **H-22a** at δ = 4.01 ppm is *cis* with a smaller coupling constant (^{3}J = 7.50 Hz). **H-22** protons equally undergo germinal coupling (^{2}J = 8.02 Hz). Phenyl protons **H-18** and **H-19** are in the aromatic region, with **H-19** being the most de-shielded resonating at δ = 7.84 ppm as a doublet integrating for two protons as expected. **H-18** resonated at the same chemical shift as **H-1** and therefore overlaps into a multiplet integrating for three (3) protons at δ = 7.32 – 7.35 ppm.

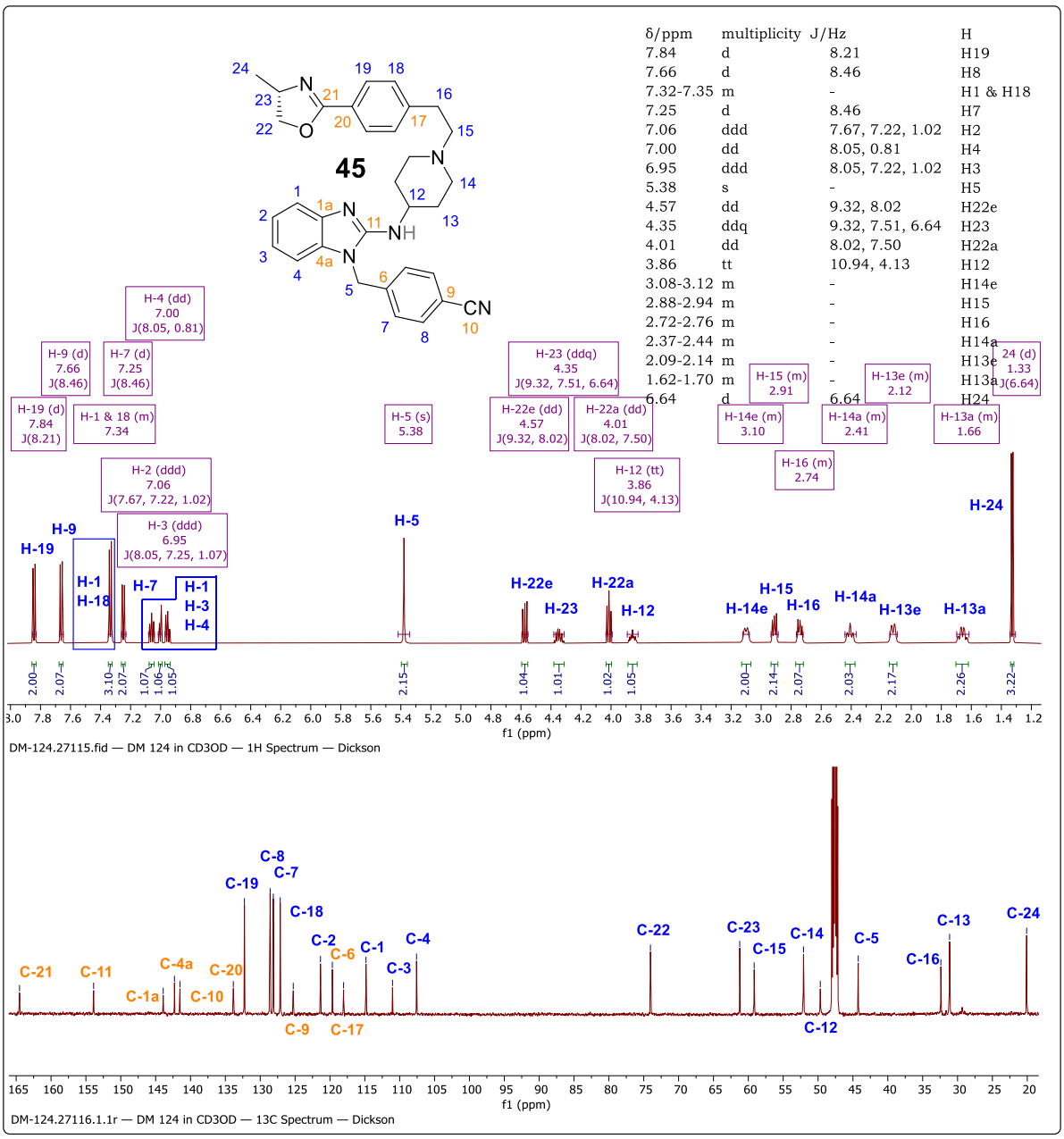

Figure 2.17: ^{1}H-NMR (*top*) and ^{13}C-NMR (*bottom*) spectra of **45** in methanol-d_4 at 400 and 101 MHz, respectively

In the ^{13}C-NMR spectrum of **45**, all the twenty-six (26) signals were consistently obtained, representing 32 carbon atoms present in the molecule. Oxazoline carbon **C-21** was the most de-shielded resonating at δ = 164.52 ppm. Other diagnostic signals include oxazoline carbons **C-22** and **C-23**, which resonated closely at δ = 74.04 and 61.23 ppm respectively.

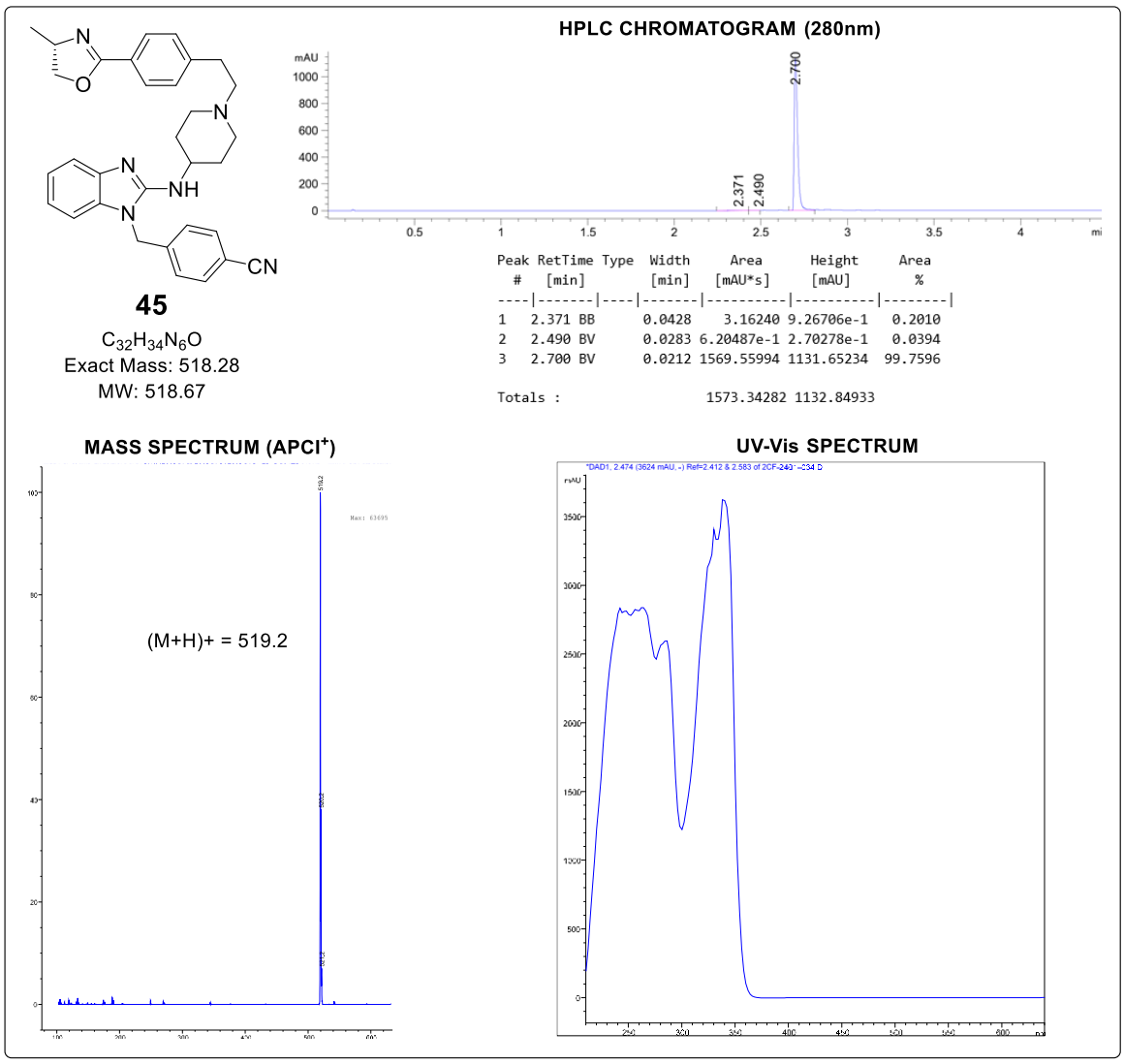

Figure 2.18: HPLC-MS chromatogram and UV-vis spectra of compound **45**

Carbon **C-21** was the most shielded, appearing in the aliphatic carbon range upfield at δ = 20.09 ppm. The rest of the signals were consistent with the structure and were unambiguously assigned according to their electronic positions and signal intensities. The HPLC-MS chromatogram and spectra of **45** (Figure 2.18) showed 99.8% purity at 2.700 min with a consistent pseudo molecular ion found at 519.2 [M+H]. The UV-Vis spectrum showed three (3) peaks depicting the absorption maxima (λ_{max}) at 240, 290 and 340 nm. Specific rotation was determined as $[\alpha]^{25}_{D}$ = +7.78°, which confirmed retention of (*S*)-configuration in the oxazoline.

2.3.6 Synthesis and Characterization of Phase I, SAR 4 Analogues

As shown in Scheme 2.13A, compounds with a varied diamine linker (**SAR 1**), were synthesized using the chemical process described in section 2.3.4. Briefly, microwave assisted S_NAr of previously prepared **12d** with a series of commercially sourced mono *N*-Boc-protected diamines, followed by Boc deprotection produced amine intermediates **56**.

A final *N*-alkylation with common intermediate **7a** afforded analogues **58** – **62** in high yields (67 – 80%; Table 2.2).

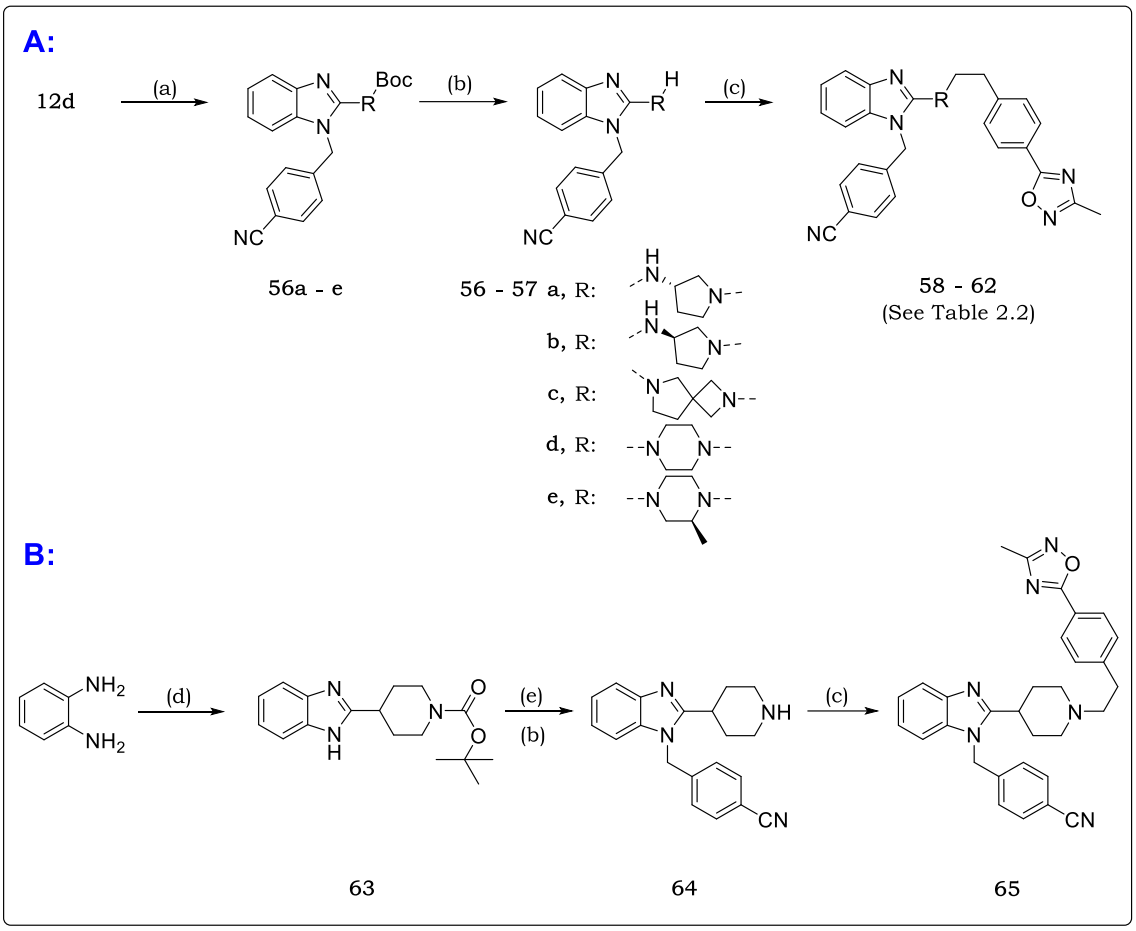

Scheme 2.13: Synthetic protocol towards phase II **SAR 4** target compounds **58 – 65**

Reagents and conditions: (a) *N*–Boc–amine, TEA, toluene, 150 °C, μW, 5–30 min (55–78%); (b) TFA, DCM, 22 °C, 2 h (75–98%); (c) **7a**, K_2CO_3, 80 °C, 10 – 24 h (67–80%); (d) *N*-Boc-4-formylpiperidine, Toluene, 24 °C, 12 h (88%); (e) 4-(bromomethyl)benzonitrile, K_2CO_3, DMF, 70 °C, 12h.

Catalyst-free oxidative cyclocondensation of aldehyde *N*-Boc-4-formylpiperidine with *O*-phenylenediamine at room temperature (24 °C) afforded 2-alkyl benzimidazole **63**. Boc deprotection, followed by S_N2 coupling of **7a** to the free amine (**64**) afforded the C-linked analogue **65** (Scheme 2.13B). The isolated yields of these analogues are summarized in Table 2.2.

Table 2.2: Isolated yields for phase I **SAR 4** analogues

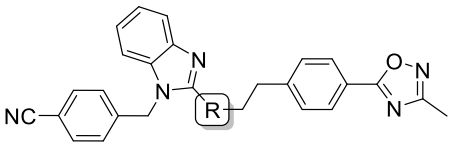

Code	R	Yield (%)	Code	R	Yield (%)
58	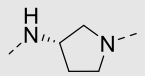	78	**61**	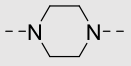	76
59	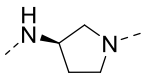	80	**62**	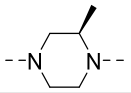	67
60		77	**65**	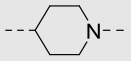	85

In this reaction, *N*-Boc-4-formylpiperidine and *O*-phenylenediamine dehydrate *via* an initial intermolecular 1,2-addition step to form an imine (Scheme 2.14). The next step is an intramolecular 1,2-addition of the imine to generate a dihydro-imidazole intermediate, which finally undergoes oxidation by air to produce the desired product.[40,41]

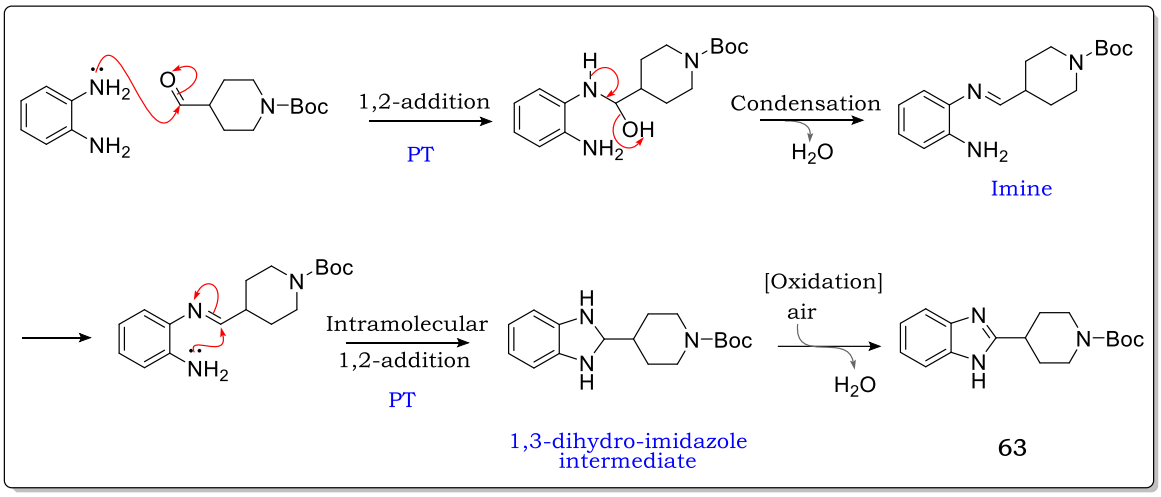

Scheme 2.14: Proposed reaction mechanisms for the formation of 2-alkyl benzimidazole **63** under catalytic-free conditions

^{1}H-NMR analysis was used to confirm the structure and successful formation of intermediates and final compounds. As an example, the spectra of **60** (Figure 2.19) showed diagnostic protons in the spiro diamine linker and all other protons were accounted for. As expected, and in the order of least shielded to the most shielded, protons **H-12** resonate as a singlet integrating for two protons (δ = 3.64 ppm) and **H-13** as a triplet because of vicinal coupling (^3J = 6.93 Hz, δ = 3.54 ppm) with **H-14** protons.

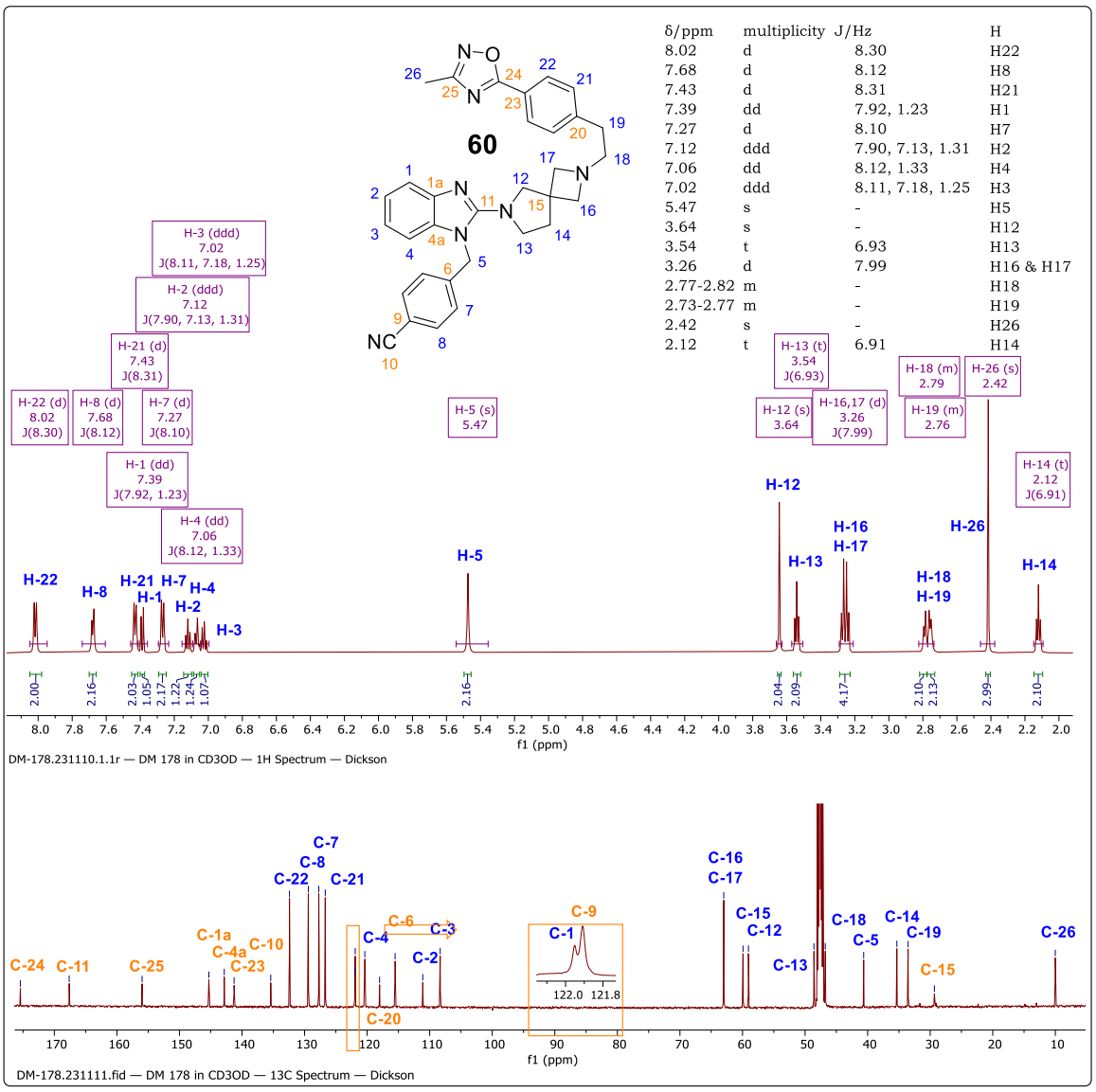

Figure 2.19: ^{1}H-NMR (*top*) and ^{13}C-NMR (*bottom*) spectra of **60** in methanol-d_4 at 400 and 101 MHz, respectively.

Protons **H-16** and **H-17** appear as two coalesced doublets (^{2}J = 7.99 Hz, δ 3.26 ppm), integrating for four protons. This is due to geminal coupling ($^{2}J_{HH}$) in the two magnetic environments. Heteronuclear single quantum coherence (HSQC) further confirmed this relationship, represented by one carbon nuclei signal (**C-16**,**17**). The most shielded protons are **H-14**, which resonate further upfield as a triplet integrating for two protons (δ = 2.12 ppm).

There were twenty-eight (28) signals in the ^{13}C-NMR spectrum of **60** (Figure 2.19). Oxadiazole carbon **C-24** (δ = 175.43 ppm) and benzimidazole **C-11** (δ = 167.62 ppm) were the most de-shielded due to their proximity with electronegative oxygen and nitrogen atoms. Spiral moiety carbons were located upfield with **C-16** and **C-17** sharing the same chemical shift environment (δ = 63.00 ppm). The methyl carbon **C-26** was the most shielded resonating at δ = 10.00 ppm.

2.3.7 Synthesis and Characterization of phase I, SAR 1_B Analogues

Maintaining the 3-methyl-1,2,4-oxadiazole moiety and the 4-aminopiperidine linker, substitution of the benzyl group was revisited. The compounds were synthesized *via* the synthetic scheme illustrated in section 2.3.4 (Scheme 2.15).

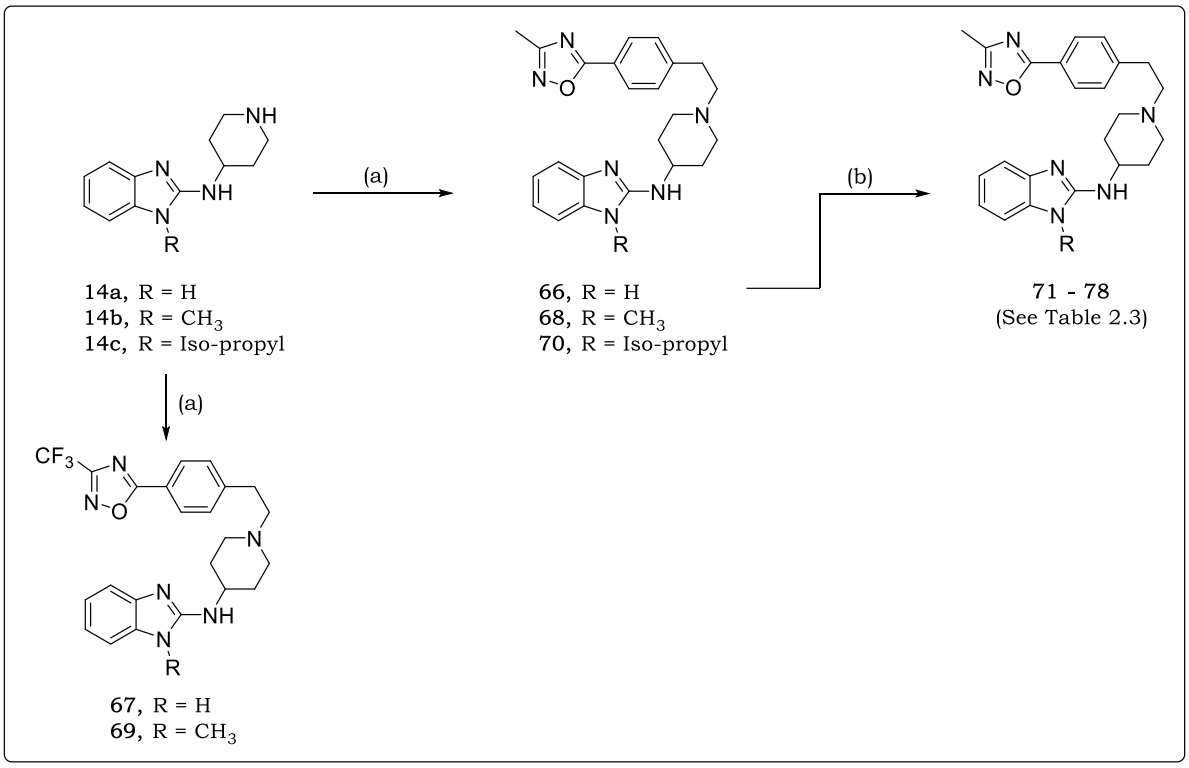

Scheme 2.15: Synthetic protocol towards **phase II**, **SAR 2** target compounds **66–78**

Reagents and conditions: (a) **7a** or **7b**, K_2CO_3, MeCN, 80 °C, 5 – 12 h (55 – 91%); (b) Alkyl bromide, DMF, 70 °C, 12 h (58 – 80%).

Briefly, S_N2 of either **7a** or **7b** with free amines **14a**–**14c** afforded **66**–**70**. Coupling of commercially available alkyl bromides with **66** afforded final compounds **71** – **78**. A summary of SAR 1_B analogues and their isolated yields is shown in Table 2.3.

Table 2.3: Isolated yields for phase I **SAR 1$_B$** analogues

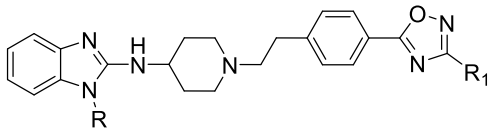

Code	R	R_1	Yield (%)
66	H	CH_3	75
67		CF_3	55
68	CH_3	CH_3	75
69		CF_3	66
70		CH_3	91
71	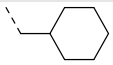		80
72	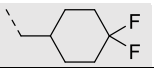		68

Code	R	R_1	Yield (%)
73	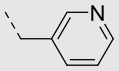	CH_3	67
74	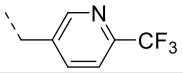		58
75	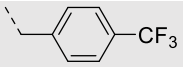		80
76	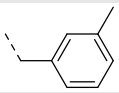		77
77	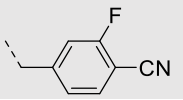		65
78	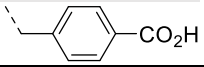		69

^{1}H-NMR was used to confirm the structure of the final compounds. Using the isopropyl analogue **70** as an example (Figure 2.20), diagnostic signals include the methyl group protons **H-19**, which resonate consistently upfield at δ = 2.43 ppm as a singlet integrating for three protons. Additionally, isopropyl protons **H-6** have the largest intensity, resonating as the most de-shielded protons at δ = 1.57 ppm as a doublet due to splitting by the **H-5** proton, which in-turn resonates as heptate/septate near-downfield at δ = 4.61 ppm (J = 6.90 Hz). With the core structure nearly the same as that of **15**, similar signature profiles were recorded in the ^{1}H-NMR spectra of this series with variations depending on the substitution.

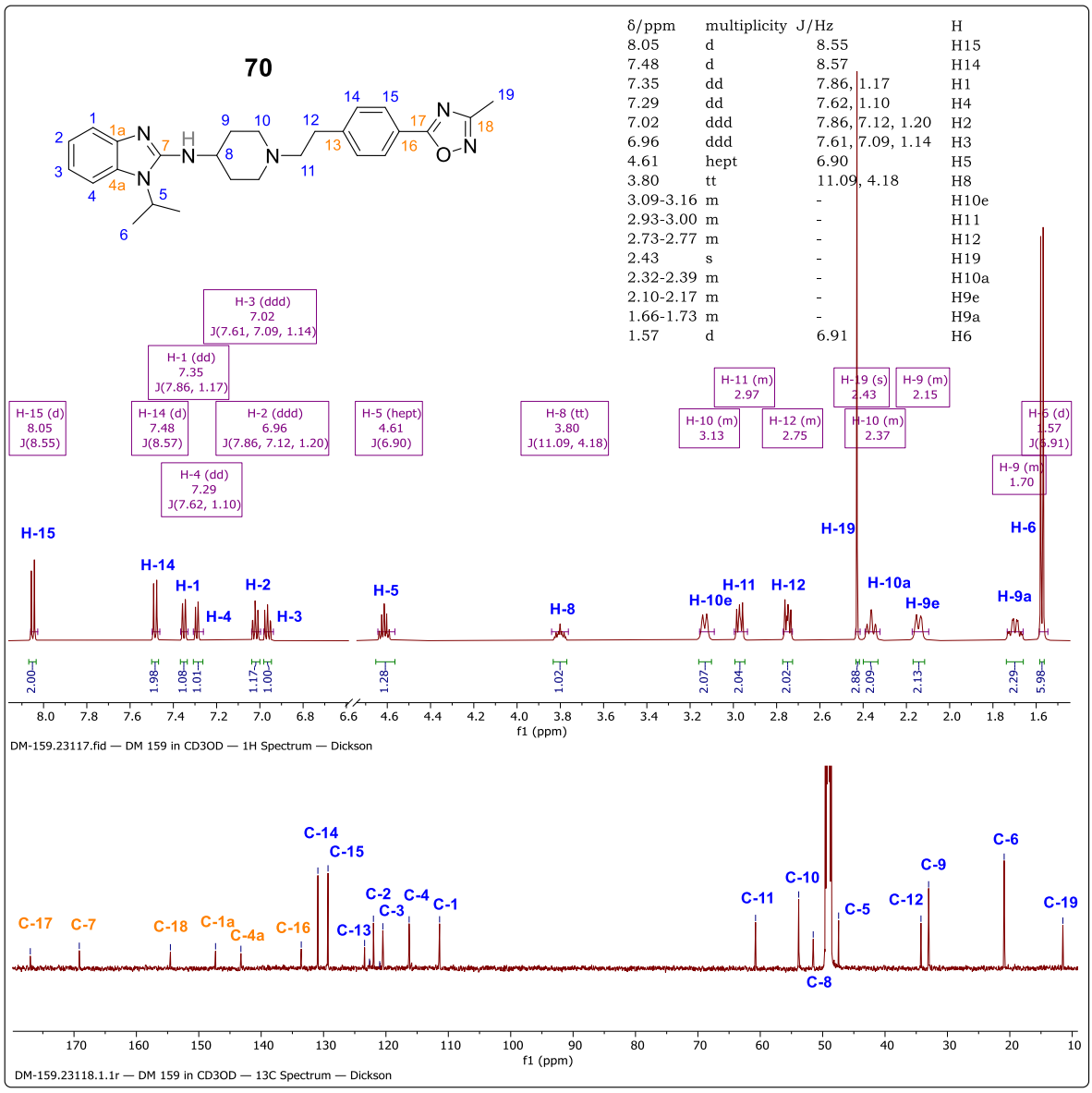

Figure 2. 20: ^{1}H-NMR (*top*) and ^{13}C-NMR (*bottom*) spectra of **70** in methanol-d_4 at 400 and 101 MHz, respectively.

The ^{13}C-NMR spectra further confirmed the structures of these analogues. For **70**, twenty-one (21) carbon signals were obtained, representing twenty-six (26) carbon atoms present in the molecule (Figure 2.20). Oxadiazole carbons **C-17** experienced the least shielding, resonating at δ = 171.01 ppm. **C-19** was the most shielded, consistently resonating in the aliphatic carbon range at δ = 11.49 ppm. In the same way, isopropyl carbons **C-6** (×2) were represented by one high intensity signal at δ = 20.90 ppm due to their similar chemical environment.

Further structural validation was achieved by the HPLC-MS chromatogram and spectra as shown in Figure 2.21.

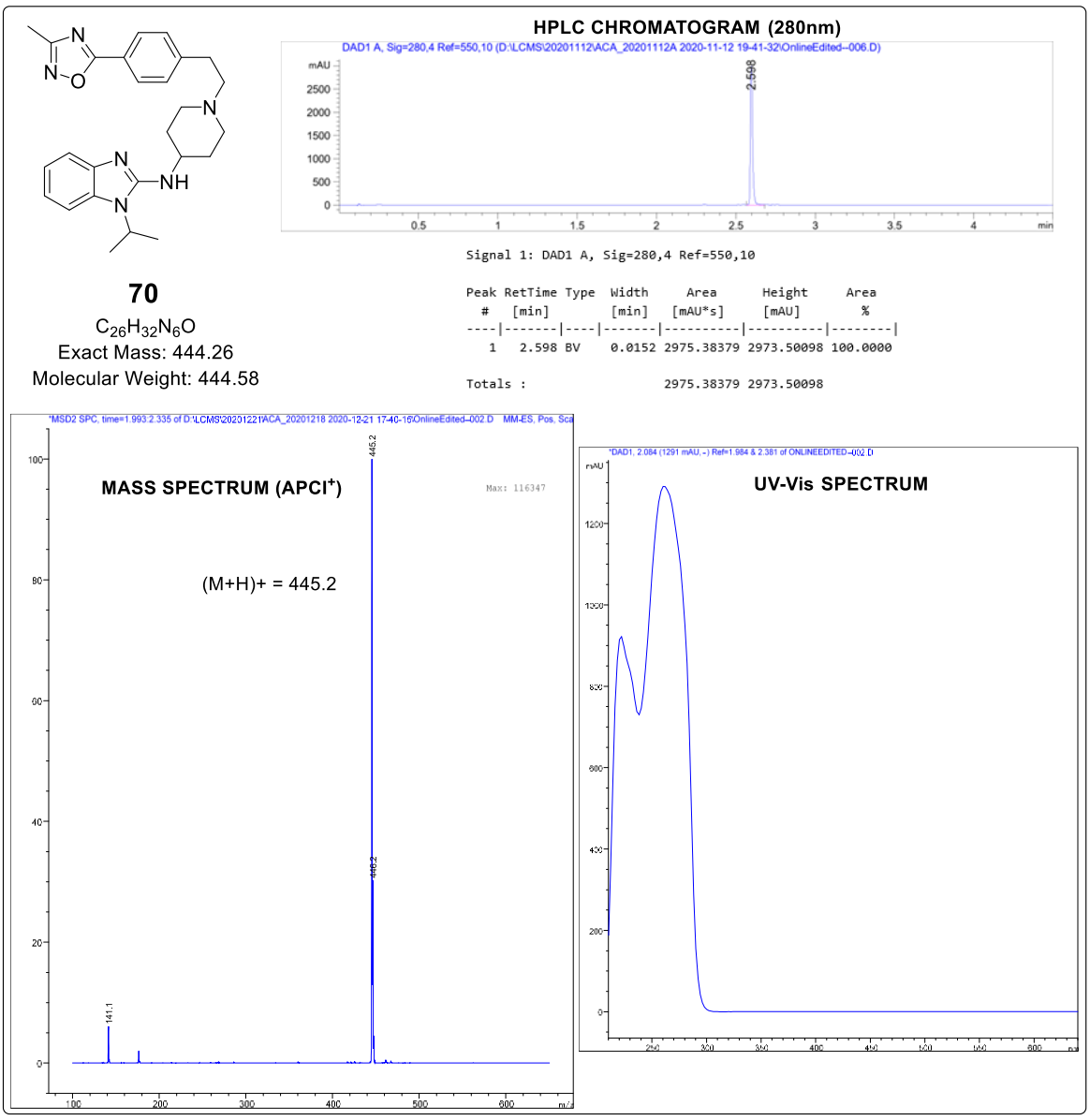

Figure 2.21: HPLC-MS chromatogram and spectra of compound **70.**

Purity was determined to be >99% based on the percentage peak area in the chromatogram. MS in positive ionization mode revealed a pseudo-molecular ion [M+H]+ of 445.2 as the base peak (100%) consistent with the calculated exact mass for $C_{26}H_{32}N_6O$. The UV-Vis spectrum revealed λ_{max} = 235 and 260 nm as the absorption maxima for this compound.

2.4 Phase II AST Analogues: Rationale & Design

The SAR and structure-property relationships (SPR) in exploratory phase I revealed that activity could be retained, solubility improved, and high metabolic stability achieved following the removal of the benzyl moiety (**66**/**67**) or its replacement with a *N*-methyl group (**68**/**69**), if a CH_3- or CF_3-substituted 1,2,4-oxadiazole was present in the lateral phenyl group. Additionally, the SAR validated the significance of the 4-amino piperidine moiety (Chapter 3). Therefore, these three structural features were maintained, and

compounds **67** and **68** were used as templates for the design of advanced phase II analogues (Figure 2.22).

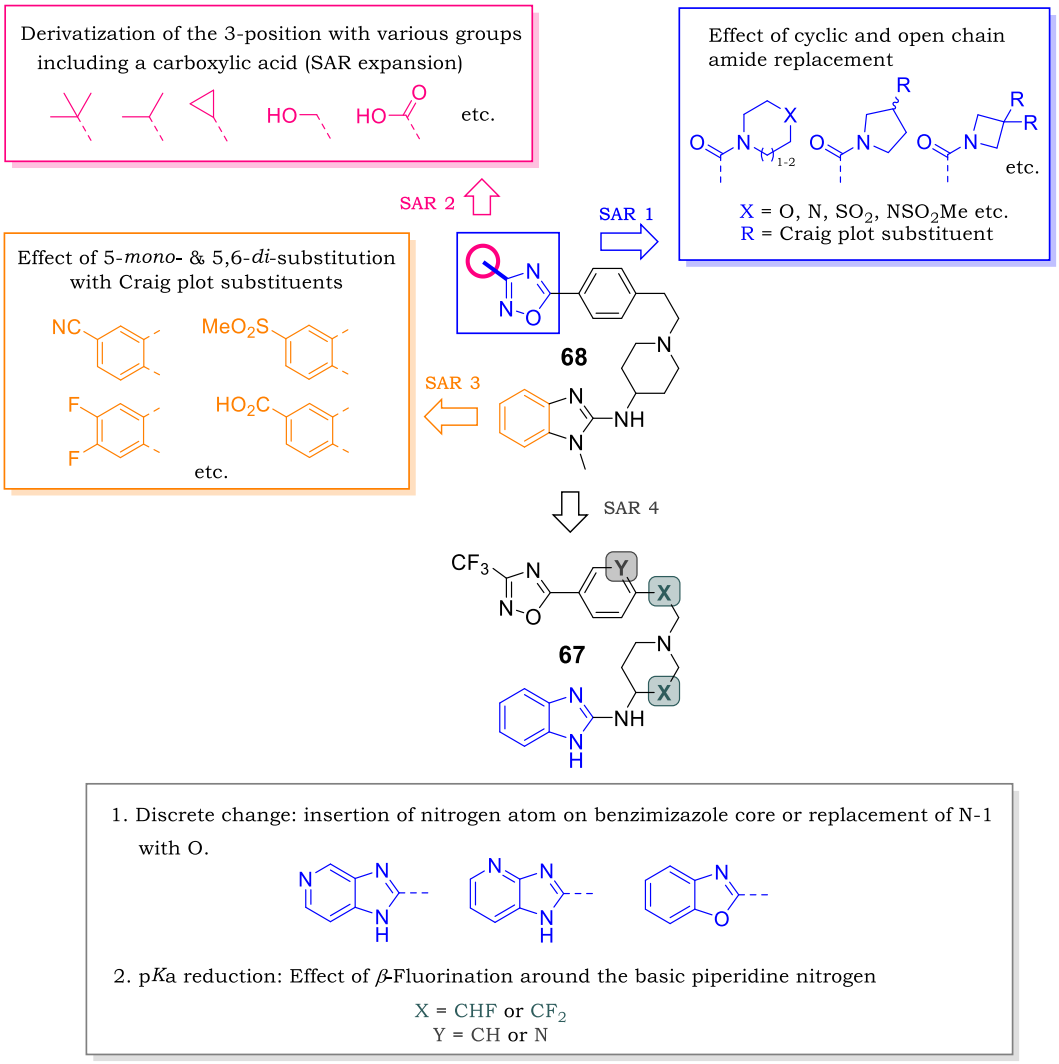

Figure 2.22: SAR-guided design of phase II AST analogue based on compounds **67** and **68**

Furthermore, removal of the benzyl moiety would result in analogues with lower MW and lower lipophilicity (clogP). Therefore, this approach was envisaged to further improve physicochemical properties and potentially reduce affinity for the hERG K+ channel relative to AST.

Amides have been extensively used as bioisosteric replacements of esters. The increased rigidity of amides makes them less likely to be metabolized. Additionally, amidation is often used as a strategy to mitigate hERG liability.[42,43] Therefore, **SAR 1** involved the design and preparation of a small and structurally diverse library of amides (Figure 2.22), which were synthesized as replacements of the oxadiazole moiety in compound **68.** A variety of open-chain and cyclic amides of different sizes was explored. Additionally, to extend the SAR in the 1,2,4-oxadiazole moiety, the 3-position was functionalized with groups that would impart varying steric and electronic effects (**SAR 2**). Synthetically accessible short aliphatic groups (i.e., *iso*-propyl, cyclopropyl, and *tert*-butyl) and water solubilizing groups (i.e., OH, SCH_3, $N(CH_3)_2$, and CO_2H) were considered.

Next, the benzimidazole ring was explored. In AST, cytochrome P450-mediated hydroxylation at benzimidazole 6-position generates a 6-hydroxy metabolite.[45] To block this site and study the effect of substitution, a series of 5- and 6-substituted benzimidazole analogues were designed (**SAR 3**) and synthesized by incorporating various Craig plot substituents. To that effect, **SAR 4** focused on discrete modifications in the benzimidazole scaffold. The SAR around the replacement of the benzimidazole heterocycle has not been investigated previously, therefore, various strategies towards reducing hERG affinity such as incorporating nitrogen in the benzimidazole ring, replacement of benzimidazole N-1 with oxygen (NH to O) were utilized. Additionally, SAR 4 involved β-fluorination around the piperidine nitrogen. This was envisaged to reduce the nitrogen basicity (p*K*a) as a strategy to reduce the hERG affinity of resulting compounds (Figure 2.22).[44]

2.5 Chemistry: Phase II

2.5.1 Synthesis of Phase II SAR 1 and 2 Analogues

The preparation of amides and oxadiazoles was initiated by the synthesis of esters **79** and **80** via nucleophilic substitution between **9** and **8** with **14b**, respectively. Hydrolysis of **79** *via* refluxing in aqueous NaOH and methanol followed by acidic workup afforded carboxylic acid **81** in quantitative yield. The next reaction involved chlorination *via* refluxing in $SOCl_2$ to quantitatively produce the common intermediate acyl chloride **82**. Amides **83–111** (Scheme 2.16A) were prepared by directly coupling commercially available amines to crude acyl chloride **82** in the presence of TEA in THF at room temperature (16–20 °C). All amides comprising the Boc protecting group were further deprotected to furnish free amines.

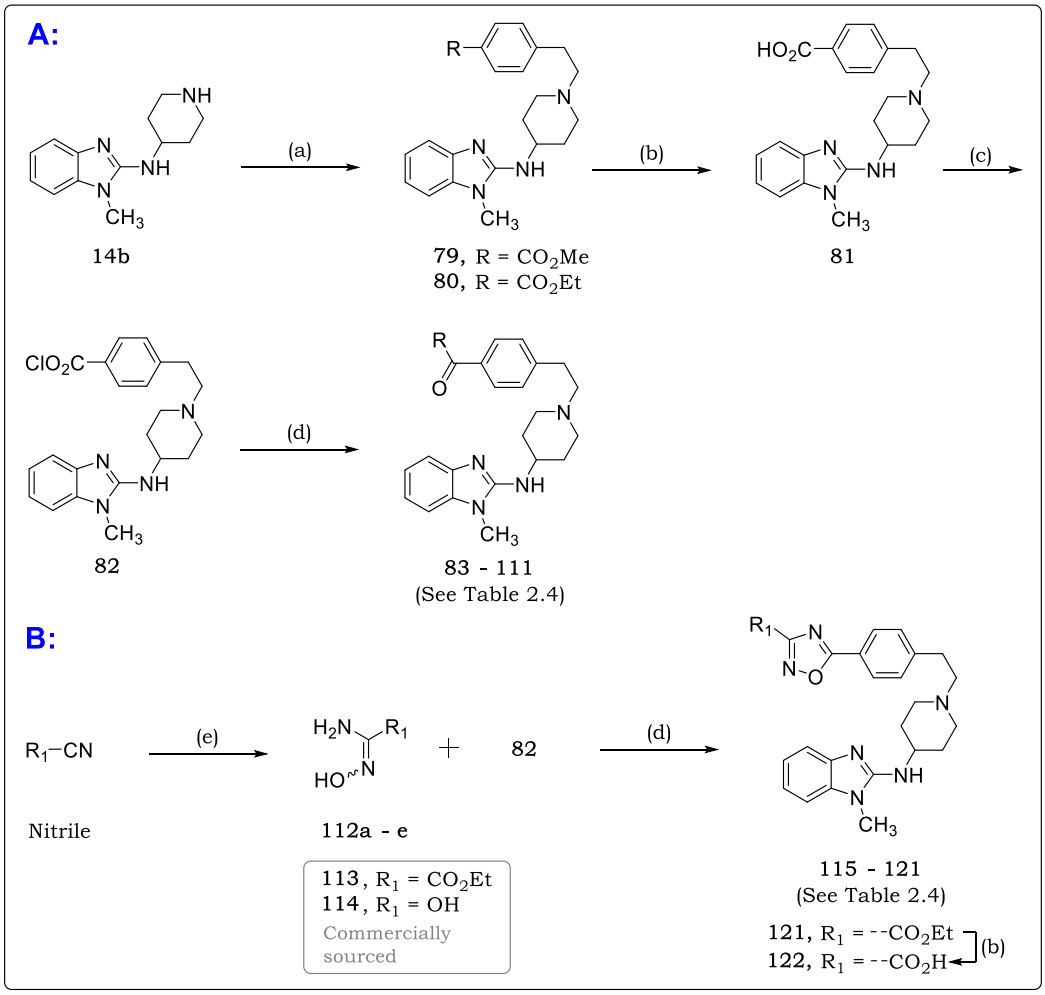

Scheme 2.16: Synthetic protocol towards phase II **SARs 1** and **2** target compounds **79–122**

Reagents and conditions: (a) **9**, K_2CO_3, 80 °C, 5 h (68%); (b) (i) 2M NaOH, MeOH (for **80**) or EtOH (for **122**), 78 °C, 2h (ii) 3N HCl, pH 2, 20 °C (98%); (iii) $SOCl_2$, 81 °C, 2 h (99%); (c) **112a–e**, **113** or **114**, TEA, THF, 20 °C, 6–10 h followed by K_2CO_3, 80 °C, 16 h (44–60% over two steps); (d) (i) 2M NaOH, EtOH, 80 °C, 15 h (ii) 3N HCl, Ph 2, 20 °C (92%); (e) *(i)* $NH_2OH{\cdot}HCl$, 8-hydroxyquinolone, TEA, ethanol, 79 °C reflux, 1.5 h, *(ii)* 21 °C, 10% HCl, Ph 3 (70–82%); (f) TFA, DCM, 20 °C, 3 h (80–89%).

To prepare 1,2,4-oxadiazoles, a series of amidoximes (**112a–e**) were first synthesized *via* treatment of respective nitriles with hydroxylamine hydrochloride by refluxing in ethanol in the presence of TEA and catalytic amounts of 8-hydroxyquinolone (Scheme 2.16B). Following an acidic work-up using 3N HCl, pure amidoximes were obtained in high yields (80–89%). Coupling of amidoximes to acyl chloride **82** resulted in *O*-acylamidoximes intermediates, which without isolation nor purification were treated with K_2CO_3 and refluxed in acetonitrile to initiate cyclocondensation, resulting in 3-substituted-5-phenyl-1,2,4-

oxadiazoles **113–121**. The 1,2,4-oxadiazole-3-carboxylic acid analogue **122** was obtained *via* hydrolysis of its ethyl ester precursor **121** in ethanol.

The isolated yields of both amides and functionalized 1,2,4-oxadiazoles (over two steps) are summarized in Table 2.4.

Table 2.4: Isolated yields for phase II **SAR 1** and **2** compounds (amides and 1,2,4-oxadiazoles)

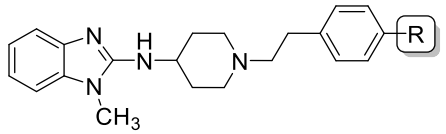

Code	R	Yield (%)
79	CO_2Me	68
80	CO_2Et	77
81	CO_2H	98
83		88
84	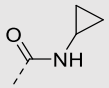	79
85	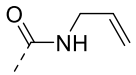	66
86	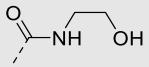	82
87	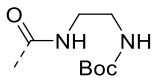	85
88	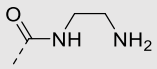	98
89	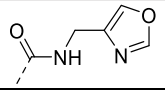	76

Code	R	Yield (%)
90	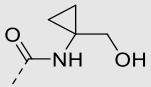	71
91	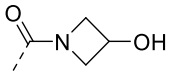	87
92	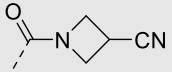	79
93	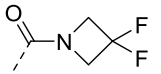	86
94	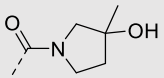	77
95	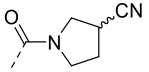	69
96	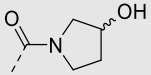	62
97	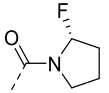	74
98	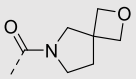	77
99	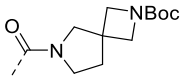	85

Code	R	Yield (%)
100	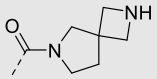	89
101	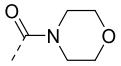	76
102	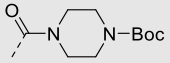	93
103	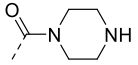	91
104	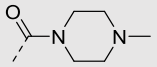	77
105	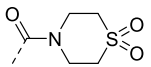	74
106	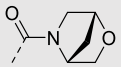	71
107	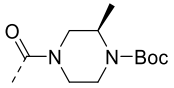	88
108	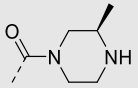	86
109	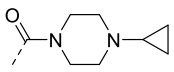	85

Code	R	Yield (%)
110	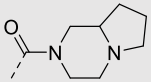	73
111	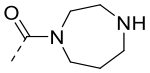	51
115	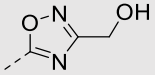	44
116	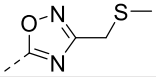	51
117	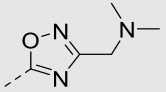	53
118	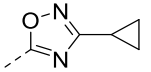	56
119	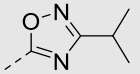	61
120	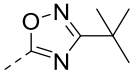	66
121	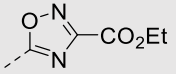	52
122	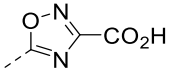	96

2.5.1.1 Characterization of Phase II SAR 1 and 2 Analogues

Mechanisms leading to the formation of these analogues are well-known and are therefore not shown. However, evidence of the formation of carboxylic acid (**81**) is presented. The stacked ^{1}H-NMR of **81** from **14b** are shown in Figure 2.23 below.

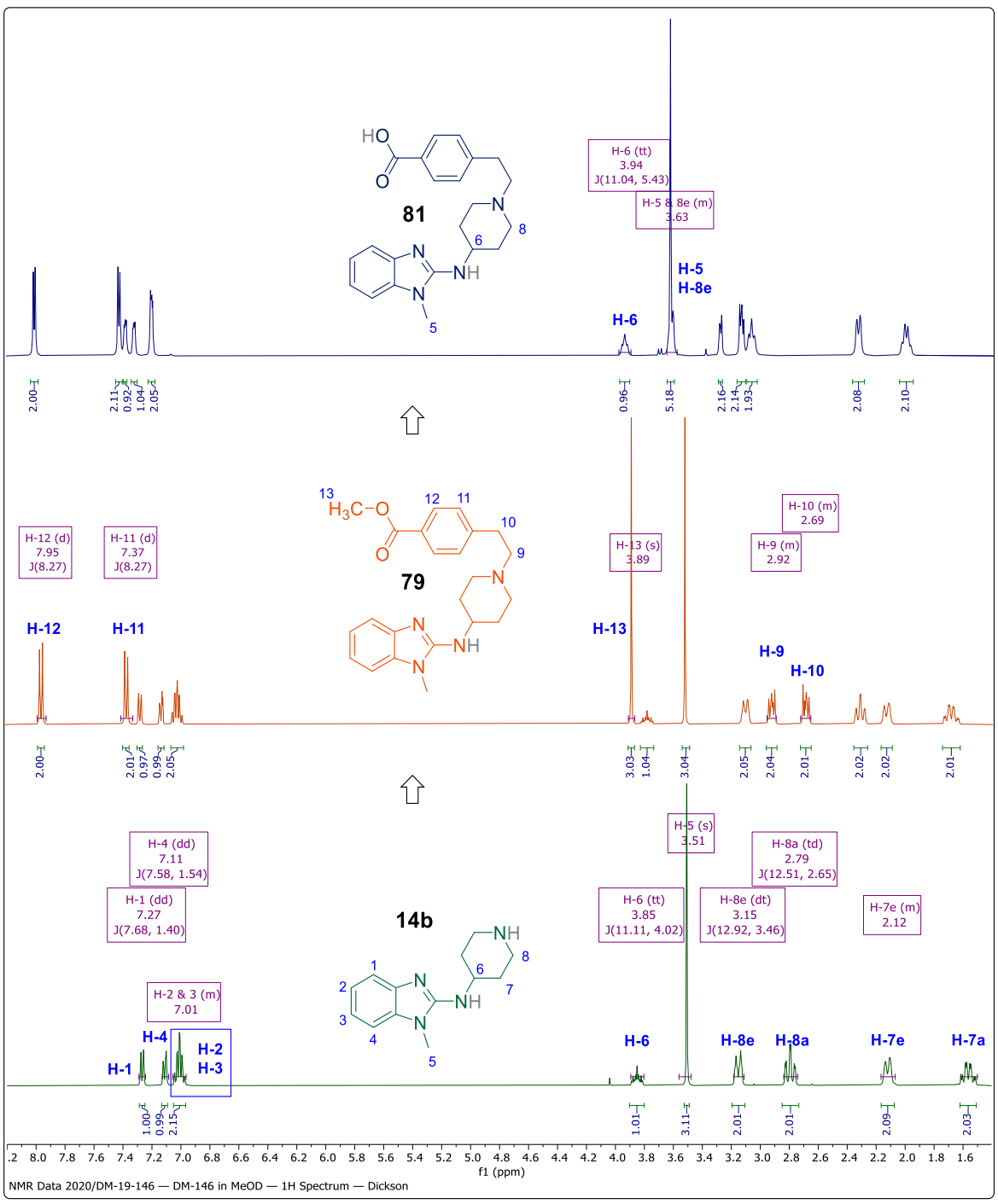

Figure 2.23: Stacked ^{1}H-NMR spectra for synthetic intermediates **14b**, **79** & **81** in methanol-d_4 at 300 MHz

Successful preparation of methyl ester **79** was confirmed by the appearance of; (i) two doublets (**H-11** and **H-12**, J = 8.27 Hz) in the aromatic region at δ = 7.37 and 7.95 ppm,

(ii) two multiplets upfield (δ = 2.92 and 2.69 ppm, respectively), each integrating for two methylene protons **H-9** and **H-10** and (iii) a methyl singlet upfield (δ = 3.89 ppm). These provided evidence of the successful synthesis of ester intermediate **79**. Formation of the hydrolysis product **81** was confirmed by the disappearance of the methyl singlet signal following ^{1}H-NMR analysis in protic solvent methanol (Figure 2.23).

The ^{1}H-NMR and ^{13}C-NMR spectra of amide **109** are shown as examples for this class of compounds. The appearance of aliphatic protons with a distinctive piperazine (**H-18** and **H-19**) proton broad singlet at δ = 2.33 ppm integrating for eight protons and the singlet at δ = 2.21 ppm representing four chemically equivalent cyclopropyl **H-21** protons is shown in Figure 2.24.

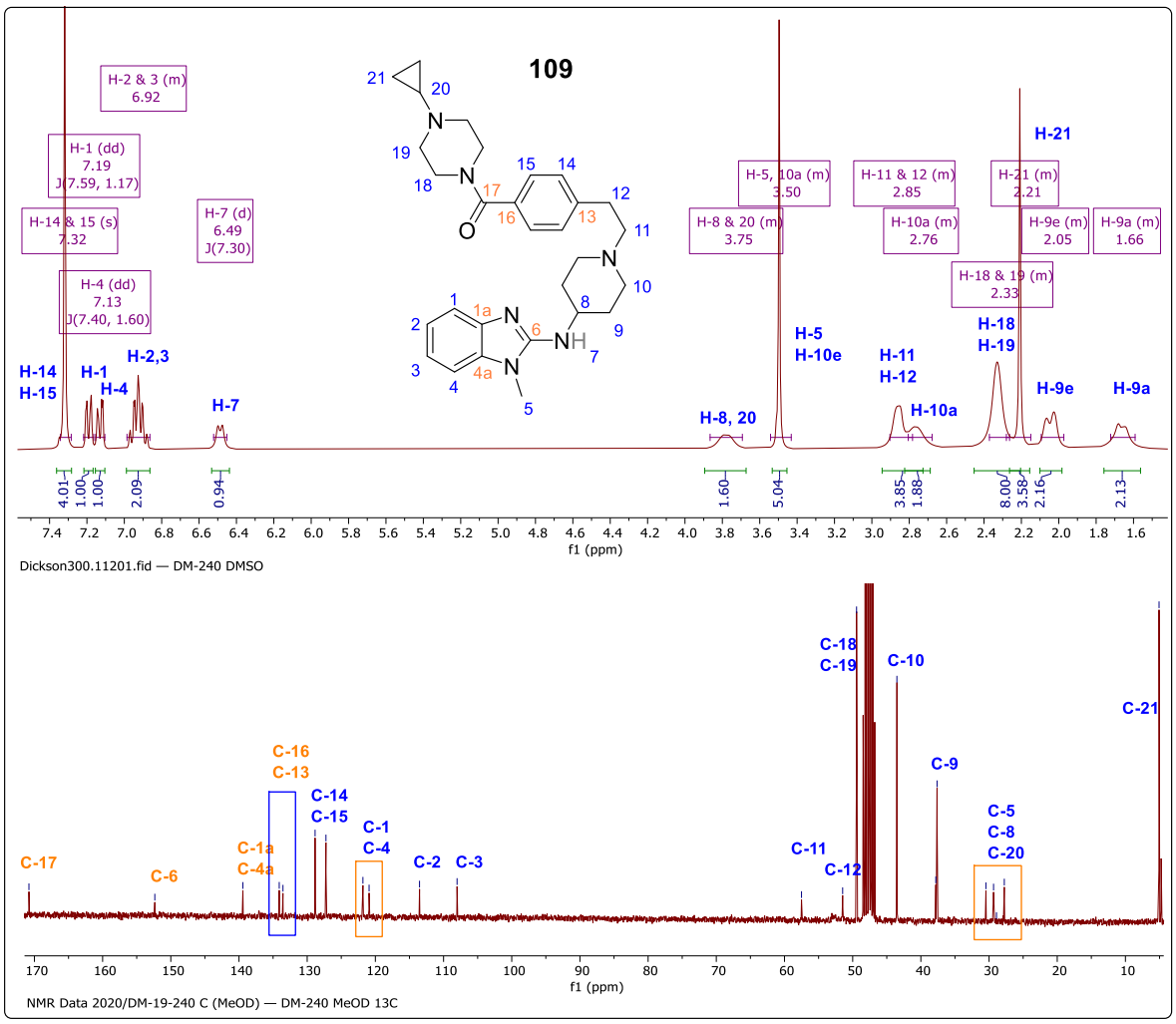

Figure 2. 24: ^{1}H-NMR (*top*) and ^{13}C-NMR (*bottom*) spectra of **109** in DMSO-d_6 and methanol-d_4 at 300 and 101 MHz respectively

Consistently, ^{13}C-NMR analysis revealed these piperazinyl (**C-18** and **C-19**) and cyclopropyl carbons (**C-21**) as distinctive singular signals at δ = 49.43 and 5.00 ppm, respectively.

2.5.2 Synthesis of Phase II SAR 3 Analogues

Two separate but converging routes (A and B) were used to synthesize 5,6-disubstituted and 5-substituted benzimidazole precursors (Scheme 2.17) below.

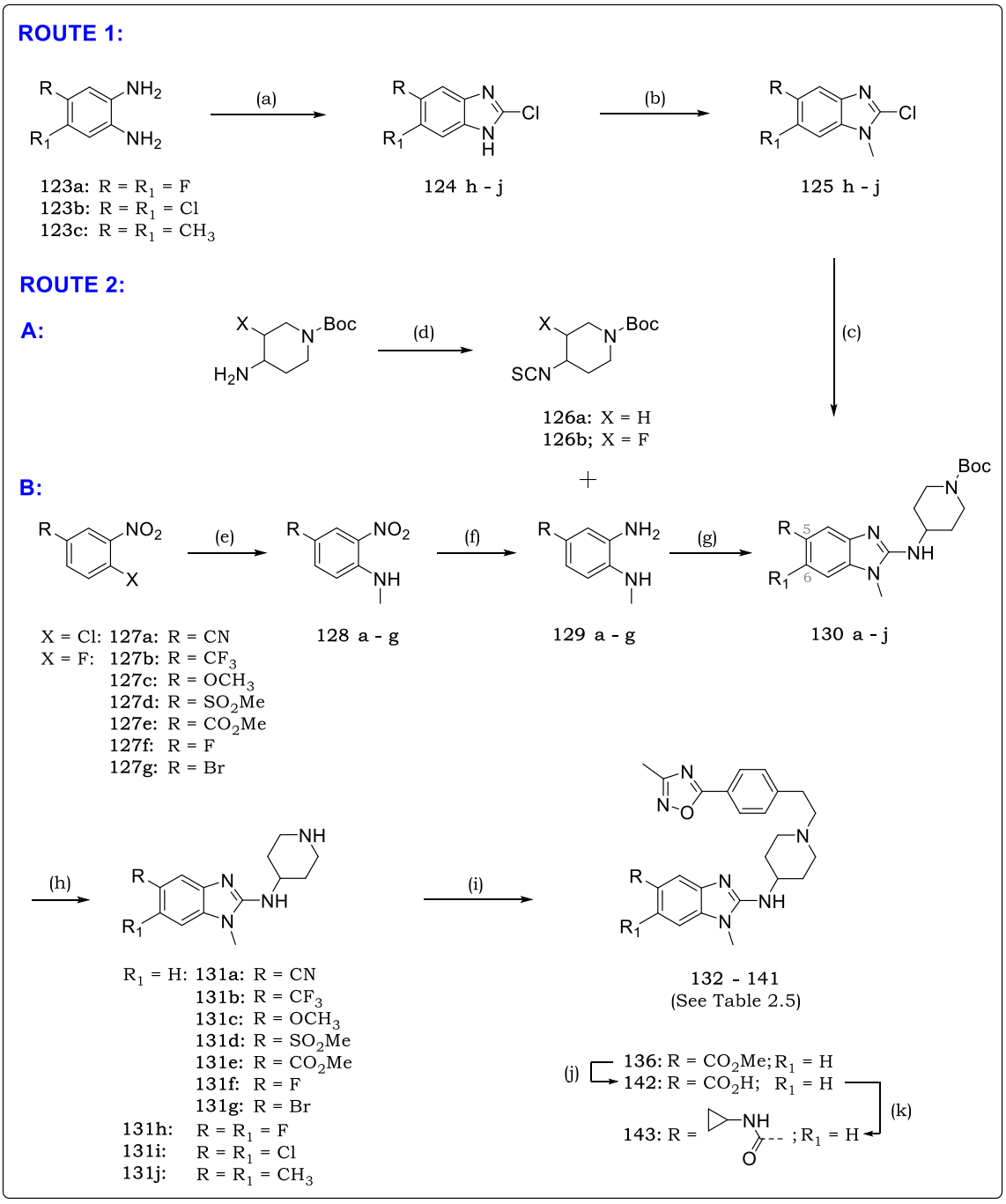

Scheme 2.17: Synthetic protocol towards phase II, **SAR 3** target compounds **132–143**

Reagents and conditions: (a) (i) CDI, DMAP, THF, 20 °C, 12 h (quant'); (ii) $POCl_3$, 110 °C, 12 h (58–93%); (b) MeI, Acetone, K_2CO_3, 23 °C, 2 h (90–97%); (c) *tert*-butyl 4-aminopiperidine-1-carboxylate, TEA, 150 °C, 2–12 h (66–85%); (d) TCDI, DMF, 23 °C, 12 h (88–97%); (e) $MeNH_2$ (2M in THF), TEA, MeCN, 65 °C, 4–18 h, (66–88%); (f) H_2, balloon, 10% Pd/C, 1:1 MeOH/EtOAc, 21 °C, 12 h (89–96%); (g) DCC, TEA, MeCN, 85 °C, 12 h (80–95%); (h) TFA, DCM, 21 °C, 3 h (71–98%); (i) **7a**, MeCN, 85 °C, 8–12 h (46–78%); (j) (i) 2M NaOH, EtOH, 25 °C, 12 h; (ii) 3N HCl, Ph 2, 20 °C (**142**, 94%); (k) Cyclopropylamine, EDCI/DMAP, DCM, 20 °C, 2 h (**143**, 48%).

Preparation of 5-substituted precursors was initiated by S_NAr reaction between methylamine (2M in THF) and an appropriate 4-substituted-1,2-halo-nitrobenzene in the presence TEA at 65 °C in MeCN (Scheme 2.17, Route 2B). The resulting 1,2-amino-nitrobenzenes were then subjected to reduction [H_2, Pd/C] to afford diamines **129 a**–**g** in high yields (89 – 96%).

N,*N*'-Dicyclohexylcarbodiimide (DCC)-mediated cyclization of the diamines **129 a**-**g** with isothiocyanate **126a** in MeCN produced 2-amino benzimidazoles **130 a**–**g** in moderate yields (48 – 79%). Intermediates **130 h**–**j** were accessed *via* an initial cyclization of appropriate and commercially available 4,5-disubstituted-1,2-diamines with carbonyldiimidazole (CDI) as shown in scheme 2.17, Route A. This was followed by chlorination using $POCl_3$ to produce corresponding 5,6-disubstituted-2-chloro-1*H*-benzimidazoles **124 h**–**j**. *N*-methylation using methyl iodide afforded 5,6-disubstituted-1-methyl-2-chlorobenzimidazoles **125 h**–**j** which were then subjected to S_NAr with *N*-Boc-4-aminopiperidine in TEA at 150 °C. Deprotection of **130 a**–**j** using TFA afforded free amines **131**, which were subsequently coupled (S_N2) with **7a** to afforded final compounds **132**–**141** in good yields (46 – 78%). The carboxylic acid analogue **142** was obtained *via* hydrolysis of ester **136** under basic conditions. Amide coupling of **136** with cyclopropylamine using EDCI/DMAP afforded amide **143**. The isolated yields of these analogues are outlined in Table 2.5.

Table 2.5: Isolated yields for phase II **SAR 3** benzimidazole-core substituted 3-methyl-1,2,4-oxadiazoles.

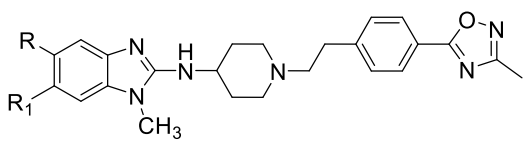

Code	R	R_1	Yield (%)
132	CN	H	69
133	CF_3	H	62
134	OCH_3	H	54
135	SO_2Me	H	64
136	CO_2Me	H	78
137	F	H	65

Code	R	R_1	Yield (%)
138	Br	H	77
139	CH_3	CH_3	48
140	F	F	53
141	Cl	Cl	46
142	CO_2H	H	94
143	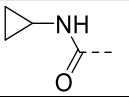	H	81

2.5.3 Mechanistic Details for the Synthesis of Phase II SAR 3 Analogues

2.5.3.1 Cyclization (Step A (i), Scheme 2.18)

Formation of the 1,3-dihydro-2-benzimidazolone intermediate results from a sequence of two nucleophilic addition-elimination reactions by the aromatic diamine nitrogen atoms and the CDI carbonyl centre (Scheme 2.18). By-product of this step are imidazole

molecules which are highly water-soluble, and the crude product is thus isolated in quantitative yield by mere filtration following the addition of water.

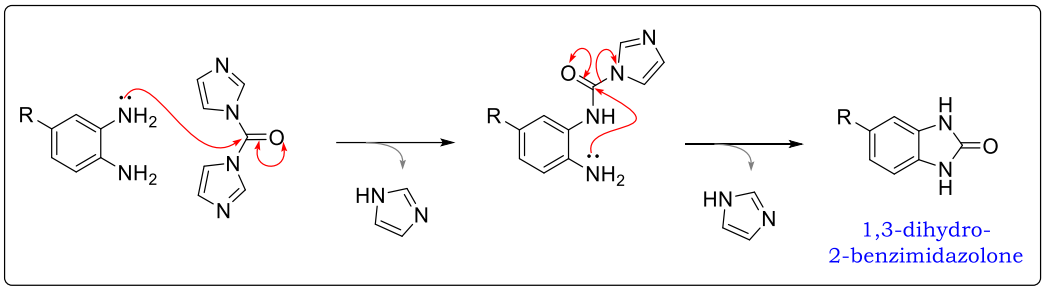

Scheme 2.18: Proposed reaction mechanism for CDI cyclization

2.5.3.2 Chlorination using POCl3 (Steps A (ii), Scheme 2.18)

Chlorination using $POCl_3$ is thought to occur *via* a 2-dichlorophosphoryl intermediate **A** (Scheme 2.19), resulting from nucleophilic attack of the phosphorus in $POCl_3$ by the oxygen atom followed by elimination of a chloride ion. The chloride ion then attacks on the electron-deficient, oxygen-bearing carbon in **A**, leading to the elimination of phosphenothioic chloride (PO_2Cl), hydrochloric acid and the desired 2-chlorobenzimidazole product.

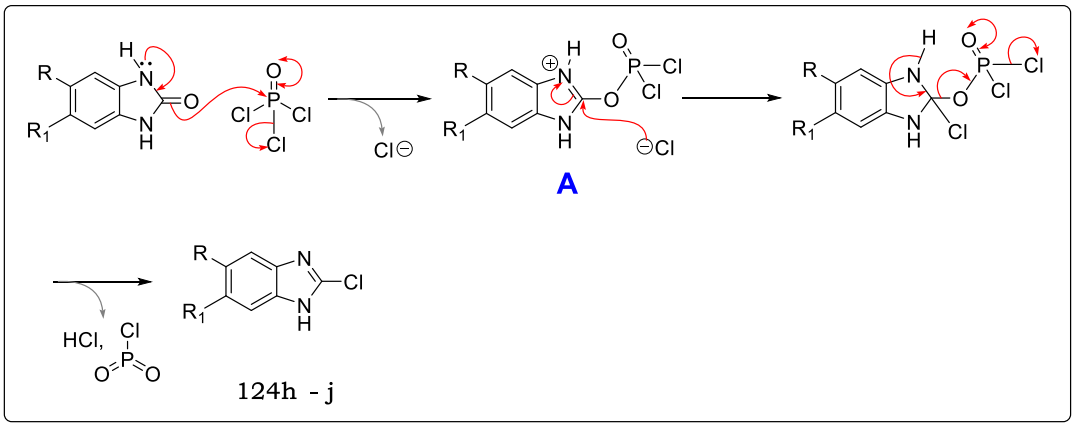

Scheme 2.19: Proposed reaction mechanism for $POCl_3$ chlorination

2.5.3.3 DCC-mediated Cyclocondensation (Step G, Scheme 2.18)

As shown in Scheme 2.20, the nucleophilic amino nitrogen of the benzene-1,2-diamine attacks the electrophilic isothiocyanate carbon to form the thiourea intermediate **B**. TEA then abstracts a proton from the aromatic-thiourea nitrogen pushing the electrons into the electron-deficient thiourea carbon. This leads to nucleophilic attack by the thiocarbonyl π-electrons onto the DCC carbodiimide carbon atom leading to the formation of intermediate **C**.

Nucleophilic cycloaddition by the second nitrogen of the diamine onto the thiourea carbon center leads to an unstable resonance stabilized anion **D**, which quickly undergoes

aromatization leading to the elimination of a thiourea by-product and formation of the desired 2-amino-1*H*-benzimidazole product. The steps that follow are *N*-Boc deprotection in acidic media and S_N2 reaction to form the final product(s) as previously described.

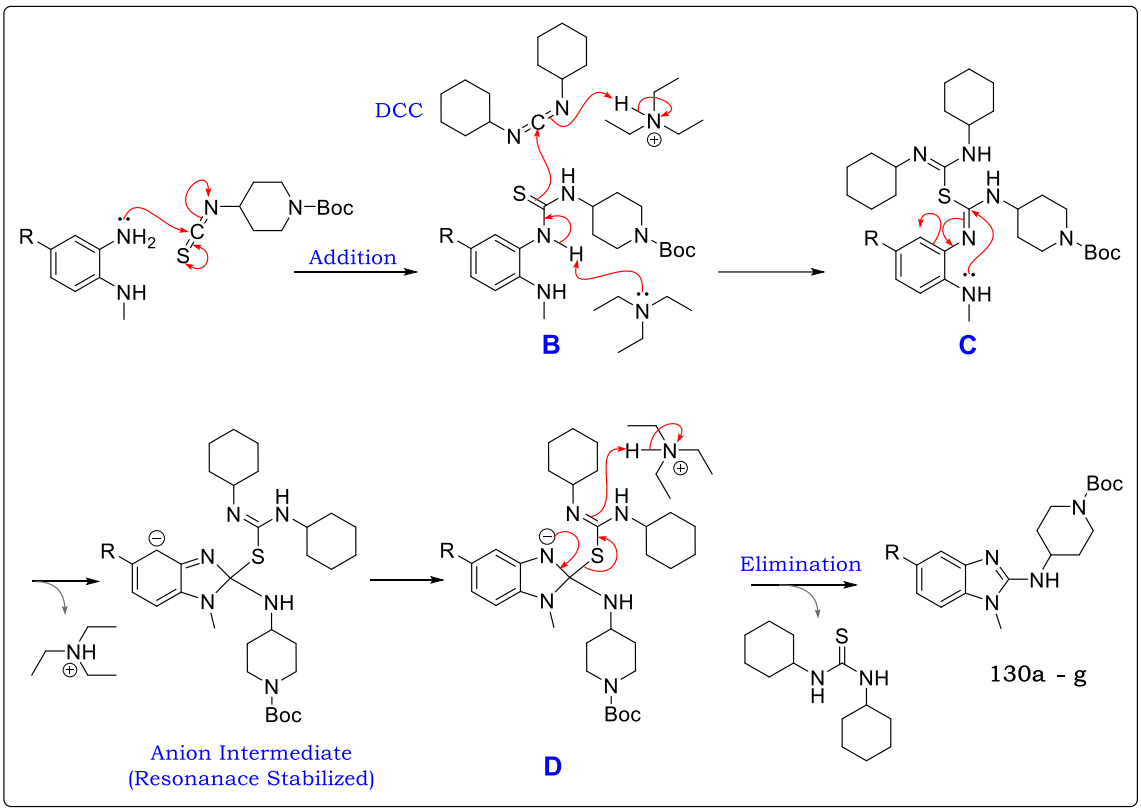

Scheme 2.20: Proposed reaction mechanism for DCC-mediated cyclocondensation

2.5.4 Characterization of Phase II SAR 3 analogues

The characterization of intermediates and final products in **SAR 3** is exemplified by the synthesis of 5-trifluoromethy-benzimidazole analogue **133**. Spectroscopic build up leading to the preparation of **131b**, a free amine intermediate is shown in the stacked ^{1}H-NMR spectra shown in Figure 2.25. The formation of *N*-methyl intermediate **128b** from the S_NAr step consistently showed three aromatic proton signals. This was confirmed by the appearance of methyl protons **H-5** (Figure 2.25) as a doublet (J = 5.56 Hz) at δ = 3.00 ppm and N-H proton (**H-4**) as a weak quartet (J = 5.56 Hz) at δ = 8.50 ppm. Following nitro reduction (**129b**), NH_2 protons (**H-5**) were observed at δ 5.00 ppm as a singlet. Formation of **130b** *via* DCC-mediated cycloaddition was confirmed by the appearance of piperidine aliphatic protons (**H-6**, **H-7**, and **H-8**), the *tert*-butyl protons (**H-9**) singlet and the 2-amino N-H (**H-5**) proton doublet downfield. Following N-Boc deprotection, the spectra of **131b** was devoid of the *tert*-butyl signal upfield, thus confirming its identity.

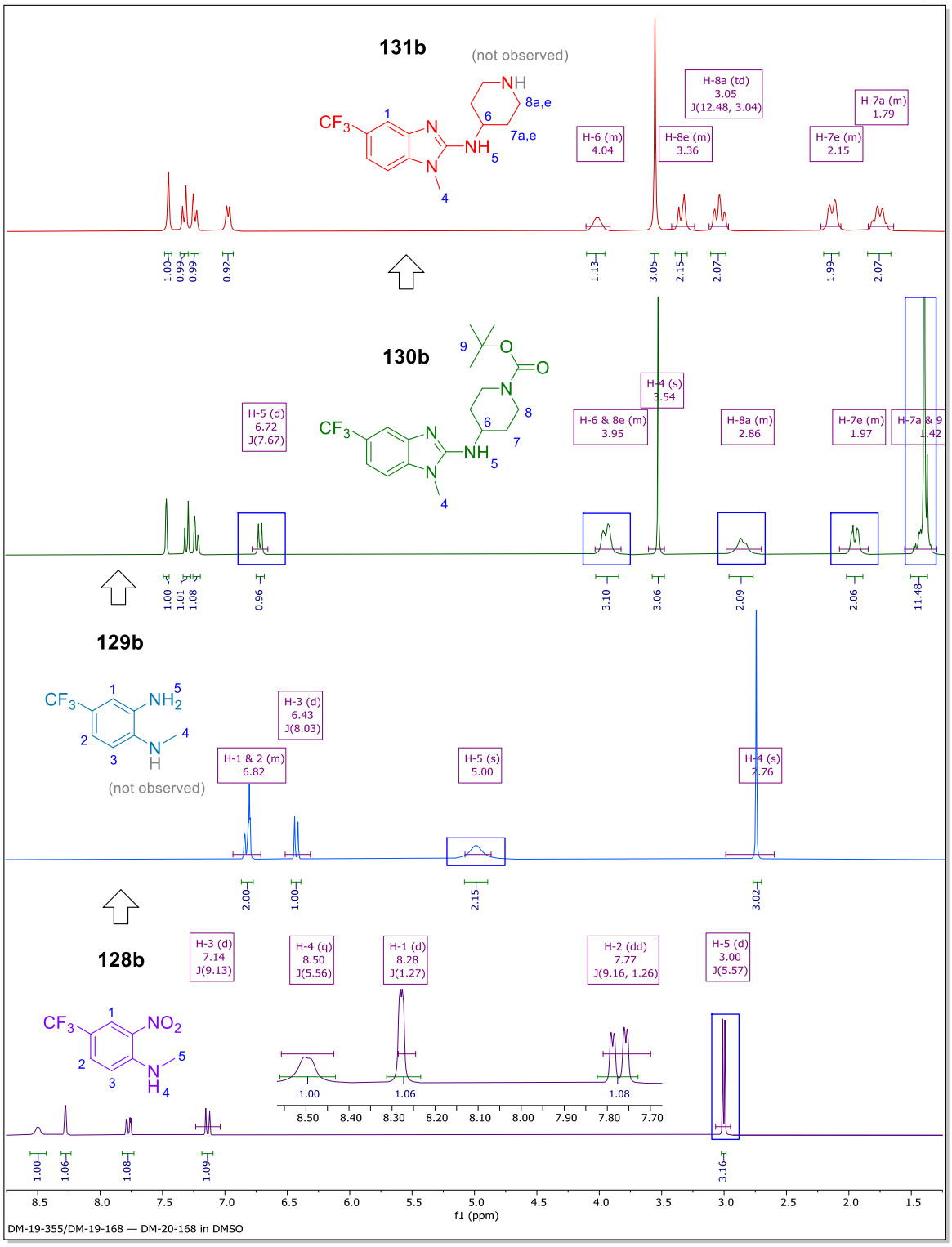

Figure 2.25: Stacked ^{1}H-NMR spectra (*from bottom to top*) from **128b** to **131b** in DMSO-d_6 at 300 MHz

Having been fully characterized, **131b** was used in the next step to prepare analogue **133**. In the ^{1}H-NMR spectra of compound **133** (Figure 2.26), the signature peaks observed in **131b** are retained, with the appearance of **H-15** and **H-16** as two doublets coupling with each other in the aromatic regions at δ = 7.50 and 8.01 ppm (J = 7.80 Hz). Methylene

protons **H-12** and **H-13** are accounted for as multiplets at δ = 2.92 and 2.41, respectively. Finally, the methyl protons **H-20** resonate as a singlet at δ = 2.08 ppm.

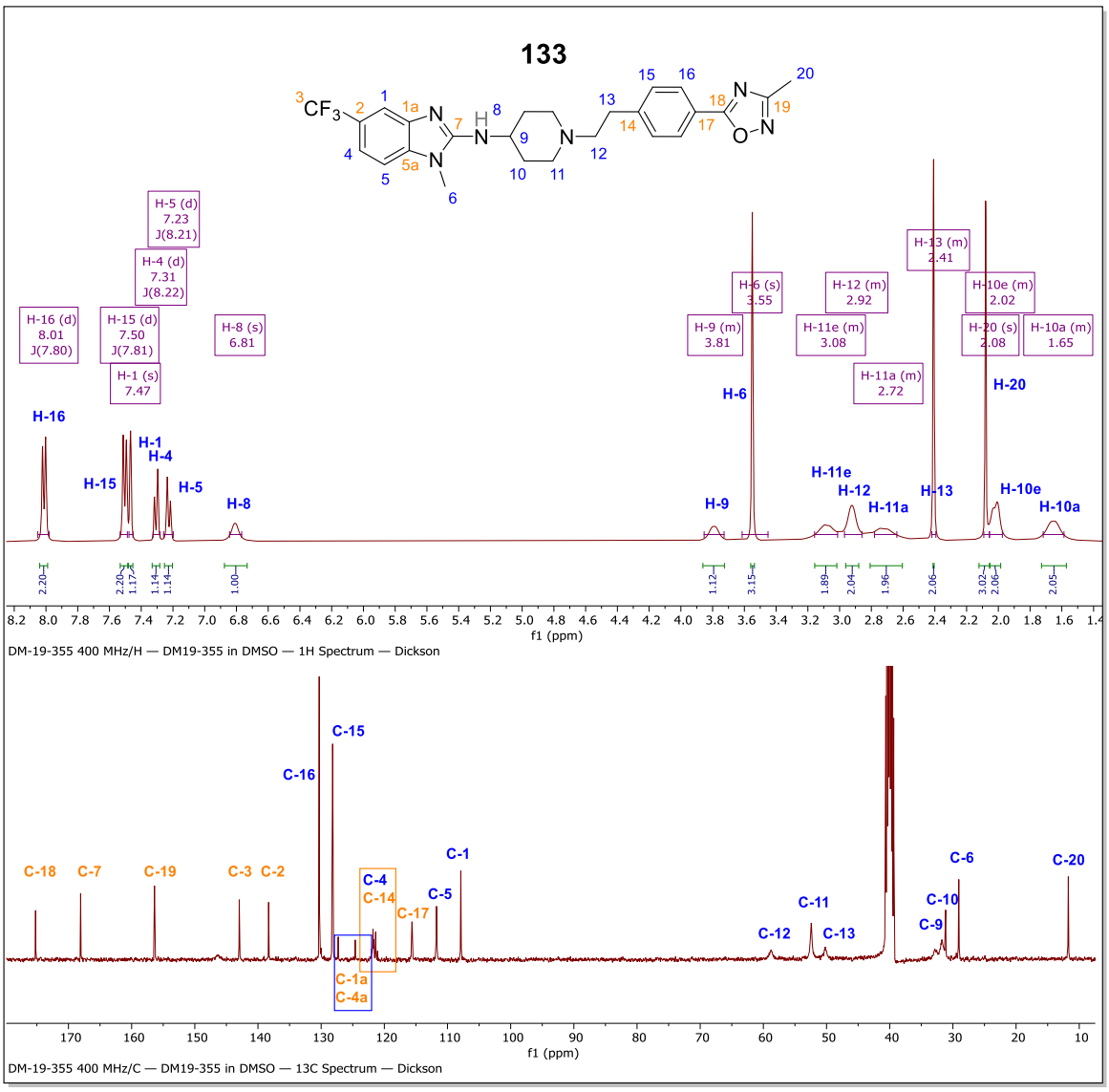

Figure 2.26: ^{1}H-NMR spectrum of **133** in DMSO-d_6 at 400 MHz

^{13}C-NMR analysis further confirmed the structure of **133** and other analogues in this series. As shown in Figure 2.26, the spectrum showed 21 signals representing 25 carbons in the molecule. The chemical shift-equivalent pairs of carbons in the phenyl ring (**C-15** and **C-16**) and the piperidine ring (**C-10** and **C-11**) resonated at the same chemical shifts. Diagnostic carbon signals were attributed to the most de-shielded oxadiazole carbons **C-18** and **C-19** resonating at δ = 175.20 and 156.38 ppm, respectively.

2.5.5 Synthesis of Phase II SAR 4 Analogues

Depending on the aromatic ring (Ar), preparation of compounds **146**–**152** involved two sequential converging routes (Scheme 2.21). In route A, titanium (IV) isopropoxide/sodium triacetoxyborohydride (Ti(O*i*Pr)$_4$/Na(OAc)$_3$BH)-mediated reductive amination between

either 2-amino benzoxazole and *N*-Boc 4-oxopiperidine or 2-amino benzimidazole and *N*-Boc-3,3-difluoro-4-oxopiperidine produced intermediates **144a** and **144b** (Scheme 2.21A) in low to high yields (24–98%). In this reaction, Ti(O*i*Pr)$_4$ acts as both a catalytic Lewis acid and as a water scavenger, as conventional reductive amination conditions (HOAc/Na(OAc)$_3$BH) could not work.

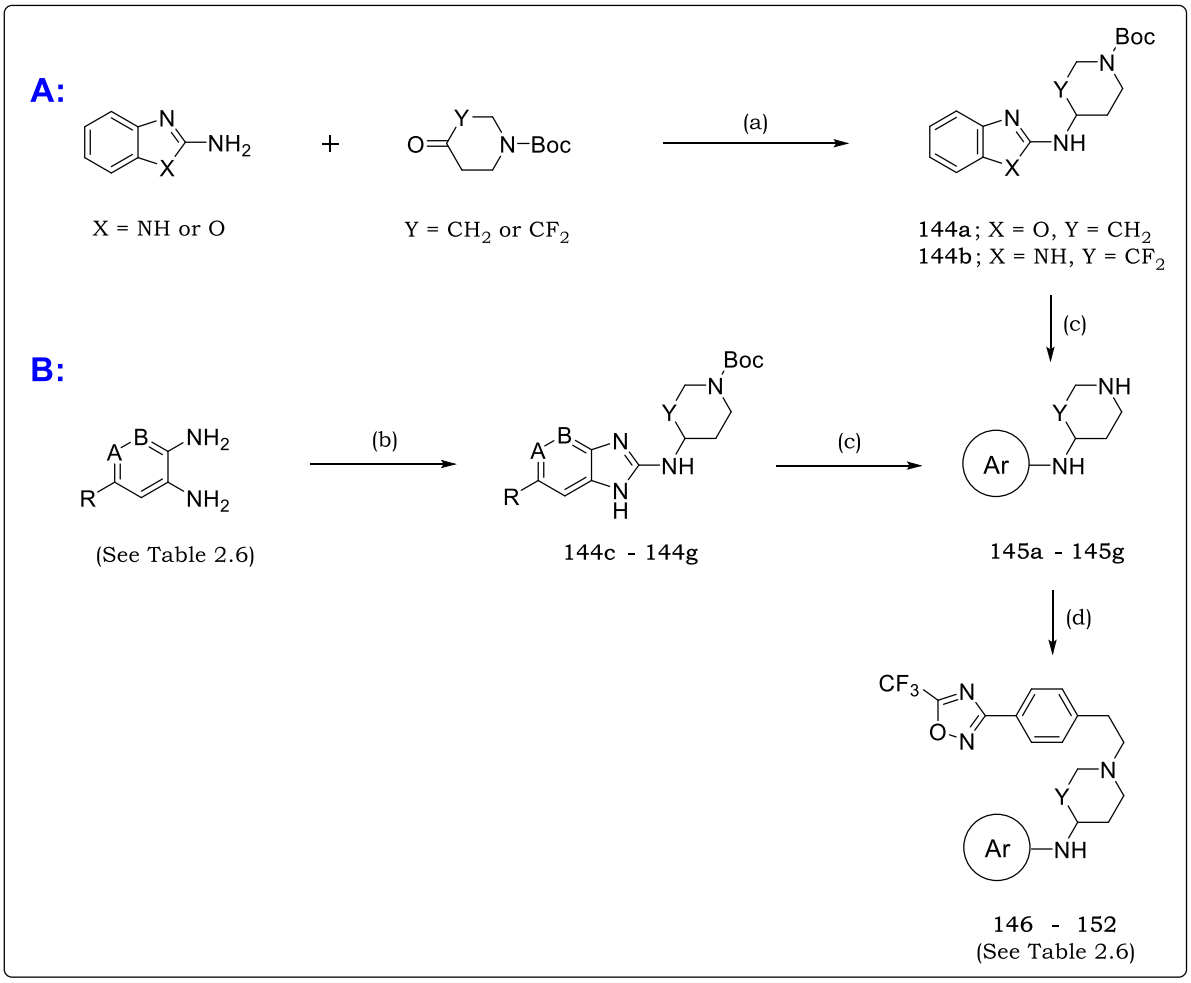

Scheme 2.21: Synthetic protocol towards phase II **SAR 4** target compounds **146–152**

Reagents and conditions: (a) (i) Ti(O*i*Pr)$_4$, THF, 18 °C, 12 h (ii) Na(OAc)$_3$BH, 18 °C, 20 h (24 – 98%); (b) **126a** or **b**, DCC, TEA, MeCN, 85 °C, 12 – 16 h (80 – 90%); (c) TFA, DCM, 24 °C, 3 h (76 – 80%); (d) **3c**, MeCN, 85 °C, 8 – 12 h (23 – 82%).

In route B, *N,N'*-dicyclohexylcarbodiimide (DCC)-mediated condensation of isothiocyanates (**126a** or **b**) with either *O*-phenylenediamine or *O*-diaminopyridines produced **144c**–**g** in high yields (80 – 90%). Following *N*-Boc deprotection of intermediates **144 a** – **g** using TFA and Amberlyst-A21, free bases **145 a** – **g** were coupled (S_N2) with **3c** to provide the final compounds **146** – **152** in low to high yields (23 – 82%).

Synthesis of **SAR 4** pyridyl compounds **156** and **157** (Scheme 2.22A) began with the preparation of aryl vinyl intermediate **153** *via* Suzuki coupling of 4,4,5,5-tetramethyl-2-vinyl-1,3,2-dioxaborolane to 6-bromonicotinonitrile. Regioselective coupling (1,2-addition)

of **153** to piperidines **14b** or **145c** was achieved using $ZnCl_2$ as a catalyst. Treatment of nitriles **154** and **155** with hydroxylamine produced an N-hydroxyl amidine intermediate which without purification, was treated with trifluoroacetic acid anhydride (TFAA) to afford oxadiazole functionalized compounds **156** and **157** in excellent yields (83%).

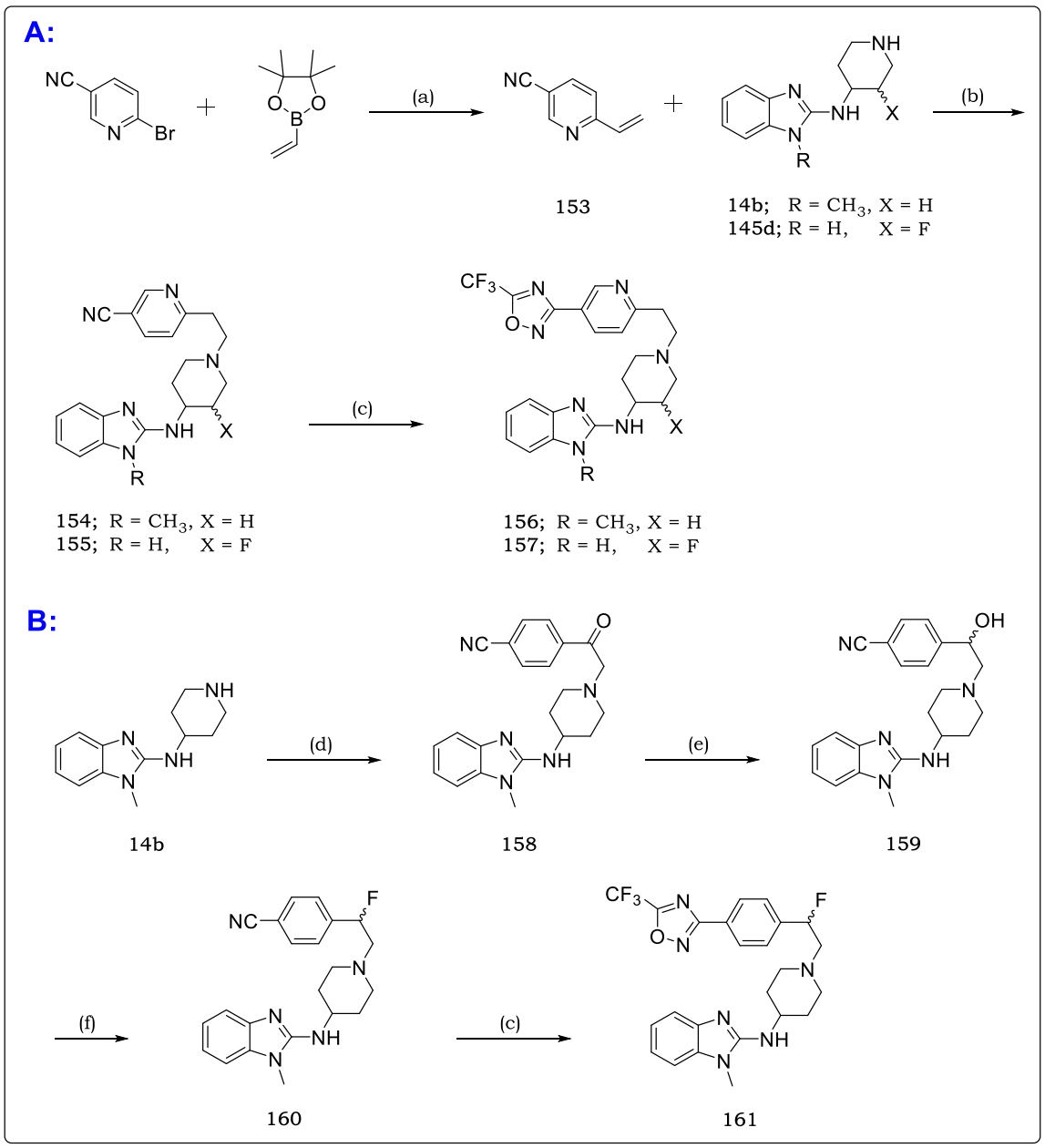

Scheme 2.22: Synthetic protocol towards phase II **SAR 4** target compounds **156, 157** and **161**

Reagents and Conditions: (a) $Pd(dppf)Cl_2$, Cs_2CO_3, 1:1 Dioxane/H_2O, 85 °C, 16 h (21%); (b) $ZnCl_2$, MeCN, 75 °C, 4 h (34 – 61%); (c) (i) $NH_2OH{\cdot}HCl$, 8-hydroxyquinolone, TEA, ethanol, 79 °C, 1.5 h (87–91 %); (ii) $(CF_3CO)_2O$, DCM, Pyridine, 16–21 °C, 1 h (48–54%) (d) 4-Cyanophenacyl bromide, K_2CO_3. MeCN, 85 °C, 5 h (74%); I $NaBH_4$, CH_3OH, 0 °C to 18 °C, 2 h (93%); (f) DAST, DCM, –70 °C to –50 °C, 0.5 h, 96%).

On the other hand, mono-fluoro compound **161** (Scheme 2.22B) was prepared following keto reduction of S_N2 product **158** followed by diethylaminosulfur trifluoride (DAST)

fluorination to produce **160**. Subsequent functionalization of the nitrile group as previously described afforded the oxadiazole compound **161** in high yield (85%). The chemical structures and isolated yields of the compounds from **SAR 4** are summarized in Table 2.6.

Table 2.6: Isolated yields for phase II **SAR 4** analogues

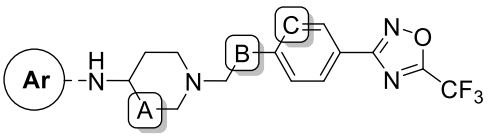

Code	Ar	A	B	C	Yield (%)
146	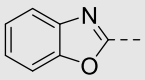				63
147	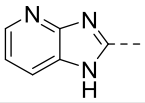				75
148	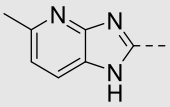	CH_2	CH_2	CH	78
149	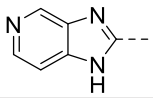				75
150	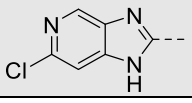				79
151	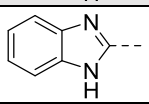	CHF	CH_2	CH	71
152		CF_2			43
157		CHF		N	48
161	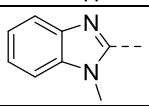	CH_2	CHF	CH	54
156			CH_2	N	48

2.5.6 Mechanistic Details for the Synthesis of Phase II SAR 4 Analogues

2.5.6.1 DAST Fluorination of Ketones (Step G, Scheme 2.23)

DAST is a fluorinating agent widely used in the preparation of nucleosides, carbohydrates, and organic compounds. Examples include fluorination of alcohols and carbonyl compounds. Fluorination of alcohols is thought to proceed *via* a 1,2-addition of hydrogen fluoride (HF) formed from the reaction between DAST and traces of water, across the C-O bond. Alternatively, the alcohol may react with DAST by nucleophilic displacement (S_N2) of fluorine on sulfur by the oxygen of the hydroxy group leading to the displacement of HF (Scheme 2.23).[46,47] Electron push from the lone pairs of electrons on nitrogen in intermediate **A** expels a fluoride ion, which consequently attacks the oxygen-bearing carbon and displaces diethylsulfuramidous fluoride (DSAF) as a by-product leading to formation of the desired α-fluoro product.

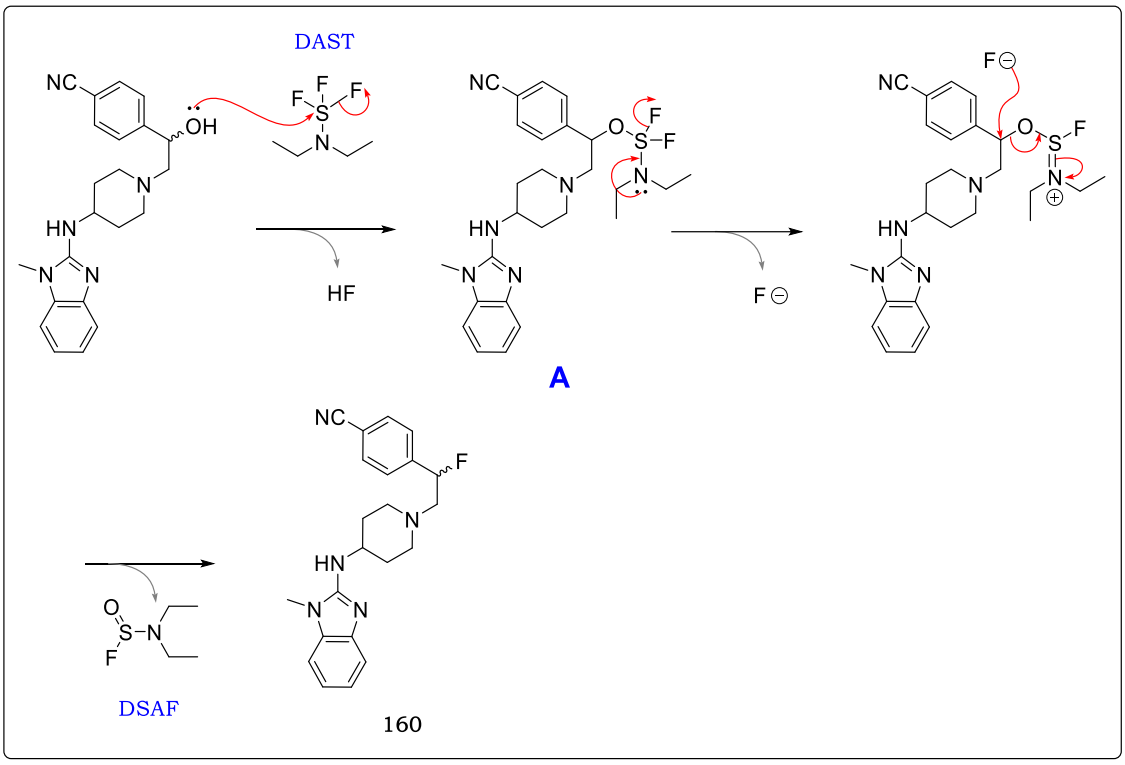

Scheme 2.23: Proposed reaction mechanism of DAST fluorination of alcohols

2.5.7 Characterization of Phase II SAR 4 Analogues

Target compound **151** is used as an example for full characterization of final compounds in this SAR (Figure 2.27). All twenty-two (22) protons were identified and accounted for, *via* ^{1}H-NMR. Consistently, aromatic protons **H-1** and **H-2**, as well as **H-12** and **H-13** each integrate for two protons resonating at δ = 7.21, 6.99, 7.44 and 8.0 ppm, respectively. The presence of the fluorine group in the piperidine ring causes significant changes in the splitting pattern of the protons in the ring in comparison with other piperidine compounds presented earlier. Briefly, **H-4** experiences both $^{3}J_{H\text{-}H}$ and $^{3}J_{H\text{-}F}$ splitting and therefore appears as a quartet of doublets (qd) at δ = 3.83 ppm. Diagnostic proton **H-8** undergoes $^{2}J_{H\text{-}F}$ splitting with a large coupling constant (J = 49.59 Hz) as observed in the doublet of triplet of doublet signal at δ = 4.49 ppm.

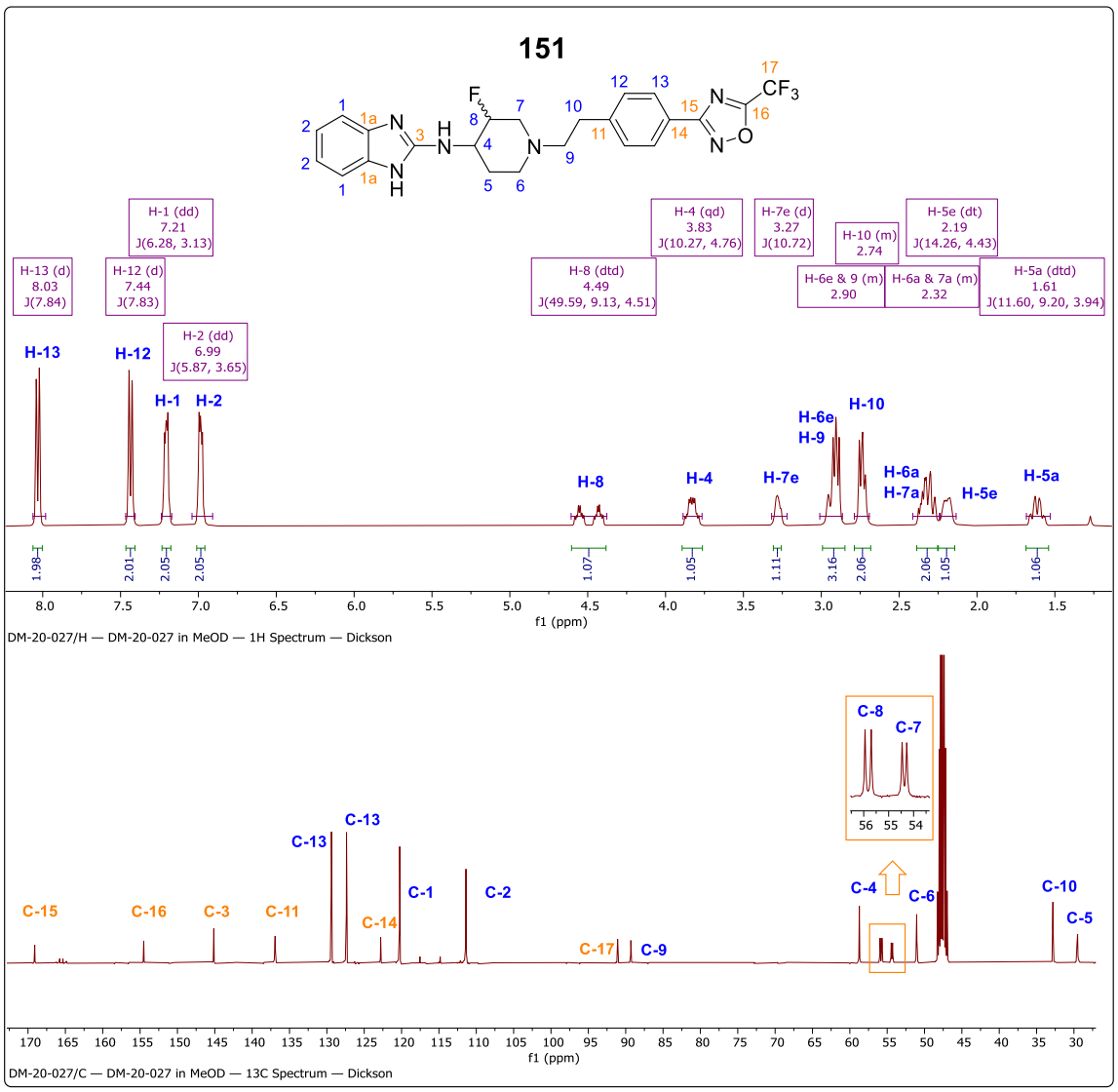

Figure 2.27: ^{1}H-NMR (*top*) ^{13}C-NMR (*bottom*) spectra of **151** in methanol-d_4 at 600 and 151 MHz, respectively

The ^{13}C-NMR spectrum of **151** (Figure 2.27) shows seventeen (17) carbon signals representative of 28 carbons present in the molecule. This is because benzimidazole carbons **C-1**, **C-2**, and **C-3** as well as phenyl carbons **C-12** and **C-13** are each represented by two carbon atoms in the same chemical environment and hence represented by one peak (signal). Fluorine bearing *α*-carbon **C-8** and β-carbon **C-7** undergo C-F splitting in the n+1 order of magnitude, where n = number of α-fluorine atoms. Therefore, diagnostically, **C-8** and **C-7** were each assigned to one of the two doublets resonating at δ = 55.82 ppm (J = 24.88 Hz) and δ = 54.37 ppm (J = 18.32 Hz). The rest of the carbons were unambiguously assigned with respect to their environment.

The HPLC-MS chromatogram of compound **151** (Figure 2.28) revealed that the compound was pure enough (98%) for biological evaluation following column chromatography.

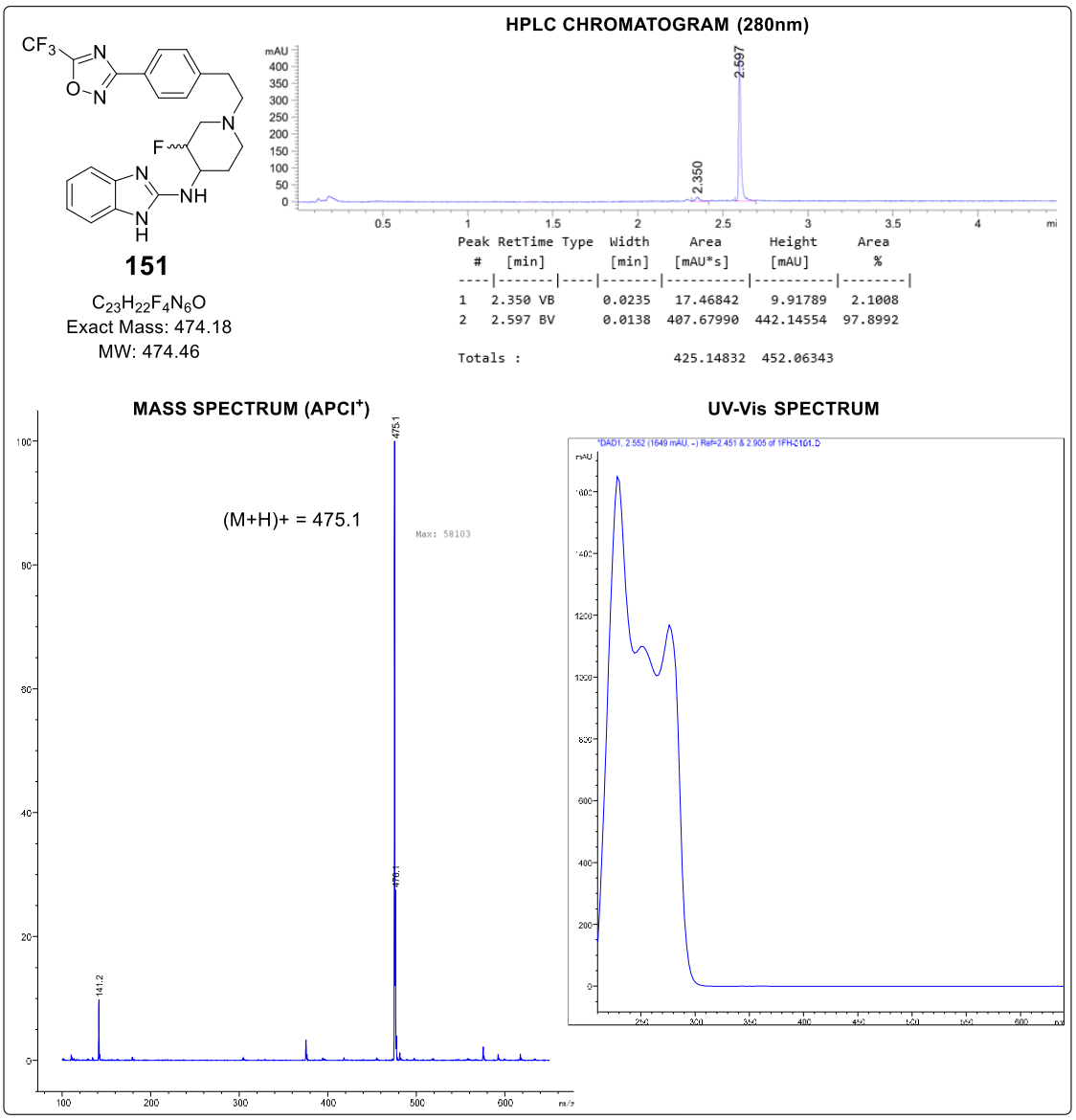

Figure 2.28: HPLC-MS chromatogram and spectra of **151**

Additionally, MS analysis showed a pseudo-molecular ion (M+H)+ of 475.1 consistent with that of the exact calculated mass of $C_{23}H_{22}F_4N_6O$. The UV-Vis absorption maxima were at 230, 255, and 280 nm.

2.6 Hybridization of AST and CQ

2.6.1 Background and Rationale

Hybridization is a strategy that is highly effective in addressing a range of issues such as drug-resistance and drug-drug interactions. AST has been used with CQ as part of a hybridization strategy to overcome *P. falciparum* resistance to CQ. Musonda and co-workers at Pfizer designed CQ-AST analogues and evaluated their activity in the CQ-resistance *P. falciparum* resistance strain (K1). The design was centered on identifying the appropriate linkage that would result in hybrids with low cross-resistance to CQ as part of a proof-of-principle study.[48]

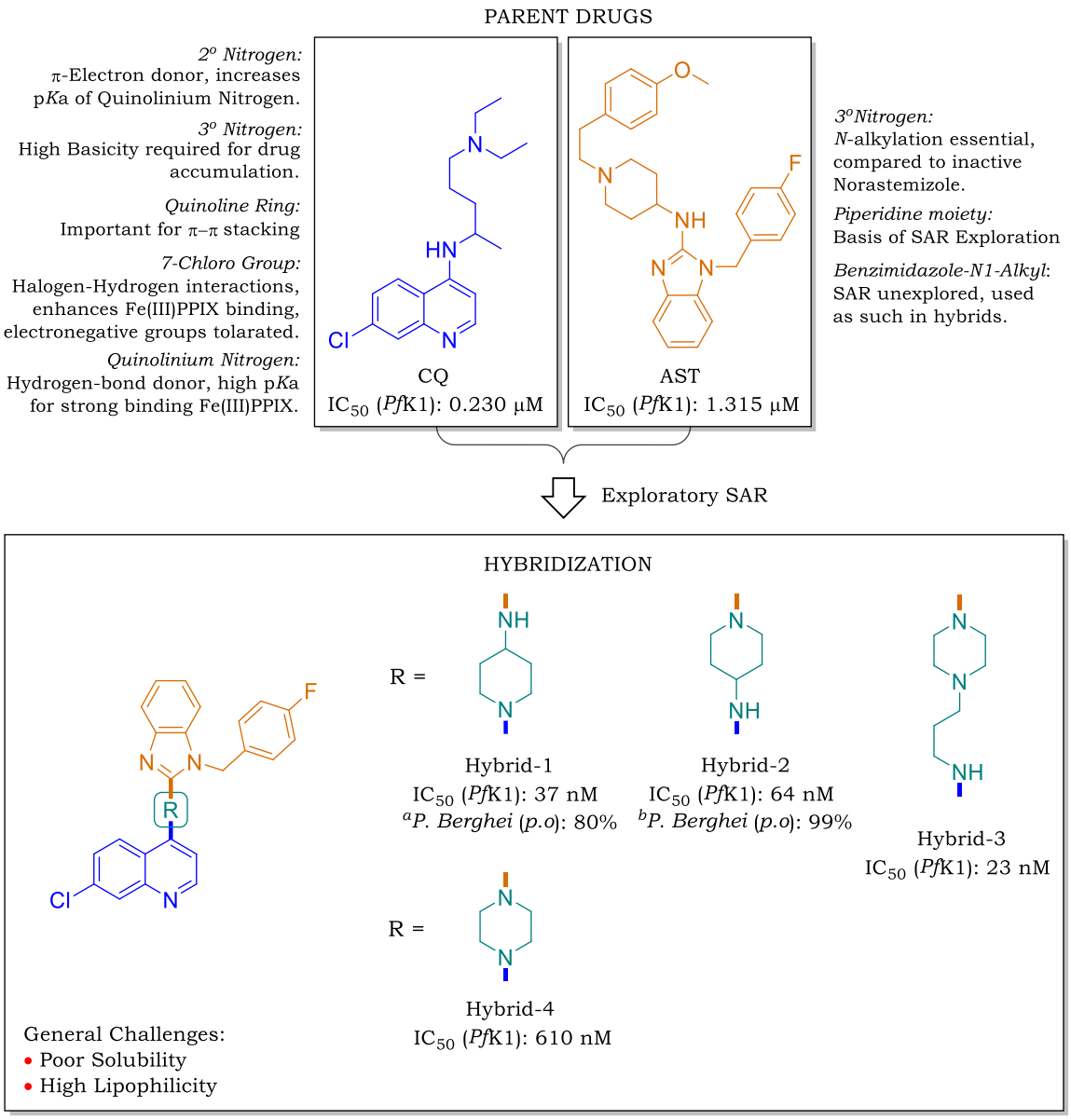

Figure 2.29: Pharmacophore details of chloroquine (CQ) and astemizole (AST), and hybridization SAR exploration carried out by Musonda *et al.*[48] [a]Dose = 4 × 20 mg.kg^{-1} for 4 days; [b]Dose = 4 × 25 mg.kg^{-1} for 4 days

Quinoline-based antimalarials such as CQ and amodiaquine (ADQ) exert their activity *via* complexation with ferriprotoporphyrin IX (Fe(III)PPIX), a by-product of the essential parasitic hemoglobin degradation pathway, thereby inhibiting the formation of hemozoin. It was therefore imperative to maintain the pharmacophoric features of the CQ portion in the hybrid (Figure 2.29). These include: the 7-chloro group that promotes π-stacking of the quinoline to the π-excessive porphyrin and halogen-hydrogen interactions,[49] and the 4-amino group (2° nitrogen) whose electron-releasing properties increase the p*K*a of the quinolinium nitrogen, thereby increasing its basicity and hydrogen-bonding capability with Fe(III)PPIX.[50] Additionally, the aliphatic 3° nitrogen had to be maintained as it is crucial for CQ accumulation in the parasitic digestive FV.

In the work from which AST's antimalarial activity was first disclosed, norastemizole (Nor-AST), an *N*-dealkylation metabolite of AST devoid of the 4-methoxyphenethyl moiety, was over 2-fold less active in a panel of three strains of *P. falciparum* (3D7, Dd2 and ItG; IC_{50} > 2.23 μM) compared to AST (IC_{50} < 0.734 μM). On the other hand, desmethylastemizole (DMAST), an O-demethylation metabolite of AST displayed over 6-fold higher activity (IC_{50} < 0.107 μM) than AST.[1] Based on this data, the low activity of nor-AST suggested the importance of alkylation of the 3° piperidine nitrogen in AST for antimalarial activity. Therefore, following a diversity study comprising various linkers between AST and CQ (Figure 2.29), a set of diaminoalkyl linkers were identified, with three frontrunner compounds showing improved potency against CQ-resistant K1 strain. Two of these hybrids demonstrated *in vivo* efficacy in the *P. berghei* mouse model of malaria.[48]

The observed high *in vitro* activity and *in vivo* efficacy of the hybrids suggest their potential for further development. However, the work (i) explored a limited SAR, (ii) delivered hybrids with poor drug-like properties such as high lipophilicity and low solubility and (iii) does not show multi-stage activity other than that against the asexual-blood stage. Therefore, the work described here will further explore the SAR of front-runner **hybrid-2** (**H-2**) in an attempt to improve its drug-like properties.

2.6.2 Design

H-2 was selected as a template for further investigation because of its reported good high *in vivo* efficacy (*P. berghei* (p.o.), 4 × 50 $mg.kg^{-1}$: 99%), low cytotoxicity in the CHO mammalian cells (IC_{50}: 9.1 μM) and high mean survival days (MSD) of infected mice (13 days).

The design of analogues was guided by previously established SARs for both CQ and AST. The role of the carbon chain length in the diaminoalkyl linker in CQ has been extensively investigated in literature, and results suggest that either shortening (two to three carbons) or lengthening (ten to twelve carbons) would lead to compounds that remain active against CQ-resistant malaria parasites. However, short spacers (four or fewer) have consistently conferred greater activity than long variants.[51–53] Therefore, the 4-aminopiperidine spacer was maintained because it is both present in AST and imparts a propyl spacer (three carbons, Figure 2.30).

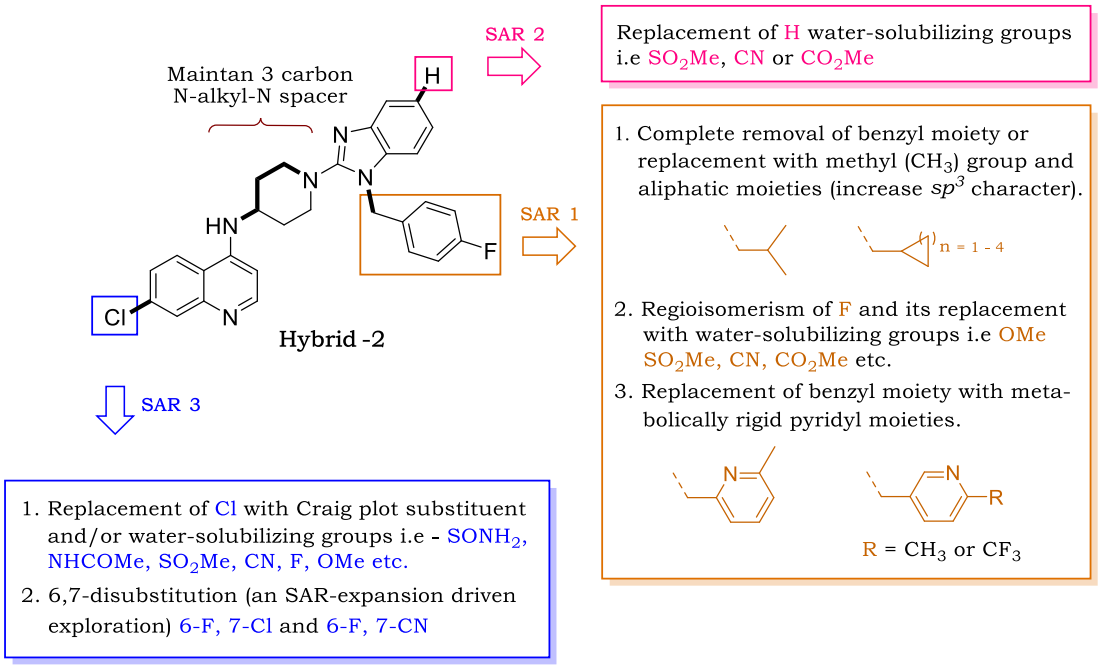

Figure 2. 30: Design of astemizole-chloroquine (AST-CQ) analogues around **hybrid-2** (**H-2**)

SAR 1 was focused on the benzyl side chain of the AST portion of the hybrid (Figure 2.30). This SAR included complete removal of the sidechain, replacement with short alkyl moieties, replacement with pyridyl moieties, regioisomerism and substitution of the 4-fluoro with water solubilizing groups and other Craig plot substituents for SAR expansion.

In **SAR 2**, the *p*-fluoro benzyl moiety was fixed, while changes were made at the 7-position of the aminoquinoline portion of the hybrid. The 7-chloro group is responsible for inhibition of hemozoin formation, although it is thought to have little influence on the strength of association with Fe(III)PPX.[54] Replacement of the 7-chloro with electron-withdrawing groups such as NO_2, CN, and CF_3 generally produces potent hemozoin-formation inhibitors comparable to those containing Cl, although this is not always associated with antiplasmodium potency. The strong electron-withdrawing effect of groups such as NO_2 at the 7-position decreases the basicity (pK_a) of quinoline nitrogen so that accumulation of the molecule in the parasite digestive FV is too low to exert strong biological activity. However, derivatives with weaker electron-withdrawing groups (i.e., CN) retain potency similar to that of Cl derivatives.[55] The lower lipophilicity of groups such as CN compared to Cl indicates the possibility of analogues with more favorable physicochemical profiles and lower toxicity. Therefore, to test this hypothesis, the 7-Cl group was substituted with water-solubilizing groups and other synthetically accessible Craig plot substituents (Figure 2.30).

2.7 Chemistry: AST-CQ Hybrids

2.7.1 Synthesis of SARs 1 and 2 Hybrids

The synthesis of **SAR 1** analogues (Scheme 2.24) was achieved following the synthetic route similar to that described in section 2.5.4. Briefly, S_NAr of appropriately substituted 2-halo nitro benzene followed by H_2/Pd reduction, CDI cyclization, and $POCl_3$ chlorination produced intermediates **165a** and **165t**–**v** (Scheme 2.25). Conversely, intermediates **165b**–**s** were prepared by direct S_N2 coupling of appropriate alkyl halide to 2-chloro benzimidazole as previously described. Direct S_NAr coupling of **165** chloro intermediates to amino intermediate **167** at high temperature using TEA afforded hybrid compounds **168**–**193** in high yields (78 – 91%). A summary of the structures and isolated yields of **SAR 1** and **2** hybrid compounds is shown in Table 2.7.

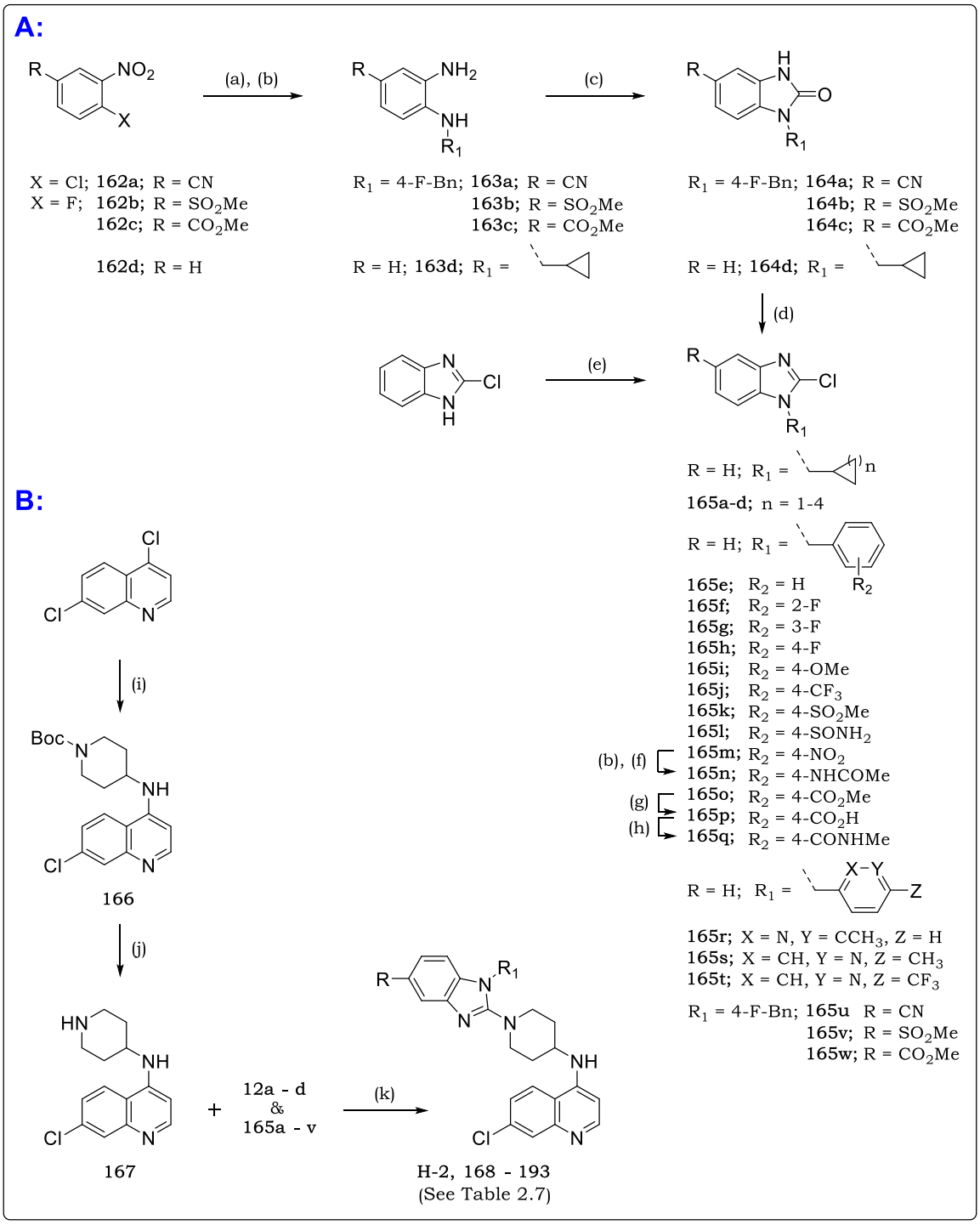

Scheme 2. 24: Synthetic protocol towards **SAR 1** and **2** hybrids (**H-2**, **168 – 193**)

Reagents and conditions: (a) (i) 4-Fluorobenzylamine (for **163a-c**) or cyclopropanemethylamine (for **163d**), TEA, MeCN, 80 °C, 2–72 h (quant'); (b) H_2 (balloon), 10% Pd/C, 1:1 MeOH/EtOAc, 27 °C, 7 h, (90–98%); (c) CDI, THF, 28 °C, 3 h (quant'); (d) $POCl_3$, neat, 110 °C, 12 h (80–90%); I Alkyl halide, K_2CO_3, Acetone, 23–60 °C, 2–36 h (88–95%); (f) Acetyl chloride, TEA, MeCN, 26 °C (88%); (g) (ii) 2M aq. KOH, MeOH, 80 °C, 2h; (ii) 3N aq. HCl, Ph = 1 (89%); (h) Methylamine (2M in THF), EDCI/DMAP, DCM, 25 °C, 2 h (76%); (i) *N*-Boc-4-aminopiperidine, TEA, 155 °C, 8 h (78%); (j) TFA, DCM, 23 °C, 2 h (98%); (k) TEA, 160 °C, 5 h (59–95%).

Table 2.7: Isolated yields for **SARs 1** and **2** analogues.

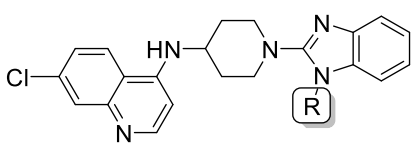

Code	R	R_1	Yield (%)
168	H		74
169	CH_3		83
170			89
171			84
172	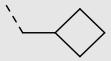		87
173	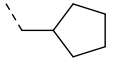		82
174	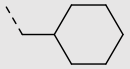		79
175		H	89
176		2-F	83
177	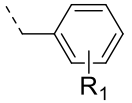	3-F	85
H-2		4-F	79
178		4-CN	80

Code	R	R_1	Yield (%)
179		4-OMe	69
180		4-CF_3	86
181		4-SO_2Me	81
182		4-$SONH_2$	59
183	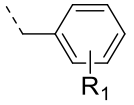	4-NO_2	72
184		4-NHCOMe	75
185		4-CO_2Me	80
186		4-CO_2H	95
187		4-CONHMe	88
188	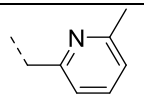		83
189	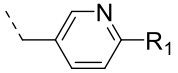	CH_3	85
190		CF_3	88

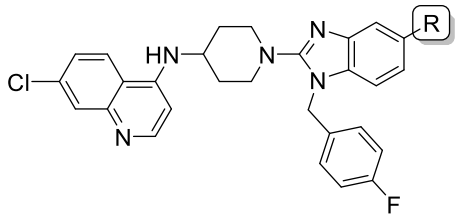

Code	R	Yield (%)
191	CN	77
192	SO_2Me	79
193	CO_2Me	73

2.7.2 Synthesis of SAR 3 Hybrids

Meldrum's acid (2,2-dimethyl-1,3-dioxane-4,6-dione; Scheme 2.25A) is a remarkable reagent with various reactivities that has found numerous applications in the preparation of nitrogen containing heterocycles. This utility is attributable to its susceptibility to both electrophilic and nucleophilic attack on C-5 and C-4/6 respectively, along with unique ring opening capability. In this case, it was used for the efficient preparation of commercially inaccessible 4-chloro-7-substituted aminoquinoline precursors required for **SAR 3** analogues.

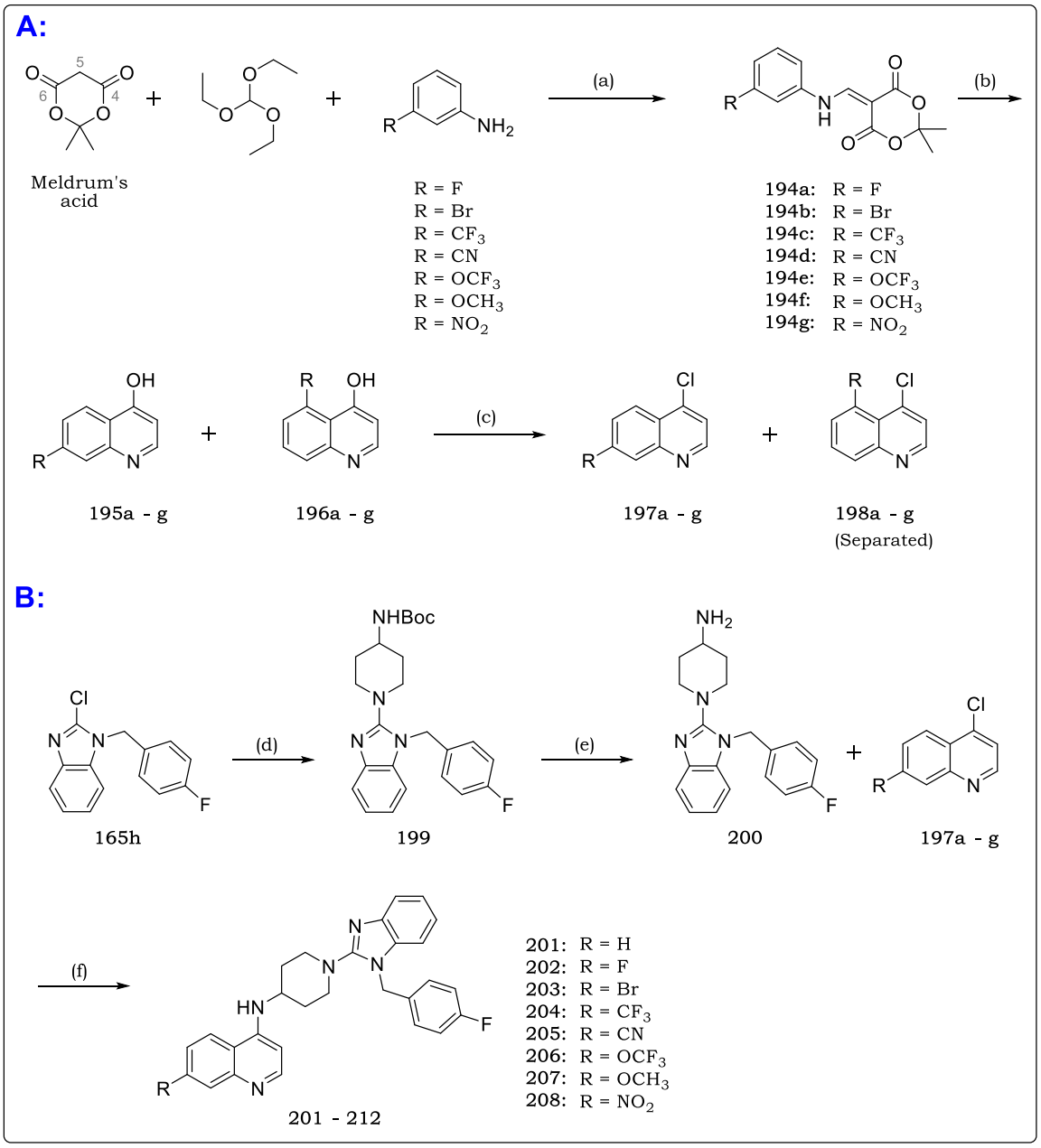

Scheme 2.25: Synthetic protocol towards **SAR 3** target compounds **201–212**

Reagents and conditions: (a) 149 °C, 3 h, (89–98%); (b) Ph_2O, 225 °C, μW, 5 min (Crude: 95–98%); (c) $POCl_3$, Toluene, 110 °C, 2 h (7-substituted, 43–98%); (d) 160 °C, 2 h (72%); I TFA, DCM, 25 °C, 2 h (98%); (f) Phenol, 120 °C, μW, 45 min (39–72%).

The condensation of 3-substituted anilines with Meldrum's acid and triethyl orthoformate (Scheme 2.25A) by stirring at 148°C under neat conditions produced enamines **194** in excellent yields (90 – 95%). After isolation, microwave assisted cyclization of enamines in diphenyl ether (Ph_2O) afforded a ~ 2:1 mixture of 7- and 5-regioisomers **195a-j** and **196a-j** respectively, which could not be separated *via* either flash chromatography or crystallization. However, following chlorination of the mixture with $POCl_3$, 7-substituted regioisomers (**197a-j**) were successfully separated from their 5-substituted regioisomers (**198a-j**) *via* column chromatography. Microwave-assisted nucleophilic aromatic substitution (S_NAr) of **197a-j** with previously prepared **200** (Scheme 2.25B) in phenol afforded the hybrid compounds **202** – **211** in high yields (70 – 85%). Hybrid compound **201** was obtained from commercially available 4-chloro-quinoline. Reduction of nitro compound **211** followed by acylation using acetyl chloride and TEA afforded amide **212**.

Respective analogues and their isolated yields are shown in Table 2.8 below.

Table 2.8: Isolated yields for **SAR 3** analogues.

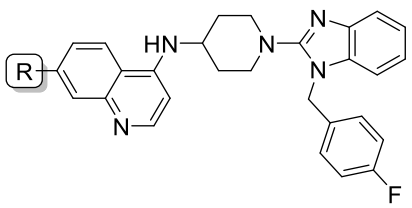

Code	R	Yield (%)	Code	R	Yield (%)
201	H	58	**205**	CN	49
202	F	44	**206**	OCF_3	59
203	Br	72	**207**	OCH_3	42
204	CF_3	63	**208**	NO_2	39

2.7.3 Reaction Mechanisms and Characterization

As shown in Scheme 2.26, the multi-component reaction involving Meldrum's acid, triethyl orthoformate and aniline precursors is thought proceed *via* the generation of a reactive 5-ethoxymethylene 1,3-dioxane-4,6-dione (otherwise called the ethoxymethylene Meldrum's acid) intermediate *in situ*.

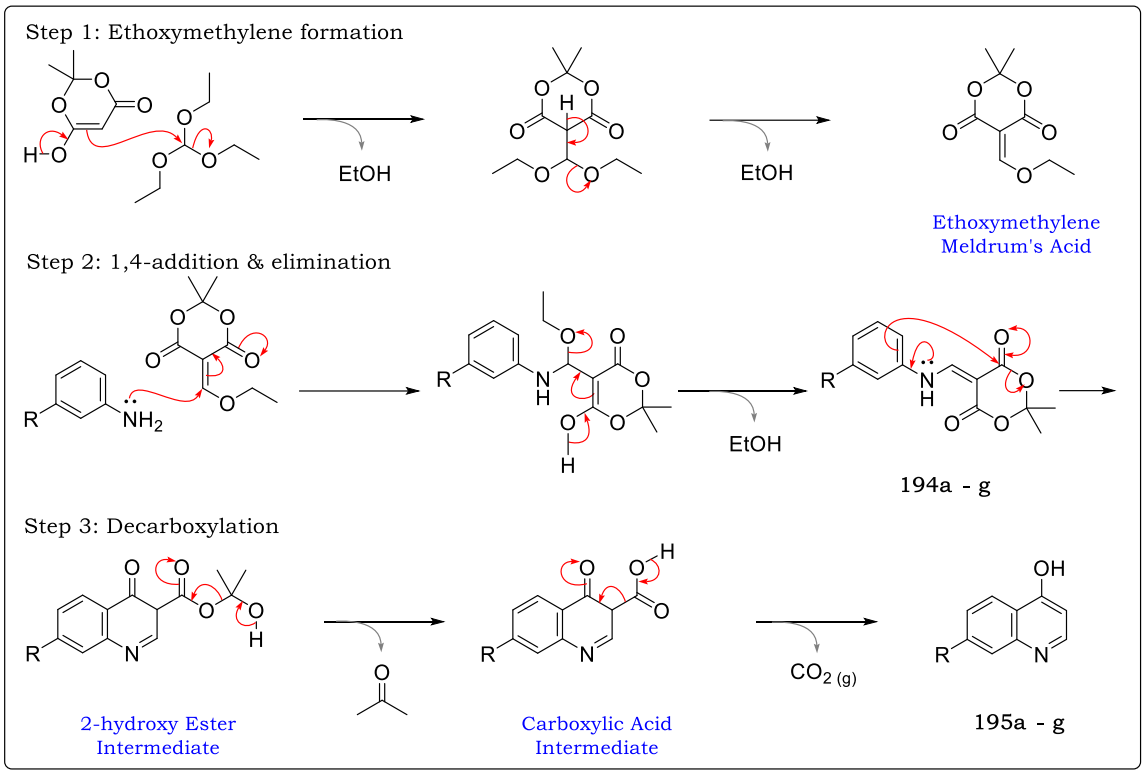

Scheme 2.26: Proposed reaction mechanisms for the formation of the 7-substituted-4-hydroxyquinoline ring *via* Meldrum's acid

The respective aniline undergoes nucleophilic addition to the reactive intermediate *via* 1,4-Michael addition, leading to the elimination of ethanol and formation of an enamine intermediate. Under microwave conditions, the enamine undergoes intramolecular cycloaddition *via* nucleophilic attack by the aromatic π-electron onto one of the electrophilic carbonyl carbons. The resulting 2-hydroxy ester intermediate quickly undergoes decomposition to form a carboxylic acid, which subsequently undergoes decarboxylation to produce 5- and 7-sustituted-4-hydroxy aminoquinoline mixture. This was without purification, subjected to chlorination using $POCl_3$.

The ^{1}H-NMR spectra for the enamine for cyano intermediate **194d** consistently showed seven proton signals. As shown in Figure 2.31, diagnostic NH (**H-5**) and enamine C-H (**H-6**) protons appear as doublets (δ = 11.30 and 8.64 ppm, J = 14.26 Hz) coupling with each other. Additionally, lactam dimethyl protons (**H-7**) are observed upfield (δ = 1.68 ppm) as a singlet integrating for six protons. Following decarboxylative ring closure and chlorination to give **197d**, quinoline protons **H-4** and **H-5** resonate at δ = 8.99 and 7.95 ppm, respectively, with a coupling constant of J = 4.84 Hz.

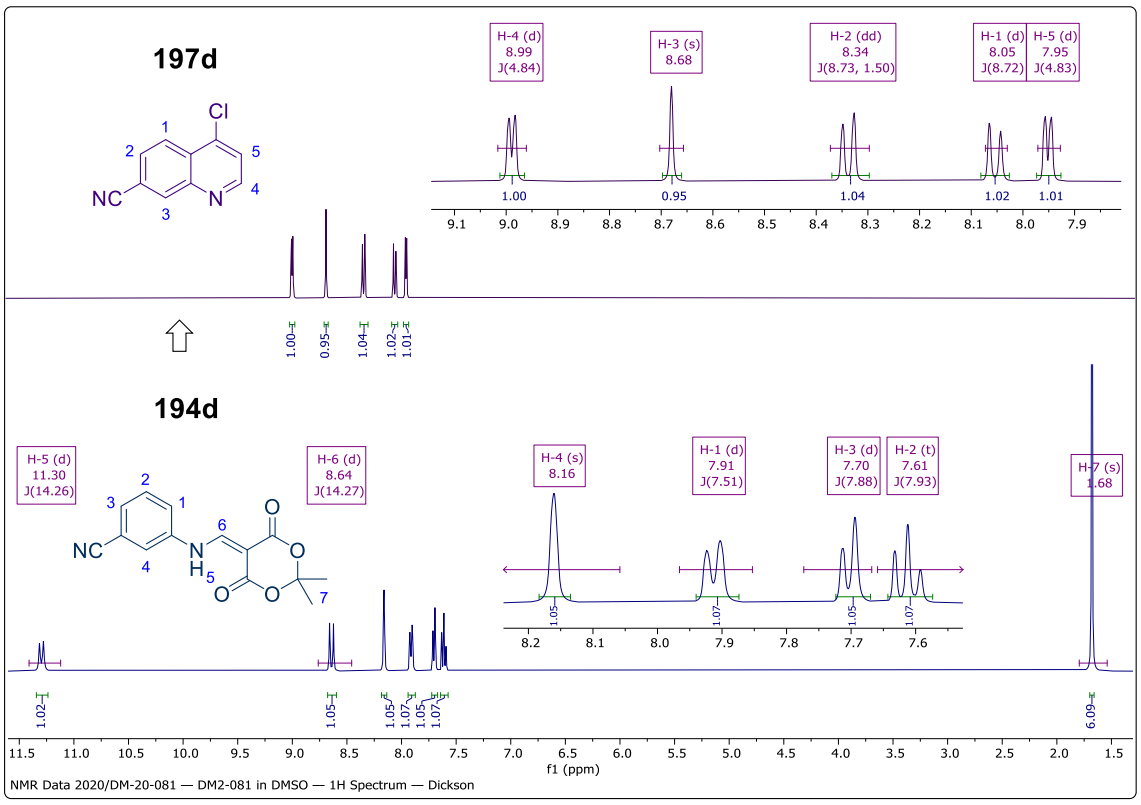

Figure 2.31: Stacked ^{1}H-NMR spectra (*bottom to top*) for synthetic intermediates **194d** – **197d** in DMSO-d_6 at 300 MHz

As an example, for the characterization of final compounds in this series, ^{1}H-NMR, and ^{13}C-NMR spectra for the cyano hybrid **205** are shown in Figure 2.32. The assignment of protons was assisted by both HSQC and homonuclear correlation spectroscopy (COSY) 2D NMR experiments in order to map and assign the protons and carbons. All twenty-five (25) protons have been accounted for with multiple signals overlapping in the aromatic region. Similarly, ^{13}C-NMR analysis shows signals of all twenty-four (24) carbon environments with the diagnostic and most shielded carbon (**C-11**) appearing upfield (δ = 30.75 ppm) representing two carbons. **C-13** is the most deshielded carbon, resonation downfield at δ = 163.07 ppm.

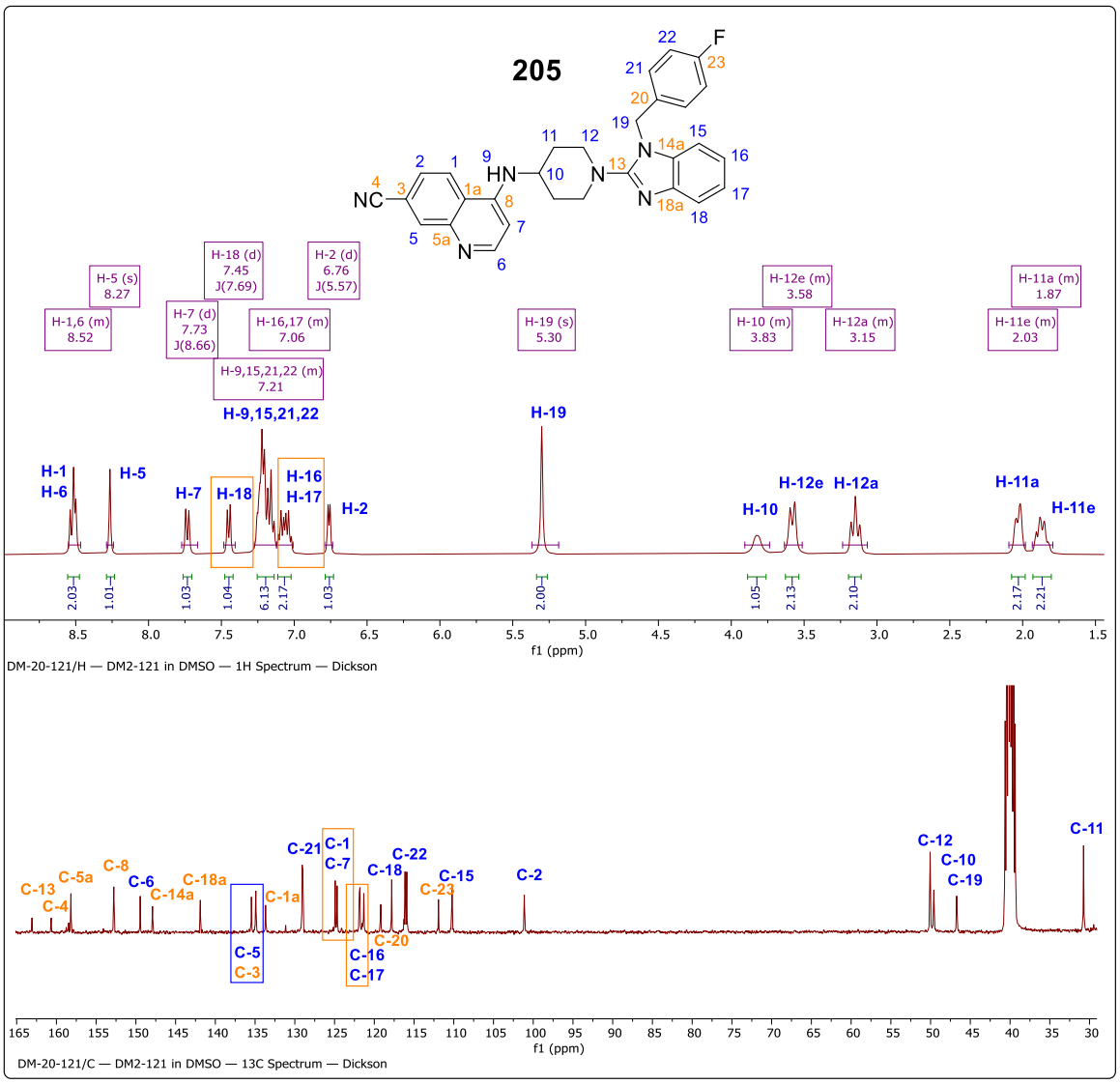

Figure 2.32: ^{1}H-NMR (*top*) ^{13}C-NMR (*bottom*) spectra of **205** in methanol-d_4 at 400 and 101 MHz, respectively

2.8 Conclusion

To conclude, this chapter has described the rationale, design, synthesis, and characterization of AST derivatives (phase I and II) and AST-CQ hybrids. The design employed both rational medicinal chemistry principles and synthetically tractable literature methodologies to efficiently access the compounds. All final compounds synthesized were fully characterized using available and accessible spectroscopic techniques such as NMR spectroscopy and chromatographic methods (TLC and HPLC-MS) including physicochemical analyses (e.g., melting points). The biological activities and other physicochemical parameters of target compounds were assessed following a project-specific progression criteria.

2.9 References

(1) Chong, C. R.; Chen, X.; Shi, L.; Liu, J. O.; Sullivan, D. J. A Clinical Drug Library Screen Identifies Astemizole as an Antimalarial Agent. *Nat. Chem. Biol.* **2006**, *2*, 415–416.

(2) Roman, G.; Crandall, I. E.; Szarek, W. A. Synthesis and Anti- Plasmodium Activity of Benzimidazole Analogues Structurally Related to Astemizole. *ChemMedChem* **2013**, *8*, 1795–1804.

(3) Tian, J.; Vandermosten, L.; Peigneur, S.; Moreels, L.; Rozenski, J.; Tytgat, J.; Herdewijn, P.; Van den Steen, P. E.; De Jonghe, S. Astemizole Analogues with Reduced HERG Inhibition as Potent Antimalarial Compounds. *Bioorg. Med. Chem.* **2017**, *25* (24), 6332–6344.

(4) Kumar, M.; Okombo, J.; Mambwe, D.; Taylor, D.; Lawrence, N.; Reader, J.; van der Watt, M.; Fontinha, D.; Sanches-Vaz, M.; Bezuidenhout, B. C.; et al. Multistage Antiplasmodium Activity of Astemizole Analogues and Inhibition of Hemozoin Formation as a Contributor to Their Mode of Action. *ACS Infect. Dis.* **2019**, *5* (2), 303–315.

(5) Tong, A. S. T.; Choi, P. J.; Blaser, A.; Sutherland, H. S.; Tsang, S. K. Y.; Guillemont, J.; Motte, M.; Cooper, C. B.; Andries, K.; Van den Broeck, W.; et al. 6-Cyano Analogues of Bedaquiline as Less Lipophilic and Potentially Safer Diarylquinolines for Tuberculosis. *ACS Med. Chem. Lett.* **2017**, *8* (10), 1019–1024.

(6) Craig, P. N. Interdependence between Physical Parameters and Selection of Substituent Groups for Correlation Studies. *J. Med. Chem.* **1971**, *14* (8), 680–684.

(7) Ertl, P. Craig Plot 2.0: An Interactive Navigation in the Substituent Bioisosteric Space. *J. Cheminform.* **2020**, *12* (1), 8.

(8) van der Westhuyzen, R.; Winks, S.; Wilson, C. R.; Boyle, G. A.; Gessner, R. K.; Soares de Melo, C.; Taylor, D.; de Kock, C.; Njoroge, M.; Brunschwig, C.; et al. Pyrrolo[3,4- c]Pyridine-1,3(2 H)-Diones: A Novel Antimycobacterial Class Targeting Mycobacterial Respiration. *J. Med. Chem.* **2015**, *58* (23), 9371–9381.

(9) Lee, S.; Yi, K. Y.; Yoo, S. E. Introduction of Heterocycles at the 2-Position of Indoline as Ester Bioisosteres. *Bull. Korean Chem. Soc.* **2004**, *25* (2), 207–212.

(10) Bilodeau, M. T.; Balitza, A. E.; Koester, T. J.; Manley, P. J.; Rodman, L. D.; Buser-Doepner, C.; Coll, K. E.; Fernandes, C.; Gibbs, J. B.; Heimbrook, D. C.; et al. Potent N -(1,3-thiazol-2-yl)Pyridin-2-Amine Vascular Endothelial Growth Factor Receptor Tyrosine Kinase Inhibitors with Excellent Pharmacokinetics and Low Affinity for the HERG Ion Channel. *J. Med. Chem.* **2004**, *47*, 6363–6372.

(11) Bourrain, S.; Collins, I.; Neduvelil, J. G.; Rowley, M.; Leeson, P. D.; Patel, S.; Patel, S.; Emms, F.; Marwood, R.; Chapman, K. L.; et al. Substituted Pyrazoles as Novel Selective Ligands for the Human Dopamine D 4 Receptor. *Bioorg. Med. Chem.* **1998**, *6* (10), 1731–1743.

(12) Jamieson, C.; Moir, E. M.; Rankovic, Z.; Wishart, G. Medicinal Chemistry of HERG Optimizations: Highlights and Hang-Ups. *J. Med. Chem.* **2006**, *49* (17), 5029–5046.

(13) Evans, M. D.; Ring, J.; Schoen, A.; Bell, A.; Edwards, P.; Berthelot, D.; Nicewonger, R.; Baldino, C. M. The Accelerated Development of an Optimized Synthesis of 1,2,4-Oxadiazoles: Application of Microwave Irradiation and Statistical Design of Experiments. *Tetrahedron Lett.* **2003**, *44* (52), 9337–9341.

(14) Borg, S.; Estenne-Bouhtou, G.; Luthman, K.; Csoeregh, I.; Hesselink, W.; Hacksell, U. Synthesis of 1,2,4-Oxadiazole-, 1,3,4-Oxadiazole-, and 1,2,4-Triazole-Derived Dipeptidomimetics. *J. Org. Chem.* **1995**, *60* (10), 3112–3120.

(15) Wang, Y.; Miller, R. L.; Sauer, D. R.; Djuric, S. W. Rapid and Efficient Synthesis of 1,2,4-Oxadiazoles Utilizing Polymer-Supported Reagents under Microwave Heating. *Org. Lett.* **2005**, *7* (5), 925–928.

(16) Adib, M.; Jahromi, A. H.; Tavoosi, N.; Mahdavi, M.; Bijanzadeh, H. R. Microwave-Assisted Efficient, One-Pot, Three-Component Synthesis of 3,5-Disubstituted 1,2,4-Oxadiazoles under Solvent-Free Conditions. *Tetrahedron Lett.* **2006**, *47* (17), 2965–2967.

(17) Grant, D.; Dahl, R.; Cosford, N. D. P. Rapid Multistep Synthesis of 1,2,4-Oxadiazoles in a Single Continuous Microreactor Sequence. *J. Org. Chem.* **2008**, *73* (18), 7219–7223.

(18) Al-Talib, M.; Tashtoush, H.; Odeh, N. Diacyl Acid Dihydrazides. *Magn. Reson. Chem.* **1990**, *28* (12), 1072–1075.

(19) Theocharis, A. B.; Alexandrou, N. E. Synthesis and Spectral Data of 4,5-Bis[5-Aryl-1,3,4-Oxadiazol-2-Yl]-1-Benzyl-1,2,3-Triazoles. *J. Heterocycl. Chem.* **1990**, *27* (6), 1685–1688.

(20) Carlsen, P. H. J.; Jørgensen, K. B. Synthesis of Unsymmetrically Substituted 4 H -1,2,4-Triazoles. *J. Heterocycl. Chem.* **1994**, *31* (4), 805–807.

(21) Liras, S.; Allen, M. P.; Segelstein, B. E. A Mild Method for the Preparation of 1,3,4-Oxadiazoles: Triflic Anhydride Promoted Cyclization of Diacylhydrazines. *Synth. Commun.* **2000**, *30* (3), 437–443.

(22) Kimura, Tomio; Ohkawa, Nobuyuki; Nakao, Akira; Nagasaki, Takayoshi; Shimozato, T. Preparation of Cyclic Tertiary Amine Compounds That Inhibit Inflammatory Cytokine Production, **2007**.

(23) Maharvi, G. M.; Fauq, A. H. A Synthesis of the γ-Secretase Inhibitor BMS-708163. *Tetrahedron Lett.* **2010**, *51* (50), 6542–6544.

(24) Yang, S.; Zhu, S.-F.; Zhang, C.-M.; Song, S.; Yu, Y.-B.; Li, S.; Zhou, Q.-L. Enantioselective Iridium-Catalyzed Hydrogenation of α-Arylcinnamic Acids and Synthesis of (S)-Equol. *Tetrahedron* **2012**, *68* (26), 5172–5178.

(25) Kühnel, E.; Laffan, D. D. P.; Lloyd-Jones, G. C.; Martínez del Campo, T.; Shepperson, I. R.; Slaughter, J. L. Mechanism of Methyl Esterification of Carboxylic Acids by

Trimethylsilyldiazomethane. *Angew. Chemie Int. Ed.* **2007**, *46* (37), 7075–7078.

(26) Rose, Yannick Stephane; Ciblat, Stephane; Kang, Ting; Rafai Far, Adel; Dietrich, Evelyne; Lafontaine, Yanick; Reddy, R. Preparation of Phosphonated Rifamycins for the Prevention and Treatment of Bone and Joint Infections, **2007**.

(27) Rosenberger, N.; Studer, A.; Takatani, N.; Nakajima, H.; Watanabe, Y. Azurin-Poly(N -Isopropylacrylamide) Conjugates by Site-Directed Mutagenesis and Their Thermosensitive Behavior in Electron-Transfer Processes. *Angew. Chemie Int. Ed.* **2009**, *48* (11), 1946–1949.

(28) Ajvazi, N.; Stavber, S. Direct Halogenation of Alcohols with Halosilanes under Catalyst- and Organic Solvent-Free Reaction Conditions. *Tetrahedron Lett.* **2016**, *57* (22), 2430–2433.

(29) Newman, S.; Bryan, C.; Perez, D.; Lautens, M. The Use of Bromotrichloromethane in Chlorination Reactions. *Synthesis (Stuttg).* **2011**, *2011* (02), 342–346.

(30) Tandiary, M.; Masui, Y.; Onaka, M. Chlorination of Benzylic and Allylic Alcohols with Trimethylsilyl Chloride Enhanced by Natural Sodium Montmorillonite. *Synlett* **2014**, *25* (18), 2639–2643.

(31) Rebek, J.; Feitler, D. Mechanism of the Carbodiimide Reaction. II. Peptide Synthesis on the Solid Phase. *J. Am. Chem. Soc.* **1974**, *96* (5), 1606–1607.

(32) Rebek, J.; Fietler, D. An Improved Method for the Study of Reaction Intermediates. The Mechanism of Peptide Synthesis Mediated by Carbodiimides. *J. Am. Chem. Soc.* **1973**, *95* (12), 4052–4053.

(33) Han, E. S.; goleman, daniel; boyatzis, Richard; Mckee, A. More Complex Spin-Spin Splitting Patterns https://chem.libretexts.org/Courses/Athabasca_University/Chemistry_350%3A_Organic_Chemistry_I/13%3A_Structure_Determination%3A_Nuclear_Magnetic_Resonance_Spectroscopy/13.12%3A_More_Complex_Spin-Spin_Splitting_Patterns (accessed Dec 12, 2020).

(34) Kosak, T. M.; Conrad, H. A.; Korich, A. L.; Lord, R. L. Ether Cleavage Re-Investigated: Elucidating the Mechanism of BBr 3 -Facilitated Demethylation of Aryl Methyl Ethers. *European J. Org. Chem.* **2015**, *2015* (34), 7460–7467.

(35) Sousa, C.; Silva, P. J. BBr 3 -Assisted Cleavage of Most Ethers Does Not Follow the Commonly Assumed Mechanism. *European J. Org. Chem.* **2013**, *2013* (23), 5195–5199.

(36) Kriek, E.; Emmelot, P. Methylation of Deoxyribonucleic Acid by Diazomethane. *Biochim. Biophys. Acta - Spec. Sect. Nucleic Acids Relat. Subj.* **1964**, *91* (1), 59–66.

(37) Lennox, A. J. J. Meisenheimer Complexes in S N Ar Reactions: Intermediates or Transition States? *Angew. Chemie Int. Ed.* **2018**, *57* (45), 14686–14688.

(38) Lambert, Joseph B; Goldstein, J. E. The Chemical-Shift Difference between the ß Axial and Equatorial Protons in Pentamethylene Heterocycles. *J. Am. Chem. Soc.* **1977**, *99*

(17), 5689–5693.

(39) Hans, R. J. 5-HMR-5 Vicinal Proton-Proton Coupling 3JHH https://www.chem.wisc.edu/areas/reich/nmr/05-hmr-05-3j.htm (accessed May 22, 2020).

(40) Chen, Y.; Leonardi, M.; Dingwall, P.; Labes, R.; Pasau, P.; Blakemore, D. C.; Ley, S. V. Photochemical Homologation for the Preparation of Aliphatic Aldehydes in Flow. *J. Org. Chem.* **2018**, *83* (24), 15558–15568.

(41) Zhang, C.; Zhang, L.; Jiao, N. Catalyst Free Approach to Benzimidazoles Using Air as the Oxidant at Room Temperature. *Green Chem.* **2012**, *14* (12), 3273.

(42) Skerlj, R.; Bridger, G.; Zhou, Y.; Bourque, E.; McEachern, E.; Danthi, S.; Langille, J.; Harwig, C.; Veale, D.; Carpenter, B.; et al. Mitigating HERG Inhibition: Design of Orally Bioavailable CCR5 Antagonists as Potent Inhibitors of R5 HIV-1 Replication. *ACS Med. Chem. Lett.* **2012**, *3* (3), 216–221.

(43) Choi, Y. J.; Seo, J. H.; Shin, K. J. Successful Reduction of Off-Target HERG Toxicity by Structural Modification of a T-Type Calcium Channel Blocker. *Bioorg. Med. Chem. Lett.* **2014**, *24* (3), 880–883.

(44) Yang, Z.-Q.; Barrow, J. C.; Shipe, W. D.; Schlegel, K.-A. S.; Shu, Y.; Yang, F. V.; Lindsley, C. W.; Rittle, K. E.; Bock, M. G.; Hartman, G. D.; et al. Discovery of 1,4-Substituted Piperidines as Potent and Selective Inhibitors of T-Type Calcium Channels. *J. Med. Chem.* **2008**, *51* (20), 6471–6477.

(45) Zhou, Z.; Vorperian, V. R.; Gong, Q.; Zhang, S.; January, C. T. Block of HERG Potassium Channels by the Antihistamine Astemizole and Its Metabolites Desmethylastemizole and Norastemizole. *J. Cardiovasc. Electrophysiol.* **1999**, *10*, 836–843.

(46) Hudlický, M. Fluorination with Diethylaminosulfur Trifluoride and Related Aminofluorosulfuranes. In *Organic Reactions*; John Wiley & Sons, Inc.: Hoboken, NJ, USA, **1988**; pp 513–637.

(47) Baptista, L.; Bauerfeldt, G. F.; Arbilla, G.; Silva, E. C. Theoretical Study of Fluorination Reaction by Diethylaminosulfur Trifluoride (DAST). *J. Mol. Struct. Theochem.* **2006**, *761* (1–3), 73–81.

(48) Musonda, C. C.; Whitlock, G. A.; Witty, M. J.; Brun, R.; Kaiser, M. Chloroquine–Astemizole Hybrids with Potent in Vitro and in Vivo Antiplasmodial Activity. *Bioorg. Med. Chem. Lett.* **2009**, *19*, 481–484.

(49) Kuter, D.; Streltsov, V.; Davydova, N.; Venter, G. A.; Naidoo, K. J.; Egan, T. J. Solution Structures of Chloroquine–Ferriheme Complexes Modeled Using MD Simulation and Investigated by EXAFS Spectroscopy. *J. Inorg. Biochem.* **2016**, *154*, 114–125.

(50) Alumasa, J. N.; Gorka, A. P.; Casabianca, L. B.; Comstock, E.; de Dios, A. C.; Roepe, P. D. The Hydroxyl Functionality and a Rigid Proximal N Are Required for Forming a Novel Non-Covalent Quinine-Heme Complex. *J. Inorg. Biochem.* **2011**, *105* (3), 467–

475.

(51) Madrid, P. B.; Sherrill, J.; Liou, A. P.; Weisman, J. L.; DeRisi, J. L.; Guy, R. K. Synthesis of Ring-Substituted 4-Aminoquinolines and Evaluation of Their Antimalarial Activities. *Bioorg. Med. Chem. Lett.* **2005**, *15* (4), 1015–1018.

(52) Ridley, R. G.; Hofheinz, W.; Matile, H.; Jaquet, C.; Dorn, A.; Masciadri, R.; Jolidon, S.; Richter, W. F.; Guenzi, A.; Girometta, M. A.; et al. 4-Aminoquinoline Analogs of Chloroquine with Shortened Side Chains Retain Activity against Chloroquine-Resistant Plasmodium Falciparum. *Antimicrob. Agents Chemother.* **1996**, *40* (8), 1846–1854.

(53) Solomon, V. R.; Haq, W.; Srivastava, K.; Puri, S. K.; Katti, S. B. Synthesis and Antimalarial Activity of Side Chain Modified 4-Aminoquinoline Derivatives. *J. Med. Chem.* **2007**, *50* (2), 394–398.

(54) Egan, T. J.; Hunter, R.; Kaschula, C. H.; Marques, H. M.; Misplon, A.; Walden, J. Structure−Function Relationships in Aminoquinolines: Effect of Amino and Chloro Groups on Quinoline−Hematin Complex Formation, Inhibition of β-Hematin Formation, and Antiplasmodial Activity. *J. Med. Chem.* **2000**, *43* (2), 283–291.

(55) Nsumiwa, S.; Kuter, D.; Wittlin, S.; Chibale, K.; Egan, T. J. Structure–Activity Relationships for Ferriprotoporphyrin IX Association and β-Hematin Inhibition by 4-Aminoquinolines Using Experimental and Ab Initio Methods. *Bioorg. Med. Chem.* **2013**, *21* (13), 3738–3748.

(56) Egan, T. J. Interactions of Quinoline Antimalarials with Hematin in Solution. *J. Inorg. Biochem.* **2006**, *100* (5–6), 916–926.

(57) Hoang, A. N.; Sandlin, R. D.; Omar, A.; Egan, T. J.; Wright, D. W. The Neutral Lipid Composition Present in the Digestive Vacuole of Plasmodium Falciparum Concentrates Heme and Mediates β-Hematin Formation with an Unusually Low Activation Energy. *Biochemistry* **2010**, *49* (47), 10107–10116.

(58) Lavis, L. D.; Raines, R. T. Bright Ideas for Chemical Biology. *ACS Chem. Biol.* **2008**, *3* (3), 142–155.

(59) Levi, J.; Cheng, Z.; Gheysens, O.; Patel, M.; Chan, C. T.; Wang, Y.; Namavari, M.; Gambhir, S. S. Fluorescent Fructose Derivatives for Imaging Breast Cancer Cells. *Bioconjug. Chem.* **2007**, *18* (3), 628–634.

(60) Wiederschain, G. Y. The Molecular Probes Handbook. A Guide to Fluorescent Probes and Labeling Technologies. *Biochem.* **2011**, *76* (11), 1276–1276.

(61) Lin, S.; Struve, W. S. Time-resolved Fluorescence of Nitrobenzoxadiazole-aminohexanoic Acid: Effect of Intermolecular Hydrogen-bonding on Non-radiative Decay. *Photochem. Photobiol.* **1991**, *54* (3), 361–365.

(62) Chattopadhyay, A. Chemistry and Biology of N-(7-Nitrobenz-2-Oxa-1,3-Diazol-4-Yl)-Labeled Lipids: Fluorescent Probes of Biological and Model Membranes. *Chem. Phys. Lipids* **1990**, *53* (1), 1–15.

(63) Dai, Z.; Dulyaninova, N. G.; Kumar, S.; Bresnick, A. R.; Lawrence, D. S. Visual Snapshots of Intracellular Kinase Activity at the Onset of Mitosis. *Chem. Biol.* **2007**, *14* (11), 1254–1260.

CHAPTER 3

BIOLOGICAL EVALUATION, SOLUBILITY, AND STRUCTURE-ACTIVITY RELATIONSHIPS

4.1 Chapter overview

This chapter discusses the biological activity and solubility of the synthesized compounds, in line with the second and fifth aims of this Ph.D. project. To ensure the progression of quality compounds only, a screening cascade (Figure 3.1) was used. The cascade established a progression-criteria, which played a critical role in prioritizing compounds based on specific cut-offs. These cut-offs are described in Figure 3.1 and reiterated at the beginning of each sub-section. The chapter begins with the discussion of *in vitro* antiplasmodium activity (asexual-blood stage) and solubility of all synthesized compounds and selected intermediates. This is followed by the *in vitro* gametocytocidal activity (sexual stages IV – V), cytotoxicity, and hERG inhibition profiles of selected compounds. Finally, the microsomal metabolic stability, *in vivo* antimalarial efficacy and pharmacokinetic (PK) profiles of front-runner compounds are presented and discussed.

3.2 *In vitro* Asexual-blood Stage Antiplasmodium Activity & Solubility

Following successful synthesis and full characterization (Chapter 2), all target compounds were subjected to HPLC-MS analysis to ensure that the purity was ≥95%, after which *in vitro* asexual blood-stage antiplasmodium activity was assessed (Figure 3.1). The activity of compounds was tested against the CQ-sensitive laboratory strain of *P. falciparum* NF54 (*Pf*NF54), and all compounds with *Pf*NF54 IC_{50} < 0.5 μM were further tested against the multi-drug resistant (MDR) *Pf* K1 strain (Figure 3.1). In these assays, compounds were tested using either a parasite lactate dehydrogenase (pLDH) assay as a marker for parasite survival, or *via* the modified [^{3}H]-hypoxanthine incorporation assay. pLDH assays were performed by the Drug Discovery and Development Centre (H3D), Division of Clinical Pharmacology, Department of Medicine, University of Cape Town, while the modified [^{3}H]-hypoxanthine incorporation assay was performed at the Swiss Tropical and Public Health Institute in Basel, Switzerland. *In vitro* activity is reported as the concentration of a compound required to achieve 50% *Pf* inhibition (IC_{50}).

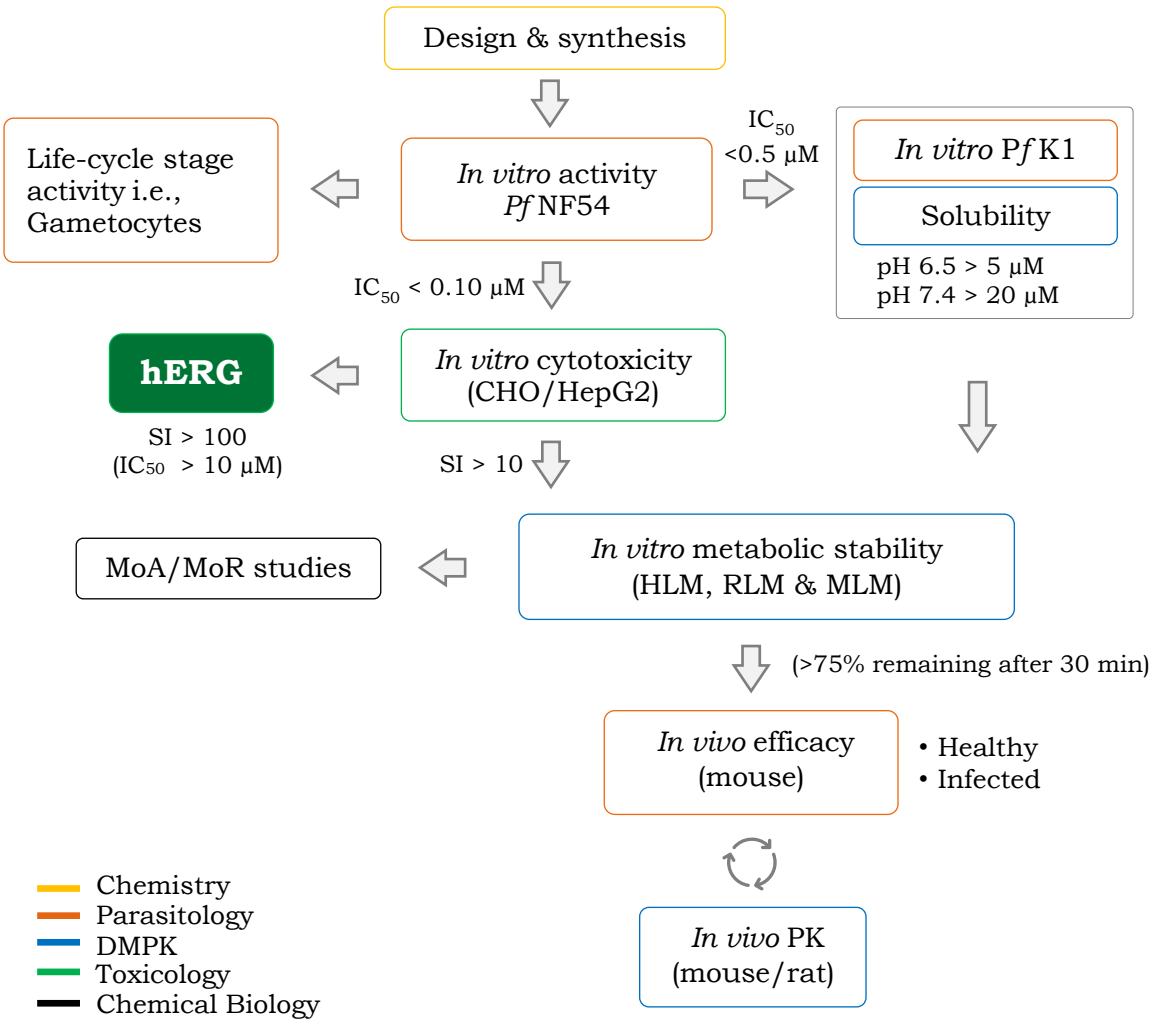

Pf: *Plasmodium falciparum*
IC_{50}: concentration required for 50% inhibition
CHO: Chinese hamster ovary cell-line
HepG2: Human epithelial cell-line
hERG: human ether-*á-go-go* related gene
DM(PK): drug metabolism and pharmacokinetics
SI: selectivity index
MLM: mouse liver microsomes
RLM: rat liver microsomes
HLM: human liver microsomes
MoA: mechanism of action
MoR: mechanism of resistance

Figure 3.1: Screening cascade and progression criteria for compounds

In parallel with *in vitro* activity, the solubility of all the compounds was assessed using a the turbidimetric solubility method, in which the turbidity of a compound that precipitates is measured spectrophotometrically following incubation in phosphate buffered saline (PBS) at pH 7.4. Solubility ($S_{7.4}$) data are expressed in micromolar (µM) units. The experimental chapter (Chapter 6) provides a detailed description of all assays used in this study.

A summary of the *in vitro* antiplasmodium activity and solubility data is shown in Tables 3.1–3.8 (AST phase I and II), Tables 3.9–3.10 (AST-CQ).

3.2.1 SAR and Solubility of Phase I AST Analogues

3.2.1.1 Phase I: Benzimidazole N-1 Substituted Analogues (SAR 1)

AST phase I analogues were developed by building on the SAR described by Roman *et al.* and De Jonghe *et al.*, using *di*-cyanated compound **17** (Table 3.1) as a starting point. In **SAR 1**, various Craig plot substituents were investigated and other modifications, including deletion of the benzyl moiety and replacement with the methyl group or pyridyl moieties, were also carried out.

Compound **17** retained antiplasmodium potency (IC_{50} = 0.156 μM), which was comparable to the hit compound AST (IC_{50} = 0.086 μM) and displayed greater solubility ($S_{7.4}$ = 100 μM). In this SAR, compounds generally had IC_{50} values > 0.100 μM, with only 2 of 16 analogues showing activity higher than AST (**18** and **29**). Notably, removal of the benzyl group (**15**, IC_{50} = 0.579 μM) led to a 7-fold loss of potency, while replacement with the methyl group was detrimental to activity (**16**, IC_{50} = 5.08 μM), an observation that within this SAR, highlights the significance of benzimidazole N-1 substitution. CN/F disubstitution on the benzyl group was generally tolerated, although potency was lowered by ~2-fold when the CN group was in the *ortho*-position (**19**, IC_{50} = 0.185 μM), compared to fluorine (**20**, IC_{50} = 0.108 μM). However, CN/F disubstitution preferentially favored *para*-CN and *meta*-F regioisomerism (**18**, IC_{50} = 0.071 μM). Craig plot substitution tends to generally favor electron withdrawing groups (EWGs). However, among the groups tested, only the CN and CF_3 groups are tolerated (**17** – **18**, **26**; IC_{50} < 0.3 μM) among electron withdrawing-hydrophilic and electron withdrawing-hydrophobic groups, respectively. Pyridyl analogues (**29** and **30**) were more active than their phenyl (**26** and **27**) match pairs, with the 4-trifluoromethyl-3-pyridyl analogue (**29**, IC_{50} = 0.025 μM) showing the highest activity in the series. *Pf*K1 data for some compounds showed potential for cross resistance (SI > 2) with existing antimalarial drugs (i.e., CQ).

As expected, analogues bearing water solubilizing groups generally exhibited moderate to high solubility ($S_{7.4}$ = 80 – 200 μM) compared to those with lipophilic substituents such as nitro or halogens ($S_{7.4}$ < 80 μM). Despite being the least active (IC_{50} > 6 μM), the carboxylic acid analogue **25** was as expected highly soluble ($S_{7.4}$ >200 μM). Methylation of the benzyl methylene linker in **17** was envisaged to push the benzyl group further out of plane with the benzimidazole ring, and increase molecular complexity (introduce three-dimensional and sp^3 character), both of which would translate into improved solubility.[1] This effect was indeed observed in the increased solubility of **28** ($S_{7.4}$ = 120 μM) compared to that of **17** ($S_{7.4}$ = 90 μM), without affecting antiplasmodium potency.

Table 3.1: *In vitro* antiplasmodium activity (*Pf*NF54 and K1) and solubility data of **phase I**, **SAR 1** analogues.

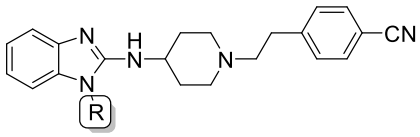

No./Lab Code	**R**	**R_1**	***Pf* IC_{50} (µM)[a,b]**		**RI[c]**	**Sol.[d] (µM)**
			NF54	**K1**		
15/DM-289	H	-	0.579	ND[e]	-	120
16/DM-290	Me	-	5.080	ND[e]	-	100
17/DM-032	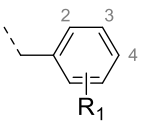	4-CN	0.156	0.176	1.12	90
18/DM-080		3-F,4-CN	0.071	0.211	2.97	40
19/DM-085		2-CN,4-F	0.185	4.013	-	50
20/DM-081		2-F,4-CN	0.108	ND[e]	-	20
21/DM-280		4-OMe	0.624	ND[e]	-	50
22/DM-274		4-SO_2Me	0.485	ND[e]	-	40
23/DM-294		4-NO_2	0.952	ND[e]	-	20
24/DM-282		4-CO_2Me	0.591	ND[e]	-	120
25/DM-283		4-CO_2H	>6	ND[e]	-	>200
26/DM-275		4-CF_3	0.253	0.384	1.52	20
27/DM-273		4-CH_3	0.565	ND[e]	-	80
28/DM-092	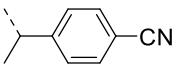	-	0.156	0.157	1.01	120
29/DM-272	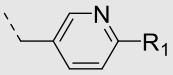	CF_3	0.025	0.082	3.28	20
30/DM-086		CH_3	0.261	ND[e]	-	50

[a]Mean from n ≥ 2 independent experiments with sensitive (*Pf*NF54) and MDR (*Pf*K1) strains
[b]Chloroquine (NF54 50% inhibitory concentration [IC_{50}] = 0.004 µM; K1 IC_{50} = 0.14 µM) was used as a reference drug
[c]Resistance index = (*Pf*K1 IC_{50}/*Pf*NF54 IC_{50})
[d]Determined using a turbidimetric method at pH 7.4. Hydrocortisone (>200 µM) and reserpine (<10 µM) were used as control drugs
[e]ND, not determined

3.2.1.2 Phase I: Lateral Phenyl Group and Ester Group Bioisosteres SAR Explorations (SARs 2 and 3)

As observed in SAR 1, substitution at the 4-phenyl position in SAR 2 was also favored by EWGs (Table 3.2). This is evident in the carboxylate analogues whose activities ranged from low to high in analogues containing carboxylic acid (CO_2H), methyl ester (CO_2Me) and ethyl

ester (CO_2Et) groups. Activity was retained in the hydroxyl analogue **32** (IC_{50} = 0.028 μM), and the runner-up trifluoromethyl analogue **35** (IC_{50} = 0.035 μM).

Comparing the hydroxyl (**32**), trifluoromethyl (**35**) and the ethyl ester (**38**) analogues, the ester group is more chemically versatile and amenable to structural mimicry by the exploration of bioisosteres, which may prove useful in mitigating its underlying susceptibility towards CYP-mediated phase one metabolism and other potential liabilities. Therefore, non-classical bioisosteres of the ethyl ester group were also explored in SAR 2. Potency was improved and/or retained in 1,2,4-oxadiazoles and oxazolines (IC_{50} = 0.021–0.104 μM), falling within the potency cut-off with respect to the progression criteria (IC_{50} <0.100 μM). However, 1,2,4-oxadiazoles were more potent than their oxazoline counterparts (Table 3.2).

Table 3.2: *In vitro* antiplasmodium activity (*Pf* NF54 and K1) and solubility data of **phase I**, **SARs 2 & 3** analogues

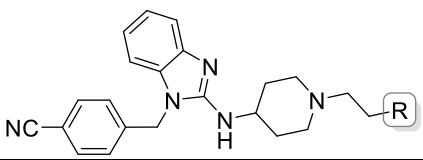

No./Lab Code	**R**	**R_1**	***Pf* IC_{50} (μM)[a,b]**		**RI[c]**	**Sol.[d] (μM)**
			NF54	**K1**		
31/DM-063	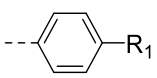	H	0.163	0.170	1.04	40
32/DM-061		OH	0.028	0.041	1.46	120
33/DM-054		SO_2Me	0.238	4.592	-	80
34/DM-286		CH_3	0.357	ND[e]	-	40
35/DM-118		CF_3	0.035	0.103	2.94	20
36/DM-285		NO_2	0.486	ND[e]	-	40
37/DM-257		CO_2Me	0.204	ND[e]	-	80
38/DM-162		CO_2Et	0.043	0.052	1.21	40
39/DM-259		CO_2H	>6	ND[e]	-	120
40/DM-113			0.089	0.221	2.49	40
41/DM-114		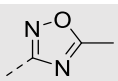	0.051	0.174	3.41	40
42/DM-129		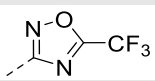	0.021	0.049	2.33	20
43/DM-120	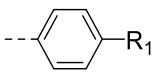	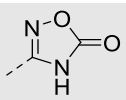	1.240	ND[e]	-	40
44/DM-128		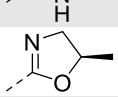	0.104	0.352	3.38	60
45/DM-124		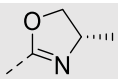	0.074	0.263	3.55	20
46/DM-039		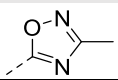	0.069	0.192	2.78	20

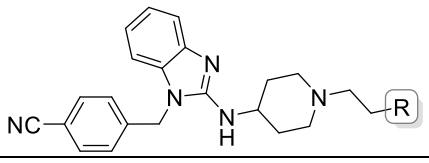

No./Lab Code	**R**	**R$_1$**	***Pf* IC$_{50}$ (µM)[a,b]**		**RI[c]**	**Sol.[d] (µM)**
			NF54	**K1**		
47/DM-050	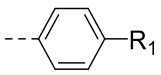	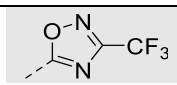	0.022	0.096	4.36	10
48/DM-036		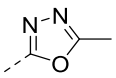	0.519	0.693	1.34	20
49/DM-049			4.152	ND[e]	-	20
50/DM-058			1.386	ND[e]	-	20
51/DM-067			1.248	ND[e]	-	<5
52/DM-065	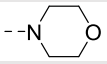		>6	ND[e]	-	10
53/DM-071	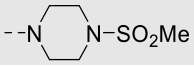		>6	ND[e]	-	40
54/DM-068	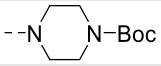		1.542	ND[e]	-	<10
55/DM-069	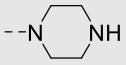		1.677	ND[e]	-	20

[a]Mean from n ≥ 2 independent experiments with sensitive (*Pf*NF54) and MDR (*Pf*K1) strains
[b]Chloroquine (NF54 50% inhibitory concentration [IC$_{50}$] = 0.004 µM; K1 IC$_{50}$ = 0.14 µM) was used as a reference drug
[c]Resistance index = (*Pf*K1 IC$_{50}$/*Pf*NF54 IC$_{50}$)
[d]Determined using a turbidimetric method at pH 7.4. Hydrocortisone (>200 µM) and reserpine (<10 µM) were used as control drugs
[e]ND, not determined

1,2,4-oxadiazole SAR revealed a gradual increase in activity following substitution at the 5-position. A 1.7-fold difference in activity was observed between unsubstituted **40** (5-H, IC$_{50}$ = 0.089 µM) and methyl substituted **41** (5-CH$_3$, IC$_{50}$ = 0.051 µM), while trifluoro methyl substituted **42** (5-CF$_3$, IC$_{50}$ = 0.021 µM) was 2.4-fold more active than **41**. This trend not only suggests the significance of substitution at the 5-position in the 1,2,4-oxadiazole moiety, but also revealed the existence of a potential lipophilicity-activity correlation at this position. To test the effect of regio-isomerism, reversed 3-substituted-1,2,4-oxadiazoles (**46** and **47**) were synthesized. 3-/5-CF$_3$- and 3-/5-CH$_3$-1,2,4-oxadiazole reverse pairs were either equipotent (**42**/**47**, IC$_{50}$ = 0.021 µM), or showed activity within a 1.4-fold difference (**41**, IC$_{50}$ = 0.051 µM; **46**, IC$_{50}$ = 0.069 µM), suggesting that potency is independent of regio-isomerism within the series.

On the other hand, 1,3,4-oxadiazole **48** (IC$_{50}$ = 0.519 µM) displayed >10-fold lower activity compared to its 1,2,4-oxadiazole match pairs (**41**, IC$_{50}$ = 0.051 µM and **46**, IC$_{50}$ = 0.069 µM). This observation may be attributed to the differences in the aromaticity and the closeness

of the two moieties in mimicking the ester group. Theoretically, 1,2,4-oxadiazoles have been experimentally proven to exhibit similar spectral properties as that of conjugate dienes, and therefore do not have significant aromaticity compared to the rather symmetrical 1,3,4-oxadiazoles,[2,3] although both satisfy Hückel's rule, which estimates whether a planar molecule will have aromatic properties based on the number of *pi* (π) electrons. This difference can also be seen in the different reactivities of the two isomers. 1,2,4-oxadiazoles are more prone to conjugate addition (like dienes or α,β-unsaturated ketones) as opposed to 1,3,4-oxadiazoles which favor substitution (like aromatic rings).[4,5] Therefore, based on this evidence, 1,2,4-oxadiazoles are more closely related to the ester group and best recapitulate sufficient hydrogen-bonding capability as opposed to π-π-stacking, hydrophobic interactions and cation-π interactions which 1,3,4-oxadiazoles exhibit due to their aromatic nature.[5,6] These properties may impart significant differences in the intrinsic interactions of the two isomers with macromolecules at the target site, which may explain the shift in potencies between the two isomeric forms.

Activity was lost in the oxadiazolone **43** (IC_{50} = 1.240 μM). This, however, is not surprising since 5-oxo-1,2,4-oxadiazoles are more closely related to carboxylic acids than they are to esters.[7] Therefore, notwithstanding the observed 5-fold higher activity of **43** compared to carboxylic acid derivative **39**, they both demonstrated low activity. Oxazolines **45** (IC_{50} = 0.074 μM) and **44** (IC_{50} = 0.104 μM) displayed comparable activities. However, the relatively higher activity observed for 4-methyl-oxazoline **45** may suggest the possible existence of SAR relating to the regio-isomerism of the methyl group. With the exception of 1,3,4-oxadiazole **48**, all other ester bioisostere analogues of **38** showed lower potential for cross-resistance with CQ than **38** (SI > 2).

In SAR 3, replacement of the phenyl moiety with heteroaromatic or aliphatic moieties resulted in loss of activity (IC_{50} > 1.2 μM), and consequently, this SAR was not pursued further as the results from these few analogues indicated the significance of the phenyl group in the AST pharmacophore.

All analogues of SAR 2 and 3 exhibited low to moderate solubility (10 – 80 μM), showing no improvement relative to AST. However, analogues containing 4-OH (**32**) and 4-CO_2H (**39**) in the lateral phenyl group displayed relatively high solubility ($S_{7.4}$ = 120 μM), attributable to the solubilizing nature of the two groups compared to 4-CN in **17** and 4-Ome in AST.

3.2.1.3 Phase I: Diaminoalkyl Linker (SAR 4) and Revisited Benzimidazole N-1 Substitution (SAR 1_B)

The identification of 3-/5-CH_3-1,2,4-oxadiazoles **41**/**46** and 3-/5-CF_3-1,2,4-oxadiazoles **42**/**47**, which exhibited higher activity and microsomal metabolic stability profiles compared to AST provided the basis for the design of SAR 4 and SAR 1_B analogues. Owing to the expectation that invaluable structural information may be harnessed from the progression

of less active compounds than highly active ones,[8,9] compound **46** (IC_{50} = 0.069 μM) was selected as the better candidate than **47** (IC_{50} = 0.021 μM) for the derivation of further SAR because its relatively lower potency would allow for concise SAR to be derived. Additionally, the chemical tractability and lower cost of materials associated with the preparation of the 3-CH_3-1,2,4-oxadiazole moiety compared to the 3-CF_3-1,2,4-oxadiazole would allow for the preparation of more analogues for a more diverse SAR.

In SAR 4, various diaminoalkyl linkers were explored as replacements for 4-aminopiperidine in **46**. Replacement with either pyrrolidine or piperazine has been shown be an effective strategy for lowering a compound's affinity for hERG channels.[10–12] However, this change produced compounds with lower activity (IC_{50} > 0.4 μM, Table 3.3). Additionally, the data revealed that the stereochemistry (*R*/*S*) of pyrrolidine had no effect on the potency of the resulting compounds (**58**/**59**, IC_{50} ~ 0.410 μM) in the CQ-sensitive *Pf*NF54 strain. However, the *R*-form (**59**, *Pf*K1 IC_{50} = 1.32 μM) is >3-fold less active than the *S*-form (**59**, *Pf*K1 IC_{50} = 0.40 μM) in the MDR *Pf*K1 strain. Interestingly, the solubility profile of pyrrolidine derivatives was 4-fold higher (**58**/**59**; $S_{7.4}$ = 80 μM), compared to that of piperidine containing **46** ($S_{7.4}$ = 20 μM). Substitution with 2,6-diazaspiro[3.4]octane (**60**, IC50 = 0.446 μM) produced comparable potency as that of pyrrolidine derivative, albeit 2-fold lower solubility was observed. Introduction of stereochemistry *via* methylation of piperazine had no effect on potency (**61**/**62**, IC_{50} ~ 1.4 μM), with respect to the I-enantiomer used.

Table 3.3: *In vitro* antiplasmodium activity (*Pf* NF54 and K1) and solubility data of **phase I**, **SAR 4** and **SAR 1$_B$** analogues.

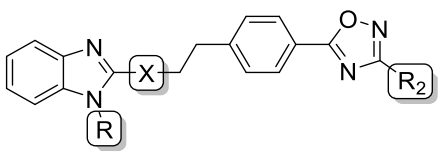

No./Lab Code	**R**	**R_1**	**X**	**R_2**	***Pf* IC_{50} (μM)[a,b]**		**RI[c]**	**Sol.[d] (μM)**
					NF54	**K1**		
58/DM-134	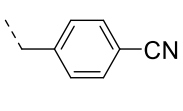	-	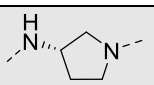	CH_3	0.400	0.403	1.01	80
59/DM-136		-	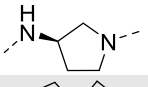		0.415	1.315	3.17	80
60/DM-178		-	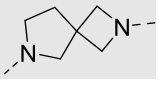		0.446	0.890	2.00	40
61/DM-188		-	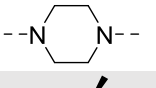		1.514	ND[e]	-	20
62/DM-187		-	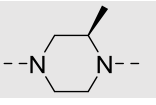		1.328	ND[e]	-	40
65/DM-322		-	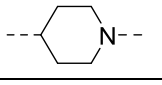		1.141	ND[e]	-	20

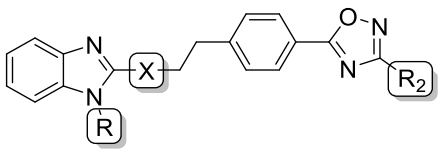

No./Lab Code	**R**	**R_1**	**X**	**R_2**	***Pf* IC_{50} (μM)[a,b]**		**RI[c]**	**Sol.[d] (μM)**
					NF54	**K1**		
66/DM-130	H	-		CH_3	0.055	0.176	3.20	80
67/DM-253	H	-		CF_3	0.012	0.040	3.33	100
68/DM-147	CH_3	-		CH_3	0.033	0.082	2.48	160
69/DM-254	CH_3	-	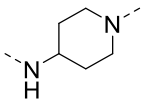	CF_3	0.066	0.048	0.73	160
70/DM-159		-		CH_3	0.702	ND[e]	-	20
71/DM-191	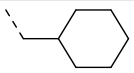	-		CH_3	0.093	ND[e]	-	80
72/DM-189	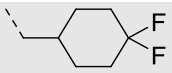	-		CH_3	0.460	ND[e]	-	20
73/DM-198	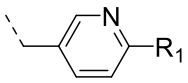	H	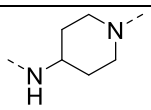	CH_3	0.304	ND	-	ND
74/DM-140		CF_3			0.044	0.173	3.93	40
75/DM-156	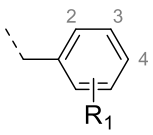	4-CF_3	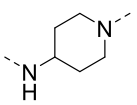	CH_3	0.030	0.104	3.47	10
76/DM-199		3-Me			0.530	ND[e]	-	20
77/DM-141		3-F, 4-CN			0.039	0.085	2.18	<10
78/DM-325		4-CO_2H			>6	ND[e]	-	80

[a]Mean from n ≥ 2 independent experiments with sensitive (*Pf*NF54) and MDR (*Pf*K1) strains
[b]Chloroquine (NF54 50% inhibitory concentration [IC_{50}] = 0.004 μM; K1 IC_{50} = 0.14 μM) was used as a reference drug
[c]Resistance index = (*Pf*K1 IC_{50}/*Pf*NF54 IC_{50})
[d]Determined using a turbidimetric method at pH 7.4. Hydrocortisone (>200 μM) and reserpine (<10 μM) were used as control drugs
[e]ND, not determined

However, the 3D character brought about by the presence of the methyl group at the α-position in piperazine translated to a 2-fold increase in aqueous solubility. Finally, the importance of the presence of the 2° amine (NH) at the 2-position of benzimidazole was highlighted, as seen in C-linked piperidine analogue **65** (IC_{50} = 1.14 μM), in which activity was 16-fold lower, compared to that of 4-aminopiperidine-linked **46** (IC_{50} = 0.069 μM).

Rather than SAR 1 explorations in which a 4-CN group was present in the lateral phenyl group, SAR 1_B sought to revisit and expand the benzyl group SAR with the 5-CH_3-1,2,4-oxadiazole moiety present (Table 3.3). This time, aromatic ring saturation was also considered, as a strategy to potentially reduce hERG affinity and increase solubility.[10,13] There was a consistent improvement in the potency associated with SAR at the benzimidazole 1-position (N-1). For instance, truncation/removal of the benzyl moiety (**66**, IC_{50} = 0.055 μM) or replacement with a methyl group (**68**, IC_{50} = 0.033 μM) was accompanied

by 18-fold and 154-fold increases in potency, respectively, compared to previously weakly active (**15**, IC_{50} = 0.579 μM) and inactive (**16**, IC_{50} = 5.08 μM) cyano match pairs. Additionally, 4-fold and 8-fold higher solubilities were observed in **66** and **68**, respectively, compared to **46** ($S_{7.4}$ = 20 μM). The phenomenon of N-methylation (or O-methylation) has being widely used in medicinal chemistry to improve solubility, therefore, the 2-fold solubility difference between desmethyl and N-methyl analogues is expected.[14] Among the benzimidazole N-methyl analogues, the hydrogen-bonding capacity of 1,2,4-oxadiazole derivative **68** translates to 1.6-fold higher solubility compared to that of CN derivative **16** despite having a higher lipophilicity. Following the preparation of corresponding 3-CF_3-1,2,4-oxadiazoles of **66** and **68**, a 5-fold increase in potency was observed, with respect to desmethyl **67** (IC_{50} = 0.012 μM), consistent with previous observation in SAR 2. However, this was not the case with N-methyl derivative **69** (IC_{50} = 0.066 μM), in which a 2-fold lower potency was observed. The significance of the oxadiazole moiety as an important structural feature in the scaffold was further validated in analogues **74** (IC_{50} = 0.044 μM), **75** (IC_{50} = 0.030 μM) and **77** (IC_{50} = 0.039 μM), in which activity was either retained or improved compared to either ester **38** (IC_{50} = 0.043 μM) or corresponding CN-substituted counterparts (**19**, IC_{50} = 0.185 μM; **26** IC_{50} = 0.253 μM; and **29** IC_{50} = 0.025 μM, respectively).

Activity was retained and solubility improved following saturation of the benzyl ring (**71**, IC_{50} = 0.093 μM). However, replacement with other saturated moieties such as isopropyl (**70**) and methyl (4,4-difluoro)cyclohexyl (**72**) was detrimental to activity (IC_{50} > 0.6 μM) and resulted in sub-optimal solubility.

Overall, exploratory phase I SAR revealed that the benzyl moiety was inconsequential within the 1,2,4-oxadiazole context. Moreover, aqueous solubility was higher, MW and lipophilicity (clog*P*) lower, and microsomal metabolic stability higher, in analogues devoid of the benzyl moiety or possessing *N*-methyl at the benzimidazole N-1 position.

3.2.2 SAR and Solubility of Phase II AST Analogues

Having established critical activity and solubility SAR from exploratory phase I SAR, front-runner compounds **67** and **68** were used as templates for the design of phase II analogues. Phase II SAR explorations would include incorporation of amides (SAR 1), extension of the functional diversity at the oxadiazole 3-position (SAR 2), exploration of substituents in the benzimidazole ring (SAR 3), as well as discreet modifications around the benzimidazole ring and reducing the pKa of the piperidine nitrogen (SAR 4).

3.2.2.1 Phase II: Amide Analogues of Compound 68 (SAR 1)

Incorporation of amides in a scaffold, also known as amidation, is one of the widely used strategies to detune hERG channel inhibition and improve solubility.[15,16] As previously described, amide analogues of AST have been previously synthesized in our research group, and sub-micromolar activity was observed (IC_{50} = 0.20 – 1.913 μM), with moderate to high

solubility (50 – 200 μM). Additionally, the piperazinyl amide MK-33 not only showed highest activity (IC_{50} = 0.20 μM), but also displayed relatively high hERG channel inhibition and selectivity (IC_{50} = 8.61 μM; SI = 43). On the basis of data, a small library of 29 diverse amides replacing the oxadiazole moiety was prepared.

However, all amides were either weakly active or inactive at the highest concentration tested (IC_{50} = 1.73 to >6 μM, Table 3.4), with no significantly discernable SAR. This included the piperazinyl amide **103** (IC_{50} = 3.41 μM) analogue of MK-33, which contained a 4-F-benzyl moiety. This observation points to the specific and intricate structural architecture required at the 4-position of the anisole moiety, and benzimidazole N-1 position in AST. Moreover, ethyl ester analogue **80** showed superior potency (IC_{50} = 0.671 μM), supporting the preference of the ethyl ester over methyl ester group or an amide group at that position. The solubility of these amides was moderate (80 – 150 μM).

Table 3.4: *In vitro* antiplasmodium activity (*Pf* NF54 and K1) and solubility data of **phase II**, **SAR 1** analogues.

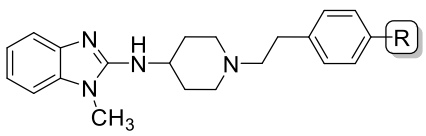

No. /Lab Code	**R**	***Pf* IC_{50} (μM)[a,b]**		**RI[c]**	**Sol.[d] (μM)**
		NF54	**K1**		
79/DM-221	CO_2Me	1.450	ND[e]	-	80
80/DM-222	CO_2Et	0.671	1.88	2.8	120
81/DM-223	CO_2H	>6	ND[e]	-	160
83/DM-248		>6	ND[e]	-	80
84/DM-233	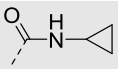	1.99	ND[e]	-	80
85/DM-244	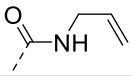	2.61	ND[e]	-	80
86/DM-242	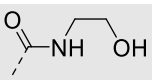	4.17	ND[e]	-	120
87/DM-243	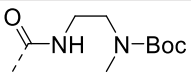	>6	ND[e]	-	160
88/DM-245	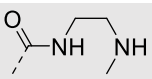	>6	ND[e]	-	100
89/DM-250	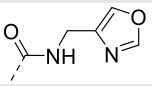	4.80	ND[e]	-	160
90/DM-225	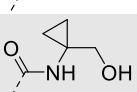	1.73	ND[e]	-	60
91/DM-238	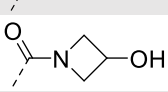	3.46	ND[e]	-	80
92/DM-231	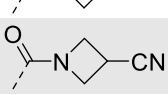	>6	ND[e]	-	60
93/DM-230	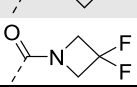	>6	ND[e]	-	40

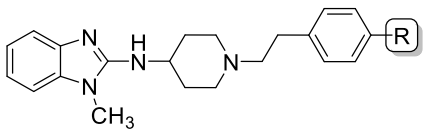

No. /Lab Code	**R**	***Pf* IC_{50} (μM)[a,b]**		**RI[c]**	**Sol.[d] (μM)**
		NF54	**K1**		
94/DM-239	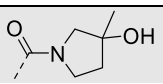	>6	ND[e]	-	80
95/DM-227	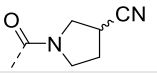	5.86	ND[e]	-	80
96/DM-226	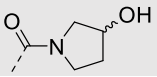	3.99	ND[e]	-	80
97/DM-228	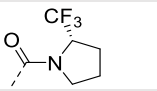	2.97	ND[e]	-	40
98/DM-237	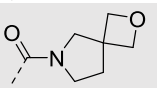	>6	ND[e]	-	60
99/DM-246	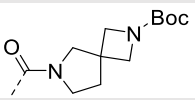	4.25	ND[e]	-	40
100/DM-247	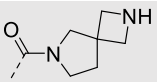	>6	ND[e]	-	160
101/DM-249	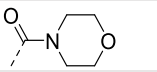	>6	ND[e]	-	80
102/DM-205	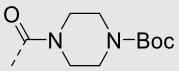	3.83	ND[e]	-	70
103/DM-208	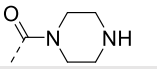	3.41	ND[e]	-	120
104/DM-212	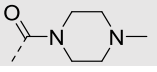	4.96	ND[e]	-	80
105/DM-213	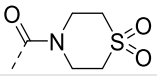	>6	ND[e]	-	80
106/DM-218	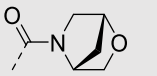	>6	ND[e]	-	100
107/DM-217	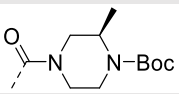	2.17	ND[e]	-	80
108/DM-219	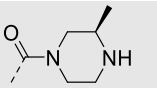	3.04	ND[e]	-	100
109/DM-240	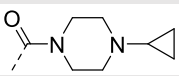	5.12	ND[e]	-	60
110/DM-229	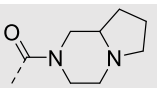	1.28	ND[e]	-	60
111/DM-236	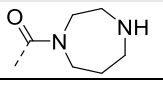	3.64	ND[e]	-	80

[a]Mean from n ≥ 2 independent experiments with sensitive (*Pf*NF54) and MDR (*Pf*K1) strains
[b]Chloroquine (NF54 50% inhibitory concentration [IC_{50}] = 0.004 μM; K1 IC_{50} = 0.14 μM) was used as a reference drug
[c]Resistance index = (*Pf*K1 IC_{50}/*Pf*NF54 IC_{50})
[d]Determined using a turbidimetric method at pH 7.4. Hydrocortisone (>200 μM) and reserpine (<10 μM) were used as control drugs
[e]ND, not determined

3.2.2.2 Phase II: Diversity Exploration of the 3-position in the 1,2,4-oxadiazole Moiety (SAR 2)

The independence of potency in relation to regio-isomerism in the 1,2,4-oxadiazole ring was established in phase I SAR 2. However, the 3- or 5-position provided an opportunity to explore structural diversity. Therefore, various small lipophilic and hydrophilic groups were introduced at the 3-position as shown in Table 3.5.

Within this largely chemistry-driven SAR, extension of the substituent to more than two carbons, as well as introduction of polar groups led to lower activities, with IC_{50} values >13-fold higher (**115**, IC_{50} = 0.567 μM), compared to **68**. However, the *tert*-butyl analogue **120** (IC_{50} = 0.064 μM) was highly active and equipotent to **69** (IC_{50} = 0.066 μM), a CF_3 substituted analogue. This is not surprising as the *tert*-butyl group has been widely used as an effective CF_3 group surrogate, among other notable bulky structural isosteres such as pentafluorosulfanyl (SF_5), bicyclo[1.1.1]pentanyl (BCP), and cyclopropyl-trifluoromethyl (cyclopropyl-CF_3).[17,18] No apparent differences in activity was observed between cyclopropyl/isopropyl (**118**/**119**, IC_{50} = 0.490 μM) groups, despite their differences in size and steric effects.[19]

Table 3.5: *In vitro* antiplasmodium activity (*Pf* NF54 and K1) and solubility data of **phase II**, **SAR 2** analogues

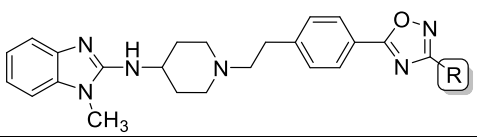

No./Lab Code	**R**	***Pf* IC_{50} (μM)[a,b]**		**RI[c]**	**Sol. (μM)[d]**
		NF54	**K1**		
115/DM-352		0.567	ND[e]	-	100
116/DM-343		0.383	ND[e]	-	80
117/DM-252		0.831	ND[e]	-	120
118/DM-341		0.484	ND[e]	-	60
119/DM-356		0.492	ND[e]	-	60
120/DM-337		0.064	0.070	1.10	60
122/DM-339		>6	ND[e]	-	120

[a]Mean from n ≥ 2 independent experiments with sensitive (*Pf*NF54) and MDR (*Pf*K1) strains
[b]Chloroquine (NF54 50% inhibitory concentration [IC_{50}] = 0.004 μM; K1 IC_{50} = 0.14 μM) was used as a reference drug
[c]Resistance index = (*Pf*K1 IC_{50}/*Pf*NF54 IC_{50})
[d]Determined using a turbidimetric method at pH 7.4. Hydrocortisone (>200 μM) and reserpine (<10 μM) were used as control drugs
[e]ND, not determined

Incorporation of a carboxylic acid moiety at this position was found to be detrimental to activity (**122**, IC_{50} > 6.0 μM), a consistent trend observed for all carboxylic acid-bearing analogues in the scaffold. These analogues exhibited moderate to high solubility (60 – 180 μM). Consistently, analogues containing water-solubilizing groups such as OH showed higher solubility compared to lipophilic alkyl groups. On the other hand, dimethylamino (**117**) and the highly solubilizing carboxylic acid (**122**) displayed the highest solubility in the series ($S_{7.4}$ = 120 μM).

3.2.2.3 Phase II: Benzimidazole Ring Substituents (SAR 3)

The next SAR investigated the effect of benzimidazole substitution (Table 3.6). The 5-position was selected for *mono*-substitutions due to the ready availability of most starting materials. Compared to AST (IC_{50} = 0.086 μM) and frontrunner **68** (IC_{50} = 0.033 μM), reduced activities were observed.

However, methyl disubstituted analogue **139** (IC_{50} = 0.163 μM) exhibited the highest overall activity, demonstrating tolerability of the group on the core structure when compared to halogen match pairs **140 (**IC_{50} = 1.16 μM) and **141** (IC_{50} = 0.514 μM). Notably, chlorine disubstitution was better tolerated than that with fluorine, and produced superior activity (2-fold) in both mono- and disubstituted analogues (**137**, IC_{50} = 0.834 μM or **140**, IC_{50} = 1.161 μM, respectively). Carboxylic acid derivative **142** (IC_{50} > 6 μM) was inactive.

Table 3.6: *In vitro* antiplasmodium activity (*Pf* NF54 and K1) and solubility data of **phase II**, **SAR 3** analogues.

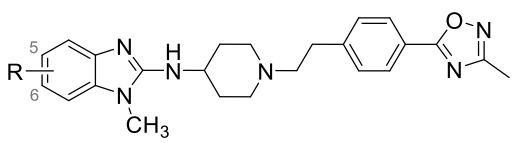

No./Lab Code	**R**	***Pf* IC_{50} (μM)[a,b]**		**RI[c]**	**Sol. (μM)[d]**
		NF54	**K1**		
132/DM-312	5-CN	0.611	1.42	2.32	80
133/DM-355	5-CF_3	0.422	ND[e]	-	40
134/DM-370	5-OMe	0.309	ND[e]	-	80
135/DM-318	5-SO_2Me	4.621	ND[e]	-	60
136/DM-400	5-CO_2Me	0.496	ND[e]	-	120
137/DM-382	5-F	0.834	ND[e]	-	80
138/DM-383	5-Br	0.720	ND[e]	-	80
139/DM-403	5,6-CH_3	0.163	ND[e]	-	60
140/DM-300	5,6-F	1.161	ND[e]	-	80

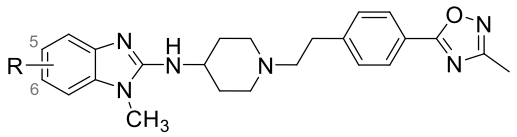

No./Lab Code	**R**	***Pf* IC$_{50}$ (μM)^{a,b}**		**RI^{c}**	**Sol. (μM)^{d}**
		NF54	**K1**		
141/DM-306	5,6-Cl	0.514	ND^{e}	-	80
142/DM-401	5-CO_2H	>6	ND^{e}	-	160
143/DM-401-01	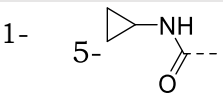	1.401	ND^{e}	-	160

^{a}Mean from n ≥ 2 independent experiments with sensitive (*Pf*NF54) and MDR (*Pf*K1) strains
^{b}Chloroquine (NF54 50% inhibitory concentration [IC$_{50}$] = 0.004 μM; K1 IC$_{50}$ = 0.14 μM) was used as a reference drug
^{c}Resistance index = (*Pf*K1 IC$_{50}$/*Pf*NF54 IC$_{50}$)
^{d}Determined using a turbidimetric method at pH 7.4. Hydrocortisone (>200 μM) and reserpine (<10 μM) were used as control drugs
^{e}ND, not determined

The availability of the carboxylic acid was used to access cyclopropyl amide **143**, which produced higher activity (IC$_{50}$ = 1.40 μM) although this remained suboptimal. The solubility profile of the analogues in this SAR was moderate to high (40 – 160 μM).

3.2.2.4 Phase II: Discreet Modifications and Reduction of Basicity (SAR 4)

In SAR 4, the first set of analogues included subtle modifications around the benzimidazole ring and the lateral phenyl group of front-runner compound **67** (IC$_{50}$ = 0.012 μM). Whereas the final set involved the incorporation of a fluorine group at the β-position around the piperidine nitrogen (β-fluorination, Table 3.7). β-fluorination around the piperidine nitrogen was envisaged to reduce the p*K*a of the nitrogen atom (Table 3.7) as a strategy to potentially reduce the hERG affinity of the resulting analogues.

Replacement the benzimidazole N-1 with O was detrimental to potency (**146**, IC$_{50}$ = 0.832 μM), whereas potency is retained or lowered following the incorporation of the nitrogen atom at either the 4- or 5-position of the benzimidazole ring. That is, 5-azabenzimidazole **149** (IC$_{50}$ = 0.017 μM), retains antiplasmodium potency, which is strikingly ~14-times higher than that of 4-azabenzimidazole **147** (IC$_{50}$ = 0.244 μM). However, although both azabenzimidazoles showed higher solubility (S$_{7.4}$ = 160 μM) compared to **67**.

Considering that *N*-containing heterocyclic fragments are susceptible to metabolism, primarily *via* aldehyde oxidase (AO)-mediated oxidation (phase I) followed by glucuronidation (phase II),[20,21] compounds **148** and **150** in which potential metabolic soft spots are blocked were prepared. The choice of blocking groups was dictated by (i) availability of starting materials and, (ii) previous SAR-3 (phase II) of tolerated groups.

Table 3.7: *In vitro* antiplasmodium activity (*Pf*NF54 and K1) and solubility data of **phase II**, **SAR 4** analogues.

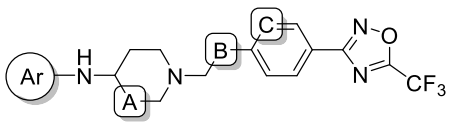

No./Lab Code	**Ar**	**A**	**B**	**C**	***Pf* IC_{50} (μM)[a,b] NF54**	**Sol. (μM)[c]**
146/DM-20-057	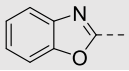	CH_2	CH_2	CH	0.832	100
147/DM-20-025	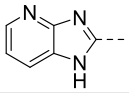				0.244	160
148/DM-20-023	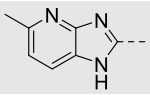				0.054	120
149/DM-20-030	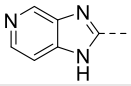				0.017	160
150/DM-20-029	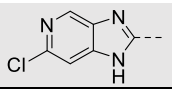				0.112	80
151/DM-20-027	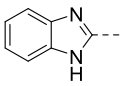		CH_2	CH	0.147	120
152/DM-20-038					0.644	80
157/DM-20-072			CH_2	N	>10	120
156/DM-20-068	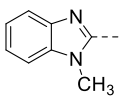	CH_2	CH_2	N	0.239	80
161/DM-20-058				CH	0.606	80

[a]Mean from n ≥ 2 independent experiments with sensitive (*Pf*NF54) and MDR (*Pf*K1) strains
[b]Chloroquine (NF54 50% inhibitory concentration [IC_{50}] = 0.004 μM; K1 IC_{50} = 0.14 μM) was used as a reference drug
[c]Determined using a turbidimetric method at pH 7.4. Hydrocortisone (>200 μM) and reserpine (<10 μM) were used as control drugs

Interestingly, 5–methyl-4-azabenzimidazole analogue **148** (IC_{50} = 0.054 μM) was ~5-fold more potent than the parent compound (**147**, IC_{50} = 0.244 μM), and showed comparable solubility. Conversely, potency and solubility were reduced in 6–chloro-5-azabenzimidazole analogue **150** (IC_{50} = 0.112 μM).

Reducing the p*K*a of the piperidine nitrogen *via* β-fluorination resulted in a loss of activity, with minimal effect on the solubility of the analogues (80 – 120 μM). Notably, this SAR revealed that piperidine ring β-monofluorination (**151**, IC_{50} = 0.147 μM) produced higher activity than highly inductive β-difluorination (**152**, IC_{50} = 0.644 μM). The combination of piperidine ring β-monofluorination and insertion of a nitrogen atom in the phenyl moiety was detrimental to potency (**157**, IC_{50} >10 μM), although solubility was optimal ($S_{7.4}$ = 120 μM). Conversely, introduction of N-heterocyclic character in the phenyl ring alone (**156**, IC_{50}

= 0.239 μM) produced moderate activity with moderate solubility ($S_{7.4}$ = 80 μM). Although there is a need to separate β-mono-fluorinated analogues into their respective diastereomers to fully derive the SARs in this approach, current data suggest that fluorine is better tolerated in the piperidine ring rather than the ethylene linker (**161**, IC_{50} = 0.606 μM). Holistically, the lower activity of the molecules in which the pKa is reduced confirms the significance of achieving sufficient basicity in the piperidine nitrogen.[22,23]

The antiplasmodium activity data of some of the intermediates in this SAR are shown in Table 3.8. Consistently, β-amino alcohol **159** (IC_{50} = 6.270 μM) was ~8.5-fold less potent than the corresponding fluoro analogue **160** (IC_{50} = 0.652 μM).

Table 3.8: *In vitro* antiplasmodium activity (*Pf*NF54) and solubility data of intermediates leading to analogues **156**, **157** and **161**.

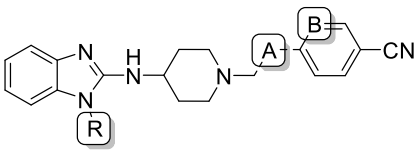

No./Lab Code	**R**	**A**	**B**	***Pf* IC_{50} (μM)[a,b] NF54**	**Sol. (μM)[c]**
159/DM-20-054	CH_3		CH	6.270	160
160/DM-20-055				0.652	100
154/DM-20-066	CH_3	CH_2	N	3.384	100
155/DM-20-071	H			6.526	120

[a]Mean from n ≥ 2 independent experiments with sensitive (*Pf*NF54) and MDR (*Pf*K1) strains
[b]Chloroquine (NF54 50% inhibitory concentration [IC_{50}] = 0.004 μM; K1 IC_{50} = 0.14 μM) was used as a reference drug
[c]Determined using a turbidimetric method at pH 7.4. Hydrocortisone (>200 μM) and reserpine (<10 μM) were used as control drugs

This may be attributed to the stronger inductive effects of the OH group compared to that of the fluoro, therefore decreasing the basicity of the piperidine nitrogen to a greater extent. Furthermore, the significance of functionalization of the cyano group to 3-/5-CF_3-1,2,4-oxadiazole is extensively demonstrated in this SAR.

3.2.3 SAR and Solubility of AST-CQ Hybrids

AST-CQ hybrid molecules were synthesized in an effort to improve physicochemical properties and expand the SAR of the hybrid molecules prepared by Musonda *et al.*[24] In this work, SAR 1 revealed that aliphatic replacements, removal of the 4-F-benzyl group, or replacement with methyl and cyclic moieties had no effect on the activity of the hybrids (IC_{50} < 0.040 μM), with the exception of iso-propyl (**170**, IC_{50} = 0.073 μM, Table 3.9). The cyclic aliphatic moieties produced interesting SARs: activity was improved with increasing aliphatic ring size, although cyclohexane and cyclopentane produced equipotent hybrids

(**173** and **174**, IC_{50} = ~0.030 μM). Conversely, solubility increased with decreasing aliphatic ring size (cyclohexyl = cyclopentyl < cyclobutyl < cyclopropyl). Interestingly, the cyclopropyl hybrid displayed the highest solubility (**171**, $S_{7.4}$ = 120 μM), while iso-propyl (**170**) and unsubstituted (**168**) hybrids produced equal moderate solubility ($S_{7.4}$ = 80 μM).

When comparing aliphatic and aromatic systems, no significant difference in activity was observed between cyclohexane **174** (IC_{50} = 0.033 μM) and benzyl **175** (IC_{50} = 0.040 μM). However, 3-F (**177**) and 4-F (**H-2**) regioisomerism was favored compared to the 2-F (**176**) position with an observed 2-fold difference.

Table 3.9: *In vitro* antiplasmodium activity (*Pf*NF54) and solubility data of **SAR 1** analogues.

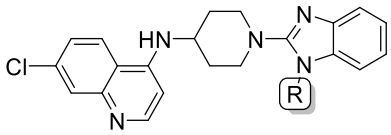

No./Lab Code	**R**	**R_1**	***Pf* IC_{50} (μM)[a,b] NF54**	**Sol.[c] (μM)**
168/DM-20-102	H	-	0.030	80
169/DM-20-116	CH_3	-	0.025	100
170/DM-20-120		-	0.073	80
171/DM-20-190		-	0.061	120
172/DM-20-155	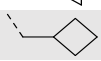	-	0.054	90
173/DM-20-154	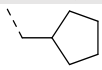	-	0.027	80
174/DM-20-153	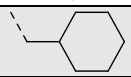	-	0.033	80
175/DM-20-196	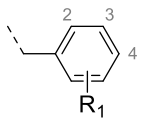	H	0.061	40
176/DM-20-147		2-F	0.078	20
177/DM-20-142		3-F	0.038	20
H-2/DM-20-160		4-F	0.040	20
178/DM-20-118		4-CN	0.034	60
179/DM-20-144		4-OMe	0.036	60
180/DM-20-149		4-CF_3	0.016	20
181/DM-20-162		4-SO_2Me	0.046	80
182/DM-20-152		4-$SONH_2$	0.245	100
183/DM-20-151		4-NO_2	0.024	80
184/DM-20-209		4-NHCOMe	0.040	100
185/DM-20-150		4-CO_2Me	0.267	80
187/DM-20-208		4-CONHMe	0.028	80
188/DM-20-159	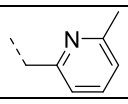	-	0.113	80

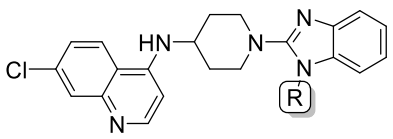

No./Lab Code	**R**	**R_1**	***Pf* IC_{50} (μM)[a,b] NF54**	**Sol.[c] (μM)**
189/DM-20-194	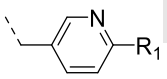	CH_3	0.045	80
190/DM-20-192		CF_3	0.044	40

[a]Mean from n ≥ 2 independent experiments with sensitive (*Pf*NF54) strain
[b]Chloroquine (NF54 50% inhibitory concentration [IC_{50}] = 0.004 μM; K1 IC_{50} = 0.14 μM) was used as a reference drug
[c]Determined using a turbidimetric method at pH 7.4. Hydrocortisone (>200 μM) and reserpine (<10 μM) were used as control drugs

Following exploration of Craig plot substituents at the 4-position, lipophilic substituents imparting negative inductive effects (EWG) such as CF_3 (**180**, IC_{50} = 0.016 μM) and NO_2 (**184**, IC_{50} = 0.040 μM) produced high activities (IC_{50} < 0.025 μM). Similarly, hydrophilic EWGs displayed high activities (IC_{50} < 0.046 μM), with the exception of methyl ester (**185**, IC_{50} = 0.267 μM) and sulfonamide (**181**, IC_{50} = 0.245 μM).

Generally, this SAR revealed that activity reduced with lipophilicity (i.e., CF_3 << NO_2 < CN < OMe etc.) although some substituents deviate from this trend. For instance, sulfonamide **181** (IC_{50} = 0.245 μM) is >8-fold less active than benzamide **187** (IC_{50} = 0.028 μM), despite having the same lipophilicity (clogP = 4.61). Noteworthy, N-phenylacetamide **184** (IC_{50} = 0.040 μM) displayed comparable activity and solubility to its reverse amide match pair, N-methyl benzamide **187** (IC_{50} = 0.028 μM). Hybrids containing water-solubilizing substituents exhibited moderate to high solubility ($S_{7.4}$ = 60 – 160 μM) compared to **H-2**. On the other hand, 2-CH_3- and 2-CF_3-5-pyridyl analogues **189** and **190**, respectively, were equipotent (IC_{50} = 0.045 μM). However, the 6-CH_3-2-pyridyl isomer **188** (IC_{50} = 0.113 μM) was 2.5-fold less potent. Notwithstanding, solubility was improved ($S_{7.4}$ > 40 μM) with methyl substituted analogues displaying higher solubility than the trifluoromethyl analogue.

In SAR 2, incorporation of lipophilic groups at the 5-position of the benzimidazole ring resulted in hybrids with comparable activity (**191** – **193**, IC_{50} < 0.053 μM, Table 3.10) to that of **H-2**. Additionally, these analogues showed higher solubility ($S_{7.4}$ > 80 μM).

In SAR 3, potential replacements of the 7-chloro (7-Cl) group in the quinoline ring were explored. Removal of the 7-Cl or its replacement with less lipophilic groups produced hybrids with lower activity (**205** – **208**, IC_{50} > 100 μM, Table 3.10). However, the bromine analogue retained high activity (**204**, IC_{50} = 0.033 μM), while the fluoro derivative was ~2.3-fold less potent (**202**, IC_{50} = 0.093 μM) than **H-2**. This observation may be attributed to the dependency of halogen bonding strength on the atomic size, electrostatics and polarization, and is well documented.[25,26] In this case, heavier halides seem preferable (F > Cl ≥ Br).

Table 3.10: *In vitro* antiplasmodium activity (*Pf*NF54 and K1) and solubility data of **SAR 2** and **3** analogues.

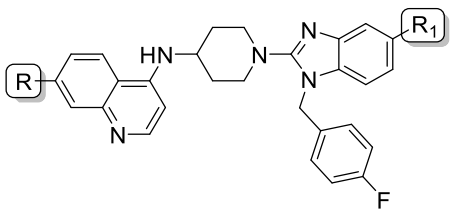

No./Lab Code	**R**	**R_1**	***Pf* IC_{50} (μM)[a,b] NF54**	**Sol.[c] (μM)**
191/DM-20-201	Cl	CN	0.029	100
192/DM-20-188		SO_2Me	0.047	120
193/DM-20-189		CO_2Me	0.053	80
201/DM-20-156	H	H	0.134	60
202/DM-20-146	F		0.093	60
203/DM-20-148	Br		0.033	40
204/DM-20-137	CF_3		0.089	20
205/DM-20-121	CN		0.225	120
206/DM-20-145	OCF_3		0.154	40
207/DM-20-122	OCH_3		0.134	80
208/DM-20-138	NO_2		0.454	80

[a]Mean from n ≥ 2 independent experiments with sensitive (*Pf*NF54) strain
[b]Chloroquine (NF54 50% inhibitory concentration [IC_{50}] = 0.004 μM; K1 IC_{50} = 0.14 μM) was used as a reference drug
[c]Determined using a turbidimetric method at pH 7.4. Hydrocortisone (>200 μM) and reserpine (<10 μM) were used as control drugs.

This assertion, and the significance of the presence of a hydrophobic halogen group at the 7-position is further evident in the lower activity of unsubstituted analogue **201** (IC_{50} = 0.134 μM). The CF_3-substituted analogue displayed 2-fold lower activity (**204**, IC_{50} = 0.089 μM).

As observed throughout this SAR study, incorporation of water-solubilizing groups increased the solubility of the hybrids as expected. However, lipophilic groups tend to be preferred for antiplasmodium potency. Removal of the benzyl moiety (**168** (IC_{50} = 0.030 μM) or its replacement with methyl group (**169**, IC_{50} = 0.030 μM) on the AST portion produced hybrids with a favorable balance of beneficial physicochemical properties (molecular weight, lipophilicity, and solubility) and antiplasmodium activity.

3.3 *In vitro* Antiplasmodium Activity versus Lipophilicity

Lipophilicity affects a wide range of molecular attributes, including potency because of its relationship with cellular binding affinity to biomolecules. Additionally, the variation of

lipophilicity within a series of designed compounds may predictably affect various ADME properties, including toxicity. As the goal of drug discovery is to achieve efficacy using a low dose and reduced administration frequency, it is important to control lipophilicity to optimize ADME properties of designed analogs in parallel with potency during early development stages. The identification of structural changes within a series that maintain or improve potency while reducing lipophilicity is therefore key to successful optimization.[27]

To achieve this, various lipophilicity dependent metrics have been developed relating to potency, ADME and other properties. In this study, lipophilic efficiency (LipE) was used to analyze the influence of lipophilicity on compound potency. LipE, also known as lipophilic ligand efficiency (LLE), normalizes potency for the lipophilicity of the molecule. It is calculated using Equation 1.

Equation 1: $LipE = pIC_{50} - logD \text{ (or clogP)}$

Where LipE is lipophilic efficiency, pIC_{50} is potency (given by: $-\log IC_{50}$ in Molar concentration, M), logD is the experimental partitioning coefficient, interchangeable with calculated lipophilicity (clogP)

A LipE plot is a vital tool for structural analysis, capturing three key molecular attributes (logD or clogP, potency, and LipE). In this plot, lipophilicity (clogP) and potency (Pic_{50}, in Molar) coincide at a 45° angle trajectory of the *x* and *y* axes of the plot, allowing for simple analysis of compound efficiency (LipE). Compounds that have the same LipE (isoefficient) are positioned on the same 45° line (LipE line). The goal of a LipE based optimization or analysis is to identify structural changes that lead to improvement of LipE (high LipE preferred) with lipophilicity that is consistent with favorable ADME and safety properties. For drug leads intended for oral administration, LipE = 5 – 7 is considered suitable.[27,28] Considering all AST analogues in this study (125 analogues), a LipE plot created to (i) furnish critical information on the chemical space occupied, (ii) interrogate and rationalize the potency-lipophilic relationships observed, and (ii) determine the suitability for development analogues based on the quality of compounds (Figure 3.2). In the AST series, the plot was divided into four quadrants based on LipE scores and were classified as low (LipE < 1), medium-low (LipE = 1 – 2), medium-high (LipE = 2 – 3), and high (LipE > 3).

3.3.1 Lipophilic Efficiency of AST Analogues (Phases I and II)

The LipE plot of all AST analogues is shown in Figure 3.2. To highlight a few structural-efficiency relationships (SERs), the transition from AST (LipE = 1.37) to the initial cyanated analogue **17** (LipE = 2.12) shows weak isopotency change (ΔLipE = +0.76). On the other hand, the transition from **17** to ethyl ester **38** and eventually the 3-CF_3-1,2,4-oxadiazole bioisostere **47**, represents an isoLipE (LipE ~ 2.17) change in which there are increases in both potency and lipophilicity with isoefficiency. However, truncation of the benzyl moiety

in **47** to produce **67** led to a ~2-fold increase in potency and reduced lipophilicity (1.12 units), which ultimately resulted in a significant efficiency gain (ΔLipE = +1.43). The significance of the oxadiazole moiety is again reflected in the isoefficiency observed following the removal of the benzyl group in **17** to produce less active cyano analogue **15** (LipE = 2.64, Δ+0.52), compared to the efficiency gain attained following the replacement of the cyano or ester group with a 1,2,4-oxadiazole moiety to produce **66** (LipE = 3.19, Δ+0.99) and **67** (LipE = 3.62, Δ+1.50). The weakly isolipophilic (ΔcLogP = 0.2) relationship between CH_3-substituted analogue (**66**) and CF_3-substituted analogue (**67**) leading to an efficiency gain (ΔLipE = +0.44) suggests that lipophilicity is a contributing factor to the observed high potency in **67** (IC_{50} = 0.012 μM), although the effect of other intrinsic structural and physicochemical factors cannot be ruled out.

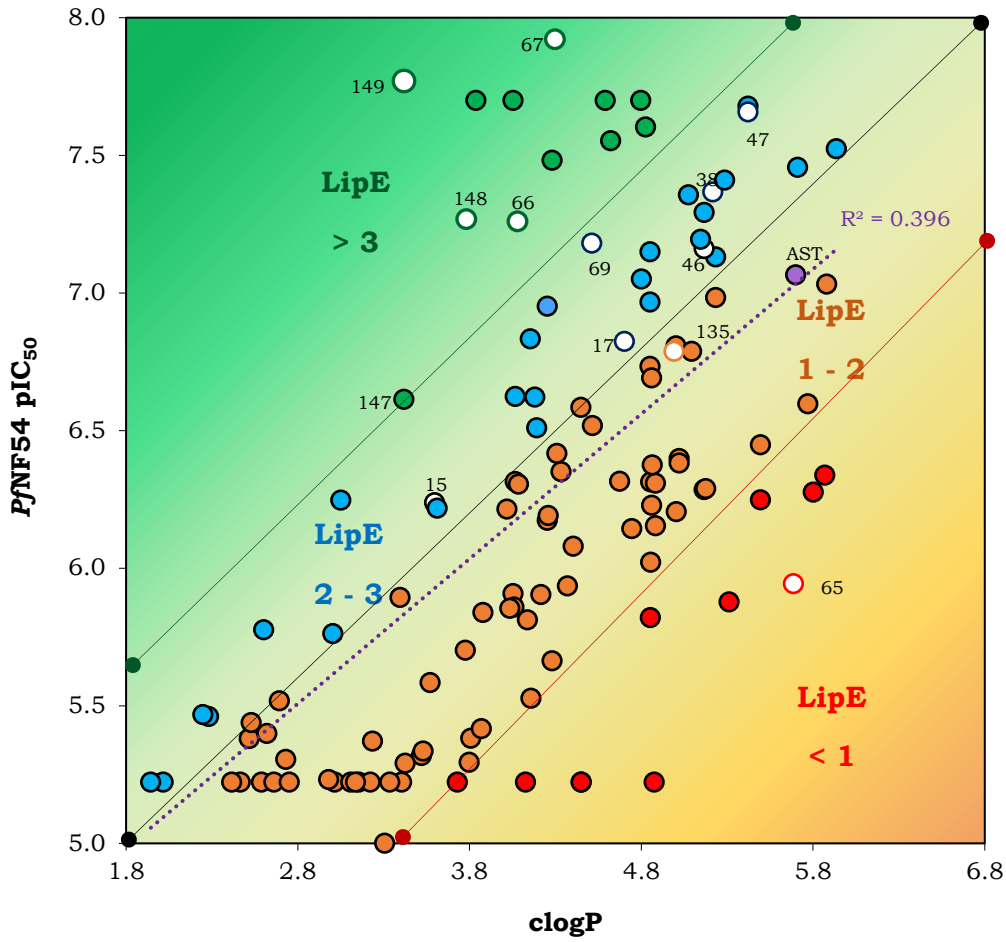

Figure 3.2: Lipophilic efficiency (LipE) plot of cLog*P* vs antiplasmodium potency, Pic_{50} [–log(*Pf*NF54 IC_{50})] of astemizole (AST) analogues. The color gradient denotes improvement of LipE from low (orange) to medium (yellow) and high (green)

Further optimization of front-runner compound **67** led to the identification of **149** (LipE = 4.35; Δ+0.73) which exhibited the highest efficiency (Figure 3.2). A weak positive correlation (r^2 = 0.396) between lipophilicity and potency (purple gradient line, Figure 3.2) was observed throughout the optimization process in both phase I and II AST analogues. Rather than

investigating *in vitro* potency or lipophilicity independently, the lipophilic efficiency of **67** (LipE = 3.62) corroborates the high *in vivo* antimalarial efficacy observed relative to that of **69** (LipE = 2.68). Additionally, this reaffirms the choice of **67** as a *bonafide* lead for further optimization towards reducing hERG affinity, resulting in **149**. Thesis data indicate that any further optimization (developability) would have to be based on 5-azabenzimidazole compound **149** (LipE = 4.35).

Statistically, most AST analogues fell within the medium range (LipE = 1 – 3) representing 74.4% of all compounds (Figure 3.3). Only 15.7% of compounds showed a favorable balance (LipE = 3 – 5) of high potency and lipophilicity. Furthermore, 10% of compounds showed poor efficiencies (LipE < 1).

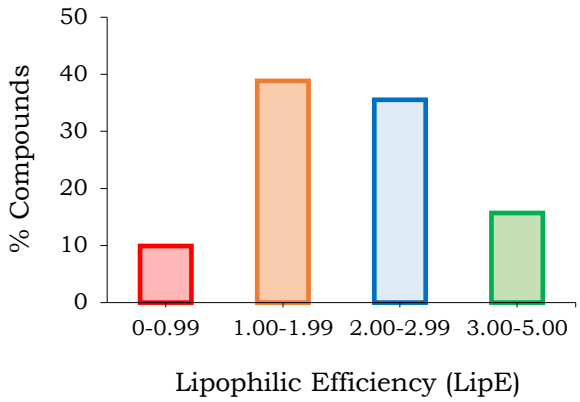

Figure 3.3: Distribution of LipE across the SAR of AST analogues

3.3.2 Lipophilic Efficiency of AST-CQ Hybrids

Lipophilic efficiency was used to conduct a qualitative analysis of AST-CQ hybrids (Figure 3.4). In this series, the LipE plot was divided into three quadrants representing low (LipE < 2), medium (LipE = 2 – 3), and high (LipE > 3) efficiency. Only four (5.1%) of the 39 hybrids showed optimal LipE: **168** (LipE = 3.20), **169** (LipE = 3.33), **181** (LipE = 2.96), and **187** (LipE = 2.95). 4-SO_2Me-benzyl and 4-CF_3-pyridyl analogues **181** and **190**, respectively, exhibited isoefficiency despite their differences in the lipophilicity.

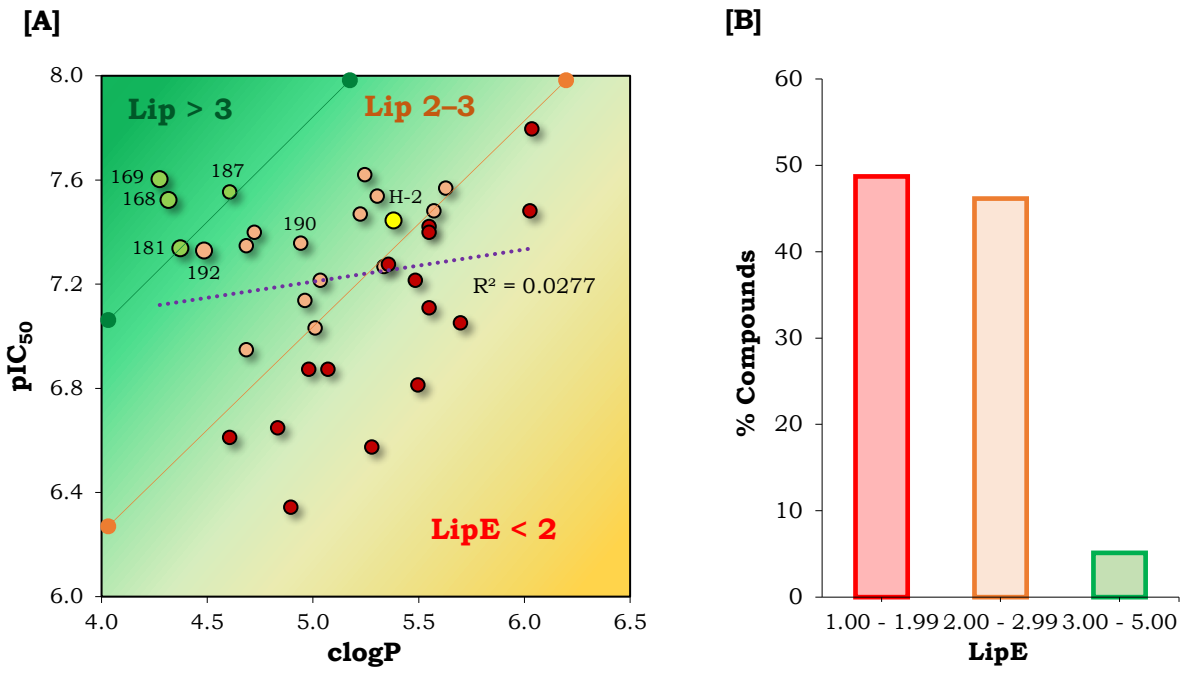

Figure 3.4: [A]; lipophilic efficiency (LipE) plot of clog*P* vs antiplasmodium potency, Pic_{50} [–log(*Pf*NF54 IC_{50})] of AST-CQ hybrids. Color gradient denotes improvement of LipE from orange (low) to yellow (medium) and green (high). [B]; LipE distribution

These data suggest that the replacement of the 4-F group in **H-2** with 4-sulfonyl (**181**) or 4-methylamide (**187**) substituents, may be a viable option for improving physicochemical properties. Additionally, the sulfonyl group is also tolerated on the benzimidazole ring (**192**, LipE = 2.84). However, removal of the benzyl group (**168**) in or its replacement with a methyl group (**169**) produced the greatest efficiency gain (ΔLipE = +1.40) and improved physicochemical properties (lower molecular weight, lower lipophilicity, and optimal solubility). Most of the analogues fell within the medium (48.7%, Figure 3.4B) and low (46.2%) LipE ranges. The LipE plot also shows a weak positive correlation between lipophilicity and potency (r^2 = 0.07).

3.4 *In vitro* Gametocytocidal Activity

In line with the new target product profiles (TPPs), towards malaria eradication (specifically target candidate profile 3 [TCP-3]), multi-stage antimalarial activity is included for new antimalarial compounds entering the pipeline. In addition to erythrocytic-stage killing, new antimalarials should also prevent relapse and block transmission *via* blockade of the liver and sexual stages, respectively.[29,30] Previous work by Kumar *et al.* in our group revealed that AST and related analogues possessed moderate sexual and good liver-stage activities.[23] Therefore, to follow up on the assessment of the potential for transmission-blocking properties, the *in vitro* gametocytocidal activity of AST, and selected analogues across most SARs were evaluated. Additionally, both early (EG, I – III) and late- or mature-stage gametocytes (LG, IV – V) were used to assess potential for stage-specificity. This work was conducted by collaborators at the Department of Biochemistry, Genetics & Microbiology,

Institute for Sustainable Malaria Control, University of Pretoria, South Africa, using a luciferase-reporter Pf NF54 line. Each compound was tested in a dual-point screen at concentrations of 1.0 and 5.0 μM (Figure 3.5).

Briefly, luciferase activity was determined *via* luciferin substrate-induced bioluminescence in parasite lysate following 48 h exposure of test compounds in parasite culture. The compounds were stratified as: High activity = >70% inhibition at 5 μM and >50% inhibition at 1 μM; Moderate activity = 50 – 70% inhibition at 5 μM and ≤50% inhibition at 1 μM; Inactive/weakly active = <70% inhibition at 5 μM and <50% inhibition at 1 μM.

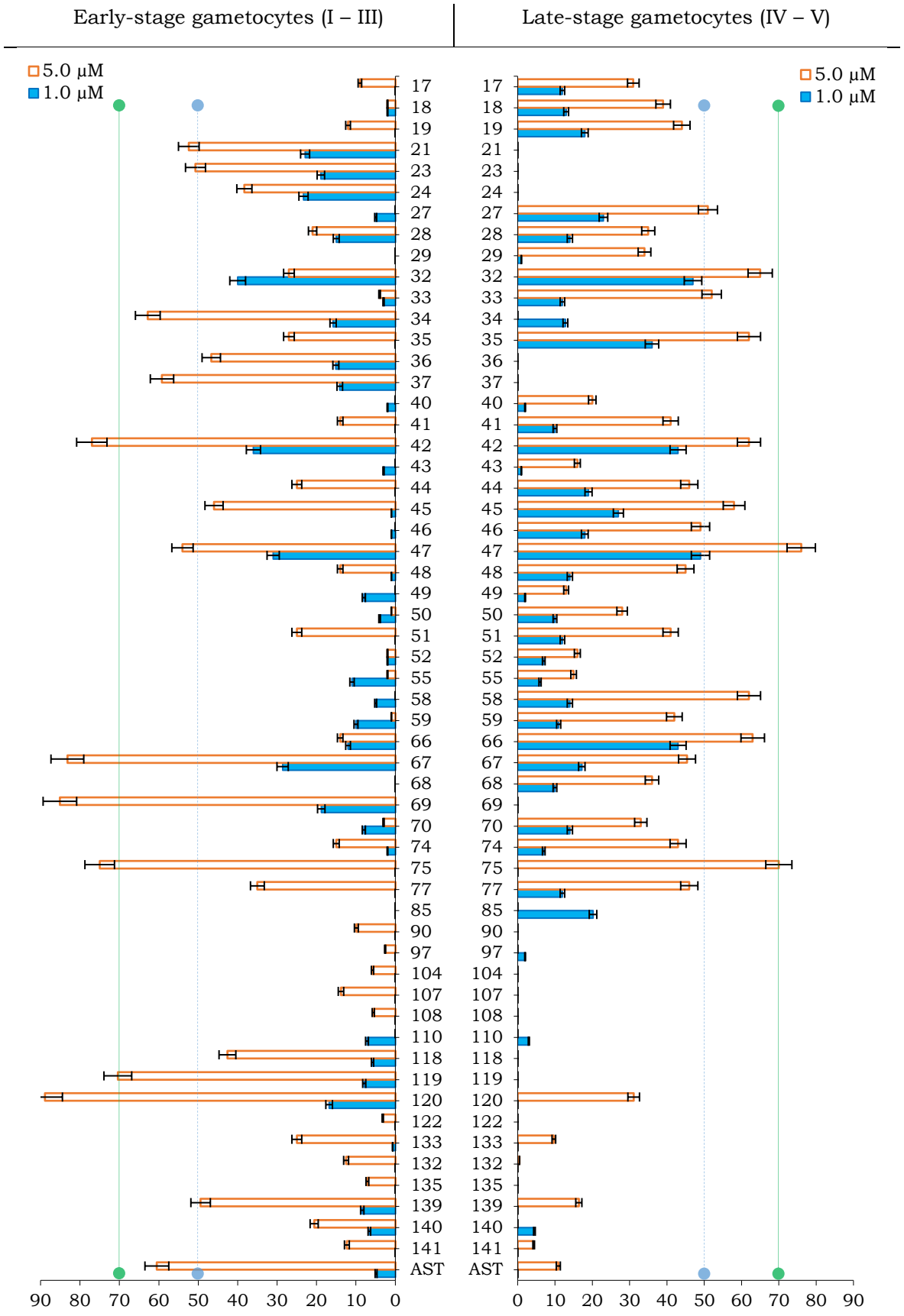

Figure 3.5: Dual-point *in vitro* gametocytocidal activity of selected compounds against luciferase (luc) *Pf*NF54 early-stages (I – III) and late-stages (IV – V) gametocytes, obtained at 1.0 µM and 5.0 µM (n = 1, one biological assay with technical triplicates). Methylene blue (EG luc at 1.0 µM = 95% inhibition, EG IC_{50} = 0.2 µM; LG luc at 1.0 µM = 92% inhibition, LG IC_{50} = 0.14 µM)

Fifty-six (56) compounds were evaluated based on their structural diversity to represent the SARs and high activity against the asexual blood stage. None of the compounds tested showed high activity against either early- or late-stage gametocytes at 1.0 µM. However, 19 compounds showed moderate to high activity at 5 µM. Compounds **42**, **47**, **67**, **69**, **75**, **119** and **120** (Figure 3.6) displayed higher activity at 5 µM compared to AST (EG luc at 5.0 µM = 60.5% inhibition, EG IC_{50} = 3.4 µM). Additionally, their IC_{50} values expected to be < 1.0 µM, which would be lower compared to those obtained for the most potent analogues in the previous study (IC_{50} = 1.9 – 4.1 µM) from our group. Moreover, it has been shown that an observed lack of whole-cell activity (*in vitro*) may not always truly reflect *in vivo* activity. However, high inhibition at low concentrations in a dual-point screen often translate to high activity.[31]

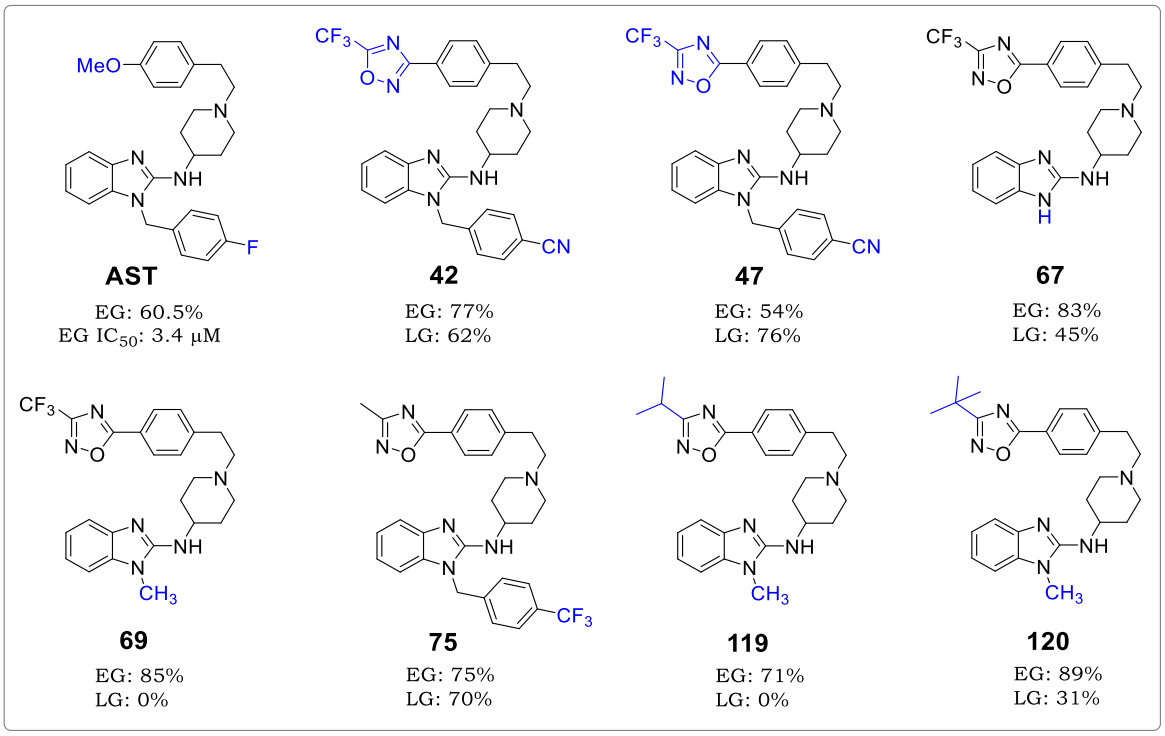

Figure 3.6: Structure of AST and compounds **42**, **47**, **67**, **69**, **75**, **119** and **120,** and their percent (%) inhibition in a dual-point screen against early-(EG) and late-stage gametocytes (LG) at 5.0 µM

The classification criteria for stage specificity were defined as compounds which display ≥ 2-fold change in dual point values between EG and LG. Noteworthy, compounds **69**, **119** and **120**, all of which lack the benzyl moiety, displayed EG specificity, while compound **75** was highly active against both stages (Figures 3.5 and 3.6). Based on this preliminary screen, compounds **47**, **67**, **69**, **75**, and **120** (asexual blood stage *Pf*IC_{50} < 0.066 µM) show the potential for dual-stage activity. Additionally, this SAR has revealed that compounds devoid of the benzyl moiety at benzimidazole N1-position (**67** – **69** and **90** – **137**) were more active against EGs compared to LGs (Figure 3.5), suggesting the possibility for tuning gametocyte stage-specificity by exploring the benzimidazole N-1 position.

3.5 *In vitro* Hemozoin Formation Inhibition (AST Analogues)

In phenotypic drug discovery (PDD), various attempts are made early during the discovery process to investigate the mode or mechanism of action (MoA) of NCEs. In this case, AST and its metabolite DMAST were previously shown by Chong *et al.* to inhibit heme crystallization, a contributing mechanism towards the MoA that was later corroborated by our group.[22,23] Therefore, it was imperative to assess this activity on new analogues and derive potential SARs.

A pyridine-based and detergent-mediated *in vitro* model that partially mimics the microenvironment of the digestive vacuole (DV) was used to quantify the ability of AST analogues to inhibit β-hematin (β-H) formation, as a surrogate for inert hemozoin formed *in vivo* during heme detoxification by the parasite. As shown in Figure 3.7, 16 of 27 compounds tested demonstrated high β-H inhibition (IC_{50} < 100 μM) compared to AST (β-H IC_{50} = 130.5 μM).

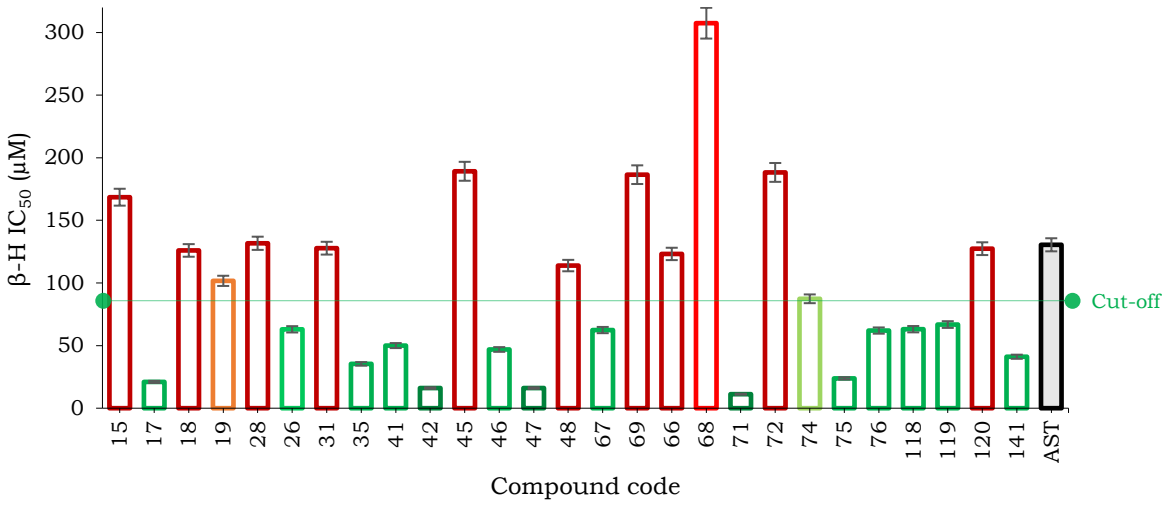

Figure 3.7: Distribution of β-H inhibition IC_{50} values of tested compounds

In phase I SAR 1 analogues containing a 4-CN-phenyl moiety, the presence of an aromatic moiety at the benzimidazole N-1 position is critical to β-H inhibition, as was for whole-cell antiplasmodium activity. For instance, there was an 8-fold increase in potency following N-alkylation of unsubstituted **15** (IC_{50} = 169 μM) to yield the compound **17** (IC_{50} = 21 μM; Figure 3.8). With respect to the nature of the aromatic moiety, substitution with CN (**17**) and CF_3 (**31**) at the 4-position are tolerated. This observation may be related to the ability of analogues with increased aromaticity to bind strongly to porphyrin *via* π–π stacking.

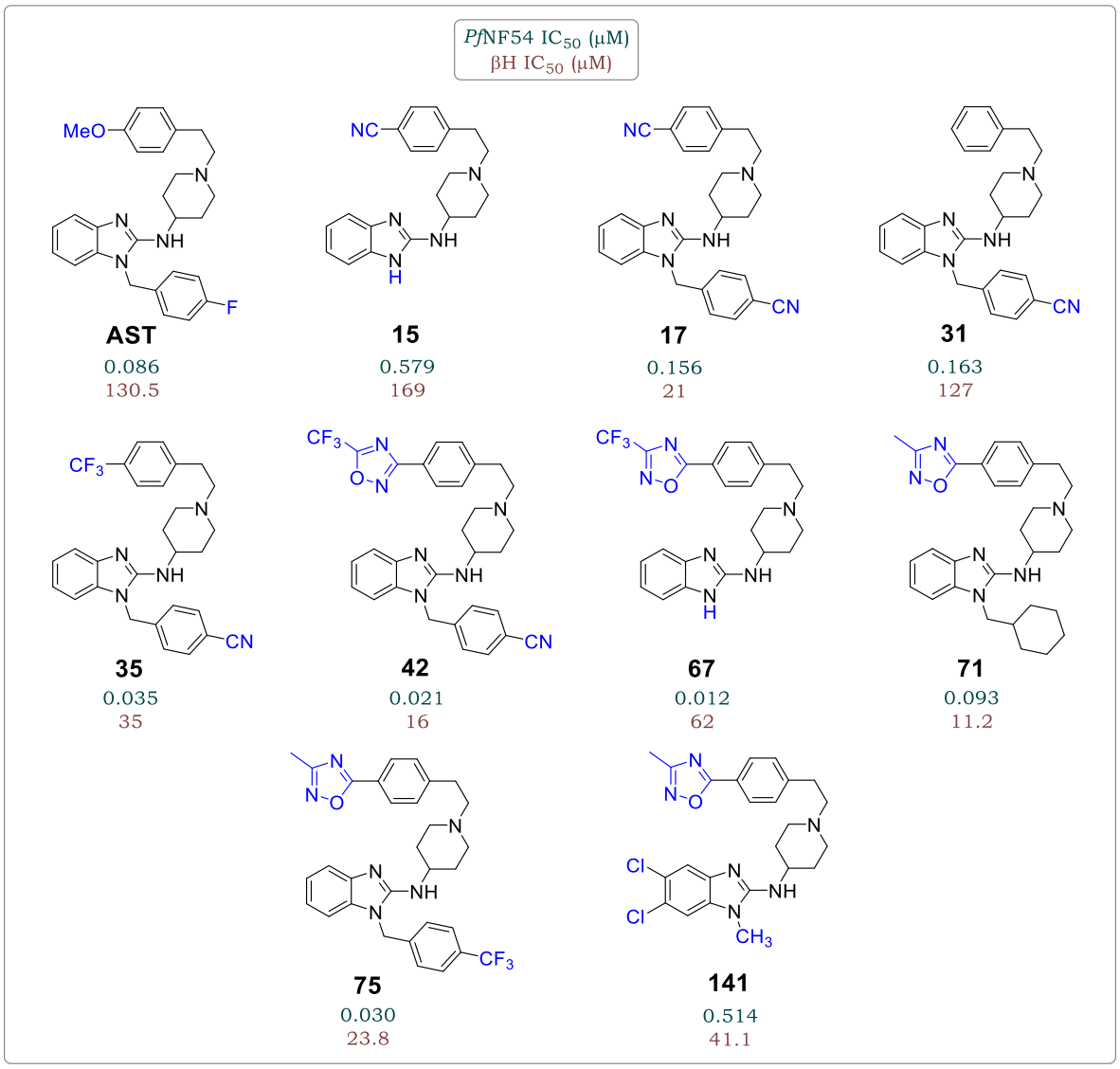

Figure 3.8: Structure of AST and compounds selected compounds with diverse β-H inhibition SAR vs whole-cell activity (*Pf* NF54)

In phase I SAR 2, EWGs such as CF_3 (**35**, IC_{50} = 35 μM) are also tolerated. Interestingly, introduction of the 3-/5-CF_3-1,2,4-oxadiazole moiety (**42** or **47**, IC_{50} = 16 μM) imparted potency lower than that of CQ (IC_{50} = 23 μM) and produced 8-fold improvement in activity compared to the unsubstituted analogue (**31**, IC_{50} = 127 μM). Unlike the cyano (CN) analogues, the presence of the 1,2,4-oxadiazole moiety (aromatic) appears to strongly compensate for the removal of the benzyl group, as doing so does not affect the β-H inhibition significantly (comparing **15** and **67**). However, even with the oxadiazole ring present, having an appropriately substituted benzyl or aliphatic (**42**, **71**, **75** and **141**) moiety at the benzimidazole N-1 position is crucial for stronger β-H inhibition activity. 5,6-Dichloro substitution on the benzimidazole core is tolerated and enhances β-H inhibition activity (**141**, IC_{50} = 41.1 μM) compared to the unsubstituted analogue (**68**, IC_{50} = 307 μM). As in CQ, this may be attributed to the capability of Cl to promote π–π stacking and facilitate halogen-hydrogen interaction between the benzimidazole ring and the porphyrin.

A weak positive correlation (r^2 = 0.0841) between β-H inhibition and activity against *Pf*NF54 (Figure 3.9) was observed. Several compounds with strong β-H activity showed low antiplasmodium activity (e.g., **141**, β-H IC_{50} = 41.1 μM; *Pf*NF54 IC_{50} = 0.514 μM). Similarly, some of the weak β-H formation inhibitors showed high antiplasmodium activity (e.g., **69**, β-H IC_{50} = 186.5 μM; *Pf*NF54 IC_{50} = 0.033 μM) irrespective of the series. Noteworthy, the most potent β-H formation inhibitor was also highly active in the parasite (**71**, β-H IC_{50} = 11.2 μM; *Pf*NF54 IC_{50} = 0.093 μM).

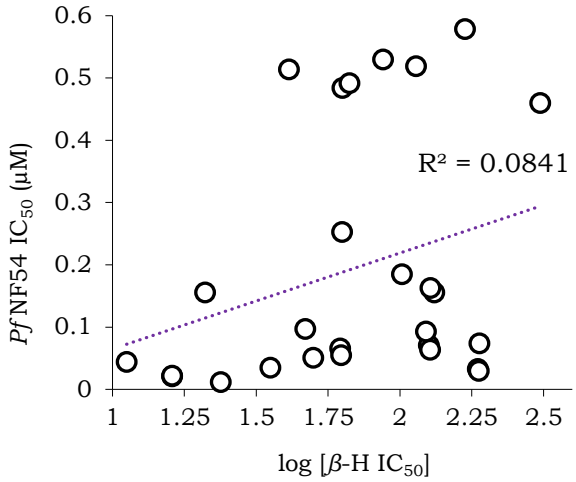

Figure 3.9: Plot showing the relationship between hemozoin formation inhibition vs antiplasmodium potency (*Pf* NF54 IC_{50} vs log [β-H IC_{50}]). Chloroquine (β-H IC_{50} = 23 μM) and Pyrimethamine (β-H IC_{50} > 300 μM) used as controls

Based on the dose-dependent effects on parasitic heme species previously shown by a less potent series (highest β-H IC_{50} = 65.2 μM) in our group earlier,[23] the data from these new analogues validate and reinforce the contribution made by inhibition of heme crystallization towards the MoA of AST analogues. However, this conclusion is made cautiously considering the limitations of this *in vitro* assay associated with recapitulating the physiological complexities of intracellular drug activity. It will be useful to carry out a dose-dependent heme-speciation assay on front-runner compounds identified from this primary screen.

3.6 *In vitro* Mammalian Cytotoxicity

To assess the potential safety of potent analogues and their selectivity for *P. falciparum*, *in vitro* cytotoxicity studies were carried out using selected analogues (*Pf*NF54 IC_{50} <1.0 μM) in two different mammalian cell lines. Toxicity studies against epithelial Chinese hamster ovary cells (CHO) were conducted at H3D, Division of Clinical Pharmacology, University of Cape Town, while those against human hepatocellular liver carcinoma (HepG2) cells were conducted at the Genetics and Microbiology department at the Institute for Sustainable Malaria Control, University of Pretoria. Using these data, Sis were determined cytotoxicity (IC_{50}) divided by antiplasmodium activity (*Pf*NF54 IC_{50}). Cytotoxicity in CHO cells were assessed using a 3-(4,5-dimethylthiazol-2-yl)-2,5-diphenyltetrazolium bromide (MTT) assay,

which measures cell survival and growth. In this assay, the formation of tetrazolium salt is used to measure proliferation and chemosensitivity using emetine as a reference compound.[32] In addition, only a small number of and potent analogues were tested in HepG2 cells. This assay was conducted at a drug concentration of 2.0 μM using a CytoSelect™ lactate dehydrogenase (LDH) cytotoxicity assay kit.[33] Detailed descriptions of both assays are provided in the experimental section (Chapter 6).

As shown in Table 3.11, most analogues exhibited marginal cytotoxicity (SI > 100) in CHO cells. However, analogues **66** and **69** showed lower selectivity's (SI = 64.7 and 48.2 respectively). HepG2 toxicity in Table 3.11 indicates the percentage cytotoxicity of a compound at the tested concentration (2.0 μM) following incubation for 48 hr. Most of the compounds showed low cytotoxicity (<50%), with the exception of compound **69** which demonstrated 51% cytotoxicity.

Table 3.11: ***In*** *vitro* cytotoxicity profiling results of selected analogues in mammalian CHO and HepG2 cell lines.

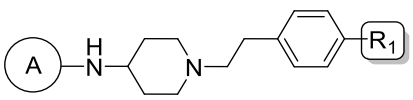

Code	A	R	R_1	CHO[a]		HepG2[a]
				IC_{50} (μM)[b]	SI[c]	
AST	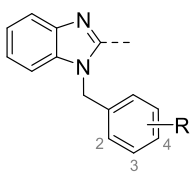	4-F	OMe	29.6	344	29.4
18		3-F, 4-CN	CN	47.4	667	ND
77		3-F, 4-CN	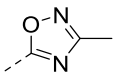	8.47	217	ND
75		4-CF_3		3.33	111	ND
29	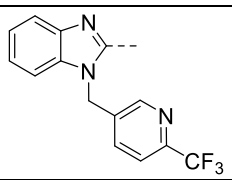	-	CN	>50	>2000	ND
74		-	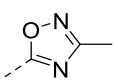	5.63	128	ND
32		-	OH	38.5	1376	ND
35		-	CF_3	5.36	153	32.0
38		-	CO_2Et	12.4	289	43.7
40	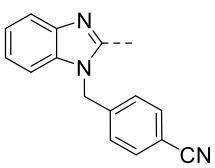	-		16.6	187	ND
41		-	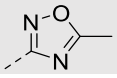	5.87	115	ND
42		-	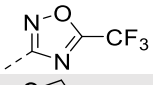	3.85	175	ND
45		-	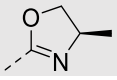	38.9	525	ND
120		-	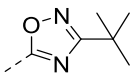	4.69	73.3	0.00

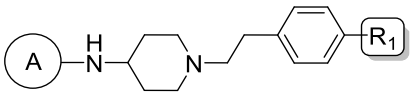

Code	A	R	R_1	CHO[a]		HepG2[a]
				IC_{50} (μM)[b]	SI[c]	
66	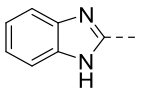	-	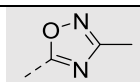	3.56	64.7	ND
67		-	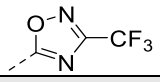	1.95	162.5	32.4
68	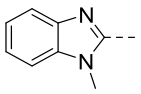	-	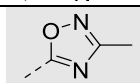	9.09	275	ND
69		-	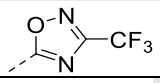	3.18	48.2	51.0
148	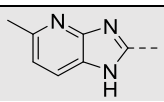	-		>50	>925	ND
149	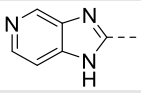	-	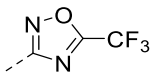	>50	<2,941	ND
150	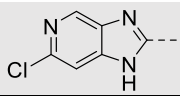	-		>50	>446	ND

[a]CHO: Chinese hamster ovary cell line; HepG2: human hepatocellular liver carcinoma cells
[b]Mean value from n = 3 independent experiments. Emetine (IC_{50} = 0.033 μM) was used as the reference drug
[c]SI: selectivity index = CHO IC_{50}/NF54 IC_{50}
[d]ND: not determined

3.7 *In vitro* hERG Potassium Channel Inhibition

The primary objective of this project was to alleviate the cardiotoxicity risk associated with AST using medicinal chemistry approaches to design analogues with reduced hERG channel activity while maintaining or improving antiplasmodium activity. hERG inhibition assays were conducted by Metrion Biosciences Limited (Cambridge, United Kingdom). In this assay, hERG K+ channels expressed in CHO cells are used, on an automated Q-patch clamp platform in triplicate at four concentrations from which a dose response-curve is drawn to calculate the hERG IC_{50}. As a caveat, IC_{50} > 10 μM (highest tested concentration) are extrapolated and should therefore be considered only as approximate indicators of hERG activity. Verapamil, a known potent blocker of hERG, was used as a positive control in the assay.

Because this project was designed address this risk, the selection of compounds for testing in the hERG inhibition assay was based on (i) the representation of analogues from each SAR in which specific hERG -reducing strategies were applied, (ii) structurally diverse compounds from each optimization stage to establish hERG SARs and (iii) "cherry-picked" compounds displaying high antiplasmodium potency, low cytotoxicity, and ideal physicochemical properties to represent best-in-class molecules.

Targeted criteria for antiplasmodium potency were *Pf*NF54 IC_{50} ≤ 0.10 μM, and a discriminatory limit of hERG $IC_{50} \geq 10$ μM, representing an SI threshold of 100 as a sufficient order of magnitude to indicate the ideal safety of a compound. Notably, the SI of AST in the *Pf*NF54 strain was 0.05 (*Pf*NF54 IC_{50} = 0.086μM; hERG IC_{50} = 0.0042 μM). The obtained results are discussed by classifying compounds based on the approach used to modulate hERG activity.

3.7.1 Furnishing Zwitterionic Character

Zwitterionic species reduce hERG affinity by limiting a compound's ability to permeate the transmembrane binding site, and therefore minimize interaction with the hERG channel. As shown in Table 3.12, incorporation of the carboxylic acid (–CO_2H) moiety in the template produced compounds with low hERG affinity (IC_{50} > 4.0 μM).

Table 3.12: *In vitro* hERG activity and *in silico* predicted clog*P* and hERG pIC_{50} of zwitterion AST analogues.

Code	Structure	hERG IC_{50} (μM)[a]	clog*P*[b]	hERG pIC_{50}[b]	SI[c]
25	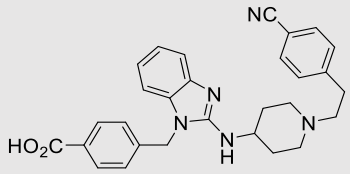	4.16	4.45	6.519	<0.7
78	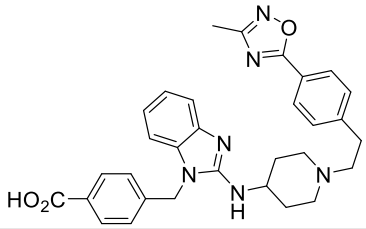	4.21	4.88	6.562	<0.7
122	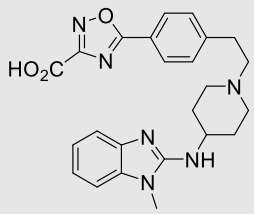	30.0	3.34	6.028	<5.0
142	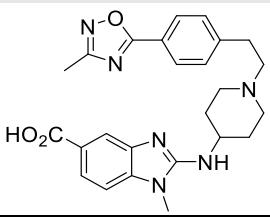	28.7	3.73	5.979	<4.7

[a]hERG: human ether-*à-go-go*-related gene. Data shown are from n = 3 independent experiments. Verapamil (IC_{50} = 0.56 ± 0.096 μM) used as a reference compound.

[b]Properties predicted using StarDrop, version 6.5.1-1 (AST: cLog*P* = 5.700; pIC_{50} = 8.265)

[c]SI: selectivity index = hERG IC_{50}/*Pf*NF54 IC_{50}

However, all analogues in this class were inactive against *P. falciparum* at the highest concentration tested (*Pf*NF54 IC_{50} > 6.0 μM, SI < 5). This was not entirely surprising because, the presence of a carboxylic acid group, is often associated with poor absorption, limited membrane permeability, and thus low whole-cell activity in the parasite. This observation was made regardless of where the $–CO_2H$ group was incorporated in the template. These results thus suggest that the zwitterion approach was ineffective as a hERG -reducing strategy in AST.

3.7.2 Lipophilicity (clog*P*) Lowering Strategies

Lipophilicity-lowering strategies are commonly used to modulate hERG channel activity because of the low propensity of lipophilic molecules to bind *via* hydrophobic interactions at the binding pocket in the hERG channel. The lipophilicity of a molecule can be reduced by incorporating groups with hydrogen-bonding potential, replacing hydrophobic groups such as halogens with less lipophilic ones, truncating or saturating aromatic groups and exploring polar bulky substitutions.

3.7.2.1 Incorporation of Water-solubilizing Groups (halogen-replacement) and Piperidine Ring Variants

In comparison to cyano analogue **17** (hERG IC_{50} = 0.05 μM), hERG affinity was reduced 2-fold by replacing the 4-CN group in the benzyl sidechain with sulfone (**22**; Table 3.13). However, the most significant effect observed (19-fold) was produced by replacing the 4-CN-benzyl group in **17**, with a 4-CF_3-3-pyridyl (**29**, hERG IC_{50} = 0.97 μM) moiety, a change that was accompanied by a ~6-fold antiplasmodium potency gain (**29**, *Pf*NF54 IC_{50} = 0.025 μM, SI = 39). This analogue represents the successful use of a lipophilicity-lowering strategy using aromatic insertion of polar atoms (phenyl to pyridyl), while exploring favorable substitution informed by antiplasmodium activity SAR (4-CN to 4-CF_3).

Table 3. 13: *In vitro* hERG activity and *in silico* predicted clog*P* and hERG pIC_{50} of AST analogues using lipophilicity lowering strategies.

Code	Structure	hERG IC_{50} (μM)[a]	clog*P*[b]	hERG pIC_{50}[b]	SI[c]
17	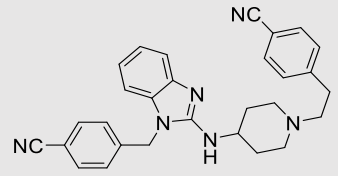	0.05	4.70	7.930	0.32
22	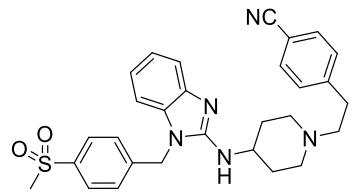	0.11	4.07	7.870	0.16

Code	Structure	hERG IC_{50} (μM)[a]	clog*P*[b]	hERG pIC_{50}[b]	SI[c]
29	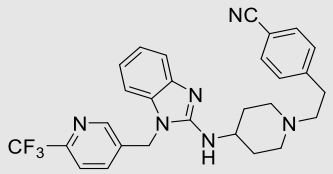	0.97	4.83	7.833	38.8
46	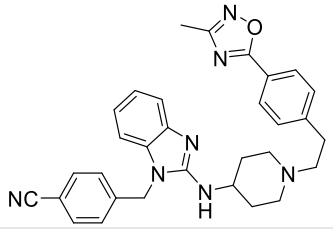	0.10	5.17	7.949	1.45
47	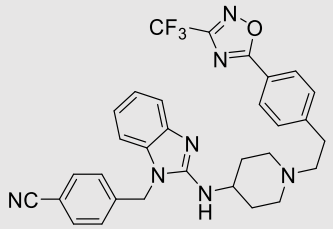	0.47	5.42	8.154	19.0
58	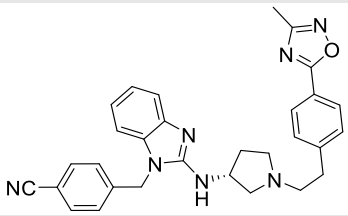	0.13	5.02	7.54	0.33
61	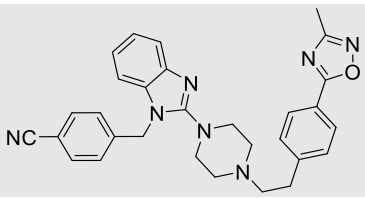	0.12	4.85	7.703	0.08
74	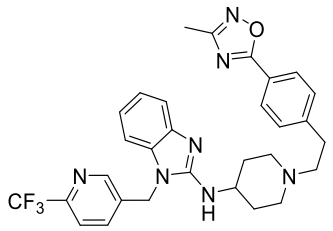	0.25	5.08	7.824	5.68

[a]hERG: human ether-*à-go-go*-related gene. Data shown are from n = 3 independent experiments. Verapamil (IC_{50} = 0.56 ± 0.096 μM) used as a reference compound.

[b]Properties predicted using StarDrop, version 6.5.1-1 (AST: cLog*P* = 5.700; pIC_{50} = 8.265)

[c]SI: selectivity index = hERG IC_{50}/*Pf*NF54 IC_{50}

Although clog*P* increased, the presence of the CF_3 group produced analogues with decreased hERG channel activity and increased antiplasmodium activity compared to those devoid of this functionality. Replacement of the lateral 4-CN group in **17** with 3-CH_3-1,2,4-oxadiazole (**46**, hERG IC_{50} = 0.10 μM) only produced a 2-fold reduction in hERG affinity. However, a ~10-fold reduction was observed in the 3-CF_3-1,2,4-oxadiazole (**47**, hERG IC_{50} = 0.47 μM) match pair. Additionally, 4-CF_3-benzyl analogue **75** (hERG IC_{50} = 0.38 μM, SI = 12) showed

a ~4-fold decrease in hERG activity than 4-CN-benzyl analogue **46** (hERG IC_{50} = 0.10 μM, SI ≈ 2). Replacement of piperidine with either pyrrolidine or piperazine has previously been used to decrease hERG activity, although this change had no effect within this scaffold (**46**, **58**, and **61**, hERG IC_{50} = 0.11 μM).

3.7.2.2 Removal of Aromatic Moiety (Ring Saturation/Truncation) and Amidation

This approach is aimed at disrupting π-π stacking interaction between the aromatic residue of the analogues and those of amino acid residues in the hERG channel. Saturation of the benzyl moiety significantly reduced hERG affinity (**71**, hERG IC_{50} = 0.89 μM, SI ~ 10, Table 3.14). However, no effect was observed following replacement of the benzyl with a methyl group in the cyanated phase I template (**16**, hERG IC_{50} = 0.09 μM). A combination of N-benzyl to N-methyl interchange, and replacement of 4-CN in the lateral phenyl group with a more hydrophilic 3-CH_3-1,2,4-oxadiazole moiety resulted in a ~4-fold decrease in hERG channel activity (**68**, hERG IC_{50} = 0.35 μM, SI = 11). Consistently, lower affinity was achieved following CH_3/CF_3 (**69**, hERG IC_{50} = 0.86 μM, SI = 13) and CH_3/*tert*-butyl (**120**, hERG IC_{50} = 1.35 μM, SI = 21) group interchange. Additionally, selectivity was further improved in desmethyl analogue **67** (hERG IC_{50} = 0.63 μM, SI = 53), showing high antiplasmodium activity (*Pf*NF54 IC_{50} = 0.012 μM) and 1100-fold increase in selectivity compared to that of AST.

Table 3.14: *In vitro* hERG activity and *in silico* predicted clog*P* and hERG pIC_{50} of AST analogues in which an aromatic group is saturated and/or removed.

Code	Structure	hERG IC_{50} (μM)[a]	clog*P*[b]	hERG pIC_{50}[b]	SI[c]
71	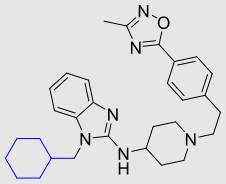	0.89	5.88	7.995	9.56
16	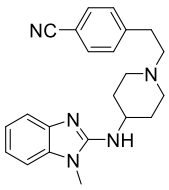	0.09	3.80	7.222	0.02
68	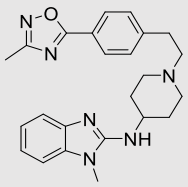	0.35	4.28	7.278	10.6

Code	Structure	hERG IC_{50} (μM)[a]	clog*P*[b]	hERG pIC_{50}[b]	SI[c]
69	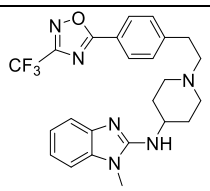	0.86	4.51	7.512	13.0
120	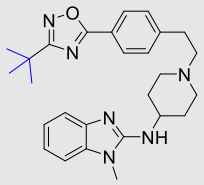	1.35	5.15	7.390	21.1
67	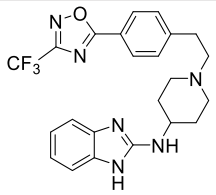	0.63	4.30	6.912	52.5
90	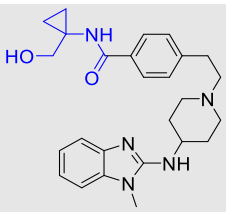	30.0	3.00	6.911	17.3
103	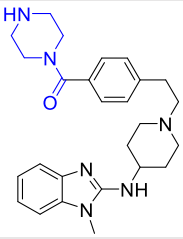	30.0	2.25	7.549	8.81
132	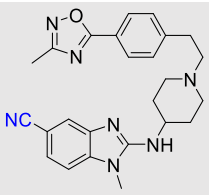	0.16	4.11	7.230	0.26
135	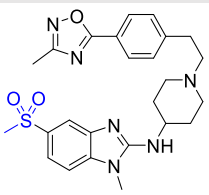	0.49	3.53	7.192	0.11

[a]hERG: human ether-*à-go-go*-related gene. Data shown are from n = 3 independent experiments. Verapamil (IC_{50} = 0.56 ± 0.096 μM) used as a reference compound.

[b]Properties predicted using StarDrop, version 6.5.1-1 (AST: cLog*P* = 5.700; pIC_{50} = 8.265)

[c]SI: selectivity index = hERG IC_{50}/*Pf*NF54 IC_{50}

The amides showed no hERG activity (**90** & **103**, IC_{50} > 10 μM), however, antiplasmodium potency was equally significantly diminished (IC_{50} > 1.0 μM). Incorporation of the sulfone group (**135**, hERG IC_{50} = 0.49 μM, SI = 0.1) in the benzimidazole ring resulted in decreased hERG activity compared to the nitrile group (**132**, hERG IC_{50} = 0.16 μM, SI = 0.3). Antiplasmodium activity was also significantly reduced in both analogues.

3.7.3 Reducing the p*K*a of Basic Nitrogen

Decreasing the p*K*a of the basic nitrogen in a hERG inhibitor has the potential to decrease hERG potency. At physiological Ph, the resulting ammonium species would not be sufficiently stable to interact (*via* π-cation) with aromatic residues lining the hERG channel binding pocket, thereby lowering the affinity of the compound for the channels.

In this project, the p*K*a of the piperidine nitrogen was reduced *via* β-fluorination. This choice of fluorine was based on its low inductive effect and its negligible effect on compound size and lipophilicity. This strategy was carried out on front-runners **67** (hERG IC_{50} = 0.63 μM, SI = 53) and **69** (hERG IC_{50} = 0.86 μM, SI = 13), both of which contain a 3-CF_3-1,2,4-oxadiazole moiety at the 4-position of the lateral phenyl group.

Mono-fluorination and di-fluorination of **67** in the piperidine ring produced **151** and **152**, with 1.6- and 2.6-fold decreases in affinity, respectively (Table 3.15). The lowest hERG affinity was achieved using a combination of piperidine β-mono-fluorination and insertion of nitrogen in lateral phenyl group (**157**, hERG IC_{50} = 1.34 μM). β-fluorination of **69** in the ethylene linker (**161**, hERG IC_{50} = 0.62 μM) was ineffective in reducing hERG affinity. Hypothetically, the theory was proven, however, ineffective because low basicity was accompanied by lower or complete loss of antiplasmodium potency. It must, however, be noted that the activities obtain from mono-fluorinated analogues may not represent concise SAR, unless they are separated into their respective diastereomers.

Table 3.15: *In vitro* hERG activity and *in silico* predicted cLog*P*, p*K*a and hERG pIC_{50} of AST analogues with reduced p*K*a of piperidine basic nitrogen.

Code	Structure	hERG IC_{50} (μM)[a]	clog*P*[b]	p*K*a[c]	hERG pIC_{50}[b]	SI[d]
151	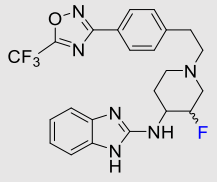	0.98	4.16	7.79	6.860	6.67
152	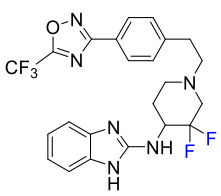	1.65	4.26	6.73	6.963	2.56

Code	Structure	hERG IC_{50} (μM)[a]	clog*P*[b]	p*Ka*[c]	hERG pIC_{50}[b]	SI[d]
159	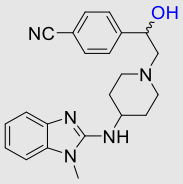	0.22	2.15	8.23	6.824	0.33
160	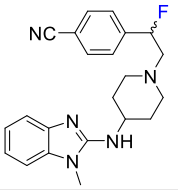	0.20	3.67	7.82	7.252	0.24
161	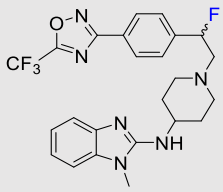	0.62	4.32	7.95	7.502	1.02
156	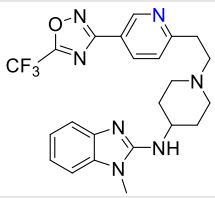	0.49	3.68	8.73	7.131	2.05
157	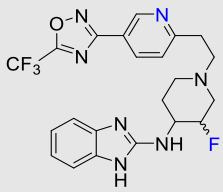	1.34	3.31	7.61	6.485	<0.14

[a]hERG: human ether-*à-go-go*-related gene. Data shown are from n = 3 independent experiments. Verapamil (IC_{50} = 0.56 ± 0.096 μM) used as a reference compound.
[b]Properties predicted using StarDrop, version 6.5.1-1 (AST: cLog*P* = 5.700; pIC_{50} = 8.265)
[c]Properties predicted using ChemDraw, version 19.0.1.28 (AST: p*K*a = 9.188)
[d]SI: selectivity index = hERG IC_{50}/*Pf*NF54 IC_{50}

3.7.4 Discreet Modifications

Subtle or discreet changes in the molecular architecture of a hERG inhibitor have the potential to significantly alter molecular properties that may affect hERG affinity without affecting antiplasmodium activity. These small discreet changes were focused on the benzimidazole ring of front-runner **67** (hERG SI = 53).

As shown in Table 3.16, replacement of the benzimidazole ring with imidazo[1,2-*a*]pyridine produced analogues with equipotent hERG activity (hERG IC_{50} = 0.66 μM, SI = 0.78). However, antiplasmodium potency was lost. Interestingly, azabenzimidazoles **147** (hERG IC_{50} = 2.72 μM) and **149** (hERG IC_{50} = 5.07 μM) showed 4.3- and 8.0-fold decrease in hERG affinity, respectively. Notably, the 5-azabenzimidazole **149** retained antiplasmodium potency (*Pf*NF54 IC_{50} = 0.017 μM) with SI = 298 compared to the closely related 4-azabenzimidazole **147** (SI = 11). The low hERG affinity of **149** represents a 6200-fold

increase in selectivity over hERG compared to that of AST. In both azabenzimidazole derivatives, α-substitution appeared to increase hERG affinity as observed in compounds **148** and **150** (Table 3.16).

Table 3.16: *In vitro* hERG activity and *in silico* predicted clog*P* and hERG pIC_{50} of AST analogues with discreetly modified benzimidazole ring.

Code	Structure	hERG IC_{50} (μM)[a]	clog*P*[b]	hERG pIC_{50}[b]	SI[d]
147	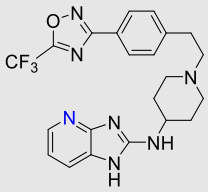	2.72	3.42	6.626	11.4
148	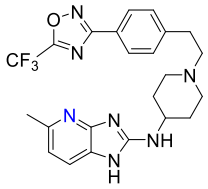	0.42	3.78	6.638	7.78
149	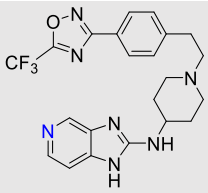	5.07	3.42	6.621	**298**
150	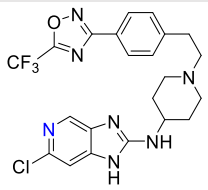	0.83	4.25	6.645	7.41

[a]hERG: human ether-*à-go-go*-related gene. Data shown are from n = 3 independent experiments. Verapamil (IC_{50} = 0.56 ± 0.096 μM) used as a reference compound.
[b]Properties predicted using StarDrop, version 6.5.1-1 (AST: cLog*P* = 5.700; pIC_{50} = 8.265)
[c]SI: selectivity index = hERG IC_{50}/*Pf*NF54 IC_{50}

3.7.5 hERG Affinity, Antiplasmodium Activity and Lipophilicity

As shown in Figure 3.10A, a weak but positive correlation (r^2 = 0.092) exists between hERG affinity and antiplasmodium potency. Generally, compounds that show high antiplasmodium activity, are also strong inhibitors of hERG K+ channels.

Likewise, a weak correlation (r^2 = 0.137) was identified between lipophilicity and hERG affinity (Figure 3.10B).

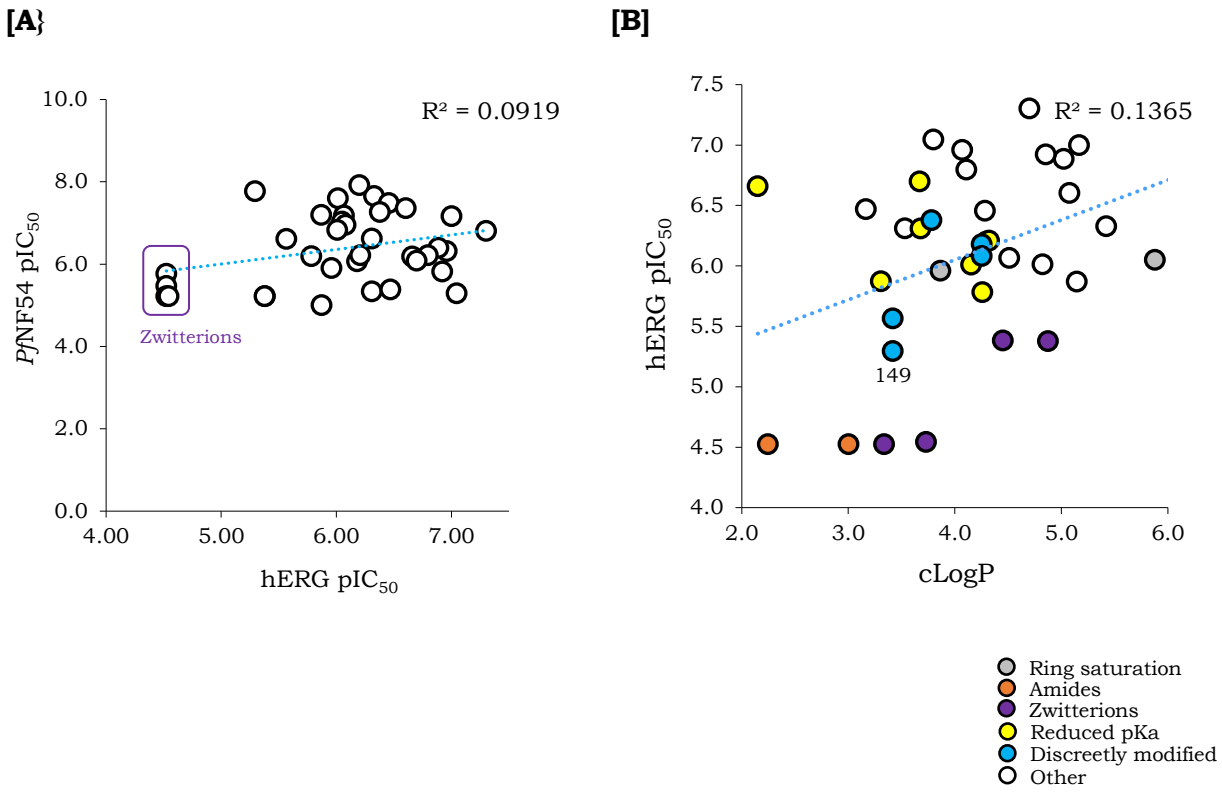

Figure 3.10: [A] Correlation plot between hERG activity (pIC_{50} = –log (hERG IC_{50}, in Molar)) and antiplasmodium potency (pIC_{50} = –log (*Pf*NF54IC_{50}, in Molar)) and [B] correlation between hERG activity (pIC_{50}) and lipophilicity (clogP)

However, it is worth mentioning that a combination of strategies (i.e., lowering lipophilicity and other discreet modifications) was required to effectively achieve a favorable balance of low hERG affinity, high antiplasmodium activity and optimal physicochemical properties.

A scoring profile (SP) plot was drawn to identify the best compounds meeting specific cut-offs/limits for antiplasmodium potency (*Pf*NF54), hERG channel activity and lipophilicity (clogP). SI = 100 was set for hERG (i.e., *Pf*NF54 IC_{50} < 0.100 µM; hERG IC_{50} > 10 µM), while clogP ≤ 4 was set as the desired value for lipophilicity. The scoring limits used in the StarDrop™ software tool are shown in Table 3.17.

Table 3.17: Parameters used for the determination of compound scoring profiles.

Property	Desired criteria		Importance
	Limits	Score	
*Pf*NF54 IC_{50} (µM)	<0.10	1.00	99%
	0.10 – 0.25	1.00 – 0.60	
	0.25 – 0.50	0.60 – 0.09	
	>0.50	<0.09	
hERG IC_{50} (µM)	>10	-	99%
clogP	≤4	-	50%

High antiplasmodium activity was of high importance to not only show potential for administration of a low dose, but also to achieve a large safety margin over hERG affinity. Compound **149** emerged as the best compound with SP = 0.24 (*Pf*NF54 IC_{50} = 0.017 µM; hERG IC_{50} = 5.07 µM and clogP = 3.42). Other noteworthy compounds include **148** (SP: 0.16), **156** (SP: 0.11) and **147** (SP: 0.10), all of which have potential for further development (Figure 3.11).

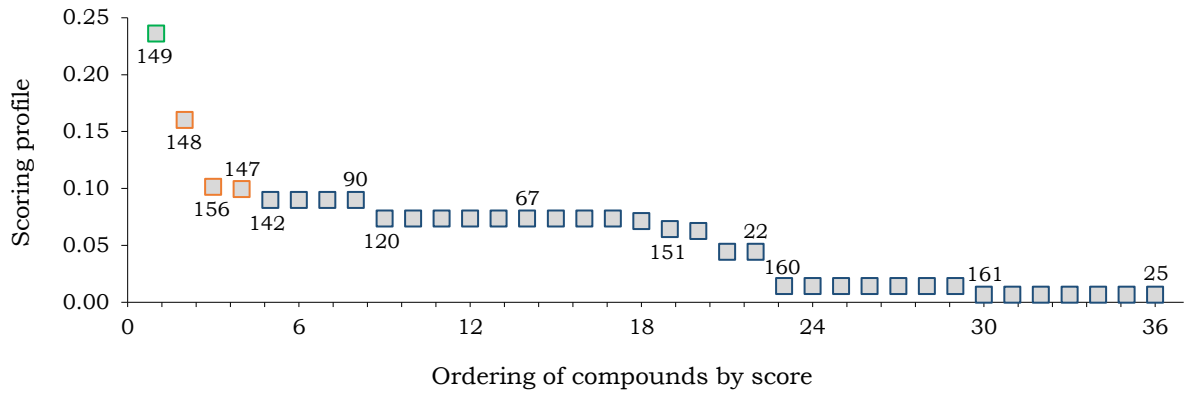

Figure 3.11: Scoring profile (SP) plot showing overall compliance with hERG affinity (IC_{50} > 10 µM), antiplasmodium potency (*Pf*NF54 IC_{50} < 0.10 µM) and lipophilicity (cLogP < 4) cut-offs. Scores calculated un using StarDrop™ software, version 6.5.1-1

3.7.6 *In silico* Predicted hERG Affinity versus *in vitro* hERG Activity

A hERG pIC_{50} model in StarDrop was used to predict hERG affinity and guide the design stage of the project. It is therefore crucial to cross-check the reliability of the tool within this series of compounds.

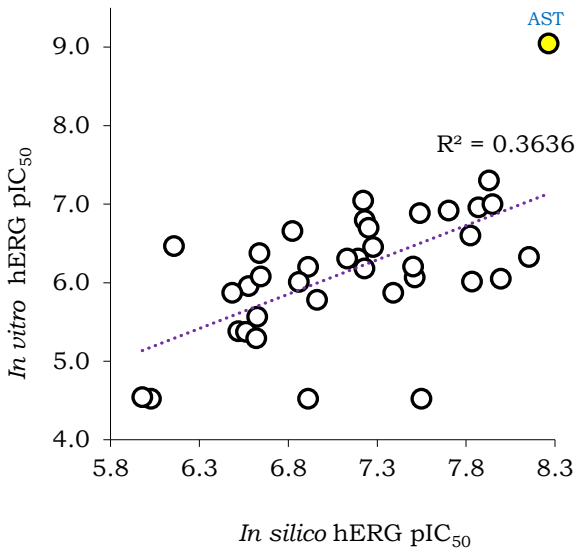

Figure 3.12: Plot showing the correlation between predicted *in silico* hERG pIC_{50} using StarDrop™ software versus experimentally determined *in vitro* hERG Pic_{50} (pIC_{50} = –log (hERG IC_{50}, in Molar))

By plotting predicted pIC_{50} values versus experimental data (Figure 3.12), a weak positive correlation (r^2 = 0.364) was identified. This low value suggests that this model should be used with caution, as significant ambiguities and inconsistencies in achieving accurate computational predictive models for hERG affinity remains a significant challenge.[34]

3.8 *In vitro* Microsomal Metabolic Stability

Metabolic stability is a measure of the susceptibility of a chemical compound towards biotransformation. *In vitro*, it is usually expressed as predicted intrinsic clearance (CL_{int}) or half-life ($t_{1/2}$). Early determination of the metabolic properties of new chemical entities (NCEs) is one of the most important steps of drug discovery as it enables rational prediction of *in vivo* drug exposure, and early assessment of the risk for drug-drug interactions related to inhibition or induction of drug metabolizing enzymes.[35,36] Drug metabolism occurs in numerous tissues including the lungs, kidneys (renal), intestines, skin, and blood. However, the liver is the primary organ responsible for drug metabolism, and accounts for the overall pharmacokinetic profile of any drug. Other routes of drug metabolism are considered to be negligible contributors.[37] Therefore, a number of *in vitro* liver models have been developed to determine the hepatic metabolic stability of drug candidates.

This study was conducted at the H3D, Division of Clinical Pharmacology, Department of Medicine, University of Cape Town, South Africa. In the assay, hepatic sub-cellular fractions called microsomes were used to determine the metabolic profile of selected compounds. Microsomes contain drug metabolizing enzymes, primarily the cytochrome P450 (CYP-450) enzymes which catalyze a wide ralnge of phase I oxidative and reductive biotransformations.[38,39] The assay was carried out by incubating test compounds with microsomes for 30 min and determining the percentage of compound which remains unchanged. Details of the assay are provided in the experimental section (Chapter 6). The metabolic stability of compounds with sub-micromolar potency ($IC_{50} \leq 0.1$ μM), favorable solubility ($S_{7.4} \geq 20$ μM) and marginal toxicity (CHO SI > 100) were evaluated in human, rat, and mouse liver microsomes (HLMs, RLMs and MLMs, respectively; Table 3.18.

Table 3.18: *In vitro* metabolic stability of selected analogues

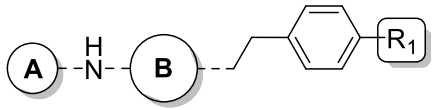

Code	A	R	B	R_1	Metabolic stability (%)[a]			Predicted $CL_{int.}$ ($\mu l.min^{-1}.mg^{-1}$)[b]			Extraction ratio (E_H)		
					H	R	M	H	R	M	H	R	M
18	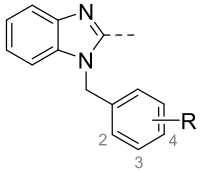	3-F,4-CN	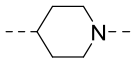	CN	41.9	5.40	24.1	72.9	243.4	118.3	0.81	0.84	0.84
73		4-CF_3		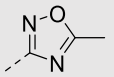	92.3	51.9	79.9	11.6	53.3	18.9	0.42	0.54	0.42
29	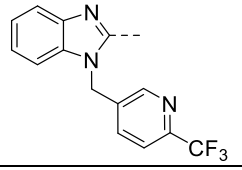	-	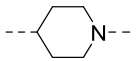	CN	43.6	36.2	8.30	71.5	84.7	207.9	0.80	0.64	0.90
74				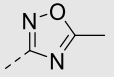	68.6	55.4	61.4	31.9	49.2	40.7	0.65	0.51	0.64
35				CF_3	82.4	44.7	36.8	16.2	67.4	83.3	0.49	0.59	0.78
38				CO_2Et	0.58	0.34	1.14	431.3	475.6	373.2	0.96	0.91	0.94
40					13.5	10.6	4.11	167.9	187.9	266.0	0.91	0.80	0.92
41	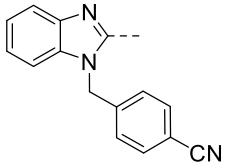	-	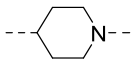	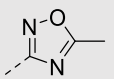	76.2	37.5	44.5	22.8	82.2	67.4	0.57	0.64	0.75
42				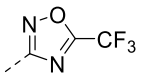	79.5	68.6	75.2	19.2	31.6	26.4	0.53	0.40	0.54
45				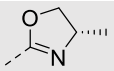	34.4	22.9	42.7	88.9	123.4	71.3	0.84	0.72	0.76
46		-		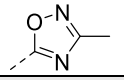	63.9	14.5	35.5	23.0	160.8	86.4	0.69	0.77	0.52
59		-	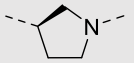		12.4	11.8	2.72	174.0	179.4	300.5	0.91	0.79	0.93

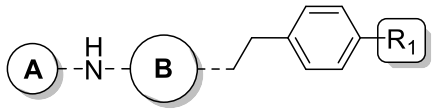

Code	A	R	B	R_1	Metabolic stability (%)[a]			Predicted $CL_{int.}$ ($\mu l.min^{-1}.mg^{-1}$)[b]			Extraction ratio (E_H)		
					H	R	M	H	R	M	H	R	M
66	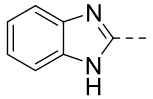	-		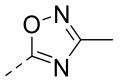	99.0	50.8	99.0	11.6	56.5	11.6	<0.42	0.54	<0.33
67		-		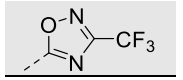	95.6	93.2	97.1	<11.6	<11.6	<11.6	<0.42	<0.30	<0.33
68		-	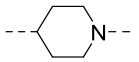	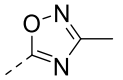	79.3	50.9	59.3	19.7	56.3	43.6	<0.42	0.53	0.45
69	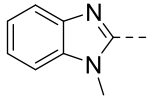	-		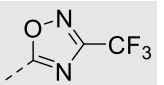	89.1	94.6	97.5	<11.6	<11.6	<11.6	<0.42	<0.30	<0.33
120		-		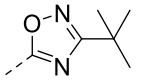	88.3	90.1	63.2	15.2	12.8	18.4	<0.40	<0.33	<0.47
147	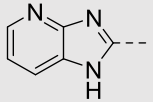	-			96.9	98.3	99.1	<11.6	<11.6	<11.6	<0.42	<0.30	<0.33
148	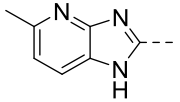	-	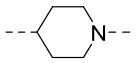	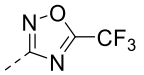	96.6	95.0	98.3	<11.6	<11.6	<11.6	<0.42	<0.30	<0.33
149	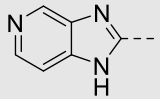	-			98.9	>99	97.8	<11.6	<11.6	<11.6	<0.42	<0.30	<0.33
150	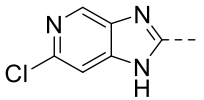	-	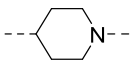	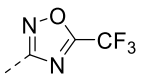	98.5	98.7	96.8	<11.6	<11.6	<11.6	<0.42	<0.30	<0.33
151	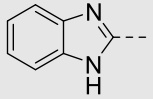	-	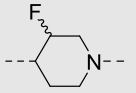	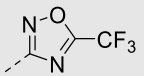	98.4	97.9	>99	<11.6	<11.6	<11.6	<0.42	<0.30	<0.33

[a]Percentage (%) of test compound remaining after 30 min incubation with human (H), rat ® or mouse (M) live microsomes.
[b]Predicted intrinsic clearance (CL_{int}) of unbound drug

Cyanated analogues **18** and **29** were unstable (CL_{int} > 71.5 µl.min^{-1}.mg^{-1}, E_H > 0.64), primarily in the rodent species. However, replacement of the phenylic 4-CN group with 4-CF_3 improved stability (i.e., **35**). The nitrile group is not readily metabolized. However, some studies have shown its susceptibility towards CYP-mediated oxidation to amides and related derivatives.[40] As expected, the ester frontrunner **38** was rapidly metabolized (CL_{int} > 370 µl.min^{-1}.mg^{-1}) in all three species. However, 2 of 8 analogues bearing an ester bioisostere showed improved stability (**42** and **73**, H/MLM > 75% remaining, CL_{int} < 26 µl.min^{-1}.mg^{-1}), which was generally higher in HLM's than in RLMs and MLM's. With the 3-methly-1,2,4-oxadiazole moiety fixed in the lateral phenyl group, substitution of CN (**46**) with CF_3 (**73**) in the benzyl moiety significantly improved stability by 1.5-fold across all species. Stability was improved following removal of the benzyl moiety (**66**, H/MLM = 99% remaining, CL_{int} = <11.6 µl.min^{-1}.mg^{-1}, E_H < 0.42). However, clearance in rat species was still high (E_H = 0.54).

Although pyrrolidine analogue **59** did not meet the progression criteria for potency (IC_{50} = 0.448 µM), its high activity within the diaminoalkyl linker SAR (phase I, SAR 4) pre-empted testing to assess the effect of linker variations toward microsomal metabolism. This test revealed loss of stability following piperidine/pyrrolidine interchange.

Interesting metabolism structure-property relationships (SPRs) can be derived regarding the ester-group bioisosteres. For instance, the 3-/5-CH_3-1,2,4-oxadiazole analogues **41**/**68** were less stable (up to 2-fold) than their 3-/5-CF_3-substituted counterparts **42**/**69**, especially in rodent species. This use of CF_3 is a proven and effective strategy for blocking metabolism.[41,42] Oxazoline **45** was less stable (HLM, CL_{int} = 88.9 µl.min^{-1}.mg^{-1}) than to oxadiazole match-pairs **42** or **46** (HLM CL_{int} < 23 µl.min^{-1}.mg^{-1}). Similarly, unsubstituted 1,2,4-oxadiazole **40** was rapidly cleared (HLM CL_{int} = 167.9 µl.min^{-1}.mg^{-1}) compared to the 5-substituted derivatives. In both cases, these observations suggest the significance of blocking the 5-position, which is clearly a metabolic soft-spot in both **40** and **45**.

Using the SPR derived from these data, the combination of (i) benzyl group truncation and (ii) metabolic soft-spot blockade by the 3-/5-CF_3 group in the oxadiazole moiety produced high metabolic stability across all three species (**67**, >93% remaining, CL_{int} = <11.6 µl.min^{-1}.mg^{-1}, E_H < 0.42). Interestingly, high stability was retained following substitution of benzimidazole with azabenzimidazole (**147** – **150**), or introduction of stereochemistry by β-fluorination of piperidine ring (**151**; Table 3.18). These transformations were carried out as strategies to mitigate hERG.

3.8.1 Metabolic Stability versus Lipophilicity

To discern the contribution of lipophilicity as a physicochemical attribute to metabolic stability, lipophilic metabolism efficiency (LipMetE) was measured. LipMetE is calculated

using Equation 2 and describes the relationship between lipophilicity and *in vitro* metabolic clearance in HLMs.[43]

Equation 2: $LipMetE = logD_{7.4}$ (or clogP) – log (CL_{int})

Where LipMetE is lipophilic metabolism efficiency, logD is the experimental partitioning coefficient between water and *n*-octanol determined at pH 7.4 (interchangeable with calculated lipophilicity, clogP) and CLint is the predicted in vitro intrinsic clearance.
By plotting logD (or clogP) versus predicted intrinsic clearance (CL_{int}), the lipophilicity-metabolism relationship can be visualized using data from the tested AST analogues (phases I and II; Figure 3.13). Similar to the analogous LipE metric discussed previously, the contribution of changes in lipophilicity to observed clearance is seen in compounds that cluster along the same or similar 45° LipMetE line.

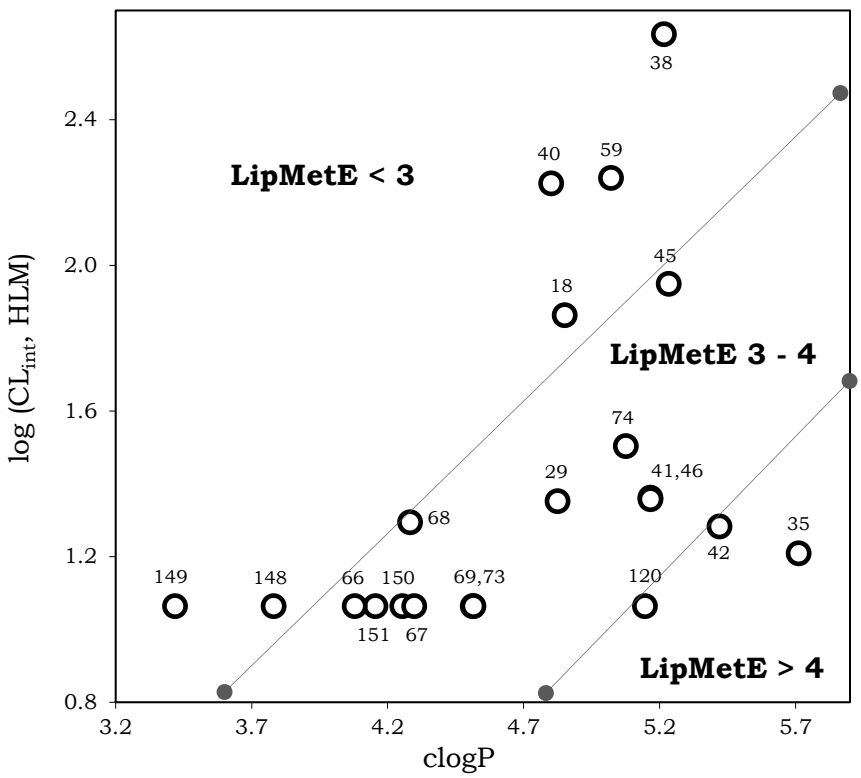

Figure 3.13: LipMetE plot of cLogP vs log(CL_{int}, HLM) of AST analogues tested *in vitro*

For this set of analogues, LipMetE values vary from 2.38 to 4.50 (Figure 3.13). The isolipophilic relationship between ethyl ester **38** and 3-/5-CH_3-1,2,4-oxadiazoles **41**/**46** (clogP ~ 5.20) shows improved metabolic stability (ΔLipMetE = +1.23), free of the influence of lipophilicity, but due to the removal of the labile ester moiety. The observed difference in clearance between 5-CH_3- (**41**) and 5-CF_3- (**42**) substituted 1,2,4-oxadiazoles match pairs (ΔLipMetE = +0.33) is clearly driven by the application of a metabolic soft-spot blocking approach, which in this case outweighs the negligible increase in lipophilicity resulting from CH_3/CF_3 interchange (ΔclogP = 0.26 units). Compared to alkyl derivatives, fluorinated derivatives show increased stability towards oxidative degradation.[41,42] In this

case, the bulky and electronegativity nature of the fluorine groups in CF_3 blocks the oxadiazole 3-/5-position soft-spot more efficiently than CH_3. Similarly, the observed 5.3-fold clearance difference between pyrrolidine (**59**) and its more stable piperidine (**46**) match pair is not driven by lipophilicity, but rather by the effect of ring size, a phenomenon that has been shown to affect metabolism.[44,45]

Removal of the benzyl moiety in **42** to produce **66**/**67** induces a 2-fold clearance improvement, which is primarily driven by a reduction of lipophilicity (ΔclogP = –1.34 units). The intrinsic clearance prediction limit for the method used is 11.0 $\mu l.min^{-1}.mg^{-1}$, and most stable compounds therefore appear isoefficient. However, this is not always the case, as the effect of reducing the lipophilicity of benzimidazole compound **67** (clogP = 4.30, LipMetE = 3.23) by incorporating a nitrogen atom in the benzimidazole ring to obtain azabenzimidazole compound **149** (clogP = 3.42, LipMetE = 2.36) can easily be seen from this plot.

3.9 *In vivo* Antimalarial Activity

To demonstrate proof-of-concept (PoC), the antimalarial efficacy of front-runner compounds with high antiplasmodium activity, low cytotoxicity and favorable ADME properties was tested in a *Plasmodium berghei*-infected mouse model. Compounds **73**, **66**, **67**, and **69** were progressed to represent the first set of front-runner analogues with favorable metabolic stability (MLMs, > 75% remaining; CL_{int} < 20 $\mu l.min^{-1}.mg^{-1}$). This study was conducted at the Swiss Tropical and Public Health Institute (Swiss TPH), Basel, Switzerland. A standard 50 $mg.kg^{-1}$ repeat dose was administered orally (*po*) to mice for four consecutive days, and antimalarial efficacy was determined according to parasitemia in infected untreated controls and treated animals (Table 3.19). In this model, curative effects are achieved if recrudescence does not occur in mice 30 days after treatment.

Compounds **67** and **69**, both of which are 3-CF_3-1,2,4-oxadiazoles, showed high parasitemia reduction (>85%) with mouse survival time/rate of 9 and 14 days, respectively. However, compound **67** was the most efficacious with 99.5% reduction in parasitemia, which correlates with *in vitro* potency (*Pf*NF54 IC_{50} = 0.012 μM), making it the first novel structural analogue of AST demonstrating PoC in an animal model. Comparatively, the reference drug CQ achieved 99.9% parasitemia reduction when administered at 4 × 30 $mg.kg^{-1}$, with a mouse survival time of 21 days.

Table 3.19: *In vivo* antimalarial activity of frontrunner compounds with chloroquine (CQ) used as a control drug.

Code	Structure	Dose ($mg.kg^{-1}$)[a]	% Activity[b,c]	MSD[c]	Mice Cured
73	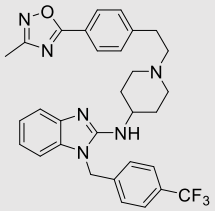	4 × 50	40.0	4	0/3
66	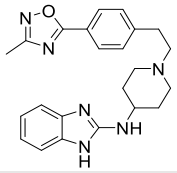	4 × 50	<39.9	4	0/3
67	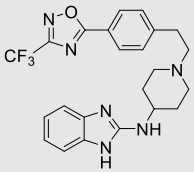	4 × 50	99.5	14	0/3
69	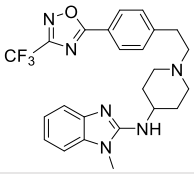	4 × 50	89.8	9	0/3
CQ	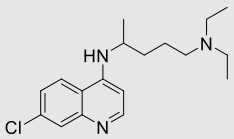	4 × 30	99.9	21	0/3

[a]Nominal dose in $mg.kg^{-1}$ administered orally (per os, *po*) once per day on 4 consecutive days (4, 24, 48, and 72 h post-infection)
[b]Activity = average parasitemia reduction compared with untreated controls
[c]MSD: mean survival days, the average lifespan of mice post infection (6 – 7 days for untreated control mice). Mice with <40% parasitemia reduction were euthanized on day 4 to prevent death from infection, otherwise occurring at day 6

The 3-CH_3-1,2,4-oxadiazoles demonstrated low efficacy regardless of whether the benzyl moiety was present or not (**73** and **66**). Based on these data, the CF_3 group appears to be a crucial part of the pharmacophore for antimalarial activity.

3.10 *In vivo* Pharmacokinetics (PK) and ADME Properties

To investigate the pharmacokinetic (PK) profiles of the structurally related compounds **67** and **69**, dried-blood spot (DBS) samples collected from *P. berghei*-infected mice (whole blood at 1h, 4h, 24h post-administration) at the Swiss TPH where subjected to pharmacokinetics (PK) analysis. The studies were conducted at the Drug Discovery and development Centre (H3D), Division of Clinical Pharmacology, Department of Medicine,

University of Cape Town (UCT). The total- and free-blood concentrations of front-runners are shown in Figure 3.14.

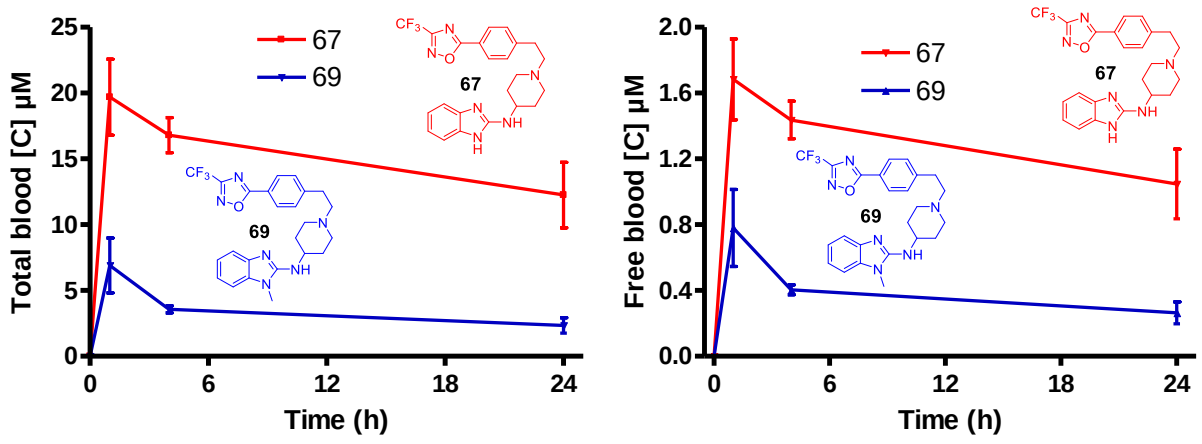

Figure 3.14: Total blood (left) and free-blood (right) concentrations of compound **66** and **69** in *P.berghei*-infected mice following oral administration at 4 × 50 mg.kg^{-1}

At 50 mg.kg^{-1} oral dose, both compounds **67** and **69** attained peak plasma concentrations within the first 2 h (Figure 3.14), reaching concentrations ~1600-fold and ~106-fold above their whole-cell activity (IC_{50} = 0.012 µM and IC_{50} = 0.066 µM), respectively. Plasma levels were maintained above the IC_{50} values for over 24 h. A similar observation was made in unbound free drug (free blood). However, the concentration of **67** was > 2-fold compared to that of **69** in both whole and free-blood, which explains the higher efficacy observed in compound **67** despite their comparable metabolic stabilities (CL_{int} = <11.6 µl.min^{-1}.mg^{-1}). Additionally, the higher efficacy may be attributed to the 5-fold difference in whole-cell activity, and the advantage that **67** has regarding possessing high gametocyte (EG/LG) activity compared to **67**, which has no LG activity.

The partitioning coefficient at pH 7.4 (log$D_{7.4}$) and solubility at pH 6.5 ($S_{6.5}$) were determined for compounds **67** and **69**, as well as **147** and **149**. Experimental log$D_{7.4}$ provides a quick and efficient snapshot of the intestinal absorption of a compound, and may be used as an alternative to *in vitro* cell culture permeability models such as the human colorectal carcinoma cells (Caco-2), with which there is a proven linear correlation.[46,47] Table 3.20 shows the logD, solubility and LipE (based of logD) of the tested compounds.

Table 3.20: ADME properties and hERG activity of front-runner compounds

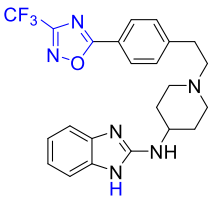
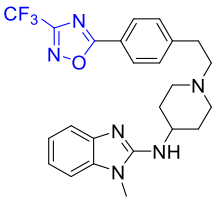
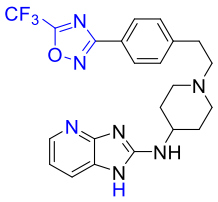
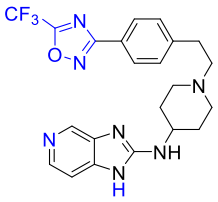

Property	67	69	147	149
log$D_{7.4}$	3.22	2.92	0.24	-0.82
$S_{6.5}$	120	140	150	195
LipE	4.70	4.26	6.71	8.59
hERG IC_{50}, μM	0.63	0.86	2.72	5.07

log$D_{7.4}$ = n-octanol-water partitioning coefficient experimentally determined at pH 7.4
S6.5 = kinetic HPLC solubility at physiological pH (6.5)
LipE = lipophilic efficiency based on experimental logD and whole-cell activity

The lower log*D* value for compound **69** (log*D* = 2.92; Table 3.20) may suggest lower membrane permeability due to low lipophilicity compared to **67** (log*D* = 3.22). This is also reflected in the higher solubility of **69**. However, both compounds have favorable log*D* values overall, and therefore permeability would not be expected to be different. And in this case, low absorption may not be a contributing factor to the observed lower efficacy of **69** compared to **67**. On the other hand, azabenzimidazoles **147** (log*D* = 0.24) and **149** (log*D* = -0.82) display much lower log*D* values, which is also reflected in their high solubility. Ideally, the permeability of **147** and **149** would be expected to be poor. However, the high solubility may compensate for their poor absorptions, and therefore this chemical space may offer an exciting opportunity for developing molecules with better ADME properties and low hERG affinity.

3.11 Chapter Summary

In this chapter, the *in vitro* antiplasmodium activity and solubility of all analogues have been discussed and SAR trends defined. Additionally, the potential for dual-stage activity in gametocytes has been highlighted, with some compounds showing stage-specific activity which was distinguished from cell toxicity *via* cytotoxicity assessment in two cell lines. To investigate the contributing MoA, selected analogues that potently inhibit β-hematin formation were identified. Although the SAR could not be defined, the high activity of some analogues corroborates previous findings implicating the interaction of AST and its analogues with the hemozoin degradation pathway. The chapter also discussed the systematic and rational utilization of bioisosterism, metabolic soft-spot blockade and other lipophilicity-reducing strategies to improve the microsomal metabolic stability of unstable front-runner ester, leading to the discovery of 1,2,4-oxadiazoles displaying high microsomal metabolic stability. A detailed account of the use of various strategies to reduce

hERG affinity has been provided, and hERG SAR trends defined, leading to the identification of a series of compounds with reduced cardiotoxicity risk associated with hERG inhibition. Finally, the chapter concludes with a discussion of the *in vivo* efficacy of front-runner compounds and provides a rationale for the observed activities *via* PK profiling and determination of ADME parameters.

3.12 References

(1) Lovering, F.; Bikker, J.; Humblet, C. Escape from Flatland: Increasing Saturation as an Approach to Improving Clinical Success. *J. Med. Chem.* **2009**, *52* (21), 6752–6756.

(2) Moussebois, C.; Oth, J. F. M. Etude Spectroscopique d'oxadiazoles-1,2,4 En Relation Avec Leur Degré d'aromaticité. *Helv. Chim. Acta* **1964**, *47* (4), 942–946.

(3) Trifonov, R. E.; Ostrovskii, V. A. Basicity of 2-Phenyl-5-R-1,3,4-Oxadiazoles. *Chem. Heterocycl. Compd.* **2006**, *42* (5), 657–664.

(4) Srivastava, Rajendra; Mauricio, Rosa; Carlos, C. 5-Butyl-3, 5-Diaryl-4, 5-Dihydro-1, 2, 4-Oxadiazoles, and a One-Step Synthesis of 4, 4-Dibutyl-2-Phenylbenzo-1, 3-Oxazine. *Heterocycles* **2000**, *53* (1), 191–195.

(5) Pitasse-Santos, P.; Sueth-Santiago, V.; Lima, M. 1,2,4- and 1,3,4-Oxadiazoles as Scaffolds in the Development of Antiparasitic Agents. *J. Braz. Chem. Soc.* **2017**.

(6) Mohammadi-Khanaposhtani, M.; Shabani, M.; Faizi, M.; Aghaei, I.; Jahani, R.; Sharafi, Z.; Shamsaei Zafarghandi, N.; Mahdavi, M.; Akbarzadeh, T.; Emami, S.; et al. Design, Synthesis, Pharmacological Evaluation, and Docking Study of New Acridone-Based 1,2,4-Oxadiazoles as Potential Anticonvulsant Agents. *Eur. J. Med. Chem.* **2016**, *112*, 91–98.

(7) Ballatore, C.; Huryn, D. M.; Smith, A. B. Carboxylic Acid (Bio)Isosteres in Drug Design. *ChemMedChem* **2013**, *8* (3), 385–395.

(8) Keserű, G. M.; Makara, G. M. Hit Discovery and Hit-to-Lead Approaches. *Drug Discov. Today* **2006**, *11* (15–16), 741–748.

(9) Boehm, H.-J.; Boehringer, M.; Bur, D.; Gmuender, H.; Huber, W.; Klaus, W.; Kostrewa, D.; Kuehne, H.; Luebbers, T.; Meunier-Keller, N.; et al. Novel Inhibitors of DNA Gyrase: 3D Structure Based Biased Needle Screening, Hit Validation by Biophysical Methods, and 3D Guided Optimization. A Promising Alternative to Random Screening. *J. Med. Chem.* **2000**, *43* (14), 2664–2674.

(10) Bilodeau, M. T.; Balitza, A. E.; Koester, T. J.; Manley, P. J.; Rodman, L. D.; Buser-Doepner, C.; Coll, K. E.; Fernandes, C.; Gibbs, J. B.; Heimbrook, D. C.; et al. Potent N -(1,3-Thiazol-2-Yl)Pyridin-2-Amine Vascular Endothelial Growth Factor Receptor Tyrosine Kinase Inhibitors with Excellent Pharmacokinetics and Low Affinity for the HERG Ion Channel. *J. Med. Chem.* **2004**, *47*, 6363–6372.

(11) Zhang, H.-C.; Derian, C. K.; McComsey, D. F.; White, K. B.; Ye, H.; Hecker, L. R.; Li, J.; Addo, M. F.; Croll, D.; Eckardt, A. J.; et al. Novel Indolylindazolylmaleimides as Inhibitors of Protein Kinase C-β: Synthesis, Biological Activity, and Cardiovascular Safety †. *J. Med. Chem.* **2005**, *48* (6), 1725–1728.

(12) Bourrain, S.; Collins, I.; Neduvelil, J. G.; Rowley, M.; Leeson, P. D.; Patel, S.; Patel, S.; Emms, F.; Marwood, R.; Chapman, K. L.; et al. Substituted Pyrazoles as Novel Selective Ligands for the Human Dopamine D 4 Receptor. *Bioorg. Med. Chem.* **1998**, *6* (10), 1731–1743.

(13) Jamieson, C.; Moir, E. M.; Rankovic, Z.; Wishart, G. Medicinal Chemistry of HERG Optimizations: Highlights and Hang-Ups. *J. Med. Chem.* **2006**, *49* (17), 5029–5046.

(14) Ritchie, T. J.; Macdonald, S. J. F.; Pickett, S. D. Insights into the Impact of N- and O-Methylation on Aqueous Solubility and Lipophilicity Using Matched Molecular Pair Analysis. *Medchemcomm* **2015**, *6* (10), 1787–1797.

(15) Price, D. A.; Armour, D.; de Groot, M.; Leishman, D.; Napier, C.; Perros, M.; Stammen, B. L.; Wood, A. Overcoming HERG Affinity in the Discovery of the CCR5 Antagonist Maraviroc. *Bioorg. Med. Chem. Lett.* **2006**, *16* (17), 4633–4637.

(16) Nair, A. G.; Wong, M. K. C.; Shu, Y.; Jiang, Y.; Jenh, C.-H.; Kim, S. H.; Yang, D.-Y.; Zeng, Q.; Shao, Y.; Zawacki, L. G.; et al. IV. Discovery of CXCR3 Antagonists Substituted with Heterocycles as Amide Surrogates: Improved PK, HERG and Metabolic Profiles. *Bioorg. Med. Chem. Lett.* **2014**, *24* (4), 1085–1088.

(17) Westphal, M. V.; Wolfstädter, B. T.; Plancher, J.-M.; Gatfield, J.; Carreira, E. M. Evaluation of Tert -Butyl Isosteres: Case Studies of Physicochemical and Pharmacokinetic Properties, Efficacies, and Activities. *ChemMedChem* **2015**, *10* (3), 461–469.

(18) Stump, B.; Eberle, C.; Schweizer, W. B.; Kaiser, M.; Brun, R.; Krauth-Siegel, R. L.; Lentz, D.; Diederich, F. Pentafluorosulfanyl as a Novel Building Block for Enzyme Inhibitors: Trypanothione Reductase Inhibition and Antiprotozoal Activities of Diarylamines. *ChemBioChem* **2009**, *10* (1), 79–83.

(19) Headley, A. D.; Ganesan, R.; Nam, J. The Effect of the Cyclopropyl Group on the Conformation of Chemotactic Formyl Tripeptides. *Bioorg. Chem.* **2003**, *31* (2), 99–108.

(20) Dalvie, D.; Di, L. Aldehyde Oxidase and Its Role as a Drug Metabolizing Enzyme. *Pharmacol. Ther.* **2019**, *201*, 137–180.

(21) Montefiori, M.; Jørgensen, F. S.; Olsen, L. Aldehyde Oxidase: Reaction Mechanism and Prediction of Site of Metabolism. *ACS Omega* **2017**, *2* (8), 4237–4244.

(22) Chong, C. R.; Chen, X.; Shi, L.; Liu, J. O.; Sullivan, D. J. A Clinical Drug Library Screen Identifies Astemizole as an Antimalarial Agent. *Nat. Chem. Biol.* **2006**, *2*, 415–416.

(23) Kumar, M.; Okombo, J.; Mambwe, D.; Taylor, D.; Lawrence, N.; Reader, J.; van der

Watt, M.; Fontinha, D.; Sanches-Vaz, M.; Bezuidenhout, B. C.; et al. Multistage Antiplasmodium Activity of Astemizole Analogues and Inhibition of Hemozoin Formation as a Contributor to Their Mode of Action. *ACS Infect. Dis.* **2019**, *5* (2), 303–315.

(24) Musonda, C. C.; Whitlock, G. A.; Witty, M. J.; Brun, R.; Kaiser, M. Chloroquine–Astemizole Hybrids with Potent in Vitro and in Vivo Antiplasmodial Activity. *Bioorg. Med. Chem. Lett.* **2009**, *19*, 481–484.

(25) Wilcken, R.; Zimmermann, M. O.; Lange, A.; Joerger, A. C.; Boeckler, F. M. Principles and Applications of Halogen Bonding in Medicinal Chemistry and Chemical Biology. *J. Med. Chem.* **2013**, *56* (4), 1363–1388.

(26) Hardegger, L. A.; Kuhn, B.; Spinnler, B.; Anselm, L.; Ecabert, R.; Stihle, M.; Gsell, B.; Thoma, R.; Diez, J.; Benz, J.; et al. Systematic Investigation of Halogen Bonding in Protein-Ligand Interactions. *Angew. Chemie Int. Ed.* **2011**, *50* (1), 314–318.

(27) Johnson, T. W.; Gallego, R. A.; Edwards, M. P. Lipophilic Efficiency as an Important Metric in Drug Design. *J. Med. Chem.* **2018**, *61* (15), 6401–6420.

(28) Edwards, M. P.; Price, D. A. Role of Physicochemical Properties and Ligand Lipophilicity Efficiency in Addressing Drug Safety Risks; 2010; pp 380–391.

(29) Olliaro, P.; Wells, T. N. C. The Global Portfolio of New Antimalarial Medicines Under Development. *Nature* **2009**, *85*, 584–595.

(30) Burrows, J. N.; Duparc, S.; Gutteridge, W. E.; Hooft van Huijsduijnen, R.; Kaszubska, W.; Macintyre, F.; Mazzuri, S.; Möhrle, J. J.; Wells, T. N. C. New Developments in Anti-Malarial Target Candidate and Product Profiles. *Malar. J.* **2017**, *16* (1), 26.

(31) Lucantoni, L.; Avery, V. Whole-Cell in Vitro Screening for Gametocytocidal Compounds. *Future Med. Chem.* **2012**, *4* (18), 2337–2360.

(32) Mosmann, T. Rapid Colorimetric Assay for Cellular Growth and Survival: Application to Proliferation and Cytotoxicity Assays. *J. Immunol. Methods* **1983**, *65* (1–2), 55–63.

(33) Verlinden, B. K.; Niemand, J.; Snyman, J.; Sharma, S. K.; Beattie, R. J.; Woster, P. M.; Birkholtz, L.-M. Discovery of Novel Alkylated (Bis)Urea and (Bis)Thiourea Polyamine Analogues with Potent Antimalarial Activities. *J. Med. Chem.* **2011**, *54* (19), 6624–6633.

(34) Kalyaanamoorthy, S.; Barakat, K. H. Development of Safe Drugs: The HERG Challenge. *Med. Res. Rev.* **2018**, *38* (2), 525–555.

(35) Baranczewski, P.; Stańczak, A.; Sundberg, K.; Svensson, R.; Wallin, A.; Jansson, J.; Garberg, P.; Postlind, H. Introduction to in Vitro Estimation of Metabolic Stability and Drug Interactions of New Chemical Entities in Drug Discovery and Development. *Pharmacol. Rep.* **2006**, *58* (4), 453—472.

(36) Masimirembwa, C. M.; Bredberg, U.; Andersson, T. B. Metabolic Stability for Drug Discovery and Development. *Clin. Pharmacokinet.* **2003**, *42* (6), 515–528.

(37) Remmer, H. The Role of the Liver in Drug Metabolism. *Am. J. Med.* **1970**, *49* (5), 617–629.

(38) *Cytochrome P-450*; de Montellano, P. R. O., Ed.; Springer US: Boston, MA, 1986.

(39) Guengerich, F. P. Cytochrome P450s and Other Enzymes in Drug Metabolism and Toxicity. *AAPS J.* **2006**, *8* (1), E101–E111.

(40) Zhang, Z.; Li, Y.; Stearns, R. A.; Ortiz de Montellano, P. R.; Baillie, T. A.; Tang, W. Cytochrome P450 3A4-Mediated Oxidative Conversion of a Cyano to an Amide Group in the Metabolism of Pinacidil. *Biochemistry* **2002**, *41* (8), 2712–2718.

(41) Jeffries, B.; Wang, Z.; Graton, J.; Holland, S. D.; Brind, T.; Greenwood, R. D. R.; Le Questel, J.-Y.; Scott, J. S.; Chiarparin, E.; Linclau, B. Reducing the Lipophilicity of Perfluoroalkyl Groups by CF 2 –F/CF 2 –Me or CF 3 /CH 3 Exchange. *J. Med. Chem.* **2018**, *61* (23), 10602–10618.

(42) Shah, P.; Westwell, A. D. The Role of Fluorine in Medicinal Chemistry. *J. Enzyme Inhib. Med. Chem.* **2007**, *22* (5), 527–540.

(43) Stepan, A. F.; Kauffman, G. W.; Keefer, C. E.; Verhoest, P. R.; Edwards, M. Evaluating the Differences in Cycloalkyl Ether Metabolism Using the Design Parameter "Lipophilic Metabolism Efficiency" (LipMetE) and a Matched Molecular Pairs Analysis. *J. Med. Chem.* **2013**, *56* (17), 6985–6990.

(44) Pescatore, G.; Kinzel, O.; Attenni, B.; Cecchetti, O.; Fiore, F.; Fonsi, M.; Rowley, M.; Schultz-Fademrecht, C.; Serafini, S.; Steinkühler, C.; et al. Optimization of a Series of Potent and Selective Ketone Histone Deacetylase Inhibitors. *Bioorg. Med. Chem. Lett.* **2008**, *18* (20), 5528–5532.

(45) Fish, P. V.; Brown, A. D.; Evrard, E.; Roberts, L. R. 7-Sulfonamido-3-Benzazepines as Potent and Selective 5-HT2C Receptor Agonists: Hit-to-Lead Optimization. *Bioorg. Med. Chem. Lett.* **2009**, *19* (7), 1871–1875.

(46) Hou, T. J.; Zhang, W.; Xia, K.; Qiao, X. B.; Xu, X. J. ADME Evaluation in Drug Discovery. 5. Correlation of Caco-2 Permeation with Simple Molecular Properties. *J. Chem. Inf. Comput. Sci.* **2004**, *44* (5), 1585–1600.

(47) Waring, M. J. Lipophilicity in Drug Discovery. *Expert Opin. Drug Discov.* **2010**, *5* (3), 235–248.

CHAPTER 4

PHYSICOCHEMICAL PROFILING AND STRUCTURE-PROPERTY RELATIONSHIPS (SPRs)

4.1 Chapter Overview

In this chapter, the physicochemical profiles of synthesized analogues are reported in the context of their influence of various drug properties. The chapter begins by highlighting the significance of physicochemical properties in drug molecules followed by an assessment of compliance to drug-likeness using the guidelines defined by Lipinski's rule-of-five (Ro5) and Verber's rules. This will be followed by an investigation of factors influencing solubility in each compound series. Lastly, structure-property relationships (SPRs) are derived citing specific examples of the impact of the approaches used to achieve optimum physicochemical profile with respect to biological activity.

4.2 Significance of Physicochemical Properties in Drug Discovery

There are many studies in literature highlighting the influence of physicochemical properties on both potency and ADME/tox profiles of drug molecules. For instance, lipophilicity affects the pharmacokinetic (PK) profile of orally administered drugs. It influences solubility, intestinal absorption, cellular permeability, plasma protein binding, metabolism, eventual excretion and as well as safety (ADME/tox).[1,2] Physicochemical and PK properties need to be optimized early in drug discovery because poor absorption and related poor PK are among the common reasons for attrition in the drug development process.[3]

The understanding of these properties has continued to evolve, with property-based design (PBD) emerging as a vital tool for medicinal chemists since the late 90's. After two decades, Lipinski's Ro5 remains as a useful guideline towards achieving 'drug-likeness' using physicochemical parameters. In their seminal paper of 1997, Lipinski *et al.* examined structural features of 'orally' administered drugs that entered phase II clinical trials by correlating their physicochemical properties namely: molecular weight (MW), lipophilicity (clog*P*) and number of hydrogen bond donors/acceptors (HBD/A) to the compounds' aqueous solubility, permeability and oral bioavailability.[4] Consequently, they devised a set of criteria/rules called the Ro5, for triaging potential drug candidates based on these descriptors. According to their rules, good oral absorption and permeability is more likely to be achieved if a compound has molecular weight (MW) ≤ 500 Daltons (Da); a clog*P* of ≤ 5; number of hydrogen-bond donors (HBD) is ≤ 5; and the number of hydrogen-bond acceptors (HBA) ≤ 10 (a multiple of 5).[1,4] However, natural products (NPs, i.e., antibiotics), compounds that are substrates to biological transporters, peptides and macrocycles belong to an oral

chemical space which are exceptions, and extend beyond the Ro5 (bRo5).[5,6] Additionally, Veber *et al.* correlated a molecule's topological polar surface area (PSA), which is closely related to logD and therefore oral bioavailability. Verber's rule suggests that compounds with TPSA ≤ 140 Å^2 and has 10 or fewer rotatable bonds, would have a high probability of achieving good oral bioavailability in the rat PK models.[7]

In general, when a compound does not 'comply' with or violates these criteria, its properties are considered to differ from those of the majority of drugs, which could suggest a higher risk of poor PK or safety outcomes *in vivo*. However, as a caveat, being similar to known drugs does not necessarily mean that a compound is more likely to become a drug. Therefore, instead of restricting physical properties to these 'rules', it is imperative to use them only as guidelines, and instead consider medicinal chemistry innovation, trends in current strategies and utilize data-driven aspects for drug-likeness (especially lipophilicity), which may in fact be specific to a project, compound series or chemical space.[8]

4.3 Evaluation of Physicochemical Properties

Lipinski's and Verber's descriptors (MW, clog*P*, HBD, HBA and TPSA) were determined and predicted using StarDrop™, an *in-silico* tool provided by Optibrium Ltd. Plotting of each of these parameters for each compound class allowed the assessment of the distribution and frequency to assess compliance or violation.

Objective 2 and specific aims 3 and 4 of this project sought to improve solubility and investigate factors that influence it. Therefore, the solubility of all the compounds was determined using the lab adapted kinetic turbidimetric method. Compared to the HPLC kinetic method, this method is less accurate due to its dependency on turbidity and the limit associated with the order of test concentrations. However, it offers a quick and cost-effective way of obtaining a solubility snapshot of compounds. Solubility was classified as low ($S_{7.4}$ < 60 μM), moderate ($S_{7.4}$ = 60 – 120 μM) and high ($S_{7.4}$ > 120 μM). Briefly, a 10 mM DMSO stock solution of the test compound was serially diluted using phosphate-buffered saline (PBS) at pH 7.4 to obtain 0, 5, 10, 20, 40, 80, 160 and 200 μM concentrations in triplicate on a 96-well microtiter plate. In order to cover the concentration gaps and increase accuracy, an additional plate containing 60, 100 and 120 μM of drug was also prepared. After equilibration and incubation at 25 °C for two (2 h, the UV-vis absorbance (Abs) was measured at 620 nm using a spectrophotometer. The readings were then be plotted against the concentration to identify the limit of solubility, indicated by the point at which Abs rose from the baseline.

To investigate factors influencing solubility, the solubility data was plotted against experimentally determined physicochemical parameters i.e., thin layer chromatography (TLC) retardation factor (R_f) values, high power/performance liquid chromatography (HPLC) retention time (t_R), melting points (m.p.) and predicted properties i.e., clog*P*.

The R_f of final compounds was determined using 10% methanol/dichloromethane solvent conditions and melting point determined using hot-stage microscopy (HSM). The details of all procedures, materials used, including the HPLC instrument conditions are fully described in chapter 6. Both predicted (*in silico*) and experimentally determined physicochemical properties of all the compounds in this thesis are presented in tables A1 to A8 of the appendix.

Table 4.1: Median values of calculated physicochemical properties in comparison to drug-likeness guidelines.

Property	Targeted criteria†	AST analogues [*n* = 122]	CQ-AST [*n* = 35]
MW	<500	470.2 (345.4–572.2)	492.7 (377.9–564.16)
clog*P*	<5	4.14 (1.94–5.94)	5.05 (4.05–6.04)
TPSA	<140	78.5 (53.4–115.8)	61.5 (45.98–91.80)
HBD	<5	1 (0–3)	1 (1–2)
HBA	<10	7 (6–9)	6 (5–8)

MW = molecular weight in Daltons; clog*P* = calculated log value of the n-octanol/water partition coefficient; TPSA = topological polar surface area in ångström (Å) units; HBD = hydrogen bond donors; HBA = hydrogen bond acceptors; AST = astemizole; CQ = chloroquine. Brackets [ ] represents the range of values for a property within the compound class; n = number of compounds in each compound class
†Targeted criteria are defined according to Lipinski's Ro5 (MW, clogP, HBD & HBA) and Verber's rule on TPSA

4.3.1 Distribution and Compliance of Physicochemical Properties: AST Analogues (Phases I and II)

As shown in Figure 4.1A, the AST series (130 analogues) had 73.8% compliance to Ro5 on MW (345.4–572.2 Da) with 45.0% of total compounds falling between 451 and 500 Da, which was also reflected in the mean value (470.2 Da, Table 4.9). An 81.4% compliance rate was observed for lipophilicity (clog*P*, Figure 4.1B), in which 43.4% and 24.8% of all the compounds fell within the 4.01–5.00 and 3.01–4.00 ranges, respectively. Only 17 compounds (12.4%) had clogP < 3, represented by mostly amides, which where inactive. It is important to watch and assess molecules that occupy the lower quadrant of clog*P*, because current trends show that lipophilicity of oral drugs has continued to decrease over time compared to other properties. Therefore associated metrics such as LipE (or LLE) as previously described, will continue to be very useful metrics in lead generation.[8,9]

Ro5 violation for both MW and clogP was hugely accounted for by compounds possessing the benzyl group or other bulky aliphatic moieties at the benzimidazole N-1 position. However, following the truncation of these groups (phase II, SARs 3–6), a dramatic reduction in both MW (mean = 439 Da) and clog*P* (mean = 3.69) was observed.

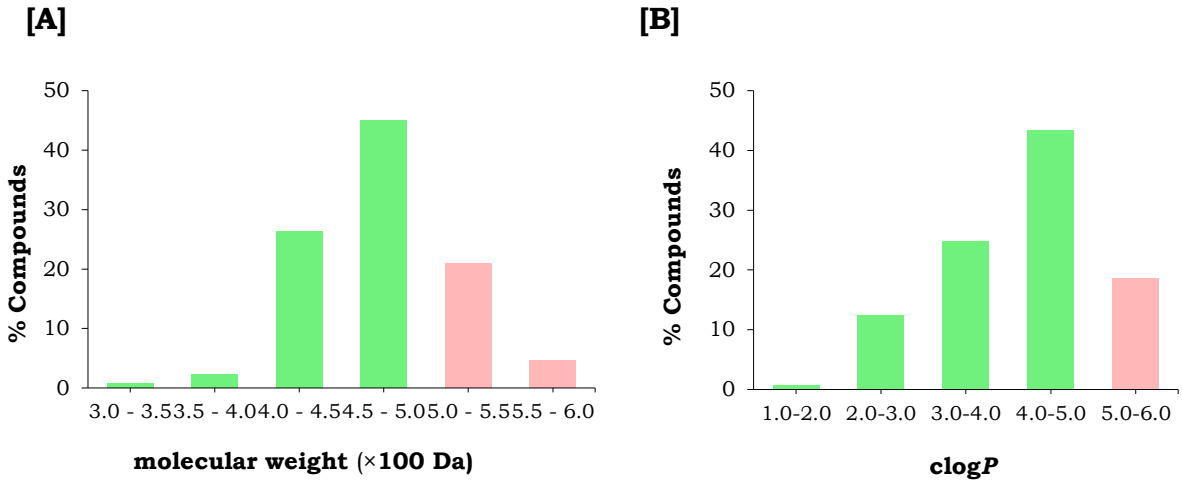

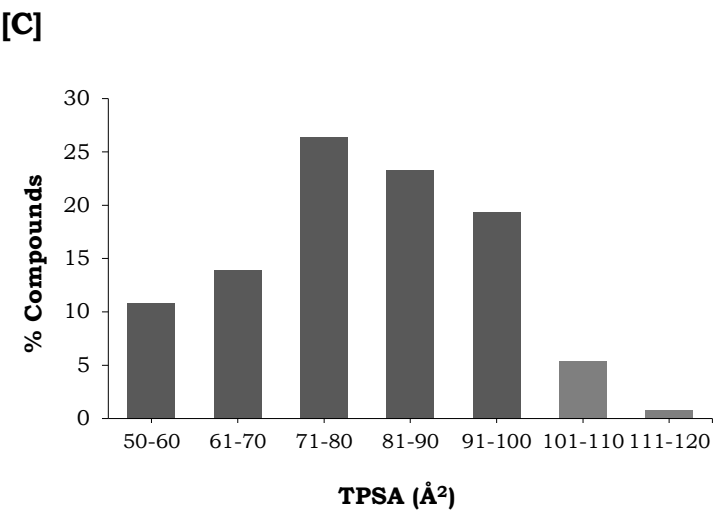

Figure 4.1: The distribution plots of: (A) molecular weight, (B) clog*P* and (C) topological polar surface area for astemizole analogues.

TPSA of all the AST analogues complied with Verber's guideline (TPSA < 140 Å^2, Figure 4.1C), with 93.8% compounds between 50 and 100 Å^2. As shown in Table A6 (Appendix), all the compounds had the number of HBD and HBA within the Ro5, each averaging one (1) and seven (7), respectively.

4.3.2 Distribution and Compliance of Physicochemical Properties: CQ-AST Hybrids

By virtue of being hybrid molecules resulting from the covalent merging of AST and CQ, the AST-CQ hybrids generally had higher molecular weights, with an average of 492.7 Da (range = 377.9 – 564.2 Da). Only 56.4% of hybrids had MW below 500 Da (Figure 4.2A), and these generally were as a result of SAR 1 modifications. N-methyl and N-desmethyl benzimidazoles **169** and **168**, respectively, account for the lower 5.1% quadrant with MW < 400 Da, while compound **192**, a 5-sulfonyl-benzimidazole derivative accounts for the higher MW quadrant (>500 Da), represented by 2.6%.

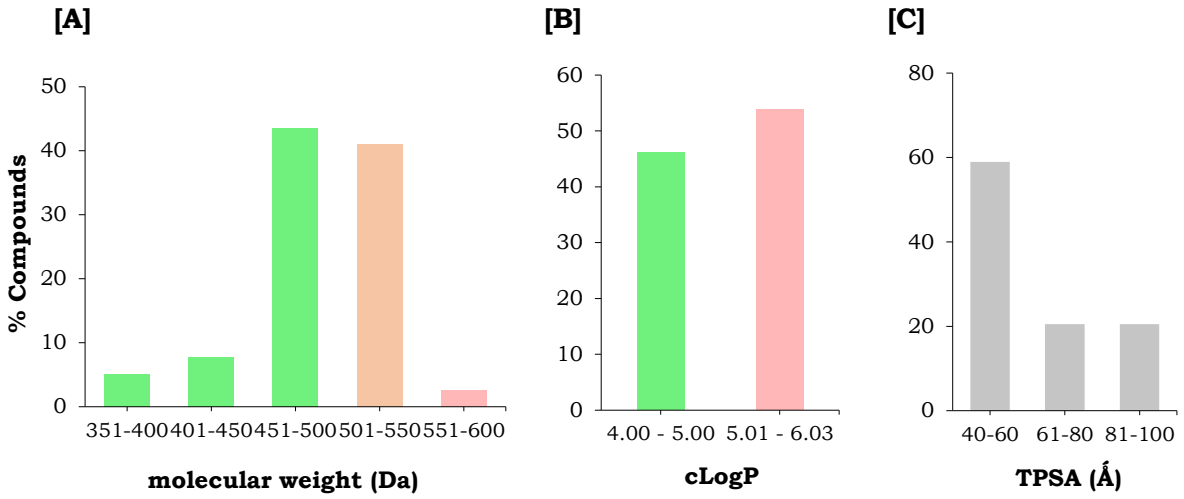

Figure 4.2: The distribution plots of: (A) molecular weight (B) cLogP and (C) topological polar surface area for astemizole-chloroquine (AST-CQ) hybrids.

Similarly, higher lipophilicities were a general characteristic of the hybrids (clog*P* = 4.05 – 6.04) with the average of clog*P* = 5 (Table 4.9). Accordingly, only 46.2% (Figure 4.2B) of the hybrids complied with the Ro5, represented mostly by compounds bearing polar groups such as CN, SO_2Me, SO_2NH_2, $CONH_2$, CONHMe and pyridyl moieties. Conversely, total compliance was achieved with Verber's guideline on polar surface area (TPSA < 100 $Å^2$, Figure 4.2C), an observation which comes as no surprise given the generally high lipophilic nature of the hybrids. This is also reflected in the high number of compounds (59%) with TPSA = 40 – 60 $Å^2$.

4.5 Structure-Property Relationships (SPRs)

4.5.1 Factors Influencing Solubility (AST Analogues and AST-CQ Hybrids)

Several strategies that are applied to improve aqueous solubility complement those used in reducing hERG affinity. Therefore, similar strategies as those described in the previous chapter for hERG, were also used to improve solubility. These included: (i) lipophilicity lowering approaches (i.e., introduction of polar substituents in the scaffold and removal of lipophilic groups such as halogens), (ii) replacement of benzyl/phenyl moieties with heterocyclics (i.e., pyridyl), (iii) disruption of crystal packing/stacking *via* removal of aromatic moieties and/or ring saturation (increase sp^3-character) and (iv) influence of crystallinity *via* the introduction of chirality. Derivation of SPRs was achieved by using

correlation plots of solubility with both measured and predicted physicochemical parameters as shown in Figures 4.3 – 4.5.

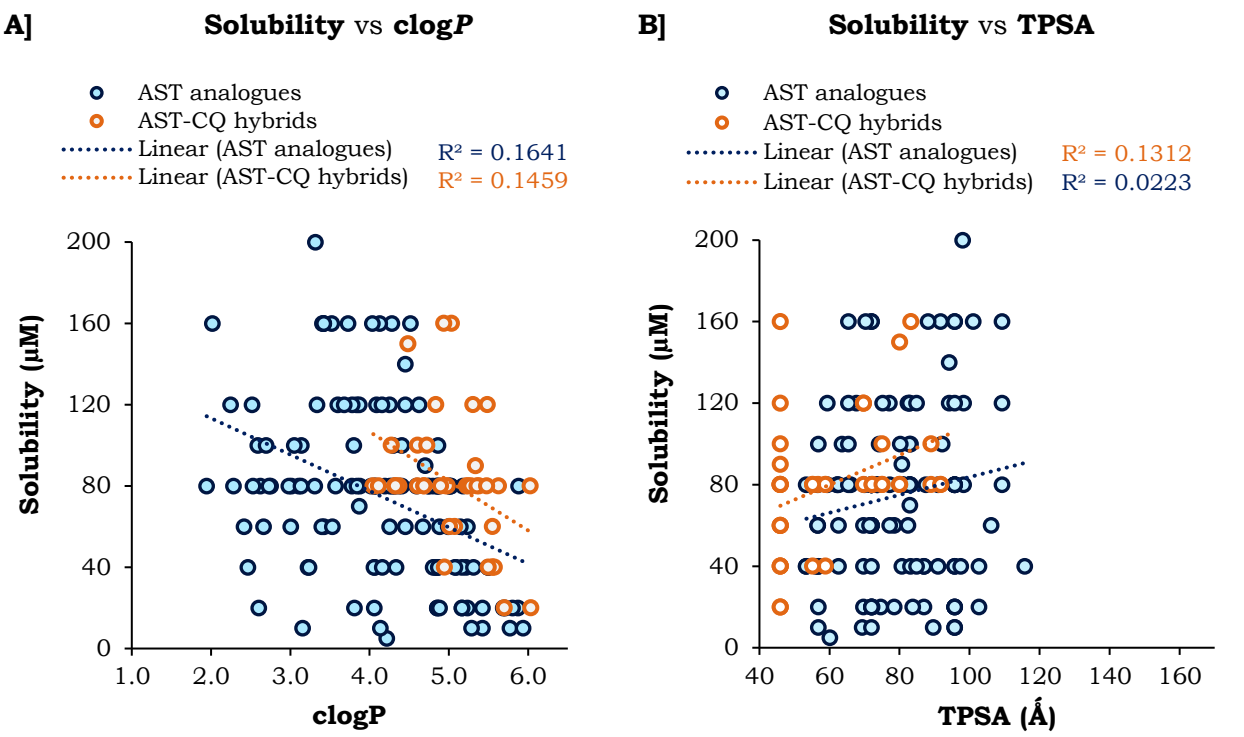

Figure 4.3: Correlation plots between solubility vs [A] lipophilicity and [B] topological polar surface area

There were similar solubility trends obtained for both AST analogues and the AST-CQ hybrids. The lipophilicity plot (Figure 4.3A) revealed that indeed reducing the lipophilicity of the compounds generally resulted in improved or higher aqueous solubility. This is reflected in the positive correlation (R^2 for AST analogues = 0.16 and R^2 for AST-CQ hybrids = 0.15) obtained, albeit rather low. For instance, replacement of the 4-F group in the benzyl group with water solubilizing groups such as sulfone (SO_2Me), sulfonamide (SO_2NH_2) or methyl ester (CO_2Me) resulted in a 2-fold or higher solubility of the hybrids. In both compound classes, lowering lipophilicity *via* aromatic ring saturation, removal or benzimidazole N-1 methylation resulted in better solubility. Methylation of heteroatoms is particularly a common strategy for improving solubility, especially in amides.[10] The lipophilicity-lowering effect on solubility is further corroborated by the TPSA plot (Figure 4.3B) in which a positive but significantly low correlation (R^2 for AST analogues = 0.03 and R^2 for AST-CQ hybrids = 0.13) was obtained.

Pyridyl replacements for benzyl or phenyl groups generally produced molecules with improved solubilities except in instances where lipophilic groups i.e., CF_3 where present on the heterocycle, in which case solubility was either maintained or reduced. Introduction of heteroatoms (i.e., nitrogen) in an all-carbon aromatic ring impart lipophilicity lowering effects, and have the ability to take part in both inter- and intramolecular hydrogen bonding (IHB) interactions, which enhance solubility and may have surprising effects on biological activity.[11,12]

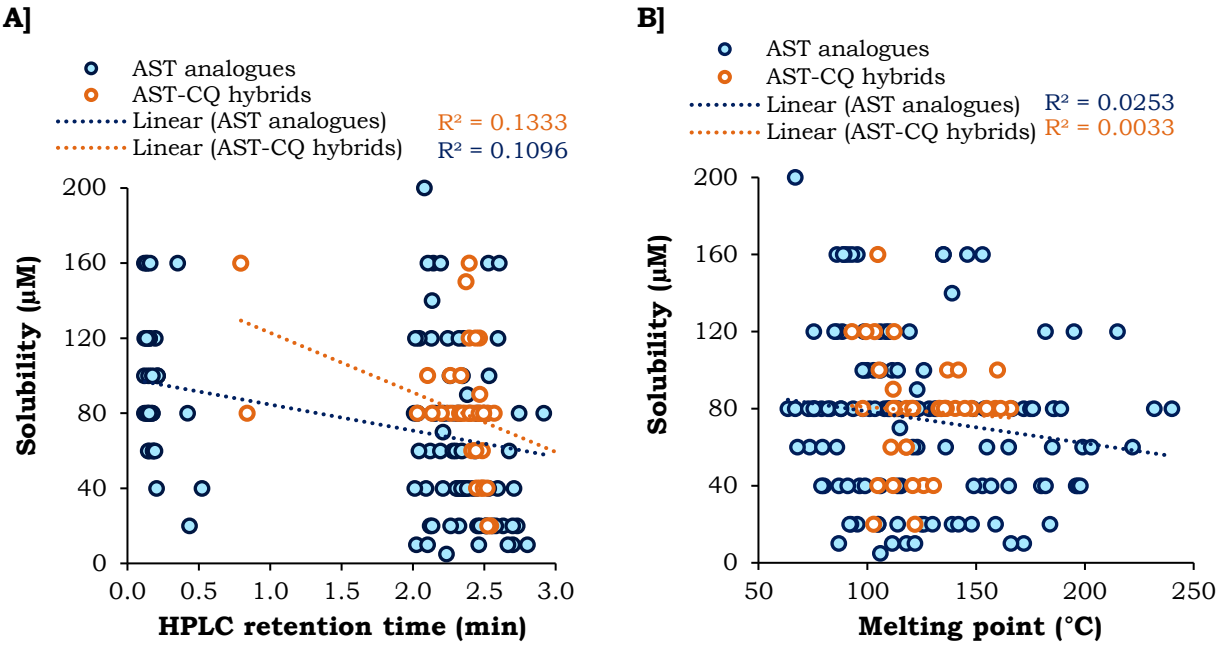

Figure 4.4: Correlation plots between solubility vs [A] HPLC retention time (t_R) and [B] melting point

There was a very weak correlation between melting point and solubility in AST analogues (R^2 = 0.03, Figure 4.4B) and none was present in AST-CQ hybrids (R^2 = 0.003). However, compounds with low melting points generally displayed higher solubilities. For instance, this phenomenon was highly observed in molecules where an aromatic moiety (i.e., benzyl) was either removed, or replaced with aliphatic moieties. Improved solubility would be theoretically achieved because of reduced molecular crystal packing *via* the reduction or disruption of aromatic π-π stacking, which is facilitated by either the removal of aromatic rings (sp^2, flat), or by the three-dimensional (3D) character brought about by chirality and increased sp^3-character in aliphatic moiety replacements.[13]

On the other hand, carboxylic acids and some pyridyl derivatives displayed moderate to high solubilities despite their relatively high melting points. In both carboxylic acids and pyridyl

compounds, higher melting points are as a result of increased crystal packing arising from their potential to take part in inter/intramolecular hydrogen bonding interactions. However, these same interactions also facilitate system polarity resulting in enhanced solubility.[14] Specific examples include compounds **142** and **149** (Figure 4.5).

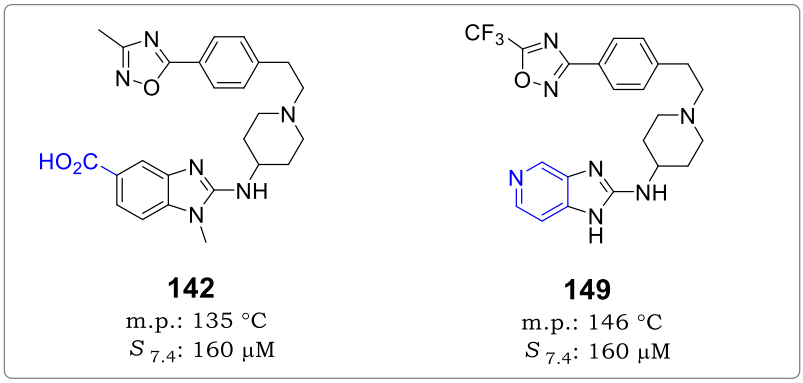

Figure 4.5: Structures of compounds **142** and **149**

As expected, compounds with lower HPLC retention times (t_R) were generally more soluble compared to those with higher t_R (R^2 for AST analogues = 0.10 and R^2 for AST-CQ hybrids = 0.13), although these correlations were significantly low.

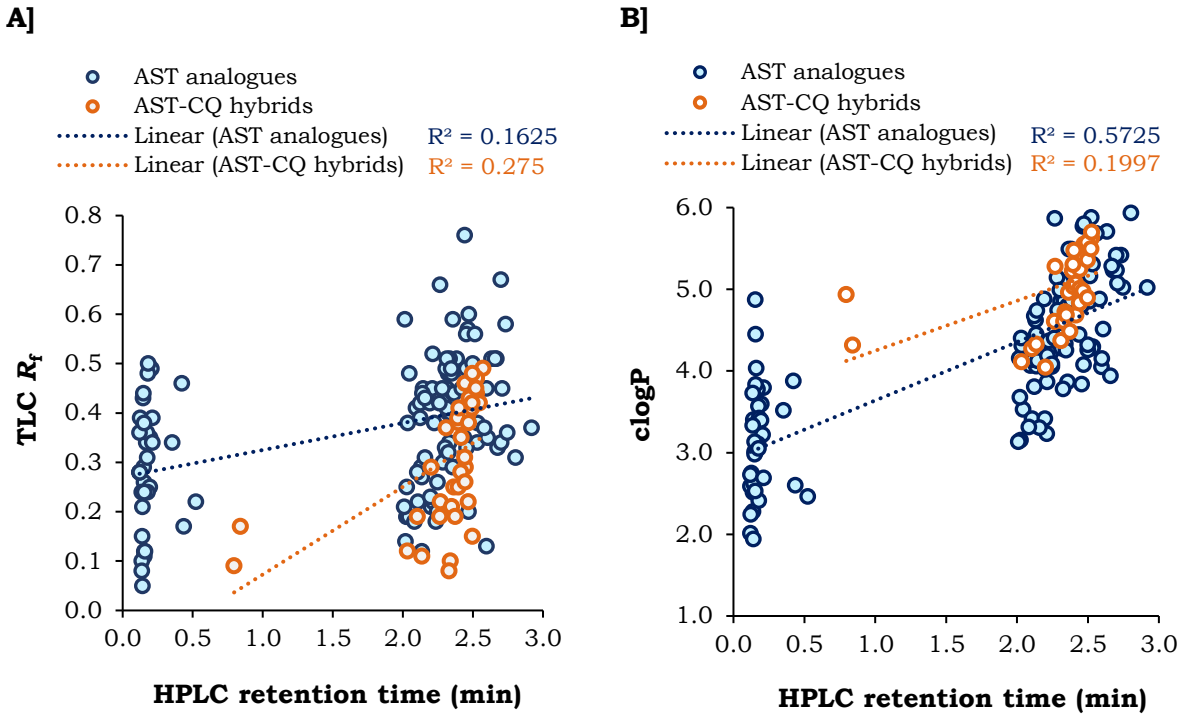

Figure 4.6: Correlation plots between [A] TLC retardation factor (R_f) vs HPLC retention time and [B] lipophilicity (clog*P*) vs HPLC retention time (t_R)

The positive correlations between TLC retardation factor (R_f)–HPLC retention times (Figure 4.6A), and lipophilicity (clog*P*)–HPLC retention times (Figure 4.6B) provides further proof that lipophilicity lowering strategies have been useful in improving the solubility of AST analogues and hybrids.

4.5.2 Physicochemical Properties and Biological Activity

4.5.2.1 Multi-parameter Optimization of AST: A Short Holistic Overview

The success of this multi-parameter optimization of AST was contingent on obtaining balance between biological activity (high antiplasmodium potency, low hERG affinity) and optimal drug-like properties (physicochemical properties). Without detailing the SAR and SPR of the obviously huge number of molecules involved, this subsection attempts to provide a summary of the progress made by highlighting specific examples leading up the current front-runner compound.

The identification of compound **149** (Figure 4.7) has been a result of the combination of various strategies and approaches, and SAR-driven progression of molecules at each SAR stage. At the outset of the project, solubility and potency were mildly enhanced following the replacement of the benzylic 4-F and anisole 4-Ome groups in AST, with less lipophilic 4-CN and polar 4-CO_2Et groups (**38**), respectively. However, despite being the best group for activity and solubility in the Craig plot-guided SAR, the ethyl ester group obviously introduced a metabolic liability.

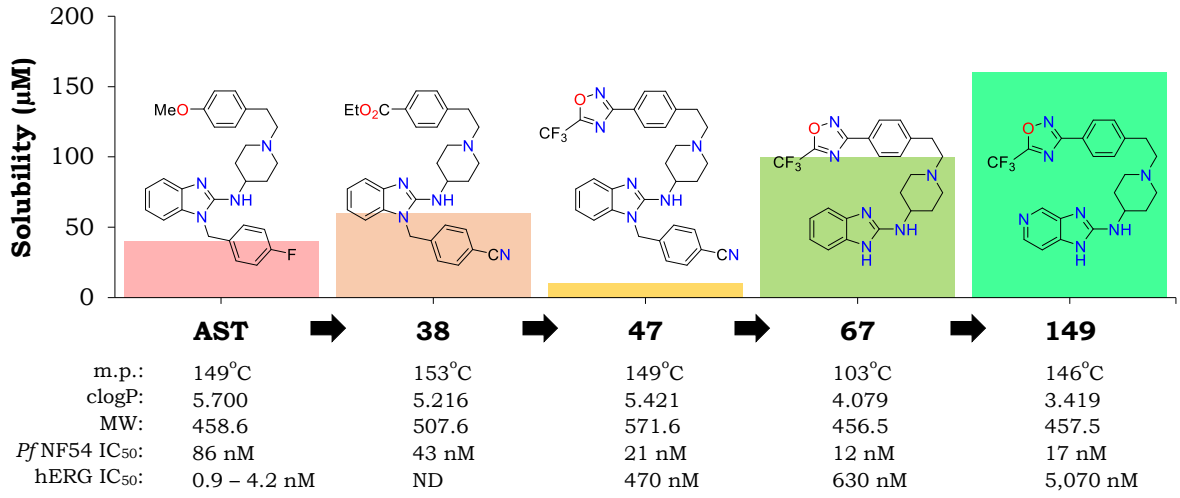

	AST	38	47	67	149
m.p.:	149°C	153°C	149°C	103°C	146°C
clogP:	5.700	5.216	5.421	4.079	3.419
MW:	458.6	507.6	571.6	456.5	457.5
Pf NF54 IC_{50}:	86 nM	43 nM	21 nM	12 nM	17 nM
hERG IC_{50}:	0.9 – 4.2 nM	ND	470 nM	630 nM	5,070 nM

Figure 4.7: Graphical representation of the progressive improvement of physicochemical properties, antiplasmodium activity and hERG affinity of AST

Following the identification metabolically stable **47**, containing the 5-CF_3-1,2,4-oxadiazole moiety as a surrogate replacement (bioisostere) for the ester group, the solubility was compromised ($S_{7.4}$ = 10 μM) due to the high lipophilicity (clog*P* = 5.7) and molecular weight (MW = 570), albeit improving both potency (*Pf* NF54 IC_{50} = 21 nM) and hERG affinity (SI = 19). However, utilization of aromatic moiety truncation as a lipophilicity and MW-lowering strategy led to **67**, with gratifyingly enhanced potency, hERG selectivity (*Pf* NF54 = 12 nM, hERG SI = 53) and moderate solubility (100 μM). Additionally, the *in vitro* activity and metabolic stability (CL_{int} <11.0 $\mu l.min^{-1}.mg^{-1}$) translated to oral *in vivo* efficacy in *P. berghei*-infected mice (99% activity when administered at 4 × 50 $mg.kg^{-1}$). Discreet modification of **67** *via* the insertion of the nitrogen at the 5-benzimidazole position resulted in closely related **149**, an equipotent, highly selective (*Pf*NF54 = 17 nM, hERG SI = 298) and soluble (160 μM) compound, without affecting microsomal metabolic stability, and other drug-like properties (i.e., MW, TPSA).

4.5.2.2 AST-CQ Hybrids

The AST benzyl group portion of the hybrid allowed for changes with minimal effects on the antiplasmodium potency, compared to other SAR changes. For instance, a 4-fold and 5-fold lipophilicity-driven rise in solubility was observed following the replacement of the 4-F-benzyl group (**H-2**, clogP = 5.55, $S_{7.4}$ = 20 μM) with a 4-SO_2Me-benzyl group (**181**, clogP =4.37, $S_{7.4}$ = 80 μM), or methyl group (**169**, clogP = 4.28, $S_{7.4}$ = 100 μM), attributable to increased polarity and removal of the aromatic moiety (reduction of crystal packing), respectively. A similar trend to the one observed for SO_2Me was also observed with CN and OMe although solubility was lower (60 μM). The highest solubility was obtained following replacement of the benzyl group with the methyl cyclopropane (**171**, $S_{7.4}$ = 120 μM, Figure 4.8).

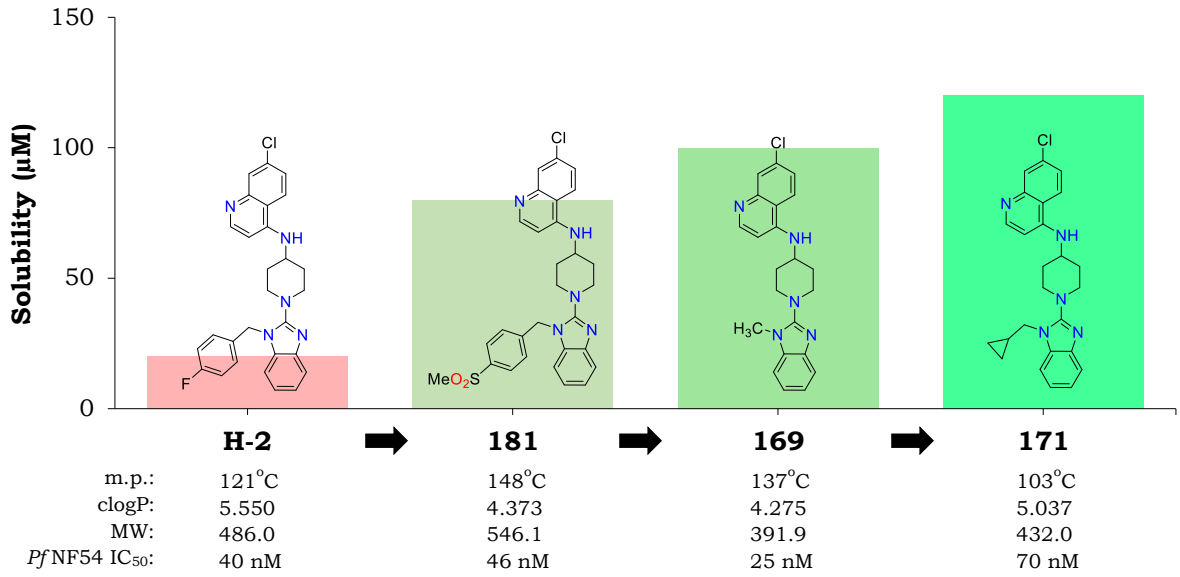

Figure 4.8: Graphical representation of the progressive improvement of physicochemical properties, while maintaining antiplasmodium activity of AST-CQ hybrids

The larger size and bulkiness of the group appears to influence the π-π stacking ability of the benzimidazole moiety to a higher extent, compared to the isopropyl group (**169**, $S_{7.4}$ = 80 µM), although the two analogues have comparable lipophilicity (clog*P* ~5). Additionally, the lower melting point (102 °C) and lipophilicity of the cyclopropyl analogue compared to hybrids containing larger groups i.e., cyclobutyl (**172**, m.p. = 112 °C, clogP = 5.34), cyclopentyl (**174**, m.p. = 136 °C, clogP = 5.63) and cyclohexyl (**174**, m.p. = 121 °C, clogP = 6.03) may explain the SPR observed within the series. Overall, the *N*-methyl (or *N*-desmethyl) and *N*-methyl cyclopropyl groups provide the best balance of antiplasmodium potency and drug-like properties (physicochemical attributes). Based on these findings, further optimizations may consider hybrids **168**, **169** and **171**, as viable starting points for further benzimidazole-CQ hybrid optimization.

4.6 Conclusion

The chapter has described the physicochemical properties and SPRs of both AST analogues and AST-CQ hybrid molecules. The profiling revealed high compliance with existing drug-like property classification guidelines such as Lipinski's Ro5 and Verber's rules. The SPRs derived showed that solubility was influenced by several physicochemical properties with low but notable correlations established with molecular lipophilicity (R^2 for AST analogues = 0.16, R^2 for AST-CQ hybrids = 0.15), which is further reflected in TPSA and inter-property correlations i.e., HPLC retention time (t_R) and TLC retardation factor (R_f). Melting point

affected solubility to a much lower extent, as evidenced by the weak correlations observed (R^2 for AST analogues = 0.03). The chapter concludes with an overview assessment of the overall effects of the optimization approaches used in the project. The success of the AST optimization is evident in azabenzimidazole **149**, which possesses relatively high solubility (160 μM) and selectivity of antiplasmodium activity over hERG affinity (SI = 298). The identification of appropriate modifications on the AST-CQ hybrid **H-2**, that favor optimal physicochemical properties and antiplasmodium activity provides viable SAR and SPR starting points for further optimization and studies.

4.7 References

(1) van de Waterbeemd, H.; Smith, D. A.; Beaumont, K.; Walker, D. K. Property-Based Design: Optimization of Drug Absorption and Pharmacokinetics. *J. Med. Chem.* **2001**, *44* (9), 1313–1333.

(2) Edwards, M. P.; Price, D. A. Role of Physicochemical Properties and Ligand Lipophilicity Efficiency in Addressing Drug Safety Risks; 2010; pp 380–391.

(3) Pollastri, M. P. Overview on the Rule of Five. *Curr. Protoc. Pharmacol.* **2010**, *49* (1).

(4) Lipinski, C. A.; Lombardo, F.; Dominy, B. W.; Feeney, P. J. Experimental and Computational Approaches to Estimate Solubility and Permeability in Drug Discovery and Development Settings. *Adv. Drug Deliv. Rev.* **1997**, *23* (1–3), 3–25.

(5) Doak, B. C.; Over, B.; Giordanetto, F.; Kihlberg, J. Oral Druggable Space beyond the Rule of 5: Insights from Drugs and Clinical Candidates. *Chem. Biol.* **2014**, *21* (9), 1115–1142.

(6) Lipinski, C. A. Rule of Five in 2015 and beyond: Target and Ligand Structural Limitations, Ligand Chemistry Structure and Drug Discovery Project Decisions. *Adv. Drug Deliv. Rev.* **2016**, *101*, 34–41.

(7) Veber, D. F.; Johnson, S. R.; Cheng, H.-Y.; Smith, B. R.; Ward, K. W.; Kopple, K. D. Molecular Properties That Influence the Oral Bioavailability of Drug Candidates. *J. Med. Chem.* **2002**, *45* (12), 2615–2623.

(8) Leeson, P. D.; Springthorpe, B. The Influence of Drug-like Concepts on Decision-Making in Medicinal Chemistry. *Nat. Rev. Drug Discov.* **2007**, *6* (11), 881–890.

(9) Waring, M. J. Lipophilicity in Drug Discovery. *Expert Opin. Drug Discov.* **2010**, *5* (3), 235–248.

(10) Leach, A. G.; Jones, H. D.; Cosgrove, D. A.; Kenny, P. W.; Ruston, L.; MacFaul, P.;

Wood, J. M.; Colclough, N.; Law, B. Matched Molecular Pairs as a Guide in the Optimization of Pharmaceutical Properties; a Study of Aqueous Solubility, Plasma Protein Binding and Oral Exposure. *J. Med. Chem.* **2006**, *49* (23), 6672–6682.

(11) Wrobleski, S. T.; Moslin, R.; Lin, S.; Zhang, Y.; Spergel, S.; Kempson, J.; Tokarski, J. S.; Strnad, J.; Zupa-Fernandez, A.; Cheng, L.; et al. Highly Selective Inhibition of Tyrosine Kinase 2 (TYK2) for the Treatment of Autoimmune Diseases: Discovery of the Allosteric Inhibitor BMS-986165. *J. Med. Chem.* **2019**, *62* (20), 8973–8995.

(12) Walker, M. A. Improvement in Aqueous Solubility Achieved via Small Molecular Changes. *Bioorg. Med. Chem. Lett.* **2017**, *27* (23), 5100–5108.

(13) Lovering, F.; Bikker, J.; Humblet, C. Escape from Flatland: Increasing Saturation as an Approach to Improving Clinical Success. *J. Med. Chem.* **2009**, *52* (21), 6752–6756.

(14) Marfo-Owusu, E.; Kato, T. Crystal Packing and Hydrogen-Bonding Studies: The Crystal and Molecular Structures of the Nonhydrate and Hydrate Forms of 2,6-Di(Propanoylamino)Pyridine. *Mol. Cryst. Liq. Cryst.* **2006**, *452* (1), 37–48.

CHAPTER 5

SUMMARY, CONCLUSIONS AND FUTURE WORK

5.1 Summary and Conclusions

5.1.1 Astemizole

The objective of this project was to disconnect the cardiotoxicity risk associated with AST, from its antimalarial properties, improve solubility and optimize drug-like properties. The project was envisaged to shed light on both structure-activity and structure-property relationships (SAR and SPR), which would be useful in further development of the template within the context of drug repositioning. SAR explorations were carried out rationally, and in two phases (phase I and II) in which the front-runner(s) from exploratory phase I, iteratively served as templates for the design of phase II analogues. Additionally, an SAR guided approach was utilized within phase II to inform the transition from one SAR to another.

The SAR design in this multi-parameter optimization was largely driven by potency. However, it was carried out and underpinned by known medicinal chemistry strategies for mitigating hERG liability, improving solubility, and maintaining drug-like properties. Various organic synthesis protocols adapted from literature were used to prepare the designed compounds . The compounds were fully characterized using NMR spectroscopy and chromatographic techniques (TLC and HPLC-MS) to ensure high purity (≥95%). Additionally, solubility and other physicochemical properties i.e., melting point were also determined. Thereafter, the compounds were evaluated for their *in vitro* antiplasmodium activity (in both sensitive and resistance *Pf* parasite strains), cytotoxicity, hERG inhibition and DMPK properties, following a sequential screening cascade in which the progression criteria at each stage were defined. Potent and soluble compounds with low cytotoxicity and high metabolic stability were progressed for *in vivo* proof-of-concept studies using the *P.berghei* mouse infection model.

As shown in Figure 5.1, the potency SAR from phase I revealed the tolerance of deactivating groups with negative inductive effects (i.e., **25**-CF_3, **35**-CN, and **38**-CO_2Et; *Pf*IC_{50}'s < 0.035 μM) as optimal replacements for the anisole methoxy group found in AST. This high activity was also extended to 1,2,3-oxadiazoles (**41**/**46** and **42**/**47**; *Pf*IC_{50}'s < 65 μM) as bioisosteres of the ethyl ester **38**. However, CF_3-substituted oxadiazole derivatives are more potent that

their CH_3 counterparts. The 4-amino piperidine cyclic linker was validated as an essential part of the antiplasmodium activity pharmacophore, as other replacements were detrimental to the potency. Nevertheless, R/S stereoisomers of pyrrolidine containing analogues produced superior, and equipotent sub-micromolar activity (**58** and **59**, *Pf*IC_{50} = 0.40 µM) within the SAR. Phase I series were characterized by poor metabolic stability (except 3-/5-CF_3-1,2,4-oxadiazole derivatives **41**/**46**) and moderate to low solubility ($S_{7.4}$ <100 µM) as summarized in Figure 5.1.

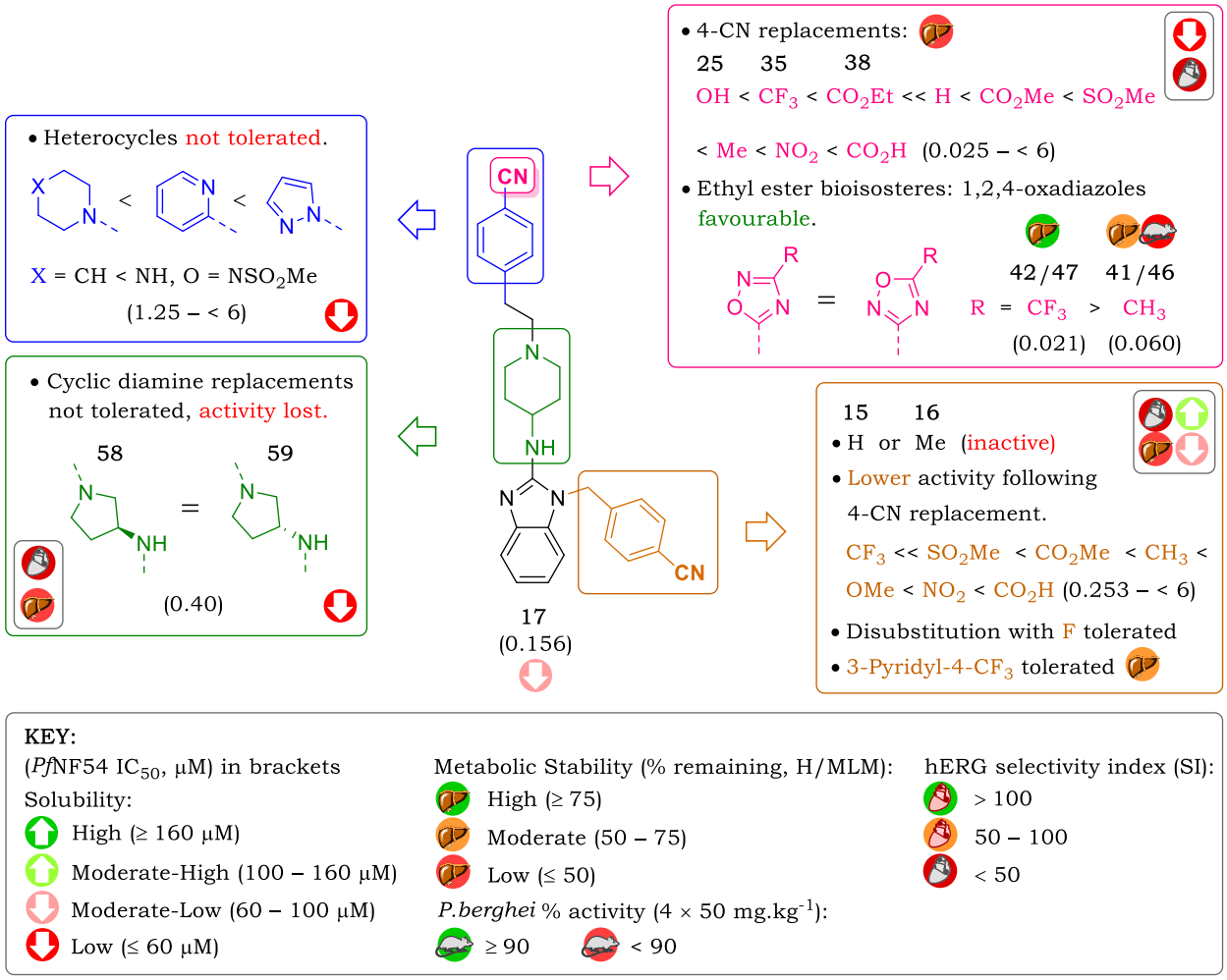

Figure 5.1: Summary of the biological activity, solubility, microsomal metabolic stability, hERG and efficacy profiles of phase I AST analogues. H/MLM = human/mouse liver microsomes

However, removal of the benzyl group (**15**), replacement with methyl (**16**) or incorporation of carboxylic moiety improved solubility, albeit at the expense of potency (*Pf*IC_{50} > 0.5 µM). Generally, hERG inhibition was still an issue in the series, characterized by low selectivity indices (SI < 20) owing to the low antiplasmodium activities of most analogues. When tested

in vivo, as an efficacy snapshot, frontrunner compound **73** demonstrated low activity (40% inhibition when administered 4 × 50 mg.kg^{-1} orally), an observation that was attributed to its moderate solubility and metabolic stability.

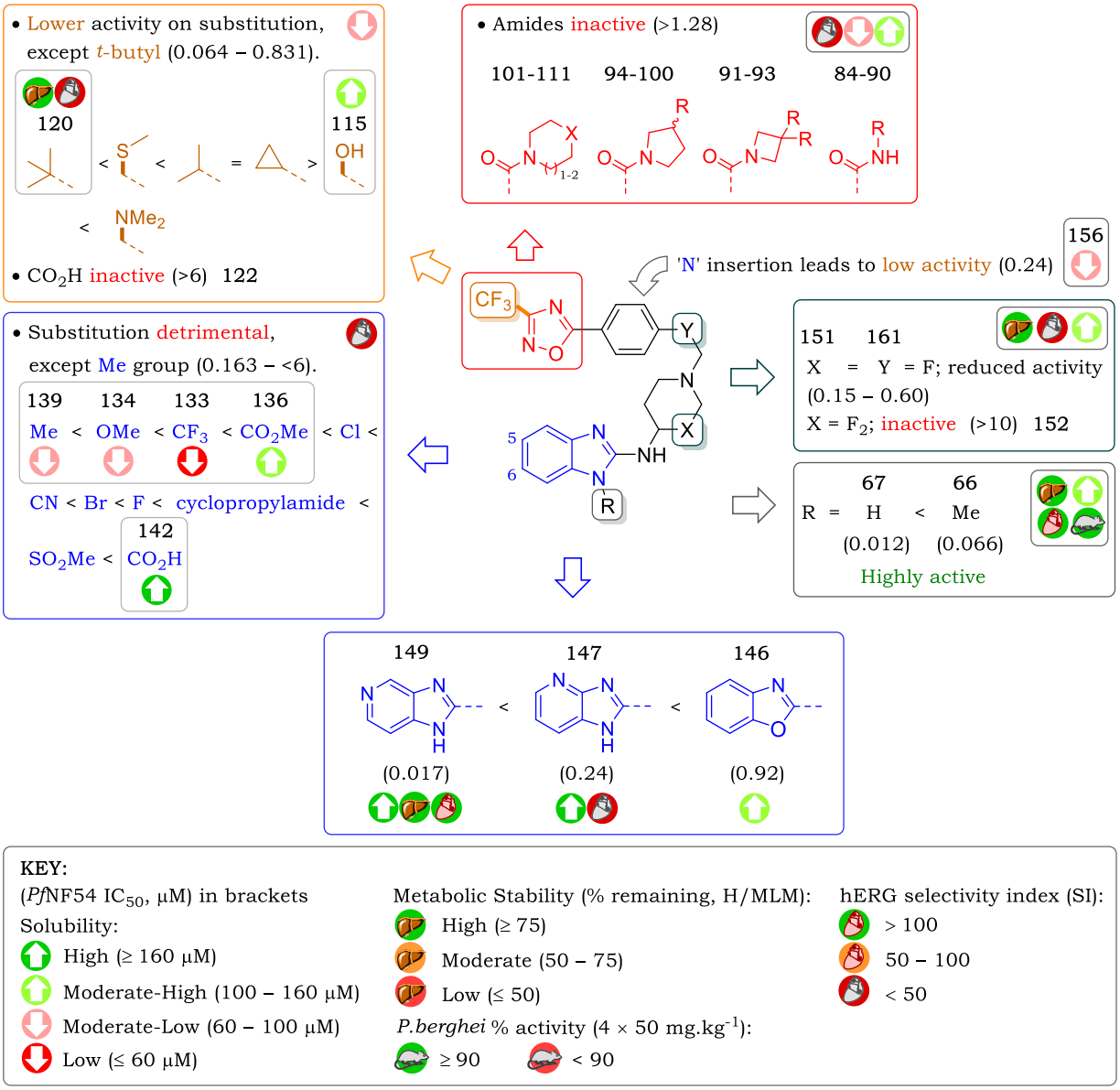

Figure 5.2: Summary of the biological activity, solubility, microsomal metabolic stability, hERG and efficacy profiles of phase II AST analogues. H/MLM = human/mouse liver microsomes

As opposed to phase I analogues, the removal of the benzyl moiety resulted in a dramatic rise in potency, and significant shifts in the solubility and metabolic stability profiles across the SARs (Figure 5.2).

For instance, N-desmethyl derivative **67** (Figure 5.2), containing a 3-CF_3-1,2,4-oxadiazole moiety, displayed nanomolar potency (*Pf*IC_{50} = 0.012 μM), moderate solubility ($S_{7.4}$ = 100 μM) and high microsomal metabolic stability (CL_{int} <11.0 μl.min^{-1}.mg^{-1}). It had relatively low cytotoxicity (CHO IC_{50} = 1.95 μM, SI = 163) and lower hERG affinity (IC_{50} = 0.63 μM, SI = 53) compared to **47** (IC_{50} = 0.47 μM, SI = 19) match pair, which bears a 4-CN-benzyl group. The hERG activity of compound **67** represented 1100-fold higher selectivity compared to AST, calculated as the ratio of the selectivity indices of **67** and AST (SI_{67}/SI_{AST} = 53/0.05). The high potency and microsomal metabolic stability of **67** translated to high *in vivo* efficacy (99% activity) when dosed orally at a 4 × 50 mg.kg^{-1} in *P.berghei*-infected mice. The mice displayed an average survival rate of fourteen (14) days post-treatment.

Further SAR explorations revealed several critical pharmacophoric features. For instance, all amide replacements of the 1,2,4-oxadiazole moiety produced low activity (**80** – **111**, *Pf*IC_{50} > 1.28 μM, Figure 5.2). Replacement or extension of the 3-CF_3/or 3-CH_3 group on the 1,2,4-oxadiazole moiety also produced lower activities (*Pf*IC_{50} = 0.38 – 0.83 μM), with the exception of the *t*-butyl group (**120**, *Pf*IC_{50} = 0.064 μM), which retained CF_3 activity, attributed to the bioisosteric relationship of the two groups. Incorporation of the carboxylic acid group at that position was detrimental to activity (**122**, *Pf*IC_{50} > 6 μM). The solubility of analogues in this SAR was generally low, with the exception of hydroxyl (**115**), dimethyl amino, and carboxylic acid (**122**) derivatives, which exhibited moderate solubilities ($S_{7.4}$ = 100 – 120 μM).

Substitution at C-5 and/or C-6 of the benzimidazole ring generally produced lower activities, especially in electron withdrawing groups i.e., SO_2Me and CO_2H (**142**). However, methyl (**139**, *Pf*IC_{50} = 0.16 μM), methoxy (**139**, *Pf*IC_{50} = 0.31 μM) and trifluoromethyl (**133**, *Pf*IC_{50} = 0.42 μM) produced notable sub-micromolar activities (Figure 5.2). Similar to other SARs, solubility was higher in analogues containing highly solubilizing groups i.e., CO_2H (**142**, $S_{7.4}$ = 160 μM) compared to other groups, although potency was compromised.

β-fluorination around the piperidine nitrogen resulted in lower activity, with piperidine mono-β-fluorination (**151**, *Pf*IC_{50} = 0.15 μM) favored compared to that in the ethylene linker (**161**, *Pf*IC_{50} = 0.60 μM). However, di-fluorination (**152**, *Pf*IC_{50} < 10 μM) is detrimental to potency. Notwithstanding this, high microsomal metabolic stability and moderate solubility were retained. Insertion of a nitrogen atom in the lateral phenyl ring reduces the potency (**156**, *Pf*IC_{50} = 0.24 μM; Figure 5.2) and no significant change in solubility was observed.

The benzimidazole ring is of particular importance for antiplasmodium activity, as loss of activity (*Pf*IC_{50} = 0.86 – 3.27 μM) was observed following its replacement with other

heterocycles such as benzoxazole (Figure 5.2). However, insertion of a nitrogen atom at C-5 and C-4 of the benzimidazole ring, to afford closely related 5- and 4-azabenzimidazoles, resulted in either retention (**149**, *Pf*IC_{50} = 0.017 μM) or only a mild reduction (**147**, *Pf*IC_{50} = 0.24 μM) of whole cell activity, respectively. Additionally, azabenzimidazoles retain microsomal metabolic stability (CL_{int} <11 $\mu l.min^{-1}.mg^{-1}$ or >99% remaining), display no cytotoxicity (CHO IC_{50} > 50 μM), and enhanced aqueous solubility ($S_{7.4}$ >120 μM) compared to the efficacious benzimidazole compound **67**.

Phase II analogues generally displayed improved hERG profiles compared to those in phase I. However, disconnection of antimalarial activity from hERG affinity was less effective in several strategies that were used. For instance, despite the low hERG activities (IC_{50}'s > 1.0 μM), the weak antiplasmodium activities of some of the analogues (i.e., amides, zwitterions, and β-fluorinated analogues around the basic nitrogen) resulted in poor selectivity's (SI < 5). Gratifyingly, discreet changes in the benzimidazole ring proved to be the most effective strategy in lowering hERG activity and obliterating cytotoxicity (CHO cells). To this end, 5-azabenzimidazole derivative **149** retained nanomolar antiplasmodium activity and produced the lowest hERG activity (IC_{50} = 5.07 μM), translating to a marginal 298 selectivity index for antiplasmodium activity. This represents 6,200-fold higher selectivity compared to AST. Coupled with its high solubility, non-cytotoxic (CHO SI > 2900) and high metabolic stability, compound **149** is most selective, highly potent and drug-like (LLE or LipE = 4.35) AST analogue in both this project, and to ever be prepared.[1,2] Further investigations on **149** i.e., gametocyte and liver stage activities, PK and *in vivo* efficacy, are warranted.

While acknowledging that a selectivity index of 300 for hERG is still not ideal for ideal safety in clinical terms, it is a significant achievement for this project. This project has revealed critical antimalarial, gametocytocidal, hERG and solubility profiles and demonstrated the potential for the repositioning of AST for malaria. The two front runners from this thesis (**67** and **149**, Figure 5.3) would be viable starting points for early lead optimization (LO) programs.

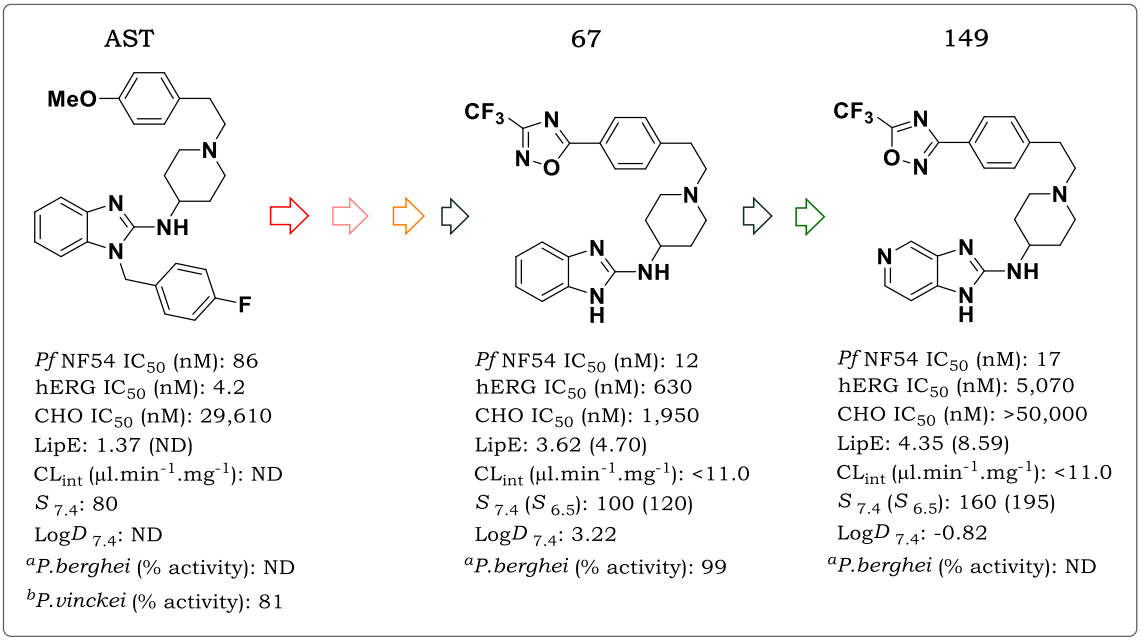

Figure 5.3: Structures and drug properties of AST and front-runner compounds **67** and **149**

$S_{7.4}$ = solubility at pH 7.4; $S_{6.5}$ = solubility at pH 6.5
LipE = lipophilic efficiency based on clogP (based on logD)
[a]50 mg.kg^{-1} dose for 4 days
[b]30 mg.kg^{-1} dose for 4 days
ND = not determined

5.1.2 AST-CQ Hybrids

The AST and CQ hybridization component of this project was aimed at improving the physicochemical properties and expand the SAR of the front-runner hybrid **H-2** (Figure 5.4) from the work of Musonda *et al.* The three (3) SARs explored furnished useful structural information on the pharmacophore of the hybrid.

Activity is retained following the removal (**168**) or replacement of the benzyl moiety with saturated aliphatic and pyridyl moieties. The hybrids substituted with aliphatic groups at benzimidazole N-1 had better solubility compared to **H-2**, with methyl analogues **169** ($S_{7.4}$ = 100 µM) and isopropyl analogues **171** ($S_{7.4}$ = 120 µM) producing the best solubility in the series. 2-CF_3/-CH_3-5-pyridyl analogues **189/190** (*Pf*IC_{50} = 0.044 µM) were equipotent and displayed higher activity than 2-pyridyl analogue **188**, although solubility was still sub-optimal ($S_{7.4}$ < 80 µM).

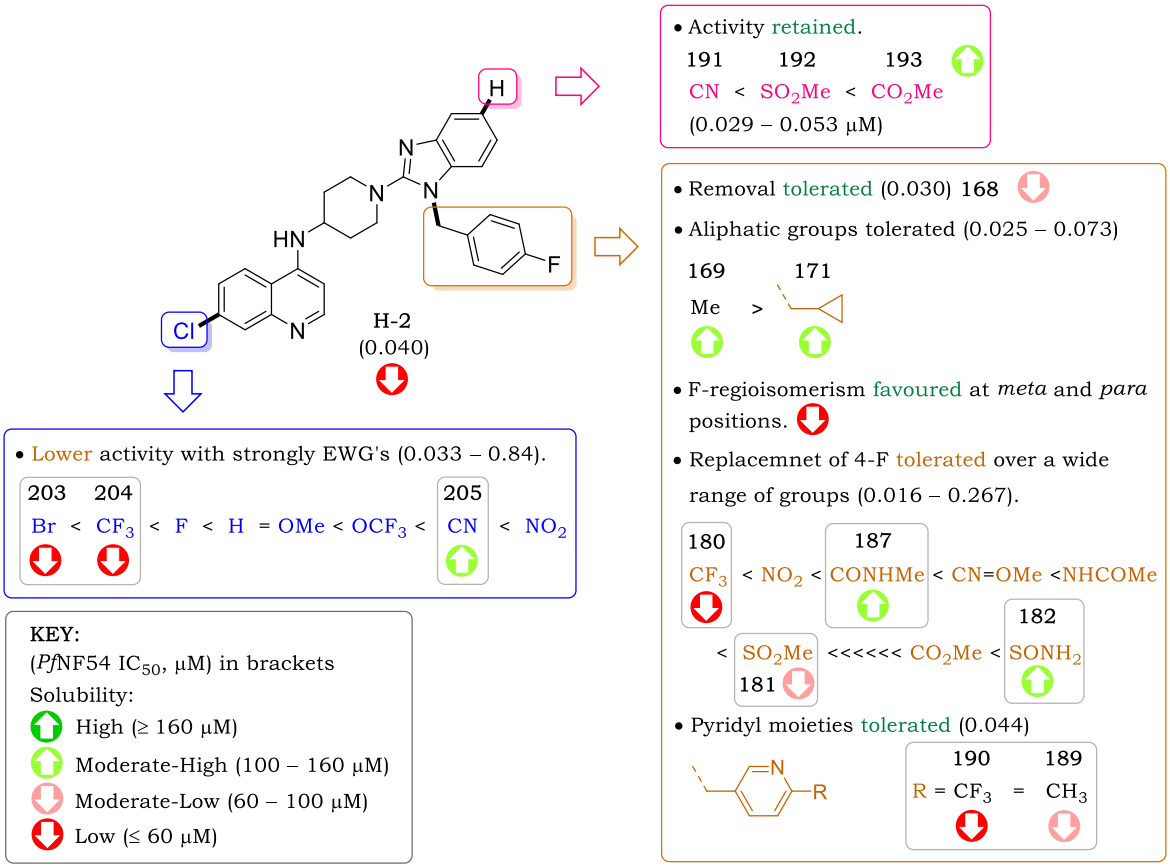

Figure 5.4: Summary of the solubility and antiplasmodium activity of AST-CQ hybrids

Regioisomerism of the fluoro group in the benzyl group is favored at the *meta* position, while activity is reduced 2-fold at the *ortho* position. Replacement of the 4-F group is tolerated over a wide range of both lipophilic and hydrophilic electron-withdrawing and donating substituents (Figure 5.4). However, solubility increased with lower lipophilicity, exemplified by sulfonamide and N-phenylacetamide (**182** and **184**, $S_{7.4}$ = 100 μM) analogues.

Activity was retained following substitution at the benzimidazole C-5 position with CN, SO_2Me and CO_2Me (**191** – **193**, *Pf*IC_{50} < 0.053 μM). Additionally, solubility was also greatly improved ($S_{7.4}$ > 80 μM). SAR involving the substitution of the quinoline 7-Cl group was consistent with that which has been reported in literature previously. Halogen, or halo group containing (i.e., OCF_3) substitutions generally produced higher activities compared to less lipophilic groups. Bromine (**204**, *Pf*IC_{50} = 0.033 μM) produced comparable activity to chlorine, while potency was 2-fold lower in the fluorine-substituted hybrid. Solubility was improved across the SAR ($S_{7.4}$ = 40 – 120 μM) with the CN-substituted (**205**) having the best solubility profile.

Hybrids **168**, **169**, **181** and **187** (Figure 5.5) emerged as front-runners with the highest lipophilic efficiencies (LipE ≥ 3). Testing of these compounds against resistant strains, and hERG inhibitory activity is warranted.

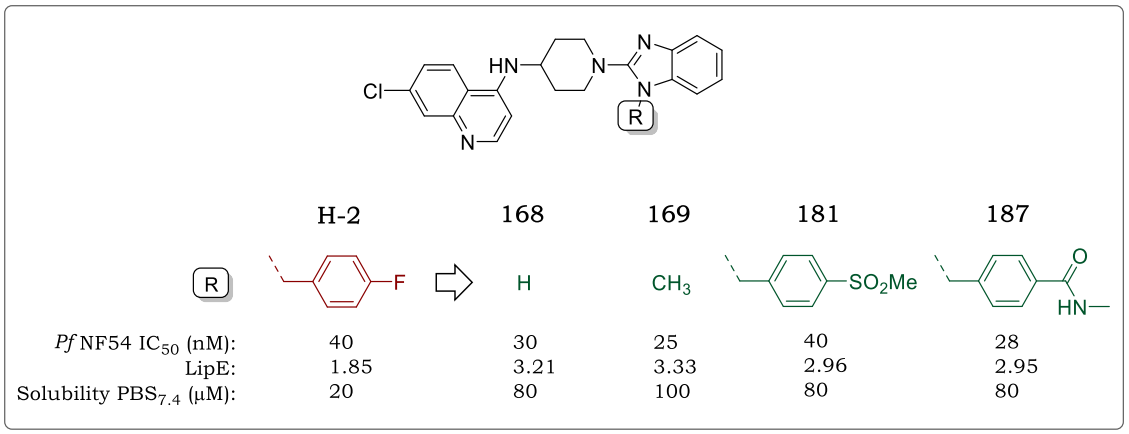

Figure 5.5: Structures and drug properties of H-2 and representative front-runner compounds **168**, **169**, **181** and **187**

5.2 Hope for a New Stride in hERG Optimization?

It is only recent (2017) that the single-particle cryogenic electron microscopy (Cryo-EM) structure of the hERG channel was solved,[3] but even then, the scarcity of the structural information regarding drug-bound and K+-bound hERG channels has limited the understanding of the underlying inhibitory mechanism, not to mention the overly promiscuous nature of the channels. This knowledge gap has forced the dependency of medicinal chemistry approaches aimed at reducing hERG liabilities on *in silico* models and SAR analysis, including the work reported in this Ph.D thesis. However, these approaches are not always effective.

Utilizing the solved hERG K+ channel structure, Asai and co-workers[4] have recently (2021) published work in which they have solved the Cryo-EM structure of $hERG_T$ K^+ channel bound and unbound with AST, detailing the interactions involved between the drug and the selectivity filter of the channels. Additionally, the team has attempted to elucidate the possible inhibition model of the channel by AST (Figure 5.6) and similar drugs.

In their model, there are four different interactions involved between AST and the hERG K+ channels within the selectivity filter, namely: (i) π-π-interactions between Y652 residue and the AST benzimidazole ring, (ii) electrostatic interactions between the charged piperidine nitrogen of AST and the highly electronegative selectivity filter, (iii) hydrogen bonding

between benzimidazole nitrogen N-3 and residue S642 and (iv) hydrophobic interactions between the AST 4-F-benzyl group and other amino acid residues i.e., T623, V625 and F656 which among others, occupy the selectivity filter from all four hERG subunits, and forming nine (9) different hydrophobic interactions (Figure 5.6F). They postulate that the anisole moiety is fluctuated and disordered.

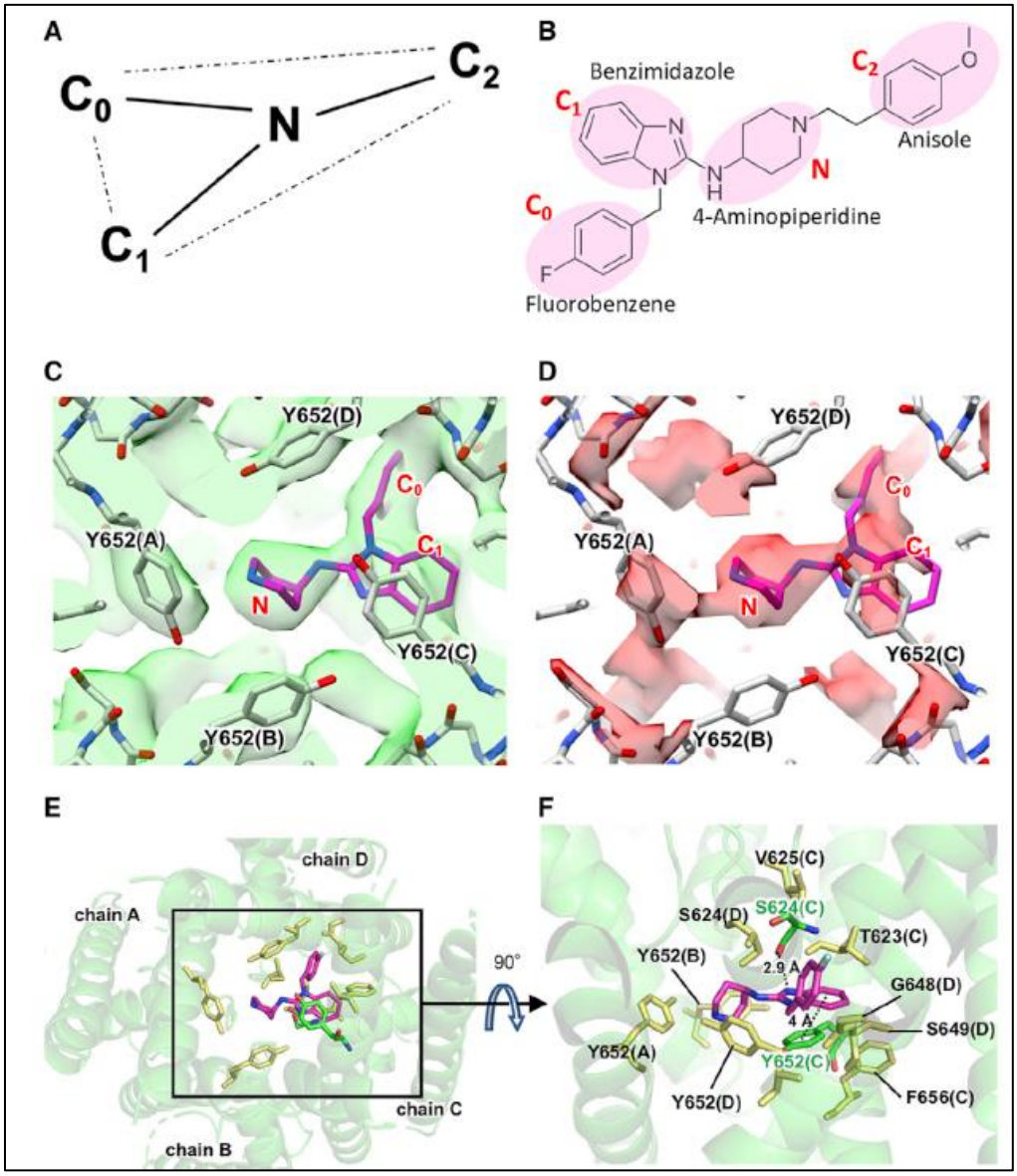

Figure 5.6: An extract from Asai *et al.*[4] showing AST binding model pharmacophore for QT-prolonging drugs. (B) Structure of AST (C_0 – C_2 and N in 'pink' are pharmacophoric points. (C and D) AST shown as 'magenta', bound to $hERG_T$ shown as 'grey'. Image C is the density map while D is the differential map. (E and F) Orthogonal views detailing the key residues involved in the binding of AST. Hydrogen bonds and π-π-interactions shown as dashed lines.

Contrary to previous findings regarding the involvement of residue F656 in hERG inhibition, this work found essentially no interactions between the residue and AST, and therefore asserted that the residue may only be involved in the inhibition as a mediator of drug penetration. Furthermore, their data show the presence of K+ within a 'plugged' selectivity filter by AST, revealing how the drug inhibits K+ conduction without inducing significant conformational changes of the hERG channel.[4]

They affirm the need for further assessment of other inhibitors bound to the channel, and the validation of pathways through-which inhibitors access hERG including the inactivation of the channels during depolarization, in order to elucidate a universal selectivity and binding mechanism for drugs.

Coupled with the hERG SAR revealed from the work in this Ph.D project, the findings of Asai *et al.* will go a long way in the design of better molecules with lower hERG affinities. Front-runner compounds from this Ph.D would serve as viable starting points for lead optimization in the context of the repositioning AST for malaria.

5.3 Future Work Recommendations

While the project has explored the AST template to a large extent, there is room for further SAR work. A summary of the proposed SAR for potential future work is shown in Figure 5.7. It is recommended that the 5-CF_3-1,2,4-oxadiazol-3-yl)phenethyl)piperidin-4-amine moiety (Portion A; Figure 5.7) is unchanged, and instead focus is drawn towards the benzimidazole or 5-azabenzimidaole (Portion B). However, the recommendation is that the structural architecture of either benzimidazole or azabenzimidazole is preserved, in order to retain antimalarial activity.

It will be wise to utilize the new information from the work of Asai *et al.*[4], regarding the putative interactions of AST with the hERG channel. An SAR exploration on focused on the (aza)benzimidazole core may include connection of portion A at the azabenzimidazole C-4 (**DM-1**) or C-6 positions (**DM-2** and **DM-3**) and blocking the original C-2 position with an alkyl group (controlling clogP is, however, critical, Figure 5.7). This change has the potential to shift the spatial orientation of the ring, and effectively prevent it from taking part in π-π-interactions in the hERG channel selectivity filter. Secondly, removal of N-3 (**DM-4**) and N-methylation of benzimidazole N-1 and N-3 (**DM-5**) may be an effective way to (i) introduce sp^3-character at C-2, thereby (ii) reducing the aromaticity (or planarity) of the moiety and

(iii) lower the hydrogen bonding capability of the two nitrogen atoms (lower p*K*a) without potentially affecting aqueous solubility significantly.[5]

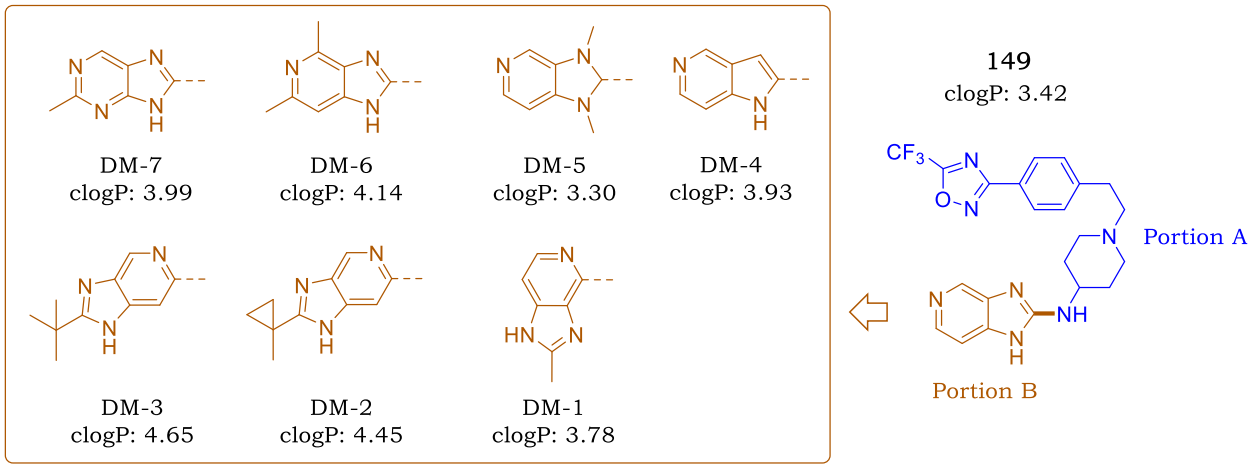

Figure 5.7: Proposed future work showing focused SAR on the azabenzimidazole core of compound **153**

Blocking of potential metabolic soft spots in **149** (**DM-6**) and replacement of the azabenzimidazole with closely related purine (**DM-5**), are all changes that may have the potential to further induce low hERG affinity. Front-runner compound 153 should be tested for *in vivo* efficacy in the same *P. berghei* model as compound 67. Additionally, the full PK study of both **67** and **149** should be carried out in both healthy and infected mice, using both the oral (*p.o.*) and intravenous (IV) routes. Furthermore, all analogues with significantly reduced hERG activity should be profiled for antihistamine activity. The activity of the AST-CQ hybrids in multi-drug resistance strains (i.e., *Pf*K1) will have to be tested in to ascertain if the hybrids retain the absence of potential to cross-resistance with CQ. Secondly, since AST is (i) associated with a cardiotoxicity risk because of its very potent hERG activity, and (ii) has been implicated in the inhibition of hemozoin biocrystallization, the hybrids should be tested in the hERG assay and assessed for β-hemozoin inhibition before any more derivatives are prepared. Additionally, metabolic stability should be determined, and front-runners progressed for *in vivo* efficacy studies in mice.

Should a hERG liability rise, SAR recommendations may involve exploring the azabenzimidazole moieties (**DM-8**) and substitution of benzimidazole with SO_2Me (**DM-9**, Figure 5.8). In the case of cross-resistance with CQ, one suggestion might be to consider incorporating a benzimidazole derived 'chemosensitizer-like' moiety such as the dihydro pyrido[1,2-*a*]benzimidazole (**DM-10**).

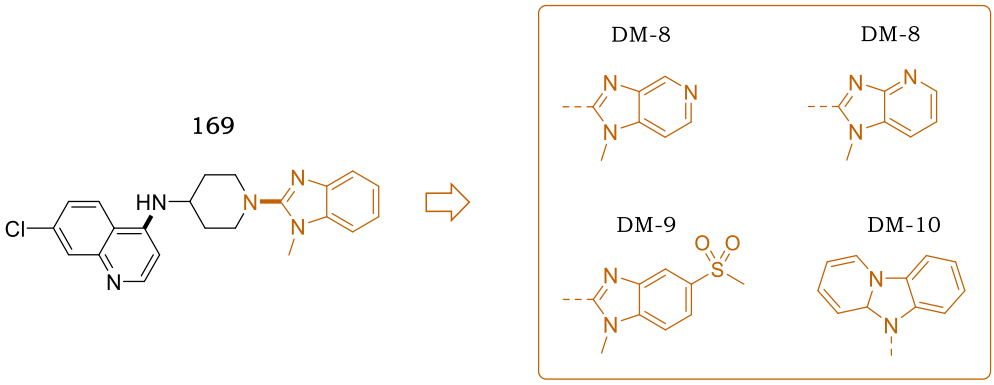

Figure 5.8: Proposed AST-CQ hybrids of **169** with potential for improved solubility and physicochemical properties

5.4 References

(1) Tian, J.; Vandermosten, L.; Peigneur, S.; Moreels, L.; Rozenski, J.; Tytgat, J.; Herdewijn, P.; Van den Steen, P. E.; De Jonghe, S. Astemizole Analogues with Reduced HERG Inhibition as Potent Antimalarial Compounds. *Bioorg. Med. Chem.* **2017**, *25* (24), 6332–6344.

(2) Roman, G.; Crandall, I. E.; Szarek, W. A. Synthesis and Anti- Plasmodium Activity of Benzimidazole Analogues Structurally Related to Astemizole. *ChemMedChem* **2013**, *8*, 1795–1804.

(3) Wang, W.; MacKinnon, R. Cryo-EM Structure of the Open Human Ether-à-Go-Go -Related K + Channel HERG. *Cell* **2017**, *169* (3), 422-430.e10.

(4) Asai, T.; Adachi, N.; Moriya, T.; Oki, H.; Maru, T.; Kawasaki, M.; Suzuki, K.; Chen, S.; Ishii, R.; Yonemori, K.; et al. Cryo-EM Structure of K+-Bound HERG Channel Complexed with the Blocker Astemizole. *Structure* **2021**.

(5) Ritchie, T. J.; Macdonald, S. J. F.; Pickett, S. D. Insights into the Impact of N- and O-Methylation on Aqueous Solubility and Lipophilicity Using Matched Molecular Pair Analysis. *Medchemcomm* **2015**, *6* (10), 1787–1797.

CHAPTER 6

EXPERIMENTAL SECTION

6.1 Chapter Overview

In this chapter, all the experimental protocols used in the thesis are described. The chapter provides supplementary information for synthetic procedures, physicochemical property analysis and biological assays which are not fully outlined in the preceding chapters. The chapter begins with a full description of the chemistry and characterization information of all synthesized intermediates and final compounds. This is then followed by the description of the biological assays used to assess the compounds, and finally, the physicochemical analysis assays (i.e., solubility and log*D*). For existing compounds, characterization data confirms the structure and matches the data in the literature, where methods were fully adapted.

6.2 Chemistry

6.2.1 Reagents & Solvents

Commercially available chemicals and reagents were purchased from Sigma Aldrich, now Merck (South Africa, SA), FluoroChem (UK), Enamine (USA) and/or Combi block (USA). Anhydrous solvents dimethylformamide (DMF), tetrahydrofuran (THF) and 4N HCl in dioxane were purchased from Merck (SA). Absolute ethanol (EtOH), methanol (MeOH), ethyl acetate (EtOAc), *n*-hexane, dichloromethane (DCM) and acetone were purchased as Analytical Reagent (AR) grade solvents from Kimix and/or Protea Chemicals Pty Ltd (SA). The High-Performance Liquid Chromatography (HPLC) grade solvents were bought from Sigma Aldrich (ammonium acetate and dimethyl sulfoxide, DMSO), Merck (Glacial acetic acid) and Microsep (acetonitrile and methanol) for Chromatography and Mass spectrometry and HPLC usage.

6.2.2 Physical & Spectroscopic Characterization

6.2.2.1 Liquid Chromatography with Mass Spectrometer (LC-MS)

Analysis was performed using an LC-MS system comprising of an Agilent 1260 Infinity Binary Pump, Agilent 1260 Infinity Diode Array Detector (DAD), Agilent 1290 Infinity Column Compartment, Agilent 1260 Infinity Standard Autos sampler, and an Agilent 6120 Quadrupole (Single) Mass Spectrometer equipped with APCI and ESI multimode ionization

source. Purities were determined by Agilent LC-MS using a Kinetex Core C18 2.6 μm column (50 × 3 mm). The aqueous phase (Mobile Phase A) was comprised of 0.4% acetic acid in 10 Mm ammonium acetate in HPLC grade (Type-1) water, while the organic phase (Mobile Phase B) was comprised of: 0.4% acetic acid, 10 Mm ammonium acetate in a 9:1 ratio of HPLC grade methanol and Type-1 water. All compounds were run with a flow rate of 0.9 ml.min^{-1}; and were confirmed to have purity of ≥ 95%.

Table 6.1: LC-MS gradient used for determining the purity (%), retention time (t_R) and mass (m/z) of compounds.

Time (min)	%A	%B	Composition	
			A	B
0.00	75	25	10 Mm ammonium acetate (NH_4Oac) buffer (0.4% Acetic acid, HOAc).	10 Mm ammonium acetate (0.4% Acetic acid) in 90% HPLC grade MeOH/H_2O.
1.00	75	25		
3.00	0	100		
4.50	0	100		
5.20	75	25		
6.00	75	25		

6.2.2.2 Nuclear Magnetic Resonance (NMR)

Spectra were recorded on Varian Mercury (^{1}H NMR on 300MHz) or Bruker (^{1}H NMR on 400 or 600 MHz and ^{13}C NMR on 101 or 151 MHz). All spectra were recorded in either deuterated dimethyl sulfoxide (DMSO-d_6), chloroform ($CDCl_3$) or methanol (MeOD-d_4) using tetramethylsilane (TMS) as an internal standard. All chemical shifts (δ) are recorded in parts per million (ppm) and are rounded off to two decimal places; Coupling constants (J) are recorded in hertz (Hz) and rounded off to two decimal places. Abbreviations used in the assigning of ^{1}H NMR signals are: br-s (broad singlet), br-d (broad doublet), br-t (broad triplet), d (doublet), m (multiplet), s (singlet), t (triplet), q (quartet), dd (doublet of doublets), ddd (doublet of doublet of doublets), ddq (doublet of doublets of quartets), td (triplet of doublets), tt (triplet of triplets). ^{13}C NMR spectra were recorded in proton-decoupled mode, and the chemical shifts are listed without assignment.

6.2.2.3 Melting Point (m.p.) and Optical Polarimetry

Melting points were determined using a Reichert-Jung Thermovar hot-stage microscope (HSM), coupled to a Reichert-Jung Thermovar digital thermometer (20 °C – 350 °C). Specific rotation was determined using the Rudolph research analytical autopol 1 automatic

polarimeter. Samples were dissolved in 2 ml methanol (AR) and read using a 1 dm path length tube at 22 °C.

6.2.3 Thin Layer Chromatography (TLC)

Thin Layer chromatographic (TLC) plates were purchased from either Merck or Sigma Aldrich's (SA or Germany) with specificity as F_{254} aluminium-backed pre-coated silica gel 60 plates. Detection and visualization of spots were performed using Ultraviolet (UV) at wavelengths 254 and 366 nm, Iodine vapours (chamber) and Ninhydrin reagent. Product purification was done with either gravity glass column chromatography or Biotage® Isolera™ One automated flash column chromatography system, using Merck Kieselgel 60:70 – 230 mesh on the Biotage equipment.

6.2.4 Synthesis & Characterization Information

General Procedure 1: Bromination of primary alcohols using *Appel* reaction

To a stirring solution of an appropriate alcohol (1.0 equiv) in DCM at 0 °C, triphenyl phosphine, PPh_3 (1.5 equiv) and carbon tetrabromide, CBr_4 (1.2 equiv) where added successively. The resulting mixture was then allowed to warm to room temperature (18 °C), at which it was stirred for 2 hr. Upon completion (monitored *via* TLC), DCM was evaporated *in vacuo* and diethyl ether (Et_2O) added to the dry residue. Insoluble materials were filtered, and the filtrate dry loaded on silica gel. Products were obtained following purification *via* flash column chromatography, using 20 – 50% EtOAc/Hexanes as an eluent.

4-(2-bromoethyl)-benzonitrile (1a)

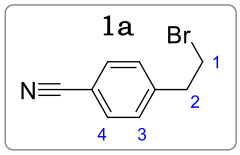

Obtained from 4-(2-hydroxyethyl)benzonitrile (10.0 g, 67.9 mmol) as a white crystalline solid (11.6 g, 81%). R_f (20% EtOAc/Hexanes) 0.74. ^{1}H NMR (300 MHz, DMSO-d_6) δ 7.78 (d, J = 8.3 Hz, 2H. H^4), 7.49 (d, J = 8.3 Hz, 2H, H^3), 3.78 (t, J = 7.0 Hz, 2H, H^1), 3.23 (t, J = 7.0 Hz, 2H, H^2). Purity: 96%, t_R = 2.753 min.

2-(2-bromoethyl)pyridine (1b)

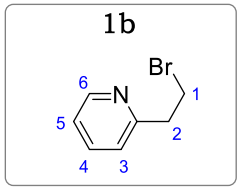

Obtained from 2-(231yridine-2-yl)ethan-1-ol (0.400 g, 3.25 mmol) as a yellow liquid (0.423 g, 70%). R_f (50% EtOAc/Hexanes) 0.50. ^{1}H NMR (300 MHz, DMSO-d_6) δ 8.52 (dd, J = 5.0, 1.4 Hz, 1H, H^6), 7.73 (td, J = 7.8, 1.4 Hz, 1H, H^4), 7.32 (dd, J = 7.8, 1.3 Hz, 1H, H^3), 7.25 (ddd, J = 7.8, 4.9, 1.3 Hz, 1H, H^5), 3.86 (t, J = 6.9 Hz, 2H, H^1), 3.28

(t, J = 6.9 Hz, 2H, H^2). LC-MS (APCI/ESI): found m/z = 186.9, 188.9 [M+H]$^+$ (cal. For C_7H_8BrN, 184.9, 186.9). LC-MS (APCI/ESI) Purity: 96%, t_R = 2.422 min.

General Procedure 2: Preparation of amidoximes from nitriles

To a solution of an appropriate nitrile (1.0 equiv) in absolute ethanol (10 – 50 ml), hydroxylamine hydrochloride ($NH_2OH{\cdot}HCl$, 1.2 equiv), triethylamine (TEA, 1.2 equiv) and catalytic amounts of 8-hydroxyquinolone (1.0 mol%) were successively added. The resulting mixture was refluxed at 79 °C for 1.5 hr. After completion (monitored *via* TLC), the solvent was evaporated *in vacuo*, the residue diluted with water. The aqueous solution was acidified to Ph 3 using 3N HCl, and the precipitate was filtered off, washed with 10% HCl and dried as the product.

If no precipitate formed, the acidic aqueous solution was extracted with EtOAc (3 × 20 – 50 ml) and combine organic phases washed with brine (1 × 5 – 20 ml), dried over anhydrous Na_2SO_4, and solvent evaporated *in vacuo* to afford the product.

4-(2-bromoethyl)-N-hydroxybenzimidamide (2)

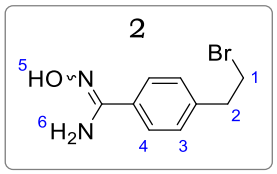

Obtained from **1a** (7.50 g, 35.7 mmol) as a light green crystalline solid (7.17 g, 82%). R_f (50% EtOAc/Hexanes) 0.25. ^{1}H NMR (300 MHz, DMSO-d_6) δ 9.57 (s, 1H, H^5), 7.61 (d, J = 8.3 Hz, 2H, H^4), 7.27 (d, J = 8.3 Hz, 2H, H^3), 5.75 (s, 2H, H^6), 3.74 (t, J = 7.1 Hz, 2H, H^1), 3.14 (t, J = 7.1 Hz, 2H, H^2). LC-MS (APCI$^+$/ESI): found m/z = 244.0, 245.0 [M+H]$^+$ (cal. For $C_9H_{11}BrN_2O$, 243.01, 244.01). Purity: 98%, t_R = 2.135 min.

N'-hydroxy-2-(methylthio) acetimidamide (112a)

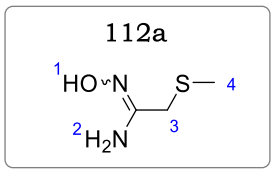

Obtained from 2-(methylthio)acetonitrile (0.250 g, 2.86 mmol) as a yellow solid (0.272 g, 79%). ^{1}H NMR (400 MHz, DMSO-d_6) δ 8.89 (s, 1H, H^1), 6.55 (s, 2H, H^2), 3.43 (s, 2H, H^3), 2.13 (s, 3H, H^4).

2-(dimethylamino)-N'-hydroxyacetimidamide (112b)

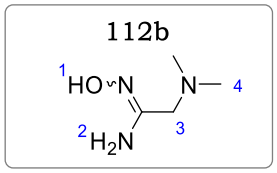

Obtained from 2-(dimethylamino)acetonitrile (0.250 g, 2.97 mmol) as a dark brown solid (0.243 g, 70%). ^{1}H NMR (400 MHz, DMSO-d_6) δ 8.90 (s, 1H, H^1), 6.53 (s, 2H, H^2), 3.35 (s, 2H, H^3), 2.24 (s, 6H, H^4).

N'-hydroxycyclopropanecarboximidamide (112c)

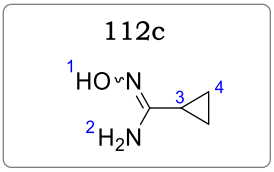

Obtained from cyclopropanecarbonitrile (0.250 g, 3.73 mmol) as a white solid (0.335 g, 90%). ^{1}H NMR (400 MHz, DMSO-d_6) δ 8.91 (s, 1H, H^1), 6.49 (s, 2H, H^2) 0.71 – 0.52 (m, 2H, H^4), 0.46 – 0.28 (m, 2H, H^4), 0.20 (p, J = 4.8 Hz, 1H, H^3).

N'-hydroxyisobutyrimidamide (112d)

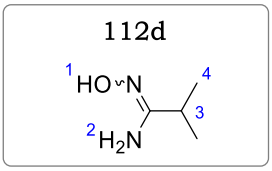

Obtained from isobutyronitrile (0.200 g, 2.89 mmol) as a pale yellow solid (0.271 g, 92%). ^{1}H NMR (400 MHz, DMSO-d_6) δ 8.90 (s, 1H, H^1), 6.51 (s, 2H, H^2), 2.55 (hept, J = 5.9 Hz, 1H, H^4), 1.05 (d, J = 5.9 Hz, 6H, H^4).

N'-hydroxypivalimidamide (112e)

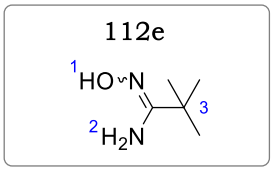

Obtained from pivalonitrile (0.250 g, 3.00 mmol) as a light green solid (0.331 g, 95%). ^{1}H NMR (400 MHz, DMSO-d_6) δ 8.90 (s, 1H, H^1), 6.55 (s, 2H, H^2), 1.43 (s, 9H, H^3).

3-(4-(2-bromoethyl)phenyl)-1,2,4-oxadiazole (3a)

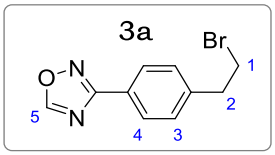

To a solution containing **2** (0.150 g, 0.62 mmol) in triethyl orthoformate ($CH(EtO)_3$, 1.5 ml) and pyridine (1.5 ml), catalytic amounts boron trifluoride etherate ($BF_3.Oet_2$) was added, and the solution stirred at 80 °C for 1 hr. After completion (monitored *via* TLC), the solvent was removed *in vacuo* and the product obtained by flash column chromatography using 10% EtOAc/Hexanes. White crystalline solid (0.080 g, 51%). R_f (40% EtOAc/Hexanes) 0.69. ^{1}H NMR (300 MHz, Methanol-d_4) δ 9.24 (s, 1H, H^5), 8.04 (d, J = 8.3 Hz, 2H, H^4), 7.43 (d, J = 8.3 Hz, 2H, H^3), 3.81 (t, J = 7.1 Hz, 2H, H^1), 3.13 (t, J = 7.0 Hz, 2H, H^2). LC (APCI$^+$/ESI): Purity: 98%, t_R = 2.412 min.

3-(4-(2-bromoethyl)phenyl)-5-methyl-1,2,4-oxadiazole (3b)

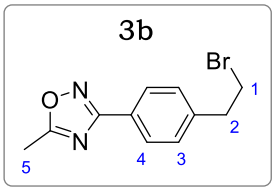

A mixture of **2** (0.100 g, 0.41 mmol) and acetyl chloride (350 µl, 0.49 mmol) was refluxed in THF at 70 °C for 30 min. At completion, the reaction mixture quenched with water (5 ml), and THF was evaporated under reduced pressure. The aqueous mixture was extracted with DCM (3 × 15 ml), combined organic extracts washed with brine (1 × 5 ml) and dried over anhydrous Na_2SO_4. Evaporating off

solvent under vacuum afforded product as white crystalline solid (0.170 g, 80%). R_f (5% MeOH/DCM) 0.62. ^{1}H NMR (300 MHz, DMSO-d_6) δ 7.68 (d, J = 8.3 Hz, 2H, H^4), 7.38 (d, J = 8.3 Hz, 2H, H^3), 3.76 (t, J = 7.0 Hz, 2H, H^1), 3.19 (t, J = 7.0 Hz, 2H, H^2), 2.17 (s, 3H, H^5). LC (APCI$^+$/ESI): Purity: 99%, t_R = 2.438 min.

3-(4-(2-bromoethyl)phenyl)-5-(trifluoromethyl)-1,2,4-oxadiazole (3c)

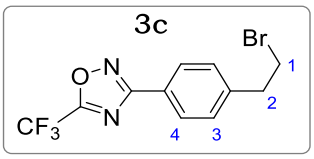

To a mixture of **2** (6.75 g, 27.8 mmol) and pyridine (3 ml) in 50 ml DCM, trifluoroacetic acid anhydride (TFAA, 4.63 ml, 33.4 mmol) was added, and the solution stirred at 22 °C for 20 min. The mixture was then poured in ice water (50 ml) and extracted with EtOAc (3 × 50 ml). The combined organic extracts were washed with brine (1 × 10 ml) and dried over anhydrous Na_2SO_4. The product was obtained after flash column chromatography using 10 – 15% EtOAc/Hexanes as a pale-yellow oil (7.15 g, 76%). R_f (40% EtOAc/Hexanes) 0.92. ^{1}HNMR (300 MHz, DMSO-d_6) δ 8.16 (d, J = 8.2, 2H, H^4), 7.49 (d, J = 8.2, 2H, H^3), 3.80 (t, J = 7.0 Hz, 2H, H^1), 3.24 (t, J = 7.0 Hz, 2H, H^2). LC (APCI$^+$/ESI): Purity: 97%, t_R = 2.631 min.

4-(2-bromoethyl)-N'-((ethoxycarbonyl)oxy)benzimidamide (3d)

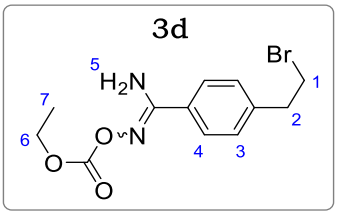

To a solution of **2** (0.050 g, 0.21 mmol) in 1.5 ml acetone, K_2CO_3 (0.031 g, 0.23 mmol) was added, and the solution kept stirring at 0 °C. Ethyl chloroformate (22 µl, 0.23mmol, dissolved in 0.5 ml cold acetone) was added to the ice-cold solution, and the resulting mixture stirred at 0 – 4 °C for 3 hr. At completion (monitored *via* TLC), the reaction mixture was diluted with 10 ml water and extracted with DCM (3 × 10 ml). The combined organic extracts were washed with brine (1 × 5 ml) and dried over anhydrous Na_2SO_4. The solvent was evaporated *in vacuo* to afford o-acylated oxime product as an off-white solid (0.070 g, 98%). R_f (50% EtOAc/Hexanes) 0.59. ^{1}H NMR (300 MHz, DMSO-d_6) δ 7.63 (d, J = 8.3 Hz, 2H, H^4), 7.35 (d, J = 8.3 Hz, 2H, H^3), 6.76 (s, 2H, H^5), 4.19 (q, J = 7.10 Hz, 2H, H^6), 3.76 (t, J = 7.05 Hz, 2H, H^1), 3.17 (t, J = 7.05 Hz, 2H, H^2), 1.26 (t, J = 7.10 Hz, 3H, H^7). LC-MS (APCI$^+$/ESI): Purity: 99%, t_R = 3.406 min.

General Procedure 3: EDCI/DMAP Amide Coupling

To a solution of 4-(2-bromoethyl) benzoic acid (1.0 equiv) in DCM under ice, DMAP (5 mol%) and EDCI (1.5 equiv) were added, and the solution stirred at room temperature (18

– 20 °C) for 15 min. The appropriate amine (1.2 equiv) was then added (dropwise if solution), and the resulting solution stirred at room temperature for 2 hr. After completion, the reaction was diluted with another aliquot of initial amount of DCM used, and the mixture washed with saturated $NaHCO_3$ (×3) followed by water (×2), then brine (×1). The DCM phase was then dried over anhydrous Na_2SO_4, and the solvent evaporated *in vacuo*. Pure products were obtained after washing the dry residue with diethyl ether.

(S)-4-(2-bromoethyl)-N-(1-hydroxypropan-2-yl)benzamide (4a)

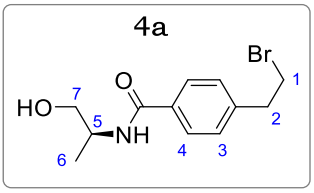

Obtained from (S)-2-aminopropan-1-ol (0.100 g, 1.31 mmol) as a white solid (0.250 g, 80%). R_f (5% MeOH/DCM), 0.40. ^{1}HNMR (300 MHz, Methanol-d_4) δ 7.78 (d, J = 8.3 Hz, 2H, H^4), 7.34 (d, J = 8.3 Hz, 2H, H^3), 4.18 (tq, J = 6.8, 6.1 Hz, 1H, H^5), 3.65 – 3.59 (m, 4H, $H^{1,7}$), 3.20 (t, J = 7.2 Hz, 2H, H^2), 1.24 (d, J = 6.1 Hz, 3H, H^6). LC-MS (APCI$^+$/ESI): found m/z = 286.0, 288.0 $[M+H]^+$ (cal. For $C_{12}H_{16}BrNO_2$, 285.04, 287.03). Purity: 96%, t_R = 2.593 min.

(S)-4-(2-bromoethyl)-N-(2-hydroxypropyl)benzamide (4b)

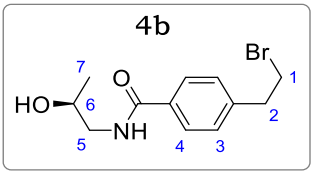

Obtained from (S)-1-aminopropan-2-ol (0.100 g, 1.31 mmol) as a white solid (0.285 g, 91%). R_f (5% MeOH/DCM), 0.38. ^{1}HNMR (300 MHz, Methanol-d_4) δ 8.12 (d, J = 8.4 Hz, 2H, H^4), 7.21 (d, J = 8.4 Hz, 2H, H^3), 3.71 (qt, J = 6.8, 6.1 Hz, 1H, H^6), 3.51 (t, J = 7.2 Hz, 2H, H^1), 3.12 (d, J = 6.1 Hz, 2H, H^5), 2.91 (t, J = 7.2 Hz, 2H, H^2), 1.22 (d, J = 6.8 Hz, 3H, H^7). LC-MS (APCI$^+$/ESI): found m/z = 286.0, 288.0 $[M+H]^+$ (cal. For $C_{12}H_{16}BrNO_2$, 285.04, 287.03). Purity: 98%, t_R = 2.508 min.

N'-acetyl-4-(2-bromoethyl)benzohydrazide (4c)

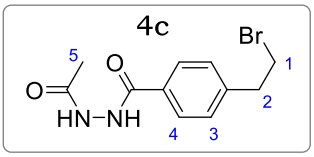

Obtained from acethydrazide (0.150 g, 1.92 mmol) as a white solid (0.358 g, 65%). R_f (5% MeOH/DCM), 0.16. ^{1}HNMR (300 MHz, Methanol-d_4) δ 7.83 (d, J = 8.3 Hz, 2H, H^4), 7.41 – 7.35 (m, 2H, H^3), 3.66 (t, J = 7.1 Hz, 2H, H^1), 3.23 (t, J = 7.1 Hz, 2H, H^2), 2.06 (s, 3H^5). Purity: 96%, t_R = 2.501 min.

N'-((4-(2-bromoethyl)benzoyl)oxy)acetimidamide (7a)

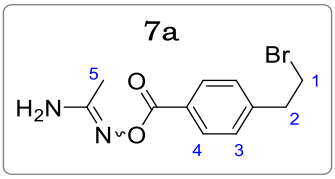

Obtained from *N*-hydroxyacetamidine (4.90 g, 62.8 mmol) as a white solid (13.48 g, 90%), washed in ether and vacuum dried. R_f(7% MeOH/DCM) 0.42. ^{1}HNMR (300 MHz, Methanol-d_4) δ 8.05 (d, J = 8.3 Hz, 2H, H^4), 7.41 (d, J = 8.3, 2H, H^3), 3.67 (t, J = 7.1 Hz, 2H, H^1), 3.24 (t, J = 7.1 Hz, 2H, H^2), 1.95 (s, 3H, H^5). LC-MS (APCI$^+$/ESI): found m/z = 284.8, 286.8 [M+H] $^+$ (cal. for $C_{11}H_{13}BrN_5O_2$, 284.8, 286.8). Purity: 96%, t_R = 2.511 min.

N-((4-(2-bromoethyl)benzoyl)oxy)-2,2,2-trifluoroacetimidamide (7b)

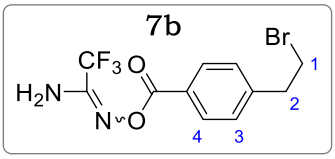

Obtained from 2,2,2-trifluoro-*N*-hydroxy ethanimidamide (3.35 g, 26.2 mmol) as a white solid (3.47 g, 78%). R_f (3% MeOH/DCM) 0.75. ^{1}H NMR (300 MHz, DMSO-d_6) δ 8.16 – 8.09 (m, 2H, H^4), 7.71 (s, 2H, H^5), 7.49 – 7.42 (m, 2H, H^3), 3.80 (t, J = 7.0 Hz, 2H, H^1), 3.24 (t, J = 7.0 Hz, 2H, H^2). LC-MS (APCI/ESI): found m/z = 337.99, 339.99 [M+H] $^+$ (cal. for $C_{11}H_{10}BrF_3N_2O_2$, 338.99, 340.99). Purity: 98%, t_R = 2.646 min.

General Procedure 4: Tosyl chloride mediated formation of oxazolines and 1,3,4-oxadiazoles from β-keto/β-hydroxy amides

To a stirred suspension of **4a** – **4c** (1.0 equiv) in DCM (5 ml), TEA (3.0 equiv) was added followed by tosyl chloride (TsCl, 2.0 equiv). The mixture was then stirred at 30 °C for 30 min. DCM was removed under vacuum, followed by addition of EtOAc (15 ml). The mixture was washed with $NaHCO_3$ (2 × 10 ml) and brine (10 ml), then dried over anhydrous Na_2SO_4 and solvent evaporated *in vacuo*. Crude solid products were purified by column chromatography using 10 – 25% EtOAc/hexanes as an eluent.

(S)-2-(4-(2-bromoethyl)phenyl)-4-methyl-4,5-dihydrooxazole (5a)

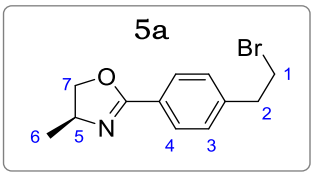

Obtained from **4a** (0.140, 0.48 mmol) as a white solid (0.092 g, 70%). R_f (40% EtOAc/Hexanes), 0.30. ^{1}HNMR (300 MHz, Methanol-d_4) δ 7.85 (d, J = 8.3 Hz, 2H, H^4), 7.33 (d, J = 8.3 Hz, 2H, H^3), 4.57 (dd, J = 9.3, 8.2 Hz, 1H, H^{7e}), 4.34 (ddq, J = 9.3, 7.7, 6.6 Hz, 1H, H^5), 4.01 (t, J = 8.0 Hz, 2H, H^{7a}), 3.63 (t, J = 7.2 Hz, 2H, H^1), 3.19 (t, J = 7.2 Hz, 2H, H^2), 1.32 (d, J = 6.6 Hz, 3H, H^6). LC-MS (APCI$^+$/ESI): found m/z = 268.0, 270.0 [M+H] $^+$ (cal. for $C_{12}H_{14}BrNO$, 267.03, 269.02). Purity: 98%, t_R = 2.745 min.

(S)-2-(4-(2-bromoethyl)phenyl)-4-methyl-4,5-dihydrooxazole (5b)

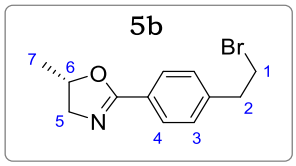

Obtained from **4b** (0.170, 0.59 mmol) as a white solid (0.136g, 85%). R_f (40% EtOAc/Hexanes) 0.32. ^{1}H NMR (300 MHz, Methanol-d_4) δ 7.99 (d, J = 8.1 Hz, 2H, H^4), 7.28 (d, J = 8.1 Hz, 2H, H^3), 4.25 (dd, J = 14.1, 8.9 Hz, 1H, H^5), 4.00 (ddq, J = 14.1, 6.3, 6.6 Hz, 1H, H^6), 3.65 (t, J = 7.3 Hz, 2H, H^1), 3.33, (dd, J = 8.9, 6.3 Hz, 1H, H^5), 3.29 (t, J = 7.3 Hz, 2H, H^2), 1.95 (d, J = 6.6 Hz, 3H, H^7). LC-MS (APCI$^+$/ESI): found m/z = 268.0, 270.0 [M+H] $^+$ (cal. for $C_{12}H_{14}BrNO$, 267.03, 269.02). Purity: 98%, t_R = 2.807 min.

2-(4-(2-bromoethyl)phenyl)-5-methyl-1,3,4-oxadiazole (5c)

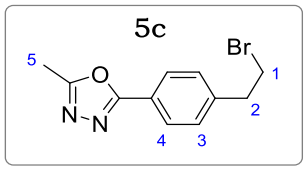

Obtained from **4c** (0.150, 0.52 mmol) as a yellow crystalline solid (0.122 g, 88%). R_f (25% EtOAc/Hexanes) 0.5. ^{1}H NMR (300 MHz, Methanol-d_4) δ 7.55 (d, J = 8.7 Hz, 2H, H^4), 7.41 (d, 2H, H^3), 3.69 (t, J = 7.1 Hz, 2H, H^1), 3.28 (t, J = 7.1 Hz, 2H, H^2), 1.99 (s, 3H, H^5). LC-MS (APCI/ESI): found m/z = 266.9, 268.9 [M+H] $^+$ (cal. For $C_{11}H_{11}BrN_2O$, 266.01, 268.00). Purity: 97%, t_R = 2.747min.

4-(2-bromoethyl)phenol (6)

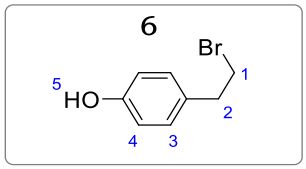

To a stirring solution of 4-methoxyphenethylbromide (0.250 g, 1.16 mmol) in 5 ml DCM at –78 °C, boron tribromide (BBr3, 720 µl, 4.19 mmol) was added. The mixture could warm to 0 °C and stirred at that temperature for 12 hours. After completion, the reaction mixture was cooled to – 50 °C and quenched by adding 2 ml water. The mixture was diluted with saturated solution of ammonium chloride, NH_4Cl (5 ml), and the resulting solution extracted with EtOAc (2 × 25 ml). Combined organic phases were dried over Na_2SO_4 and solvent evaporated under vacuum. The product was obtained after flash chromatography using 10% EtOAc/Hexane as a light-yellow solid (0.107 g, 46%). R_f (25% EtOAc/Hexanes) 0.50. ^{1}H NMR (300 MHz, DMSO-d_6) δ 9.23 (s, 1H, H^5), 7.05 (d, J = 8.5 Hz, 2H, H^4), 6.69 (d, J = 8.5 Hz, 2H, H^3), 3.63 (t, J = 7.4 Hz, 2H, H^1), 2.99 (t, J = 7.4 Hz, 2H, H^2). LC-MS (APCI/ESI) Purity: 99%, t_R = 2.356 min.

Ethyl 4-(2-bromoethyl)benzoate (8)

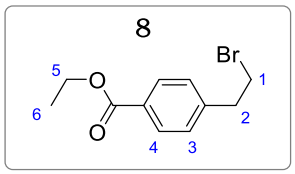

A solution of 4-(2-bromoethyl) benzoic acid (0.500 g, 0.22 mmol) and 9.5N aqueous HCl (5 ml) in absolute ethanol (10 ml) was refluxed at 80 °C for 2 hr. The mixture was then cooled to room temperature (22 °C) and the solvent evaporated *in vacuo*. The aqueous residue was diluted with 25 ml saturated $NaHCO_3$ and extracted with EtOAc (3 × 25 ml). Combined organic extracts were washed with water (2 × 15 ml), followed by brine (1 × 10 ml), and dried over anhydrous Na_2SO_4. After flash column chromatography using 20% EtOAc/Hexanes as eluent, the product obtained as a yellow oil (0.476 g, 85%). R_f(30% EtOAc/Hexanes), 0.79. ^{1}H NMR (300 MHz, Methanol-d_4) δ 7.96 (d, J = 8.3 Hz, 1H, H^4), 7.37 (d, J = 8.3 Hz, 2H, H^3), 4.35 (q, J = 7.1 Hz, 2H, H^5), 3.79 (t, J = 7.0 Hz, 2H, H^1), 3.12 (t, J = 7.0 Hz, 2H, H^2), 1.38 (t, J = 7.1 Hz, 3H, H^6). LC-MS (APCI$^+$/ESI) Purity: 99%, t_R = 2.543 min.

Methyl 4-(2-bromoethyl) benzoate (9)

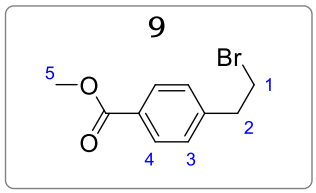

To a solution of 4-(2-bromoethyl) benzoic acid (7.00 g, 30.6 mmol) in 4:1 toluene/MeOH (60 ml) under ice, trimethylsilyldiazomethane (2M solution in hexane) was added dropwise until the yellow colour no longer dissipated (about 28 ml added in 25 minutes). The mixture was evaporated to dryness *in vacuo*, followed by purification by flash column chromatography using 20% EtOAc/Hexanes as eluent. Product obtained as a colorless oil (7.21 g, 97%). R_f (20% EtOAc/Hexanes) 0.45. ^{1}H NMR (400 MHz, DMSO-d_6) δ 7.96 (d, J = 8.4 Hz, 2H, H^1), 7.20 (d, J = 8.4 Hz, 2H, H^2), 3.85 (s, 3H, H^5), 3.54 (t, J = 4.4 Hz, 2H, H^4), 3.14 (t, J = 4.4 Hz, 2H, H^3). LC-MS (APCI$^+$/ESI): found m/z = 242.9, 244.9 [M+H]$^+$ (cal. For $C_{10}H_{11}BrO_2$, 241.99, 243.99). Purity: 99%, t_R = 2.568 min.

4-N-Boc-(2-hydroxyethyl) piperazine (10)

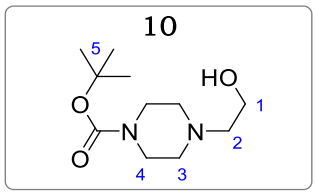

To a stirring solution of 1-(2-hydroxyethyl) piperazine (0.50 g, 3.8 mmol) in 7 ml THF at 0°C, di-*tert*-butyl dicarbonate (Boc_2O, 0.922 g, 4.2 mmol) was added and the mixture stirred at 0 °C for 15 min. The mixture was then allowed to warm to ambient temperature (18 °C) and stirred further for 2 hr. The solvent was evaporated to about half the original volume, followed by addition of water (7 ml). The solution was extracted with DCM (3 × 25 ml), combined organic phases washed with brine (1 × 10 ml) and further dried over anhydrous Na2SO_4. Solvent was evaporated under

vacuum to give product as a light brown to brick reddish oil (0.866 g, 98%). R_f (10% MeOH/DCM) 0.35. ^{1}H NMR (300 MHz, $CDCl_3$) δ 3.56 (t, J = 6.9 Hz, 2H, H^1), 3.41 (m, J = 5.1 Hz, 4H, H^4), 2.71 (t, J = 6.9 Hz, 2H, H^2), 2.44 (m, J = 5.0 Hz, 4H, H^3), 1.43 (s, 9H, H^5).

General Procedure 5: Reduction of ketones to 2° alcohols using $NaBH_4$

Sodium borohydride ($NaBH_4$, 0.5 equiv) was added to a stirring solution of ketone (1.0 equiv) in 5 ml MeOH on an ice bath (0 – 3 °C). The reaction mixture was stirred at room temperature (18 °C) for 2 hr. The mixture was diluted with 20 ml water and extracted with DCM (3 × 20 ml). Combined organic phases where further washed with brine (1 × 10 ml), followed by drying over anhydrous Na_2SO_4. The solvent was evaporated under vacuum to give products. Flash column chromatography was conducted if required.

4-(1-hydroxyethyl)benzonitrile (11a)

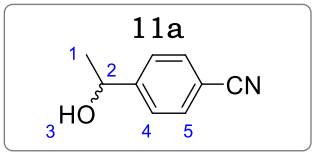

Obtained from 4-acetylbenzonitrile (0.500 g, 3.44 mmol) as a light-yellow oil (0.421 g, 83%). ^{1}H NMR (300 MHz, DMSO-d_6) δ 7.77 (d, J = 8.3 Hz, 2H, H^5), 7.54 (d, J = 8.3 Hz, 2H, H^4), 5.39 (d, J = 4.3 Hz, 1H, H^3), 4.80 (qd, J = 6.5, 4.3 Hz, 1H, H^2), 1.32 (d, J = 6.5 Hz, 3H, H^1). Purity: 99%, t_R = 2.486 min.

4-(1-bromoethyl)benzonitrile (11b)

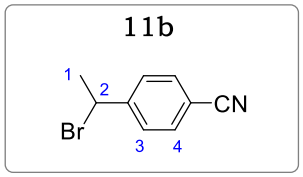

A mixture of **11a** (0.180 g, 1.22 mmol) and bromotrimethyl silane, TMSBr (0.178 ml, 1.35 mmol) was stirred at room temperature (18 °C) for 2 hr. Upon completion, volatile $(TMS)_2O$ was evaporated under reduced pressure and DCM (10 ml) added. Flash column chromatography was performed using DCM to afford the pure product as a light-yellow oil (0.185 g, 72%). R_f (3% MeOH/DCM) 0.73. ^{1}H NMR (300 MHz, DMSO-d_6) δ 7.84 (d, J = 8.5 Hz, 2H, H^4), 7.70 (d, J = 8.5 Hz, 2H, H^3), 5.54 (q, J = 6.9 Hz, 1H, H^2), 1.98 (d, J = 6.9 Hz, 3H, H^1). Purity: 99%, t_R = 2.782 min.

6-vinylnicotinonitrile (122)

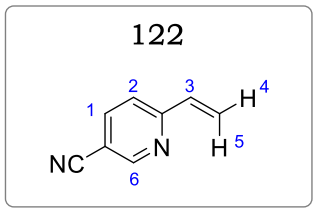

To a solution of 6-bromonicotinonitrile (2.0 g, 10.9 mmol) in 1:1 1,4-dioxane/water (10 ml), (1,1'-bis(diphenyl phosphino) ferrocene) palladium(II) dichloride, $Pd(dppf)Cl_2$ (0.1 equiv) and caesium carbonate, Cs_2CO_3 (3.0 equiv) were added, and the

solution stirred at 23 °C for 15 min with degassing using N_2. Boronic ester 4,4,5,5-tetramethyl-2-vinyl-1,3,2,-dioxaborolane (1.5 equiv) was then added to the degassed mixture, and the resulting reaction mixture stirred at 85 °C for 16 hr under N_2 atmosphere. The reaction was cooled and extracted with EtOAc (3 × 30 ml), combined organic phase dried on anhydrous Na_2SO_4 and concentrated *in vacuo*. The crude material was purified by flash chromatography and isolated at 10 – 15% EtOAc/Hexane as brown crystalline solid (0.298 g, 21%). R_f(20% EtOAc/Hexane), 0.49. ^{1}H NMR (400 MHz, DMSO-d_6) δ 8.85 (d, J = 2.1 Hz, 1H, H^6), 8.13 (dd, J = 8.2, 2.1 Hz, 1H, H^1), 7.66 (d, J = 8.2 Hz, 1H, H^2), 6.91 (dd, J = 17.5, 10.9 Hz, 1H, H^3), 6.43 (d, J = 17.5 Hz, 1H, H^5), 5.71 (d, J = 10.8 Hz, 1H, H^4). LC-MS (APCI$^+$/ESI): found m/z = 131.0 $[M+H]^+$ (cal. For $C_8H_6N_2$, 130.05). Purity: 96%, t_R = 2.485 min.

General Procedure 6: Synthesis of isothiocyanates from primary amines

To a solution of appropriate amine (1.0 equiv) in DMF at 0 °C, 1,1'-thiocarbonyldiimidazole, TCDI (1.1 equiv), dissolved in an aliquot of DMF was added. The resulting reaction mixture could rise to room temperature (24 °C) and stirred for 20 hr at that temperature. The solvent was taken off *in vacuo*, the residue dissolved in EtOAc, and washed with water (×4). The solvent was removed *in vacuo*, and residue triturated with hexane and filtered. The filtrate was treated with activated charcoal and filtered through Celite. Removal of solvent gave pure products.

Tert-butyl 4-isothiocyanatopiperidine-1-carboxylate (126a)

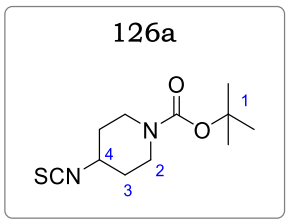

Obtained from tert-butyl 4-aminopiperidine-1-carboxylate (8.00 g, 39.9 mmol) as a colourless oil (7.52 g, 78%). ^{1}H NMR (400 MHz, DMSO-d_6) δ 4.11 – 3.98 (m, 2H, H^2), 3.69 (tt, J = 11.3, 4.1 Hz, 1H, H^4), 3.09 – 2.94 (m, 2H, H^2), 2.17 – 2.05 (m, 2H, H^3), 1.92 – 1.83 (m, 2H, H^3), 1.45 (s, 9H, H^1).

Tert-butyl 3-fluoro-4-isothiocyanatopiperidine-1-carboxylate (126b)

126b

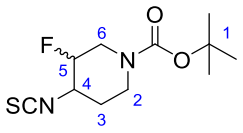

Obtained from tert-butyl 4-amino-3-fluoropiperidine-1-carboxylate (1.00 g, 4.60 mmol) as a yellow oil (0.631 g, 53%). ^{1}H NMR (400 MHz, DMSO-d_6) δ 4.73 (dtd, J = 48.8, 9.1, 4.5, 1H Hz, H^5), 4.39 (qd, J = 10.3, 4.2 Hz, 1H, H^4), 3.61 – 3.60 (m, 1H, H^{6e}), 3.55 – 3.51 (td, J = 12.1, 4.3 Hz, 1H, H^{2e}), 3.01 – 2.90 (m, 2H, H^{2a,6a}), 1.83 (dt, J =13.5, 4.2 Hz, 1H, H^{3e}), 1.75 (dtd, J = 12.1, 9.5, 3.9 Hz, 1H, H^{3a}), 1.41 (s, 9H, H^1).

General Procedure 7: Nucleophilic Aromatic Substitution (S_NAr) and Nitro group Reduction

Step 1, S_NAr: A *o*-halo-nitro precursor (1.0 equiv), an appropriate amine (1.2 equiv), and K_2CO_3 (1.5 equiv) were mixed in MeCN (10 – 15 ml). TEA (1.5 equiv) was added, and the resulting mixture stirred at 65 °C for 4 – 18 hr. After completion, the mixture was cooled to room temperature (18 °C), followed by the addition of water (10 – 15 ml) and EtOAc (15 – 25 ml). The mixture was separated, and the aqueous phase further extracted with EtOAc (3 × 15 ml). Combined organic phases were dried over anhydrous Na_2SO_4, and solvent evaporated *in vacuo*. Pure *o*-amino-nitro intermediates were obtained following recrystallization from ethanol and used in the next step.

Step 2, Nitro group (NO_2) Reduction: To a solution of the crude *o*-amino-nitro intermediates (1.0 equiv) in 1:1 MeOH/EtOAc (10 – 25 ml) was added 10% Pd/C (0.1 equiv), and the reaction mixture was stirred at 21 °C under a hydrogen (H_2) atmosphere using a double padded balloon. After 12 – 36 hr, TLC indicated reaction completion. The reaction mixture was filtered through a bed of Celite, and the filtrate concentrated *in vacuo* to afford products. If required, flash column chromatography using 20 – 70% EtOAc/Hexanes was performed.

3-amino-4-(methylamino)benzonitrile (129a)

129a

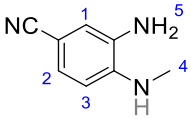

Obtained from 4-chloro-3-nitrobenzonitrile (0.500 g, 2.74 mmol) and methylamine (2M solution in THF, 1.64 ml, 3.29 mmol), as a dark brown solid (0.319 g, 79% over two steps). R_f (40% EtOAc/Hexane) 0.32. ^{1}H NMR (300 MHz, DMSO-d_6) δ 7.58 (d, J = 1.6 Hz, 1H, H^1),

7.28 (dd, *J* = 8.0, 1.6 Hz, 1H, H[2]), 6.21 (d, *J* = 8.0 Hz, 1H, H[3]), 5.02 (s, 2H, H[5]), 2.71 (s, 3H, H[4]). Purity: 99%, t_R = 0.153 min.

_N_1-methyl-4-(trifluoromethyl)benzene-1,2-diamine (129b)

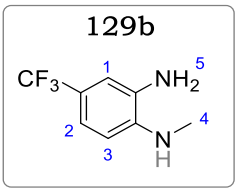

Obtained from 1-fluoro-2-nitro-4-(trifluoromethyl)benzene (0.500 g, 2.39 mmol) and methylamine (2M solution in THF, 1.43 ml, 2.86 mmol), as a dark brown solid (0.395 g, 87% over two steps). R_f (20% EtOAc/Hexane) 0.36. ^{1}H NMR (300 MHz, DMSO-d_6) δ 6.86 – 6.80 (m, 2H, H[1,2]), 6.43 (d, *J* = 8.0 Hz, 1H, H[3]), 5.00 (s, 2H, H[5]), 2.76 (s, 3H, H[4]). Purity: 98%, t_R = 0.212 min.

4-methoxy-N1-methylbenzene-1,2-diamine (129c)

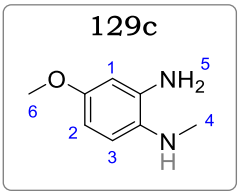

Obtained from 1-fluoro-4-methoxy-2-nitrobenzene (0.500 g, 2.92 mmol) and methylamine (2M solution in THF, 1.75 ml, 3.50 mmol), as a blackish solid (0.293 g, 66% over two steps). R_f (40% EtOAc/Hexane) 0.31. ^{1}H NMR (300 MHz, DMSO-d_6) δ 6.80 (d, *J* = 1.2 Hz, 1H, H[1]), 6.48 (dd, *J* = 8.3, 1.2 Hz, 1H, H[2]), 6.23 (d, *J* = 8.3 Hz, 1H, H[3]), 5.05 (s, 2H, H[5]), 3.91 (s, 3H, H[6]), 2.69 (s, 3H, H[4]). Purity: 97%, t_R = 0.182 min.

***N1*-methyl-4-(methylsulfonyl)benzene-1,2-diamine (129d)**

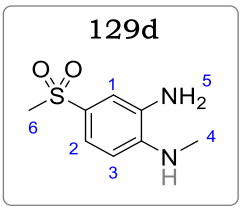

Obtained from 1-fluoro-4-(methylsulfonyl)-2-nitrobenzene (0.500 g, 2.28 mmol) and methylamine (2M solution in THF, 1.37 ml, 2.73 mmol), as a brown solid (0.388 g, 85% over two steps). R_f (40% EtOAc/Hexane) 0.45. ^{1}H NMR (300 MHz, DMSO-d_6) δ 7.40 – 7.38 (m, 2H, H[1,2]), 6.82 (d, *J* = 8.1 Hz, 1H, H[3]), 5.03 (s, 2H, H[5]), 3.01 (s, 3H, H[6]), 2.75 (s, 3H, H[4]). Purity: 97%, t_R = 0.220 min.

Methyl 3-amino-4-(methylamino)benzoate (129e)

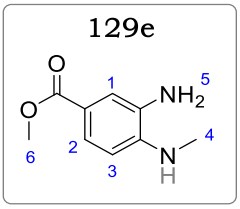

Obtained from methyl 4-fluoro-3-nitrobenzoate (0.500 g, 2.51 mmol) and methylamine (2M solution in THF, 1.50 ml, 3.01 mmol), as a yellow solid (0.348 g, 77% over two steps). R_f (40% EtOAc/Hexane) 0.39. ^{1}H NMR (300 MHz, DMSO-d_6) δ 8.05 (d, *J* = 1.1 Hz, 1H, H[1]), 7.68 (dd, *J* = 8.2, 1.0 Hz, 1H, H[2]), 6.88 (d, *J* = 8.2 Hz, 1H, H[3]), 4.99 (s, 2H, H[5]), 3.88 (s, 3H, H[6]), 2.70 (s, 3H, H[4]). Purity: 99%, t_R = 0.197 min.

4-fluoro-N1-methylbenzene-1,2-diamine (129f)

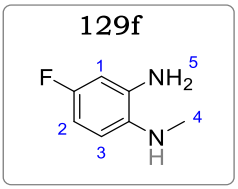

Obtained from 1,4-difluoro-2-nitrobenzene (0.500 g, 3.14 mmol) and methylamine (2M solution in THF, 1.88 ml, 3.77 mmol), as a dark oil (0.347 g, 79% over two steps). R_f(20% EtOAc/Hexane) 0.42. ^{1}H NMR (300 MHz, DMSO-d_6) δ 6.98 (d, J = 1.2 Hz, 1H, H^1), 6.25 – 6.49 (m, 2H, H^{2,3}), 5.03 (s, 2H, H^5), 2.68 (s, 3H, H^4). Purity: 99%, t_R = 0.283 min.

4-bromo-N1-methylbenzene-1,2-diamine (129g)

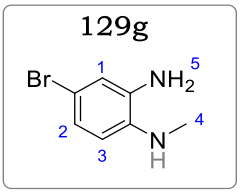

Obtained from 4-bromo-1-fluoro-2-nitrobenzene (0.500 g, 2.30 mmol) and methylamine (2M solution in THF, 1.38 ml, 2.76 mmol), as a dark brown solid (0.370 g, 81% over two steps). R_f (20% EtOAc/Hexane) 0.38. ^{1}H NMR (300 MHz, DMSO-d_6) δ 7.01 (d, J = 1.0 Hz, 1H, H^1), 6.78 – 6.71 (m, 2H, H^{2,3}), 5.05 (s, 2H, H^5), 2.69 (s, 3H, H^4). Purity: 99%, t_R = 0.291 min.

3-amino-4-((4-fluorobenzyl)amino)benzonitrile (163a)

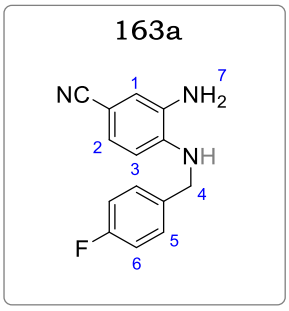

Obtained from 4-chloro-3-nitrobenzonitrile (0.250 g, 1.37 mmol) and 4-fluorobenzylamine (0.205 g, 1.64 mmol), as a brownish solid (0.293 g, 89% over two steps). R_f (50% EtOAc/Hexane) 0.21. ^{1}H NMR (300 MHz, DMSO) δ 7.88 (d, J = 1.1 Hz, 1H, H^1), 7.71 (dd, J = 8.0, 1.1 Hz, 1H, H^2), 7.44 (d, J = 7.8 Hz, 2H, H^6), 7.20 (d, J = 7.8 Hz, 2H, H^5), 6.92 (d, J = 8.0 Hz, 1H, H^3), 5.06 (s, 2H, H^7), 4.90 (d, J = 5.9 Hz, 2H, H^4). LC-MS (APCI$^+$/ESI): found m/z = 242.1 [M+H]$^+$ (cal. For $C_{14}H_{12}FN_3$, 241.10). Purity: 98%, t_R = 0.208 min.

N1-(4-fluorobenzyl)-4-(methylsulfonyl)benzene-1,2-diamine (163b)

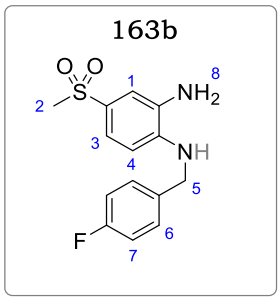

Obtained from 1-fluoro-4-(methylsulfonyl)-2-nitrobenzene (0.250 g, 1.14 mmol) and 4-fluorobenzylamine (0.171 g, 1.36 mmol), as a dark brown solid (0.310 g, 92% over two steps). R_f (50% EtOAc/Hexane) 0.23. ^{1}H NMR (300 MHz, DMSO-d_6) δ 7.51 – 7.47 (m, 2H, H^{1,3}), 7.49 (d, J = 8.0 Hz, 2H, H^7), 7.25 (d, J = 8.0 Hz, 2H, H^6), 6.97 (d, J = 7.8 Hz, 1H, H^4), 5.01 (s, 2H, H^8), 4.88 (d, J = 5.9 Hz, 2H, H^5), 2.69 (s, 3H, H^2). LC-MS (APCI$^+$/ESI): found m/z = 295.1 [M+H]$^+$ (cal. For $C_{14}H_{15}FN_2O_2S$, 294.08). Purity: 98%, t_R = 0.189 min.

Methyl 3-amino-4-((4-fluorobenzyl)amino)benzoate (163c)

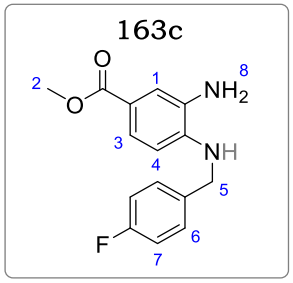

Obtained from methyl 4-fluoro-3-nitrobenzoate (0.250 g, 1.26 mmol) and 4-fluorobenzylamine (0.188 g, 1.50 mmol), as a brown solid (0.310 g, 90% over two steps). R_f (50% EtOAc/Hexane) 0.28. ^{1}H NMR (300 MHz, DMSO-d_6) δ 8.10 – 8.01 (m, 2H, H^{1,3}), 7.87 (d, J = 8.3 Hz, 2H, H^7), 7.38 (d, J = 8.3 Hz, 2H, H^6), 7.08 (d, J = 7.9 Hz, 1H, H^4), 4.99 (s, 2H, H^8), 4.85 (d, J = 6.1 Hz, 2H, H^5), 3.85 (s, 3H, H^2). LC-MS (APCI$^+$/ESI): found m/z = 275.1 [M+H]$^+$ (cal. For $C_{15}H_{15}FN_2O_2$, 274.11). Purity: 98%, t_R = 0.201 min.

N1-(cyclopropyl methyl)benzene-1,2-diamine (163d)

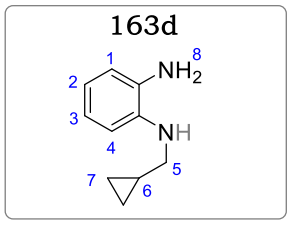

Obtained from 1-fluoro-2-nitrobenzene (0.250 g, 1.76 mmol) and cyclopropylmethanamine (0.150 g, 2.11 mmol), as a brown solid (0.272 g, 95% over two steps). R_f (50% EtOAc/Hexane) 0.24. ^{1}H NMR (300 MHz, DMSO) δ 7.01 (dd, J = 8.2, 1.1 Hz, 1H, H^1), 6.32 (dd, J = 8.0, 1.5 Hz, 1H, H^4), 6.18 – 6.10 (m, 2H, H^{2,3}), 5.10 (s, 2H, H^8), 4.91 (d, J = 6.0 Hz, 2H, H^5), 3.10 – 3.05 (m, 1H, H^6), 1.81 – 1.74 (m, 4H, H^7). LC-MS (APCI$^+$/ESI): found m/z = 163.1 [M+H]$^+$ (cal. For $C_{10}H14N_2$, 162.12). Purity: 98%, t_R = 0.258 min.

General Procedure 8: Synthesis of 2-chlorobenzimidazoles *via* CDI ring closure, followed by $POCl_3$ chlorination

Step1. **CDI Closure**: A mixture of either commercially obtained (**123a–123c**) or synthesized benzene-1,2-diamine precursors (**167a–167d**), carbonyl diimidazole, CDI (1.5 equiv) and catalytic amounts of DMAP (1.0 mol%) was dissolved in dry THF (10 ml), and the resulting mixture stirred at 22 °C for 2 – 12 hr. After completion (monitored *via* TLC), the solvent was evaporated *in vacuo* and water (30 ml) added to the resulting residue.

Benzimidazol-2-one products were obtained quantitatively, after filtering and subsequent oven drying.

Step2. **$POCl_3$ Chlorination**: Crude 245enzimidazole-2-one products (1.0 equiv) were treated with $POCl_3$ (5.0 equiv) in a seal tube and stirred at 110 °C for 12 h. The reaction mixture was then cooled to room temperature (22 °C), and excess $POCl_3$ evaporated under reduced pressure. The residue was then taken up in EtOAc (20 ml) and neutralized with 15% NaOH under ice cooling (0 °C) while stirring. After separation, the aqueous phase was further extracted with EtOAc (3 × 20 ml). The combined organic extracts were then washed with brine solution (10 ml), dried over anhydrous Na_2SO_4 and solvent evaporated *in vacuo*. Pure products were obtained after flash chromatography using 20 – 50% EtOAc/Hexanes as eluent.

2-chloro-5,6-difluoro-1H-benzo[d]imidazole (124h)

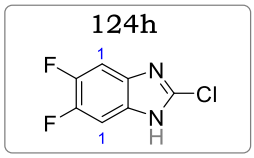

Obtained from 4,5-difluorobenzene-1,2-diamine, **123a** (0.250g, 1.73 mmol) as a reddish solid (0.278 g, 84%). R_f(5% MeOH/DCM), 0.76. ^{1}H NMR (300 MHz, Methanol-d_4) δ 7.54 (d, J = 6.8 Hz, 2H, H^1). LC-MS (APCI$^+$/ESI): found m/z = 189.0, 191.0 $[M+H]^+$ (cal. For $C_7H_3ClF_2N_2$, 188.00, 189.99). Purity: 98%, t_R = 2.632 min.

2,5,6-trichloro-1H-benzo[d]imidazole (124i)

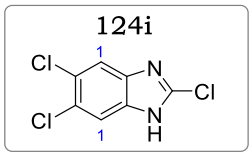

Obtained from 4,5-dichlorobenzene-1,2-diamine, **123b** (0.250g, 1.41 mmol) as a light green solid (0.215 g, 69%). R_f (5% MeOH/DCM), 0.81. ^{1}H NMR (300 MHz, Methanol-d_4) δ 7.51 (s, 2H, H^1). LC-MS (APCI$^+$/ESI): found m/z = 221.0, 223.0 $[M+H]^+$ (cal. For $C_7H_3ClF_2N_2$, 219.94, 221.93). Purity: 97%, t_R = 2.687 min.

2-chloro-5,6-dimethyl-1H-benzo[d]imidazole (124j)

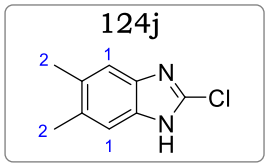

Obtained from 4,5-dimethylbenzene-1,2-diamine, **123c** (0.250g, 1.83 mmol) as a brown solid (0.259 g, 77%). R_f(5% MeOH/DCM), 0.48. ^{1}H NMR (300 MHz, Methanol-d_4) δ 7.23 (s, 2H, H^1), 2.68 (s, 6H, H^2). LC-MS (APCI$^+$/ESI): found m/z = 181.0, 183.0 $[M+H]^+$ (cal. For $C_9H_9ClN_2$, 180.05, 182.04). Purity: 97%, t_R = 2.568 min.

2-chloro-1-(cyclobutyl methyl)-1H-benzo[d]imidazole (165a)

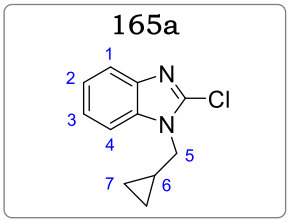

Obtained from **163d** (0.200 g, 1.22 mmol) as a white solid (0.232 g, 92%). R_f (4% MeOH/DCM), 0.63. ^{1}H NMR (400 MHz, DMSO-d_6) δ 7.44 (dd, J = 8.1, 1.5 Hz, 1H, H^1), 7.28 (dd, J = 8.0, 1.5 Hz, 1H, H^4), 6.80 (ddd, J = 8.1, 7.0, 1.0 Hz, 1H, H^2), 6.71 (ddd, J = 8.0, 7.0, 1.1, 1H, H^3), 4.80 (d, J = 6.8 Hz, 1H, H^5), 3.11 – 3.08 (m, 1H, H^6), 1.92 – 1.79 (m, 4H, H^7). LC-MS (APCI$^+$/ESI): found m/z = 207.1 [M+H]$^+$ (cal. For $C_{11}H_{11}ClN_2$, 206.06). Purity: 98%, t_R = 2.501 min.

2-chloro-1-(4-fluorobenzyl)-1H-benzo[d]imidazole-5-carbonitrile (165u)

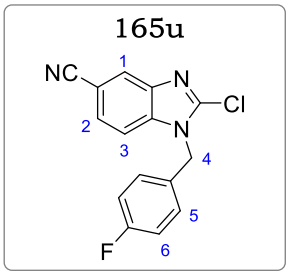

Obtained from **163a** (0.250 g, 1.03 mmol) as a pale yellow solid (0.206 g, 69% over two steps). R_f(5% MeOH/DCM) 0.48. ^{1}H NMR (300 MHz, Methanol-d_4) δ 8.03 (d, J = 0.9 Hz, 1H, H^1), 7.91 (dd, J = 8.0, 0.9 Hz, 1H, H^2), 7.60 (d, J = 8.2 Hz, H^6), 7.45 (d, J = 8.2 Hz, 2H, H^5), 7.29 (d, J = 8.0 Hz, 1H, H^3), 5.60 (s, 2H, H^4). LC-MS (APCI$^+$/ESI): found m/z = 286.0, 288.0 [M+H]$^+$ (cal. For $C_{15}H_9ClFN_3$, 285.05, 287.04). Purity: 98%, t_R = 0.213 min.

2-chloro-1-(4-fluorobenzyl)-5-(methylsulfonyl)-1H-benzo[d]imidazole (165v)

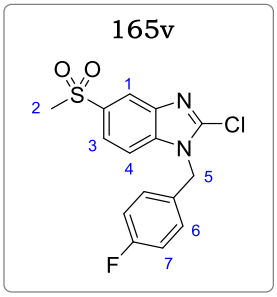

Obtained from **163b** (0.250 g, 0.85 mmol) as a white solid (0.208 g, 72% over two steps). R_f(5% MeOH/DCM) 0.42. ^{1}H NMR (300 MHz, Methanol-d_4) δ 7.93 – 7.86 (m, 2H, H^{1,3}), 7.58 (d, J = 8.1 Hz, H^7), 7.49 (d, J = 8.1 Hz, 2H, H^6), 7.33 (d, J = 7.8 Hz, 1H, H^4), 5.59 (s, 2H, H^5), 2.81 (s, 3H, H^2). LC-MS (APCI$^+$/ESI): found m/z = 339.0, 341.0 [M+H]$^+$ (cal. for $C_{15}H_{12}ClFN_2O_2S$, 338.03, 340.03). Purity: 98%, t_R = 0.198 min.

Methyl 2-chloro-1-(4-fluorobenzyl)-1H-benzo[d]imidazole-5-carboxylate (165w)

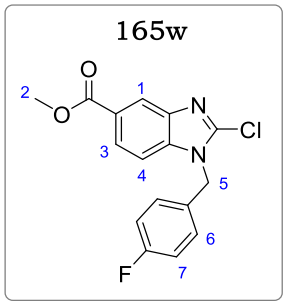

Obtained from **163c** (0.250 g, 0.91 mmol) as a white solid (0.219 g, 75% over two steps). R_f(5% MeOH/DCM) 0.39. ^{1}H NMR (300 MHz, Methanol-d_4) δ 7.89 – 7.85 (m, 2H, H^{1,3}), 7.66 (d, J = 8.3 Hz, H^7), 7.43 (d, J = 8.3 Hz, 2H, H^6), 7.29 (d, J = 8.0 Hz, 1H, H^4), 5.60 (s, 2H, H^5), 2.89 (s, 3H, H^2). LC-MS (APCI$^+$/ESI): found m/z = 319.0, 321.0 [M+H]$^+$ (cal. for $C_{16}H_{12}ClFN_2O_2$, 318.06, 320.05). Purity: 98%, t_R = 0.188 min.

General Procedure 9: N-alkylation of 2-chlorobenzimidazoles

A mixture of 2-chlorobenzimidazole, or **124h** – **124j** (1.0 equiv), alkyl halide (1.2 equiv) and K_2CO_3 (2.0 equiv) was either refluxed at 60 °C or stirred at room temperature (15 – 22 °C) in acetone for 2 – 12 hours. After completion (monitored *via* TLC), the solvent was removed *in vacuo*. Water was added to the residue, followed by extracting with DCM (×3). Combined organic layers were washed with brine (×3), dried over anhydrous Na_2SO_4, and the solvent evaporated *in vacuo* to give crude residue, which was triturated with *n*-pentane to afford the pure products.

2-Chloro-1-methyl-1H-benzo[*d*]imidazole (12b).

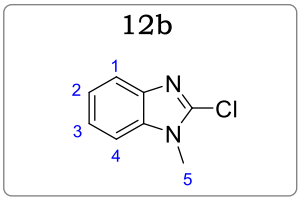

Obtained from 2-chlorobenzimidazole (15.0 g, 98.3 mmol) and methyl iodide (7.35 ml, 118 mmol), as a yellow solid (15.8 g, 96%). R_f(5% MeOH/DCM) 0.85. ^{1}H NMR (600 MHz, Methanol-d_4) δ 7.57 (dd, J = 8.5, 1.1 Hz, 1H, H^1), 7.47 (dd, J = 8.1, 1.1 Hz, 1H, H^4), 7.33 (ddd, J = 8.5, 7.3, 1.1 Hz, 1H, H^2), 7.28 (ddd, J = 8.1, 7.3, 1.2 Hz, 1H, H^3), 3.82 (s, 3H, H^5). LC-MS (APCI$^+$/ESI): found m/z = 167.0, 169.1 [M – H]$^-$ (cal. for $C_8H_7ClN_2$, 166.03, 168.03). Purity: 99%, t_R = 2.474 min.

2-Chloro-1-isopropyl-1H-benzo[*d*]imidazole (12c)

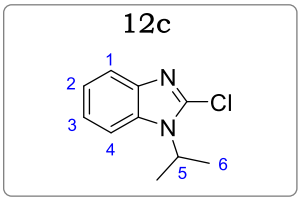

Obtained from 2-chlorobenzimidazole (0.400 g, 2.62 mmol) and 2-iodopropane (320 µl, 3.14 mmol), as a light/pale green solid (0.436 g, 85%). R_f(5% MeOH/DCM) 0.81. ^{1}H NMR (600 MHz, Methanol-d_4) δ 7.68 (dd, J = 8.1, 1.4 Hz, 1H, H^1), 7.58 (dd, J = 7.7, 1.5 Hz, 1H, H^4), 7.30 (ddd, J = 8.1, 7.3, 1.4 Hz, 1H, H^2), 7.26 (ddd, J = 7.8, 7.2, 1.3 Hz, 1H, H^3), 5.00 (sept, J = 7.0 Hz, 1H, H^5), 1.65 (d, J = 7.0 Hz, 6H, H^6). LC-MS (APCI$^+$/ESI): found m/z = 195.1, 197.1 [M – H]$^-$ (cal. for $C_{10}H_{11}ClN_2$, 194.06, 196.04). Purity: 99%, t_R = 2.690 min.

4-((2-chloro-1-benzo[*d*]imidazol-1-yl) methyl)benzonitrile (12d)

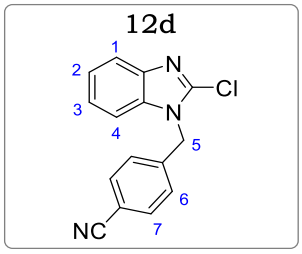

Obtained from 2-chlorobenzimidazole (7.00 g, 45.8 mmol) and 4-(bromomethyl)benzonitrile (10.8 g, 55.1 mmol), as a white crystalline solid (12.1 g, 98%). R_f (5% MeOH/DCM) 0.65. ^{1}H NMR (400 MHz, Methanol-d_4) δ 7.68 (d, J = 8.4 Hz, 2H, H^7), 7.63 (dd, J = 6.0, 0.8 Hz, 1H, H^1), 7.39 (dd, J = 6.5, 1.0 Hz, 1H, H^4), 7.34 (d, J = 8.4 Hz, 2H, H^6), 7.31 – 7.27 (m, 2H, H^{2,3}), 5.59 (s, 2H, H^5). LC-MS (APCI$^+$/ESI): found m/z = 267.9, 269.9 [M+H]$^+$ (cal. for $C_{15}H_{10}ClN_3$, 267.06, 269.05). Purity: 99%, t_R = 2.505 min.

2-chloro-5,6-difluoro-1-methyl-1H-benzo[d]imidazole (125h)

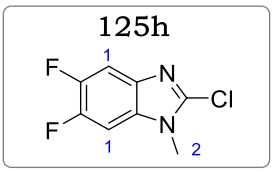

Obtained from **124h** (0.250 g, 1.32 mmol) and methyl iodide (99 µl, 1.58 mmol), as a pale/light green solid (0.212 g, 79%). R_f (5% MeOH/DCM), 0.93. ^{1}H NMR (400 MHz, Methanol-d_4) δ 7.42 (dd, J = 7.4, 5.3 Hz, 1H, H^1), 7.27 (dd, J = 7.5, 5.5 Hz, 1H, H^2), 3.83 (s, 3H, H^3). LC-MS (APCI$^+$/ESI): found m/z = 203.0, 205.0 [M+H]$^+$ (cal. for $C_8H_5ClF_2N_2$, 202.01, 204.01). Purity: 99%, t_R = 2.587 min.

2,5,6-trichloro-1-methyl-1H-benzo[d]imidazole (125i)

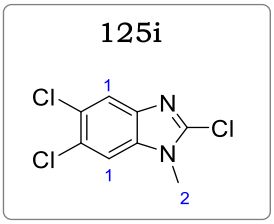

Obtained from **124i** (0.200 g, 0.90 mmol) and methyl iodide (67 µl, 1.08 mmol), as a light purple solid (0.147 g, 69%). R_f (5% MeOH/DCM), 0.90. ^{1}H NMR (400 MHz, Methanol-d_4) δ 7.51 (s, 1H, H^1), 7.38 (s, 1H, H^2), 3.83 (s, 3H, H^3). LC-MS (APCI$^+$/ESI): found m/z = 234.9, 236.9 [M+H]$^+$ (cal. for $C_8H_5Cl_3N_2$, 233.95, 235.95). Purity: 98%, t_R = 2.501min.

2-chloro-1,5,6-trimethyl-1H-benzo[d]imidazole (125j)

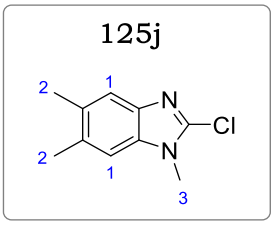

Obtained from **124j** (0.240 g, 1.31 mmol) and methyl iodide (99 µl, 1.58 mmol), as a pale yellow solid (0.195 g, 76%). R_f (5% MeOH/DCM), 0.83. ^{1}H NMR (400 MHz, Methanol-d_4) δ 7.28 (s, 1H, H^1), 7.19 (s, 1H, H^4), 3.83 (s, 3H, H^5), 2.44 (s, 3H, H^2), 2.40 (s, 3H, H^3). LC-MS (APCI$^+$/ESI): found m/z = 195.0, 197.0 [M+H]$^+$ (cal. For $C_{10}H_{11}ClN_2$, 194.06, 196.06). Purity: 97%, t_R = 2.444 min.

2-chloro-1-(cyclobutyl methyl)-1H-benzo[d]imidazole (165a)

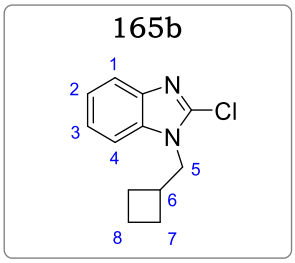

Obtained from 2-chlorobenzimidazole (0.150 g, 0.98 mmol) and (bromomethyl)cyclobutane (0.175 g, 1.18 mmol) as a white solid (0.201 g, 93%). R_f (6% MeOH/DCM), 0.80. ^{1}H NMR (400 MHz, DMSO-d_6) δ 7.59 (dd, J = 7.9, 1.3 Hz, 1H, H^1), 7.32 (dd, J = 8.0, 1.5 Hz, 1H, H^4), 6.83 – 6.70 (m, 2H, H^{2,3}), 4.89 (d, J = 6.2 Hz, 1H, H^5), 3.08 (m, 1H, H^6), 1.89 – 1.73 (m, 6H, H^{7,8}). LC-MS (APCI$^+$/ESI): found m/z = 221.1 [M+H]$^+$ (cal. For $C_{12}H_{13}ClN_2$, 220.08). Purity: 98%, t_R = 2.593 min.

2-chloro-1-(cyclopentyl methyl)-1H-benzo[d]imidazole (165c)

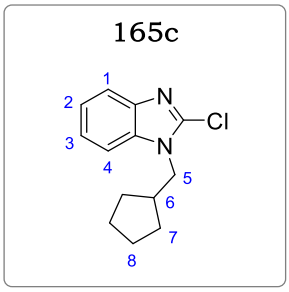

Obtained from 2-chlorobenzimidazole (0.150 g, 0.98 mmol) and (bromomethyl)cyclopentane (0.192 g, 1.18 mmol) as a white solid (0.213 g, 93%). R_f (6% MeOH/DCM), 0.67. ^{1}H NMR (300 MHz, DMSO-d_6) δ 7.66 (dd, J = 8.1, 1.1 Hz, 1H, H^1), 7.38 (dd, J = 8.0, 1.5 Hz, 1H, H^4), 6.88 – 6.72 (m, 2H, H^{2,3}), 4.28 (d, J = 6.0 Hz, 1H, H^5), 2.94 – 2.89 (m, 1H, H^6), 1.75 – 1.69 (m, 4H, H^7), 1.55 – 1.49 (m, 4H, H^8). LC-MS (APCI$^+$/ESI): found m/z = 235.1 [M+H]$^+$ (cal. For $C_{13}H_{15}ClN_2$, 234.09). Purity: 98%, t_R = 2.588 min.

2-chloro-1-(cyclohexyl methyl)-1H-benzo[d]imidazole (165d)

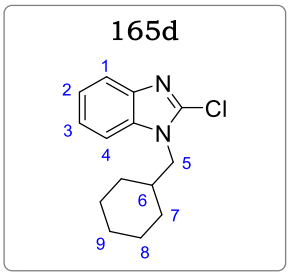

Obtained from 2-chlorobenzimidazole (0.150 g, 0.98 mmol) and (bromomethyl)cyclohexane (0.208 g, 1.18 mmol) as a White solid (0.233 g, 96%). R_f (6% MeOH/DCM), 0.65. ^{1}H NMR (300 MHz, DMSO-d_6) δ 7.54 (dd, J = 7.9, 1.1 Hz, 1H, H^1), 7.35 (dd, J = 8.0, 1.2 Hz, 1H, H^4), 6.88 – 6.75 (m, 2H, H^{2,3}), 4.91 (d, J = 5.8 Hz, 1H, H^5), 2.88 – 2.85 (m, 1H, H^6), 1.85 – 1.79 (m, 4H, H^7), 1.66 – 1.61 (m, 5H, H^{8,9}). LC-MS (APCI$^+$/ESI): found m/z = 249.1 [M+H]$^+$ (cal. For $C_{14}H_{17}ClN_2$, 248.11). Purity: 98%, t_R = 2.597 min.

1-benzyl-2-chloro-1H-benzo[d]imidazole (165e)

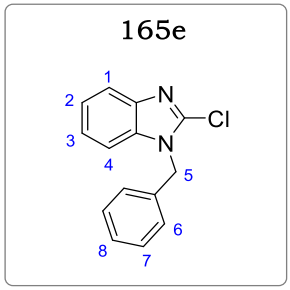

Obtained from 2-chlorobenzimidazole (0.200 g, 1.31 mmol) and (chloromethyl)benzene (0.200 g, 1.57 mmol) as a white crystalline solid (0.314 g, 91%). R_f (4% MeOH/DCM) 0.61. ^{1}H NMR (300 MHz, Methanol-d_4) δ 7.72 (dd, J = 8.0, 1.5 Hz, 1H, H^1), 7.61 – 7.48 (m, 4H, H^{4,7,8}), 7.36 - 7.22 (m, 4H, H^{2,3,6}), 7.34 (d, J = 8.4 Hz, 2H, H^6), 7.31 – 7.27 (m, 2H, H^{2,3}), 5.61 (s, 2H, H^5). LC-MS (APCI$^+$/ESI): found m/z = 243.0, 245.0 [M+H]$^+$ (cal. For $C_{14}H_{11}ClN_2$, 242.06, 264.06). Purity: 99%, t_R = 2.508 min.

2-chloro-1-(2-fluorobenzyl)-1H-benzo[d]imidazole (165f)

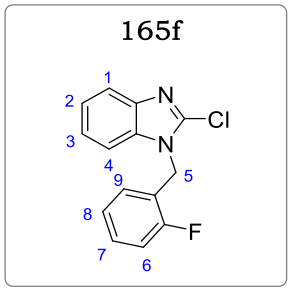

Obtained from 2-chlorobenzimidazole (0.200 g, 1.31 mmol) and 1-(bromomethyl)-2-fluorobenzene (0.296 g, 1.57 mmol) as a white crystalline solid (0.336 g, 98%). R_f (4% MeOH/DCM) 0.62. ^{1}H NMR (300 MHz, Methanol-d_4) δ 7.75 – 7.60 (m, 3H, H^{1,6,7}), 7.58 – 7.43 (m, 3H, H$^{4,8.9}$), 7.39 – 7.19 (m, 1H, H^{2,3}), 5.56 (s, 2H, H^5). LC-MS (APCI$^+$/ESI): found m/z = 261.0, 263.0 [M+H]$^+$ (cal. For $C_{14}H_{10}ClFN_2$, 260.05, 262.05). Purity: 99%, t_R = 2.587 min.

2-chloro-1-(3-fluorobenzyl)-1H-benzo[d]imidazole (165g)

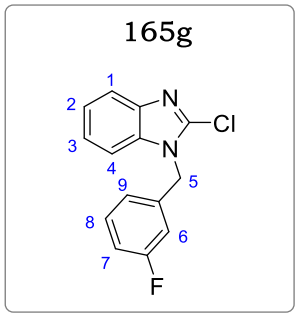

Obtained from 2-chlorobenzimidazole (0.200 g, 1.31 mmol) and 1-(bromomethyl)-3-fluorobenzene (0.296 g, 1.57 mmol) as a white solid (0.326 g, 95%). R_f (4% MeOH/DCM) 0.60. ^{1}H NMR (300 MHz, Methanol-d_4) δ 7.69 – 7.62 (m, 2H, H^{1,8}), 7.52 (dt, J = 7.5, 1.3 Hz, 1H, H^9), 7.49 – 7.42 (m, 2H, H^{4,7}), 7.36 – 7.20 (m, 1H, H^{2,3,6}), 5.60 (s, 2H, H^5). LC-MS (APCI$^+$/ESI): found m/z = 261.0, 263.0 [M+H]$^+$ (cal. For $C_{14}H_{10}ClFN_2$, 260.05, 262.05). Purity: 99%, t_R = 2.601 min.

2-chloro-1-(4-fluorobenzyl)-1H-benzo[d]imidazole (165h)

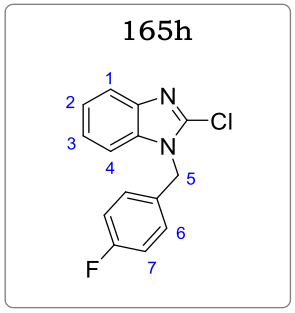

Obtained from 2-chlorobenzimidazole (3.00 g, 19.7 mmol) and 1-(bromomethyl)-4-fluorobenzene (4.46 g, 23.6 mmol) as a white solid (4.95 g, 97%). R_f(5% MeOH/DCM) 0.61. ^{1}H NMR (300 MHz, Methanol-d_4) δ 7.62 (d, J = 8.0 Hz, 2H, H^7), 7.55 (dd, J = 7.5, 0.8 Hz, 1H, H^1), 7.33 (dd, J = 7.0, 1.0 Hz, 1H, H^4), 7.25 (d, J = 8.0 Hz, 2H, H^6), 7.20 – 6.98 (m, 2H, H^{2,3}), 5.56 (s, 2H, H^5). LC-MS (APCI$^+$/ESI): found m/z = 261.0, 263.0 [M+H]$^+$ (cal. for $C_{15}H_{10}ClN_3$, 260.05, 262.05). Purity: 99%, t_R = 2.593 min.

2-chloro-1-(4-methoxybenzyl)-1H-benzo[d]imidazole (165i)

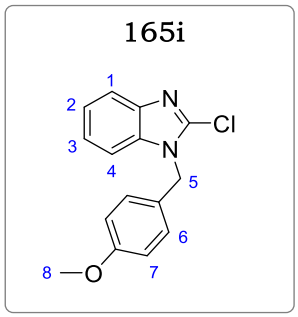

Obtained from 2-chlorobenzimidazole (0.200 g, 1.31 mmol) and 1-(bromomethyl)-4-methoxybenzene (0.316 g, 1.57 mmol) as a white solid (0.278 g, 90%). R_f (5% MeOH/DCM) 0.56. ^{1}H NMR (300 MHz, Methanol-d_4) δ 7.69 (d, J = 8.3 Hz, 2H, H^7), 7.58 (dd, J = 7.1, 1.1 Hz, 1H, H^1), 7.39 (dd, J = 7.0, 1.0 Hz, 1H, H^4), 7.30 (d, J = 8.4 Hz, 2H, H^6), 7.27 – 7.21 (m, 2H, H^{2,3}), 5.59 (s, 2H, H^5), 3.32 (s, 3H, H^8). LC-MS (APCI$^+$/ESI): found m/z = 273.1, 275.1 [M+H]$^+$ (cal. For $C_{15}H_{13}ClN_2O$, 272.07, 274.07). Purity: 99%, t_R = 2.495 min.

2-chloro-1-(4-(trifluoromethyl)benzyl)-1H-benzo[d]imidazole (165j)

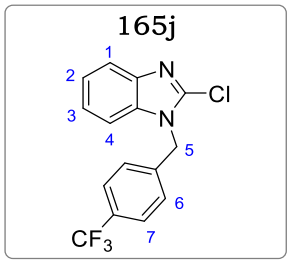

Obtained from 2-chlorobenzimidazole (0.200 g, 1.31 mmol) and 1-(bromomethyl)-4-methoxybenzene (0.316 g, 1.57 mmol) as a white solid (0.359 g, 98%). R_f(5% MeOH/DCM) 0.68. ^{1}H NMR (300 MHz, Methanol-d_4) δ 7.63 (d, J = 8.0 Hz, 2H, H^7), 7.52 (dd, J = 7.8, 1.2 Hz, 1H, H^1), 7.39 (dd, J = 7.9, 1.0 Hz, 1H, H^4), 7.30 (d, J = 8.0 Hz, 2H, H^6), 7.25 – 7.19 (m, 2H, H^{2,3}), 5.58 (s, 2H, H^5). LC-MS (APCI$^+$/ESI): found m/z = 311.0, 313.0 [M+H]$^+$ (cal. For $C_{15}H_{10}ClF_3N_2$, 310.05, 312.05). Purity: 99%, t_R = 2.598 min.

2-chloro-1-(4-(methylsulfonyl)benzyl)-1H-benzo[d]imidazole (165k)

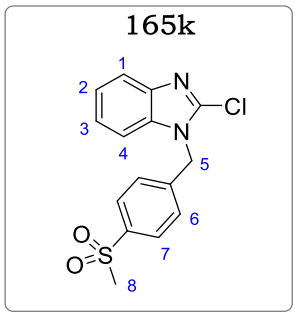

Obtained from 2-chlorobenzimidazole (0.200 g, 1.31 mmol) and 1-(bromomethyl)-4-(methylsulfonyl)benzene (0.391 g, 1.57 mmol) as a white solid (0.375 g, 89%). R_f(5% MeOH/DCM) 0.58. ^{1}H NMR (400 MHz, Methanol-d_4) δ 7.69 (d, J = 8.2 Hz, 2H, H^7), 7.49 (dd, J = 7.5, 1.0 Hz, 1H, H^1), 7.32 (d, J = 8.2 Hz, 2H, H^6), 7.26 (dd, J = 7.8, 1.3 Hz, 1H, H^4), 7.20 – 7.11 (m, 2H, H^{2,3}), 5.60 (s, 2H, H^5), 3.39 (s, 3H, H^8). LC-MS (APCI$^+$/ESI): found m/z = 321.0, 323.09 [M+H]$^+$ (cal. For $C_{15}H_{13}ClN_2O_2S$, 320.04, 322.04). Purity: 99%, t_R = 2.495 min.

4-((2-chloro-1H-benzo[d]imidazol-1-yl)methyl)benzene sulfonamide (165l)

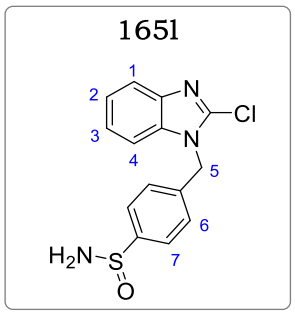

Obtained from 2-chlorobenzimidazole (0.200 g, 1.31 mmol) and 4-(bromomethyl)benzenesulfonamide (0.367 g, 1.57 mmol) as a white solid (0.341 g, 85%). R_f(5% MeOH/DCM) 0.53. ^{1}H NMR (300 MHz, Methanol-d_4) δ 7.75 (d, J = 8.0 Hz, 2H, H^7), 7.53 (dd, J = 7.2, 1.0 Hz, 1H, H^1), 7.42 (d, J = 8.0 Hz, 2H, H^6), 7.29 (dd, J = 7.5, 1.3 Hz, 1H, H^4), 7.22 – 7.15 (m, 2H, H^{2,3}), 5.58 (s, 2H, H^5). LC-MS (APCI$^+$/ESI): found m/z = 306.0, 308.0 [M+H]$^+$ (cal. for $C_{14}H_{12}ClN_3OS$, 305.04, 307.04). Purity: 99%, t_R = 2.435 min.

2-chloro-1-(4-nitrobenzyl)-1H-benzo[d]imidazole (165m)

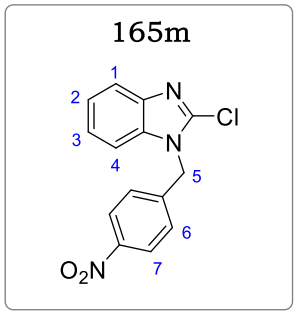

Obtained from 2-chlorobenzimidazole (0.400 g, 2.62 mmol) and 1-(bromomethyl)-4-nitrobenzene (0.680 g, 3.14 mmol) as a pale-yellow solid (0.734 g, 97%). R_f(5% MeOH/DCM) 0.70. ^{1}H NMR (300 MHz, Methanol-d_4) δ 7.73 (d, J = 7.9 Hz, 2H, H^7), 7.58 (dd, J = 6.9, 1.0 Hz, 1H, H^1), 7.40 (dd, J = 6.5, 1.0 Hz, 1H, H^4), 7.30 (d, J = 7.9 Hz, 2H, H^6), 7.28 – 7.20 (m, 2H, H^{2,3}), 5.60 (s, 2H, H^5). LC-MS (APCI$^+$/ESI): found m/z = 287.9, 289.9 [M+H]$^+$ (cal. for $C_{14}H_{10}ClN_3O_2$, 287.05, 289.05). Purity: 99%, t_R = 2.558 min.

Methyl 4-((2-chloro-1H-benzo[d]imidazol-1-yl)methyl)benzoate (165o)

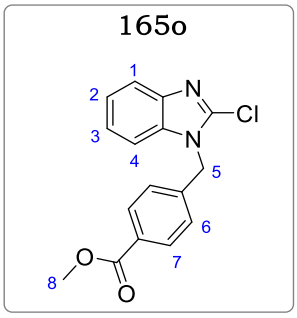

Obtained from 2-chlorobenzimidazole (0.400 g, 2.62 mmol) and methyl 4-(bromomethyl)benzoate (0.720 g, 3.14 mmol) as a white solid (0.774 g, 98%). R_f (5% MeOH/DCM) 0.60. ^{1}H NMR (400 MHz, Methanol-d_4) δ 7.73 (d, J = 8.2 Hz, 2H, H^7), 7.66 (dd, J = 6.9, 1.3 Hz, 1H, H^1), 7.41 (dd, J = 6.5, 1.1 Hz, 1H, H^4), 7.35 (d, J = 8.2 Hz, 2H, H^6), 7.30 – 7.25 (m, 2H, H^{2,3}), 5.58 (s, 2H, H^5), 3.89 (s, 3H, H^8). LC-MS (APCI$^+$/ESI): found m/z = 301.1, 303.1 [M+H]$^+$ (cal. for $C_{16}H_{13}ClN_3O_2$, 300.07, 302.06). Purity: 99%, t_R = 2.515 min.

2-chloro-1-((6-methylpyridin-2-yl)methyl)-1H-benzo[d]imidazole (165r)

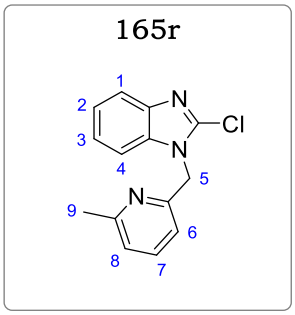

Obtained from 2-chlorobenzimidazole (0.200 g, 1.31 mmol) and 2-(bromomethyl)-6-methylpyridine hydrobromide (0.420 g, 1.57 mmol) as a dark purple solid (0.281 g, 83%). R_f(5% MeOH/DCM) 0.52. ^{1}H NMR (300 MHz, Methanol-d_4) δ 7.53 (t, J = 8.0 Hz, 1H, H^7), 7.47 (dd, J = 7.2, 1.3 Hz, 1H, H^1), 7.39 (dd, J = 6.8, 1.0 Hz, 1H, H^4), 7.30 – 7.18 (m, 4H, H^{2,3,6,8}), 5.60 (s, 2H, H^5), 2.35 (s, 3H, H^9). LC-MS (APCI$^+$/ESI): found m/z = 258.0, 260.0 [M+H]$^+$ (cal. For $C_{14}H_{12}ClN_3$, 257.07, 259.07). Purity: 99%, t_R = 2.487 min.

2-chloro-1-((6-methylpyridin-3-yl)methyl)-1H-benzo[d]imidazole (165s)

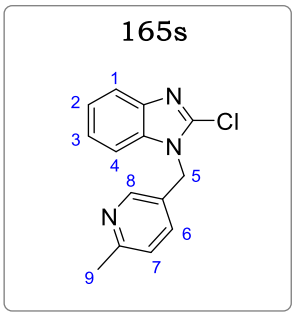

Obtained from 2-chlorobenzimidazole (0.200 g, 1.31 mmol) and 5-(bromomethyl)-2-methylpyridine hydrobromide (0.420 g, 1.57 mmol) as a purple solid (0.271 g, 80%). R_f(5% MeOH/DCM) 0.50. ^{1}H NMR (300 MHz, Methanol-d_4) δ 8.21 (d, J = 1.9 Hz, 1H, H^8), 7.88 (dd, J = 8.0, 1.9 Hz, 1H, H^6), 7.49 - 7.42 (m, 1H, H^{1,7}), 7.37 (dd, J = 7.1, 1.2 Hz, 1H, H^4), 7.29 – 7.22 (m, 4H, H^{2,3}), 5.58 (s, 2H, H^5), 2.36 (s, 3H, H^9). LC-MS (APCI$^+$/ESI): found m/z = 258.0, 260.0 [M+H]$^+$ (cal. For $C_{14}H_{12}ClN_3$, 257.07, 259.07). Purity: 98%, t_R = 2.490 min.

2-chloro-1-((6-(trifluoromethyl)253yridine-3-yl)methyl)-1H-benzo[d]imidazole (165t)

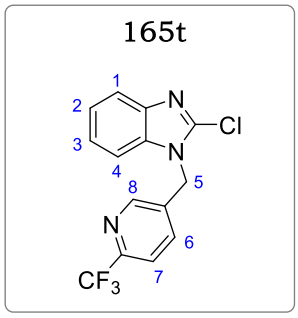

Obtained from 2-chlorobenzimidazole (0.200 g, 1.31 mmol) and 5-(bromomethyl)-2-(trifluoromethyl)pyridine (0.376 g, 1.57 mmol) as a white solid (0.402 g, 98%). R_f(5% MeOH/DCM) 0.56. ^{1}H NMR (300 MHz, Methanol-d_4) δ 8.12 (d, J = 1.3 Hz, 1H, H^8), 7.92 (dd, J = 7.5, 1.3 Hz, 1H, H^6), 7.53 – 7.50 (m, 1H, H^{1,7}), 7.41 (dd, J = 7.5, 1.3 Hz, 1H, H^4), 7.30 – 7.24 (m, 4H, H^{2,3}), 5.60 (s, 2H, H^5). LC-MS (APCI$^+$/ESI): found m/z = 312.0, 314.0 [M+H]$^+$ (cal. For $C_{14}H_9ClF_3N_3$, 311.04, 313.04). Purity: 99%, t_R = 2.532 min.

N-(4-((2-chloro-1H-benzo[d]imidazol-1-yl)methyl)phenyl)acetamide (165n)

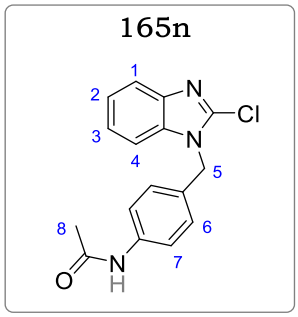

Compound **165m** (0.400g, 1.38 mmol) was subjected to nitro group reduction following general procedure 2, step 2. After which, the amine product **165m'** (0.356 g, 1.38 mmol) was dissolved in dry THF (5 ml) and cooled to 0 °C and TEA (1.5 equiv) added. While stirring, acetyl chloride (1.2 equiv) was added dropwise. The reaction was quenched with water (5 ml) and the resulting mixture extracted with EtOAc (3 × 15 ml). Combined EtOAc phase was washed with brine and dried over anhydrous Na_2SO_4. The solvent was evaporated in vacuo, to obtain the product as a light brown solid (0.264 g, 98%). R_f(5% MeOH/DCM) 0.42. ^{1}H NMR (300 MHz, Methanol-d_4) δ 7.65 – 7.59 (m, 2H, H^{1,7}), 7.42 (dd, J = 6.9, 1.0 Hz, 1H, H^4), 7.31 (d, J = 8.2 Hz, 2H, H^6), 7.29 – 7.22 (m, 2H, H^{2,3}), 5.60 (s, 2H, H^5), 2.19 (s, 3H, H^8). LC-MS (APCI$^+$/ESI): found m/z = 300.1, 302.1 [M+H]$^+$ (cal. for $C_{16}H_{14}ClN_3O$, 299.08, 301.08). Purity: 99%, t_R = 2.450 min.

4-((2-chloro-1H-benzo[d]imidazol-1-yl)methyl)benzoic acid (165p)

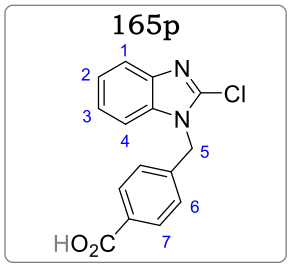

Compound **165o** (0.400 g, 1.31 mmol) was dissolved in methanol (15 ml) and 2M KOH added (3.3 ml, 6.55 mmol). The resulting mixture was refluxed at 79 °C for 2 hr. After completion, the solution was cooled to 0 °C, and while stirring the mixture was acidified with 3N HCl to pH 2. The carboxylic acid precipitate was filtered and dried as an off white solid (0.378 g, 98%). R_f (5% MeOH/DCM) ~0.05. ^{1}H NMR (300 MHz, Methanol-d_4) δ 7.78 (d, J = 8.2 Hz, 2H, H^7), 7.61 (dd, J = 8.3, 1.5 Hz, 1H, H^1), 7.42 (dd, J = 7.1, 1.3 Hz, 1H, H^4), 7.32 (d, J = 8.2 Hz, 2H, H^6), 7.30 – 7.25 (m, 2H, H^{2,3}), 5.59 (s, 2H, H^5), 4.00 (s, 3H, H^8). LC-MS (APCI$^+$/ESI): found

m/z = 287.1, 289.1 $[M+H]^+$ (cal. for $C_{15}H_{11}ClN_2O_2$, 286.05, 288.05). Purity: 99%, t_R = 0.289 min.

4-((2-chloro-1H-benzo[d]imidazol-1-yl)methyl)-N-methyl benzamide (165q)

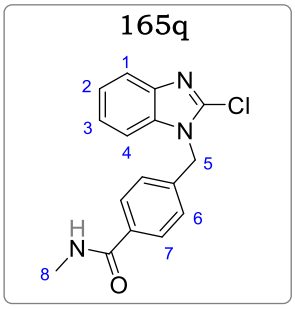

Following EDCI/DMAP amide coupling in general procedure 3, obtained from**165p** (0.200, 0.69 mmol) and methylamine (2M in THF, 1.2 equiv) as a brown solid (0.125 g, 98%). R_f (5% MeOH/DCM) 0.40. ^{1}H NMR (300 MHz, Methanol-d_4) δ 7.69 – 7.55 (m, 2H, $H^{1,7}$), 7.39 (dd, *J* = 7.1, 1.0 Hz, 1H, H^4), 7.32 (d, *J* = 8.4 Hz, 2H, H^6), 7.28 – 7.22 (m, 2H, $H^{2,3}$), 5.58 (s, 2H, H^5), 4.02 (s, 3H, H^8). LC-MS (APCI$^+$/ESI): found *m/z* = 300.1, 302.1 $[M+H]^+$ (cal. for $C_{16}H_{14}ClN_3O$, 299.08, 301.08). Purity: 99%, t_R = 2.461 min.

General Procedure 10: Preparation of Meldrum acid Enamine Intermediates

A solution of 2,2-dimethyl-1,3-dioxane-4,6-dione (1.5 equiv) in triethyl orthoformate (5 equiv) was refluxed at 148 °C for 1 h. The mixture was then cooled to room temperature and an appropriate 3-substituted aniline (1.0 equiv) was added to the solution. The mixture was further refluxed at 148 °C for 2 h, then cooled to room temperature (25 °C). The precipitates were filtered and washed with diethyl ether to give pure products.

5-(((3-fluorophenyl)amino)methylene)-2,2-dimethyl-1,3-dioxane-4,6-dione (198a)

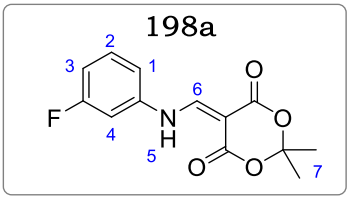

Obtained from 3-fluoroaniline (1.00 g, 9.0 mmol) as a yellow solid (2.26 g, 95%). R_f(20% EtOAc/Hexane), 0.45. ^{1}H NMR (400 MHz, DMSO-d_6) δ 11.25 (d, *J* = 14.4 Hz, 1H, H^5), 8.59 (d, *J* = 14.4 Hz, 1H, H^6), 7.58 (d, *J* = 10.8 Hz, 1H, H^4), 7.51 – 7.37 (m, 2H, $H^{1,3}$), 7.09 (td, *J* = 8.1, 2.3 Hz, 1H, H^2), 1.68 (s, 6H). LC-MS (APCI$^+$/ESI): found m/z = 266.1 $[M+H]^+$ (cal. For $C_{13}H_{12}FNO_4$, 265.08). Purity: 98%, t_R = 2.468 min.

5-(((3-bromophenyl)amino)methylene)-2,2-dimethyl-1,3-dioxane-4,6-dione (198b)

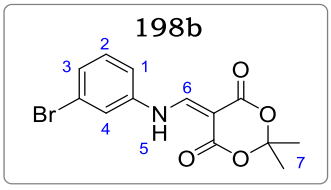

Obtained from 3-bromoaniline (1.00 g, 5.81 mmol) as a yellow crystalline solid (1.82 g, 98%). R_f(20% EtOAc/Hexane), 0.38. ^{1}H NMR (400 MHz, DMSO-d_6) δ 11.23 (d, *J* = 14.1 Hz, 1H, H^5), 8.57 (d, *J* = 14.1 Hz, 1H, H^6), 7.90 (t, *J* = 2.2 Hz, 1H, H^4), 7.58 (d, *J* = 8.0 Hz, 1H, H^1), 7.44 (d, *J* = 8.0 Hz, 1H, H^3), 7.37 (t, *J*

= 8.0 Hz, 1H, H^2), 1.67 (s, 6H, H^7). LC-MS (APCI$^+$/ESI): found m/z = 326.0, 328.0 $[M+H]^+$ (cal. For $C_{13}H_{12}BrNO_4$, 324.99, 326.99). Purity: 98%, t_R = 2.462 min.

2,2-dimethyl-5-(((3-(trifluoromethyl)phenyl)amino)methylene)-1,3-dioxane-4,6-dione (198c)

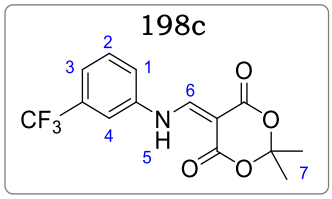

Obtained from 3-(trifluoromethyl)aniline (1.00 g, 6.21 mmol) as a brown solid (1.92 g, 98%). R_f(20% EtOAc/Hexane), 0.41. ^{1}H NMR (400 MHz, DMSO-d_6) δ 11.25 (d, J = 14.0 Hz, 1H, H^5), 8.57 (d, J = 14.0 Hz, 1H, H^6), 8.09 (dd, J = 2.0, 1.3 Hz, 1H, H^4), 7.92 – 7.81 (m, 1H, H^1), 7.69 (ddd, J = 7.8, 2.0, 1.5 Hz, 1H, H^3), 7.59 (dd, J = 7.9, 6.9 Hz, 1H, H^2),1.67 (s, 6H, H^7). LC-MS (APCI$^+$/ESI): found m/z = 316.1 $[M+H]^+$ (cal. For $C_{14}H_{12}F_3NO_4$, 315.07). Purity: 99%, t_R = 2.402 min.

3-(((2,2-dimethyl-4,6-dioxo-1,3-dioxan-5-ylidene)methyl) amino) benzonitrile (198d)

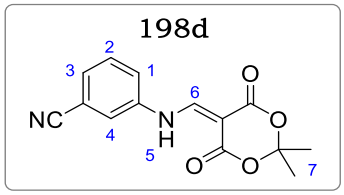

Obtained from 3-aminobenzonitrile (1.00 g, 8.46 mmol) as a yellow solid (2.21 g, 96%). R_f(20% EtOAc/Hexane), 0.25. ^{1}H NMR (400 MHz, DMSO-d_6) δ 11.30 (d, J = 14.3 Hz, 1H, H^5), 8.64 (d, J = 14.3 Hz, 1H, H^6), 8.16 (t, J = 1.9 Hz, 1H, H^4), 7.97 – 7.85 (m, 1H, H^1), 7.77 – 7.67 (m, 1H, H^3), 7.61 (t, J = 7.9 Hz, 1H, H^2), 1.68 (s, 6H, H^7). LC-MS (APCI$^+$/ESI): found m/z = 273.0 $[M+H]^+$ (cal. For $C_{14}H_{12}N_2O_4$, 272.08). Purity: 98%, t_R = 2.231 min.

2,2-dimethyl-5-(((3-(trifluoromethoxy)phenyl)amino)methylene)-1,3-dioxane-4,6-dione (198e)

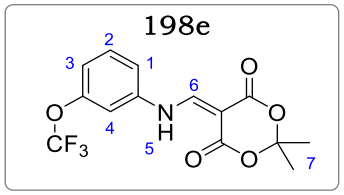

Obtained from 3-(trifluoromethoxy)aniline (1.00 g, 5.64 mmol) as a yellow solid (1.83 g, 98%). R_f(20% EtOAc/Hexane), 0.39. NMR (400 MHz, DMSO-d_6) δ 11.28 (d, J = 14.5 Hz, 1H, H^5), 8.61 (d, J = 14.5 Hz, 1H, H^6), 7.33 (t, J = 8.2 Hz, 1H, H^2), 7.18 (t, J = 2.1 Hz, 1H, H^4), 7.09 (dd, J = 8.2, 2.1 Hz, 1H, H^1), 6.89 (dd, J = 8.2, 2.1 Hz, 1H, H^3), 1.69 (s, 6H, H^7). LC-MS (APCI$^+$/ESI): found m/z = 332.1 $[M+H]^+$ (cal. For $C_{14}H_{12}F_3NO_5$, 331.07). Purity: 98%, t_R = 2.495 min.

5-(((3-methoxyphenyl)amino)methylene)-2,2-dimethyl-1,3-dioxane-4,6-dione (198f)

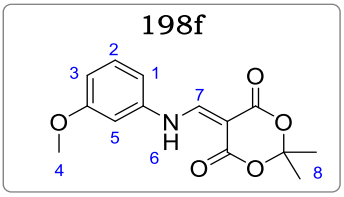

Obtained from 3-methoxyaniline (1.00 g, 8.12 mmol) as a yellow solid (2.09 g, 93%). R_f(20% EtOAc/Hexane), 0.30. NMR (400 MHz, DMSO-d_6) δ 11.21 (d, J = 14.5 Hz, 1H, H^6), 8.60 (d, J = 14.5 Hz, 1H, H^7), 7.33 (t, J = 8.3 Hz, 1H, H^2), 7.20 (t, J = 2.1 Hz, 1H, H^5), 7.11 (dd, J = 8.3, 2.1 Hz, 1H, H^1), 6.83 (dd, J = 8.3, 2.1 Hz, 1H, H^3), 3.80 (s, 3H, H^4), 1.67 (s, 6H, H^8). LC-MS (APCI$^+$/ESI): found m/z = 278.1 $[M+H]^+$ (cal. For $C_{14}H_{15}NO_5$, 277.10). Purity: 98%, t_R = 2.304 min.

2,2-dimethyl-5-(((3-nitrophenyl)amino)methylene)-1,3-dioxane-4,6-dione (198g)

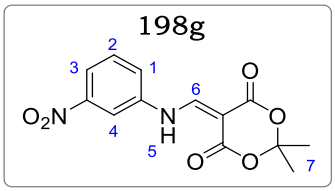

Obtained from 3-nitroaniline (1.00 g, 7.24 mmol) as a yellow solid (2.07 g, 98%). R_f(20% EtOAc/Hexane), 0.35. NMR (400 MHz, DMSO-d_6) δ 11.19 (d, J = 14.3 Hz, 1H, H^5), 8.59 (d, J = 14.3 Hz, 1H, H^6), 7.33 (t, J = 8.0 Hz, 1H, H^2), 7.26 (t, J = 1.9 Hz, 1H, H^4), 7.10 (dd, J = 8.0, 1.9 Hz, 1H, H^1), 6.93 (dd, J = 8.0, 1.8 Hz, 1H, H^3), 1.68 (s, 6H, H^7). LC-MS (APCI$^+$/ESI): found m/z = 293.1 $[M+H]^+$ (cal. for $C_{13}H_{12}N_2O_6$, 292.07). Purity: 98%, t_R = 2.300 min.

General Procedure 11: Preparation of 4-chloroquinoline intermediates

A mixture of Meldrum's acid enamine (**198a – j**) and diphenyl ether (10 ml) were irradiated under microwave at 225 °C for 5 min. Diethyl ether (10 ml) was added to the mixture, and the resulting precipitates were collected and washed with ether to give a mixture of 7- and 5-substututed quinolin-4-ols in quantitative yields.

Without purification nor characterization, these intermediates were suspended in dry toluene (5 ml) and $POCl_3$ (2 equiv) was added. The mixture was stirred for 2 h at 100 °C, then cooled to room temperature (23 °C). Excess $POCl_3$ was quenched by adding ice water (5 ml) and the resulting aqueous mixture was extracted with DCM (3 × 20 ml). The organic phase was dried over anhydrous Na_2SO_4, and the solvent was removed *in vacuo*. The 7-chloroquinoline products were separated by flash chromatography using 8 – 20% EtOAc/Hexane.

4-chloro-7-fluoroquinoline (201a)

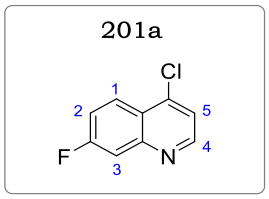

Obtained from **198a** (1.00 g, 3.77 mmol) as a white solid (0.504 g, 73%). R_f(20% EtOAc/Hexane), 0.41. ^{1}H NMR (400 MHz, DMSO-d_6) δ 8.85 (d, J = 4.2 Hz, 1H, H^4), 8.24 (dd, J = 9.5, 1.5 Hz, 1H, H^3), 7.85 (dd, J = 9.2, 2.2 Hz, 1H, H^1), 7.74 (d, J = 4.2 Hz, 1H, H^5), 7.72 – 7.65 (m, 1H, H^2). LC-MS (APCI$^+$/ESI): found m/z = 182.0, 184.0 $[M+H]^+$ (cal. For C_9H_5ClFN, 181.01, 183.00). Purity: 99%, t_R = 2.435 min.

7-bromo-4-chloroquinoline (201b)

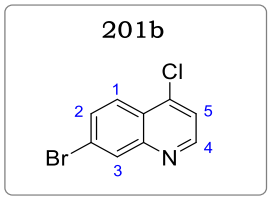

Obtained from **198b** (1.00 g, 3.07 mmol) as a white solid (0.586 g, 79%). R_f(20% EtOAc/Hexane), 0.38. ^{1}H NMR (400 MHz, DMSO-d_6) δ 8.87 (d, J = 4.8 Hz, 1H, H^4), 8.32 (d, J = 1.7 Hz, 1H, H^3), 8.13 (dd, J = 8.9, 1.7 Hz, 1H, H^2), 7.90 (d, J = 8.9 Hz, 1H, H^1), 7.82 (d, J = 4.8 Hz, 1H, H^5). LC-MS (APCI$^+$/ESI): found m/z = 241.9, 243.9 $[M+H]^+$ (cal. For C_9H_5BrClN, 240.9, 242.9). Purity: 99%, t_R = 2.567 min.

4-chloro-7-(trifluoromethyl)quinoline (201c)

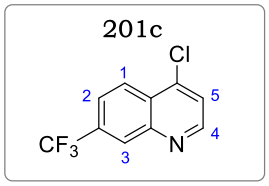

Obtained from **198c** (1.00 g, 3.17 mmol) as a white solid (0.436 g, 59%). R_f(20% EtOAc/Hexane), 0.35. ^{1}H NMR (600 MHz, DMSO-d_6) δ 9.00 (d, J = 4.7 Hz, 1H, H^4), 8.47 – 8.38 (m, 2H, H^{1,3}), 8.03 (dd, J = 8.7, 1.9 Hz, 1H, H^2), 7.96 (d, J = 4.7 Hz, 1H, H^5). LC-MS (APCI$^+$/ESI): found m/z = 232.0, 234.0 $[M+H]^+$ (cal. For $C_{10}H_5ClF_3N$, 231.01, 233.00). Purity: 98%, t_R = 2.523 min.

4-chloroquinoline-7-carbonitrile (201d)

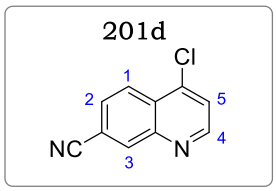

Obtained from **198d** (1.00 g, 3.68 mmol) as a white solid (0.454 g, 65%). R_f(20% EtOAc/Hexane), 0.32. ^{1}H NMR (400 MHz, DMSO-d_6) δ 8.99 (d, J = 4.8 Hz, 1H, H^4), 8.68 (d, J = 1.5 Hz, 1H, H^3), 8.34 (dd, J = 8.7, 1.5 Hz, 1H, H^2), 8.05 (d, J = 8.7 Hz, 1H, H^1), 7.95 (d, J = 4.8 Hz, 1H, H^5). LC-MS (APCI$^+$/ESI): found m/z = 189.0, 191.0 $[M+H]^+$ (cal. For $C_{10}H_5ClN_2$, 188.01, 190.01). Purity: 98%, t_R = 2.301 min.

4-chloro-7-(trifluoromethoxy)quinoline (201e)

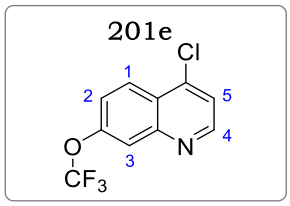

Obtained from **198e** (1.00 g, 3.02 mmol) as a white solid (0.421 g, 56%). R_f(20% EtOAc/Hexane), 0.40. ^{1}H NMR (400 MHz, DMSO-d_6) δ 8.92 (d, J = 4.8 Hz, 1H, H^4), 8.34 (dd, J = 9.2, 1.5 Hz, 1H, H^2), 8.02 (d, J = 1.5 Hz, 1H, H^3), 7.84 (d, J = 4.8 Hz, 1H, H^5), 7.77

(d, J = 9.2 Hz, 1H, H[1]). LC-MS (APCI$^+$/ESI): found m/z = 248.0, 250.0 $[M+H]^+$ (cal. For $C_{10}H_5ClF_3NO$, 247.00, 249.00). Purity: 98%, t_R = 2.568 min.

4-chloro-7-methoxyquinoline (201f)

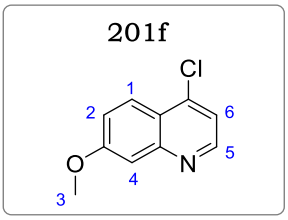

Obtained from **198f** (1.00 g, 3.61 mmol) as a white solid (0.338 g, 48%). R_f(20% EtOAc/Hexane), 0.25. ^{1}H NMR (600 MHz, DMSO) δ 8.75 (d, J = 4.8 Hz, 1H, H[5]), 8.09 (d, J = 9.2 Hz, 1H, H[1]), 7.58 (d, J = 4.8 Hz, 1H, H[6]), 7.47 (d, J = 2.6 Hz, 1H, H[4]), 7.40 (dd, J = 9.2, 2.6 Hz, 1H, H[2]), 3.95 (s, 3H, H[3]). LC-MS (APCI$^+$/ESI): found m/z = 194.0, 196.0 $[M+H]^+$ (cal. For $C_{10}H_8ClNO$, 193.03, 195.03). Purity: 98%, t_R = 2.326 min.

4-chloro-7-nitroquinoline (201g)

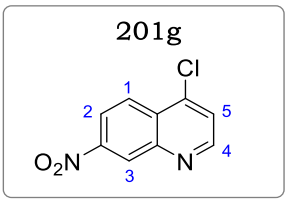

Obtained from **198g** (1.00 g, 3.42 mmol) as a white solid (0.453 g, 63%). R_f(20% EtOAc/Hexane), 0.38. ^{1}H NMR (600 MHz, DMSO-d_6) δ 9.06 (d, J = 4.7 Hz, 1H, H[4]), 8.87 (d, J = 1.1 Hz, 1H, H[3]), 8.50 – 8.43 (m, 2H, H[1,2]), 8.02 (d, J = 4.7 Hz, 1H, H[5]). LC-MS (APCI$^+$/ESI): found m/z = 209.0, 211.0 $[M+H]^+$ (cal. for $C_9H_5ClN_2O_2$, 208.00, 210.00). Purity: 98%, t_R = 2.495 min.

General Procedure 12: Preparation of 2-aminobenzimidazoles *via* S_NAr between amines and 2-chlorobenzimidazoles

A mixture of an appropriate 2-chlorobenzimidazole (1.0 equiv), an appropriate mono *N*-*tert*-butyl or *N*-ethyl carboxylate protected cyclic diamine (1.5 equiv), and TEA (2.0 equiv) was stirred at 155 °C in a seal tube for 6 – 36 hours. Alternatively, the mixture would be irradiated in a microwave reactor for 5 – 30 minutes at 150 °C, using toluene as solvent. After completion (monitored *via* TLC), the residue was cooled and diluted with 10% MeOH/DCM. The mixture was washed with saturated $NaHCO_3$ solution (×3), then brine (×1), and dried over anhydrous Na_2SO_4. The solvent was evaporated *in vacuo* to obtain a crude residue which was either triturated with *n*-pentane (or diethyl ether) or purified *via* flash column chromatography to afford the pure products.

Ethyl 4-((1*H*-benzo[*d*]imidazol-2-yl)amino)piperidine-1-carboxylate (13a)

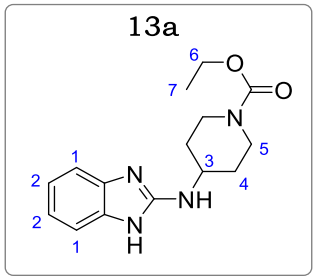

Obtained from 2-chlorobenzimidazole (5.0 g, 32.8 mmol) and ethyl 4-aminopiperidine-1-carboxylate (8.46 g, 49.1 mmol), as a light brown solid (8.22 g, 79%). R_f (10% MeOH/DCM), 0.35. ^{1}H NMR (600 MHz, Methanol-d_4) δ 7.18 (dd, J = 5.8, 3.2 Hz, 2H, H^2), 6.95 (dd, J = 5.8, 3.2 Hz, 2H, H^1), 4.11 (q, J = 7.1 Hz, 2H, H^6), 4.09 (m, 2H, H^5), 3.80 (tt, J = 10.6, 4.0 Hz, 1H, H^3), 3.05 – 2.99 (m, 2H, H^5), 2.08 – 2.01 (m, 2H, H^4), 1.48 – 1.39 (m, 2H, H^4), 1.25 (t, J = 7.1 Hz, 3H, H^7). LC-MS (APCI$^+$/ESI): found m/z = 289.0 [M+H]$^+$ (cal. For $C_{15}H_{20}N_4O_2$, 288.16). Purity: 98%, t_R = 2.258 min.

2-chloro-1-methyl-1H-benzo[*d*]imidazole (13b)

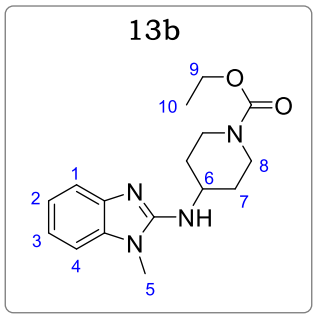

Obtained from **12b** (13 g, 77.4 mmol) and ethyl 4-aminopiperidine-1-carboxylate (20.0 g, 116 mmol), as a brown crystalline solid (19.8 g, 85%). R_f (5% MeOH/DCM), 0.48. ^{1}H NMR (400 MHz, Methanol-d_4) δ 7.28 (dd, J = 7.7, 0.9 Hz, 1H, H^1), 7.12 (dd, J = 7.9, 1.0 Hz, 1H, H^4), 7.04 (ddd, J = 7.7, 7.1, 0.9 Hz, 1H, H^2), 6.99 (ddd, J = 8.0, 7.1, 1.1 Hz, 1H, H^3), 4.51 – 4.44 (m, 2H, H^8), 4.13 (q, J = 7.1 Hz, 2H, H^9), 3.92 (tt, J = 11.1, 4.0 Hz, 1H, H^6), 3.51 (s, 3H, H^5), 3.07 – 2.95 (m, 2H, H^8), 2.09 – 1.99 (m, 2H, H^7), 1.50 - 1.51 (m, 2H, H^7), 1.27 (t, J = 7.1 Hz, 3H, H^{10}). LC-MS (APCI$^+$/ESI): found m/z = 303.2 [M+H]$^+$ (cal. For $C_{16}H_{22}N_4O_2$, 302.17). Purity: 99%, t_R = 2.381 min.

Ethyl 4-((1-isopropyl-1H-benzo[*d*]imidazol-2-yl) amino) piperidine-1-carboxylate (13c)

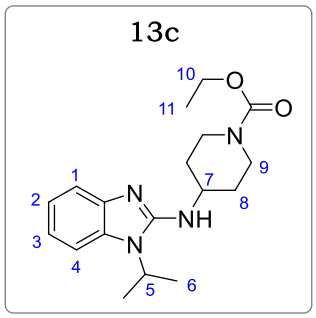

Obtained from **12c** (0.400 g, 2.04 mmol) and ethyl 4-aminopiperidine-1-carboxylate (0.526 g, 3.06 mmol), as a brown solid (0.538 g, 80%). R_f (5% MeOH/DCM), 0.55. ^{1}H NMR (400 MHz, Methanol-d_4) δ 7.34 (dd, J = 7.6, 1.2 Hz, 1H, H^1), 7.29 (dd, J = 7.7, 1.2 Hz, 1H, H^4), 7.02 (ddd, J = 7.7, 7.2, 1.3 Hz, 1H, H^3), 6.96 (ddd, J = 7.6, 7.2, 1.3 Hz, 1H, H^2), 4.58 (sept, J = 6.9 Hz, 1H, H^5), 4.20 – 4.07 (m, 4H, H^{9,10}), 3.92 (tt, J = 10.8, 4.0 Hz, 1H, H^7), 3.06 – 2.95 (m, 2H, H^9), 2.13 – 2.06 (m, 2H, H^8), 1.56 (d, J = 6.9 Hz, 6H, H^6), 1.54 – 1.43 (m, 2H, H^8), 1.27 (t, J = 7.1 Hz, 3H, H^{11}). LC-MS (APCI$^+$/ESI): found m/z = 331.2 [M+H]$^+$ (cal. For $C_{18}H_{26}N_4O_2$, 330.21). Purity: 99%, t_R = 2.501 min.

***Tert*-butyl 4-((1-(4-cyanobenzyl)-1H-benzo[*d*]imidazol-2-yl) amino) piperidine-1-carboxylate (13d)**

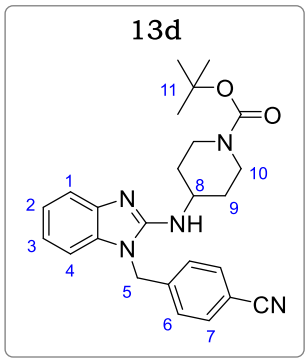

Obtained from **12d** (9.00 g, 33.5 mmol) and *tert*-butyl 4-aminopiperidine-1-carboxylate (10.1 g, 50.2 mmol), as a light brown solid (8.67 g, 60%). R_f(10% MeOH/DCM), 0.68. ^{1}H NMR (600 MHz, Methanol-d_4) δ 7.64 (d, J = 8.6 Hz, 2H, H^7), 7.32 (dd, J = 7.9, 1.1 Hz, 1H, H^1), 7.22 (d, J = 8.6 Hz, 2H, H^6), 7.04 (ddd, J = 7.9, 7.2, 1.3 Hz, 1H, H^2), 6.97 (dd, J = 8.2, 1.3 Hz, 1H, H^4), 6.93 (ddd, J = 8.2, 7.2, 1.1 Hz, 1H, H^3), 5.34 (s, 2H, H^5), 4.07 – 4.02 (m, 2H, H^{10}), 3.94 (tt, J = 11.0, 4.0 Hz, 1H, H^8), 2.99 – 2.88 (m, 2H, H^{10}), 2.05 – 2.00 (m, 2H, H^9), 1.51 – 1.32 (m, 11H, H^{9,11}). LC-MS (APCI$^+$/ESI): found m/z = 432.2 [M+H] $^+$ (cal. For $C_{25}H_{29}N_5O_2$, 431.23). Purity: 98%, t_R = 2.673 min.

***Tert*-butyl (R)-3-((1-(4-cyanobenzyl)-1H-benzo[*d*]imidazol-2-yl)amino)pyrrolidine-1-carboxylate (56a)**

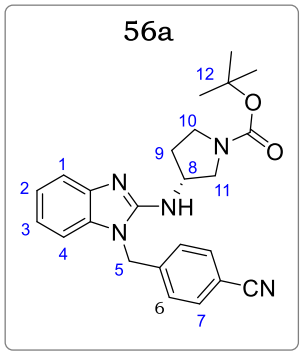

Obtained from **12d** (0.300 g, 1.12 mmol) and *tert*-butyl *(S)*-3-aminopyrrolidine-1-carboxylate (293 µl, 1.68 mmol) as a light brown solid (0.304 g, 65%). R_f(10% MeOH/DCM), 0.50. ^{1}H NMR (600 MHz, Methanol-d_4) δ 7.70 (d, J = 8.3 Hz, 2H, H^7), 7.49 (dd, J = 7.9, 1.2 Hz, 1H, H^1), 7.38 (d, J = 8.3 Hz, 2H, H^6), 7.32 (ddd, J = 7.9, 7.0, 1.4 Hz, 1H, H^2), 7.28 (dd, J = 8.1, 1.2 Hz, 1H, H^4), 7.25 (ddd, J = 8.1, 7.0, 1.4 Hz, 1H, H^3), 5.62 (s, 2H, H^5), 4.70 (tt, J = 6.8, 4.2 Hz, 1H, H^8), 3.73 (dd, J = 12.9, 6.8 Hz, 1H, H^{11}), 3.55 – 3.47 (m, 2H, H^{10,11}), 3.40 (ddd, J = 11.5, 8.4, 5.7 Hz, 1H, H^{10}), 2.55 (ddd, J = 15.0, 8.4, 6.8 Hz, 1H, H^9), 2.29 (ddd, J = 11.5, 8.2, 4.1 Hz, 1H, H^9), 1.48 (s, 9H, H^{12}). LC-MS (APCI$^+$/ESI): found m/z = 418.2 [M+H] $^+$ (cal. for $C_{24}H_{27}N_5O_2$, 417.22). Purity: 99%, t_R = 2.801 min.

***Tert*-butyl (S)-3-((1-(4-cyanobenzyl)-1H-benzo[*d*]imidazol-2-yl) amino) pyrrolidine-1-carboxylate (56b**)

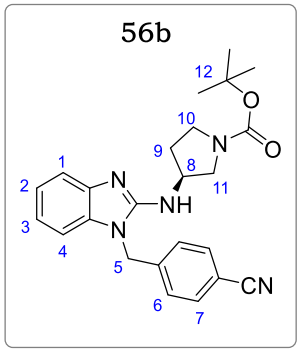

Obtained from **12d** (0.200 g, 0.75 mmol) and tert-butyl *(R)*-3-aminopyrrolidine-1-carboxylate (192 µl, 1.12 mmol) as a light brown solid (0.243 g, 78%). R_f(10% MeOH/DCM), 0.50. ^{1}H NMR (600 MHz, Methanol-d_4) δ 7.68 (d, J = 8.4 Hz, 2H, H^7), 7.43 (dd, J = 7.8, 1.2 Hz, 1H, H^1), 7.39 (d, J = 8.4 Hz, 2H, H^6), 7.30 (ddd, J = 7.8, 7.0, 1.2 Hz, 1H, H^2), 7.26 (dd, J = 8.0, 1.2 Hz, 1H, H^4), 7.21 (ddd, J = 8.0, 7.0, 1.4 Hz, 1H, H^3), 5.63 (s, 2H, H^5), 4.66 (tt, J = 7.1, 4.0 Hz, 1H, H^8), 3.70 (dd, J = 12.5, 7.1 Hz, 1H, H^{11}), 3.57 – 3.48 (m, 2H, H^{10,11}), 3.35 (ddd, J = 10.5, 8.9, 5.0 Hz, 1H, H^{10}), 2.53 (ddd, J = 15.0, 8.9, 7.1 Hz, 1H, H^9), 2.21 (ddd, J = 11.5, 8.9, 4.0 Hz, 1H, H^9), 1.46 (s, 9H, H^{12}). LC-MS (APCI$^+$/ESI): found m/z = 418.2 [M+H] $^+$ (cal. for $C_{24}H_{27}N_5O_2$, 417.22). Purity: 98%, t_R = 2.876 min.

Tert-butyl-6-(1-(4-cyanobenzyl)-1-benzo[_d_]imidazol-2-yl)-2,6-diazaspiro[3.4]octane-2-carboxylate (56c)

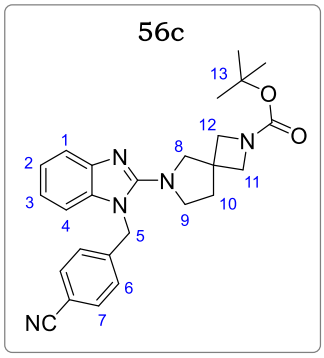

Obtained from **12d** (0.151 g, 0.57 mmol) and tert-butyl 2,6-diazaspiro [3.4] octane-2-carboxylate (181 g, 0.85 mmol) after irradiation under microwave for 6 min, as a white crystal (0.173 g, 55%). R_f(7% MeOH/DCM), 0.63. ^{1}H NMR (600 MHz, Methanol-d_4) δ 7.69 (d, J = 8.3 Hz, 2H, H^7), 7.40 (dd, J = 7.9, 1.2 Hz, 1H, H^1), 7.28 (d, J = 8.3 Hz, 2H, H^6), 7.13 (ddd, J = 7.9, 7.4, 1.2 Hz, 1H, H^2), 7.10 (dd, J = 8.0, 1.3 Hz, 1H, H^4), 7.04 (ddd, J = 8.0, 7.4, 1.2 Hz, 1H, H^3), 5.49 (s, 2H, H^5), 3.84 (br-s, 4H, H^{11,12}), 3.69 (s, 2H, H^8), 3.58 (t, J = 6.9 Hz, 2H, H^9), 2.15 (t, J = 6.9 Hz, 2H, H^{10}), 1.43 (s, 9H, H^{13}). LC-MS (APCI$^+$/ESI): found m/z = 444.2 [M+H] $^+$ (cal. for $C_{26}H_{29}N_5O_2$, 443.23). Purity: 99%, t_R = 2.409 min

Tert-butyl 4-(1-(4-cyanobenzyl)-1H-benzo[_d_]imidazol-2-yl)piperazine-1-carboxylate (56d)

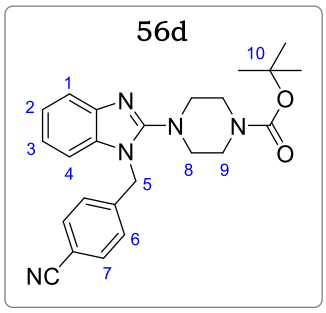

Following general procedure 4, obtained from **12d** (0.500 g, 1.87 mmol) and tert-butyl piperazine-1-carboxylate (0.522 g, 2.80 mmol) after irradiation under microwave for 6 min. Pale yellow solid (0.593 g, 76%). R_f (10% MeOH/DCM), 0.48. ^{1}H NMR (600 MHz, Methanol-d_4) δ 7.69 (d, J = 8.4 Hz, 2H, H^7), 7.53 (dd, J = 7.9, 0.9 Hz, 1H, H^1), 7.32 (d, J = 8.4 Hz, 2H, H^6), 7.19 (ddd, J = 7.9, 5.8, 1.0 Hz, 1H, H^2), 7.15 – 7.12 (m, 2H, H^{3,4}), 5.44 (s, 2H, H^5), 3.61 – 3.49 (br, 4H, H^9), 3.21 – 3.12 (m, 4H, H^8), 1.47 (s, 9H, H^{10}). LC-MS (APCI$^+$/ESI): found m/z = 418.2 [M+H] $^+$ (cal. for $C_{24}H_{27}N_5O_2$, 417.22). Purity: 99%, t_R = 2.574 min.

Tert-butyl (R)-4-(1-(4-cyanobenzyl)-1H-benzo[_d_]imidazol-2-yl)-2-methylpiperazine-1-carboxylate (56e)

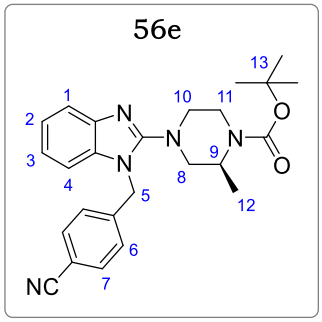

Obtained from **12d** (0.250 g, 0.93 mmol) and *tert*-butyl *(R)*-2-methylpiperazine-1-carboxylate (0.281 g, 1.40 mmol) after irradiation under microwave for 25 min, as a white solid (0.290 g, 72%). R_f (10% MeOH/DCM), 0.55. ^{1}H NMR (600 MHz, Methanol-d_4) δ 7.69 (d, J = 8.7 Hz, 2H, H^7), 7.53 (dd, J = 8.0, 0.9 Hz, 1H, H^1), 7.28 (d, J = 8.7 Hz, 2H, H^6), 7.20 (ddd, J = 8.0, 6.8, 1.6 Hz, 1H, H^2), 7.17 (dd, J = 8.1, 1.6 Hz, 1H, H^4), 7.14 (ddd, J = 8.1, 6.8, 1.1 Hz, 1H, H^3), 5.47 (s, 2H, H^5), 4.32 – 4.25 (m, 1H, H^9), 3.93 – 3.88 (m, 1H, H^{11}), 3.45 – 3.38 (m, 1H, H^{10a}), 3.29 – 3.23 (m, 1H, H^{11}), 3.22 (dd, J = 12.3, 2.0 Hz, 1H, H^{8e}), 3.13 (dd, J = 12.3, 3.7 Hz, 1H, H^{8a}), 2.97 (td, J = 12.2, 3.4 Hz, 1H, H^{10e}), 1.46 (s, 9H, H^{13}), 1.19 (d, J = 6.8 Hz, 3H, H^{12}). LC-MS (APCI$^+$/ESI): found m/z = 432.2 [M+H]$^+$ (cal. for $C_{25}H_{29}N_5O_2$, 431.23). Purity: 99%, t_R = 2.599 min.

Ethyl 4-((5,6-difluoro-1-methyl-1H-benzo[d]imidazol-2-yl) amino) piperidine-1-carboxylate (130h)

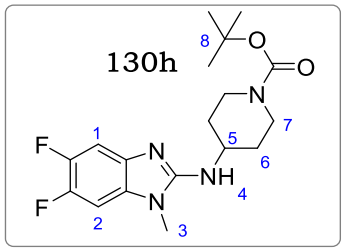

Obtained from **125h** (0.180 g, 0.88 mmol) and *tert*-butyl 4-aminopiperidine-1-carboxylate (0.265 g, 1.32 mmol), as a brown solid (0.184 g, 57%). R_f (5% MeOH/DCM), 0.78. ^{1}H NMR (400 MHz, DMSO-d_6) δ 7.40 (dd, J = 7.4, 5.3 Hz, 1H, H^1), 7.32 (dd, J = 7.5, 5.5 Hz, 1H, H^2), 6.69 (d, J = 7.6 Hz, 1H, H^4), 4.51 – 4.42 (m, 2H, H^{7e}), 3.91 (tt, J = 11.2, 4.0 Hz, 1H, H^5), 3.52 (s, 3H, H^3), 3.09 – 2.98 (m, 2H, H^{7a}), 2.15 – 2.06 (m, 2H, H^{6e}), 1.59 – 1.51

(m, 2H, H^{6a}), 1.39 (s, 9H, H^{8}). LC-MS ($APCI^+$/ESI): found m/z = 367.2 $[M+H]^+$ (cal. for $C_{18}H_{24}F_2N_4O_2$, 366.19). Purity: 98%, t_R = 2.579 min.

Ethyl 4-((5,6-dichloro-1-methyl-1H-benzo[d]imidazol-2-yl) amino) piperidine-1-carboxylate (130i)

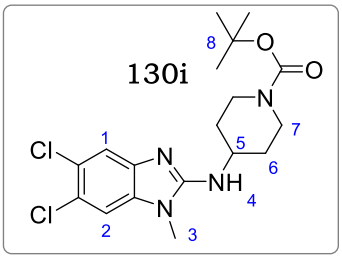

Obtained from **125i** (0.130 g, 0.55 mmol) and *tert*-butyl 4-aminopiperidine-1-carboxylate (0.166 g, 0.83 mmol), as a light brown solid (0.143 g, 65%). R_f (5% MeOH/DCM), 0.79. ^{1}H NMR (400 MHz, DMSO-d_6) δ 8.12 (s, 1H, H^1), 8.03 (s, 1H, H^2), 6.70 (d, J = 7.3 Hz, 1H, H^4), 4.51 – 4.46 (m, 2H, H^{7e}), 3.92 (tt, J = 10.9, 4.1 Hz, 1H, H^5), 3.52 (s, 3H, H^3), 3.10 – 3.02 (m, 2H, H^{7a}), 2.09 – 2.00 (m, 2H, H^{6e}), 1.52 – 1.47 (m, 2H, H^{6a}), 1.39 (s, 9H, H^8). LC-MS ($APCI^+$/ESI): found m/z = 399.1, 401.1 $[M+H]^+$ (cal. for $C_{18}H_{24}Cl_2N_4O_2$, 398.13, 400.12). Purity: 96%, t_R = 2.530 min.

Ethyl 4-((1,5,6-trimethyl-1H-benzo[d]imidazol-2-yl) amino) piperidine-1-carboxylate (130j)

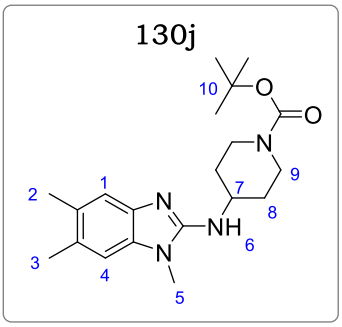

Obtained from **125j** (0.180 g, 0.91 mmol) and *tert*-butyl 4-aminopiperidine-1-carboxylate (0.276 g, 1.38 mmol), as a light brown solid (0.225 g, 69%). R_f (5% MeOH/DCM), 0.69. ^{1}H NMR (400 MHz, DMSO-d_6) δ 7.37 (s, 1H, H^1), 7.22 (s, 1H, H^4), 6.65 (d, J = 7.2 Hz, 1H, H^6), 4.54 – 4.46 (m, 2H, H^{9e}), 3.92 (tt, J = 10.9, 4.2 Hz, 1H, H^7), 3.51 (s, 3H, H^5), 3.07 – 2.99 (m, 2H, H^{9a}), 2.24 (s, 3H, H^2), 2.19 (s, 3H, H^3), 2.11 – 1.10 (m, 2H, H^{8e}), 1.51 – 1.44 (m, 2H, H^{8a}), 1.32 (s, 9H, H^{10}). ^{13}C NMR (151 MHz, DMSO-d_6) δ 155.37, 148.83, 141.43, 134.66, 131.86, 130.93, 115.73, 60.87, 50.80 (2C), 48.30, 32.18, 31.09 (2C), 19.89, 19.62, 13.93 (3C). LC-MS ($APCI^+$/ESI): found m/z = 359.2 $[M+H]^+$ (cal. for $C_{20}H_{30}N_4O_2$, 358.24). Purity: 98%, t_R = 2.499 min.

Tert-butyl 4-((7-chloroquinolin-4-yl)amino)piperidine-1-carboxylate (170)

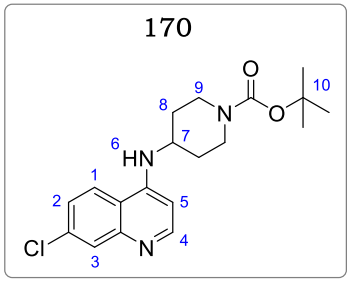

Obtained from 4,7-dichloroquine (5.00 g, 25.2 mmol) and *tert*-butyl 4-aminopiperidine-1-carboxylate (7.60 g, 37.9 mmol), as a pale-yellow solid (7.11 g, 78%). R_f (10% MeOH/DCM), 0.59. ^{1}H NMR (400 MHz, DMSO-d_6) δ 8.38 (d, J = 5.4 Hz, 1H, H^4), 8.24 (d, J = 9.0 Hz, 1H, H^1), 7.94 (d, J = 2.2 Hz, 1H, H^3), 7.55 (d, J = 5.4 Hz, 1H, H^5), 6.96 (dd, J = 9.0, 2.2 Hz, 1H, H^2), 6.61 (d, J = 5.5 Hz, 1H, H^6), 4.04 – 3.89 (m, 2H, H^{9e}), 3.73 (tt, J = 10.6, 4.0 Hz, 1H, H^7), 2.97 – 2.81 (m, 2H, H^{9e}), 1.94 (td, J = 12.7 Hz, 2H, H^{8e}), 1.54 – 1.34 (m, 11H, H^{8a,10}). LC-MS (APCI$^+$/ESI): found m/z = 362.1 [M+H]$^+$ (cal. for $C_{19}H_{24}ClN_3O_2$, 361.16). Purity: 99%, t_R = 2.564 min.

Tert-butyl (1-(1-(4-fluorobenzyl)-1H-benzo[d]imidazol-2-yl) piperidin-4-yl)carbamate (203)

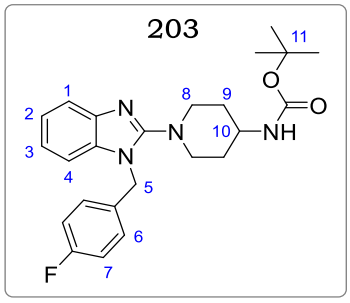

Obtained from **169h** (4.00 g, 15.2 mmol) and *tert*-butyl piperidin-4-ylcarbamate (4.58 g, 22.9 mmol), as a pale-yellow solid (4.64 g, 72%). R_f (10% MeOH/DCM), 0.52. ^{1}H NMR (400 MHz, Methanol-d_4) δ 7.63 (d, J = 8.2 Hz, 2H, H^7), 7.48 (dd, J = 8.0, 1.3 Hz, 1H, H^1), 7.29 (d, J = 8.2 Hz, 2H, H^6), 7.16 (ddd, J = 8.0, 6.6, 1.2 Hz, 1H, H^2), 7.10 – 7.03 (m, 2H, H^{3,4}), 5.48 (s, 2H, H^5), 3.61 – 3.49 (m, 4H, H^8), 3.29 (tt, J = 11.0, 3.9 Hz, 1H, H^{10}), 3.21 – 3.18 (m, 2H, H^{9e}), 3.01 – 2.93 (m, 2H, H^{9a}), 1.46 (s, 9H, H^{11}). LC-MS (APCI$^+$/ESI): found m/z = 425.2 [M+H] $^+$ (cal. for $C_{24}H_{29}FN_4O_2$, 424.23). Purity: 99%, t_R = 2.522 min.

General Procedure 13: Preparation of 2-aminobenzimidazoles *via* DCC-mediated cyclocondensation of aromatic 1,2-diamines with isothiocyanates

To a solution of commercially sourced or synthesized aromatic 1,2-diamines (**129a**–**129g**, 1.0 equiv) in 15 ml MeCN, isothiocyanate (**126a** – **126b**, 1.1 equiv) and TEA (1.2 equiv) were added, and the mixture refluxed at 85 °C for 1 hr. DCC (1.2 equiv) was then added, and the reaction mixture was refluxed at 85 °C for 11 hr. After completion (monitored *via* TLC), MeCN was evaporated *in vacuo*, and the residue adsorbed on silica gel. Pure products were obtained after purification *via* flash chromatography using 10% MeOH/DCM as eluent.

Tert-butyl 4-((5-cyano-1-methyl-1H-benzo[d]imidazol-2-yl) amino) piperidine-1-carboxylate (130a)

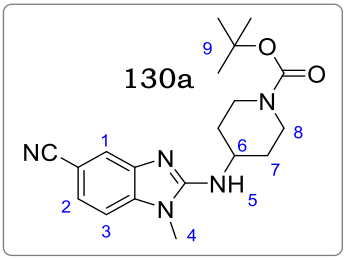

Obtained from **129a** (0.280 g, 1.90 mmol) and **126a** (0.507 g, 2.10 mmol), as a light brown solid (0.573 g, 85%). R_f(5% MeOH/DCM), 0.53. ^{1}H NMR (400 MHz, DMSO-d_6) δ 7.97 (d, J = 1.4 Hz, 1H, H^1), 7.78 (d, J = 7.5 Hz, 1H, H^3), 7.52 (dd, J = 7.5, 1.4 Hz, 1H, H^2), 6.75 (d, J = 7.5 Hz, 1H, H^5), 4.49 – 4.41 (m, 2H, H^{8e}), 3.94 (tt, J = 10.8, 4.0 Hz, 1H, H^6), 3.50 (s, 3H, H^4), 3.08 – 2.95 (m, 2H, H^{8a}), 2.10 – 2.01 (m, 2H, H^{7e}), 1.50 – 1.43 (m, 2H, H^{7a}), 1.43 (s, 9H, H^9). LC-MS (APCI$^+$/ESI): found m/z = 356.2 [M+H]$^+$ (cal. For $C_{19}H_{25}N_5O_2$, 355.20). Purity: 99%, t_R = 2.397 min.

Ethyl 4-((1-methyl-5-(trifluoromethyl)-1H-benzo[d]imidazol-2-yl) amino) piperidine-1-carboxylate (130b)

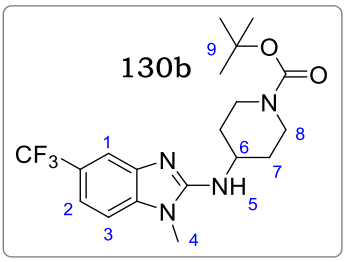

Obtained from **129b** (0.300 g, 1.57 mmol) and **126a** (0.420 g, 1.73 mmol), as an off white solid (0.520 g, 83%). R_f(5% MeOH/DCM), 0.73. ^{1}H NMR (300 MHz, DMSO-d_6) δ 7.47 (d, J = 1.6 Hz, 1H, H^1), 7.31 (d, J = 8.2 Hz, 1H, H^3), 7.23 (dd, J = 8.2, 1.6 Hz, 1H, H^2), 6.72 (d, J = 7.7 Hz, 1H, H^5), 4.04 – 3.84 (m, 3H, H^{6,8e}), 3.54 (s, 3H, H^4), 3.00 – 2.72 (m, 2H, H^{8a}), 2.09 – 1.86 (m, 2H, H^{7e}), 1.57 – 1.32 (m, 11H, H^{7a,9}). LC-MS (APCI$^+$/ESI): found m/z = 399.2 [M+H]$^+$ (cal. For $C_{17}H_{21}F_3N_4O_2$, 398.19). Purity: 99%, t_R = 2.588 min.

Tert-butyl 4-((5-methoxy-1-methyl-1H-benzo[d]imidazol-2-yl) amino) piperidine-1-carboxylate (130c)

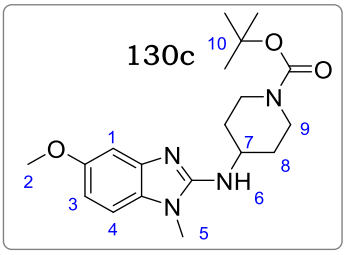

Obtained from **129c** (0.250 g, 1.64 mmol) and **126a** (0.437 g, 1.81 mmol), as a light brown solid (0.501 g, 85%). R_f(5% MeOH/DCM), 0.51. ^{1}H NMR (400 MHz, DMSO-d_6) δ 7.43 (d, J = 1.4 Hz, 1H, H^1), 7.25 (dd, J = 7.5, 1.4 Hz, 1H, H^3), 7.16 (d, J = 7.5 Hz, 1H, H^4), 6.69 (d, J = 7.9 Hz, 1H, H^6), 4.50 – 4.43 (m, 2H, H^{9e}), 3.91 (tt, J = 11.0, 4.1 Hz, 1H, H^7), 3.86 (s, 3H, H^5), 3.51 (s, 3H, H^2), 3.07 – 2.96 (m, 2H, H^{9a}), 2.10 – 1.99 (m, 2H, H^{8e}), 1.51 – 1.45 (m, 2H, H^{8a}), 1.41 (s, 9H, H^{10}). LC-MS (APCI$^+$/ESI): found m/z = 361.2 [M+H]$^+$ (cal. For $C_{19}H_{28}N_4O_3$, 360.22). Purity: 97%, t_R = 2.393 min.

Tert-butyl 4-((1-methyl-5-(methylsulfonyl)-1H-benzo[d]imidazol-2-yl) amino) piperidine-1-carboxylate (130d)

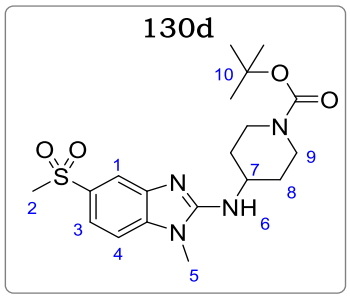

Obtained from **129d** (0.300 g, 1.50 mmol) and **126a** (0.400 g, 1.64 mmol), as a light brown solid (0.538 g, 88%). R_f (5% MeOH/DCM), 0.57. ^{1}H NMR (400 MHz, DMSO-d_6) δ 8.03 (d, J = 1.1 Hz, 1H, H^1), 7.83 (d, J = 7.8 Hz, 1H, H^4), 7.41 (dd, J = 7.8, 1.1 Hz, 1H, H^3), 6.73 (d, J = 7.9 Hz, 1H, H^6), 4.50 – 4.43 (m, 2H, H^{9e}), 3.92 (tt, J = 10.9, 4.1 Hz, 1H, H^7), 3.61 (s, 3H, H^2), 3.49 (s, 3H, H^5), 3.10 – 3.01 (m, 2H, H^{9a}), 2.10 – 2.00 (m, 2H, H^{8e}), 1.51 – 1.44 (m, 2H, H^{8a}), 1.44 (s, 9H, H^{10}). LC-MS (APCI$^+$/ESI): found m/z = 409.2 [M+H]$^+$ (cal. For $C_{19}H_{28}N_4O_2S$, 408.18). Purity: 96%, t_R = 2.492 min.

Methyl 2-((1-(tert-butoxycarbonyl) piperidin-4-yl) amino)-1-methyl-1H-benzo[d]imidazole-5-carboxylate (130e)

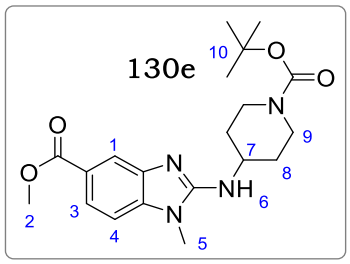

Obtained from **129e** (0.250 g, 1.38 mmol) and **126a** (0.370 g, 1.53 mmol), as an off white solid (0.434 g, 81%). R_f (5% MeOH/DCM), 0.55. ^{1}H NMR (400 MHz, DMSO-d_6) δ 8.10 (d, J = 1.3 Hz, 1H, H^1), 7.89 (dd, J = 7.7, 1.3 Hz, 1H, H^3), 7.58 (d, J = 7.7 Hz, 1H, H^4), 6.75 (d, J = 7.6 Hz, 1H, H^6), 4.49 – 4.42 (m, 2H, H^{9e}), 3.91 (tt, J = 10.9, 4.2 Hz, 1H, H^7), 3.78 (s, 3H, H^2), 3.51 (s, 3H, H^5), 3.08 – 2.98 (m, 2H, H^{9a}), 2.08 – 2.01 (m, 2H, H^{8e}), 1.50 – 1.42 (m, 2H, H^{8a}), 1.40 (s, 9H, H^{10}). LC-MS (APCI$^+$/ESI): found m/z = 389.2 [M+H]$^+$ (cal. for $C_{20}H_{28}N_4O_4$, 388.21). Purity: 98%, t_R = 2.403 min.

Ethyl 4-((5-fluoro-1-methyl-1H-benzo[d]imidazol-2-yl) amino) piperidine-1-carboxylate (130f)

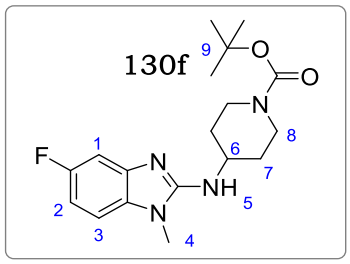

Obtained from **129f** (0.250 g, 1.78 mmol) and **126a** (0.475 g, 1.96 mmol), as a light brown solid (0.545 g, 88%). R_f (5% MeOH/DCM), 0.53. ^{1}H NMR (400 MHz, DMSO-d_6) δ 7.49 (dd, J = 8.5, 1.3 Hz, 1H, H^1), 7.39 (dd, J = 7.9, 1.5 Hz, 1H, H^3), 6.85 (ddd, J = 8.0, 7.9, 1.3 Hz, 1H, H^2), 6.68 (d, J = 7.1 Hz, 1H, H^5), 4.54 – 4.46 (m, 2H, H^{8e}), 3.93 (tt, J = 11.2, 4.1 Hz, 1H, H^6), 3.52 (s, 3H, H^4), 3.01 – 2.93 (m, 2H, H^{8a}), 2.15 – 2.08 (m, 2H, H^{7e}), 1.56 – 1.49 (m, 2H, H^{7a}), 1.38 (s, 9H, H^9). LC-MS (APCI$^+$/ESI): found m/z = 349.2 [M+H]$^+$ (cal. for $C_{18}H_{25}FN_4O_2$, 348.20). Purity: 99%, t_R = 2.553 min.

Ethyl 4-((5-bromo-1-methyl-1H-benzo[d]imidazol-2-yl) amino) piperidine-1-carboxylate (130g)

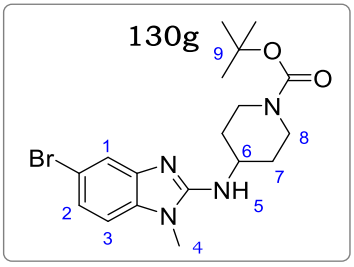

Obtained from **129g** (0.250 g, 1.24 mmol) and **126a** (0.331 g, 1.37 mmol), as a dark brown solid (0.422 g, 83%). R_f (5% MeOH/DCM), 0.62. ^{1}H NMR (400 MHz, DMSO-d_6) δ 7.35 (d, J = 1.3 Hz, 1H, H^1), 7.28 (d, J = 7.8 Hz, 1H, H^3), 7.13 (dd, J = 7.8, 1.3 Hz, 1H, H^2), 6.71 (d, J = 7.1 Hz, 1H, H^5), 4.51 – 4.43 (m, 2H, H^{8e}), 3.92 (tt, J = 10.9, 4.0 Hz, 1H, H^6), 3.51 (s, 3H, H^4), 3.07 – 2.98 (m, 2H, H^{8a}), 2.10 – 2.01 (m, 2H, H^{7e}), 1.59 – 1.51 (m, 2H, H^{7a}), 1.42 (s, 9H, H^9). LC-MS (APCI$^+$/ESI): found m/z = 409.1, 411.1 [M+H]$^+$ (cal. For $C_{18}H_{25}BrN_4O_2$, 408.12, 410.11). Purity: 98%, t_R = 2.591 min.

Tert-butyl 4-((1H-imidazo[4,5-b]pyridine-2-yl)amino)piperidine-1-carboxylate (144c)

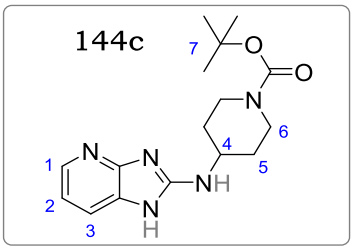

Obtained from pyridine-2,3-diamine (0.200 g, 1.83 mmol) and **126a** (0.489 g, 2.02 mmol), as a an off white solid (0.516 g, 89%). R_f (10% MeOH/DCM), 0.22. ^{1}H NMR (400 MHz, Methanol-d_4) δ 8.53 (dd, J = 5.0, 1.4 Hz, 1H, H^1), 7.63 (dd, J = 8.2, 1.3 Hz, 1H, H^3), 7.19 (dd, J = 8.2, 5.0 Hz, 1H, H^2), 4.11 – 4.05 (m, 2H, H^{6e}), 3.83 (tt, J = 10.6, 4.0 Hz, 1H, H^4), 3.06 – 2.98 (m, 2H, H^{6a}), 2.11 – 2.03 (m, 2H, H^{5e}), 1.58 – 1.51 (m, 2H, H^{5a}), 1.38 (s, 9H, H^7). LC-MS (APCI$^+$/ESI): found m/z = 318.2 [M+H] $^+$ (cal. For $C_{16}H_{23}N_5O_2$, 317.19). Purity: 98%, t_R = 2.169 min.

Tert-butyl 4-((5-methyl-1H-imidazo[4,5-b]pyridin-2-yl)amino)piperidine-1-carboxylate (144d)

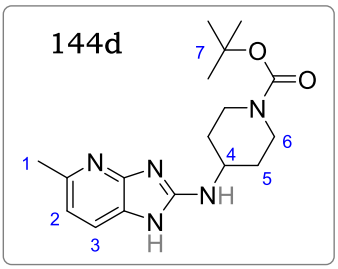

Obtained from 6-methylpyridine-2,3-diamine (0.200 g, 1.62 mmol) and **126a** (0.433 g, 1.78 mmol), as a pale orange solid (0.500 g, 93%). R_f (10% MeOH/DCM), 0.29. ^{1}H NMR (400 MHz, Methanol-d_4) δ 7.29 (d, J = 8.3 Hz, 1H, H^3), 6.50 (d, J = 8.3 Hz, 1H, H^2), 4.09 – 4.01 (m, 2H, H^{6e}), 3.81 (tt, J = 10.6, 4.0 Hz, 1H, H^4), 3.02 – 2.93 (m, 2H, H^{6a}), 2.25 (s, 3H, H^1), 2.09 – 2.01 (m, 2H, H^{5e}), 1.62 – 1.55 (m, 2H, H^{5a}), 1.40 (s, 9H, H^7). LC-MS (APCI$^+$/ESI): found m/z = 332.2 [M+H] $^+$ (cal. for $C_{17}H_{25}N_5O_2$, 331.20). Purity: 98%, t_R = 2.208 min.

***Tert*-butyl 4-((1H-imidazo[4,5-c]pyridin-2-yl)amino)piperidine-1-carboxylate (144e)**

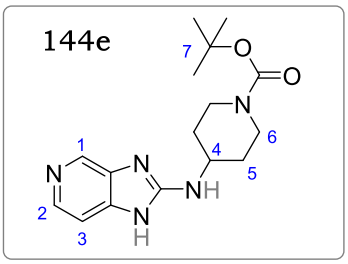

Obtained from pyridine-3,4-diamine (0.200 g, 1.83 mmol) and **126a** (0.489 g, 2.02 mmol), as a white solid (0.481 g, 83%). R_f (10% MeOH/DCM), 0.22. ^{1}H NMR (400 MHz, Methanol-d_4) δ 8.79 (d, J = 1.8 Hz, 1H, H^1), 8.23 (dd, J = 5.1, 1.8 Hz, 1H, H^2), 7.38 (d, J = 5.1 Hz, 1H, H^3), 4.10 – 4.03 (m, 2H, H^{6e}), 3.82 (tt, J = 10.8, 4.1 Hz, 1H, H^4), 3.09 – 3.01 (m, 2H, H^{6a}), 2.14 – 2.08 (m, 2H, H^{5e}), 1.60 – 1.53 (m, 2H, H^{5a}), 1.43 (s, 9H, H^7). LC-MS (APCI$^+$/ESI): found m/z = 318.2 [M+H] $^+$ (cal. for $C_{16}H_{23}N_5O_2$, 317.19). Purity: 98%, t_R = 2.098 min.

Tert-butyl 4-((6-chloro-1H-imidazo[4,5-c]pyridin-2-yl)amino)piperidine-1-carboxylate (144f)

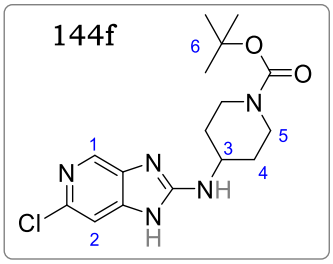

Obtained from 6-chloropyridine-3,4-diamine (0.200 g, 1.39 mmol) and **126a** (0.371 g, 1.53 mmol), as a white solid (0.392 g, 80%). R_f (10% MeOH/DCM), 0.34. ^{1}H NMR (400 MHz, Methanol-d_4) δ 8.81 (s, 1H, H^1), 7.55 (s, 1H, H^2), 4.09 – 4.01 (m, 2H, H^{5e}), 3.80 (tt, J = 10.8, 4.1 Hz, 1H, H^3), 3.10 – 3.03 (m, 2H, H^{5a}), 2.11 – 2.07 (m, 2H, H^{4e}), 1.58 – 1.51 (m, 2H, H^{4a}), 1.42 (s, 9H, H^6). LC-MS (APCI$^+$/ESI): found m/z = 352.2, 354.2 [M+H] $^+$ (cal. for $C_{16}H_{22}ClN_5O_2$, 351.15, 353.14). Purity: 98%, t_R = 2.355 min.

Tert-butyl 4-((1H-benzo[d]imidazol-2-yl)amino)-3-fluoropiperidine-1-carboxylate (144g)

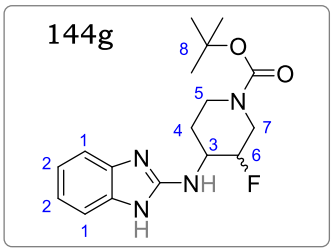

Obtained from benzene-1,2-diamine (0.200 g, 1.85 mmol) and **126b** (0.530 g, 2.03 mmol), as a white solid (0.482 g, 78%). R_f (6% MeOH/DCM), 0.38. ^{1}H NMR (400 MHz, Methanol-d_4) δ 7.22 (dd, J = 5.9, 3.2 Hz, 2H, H^2), 6.98 (dd, J = 5.9, 3.2 Hz, 2H, H^1), 4.33 (dtd, J = 48.8, 9.1, 4.2 Hz, 1H, H^6), 3.81 (qd, J = 11.2, 4.3 Hz, 1H, H^3), 3.33 (d, J = 10.1 Hz, 1H, H^{7e}), 2.98 – 2.93 (m, 1H, H^{5e}), 2.89 – 2.80 (m, 2H, H^{7a,5a}), 2.19 – 2.11 (m, 1H, H^{4e}), 1.49 – 1.41 (m, 1H, H^{4a}), 1.32 (s, 9H, H^8). LC-MS (APCI$^+$/ESI): found m/z = 335.2 [M+H] $^+$ (cal. For $C_{17}H_{23}FN_4O_2$, 334.18). Purity: 98%, t_R = 2.365 min.

General Procedure 14: Reductive amination using titanium isopropoxide

A solution of aryl amine (1.0 equiv) and ketone (1.2 equiv) in anhydrous THF (10 ml) was degassed by purging with N_2 for 15 min. Titanium isopropoxide, Ti(*i*OPr)$_4$ (3.0 equiv) was then added, and the resulting mixture degassed further for 15 min. The reaction was stirred under nitrogen atmosphere for 12 h at 23 °C. When the amine was consumed, or the reaction could not proceed further, sodium triacetoxy borohydride, Na(OAc)$_3$BH (1.0 equiv) was added, and the resulting mixture stirred at 23 °C for 6 hr. The reaction was quenched by adding saturated $NaHCO_3$ (15 ml), after which the resulting mixture was extracted with EtOAc (3 × 30 ml). Combined organic phases were washed with water (2 × 10 ml), and then by brine (10 ml). Pure products were obtained following purification *via* column chromatography with 4 – 5% MeOH/DCM as eluent.

Tert-butyl 4-((1H-indol-2-yl)amino)piperidine-1-carboxylate (144a)

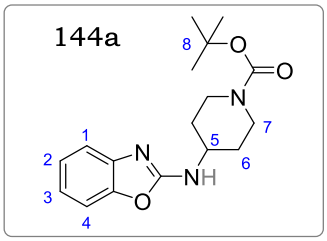

Obtained from 2-aminobenzoxazole (0.250 g, 1.86 mmol) and *tert*-butyl 4-oxopiperidine-1-carboxylate (0.445 g, 2.23 mmol) as a white solid (0.577 g, 98%). R_f(6% MeOH/DCM), 0.47. ^{1}H NMR (600 MHz, Methanol-d_6) δ 7.41 (dd, J = 8.2, 1.2 Hz, 1H, H^4), 7.29 (dd, J = 7.8, 1.3 Hz, 1H, H^1), 7.10 (ddd, J = 8.2, 7.0, 1.1 Hz, 1H, H^3), 6.85 (ddd, J = 7.8, 7.0, 1.2 Hz), 4.09 – 4.01 (m, 2H, H^{7e}), 3.82 (tt, J = 11.2, 4.0 Hz, 1H, H^5), 2.98 – 2.90 (m, 2H, H^{7a}), 2.10 – 1.99 (m, 2H, H^{6e}), 1.58 – 1.51 (m, 2H, H^{6a}), 1.42 (s, 9H, H^8). LC-MS (APCI$^+$/ESI): found m/z = 318.2 [M+H]$^+$ (cal. For $C_{17}H_{23}N_3O_3$, 317.17). Purity: 97%, t_R = 2.334 min.

Tert-butyl 4-((1H-benzo[d]imidazol-2-yl)amino)-3,3-difluoropiperidine-1-carboxylate (144b)

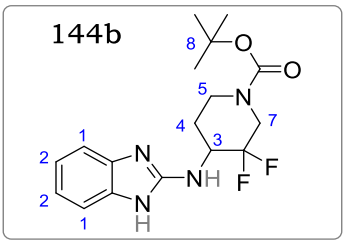

Obtained from 2-aminobenzimidazole (0.650 g, 4.88 mmol) and tert-butyl 3,3-difluoro-4-oxopiperidine-1-carboxylate (1.38 g, 5.86 mmol) as a white solid (0.395 g, 23%). R_f(6% MeOH/DCM), 0.41. ^{1}H NMR (400 MHz, Methanol-d_4) δ 7.28 (dd, J = 5.6, 3.1 Hz, 2H, H^2), 7.01 (dd, J = 5.6, 3.1 Hz, 2H, H^1), 4.09 – 3.98 (m, 2H, H^{3,6e}), 3.01 – 2.95 (m, 1H, H^{5e}), 2.88 – 2.79 (m, 2H, H^{5a,6a}), 2.15 – 2.09 (m, 1H, H^{4e}), 1.51 – 1.48 (m, 1H, H^{4a}), 1.40 (s, 9H, H^7). LC-MS (APCI$^+$/ESI): found m/z = 353.2 [M+H] $^+$ (cal. For $C_{17}H_{22}F_2N_4O_2$, 352.17). Purity: 98%, t_R = 2.487 min.

Tert-butyl 4-(1H-benzo[d]imidazol-2-yl)piperidine-1-carboxylate (63)

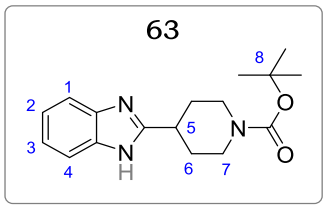

To a stirring solution of *N*-Boc-4-formylpiperidine (0.400 g, 1.88 mmol) and freshly activated 4Å molecular sieves in toluene (10 ml) at 24°C was added *o*-phenylenediamine (0.305 g, 2.82 mmol). The reaction mixture was then bubbled with one balloon of oxygen (O_2) and stirred at room temperature (24°C) for 12 h. Molecular sieves were filtered over filter paper, and the filtrate was concentrated under vacuum before being purified *via* flash chromatography with 6 – 7% MeOH/DCM to afford the product. Pale yellow solid (0.401 g, 85%). R_f(10% MeOH/DCM), 0.51. ^{1}H NMR (400 MHz, Methanol-d_4) δ 7.21 (dd, J = 5.6, 3.1 Hz, 2H, $H^{1,4}$), 6.92 (dd, J = 5.6, 3.1 Hz, 2H, $H^{2,3}$), 4.10 – 4.06 (m, 2H, H^{7e}), 3.82 (tt, J = 10.8, 4.2 Hz, 1H, H^5), 3.09 – 3.01 (m, 2H, H^{7a}), 2.10 – 2.03 (m, 2H, H^{6e}), 1.51 – 1.45 (m, 2H, H^{6a}), 1.39 (s, 9H, H^8). LC-MS (APCI$^+$/ESI): found m/z = 302.2 [M+H] $^+$ (cal. For $C_{17}H_{23}N_3O_2$, 301.18). Purity: 98%, t_R = 2.402 min.

Tert-butyl 4-(1-(4-cyanobenzyl)-1H-benzo[d]imidazol-2-yl)piperidine-1-carboxylate (63')

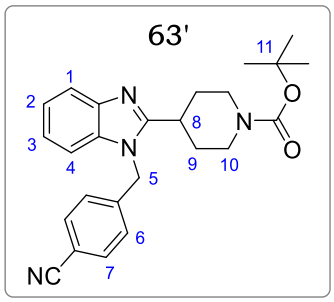

A mixture of **63** (0.200 g, 0.66 mmol) a with 4-(bromomethyl)benzonitrile (0.196 g, 0.80 mmol) and K_2CO_3 (0.110 g, 0.80 mmol) in DMF (5 ml) was stirred at 70°C for 8 hours. After completion, DMF was taken off using the gene-vac and the residue take up in 10% MeOH/DCM and filtered. Flash column chromatography at 5 – 7% MeOH/DCM afforded the product. Yellow solid (0.591 g, 88%). R_f (8% MeOH/DCM), 0.59. ^{1}H NMR (400 MHz, Methanol-d_4) δ 7.59 (d, J = 8.2 Hz, 2H, H^7), 7.29 (dd, J = 8.0, 1.3 Hz, 1H, H^1), 7.18 (d, J = 8.2 Hz, 2H, H^6), 6.98 (ddd, J = 8.0, 7.2, 1.2 Hz, 1H, H^2), 6.88 (dd, J = 8.2, 1.3 Hz, 1H, H^4), 6.79 (ddd, J = 8.2, 7.2, 1.1 Hz, 1H, H^3), 5.35 (s, 2H, H^5), 4.05 – 3.99 (m, 2H, H^{10e}), 3.91 (tt, J = 11.2, 4.3 Hz, 1H, H^8), 2.97 – 2.89 (m, 2H, H^{10a}), 2.02 – 1.97 (m, 2H, H^{9e}), 1.49 – 1.35 (m, 11H, $H^{9a,11}$). LC-MS (APCI$^+$/ESI): found m/z = 417.2 [M+H] $^+$ (cal. For $C_{25}H_{28}N_4O_2$, 416.22). Purity: 98%, t_R = 2.644 min.

General Procedure 15: N-ethyl and N-*tert*-butyl (Boc) carboxylate deprotection

N-ethyl and N-*tert*-butyl (Boc) carboxylate intermediates were refluxed in 48% HBr solution for 2 hr at 120 °C and stirred in DCM with TFA (10 equiv) for 1 hr at 23 °C, respectively.

a) **48% Aqueous HBr workup**: After completion, the reaction mixture was cooled and diluted with deionized water, followed by neutralizing with 15% NaOH. The

aqueous solution was extracted with DCM, and the combined organic layers washed with brine and dried over anhydrous Na_2SO_4. Evaporating off the solvent *in vacuo* and washing residue in diethyl ether afforded the free amines.

b) **TFA workup**: After completion, DCM and TFA were evaporated *in vacuo* and the residue taken up 50% MeOH/DCM and stirred with Amberlyst A-21 free base resin at room temperature (23°C) until pH was neutral. The mixture was then filtered, and the filtrate evaporated *in vacuo* to afford free amines.

N-(piperidin-4-yl)-1H-benzo[*d*]imidazol-2-amine (14a)

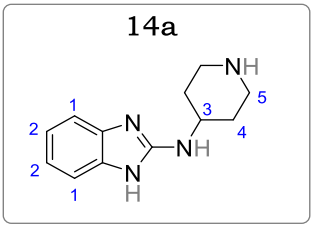

Obtained from **13a** (8.00 g, 28.0 mmol) as a white crystalline solid (3.52 g, 58%). R_f (10% MeOH/DCM), 0.08. ^{1}H NMR (600 MHz, Methanol-d_4) δ 7.43 (dd, J = 6.0, 3.1 Hz, 2H, H^2), 7.30 (dd, J = 6.0, 3.1 Hz, 2H, H^1), 4.03 (tt, J = 10.6, 4.1 Hz, 1H, H^3), 3.59 – 3.54 (m, 2H, H^{5e}), 3.30 – 3.24 (m, 2H, H^{5a}), 2.39 – 2.33 (m, 2H, H^{4e}), 2.04 – 1.96 (m, 2H, H^{4a}). LC-MS (APCI$^+$/ESI): found m/z = 217.2 [M+H] $^+$ (cal. For $C_{12}H_{16}N_4$, 216.29). Purity: 98%, t_R = 0.621 min.

1-Methyl-N-(piperidin-4-yl)-1H-benzo[*d*]imidazol-2-amine (14b)

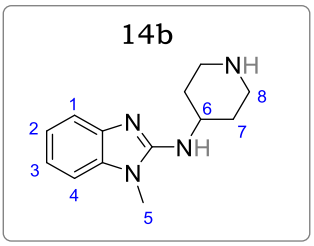

Obtained from **13b** (18.0 g, 59.6 mmol) as a white solid (12.2 g, 89%). R_f (10% MeOH/DCM), 0.17. ^{1}H NMR (400 MHz, Methanol-d_4) δ 7.27 (dd, J = 7.9, 1.2 Hz, 1H, H^1), 7.11 (dd, J = 7.6, 1.5 Hz, 1H, H^4), 7.05 – 6.96 (m, 2H, H^{2,3}), 3.85 (tt, J = 11.1, 4.0 Hz, 1H, H^6), 3.51 (s, 3H, H^5), 3.22 – 3.10 (m, 2H, H^{8e}), 2.79 (td, J = 12.5, 2.6 Hz, 2H, H^{8a}), 2.23 – 2.00 (m, 2H, H^{7e}), 1.56 (dtd, J = 13.4, 12.0, 4.0 Hz, 2H, H^{7a}). LC-MS (APCI$^+$/ESI): found m/z = 231.2 [M+H] $^+$ (cal. For $C_{13}H_{18}N_4$, 230.15). Purity: 99%, t_R = 0.703 min.

1-Isopropyl-N-(piperidin-4-yl)-1H-benzo[*d*]imidazol-2-amine (14c)

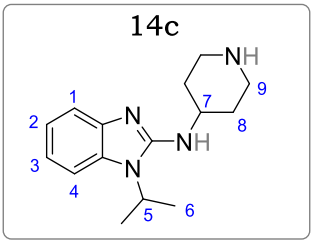

Obtained from **13c** (0.500 g, 1.52 mmol) as a white solid (0.336 g, 86%). R_f (10% MeOH/DCM), 0.23. ^{1}H NMR (400 MHz, Methanol-d_4) δ 7.37 (dd, J = 7.7, 1.2 Hz, 1H, H^1), 7.30 (dd, J = 8.0, 1.2 Hz, 1H, H^4), 6.96 (ddd, J = 8.0, 7.2, 1.3 Hz, 1H, H^3), 6.77 (ddd, J = 7.7, 7.2, 1.3 Hz, 1H, H^2), 4.55 (hept, J = 6.8 Hz, 1H, H^5), 4.20 (tt, J = 10.8, 4.0 Hz, 1H, H^7), 3.98 – 3.91 (m, 2H, H^{9e}), 3.05 – 2.96 (m, 2H, H^{9a}), 2.11 – 2.03 (m, 2H, H^{8e}), 1.59 (d, J = 6.8 Hz, 6H, H^6), 1.55

– 1.47 (m, 2H, H^{8a}). LC-MS (APCI$^+$/ESI): found m/z = 259.2 $[M+H]^+$ (cal. For $C_{15}H_{22}N_4$, 258.18). Purity: 99%, t_R = 0.877 min.

4-((2-(piperidin-4-ylamino)-1H-benzo[*d*]imidazol-1-yl) methyl) benzonitrile (14d)

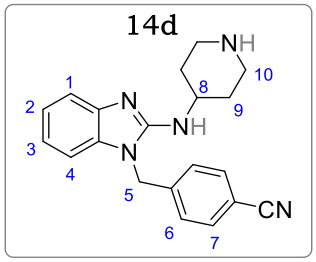

Obtained from **13d** (8.50 g, 28.0 mmol) as a light yellow solid (6.40 g, 98%). R_f(10% MeOH/DCM), 0.05. ^{1}H NMR (400 MHz, Methanol-d_4) δ 7.67 (d, J = 8.4 Hz, 2H, H^7), 7.32 (dd, J = 7.9, 0.9 Hz, 1H, H^1), 7.25 (d, J = 8.4 Hz, 2H, H^6), 7.05 (ddd, J = 7.9, 7.1, 1.1 Hz, 1H, H^2), 6.99 (dd, J = 8.0, 1.5 Hz, 1H, H^4), 6.94 (ddd, J = 8.0, 7.1, 1.1 Hz, 1H, H^3), 5.37 (s, 2H, H^5), 3.89 (tt, J = 11.1, 4.1 Hz, 1H, H^8), 3.07 (dt, J = 12.9, 3.6 Hz, 2H, H^{10e}), 2.74 (td, J = 12.5, 2.6 Hz, 2H, H^{10a}), 2.11 – 2.01 (m, 2H, H^{9e}), 1.46 (dtd, J = 13.3, 11.9, 4.07 Hz, 2H, H^{9a}). LC-MS (APCI$^+$/ESI): found m/z = 332.2 $[M+H]^+$ (cal. For $C_{20}H_{25}N_5O$, 331.18). Purity: 99%, t_R = 0.303 min.

(R)-4-((2-(Pyrrolidine-3-ylamino)-1H-benzo[*d*]imidazol-1-yl)methyl) benzonitrile (57a)

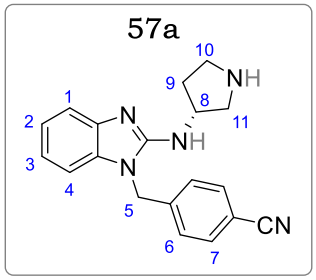

Obtained from **56a** (0.280 g, 0.67 mmol) as a pale-yellow solid (0.181 g, 85%). R_f(10% MeOH/DCM), 0.10. ^{1}H NMR (600 MHz, Methanol-d_4) δ 7.73 (d, J = 8.4 Hz, 2H, H^7), 7.55 (dd, J = 8.0, 1.2 Hz, 1H, H^1), 7.43 (d, J = 8.4 Hz, 2H, H^6), 7.38 (ddd, J = 8.0, 7.1, 1.5 Hz, 1H, H^2), 7.31 (dd, J = 8.2, 1.2 Hz, 1H, H^4), 7.29 (ddd, J = 8.2, 7.1, 1.4 Hz, 1H, H^3), 5.60 (s, 2H, H^5), 4.69 (tt, J = 6.7, 4.3 Hz, 1H, H^8), 3.79 (dd, J = 12.8, 6.7 Hz, 1H, H^{11e}), 3.61 – 3.55 (m, 2H, $H^{10e,11a}$), 3.52 (ddd, J = 11.5, 8.2, 5.7 Hz, 1H, H^{10a}), 2.56 (ddd, J = 14.7, 8.2, 6.7 Hz, 1H, H^{9e}), 2.31 (ddd, J = 11.5, 8.2, 4.3 Hz, 1H, H^{9a}). LC-MS (APCI$^+$/ESI): found m/z = 318.2 $[M+H]^+$ (cal. For $C_{19}H_{19}N_5$, 317.16). Purity: 99%, t_R = 2.499 min.

(S)-4-((2-(pyrrolidin-3-ylamino)-1H-benzo[*d*]imidazol-1-yl) methyl) benzonitrile (57b)

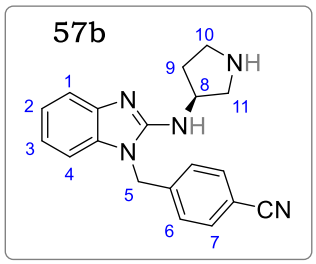

Obtained from **56b** (0.200 g, 0.47 mmol) as a pale-yellow solid (0.114 g, 75%). R_f(10% MeOH/DCM), 0.11. ^{1}H NMR (600 MHz, Methanol-d_4) δ 7.70 (d, J = 8.3 Hz, 2H, H^7), 7.41 (dd, J = 7.8, 1.2 Hz, 1H, H^1), 7.35 (d, J = 8.3 Hz, 2H, H^6), 7.29 (ddd, J = 7.8, 7.2, 1.2 Hz, 1H, H^2), 7.24 (dd, J = 8.1, 1.2 Hz, 1H, H^4), 7.19 (ddd, J = 8.1, 7.2, 1.4 Hz, 1H, H^3), 5.64 (s, 2H, H^5), 4.62 (tt, J = 7.0, 4.1 Hz, 1H, H^8), 3.66 (dd, J = 12.3, 7.0 Hz, 1H, H^{11e}), 3.55 – 3.46 (m, 2H, $H^{10e,11a}$), 3.30 (ddd, J = 10.9, 8.5, 5.1 Hz, 1H, H^{10a}), 2.52 (ddd, J = 15.0, 8.5, 7.0 Hz, 1H, H^{9e}), 2.19

(ddd, J = 11.5, 8.5, 4.1 Hz, 1H, H^{9a}). LC-MS (APCI$^+$/ESI): found m/z = 318.2 $[M+H]^+$ (cal. for $C_{19}H_{19}N_5$, 317.16). Purity: 97%, t_R = 2.401 min.

4-((2-(2,6-diazaspiro[3.4]octan-6-yl)-1H-benzo[*d*]imidazol-1-yl) methyl) benzonitrile (57c)

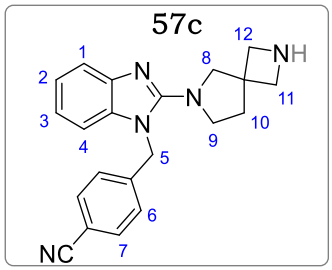

Obtained from **56c** (0.160 g, 0.36 mmol) as a pale-yellow solid (0.121 g, 98%). R_f (10% MeOH/DCM), 0.10. ^{1}H NMR (600 MHz, Methanol-d_4) δ 7.70 (d, J = 8.1 Hz, 2H, H^7), 7.38 (dd, J = 7.8, 1.2 Hz, 1H, H^1), 7.25 (d, J = 8.1 Hz, 2H, H^6), 7.10 (ddd, J = 7.8, 7.2, 1.2 Hz, 1H, H^2), 7.08 (dd, J = 8.1, 1.3 Hz, 1H, H^4), 7.02 (ddd, J = 8.1, 7.2, 1.2 Hz, 1H, H^3), 5.45 (s, 2H, H^5), 3.77 (br-s, 4H, $H^{11,12}$), 3.71 (s, 2H, H^8), 3.50 (t, J = 6.8 Hz, 2H, H^9), 2.11 (t, J = 6.8 Hz, 2H, H^{10}). LC-MS (APCI$^+$/ESI): found m/z = 344.1 $[M+H]^+$ (cal. for $C_{21}H_{21}N_5$, 343.18). Purity: 99%, t_R = 0.426 min.

4-((2-(piperazin-1-yl)-1H-benzo[*d*]imidazol-1-yl)methyl)benzonitrile (57d)

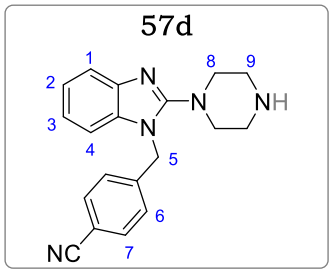

Obtained from **56d** (0.500 g, 1.20 mmol) as a pale-yellow solid (0.353 g, 93%). R_f (10% MeOH/DCM), 0.12. ^{1}H NMR (400 MHz, Methanol-d_4) δ 7.63 (d, J = 8.3 Hz, 2H, H^7), 7.50 (dd, J = 7.7, 0.9 Hz, 1H, H^1), 7.31 (d, J = 8.3 Hz, 2H, H^6), 7.19 (ddd, J = 7.7, 6.1, 1.0 Hz, 1H, H^2), 7.12 – 7.07 (m, 2H, $H^{3,4}$), 5.39 (s, 2H, H^5), 3.58 – 3.39 (br, 4H, H^9), 3.20 – 3.11 (m, 4H, H^8). LC-MS (APCI$^+$/ESI): found m/z = 318.1 $[M+H]^+$ (cal. for $C_{19}H_{19}N_5$, 317.16). Purity: 98%, t_R = 2.134 min.

(S)-4-((2-(3-methylpiperazin-1-yl)-1H-benzo[*d*]imidazol-1-yl)methyl)benzonitrile (57e)

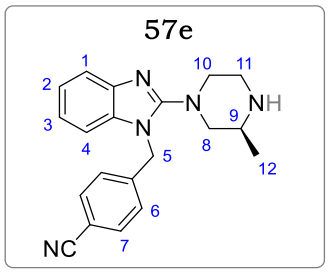

Obtained from **56e** (0.280 g, 0.65 mmol) as a yellow solid (0.210 g, 98%). R_f (10% MeOH/DCM), 0.15. ^{1}H NMR (600 MHz, Methanol-d_4) δ 7.62 (d, J = 8.5 Hz, 2H, H^7), 7.49 (dd, J = 7.9, 0.9 Hz, 1H, H^1), 7.22 (d, J = 8.5 Hz, 2H, H^6), 7.20 (ddd, J = 7.9, 6.9, 1.2 Hz, 1H, H^2), 7.15 (dd, J = 8.1, 1.2 Hz, 1H, H^4), 7.14 (ddd, J = 8.1, 6.9, 1.1 Hz, 1H, H^3), 5.43 (s, 2H, H^5), 4.30 – 4.21 (m, 1H, H^9), 3.89 – 3.82 (m, 1H, H^{11e}), 3.33 – 3.20 (m, 1H, H^{10e}), 3.01 – 2.93 (m, 1H, H^{11a}), 2.66 (dd, J = 13.0, 2.2 Hz, 1H, H^{8e}), 2.43 (dd, J = 12.9, 3.7 Hz, 1H, H^{8a}), 2.22

(td, J = 12.7, 3.6 Hz, 1H, H^{10a}), 1.18 (d, J = 6.9 Hz, 3H, H^{12}). LC-MS (APCI$^+$/ESI): found m/z = 332.2 $[M+H]^+$ (cal. for $C_{20}H_{21}N_5$, 331.18). Purity: 96%, t_R = 2.094 min.

4-((2-(piperidin-4-yl)-1H-benzo[d]imidazol-1-yl)methyl)benzonitrile (64)

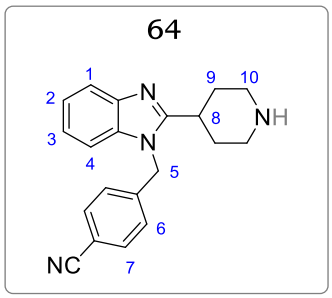

Obtained from **63'** (0.500 g, 1.20 mmol) as a pale-yellow solid (0.372 g, 98%). R_f (10% MeOH/DCM), 0.21. ^{1}H NMR (400 MHz, Methanol-d_4) δ 7.49 (d, J = 8.0 Hz, 2H, H^7), 7.33 (dd, J = 7.7, 1.1 Hz, 1H, H^1), 7.26 (d, J = 8.0 Hz, 2H, H^6), 7.18 (ddd, J = 7.7, 6.5, 1.0 Hz, 1H, H^2), 7.08 – 6.98 (m, 2H, $H^{3,4}$), 5.41 (s, 2H, H^5), 3.55 – 3.40 (br, 4H, H^{10}), 3.29 (tt, J = 10.2, 3.8 Hz, 1H, H^8), 3.18 – 3.12 (m, 4H, H^9). LC-MS (APCI$^+$/ESI): found m/z = 317.2 $[M+H]^+$ (cal. for $C_{20}H_{20}N_4$, 316.17). Purity: 98%, t_R = 2.208 min.

1-methyl-2-(piperidin-4-ylamino)-1H-benzo[d]imidazole-5-carbonitrile (131a)

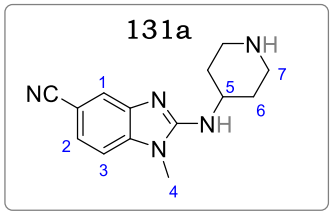

Obtained from **130a** (0.500 g, 1.41 mmol) as an off white solid (0.319 g, 89%). R_f(5% MeOH/DCM), 0.13. ^{1}H NMR (400 MHz, Methanol-d_4) δ 7.97 (d, J = 1.4 Hz, 1H, H^1), 7.78 (d, J = 7.5 Hz, 1H, H^3), 7.52 (dd, J = 7.5, 1.4 Hz, 1H, H^2), 3.94 (tt, J = 10.8, 4.0 Hz, 1H, H^5), 3.50 (s, 3H, H^4), 3.21 – 3.13 (m, 2H, H^{7e}), 3.08 – 2.99 (m, 2H, H^{7a}), 2.09 – 1.98 (m, 2H, H^{6e}), 1.52 – 1.39 (m, 2H, H^{6a}). LC-MS (APCI$^+$/ESI): found m/z = 256.2 $[M+H]^+$ (cal. for $C_{14}H_{17}N_5$, 255.15). Purity: 99%, t_R = 0.699 min.

1-methyl-N-(piperidin-4-yl)-5-(trifluoromethyl)-1H-benzo[d]imidazol-2-amine (131b)

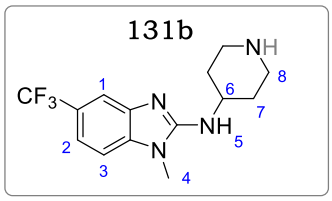

Obtained from **130b** (0.480 g, 1.21 mmol) as a white solid (0.348 g, 97%). R_f(5% MeOH/DCM), 0.17. ^{1}H NMR (300 MHz, DMSO-d_6) δ 7.46 (d, J = 1.3 Hz, 1H, H^1), 7.33 (d, J = 8.2 Hz, 1H, H^3), 7.25 (dd, J = 8.2, 1.3 Hz, 1H, H^2), 6.98 (d, J = 7.1 Hz, 1H, H^5), 4.12 – 3.93 (m, 1H, H^6), 3.56 (s, 3H, H^4), 3.44 – 3.25 (m, 2H, H^{8e}), 3.05 (td, J = 12.5, 3.0 Hz, 2H, H^{8a}), 2.24 – 2.08 (m, 2H, H^{7a}), 1.87 – 1.66 (m, 2H, H^{7e}). LC-MS (APCI$^+$/ESI): found m/z = 299.1 $[M+H]^+$ (cal. for $C_{14}H_{17}F_3N_4$, 298.14). Purity: 99%, t_R = 0.813 min.

5-methoxy-1-methyl-N-(piperidin-4-yl)-1H-benzo[d]imidazol-2-amine (131c)

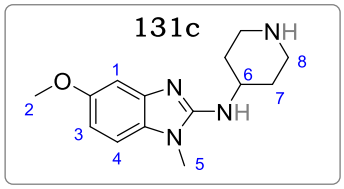

Obtained from **130c** (0.470 g, 1.31 mmol) as a light brown solid (0.322 g, 95%). R_f(5% MeOH/DCM), 0.10. ^{1}H NMR (400 MHz, Methanol-d_4) δ 7.44 (d, J = 1.1 Hz, 1H, H^1), 7.27 (dd, J = 7.5, 1.1 Hz, 1H, H^3), 7.17 (d, J = 7.5 Hz, 1H, H^4), 3.92 (tt, J = 11.0, 4.1 Hz, 1H, H^6), 3.85 (s, 3H, H^2), 3.52 (s, 3H, H^5), 3.19 – 3.11 (m, 2H, H^{8e}), 3.07 – 2.98 (m, 2H, H^{8a}), 2.10 – 2.01 (m, 2H, H^{7e}), 1.53 – 1.41 (m, 2H, H^{7a}). LC-MS (APCI$^+$/ESI): found m/z = 261.2 [M+H] $^+$ (cal. for $C_{14}H_{20}N_4O$, 260.16). Purity: 99%, t_R = 0.690 min.

1-methyl-5-(methylsulfonyl)-N-(piperidin-4-yl)-1H-benzo[d]imidazol-2-amine (131d)

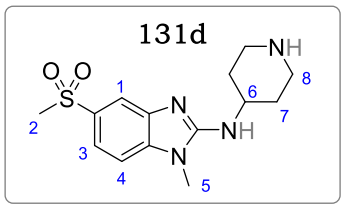

Obtained from **130d** (0.490 g, 1.20 mmol) as a light brown solid (0.314 g, 85%). R_f(5% MeOH/DCM), 0.09. ^{1}H NMR (400 MHz, Methanol-d_4) δ 7.89 (d, J = 1.3 Hz, 1H, H^1), 7.81 (d, J = 7.8 Hz, 1H, H^4), 7.40 (dd, J = 7.8, 1.3 Hz, 1H, H^3), 3.91 (tt, J = 10.9, 4.1 Hz, 1H, H^6), 3.52 (s, 3H, H^5), 3.38 (s, 3H, H^2), 3.19 – 3.12 (m, 2H, H^{8e}), 3.07 – 2.98 (m, 2H, H^{8a}), 2.09 – 2.00 (m, 2H, H^{7e}), 1.51 – 1.43 (m, 2H, H^{7a}). LC-MS (APCI$^+$/ESI): found m/z = 309.1 [M+H] $^+$ (cal. for $C_{14}H_{20}N_4O_2S$, 308.13). Purity: 97%, t_R = 0.643 min

Methyl 1-methyl-2-(piperidin-4-ylamino)-1H-benzo[d]imidazole-5-carboxylate (131e)

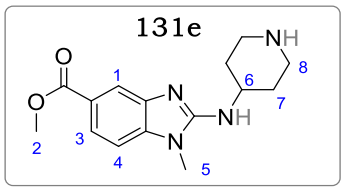

Obtained from **130e** (0.495 g, 1.28 mmol) as an off white solid (0.341 g, 93%). R_f(5% MeOH/DCM), 0.08. ^{1}H NMR (400 MHz, Methanol-d_4) δ 8.12 (d, J = 1.3 Hz, 1H, H^1), 7.90 (dd, J = 7.7, 1.3 Hz, 1H, H^3), 7.57 (d, J = 7.7 Hz, 1H, H^4), 3.90 (tt, J = 10.9, 4.2 Hz, 1H, H^6), 3.79 (s, 3H, H^2), 3.52 (s, 3H, H^5), 3.20 – 3.13 (m, 2H, H^{8e}), 3.09 – 3.01 (m, 2H, H^{8a}), 2.08 – 2.02 (m, 2H, H^{7e}), 1.51 – 1.43 (m, 2H, H^{7a}). LC-MS (APCI$^+$/ESI): found m/z = 289.2 [M+H] $^+$ (cal. for $C_{15}H_{20}N_4O_2$, 288.16). Purity: 98%, t_R = 0.661 min.

5-fluoro-1-methyl-N-(piperidin-4-yl)-1H-benzo[d]imidazol-2-amine (131f)

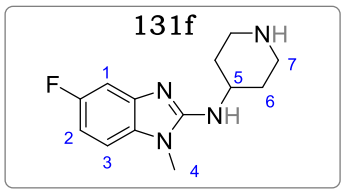

Obtained from **130f** (0.490 g, 1.41 mmol) as a light brown solid (0.342 g, 98%). R_f(5% MeOH/DCM), 0.11. ^{1}H NMR (400 MHz, Methanol-d_4) δ 7.51 (dd, J = 8.2, 1.3 Hz, 1H, H^1), 7.40 (dd, J = 7.9, 1.5 Hz, 1H, H^3), 6.87 (ddd, J = 8.0, 7.9, 1.3 Hz, 1H, H^2), 3.92 (tt, J = 11.2, 4.1 Hz, 1H, H^5), 3.52 (s, 3H, H^4),

3.19 – 3.10 (m, 2H, H^{7e}), 3.04 – 2.93 (m, 2H, H^{7a}), 2.09 – 2.00 (m, 2H, H^{6e}), 1.50 – 1.39 (m, 2H, H^{6a}). LC-MS (APCI$^+$/ESI): found m/z = 249.2 $[M+H]^+$ (cal. for $C_{13}H_{17}FN_4$, 248.14). Purity: 97%, t_R = 0.802 min.

5-bromo-1-methyl-N-(piperidin-4-yl)-1H-benzo[d]imidazol-2-amine (131g)

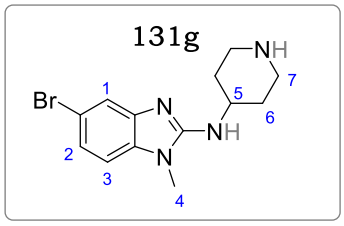

Obtained from **130g** (0.380 g, 0.93 mmol) as a brown solid (0.273 g, 95%). R_f(5% MeOH/DCM), 0.12. ^{1}H NMR (400 MHz, Methanol-d_4) δ 7.35 (d, J = 1.3 Hz, 1H, H^1), 7.28 (d, J = 7.8 Hz, 1H, H^3), 7.13 (dd, J = 7.8, 1.3 Hz, 1H, H^2), 3.92 (tt, J = 10.9, 4.0 Hz, 1H, H^5), 3.51 (s, 3H, H^4), 3.20 – 3.12 (m, 2H, H^{7e}), 3.07 – 2.99 (m, 2H, H^{7a}), 2.10 – 2.00 (m, 2H, H^{6e}), 1.49 – 1.38 (m, 2H, H^{6a}). LC-MS (APCI$^+$/ESI): found m/z = 309.1 $[M+H]^+$ (cal. for $C_{13}H_{17}BrN_4$, 308.06, 310.06). Purity: 98%, t_R = 0.856 min.

5,6-difluoro-1-methyl-N-(piperidin-4-yl)-1H-benzo[d]imidazol-2-amine (131h)

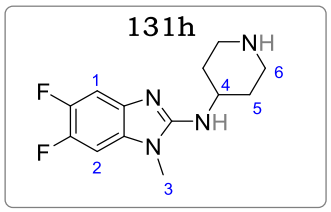

Obtained from **130h** (0.160 g, 0.44 mmol) as a light brown solid (0.108 g, 93%). R_f(5% MeOH/DCM), 0.13. ^{1}H NMR (400 MHz, Methanol-d_4) δ 7.45 (dd, J = 7.4, 5.3 Hz, 1H, H^1), 7.34 (dd, J = 7.5, 5.5 Hz, 1H, H^2), 3.92 (tt, J = 11.2, 4.0 Hz, 1H, H^4), 3.52 (s, 3H, H^3), 3.19 – 3.10 (m, 2H, H^{6e}), 3.05 – 2.96 (m, 2H, H^{6a}), 2.10 – 1.98 (m, 2H, H^{5e}), 1.49 – 1.38 (m, 2H, H^{5a}). LC-MS (APCI$^+$/ESI): found m/z = 267.1 $[M+H]^+$ (cal. for $C_{13}H_{16}F_2N_4$, 266.13). Purity: 96%, t_R = 0.822 min.

5,6-dichloro-1-methyl-N-(piperidin-4-yl)-1H-benzo[d]imidazol-2-amine (131i)

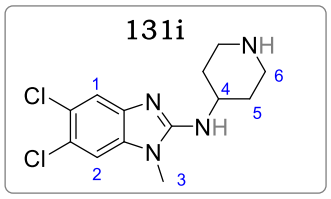

Obtained from **130i** (0.130 g, 0.33 mmol) as a brown solid (0.084 g, 86%). R_f(5% MeOH/DCM), 0.14. ^{1}H NMR (400 MHz, Methanol-d_4) δ 8.15 (s, 1H, H^1), 8.04 (s, 1H, H^2), 3.92 (tt, J = 10.9, 4.1 Hz, 1H, H^4), 3.51 (s, 3H, H^3), 3.21 – 3.12 (m, 2H, H^{6e}), 3.09 – 3.01 (m, 2H, H^{6a}), 2.09 – 2.00 (m, 2H, H^{5e}), 1.48 – 1.37 (m, 2H, H^{5a}). LC-MS (APCI$^+$/ESI): found m/z = 299.1, 301.1 $[M+H]^+$ (cal. for $C_{13}H_{16}Cl_2N_4$, 298.08, 300.07). Purity: 99%, t_R = 0.811 min.

1,5,6-trimethyl-*N*-(piperidin-4-yl)-1H-benzo[d]imidazol-2-amine (131j)

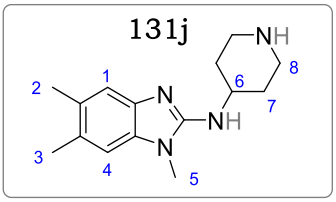

Obtained from **130j** (0.200 g, 0.56 mmol) as a light brown solid (0.127 g, 88%). R_f(5% MeOH/DCM) 0.12. ^{1}H NMR (400 MHz, Methanol-d_4) δ 7.39 (s, 1H, H^1), 7.28 (s, 1H, H^4), 3.91 (tt, J = 10.9, 4.1 Hz, 1H, H^6), 3.51 (s, 3H, H^5), 3.20 – 3.11 (m, 2H, H^{8e}), 3.06 – 2.98 (m, 2H, H^{8a}), 2.26 (s, 3H, H^2), 2.20 (s, 3H, H^3), 2.09 – 1.98 (m, 2H, H^{7e}), 1.50 – 1.39 (m, 2H, H^{7a}). LC-MS (APCI$^+$/ESI): found m/z = 259.2 [M+H]$^+$ (cal. For $C_{15}H_{22}N_4$, 258.18). Purity: 98%, t_R = 0.733 min.

***N*-(piperidin-4-yl)benzo[d]oxazol-2-amine (145a)**

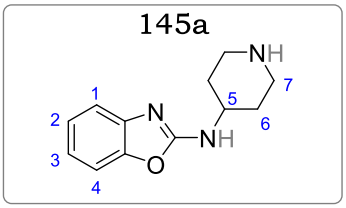

Obtained from **144a** (0.500 g, 1.58 mmol) as a white crystalline solid (0.329 g, 96%). R_f(10% MeOH/DCM), 0.10. ^{1}H NMR (400 MHz, Methanol-d_4) δ 7.38 (dd, J = 8.0, 1.0 Hz, 1H, H^4), 7.22 (dd, J = 7.8, 1.2 Hz, 1H, H^1), 7.08 (ddd, J = 8.0, 7.0, 1.1 Hz, 1H, H^3), 6.79 (ddd, J = 7.8, 7.0, 1.1 Hz), 3.92 (tt, J = 11.0, 4.0 Hz, 1H, H^5), 3.79 – 3.70 (m, 2H, H^{7e}), 3.09 – 2.99 (m, 2H, H^{7a}), 2.08 – 1.97 (m, 2H, H^{6e}), 1.46 – 1.37 (m, 2H, H^{6a}). LC-MS (APCI$^+$/ESI): found m/z = 218.1 [M+H]$^+$ (cal. for $C_{12}H_{15}N_3O$, 217.12). Purity: 99%, t_R = 0.559 min.

***N*-(3,3-difluoropiperidin-4-yl)-1H-benzo[d]imidazol-2-amine (145b)**

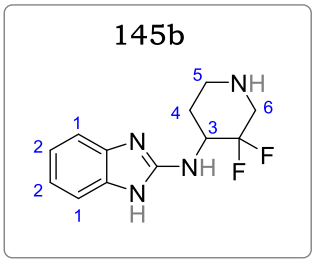

Obtained from **144b** (0.350 g, 1.00 mmol) as a white solid (0.245 g, 98%). R_f(10% MeOH/DCM), 0.21. ^{1}H NMR (400 MHz, Methanol-d_4) δ 7.21 (dd, J = 5.6, 3.2 Hz, 2H, H^2), 6.98 (dd, J = 5.6, 3.2 Hz, 2H, H^1), 4.11 – 3.99 (m, 2H, H^{3,6e}), 2.99 – 2.86 (m, 1H, H^{5e}), 2.65 – 2.49 (m, 2H, H^{5a,6a}), 2.11 – 2.05 (m, 1H, H^{4e}), 1.48 – 1.39 (m, 1H, H^{4a}). LC-MS (APCI$^+$/ESI): found m/z = 253.1 [M+H]$^+$ (cal. for $C_{12}H_{14}F_2N_4$, 252.12). Purity: 98%, t_R = 0.356 min.

***N*-(piperidin-4-yl)-1H-imidazo[4,5-*b*]pyridin-2-amine (145c)**

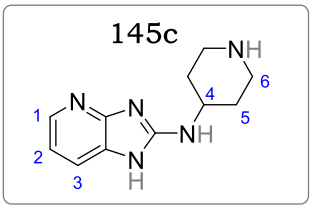

Obtained from **144c** (0.480 g, 1.51 mmol) as a white solid (0.322 g, 98%). R_f(10% MeOH/DCM), 0.18. ^{1}H NMR (400 MHz, Methanol-d_4) δ 8.39 (dd, J = 5.3, 1.5 Hz, 1H, H^1), 7.58 (dd, J = 8.0, 1.5 Hz, 1H, H^3), 7.13 (dd, J = 8.0, 5.3 Hz, 1H, H^2), 3.89 (tt, J = 10.9, 3.8 Hz, 1H, H^4), 3.95 – 3.86 (m, 2H, H^{6e}), 3.08 – 2.98

(m, 2H, H^{6a}), 2.03 – 1.94 (m, 2H, H^{5e}), 1.54 – 1.43 (m, 2H, H^{5a}). LC-MS (APCI$^+$/ESI): found m/z = 218.1 [M+H]$^+$ (cal. for $C_{11}H_{15}N_5$, 217.13). Purity: 98%, t_R = 0.359 min.

5-methyl-*N*-(piperidin-4-yl)-1H-imidazo[4,5-*b*]pyridin-2-amine (145d)

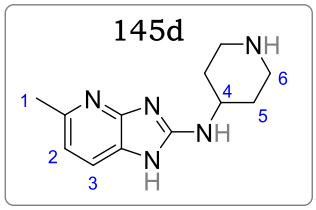

Obtained from **144d** (0.470 g, 1.42 mmol) as a pale orange solid (0.321 g, 98%). R_f(10% MeOH/DCM), 0.18. ^{1}H NMR (400 MHz, Methanol-d_4) δ 7.21 (d, J = 8.1 Hz, 1H, H^3), 6.53 (d, J = 8.1 Hz, 1H, H^2), 3.90 (tt, J = 10.8, 3.9 Hz, 1H, H^4), 3.98 – 3.89 (m, 2H, H^{6e}), 3.01 – 2.93 (m, 2H, H^{6a}), 2.33 (s, 3H, H^1), 2.05 – 1.96 (m, 2H, H^{5e}), 1.59 – 1.50 (m, 2H, H^{5a}). LC-MS (APCI$^+$/ESI): found m/z = 232.2 [M+H]$^+$ (cal. for $C_{12}H_{17}N_5$, 231.15). Purity: 98%, t_R = 0.298 min.

***N*-(piperidin-4-yl)-1H-imidazo[4,5-c]279yridine-2-amine (145e)**

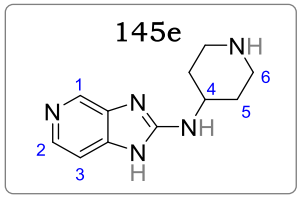

Obtained from **144e** (0.450 g, 1.42 mmol) as a white solid (0.300 g, 98%). R_f (10% MeOH/DCM), 0.12. ^{1}H NMR (400 MHz, Methanol-d_4) δ 8.56 (d, J = 1.5 Hz, 1H, H^1), 8.19 (dd, J = 5.3, 1.5 Hz, 1H, H^2), 7.29 (d, J = 5.3 Hz, 1H, H^3), 3.91 (tt, J = 10.9, 4.0 Hz, 1H, H^4), 4.01 – 3.92 (m, 2H, H^{6e}), 2.98 – 2.89 (m, 2H, H^{6a}), 2.08 – 1.97 (m, 2H, H^{5e}), 1.59 – 1.51 (m, 2H, H^{5a}). LC-MS (APCI$^+$/ESI): found m/z = 218.1 [M+H]$^+$ (cal. For $C_{11}H_{15}N_5$, 217.13). Purity: 98%, t_R = 0.246 min.

6-chloro-*N*-(piperidin-4-yl)-1H-imidazo[4,5-c]279yridine-2-amine (145f)

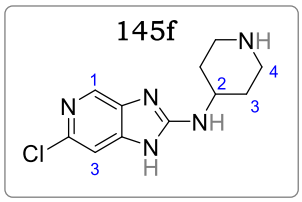

Obtained from **144f** (0.370 g, 1.05 mmol) as a white solid (0.252 g, 95%). R_f (10% MeOH/DCM), 0.19. ^{1}H NMR (400 MHz, Methanol-d_4) δ 8.56 (s, 1H, H^1), 7.66 (s, 1H, H^2), 3.89 (tt, J = 10.7, 3.9 Hz, 1H, H^3), 3.96 – 3.85 (m, 2H, H^{5e}), 3.05 – 2.93 (m, 2H, H^{5a}), 2.08 – 1.99 (m, 2H, H^{4e}), 1.56 – 1.48 (m, 2H, H^{4a}). LC-MS (APCI$^+$/ESI): found m/z = 252.1, 254.1 [M+H]$^+$ (cal. For $C_{11}H_{14}ClN_5$, 251.09, 253.09). Purity: 99%, t_R = 0.256 min.

***N*-(3-fluoropiperidin-4-yl)-1H-benzo[d]imidazol-2-amine (145g)**

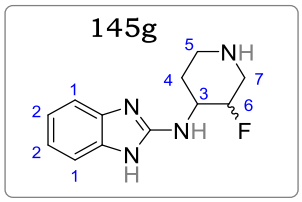

Obtained from **144g** (0.470 g, 1.41 mmol) as a white solid (0.256 g, 78%). R_f (10% MeOH/DCM), 0.19. ^{1}H NMR (400 MHz, Methanol-d_4) δ 7.19 (dd, J = 5.5, 3.1 Hz, 2H, H^2), 6.85 (dd, J = 5.5, 3.1 Hz, 2H, H^1), 4.30 (dtd, J = 49.3, 10.3, 4.5 Hz, 1H, H^6), 3.79 (qd, J = 11.0, 4.2 Hz, 1H, H^3), 3.18 (d, J = 11.6 Hz, 1H, H^{7e}), 2.90 – 2.81 (m, 1H, H^{5e}), 2.73 – 2.58 (m, 2H, $H^{7a,5a}$), 2.03 – 1.91 (m, 1H, H^{4e}), 1.44 – 1.36

(m, 1H, H^{4a}). LC-MS (APCI$^+$/ESI): found m/z = 235.1 [M+H] $^+$ (cal. For $C_{12}H_{15}FN_4$, 234.13). Purity: 98%, t_R = 0.295 min.

7-chloro-N-(piperidin-4-yl)quinolin-4-amine (171)

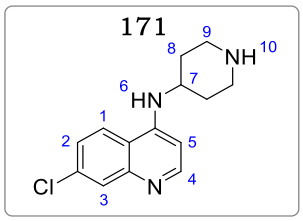

Obtained from **170** (7.00 g, 19.4 mmol) as a pale-yellow solid (4.95 g, 98%). R_f (10% MeOH/DCM), 0.13. ^{1}H NMR (400 MHz, DMSO) δ 8.78 (s, 1H, H^{10}), 8.56 – 8.34 (m, 2H, $H^{1,4}$), 7.85 (s, 1H, H^3), 7.77 (d, J = 6.4 Hz, 1H, H^5), 7.56 (d, J = 8.5 Hz, 1H, H^2), 6.77 (d, J = 6.0 Hz, 1H, H^6), 3.95 (tt, J = 11.1, 4.2 Hz, 1H, H^7), 3.56 – 3.25 (m, 2H, H^{9e}), 3.07 (td, J = 12.4, 3.5 Hz, 2H, H^{9a}), 2.18 – 2.01 (m, 2H, H^{8e}), 1.82 (dtd, J = 12.4, 10.8, 3.9 Hz, 2H, H^{8a}). LC-MS (APCI$^+$/ESI): found m/z = 262.1 $[M+H]^+$ (cal. for $C_{14}H_{16}ClN_3$, 261.10). Purity: 99%, t_R = 0.179 min.

1-(1-(4-fluorobenzyl)-1H-benzo[d]imidazol-2-yl)piperidin-4-amine (204)

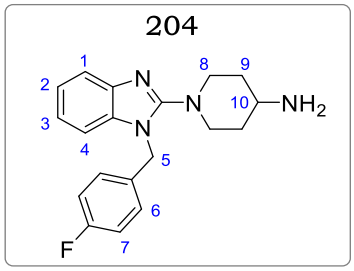

Obtained from **203** (4.50 g, 10.6 mmol) as a pale-yellow solid (3.37 g, 98%). R_f (10% MeOH/DCM), 0.12. ^{1}H NMR (400 MHz, Methanol-d_4) δ 7.70 (d, J = 8.1 Hz, 2H, H^7), 7.36 (dd, J = 7.8, 1.2 Hz, 1H, H^1), 7.25 (d, J = 8.1 Hz, 2H, H^6), 7.07 (ddd, J = 7.8, 6.5, 1.2 Hz, 1H, H^2), 6.95 – 6.88 (m, 2H, $H^{3,4}$), 5.42 (s, 2H, H^5), 3.56 (dt, J = 11.9, 3.9 Hz, 2H, H^{8e}), 3.48 – 3.41 (m, 3H, $H^{8a,10}$), 3.19 – 3.10 (m, 2H, H^{9e}), 2.21 – 2.15 (m, 2H, H^{9a}). LC-MS (APCI$^+$/ESI): found m/z = 325.2 $[M+H]^+$ (cal. for $C_{19}H_{21}FN_4$, 324.18). Purity: 98%, t_R = 0.159 min.

General Procedure 16: Bimolecular Nucleophilic Substitution (S_N2), Synthesis of Target Compounds

A solution of appropriate amine (1.0 equiv) and K_2CO_3 (1.5 equiv) in MeCN was stirred under reflux at 80 °C for 30 minutes. An appropriate alkyl bromide (1.2 equiv) was then added, and the resulting mixture further stirred under reflux at 85 °C for 5 – 24 hours. After completion, MeCN was taken off under reduced pressure, the residue taken up in 10% MeOH/DCM and filtered. The filtrate was adsorbed on silica gel, after which column chromatography was performed using a 3 – 10% MeOH/DCM gradient as eluent, to afford final compounds.

4-(2-(4-((1H-benzo[d]imidazol-2-yl)amino)piperidin-1-yl)ethyl)benzonitrile (15)

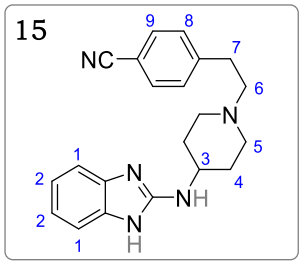

Obtained from **14a** (2.50 g, 11.6 mmol) and **1a** (2.91 g, 13.9 mmol) as a pale-yellow solid (3.40 g, 85%); m.p.: 88 – 89 °C; R_f (10% MeOH/DCM), 0.35. ^{1}H NMR (400 MHz, Methanol-d_4) δ 7.65 (d, J = 8.3 Hz, 2H, H^9), 7.44 (d, J = 8.3 Hz, 2H, H^8), 7.20 (dd, J = 5.8, 3.2 Hz, 2H, H^1), 6.98 (dd, J = 5.8, 3.2 Hz, 2H, H^2), 3.68 (tt, J = 10.7, 4.2 Hz, 1H, H^3), 3.12 – 3.02 (m, 2H, H^{5e}), 2.99 – 2.88 (m, 2H, H^6), 2.74 – 2.65 (m, 2H, H^7), 2.35 (td, J = 11.8, 2.6 Hz, 2H, H^{5a}), 2.17 – 2.04 (m, 2H, H^{4e}), 1.70 – 1.58 (m, 2H, H^{4a}). ^{13}C NMR (101 MHz, Methanol-d_4) δ 154.17, 146.02, 137.01, 131.98 (2C), 129.49 (2C), 120.18 (2C), 118.44, 111.29 (2C), 109.68, 59.02, 51.93 (2C), 49.32, 32.73, 31.58 (2C). LC-MS (APCI$^+$/ESI): found m/z = 346.2 [M+H] $^+$ (cal. For $C_{21}H_{23}N_5$, 345.20). Purity: 99%, t_R = 0.196 min.

4-(2-(4-((1-methyl-1H-benzo[d]imidazol-2-yl)amino)piperidin-1-yl)ethyl) benzonitrile (16)

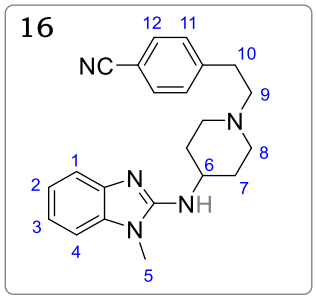

Obtained from **14b** (0.100 g, 0.43 mmol) and **1a** (0.110 g, 0.52 mmol) as a pale yellow solid (0.129 g, 84%); m.p.: 111 – 112 °C; R_f (10% MeOH/DCM) 0.39. ^{1}H NMR (400 MHz, Methanol-d_4) δ 7.44 (d, J = 8.3 Hz, 2H, H^{12}), 7.23 (d, J = 8.3 Hz, 2H, H^{11}), 7.06 (dd, J = 7.2, 1.1 Hz, 1H, H^1), 6.92 (dd, J = 7.5, 1.6 Hz, 1H, H^4), 6.85 – 6.76 (m, 2H, H^{2,3}), 3.57 (tt, J = 11.1, 4.2 Hz, 1H, H^6), 3.31 (s, 3H, H^5), 2.94 – 2.85 (m, 2H, H^{8e}), 2.77 – 2.69 (m, 2H, H^9), 2.52 – 2.45 (m, 2H, H^{10}), 2.11 (td, J = 12.0, 2.4 Hz, 1H, H^{8a}), 1.97 – 1.88 (m, 2H, H^{7e}), 1.47 (dtd, J = 12.2, 11.5, 3.8 Hz, 2H, H^{7a}). ^{13}C NMR (101 MHz, Methanol-d_4) δ 154.23, 146.12, 140.98, 134.53 (2C), 131.97 (2C), 129.50, 120.75, 119.31, 118.45, 114.34, 109.65, 106.97, 59.09, 52.28 (2C), 49.87, 32.79, 31.58 (2C), 27.18. LC-MS (APCI$^+$/ESI): found m/z = 360.2 [M+H] $^+$ (cal. For $C_{22}H_{25}N_5$, 359.21). Purity: 99%, t_R= 0.212 min.

4-(2-(4-((1-(4-cyanobenzyl)-1H-benzo[d]imidazol-2-yl)amino)piperidin-1-yl) ethyl) benzonitrile (17)

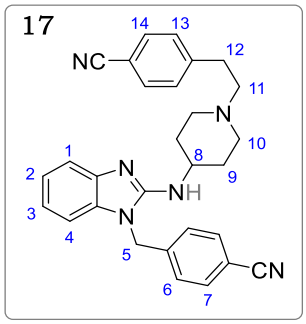

Obtained from **14d** (0.100 g, 0.30 mmol) and **1a** (0.076 g, 0.36 mmol) as a white solid (0.119 g, 86%). M.p.: 122 – 124 °C; R_f (10% MeOH/DCM) 0.40. ^{1}H NMR (300 MHz, DMSO-d_6) δ 7.79 (d, J = 8.3 Hz, 2H, H^{14}), 7.73 (d, J = 8.3 Hz, 2H, H^{13}), 7.45 (d, J = 8.2 Hz, 2H, H^7), 7.27 (d, J = 8.2 Hz, 2H, H^6), 7.21 (dd, J = 7.6, 1.3 Hz, 1H, H^1), 7.01 (dd, J = 7.7, 1.2 Hz, 1H, H^2), 6.97 – 6.91 (m, 1H, H^4), 6.86 – 6.79 (m, 1H, H^3), 5.38 (s, 2H, H^5), 4.01 (tt, J = 10.5, 3.7 Hz, 1H, H^8), 3.75 – 3.69 (m, 2H, H^{10}), 2.90 – 2.89 (m, 2H, H^{11}), 2.83 – 2.75 (m, 2H, H^{12}), 2.56 – 2.48 (m, 2H, H^{10}), 2.08 – 1.98 (m, 2H, H^9), 1.95 – 1.86 (d, J = 12.8 Hz, 2H, H^9). ^{13}C NMR (101 MHz, DMSO-d_6) δ 154.49, 147.47, 144.34, 143.48, 143.30, 134.72, 132.97 (2C), 132.46 (2C), 130.28 (2C), 128.10 (2C), 121.17, 119.50, 118.98, 115.62, 110.56, 109.13, 108.13, 59.12, 52.59 (2C), 50.50, 44.60, 33.39, 32.32(2C). LC-MS (APCI+/ESI): found m/z = 461.2 [M+H]$^+$ (cal. For $C_{29}H_{28}N_6$, 460.24). Purity: 98%, t_R = 2.382min.

4-((2-((1-phenethylpiperidin-4-yl)amino)-benzimidazoyl)methyl)benzonitrile (31)

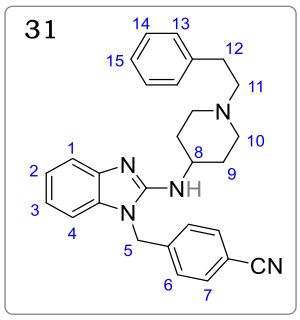

Obtained from **14d** (0.080 g, 0.24 mmol) and (2-bromoethyl)benzene (0.054 g, 0.30 mmol) as a pale yellow crystalline solid (0.078 g, 75%). M.p.: 105 – 107 °C; R_f (10% MeOH/DCM) 0.32. ^{1}H NMR (400 MH z, Methanol-d_4) δ δ 7.67 (d, J = 8.6 Hz, 2H, H^7), 7.34 (dd, J = 7.9, 0.9 Hz, 1H, H^1), 7.30 – 7.16 (m, 7H, H^{6,13,14,15}), 7.06 (ddd, J = 8.6, 7.1, 1.4 Hz, 1H, H^2), 7.00 (dd, J = 7.9, 1.5 Hz, 1H, H^4), 6.95 (ddd, J = 7.9, 7.1, 1.1 Hz, 1H, H^3), 5.38 (s, 2H, H^5), 3.86 (tt, J = 11.0, 4.2 Hz, 1H, H^8), 3.13 – 3.06 (m, 2H, H^{10e}), 2.88 – 2.81 (m, 2H, H^{11}), 2.74 – 2.67 (m, 2H, H^{12}), 2.43 – 2.34 (m, 2H, H^{10a}), 2.17 – 2.07 (m, 2H, H^{9e}), 1.72 – 1.58 (m, 2H, H^{9a}). ^{13}C NMR (151 MHz, Methanol-d_4) δ 154.02, 143.26, 142.00, 136.25, 135.98, 133.31, 131.78 (2C), 128.96 (2C), 128.22 (2C), 127.32 (2C), 122.04, 119.56, 118.65, 114.96, 111.56, 108.09, 60.01, 52.32 (2C), 49.39, 44.56, 31.83, 31.13 (2C). LC-MS (APCI+/ESI): found m/z = 435.1 [M+H] $^+$ (cal. For $C_{28}H_{29}N_5$, 435.24). Purity: 99%, t_R = 2.313 min.

4-((2-((1-(4-hydroxyphenethyl)piperidin-4-yl)amino)-1-benzimidazyl) methyl) benzonitrile (32)

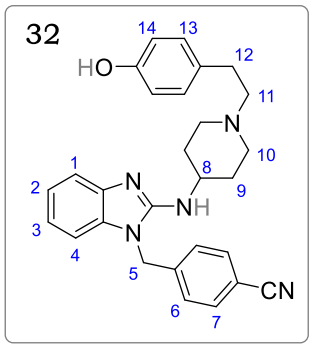

Obtained from **14d** (0.070 g, 0.21 mmol) and **6** (0.055 g, 0.27 mmol) as a pale yellow crystalline solid (0.060g, 63%). M.p.: not determined; R_f (10% MeOH/DCM) 0.29. ^{1}H NMR (400 MHz, Methanol-d_4) δ 7.67 (d, J = 8.5 Hz, 2H, H^{14}), 7.35 (d, J = 7.9, 2H, H^7), 7.26 (d, J = 8.5 Hz, 2H, H^{13}), 7.12 – 7.07 (m, 3H, H^{1,6}), 7.02 (ddd, J = 7.6, 7.1, 1.1 Hz, 1H, H^2), 6.95 (dd, J = 8.1, 1.1 Hz, 1H, H^4), 6.75 (ddd, J = 8.0, 7.1 Hz, 1H, H^3), 5.41 (s, 2H, H^5), 3.96 (tt, J = 10.7, 4.0 Hz, 1H, H^8), 3.38 (td, J = 12.5, 3.1 Hz, 2H, H^{10a}), 3.01 – 2.95 (m, 2H, H^{11}), 2.90 – 2.79 (m, 4H, H^{10e,12}), 2.24 – 2.18 (m, 2H, H^9), 1.81 – 1.78 (m, 2H, H^9). ^{13}C NMR (151 MHz, Methanol-d_4) δ 155.63, 143.25, 140.05, 136.58, 135.56, 133.18, 132.33 (2C), 128.23 (2C), 128.08 (2C), 126.35 (2C), 121.22, 119.45, 119.04, 115.07, 110.25, 107.89, 60.35, 52.65 (2C), 49.55, 44.38, 31.85, 30.64 (2C). LC-MS (APCI+/ESI): found m/z = 452.1 [M+H]$^+$ (cal. For $C_{28}H_{29}N_5O$, 451.24). Purity: 98%, t_R = 2.130 min.

4-((2-((1-(4-(methylsulfonyl) phenethyl) piperidin-4-yl) amino)-1H-benzo[d]imidazol-1-yl) methyl) benzonitrile (33)

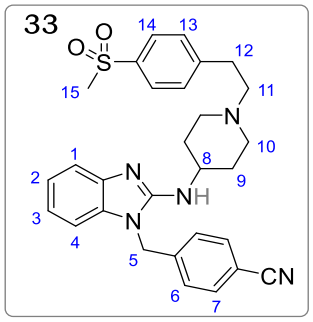

Obtained from **14d** (0.080 g, 0.24 mmol) and 1-(2-bromoethyl)-4-(methylsulfonyl)benzene (0.076 g, 0.29 mmol) as a white crystalline solid (0.108 g, 88%). M.p.: 231 – 233 °C; R_f (10% MeOH/DCM) 0.31. ^{1}H NMR (600 MH z, DMSO-d_6) δ 7.82 (d, J = 7.9 Hz, 2H, H^{14}), 7.79 (d, J = 8.0 Hz, 2H, H^7), 7.52 (d, J = 7.9 Hz, 2H, H^{13}), 7.27 (d, J = 8.0 Hz, 2H, H^6), 7.22 (dd, J = 7.8, 1.5 Hz, 1H, H^1), 7.01 (dd, J = 7.8, 1.3 Hz, 1H, H^4), 6.94 (ddd, J = 7.8, 7.2, 1.2 Hz, 1H, H^2), 6.83 (ddd, J = 7.8, 7.2, 1.1 Hz, 1H, H^3), 5.39 (s, 2H, H^5), 3.76 (tt, J = 10.3, 4.0 Hz, 1H, H^8), 3.18 (s, 3H, H^{15}), 2.94 – 2.89 (m, 2H, H^{10e}), 2.87 – 2.83 (m, 2H, H^{11}), 2.62 – 2.54 (m, 2H, H^{12}), 2.13 – 2.05 (m, 2H, H^{10a}), 2.00 – 1.93 (m, 2H, H^{9e}), 1.55 – 1.45 (m, 2H, H^{9a}). ^{13}C NMR (151 MHz, DMSO-d_6) δ 154.44, 143.48, 143.27, 138.89, 134.69, 132.97 (2C), 130.04 (2C), 128.07 (2C), 127.27 (2C), 121.13, 119.11, 118.94, 115.58, 110.51, 108.11, 59.27, 52.58, 50.46 (2C), 44.53, 44.07, 33.10, 32.28 (2C), 16.88. LC-MS (APCI+/ESI): found m/z = 514.2 [M+H]$^+$ (cal. For $C_{29}H_{31}N_5O_2S$, 513.22). Purity: 99%, t_R = 2.157 min.

4-((2-((1-(4-methylphenethyl)piperidin-4-yl)amino)-1H-benzo[d]imidazol-1-yl) methyl) benzonitrile (34)

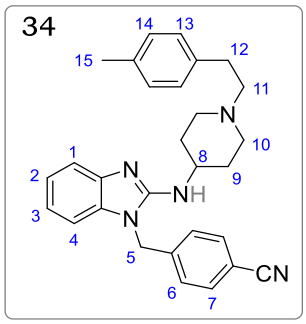

Obtained from **14d** (0.080 g, 0.24 mmol) and 1-(2-bromoethyl)-4-methylbenzene (0.058 g, 0.29 mmol) as a pale yellow crystalline solid (0.082 g, 76%). M.p.: 179 – 181 °C; R_f (10% MeOH/DCM) 0.44. ^{1}H NMR (600 MH z, Methanol-d_4) δ 7.66 (d, J = 8.5 Hz, 2H, H^7), 7.34 (dd, J = 7.9, 1.2 Hz, 1H, H^1), 7.25 (d, J = 8.5 Hz, 2H, H^6), 7.10 (br-s, 4H, H^{13,14}), 7.06 (ddd, J = 8.0, 7.2, 1.3 Hz, 1H, H^2), 7.01 (dd, J = 7.6, 1.2 Hz, 1H, H^4), 6.95 (ddd, J = 7.6, 1.5 Hz, 1H, H^3), 5.38 (s, 2H, H^5), 3.87 (tt, J = 10.9, 4.6 Hz, 1H, H^8), 3.19 – 3.12 (m, 2H, H^{10e}), 2.84 – 2.81 (m, 2H, H^{11}), 2.78 – 2.72 (m, 2H, H^{12}), 2.51 – 2.44 (m, 2H, H^{10a}), 2.29 (s, 3H, H^{15}), 2.18 – 2.08 (m, 2H, H^{9e}), 1.68 (dtd, J = 12.1, 11.1, 3.6 Hz, 2H, H^{9a}). ^{13}C NMR (151 MHz, Methanol-d_4) δ 153.84, 142.27, 141.48, 135.86, 135.61, 133.83, 132.24 (2C), 128.80 (2C), 128.14 (2C), 127.09 (2C), 121.34, 119.66, 118.01, 114.83, 111.01, 107.58, 59.63, 52.01 (2C), 49.43, 44.22, 31.79, 30.84 (2C), 19.61. LC-MS (APCI+/ESI): found m/z = 450.2 [M+H]$^+$ (cal. For $C_{29}H_{31}N_5$, 449.26). Purity: 99%, t_R = 2.365 min.

4-((2-((1-(4-(trifluoromethyl)phenethyl)piperidin-4-yl)amino)-1H-benzo[d]imidazol-1-yl) methyl) benzonitrile (35)

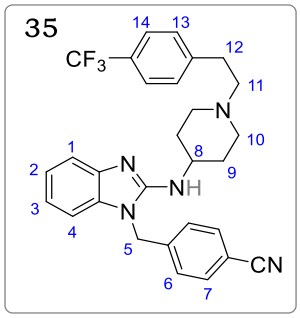

Obtained from **14d** (0.080 g, 0.24 mmol) and 1-(2-bromoethyl)-4-(trifluoromethyl)benzene (0.073 g, 0.29 mmol) as a pale yellow crystalline solid (0.095 g, 79%). M.p.: 92 – 93 °C; R_f (10% MeOH/DCM) 0.51. ^{1}H NMR (400 MHz, Methanol-d_4) δ 7.66 (d, J = 8.4 Hz, 2H, H^{14}), 7.58 (d, J = 8.0 Hz, 2H, H^7), 7.42 (d, J = 8.4 Hz, 2H, H^{13}), 7.33 (dd, J = 8.0, 1.2 Hz, 1H, H^1), 7.25 (d, J = 8.0 Hz, 2H, H^6), 7.06 (ddd, J = 8.0, 7.3, 1.2 Hz, 1H, H^6), 7.00 (dd, J = 8.1, 1.3 Hz, 1H, H^4), 6.95 (ddd, J = 8.1, 7.3, 1.1 Hz, 1H, H^3), 5.38 (s, 2H, H^5), 3.84 (tt, J = 10.9, 4.1 Hz, 1H, H^8), 3.08 – 3.02 (m, 2H, H^{10e}), 2.94 – 2.89 (m, 2H, H^{11}), 2.72 – 2.64 (m, 2H, H^{12}), 2.36 – 2.30 (m, 2H, H^{10a}), 2.13 – 2.05 (m, 2H, H^{9e}), 1.63 (dtd, J = 11.8, 10.0, 3.8 Hz, 2H, H^{9a}). ^{13}C NMR (151 MHz, Methanol-d_4) δ 153.93, 144.51, 142.30, 141.56, 133.84, 132.23 (2C), 128.96 (2C), 128.26 (q, J = 22.3 Hz), 127.11 (2C), 124.93 (2C), 123.53, 121.30, 119.57, 118.02, 114.79, 110.99, 107.51, 59.30, 52.12 (2C), 49.85, 44.19, 32.43, 30.77 (2C). LC-MS (APCI+/ESI): found m/z = 504.2 [M+H]$^+$ (cal. For $C_{29}H_{28}F_3N_5$, 503.23). Purity: 99%, t_R = 2.633 min.

4-((2-((1-(4-nitrophenethyl)piperidin-4-yl)amino)-1H-benzimidazol-1-yl) methyl) benzonitrile (36)

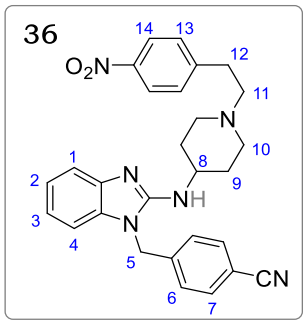

Obtained from **14d** (0.080 g, 0.24 mmol) and 1-(2-bromoethyl)-4-nitrobenzene (0.067 g, 0.29 mmol) as a light orange solid (0.089 g, 77%). M.p.: 86 – 88 °C; R_f(10% MeOH/DCM) 0.49. ^{1}H NMR (600 MHz, Methanol-d_4) δ 8.16 (d, J = 8.0 Hz, 2H, H^{14}), 7.66 (d, J = 7.7 Hz, 2H, H^7), 7.48 (d, J = 8.0 Hz, 2H, H^{13}), 7.33 (dd, J = 7.9, 1.2 Hz, 1H, H^1), 7.25 (d, J = 7.7 Hz, 2H, H^6), 7.06 (ddd, J = 7.9, 7.0, 1.2 Hz, 1H, H^2), 7.00 (dd, J = 8.0, 1.2 Hz, 1H, H^4), 6.95 (ddd, J = 8.0, 7.0, 1.4 Hz, 1H, H^3), 5.38 (s, 2H, H^5), 3.84 (tt, J = 11.2, 5.4 Hz, 1H, H^8), 3.06 – 3.00 (m, 2H, H^{10e}), 2.99 – 2.93 (m, 2H, H^{11}), 2.73 – 2.65 (m, 2H, H^{12}), 2.37 – 2.28 (m, 2H, H^{10a}), 2.12 – 2.08 (m, 2H, H^{9e}), 1.63 (dtd, J = 12.2, 11.7, 3.3 Hz, 2H, H^{9a}). ^{13}C NMR (151 MHz, Methanol-d_4) δ 153.92, 148.04, 146.57, 142.32, 141.52, 133.84, 132.25 (2C), 129.46 (2C), 127.13 (2C), 123.16 (2C), 121.32, 119.60, 118.06, 114.80, 110.94, 107.53, 58.94, 52.05 (2C), 49.82, 44.21, 32.40, 31.32 (2C). LC-MS (APCI+/ESI): found m/z = 481.2 [M+H]$^+$ (cal. For $C_{28}H_{28}N_6O_2$, 480.23). Purity: 99%, t_R = 2.306 min.

Methyl 4-(2-(4-((1-(4-cyanobenzyl)-1H-benzo[d]imidazol-2-yl)amino)piperidin-1-yl)ethyl)benzoate (37)

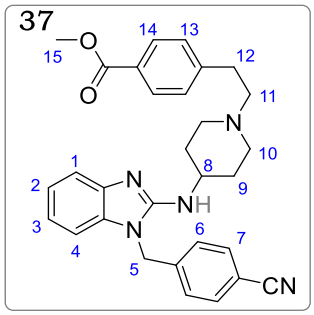

Obtained from **14d** (0.200 g, 0.60 mmol) and **9** (0.176 g, 0.72 mmol) as a pale-yellow solid (0.263 g, 89%); m.p.: 166 – 167 °C; R_f(10% MeOH/DCM) 0.34. ^{1}H NMR (600 MHz, Methanol-d_4) δ 7.94 (d, J = 8.3 Hz, 2H, H^{14}), 7.66 (d, J = 8.4 Hz, 2H, H^7), 7.37 – 7.30 (m, 3H, H^{1,13}), 7.25 (d, J = 8.4 Hz, 2H, H^6), 7.06 (ddd, J = 7.7, 7.3, 1.3 Hz, 1H, H^2), 7.00 (dd, J = 7.8, 1.3 Hz, 1H, H^4), 6.95 (ddd, J = 7.8, 7.3, 1.1 Hz, 1H, H^3), 5.37 (s, 2H, H^5), 3.88 (s, 3H, H^{15}), 3.83 (tt, J = 10.9, 4.1 Hz, 1H, H^8), 3.07 – 3.00 (m, 2H, H^{10e}), 2.92 – 2.88 (m, 2H, H^{11}), 2.70 – 2.64 (m, 2H, H^{12}), 2.35 – 2.28 (m, 2H, H^{10a}), 2.12 – 2.06 (m, 2H, H^{9e}), 1.67 – 1.58 (m, 2H, H^{9a}). ^{13}C NMR (151 MHz, Methanol-d_4) δ 167.12, 153.94, 145.77, 142.31, 141.59, 133.85 (2C), 132.23 (2C), 129.33 (2C), 128.53 (2C), 127.94, 127.10, 121.29, 119.55, 118.02, 114.79, 110.99, 107.50, 59.34, 52.13 (2C), 51.08, 49.88, 44.18, 32.67, 31.37 (2C). LC-MS (APCI$^+$/ESI): found m/z = 494.2 [M+H]$^+$ (cal. For $C_{30}H_{31}N_5O_2$, 493.25). Purity: 99%, t_R = 2.330 min.

Ethyl 4-(2-(4-((1-(4-cyanobenzyl)-1H-benzo[*d*]imidazol-2-yl) amino) piperidin-1-yl) ethyl) benzoate (38)

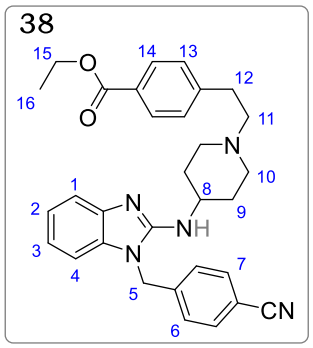

Obtained from **14d** (0.150 g, 0.45 mmol) and **8** (0.140 g, 0.54 mmol) as a pale-yellow solid (0.125 g, 55%); m.p.: 152 – 154 °C; R_f (10% MeOH/DCM) 0.45. ^{1}H NMR (400 MHz, Methanol-d_4) δ 7.95 (d, J = 8.2 Hz, 2H, H^{14}), 7.67 (d, J = 8.5 Hz, 2H, H^7), 7.36 (d, J = 8.2 Hz, 2H, H^{13}), 7.33 (dd, J = 7.9, 0.9 Hz, 1H, H^1), 7.25 (d, J = 8.5 Hz, 2H, H^6), 7.06 (ddd, J = 7.9, 7.3, 1.1 Hz, 1H, H^2), 7.01 (dd, J = 8.0, 1.1 Hz, 1H, H^4), 6.95 (ddd, J = 8.0, 7.3, 1.1 Hz, 1H, H^3), 5.38 (s, 2H, H^5), 4.35 (q, J = 7.1 Hz, 2H, H^{15}), 3.85 (tt, J = 10.9, 4.1 Hz, 1H, H^8), 3.09 – 3.05 (m, 2H, H^{10}), 2.93 – 2.90 (m, 2H, H^{11}), 2.74 – 2.69 (m, 2H, H^{12}), 2.40 – 2.33 (m, 2H, H^{10}), 2.14 – 2.09 (m, 2H, H^9), 1.68 – 1.60 (m, 2H, H^9), 1.38 (t, J = 7.1 Hz, 3H, H^{16}). ^{13}C NMR (151 MHz, Methanol-d_4) δ 167.54, 154.80, 146.40, 143.20, 142.42, 134.74, 133.14 (2C), 130.20 (2C), 129.41 (2C), 129.21 (2C), 128.00, 122.21, 120.50, 118.92, 115.69, 111.91, 108.43, 61.52, 60.13, 53.01 (2C), 50.68, 45.11, 33.46, 32.16 (2C), 14.08. LC-MS (APCI$^+$/ESI): found m/z = 508.2 [M+H] $^+$ (cal. For $C_{31}H_{33}N_5O_2$, 507.26). Purity: 99%, t_r = 2.419 min.

4-(2-(4-((1-(4-cyanobenzyl)-1H-benzo[d]imidazol-2-yl)amino)piperidin-1-yl) ethyl) benzoic acid (39)

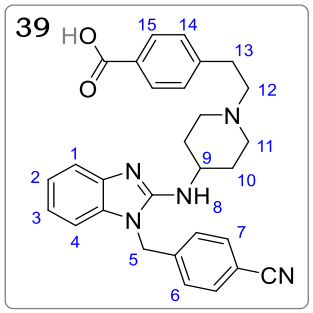

To a solution of **37** (0.180 g, 0.37 mmol) in 10 ml methanol, 2M aqueous KOH (912 µl, 1.82 mmol) was added, and the resulting mixture stirred at 79 °C for 2 hr. Following completion, the reaction mixture was cooled to 0 °C, and acidified to pH 2 while stirring. The product was filtered and obtained after recrystallization in methanol and drying, as a white solid (0.170 g, 96%); m.p.: 181 – 183 °C; R_f (10% MeOH/DCM), 0.11. ^{1}H NMR (600 MHz, DMSO-d_6) δ 7.88 (d, J = 8.0 Hz, 2H, H^{15}), 7.79 (d, J = 8.1 Hz, 2H, H^7), 7.37 (d, J = 8.0 Hz, 2H, H^{14}), 7.28 (d, J = 8.1 Hz, 2H, H^6), 7.23 (dd, J = 8.0, 1.2 Hz, 1H, H^1), 7.02 (dd, J = 7.9, 1.3 Hz, 1H, H^4), 6.95 (ddd, J = 8.0, 7.3, 1.2 Hz, 1H, H^2), 6.84 (ddd, J = 7.9, 7.3, 1.2 Hz, 1H, H^3), 6.78 (d, J = 3.9 Hz, 1H, H^8), 5.42 (s, 2H, H^5), 3.86 (tt, J = 10.3, 4.2 Hz, 1H, H^9), 3.17 – 3.10 (m, 2H, H^{11e}), 2.96 – 2.90 (m, 2H, H^{12}), 2.86 – 2.79 (m, 2H, H^{13}), 2.45 – 2.52 (m, 2H, H^{11a}), overlap with DMSO signal), 2.08 – 2.00 (m, 2H, H^{10e}), 1.73 – 1.63 (m, 2H, H^{10a}). ^{13}C NMR (151 MHz, DMSO-d_6) δ 167.77, 154.33, 143.45, 143.07, 134.65, 132.97 (2C), 129.90 (2C), 129.85 (2C), 129.42 (2C), 129.29,

128.08, 127.45, 121.21, 119.03, 115.61, 110.52, 108.22, 58.29, 51.96 (2C), 49.52, 44.61, 32.07, 31.05 (2C). LC-MS (APCI$^+$/ESI): found m/z = 480.2 [M+H] $^+$ (cal. For $C_{29}H_{29}N_5O_2$, 479.23). Purity: 96%, t_R = 0.155 min.

4-((2-((1-(4-(1,2,4-oxadiazol-3-yl) phenethyl) piperidin-4-yl) amino)-1-benzo[*d*]imidazol-1-yl) methyl) benzonitrile (40)

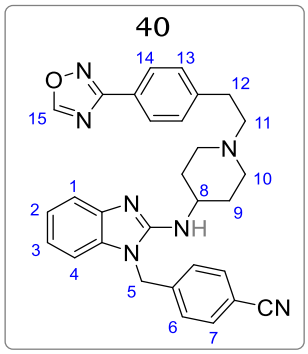

Obtained from **14d** (0.080 g, 0.24 mmol) and **3a** (0.073 g, 0.29 mmol) as a pale-yellow solid (0.087 g, 72%); m.p.: 98 – 100 °C; R_f (10% MeOH/DCM), 0.59. ^{1}H NMR (600 MHz, Methanol-d_4) δ 7.65 (d, J = 8.7 Hz, 2H, H^{14}), 7.63 (dd, J = 8.0 Hz, 2H, H^7), 7.42 (d, J = 8.7 Hz, 2H, H^{13}), 7.33 (dd, J = 7.9, 1.1 Hz, 1H, H^1), 7.24 (d, J = 8.0 Hz, 2H, H^6), 7.06 (ddd, J = 7.9, 7.2, 1.0 Hz, 1H, H^2), 7.00 (dd, J = 8.0, 1.0 Hz, 1H, H^4), 6.95 (ddd, J = 8.0, 7.2, 1.1 Hz, 1H, H^3), 5.37 (s, 2H, H^5), 3.84 (tt, J = 11.1, 4.2 Hz, 1H, H^8), 3.06 – 3.01 (m, 2H, H^{10}), 2.94 – 2.87 (m, 2H, H^{11}), 2.70 – 2.66 (m, 2H, H^{12}), 2.36 – 2.30 (m, 2H, H^{10}), 2.12 – 2.08 (m, 2H, H^9), 1.67 – 1.58 (m, 2H, H^9). ^{13}C NMR (151 MHz, Methanol-d_4) δ 154.10, 145.93, 142.30, 141.53, 140.68, 133.85, 132.25 (2C), 131.97 (2C), 129.47 (2C), 127.13 (2C), 121.34, 119.63, 118.44, 118.05, 114.82, 111.01, 109.67, 107.56, 58.97, 52.10 (2C), 49.83, 44.23, 32.67, 31.33 (2C). LC-MS (APCI$^+$/ESI): found m/z = 504.2 [M+H] $^+$ (cal. For $C_{30}H_{29}N_7O$, 503.24). Purity: 97%, t_R = 2.356 min.

4-((2-((1-(4-(5-methyl-1,2,4-oxadiazol-3-yl) phenethyl) piperidin-4-yl) amino)-1H-benzo[*d*]imidazol-1-yl) methyl) benzonitrile (41)

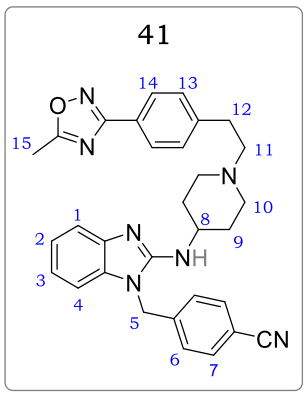

Obtained from **14d** (0.080 g, 0.24 mmol) and **3b** (0.077 g, 0.29 mmol) as a pale-yellow solid (0.076 g, 61%); m.p.: 148 – 150 °C; R_f (10% MeOH/DCM) 0.48. ^{1}H NMR (600 MHz, Methanol-d_4) δ 8.02 (d, J = 7.9 Hz, 2H, H^{14}), 7.70 (d, J = 8.0 Hz, 2H, H^7), 7.47 (d, J = 7.9 Hz, 2H, H^{13}), 7.41 (dd, J = 7.9, 0.9 Hz, 1H, H^1), 7.30 (d, J = 8.0 Hz, 2H, H^6), 7.17 (ddd, J = 7.9, 7.1, 1.0 Hz, 1H, H^2), 7.12 (dd, J = 8.0, 1.0 Hz, 1H, H^4), 7.08 (ddd, J = 8.0, 7.1, 1.0 Hz, 1H, H^3), 5.46 (s, 2H, H^5), 4.04 (tt, J = 10.5, 4.1 Hz, 1H, H^8), 3.75 – 3.63 (m, 2H, H^{10}), 3.44 – 3.38 (m, 2H, H^{11}), 3.26 – 3.18 (m, 2H, H^{12}), 3.18 – 3.12 (m, 2H, H^{10}), 2.65 (s, 3H, H^{15}), 2.40 – 2.31 (m, 2H, H^9), 1.99 – 1.89 (m, 2H, H^9). ^{13}C NMR (151 MHz, Methanol-d_4) δ 177.47, 167.78, 152.31, 141.41, 139.89, 132.95, 132.38 (2C), 129.12 (2C), 127.43 (2C), 127.07 (2C), 125.74, 122.33, 121.13,

119.23, 117.95, 114.13, 111.28, 108.49, 57.10, 51.63 (2C), 44.63, 30.15, 29.19 (2C), 29.09, 10.64. LC-MS (APCI$^+$/ESI): found m/z = 518.2 [M+H]$^+$ (cal. For $C_{31}H_{31}N_7O$, 517.26). Purity: 97%, t_R = 2.447 min.

4-((2-((1-(4-(5-(trifluoromethyl)-1,2,4-oxadiazol-3-yl) phenethyl) piperidin-4-yl) amino)-1H-benzo[*d*]imidazol-1-yl) methyl) benzonitrile (42)

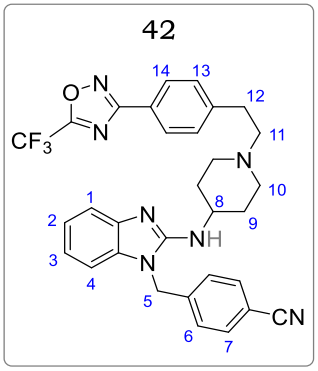

Obtained from **14d** (0.080 g, 0.24 mmol) and **3c** (0.093 g, 0.29 mmol) as a pale-yellow solid (0.107 g, 78%); m.p.: 125 – 126 °C; R_f (10% MeOH/DCM) 0.58. ^{1}H NMR (600 MHz, Methanol-d_4) δ 8.05 (d, J = 8.3 Hz, 2H, H^{14}), 7.67 (d, J = 8.4 Hz, 2H, H^7), 7.46 (d, J = 8.3 Hz, 2H, H^{13}), 7.33 (dd, J = 7.8, 0.9 Hz, 1H, H^1), 7.25 (d, J = 8.4 Hz, 2H, H^6), 7.06 (ddd, J = 7.8, 7.3, 1.0 Hz, 1H, H^2), 7.01 (dd, J = 8.0, 1.1 Hz, 1H, H^4), 6.95 (ddd, J = 8.0, 7.3, 1.1 Hz, 1H, H^3), 5.38 (s, 2H, H^5), 3.85 (tt, J = 10.9, 4.1 Hz, 1H, H^8), 3.12 – 3.05 (m, 2H, H^{10}), 2.97 – 2.91 (m, 2H, H^{11}), 2.77 – 2.70 (m, 2H, H^{12}), 2.41 – 2.33 (m, 2H, H^{10}), 2.14 – 2.09 (m, 2H, H^9), 1.71 – 1.60 (m, 2H, H^9). ^{13}C NMR (151 MHz, Methanol-d_4) δ 169.07, 165.92 (q, J = 23.9 Hz), 153.92, 144.84, 142.32, 141.55, 133.86, 132.26 (2C), 129.34 (2C), 127.46 (2C), 127.13 (2C), 122.94, 121.33, 119.61, 118.04, 117.07, 115.27, 111.02, 107.55, 59.27, 52.14 (2C), 49.82, 44.23, 32.59, 31.31 (2C). LC-MS (APCI$^+$/ESI): found m/z = 572.2 [M+H]$^+$ (cal. For $C_{31}H_{28}F_3N_7O$, 571.23). Purity: 97%, t_R = 2.732 min.

4-((2-((1-(4-(5-oxo-4,5-dihydro-1,2,4-oxadiazol-3-yl) phenethyl) piperidin-4-yl) amino)-1H-benzo[*d*]imidazol-1-yl) methyl) benzonitrile (43)

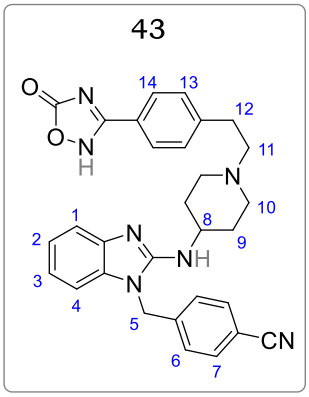

Obtained from **14d** (0.080 g, 0.24 mmol) and **3d** (0.091 g, 0.29 mmol) as a white solid (0.085 g, 68%); m.p.: 181 – 183 °C; R_f (10% MeOH/DCM) 0.13. ^{1}H NMR (600 MHz, Methanol-d_4) δ 7.78 (d, J = 8.3 Hz, 2H, H^{14}), 7.67 (d, J = 8.5 Hz, 2H, H^7), 7.39 (d, J = 8.3 Hz, 2H, H^{13}), 7.36 (dd, J = 7.9, 1.0 Hz, 1H, H^1), 7.26 (d, J = 8.5 Hz, 2H, H^6), 7.10 (ddd, J = 7.9, 7.3, 1.1 Hz, 1H, H^2), 7.04 (dd, J = 8.1, 1.1 Hz, 1H, H^4), 6.99 (ddd, J = 8.1, 7.3, 1.1 Hz, 1H, H^3), 5.42 (s, 2H, H^5), 4.00 (tt, J = 10.7, 4.0 Hz, 1H, H^8), 3.53 – 3.47 (m, 2H, H^{10}), 3.22 – 3.18 (m, 2H, H^{11}), 3.09 – 3.05 (m, 2H, H^{12}), 3.02 – 2.95 (m, 2H, H^{10}), 2.31 – 2.26 (m, 2H, H^9), 1.91 – 1.83 (m, 2H, H^9). ^{13}C NMR (151 MHz, Methanol-d_4) δ 163.99, 153.43, 142.08, 140.79, 140.44, 133.71, 132.29

(2C), 128.91 (2C), 127.10 (2C), 126.43 (2C), 125.94, 121.60, 120.08, 118.02, 114.83, 111.07, 107.88, 57.60, 51.58 (2C), 48.28, 48.16, 44.40, 30.71, 29.56 (2C). LC-MS (APCI$^+$/ESI): found m/z = 520.2 [M+H] $^+$ (cal. For $C_{30}H_{29}N_7O_2$, 519.24). Purity: 98%, t_R = 2.595 min.

(S)-4-((2-((1-(4-(5-methyl-4,5-dihydrooxazol-2-yl) phenethyl) piperidin-4-yl) amino)-1H-benzo[*d*]imidazol-1-yl) methyl) benzonitrile (44)

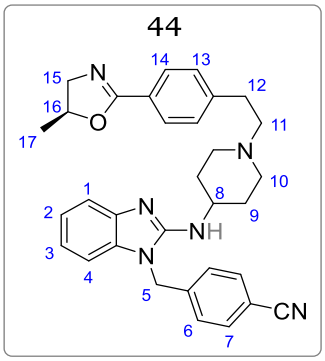

Obtained from **14d** (0.050 g, 0.15 mmol) and **5a** (0.049 g, 0.18 mmol) as a pale-yellow solid (0.045 g, 58%); m.p.: 67 – 69 °C; R_f(10% MeOH/DCM), 0.33. ^{1}H NMR (400 MHz, Methanol-d_4) δ 7.83 (d, J = 8.2 Hz, 2H, H^{14}), 7.67 (d, J = 8.3 Hz, 2H, H^7), 7.36 – 7.30 (m, 3H, H^{13,1}), 7.25 (d, J = 8.3 Hz, 2H, H^6), 7.06 (ddd, J = 7.9, 7.2, 1.4 Hz, 1H, H^2), 7.01 (dd, J = 8.2, 1.2 Hz, 1H, H^4), 6.96 (ddd, J = 8.2, 7.2, 1.4 Hz, 1H, H^3), 5.38 (s, 2H, H^5), 4.91 (ddq, J = 14.3, 9.3, 6.3 Hz, 1H, H^{16}), 4.11 (dd, J = 14.3, 7.4 Hz, 1H, H^{15}), 3.85 (tt, J = 11.0, 5.5 Hz, 1H, H^8), 3.57 (dd, J = 9.3, 7.4 Hz, 1H, H^{15}), 3.11 – 3.03 (m, 2H, H^{10}), 2.95 – 2.85 (m, 2H, H^{11}), 2.76 – 2.66 (m, 2H, H^{12}), 2.42 – 2.32 (m, 2H, H^{10}), 2.15 – 2.06 (m, 2H, H^9), 1.71 – 1.58 (m, 2H, H^9), 1.42 (d, J = 6.3 Hz, 3H, H^{17}). ^{13}C NMR (101 MHz, Methanol-d_4) δ 164.81, 153.92, 143.99, 142.30, 141.56, 133.87, 132.25 (2C), 128.53 (2C), 127.99 (2C), 127.13 (2C), 125.45, 121.32, 119.61, 118.03, 114.84, 111.03, 107.55, 76.71, 60.25, 59.26, 52.11 (2C), 49.78, 44.25, 32.51, 31.25 (2C), 19.76. LC-MS (APCI$^+$/ESI): found m/z = 519.2 [M+H] $^+$ (cal. For $C_{32}H_{34}N_6O$, 518.28). Purity: 98%, t_R= 2.676 min. Specific rotation, $[\alpha]^{25}_D$ = +8.11°

(S)-4-((2-((1-(4-(4-methyl-4,5-dihydrooxazol-2-yl) phenethyl) piperidin-4-yl) amino)-1H-benzo[*d*]imidazol-1-yl) methyl) benzonitrile (45)

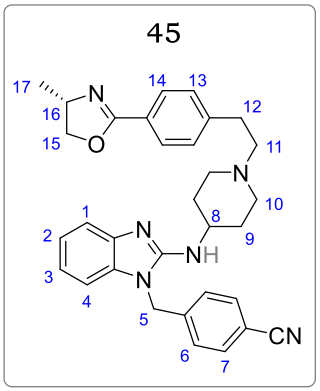

Obtained from **14d** (0.047 g, 0.14 mmol) and **5b** (0.047 g, 0.17 mmol) as a pale pale-yellow solid (0.061 g, 81%); m.p.: 104 – 106 °C; R_f (10% MeOH/DCM), 0.34. ^{1}H NMR (400 MHz, Methanol-d_4) δ 7.84 (d, J = 8.2 Hz, 2H, H^{14}), 7.66 (d, J = 8.5 Hz, 2H, H^7), 7.35 – 7.32 (m, 3H, H^{13,1}), 7.25 (d, J = 8.5 Hz, 2H, H^6), 7.06 (ddd, J = 7.7, 7.2, 1.0 Hz, 1H, H^2), 7.00 (dd, J = 8.1, 0.8 Hz, 1H, H^4), 6.95 (ddd, J = 8.1, 7.3, 1.1 Hz, 1H, H^3), 5.38 (s, 2H, H^5), 4.57 (dd, J = 9.3, 8.0 Hz, 1H, H^{15}), 4.35 (ddq, J = 9.3, 7.5, 6.6 Hz, 1H, H^{16}), 4.01 (dd, J = 8.0, 7.5 Hz, 1H, H^{15}), 3.86

(tt, J = 10.9, 4.1 Hz, 1H, H^8), 3.12 – 3.08 (m, 2H, H^{10}), 2.93 – 2.89 (m, 2H, H^{11}), 2.76 – 2.72 (m, 2H, H^{12}), 2.44 – 2.37 (m, 2H, H^{10}), 2.14 – 2.09 (m, 2H, H^9), 1.70 – 1.62 (m, 2H, H^9), 1.33 (d, J = 6.6 Hz, 3H, H^{17}). ^{13}C NMR (151 MHz, Methanol-d_4) δ 164.50, 153.88, 143.90, 142.29, 141.50, 133.85, 132.26 (2C), 128.57 (2C), 128.11 (2C), 127.12 (2C), 125.25, 121.35, 119.64, 118.04, 114.82, 111.02, 107.58, 74.04, 61.23, 59.16, 52.08 (2C), 49.68, 44.25, 32.39, 31.14 (2C), 20.09. LC-MS (APCI$^+$/ESI): found m/z = 519.2 $[M+H]^+$ (cal. For $C_{32}H_{34}N_6O$, 518.28). Purity: 98%, t_R = 2.700 min. Specific rotation, $[\alpha]^{25}_D$ = +7.78°

4-((2-((1-(4-(3-methyl-1,2,4-oxadiazol-5-yl)phenethyl)piperidin-4-yl)amino)-1H-benzo[d]imidazol-1-yl)methyl)benzonitrile (46)

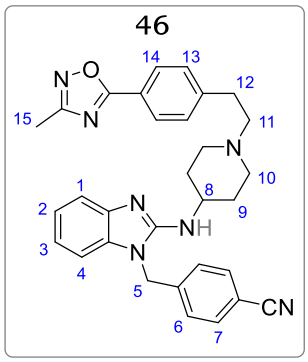

Obtained from **14d** (0.100 g, 0.30 mmol) and **7a** (0.103 g, 0.36 mmol) as a pale yellow solid (0.100 g, 65%). M.p.: 147 – 149 °C; R_f (10% MeOH/DCM), 0.56. ^{1}H NMR (300 MHz, Methanol-d_4) δ 8.05 (d, J = 8.3 Hz, 2H, H^{14}), 7.68 (d, J = 7.9 Hz, 2H, H^7), 7.47 (d, J = 8.3 Hz, 2H, H^{13}), 7.33 (dd, J = 7.8, 1.0 Hz, 1H, H^1), 7.28 – 7.23 (m, 2H, $H^{2,6}$), 7.08 (dd, J = 7.9, 0.9 Hz, 1H, H^4), 7.02 – 6.91 (m, 1H, H^3), 5.39 (s, 2H, H^5), 3.90 – 3.78 (m, 2H, H^{10}), 3.07 – 2.98 (m, 2H, H^{11}), 2.95 – 2.88 (m, 2H, H^{12}), 2.71 – 2.63 (m, 2H, H^{10}), 2.43 (s, 3H, H^{15}), 2.34 – 2.36 (m, 2H, H^9), 2.11 – 2.06 (m, 2H, H^9). ^{13}C NMR (101 MHz, Methanol-d_4) δ 175.43, 164.40, 153.97, 144.61, 142.33, 141.62, 133.90, 132.27 (2C), 129.32 (2C), 127.15 (2C), 126.55 (2C), 121.32, 119.61, 118.04, 114.87, 112.03, 111.05, 107.54, 59.27, 52.13 (2C), 49.88, 44.27, 32.64, 31.38 (2C), 9.05. LC-MS (APCI+/ESI): found m/z = 517.9 $[M+H]^+$ (cal. For $C_{31}H_{31}N_7O$, 517.24). HPLC Purity: 98%, t_R = 2.453 min.

4-((2-((1-(4-(3-(trifluoromethyl)-1,2,4-oxadiazol-5-yl)phenethyl)piperidin-4-yl)amino)-1-benzimidazol-1-yl)methyl)benzonitrile (47)

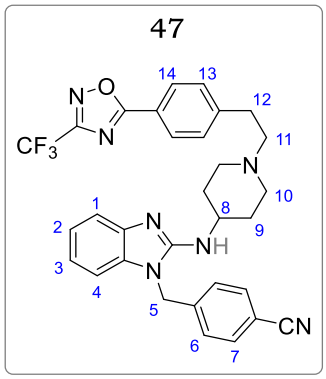

Obtained from **14d** (0.100 g, 0.30 mmol) and **7b** (0.122 g, 0.36 mmol) as a white solid (0.128 g, 75%). M.p.: 117 – 119 °C; R_f (10% MeOH/DCM), 0.67. ^{1}H NMR (300 MHz, Methanol-d_4) δ 8.12 (d, J = 8.3 Hz, 2H, H^{14}), 7.68 (d, J = 8.2 Hz, 2H, H^7), 7.53 (d, J = 8.3 Hz, 2H, H^{13}), 7.33 (dd, J = 7.7, 1.1 Hz, 1H, H^1), 7.26 – 7.17 (m, 2H, $H^{2,6}$), 7.05 (dd, J = 7.9, 1.2, 1H, H^4), 7.01 – 6.92 (m, 1H, H^3), 5.39 (s, 2H, H^5), 3.86 (tt, J = 10.9, 3.8 Hz, 1H, H^8), 3.05 – 2.97 (m, 2H, H^{10}), 2.97 – 2.89 (m, 2H, H^{11}), 2.72 – 2.67

(m, 2H, H^{12}), 2.33 – 2.25 (m, 2H, H^{10}), 2.10 – 2.02 (m, 2H, H^{9}), 1.72 – 1.55 (m, 2H, H^{9}). ^{13}C NMR (151 MHz, Methanol-d_4) δ 168.93, 165.33 (q, J = 24.0 Hz), 154.01, 144.75, 142.46, 141.97, 134.02, 132.45 (2C), 129.45 (2C), 127.88 (2C), 127.58 (2C), 123.03, 121.67, 119.69, 118.12, 116.99, 115.31, 111.13, 107.58, 59.33, 52.20 (2C), 49.95, 44.44, 32.62, 31.24 (2C). LC-MS (APCI+/ESI): found m/z = 571.9 $[M+H]^+$ (cal. For $C_{31}H_{28}F_3N_7O$, 571.23). HPLC Purity: 97%, t_R = 2.699 min.

4-((2-((1-(4-(5-methyl-1,3,4-oxadiazol-2-yl)phenethyl)piperidin-4-yl)amino)-1H-benzo[d]imidazol-1-yl)methyl)benzonitrile (48)

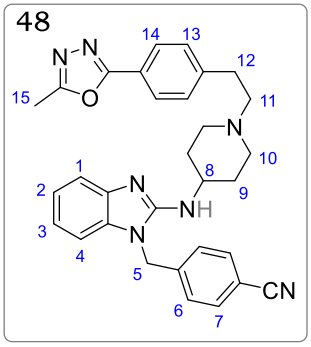

Obtained from **14d** (0.100 g, 0.30 mmol) and **7a** (0.096 g, 0.36 mmol) as a white solid (0.074 g, 48%). M.p.: 125 – 127 °C; R_f (10% MeOH/DCM), 0.56. ^{1}H NMR (300 MHz, Methanol-d_4) δ 7.95 (d, J = 8.3 Hz, 2H, H^{14}), 7.67 (d, J = 8.1 Hz, 2H, H^{7}), 7.45 (d, J = 8.3 Hz, 2H, H^{13}), 7.34 (dd, J = 7.9, 1.2, 1H, H^{1}), 7.25 (d, J = 8.0 Hz, 2H, H^{6}), 7.06 (td, J = 7.5, 1.6 Hz, 1H, H^{2}), 7.03 – 6.92 (m, 2H, $H^{3,4}$), 5.38 (s, 2H, H^{5}), 3.84 (tt, J = 10.8, 3.9 Hz, 1H, H^{8}), 3.06 – 2.98 (m, 2H, H^{10}), 2.93 – 2.86 (m, 2H, H^{11}), 2.71 – 2.63 (m, 2H, H^{12}), 2.61 (s, 3H, H^{15}), 2.35 – 2.27 (m, 2H, H^{10}), 2.11 – 2.03 (m, 2H, H^{9}), 1.73 – 1.55 (m, 2H, H^{9}). ^{13}C NMR (101 MHz, Methanol-d_4) δ 164.40, 153.97, 144.61, 142.33, 141.62, 138.43, 133.90, 132.27(2C), 129.32 (2C), 127.15 (2C), 126.55 (2C), 121.32, 119.61, 118.04, 114.87, 112.34, 111.05, 107.54, 59.27, 52.13 (2C), 49.88, 44.27, 32.64, 31.38 (2C), 9.25. LC-MS (APCI+/ESI): found m/z = 517.9 $[M+H]^+$ (cal. For $C_{31}H_{31}N_7O$, 517.24). HPLC Purity: 97%, t_R = 2.514 min.

4-((2-((1-(2-(1H-pyrazyl)ethyl)piperidin-4-yl)amino)-1-benzimidazyl) methyl) benzonitrile (49)

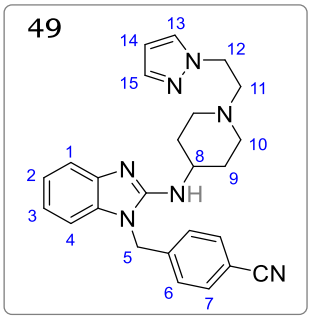

Obtained from **14d** (0.084 g, 0.25 mmol) and 2-bromoethyl-1*H*-pyrazole (0.054 g, 0.30 mmol) as a yellow solid (0.057g, 53%). M.p.: 129 – 131 °C; R_f (10% MeOH/DCM) 0.42. ^{1}H NMR (300 MHz, DMSO-d_6) δ 7.79 (d, J = 8.3 Hz, 2H, H^{7}), 7.71 (dd, J = 7.3, 1.9 Hz, 1H, H^{13}), 7.40 (dd, J = 7.3, 1.8 Hz, 1H, H^{15}), 7.27 (d, J = 8.3 Hz, 2H, H^{6}), 7.22 (dd, J = 7.4, 7.3 Hz, 1H, H^{14}), 7.01 (dd, J = 7.5, 1.3, 1H, H^{1}), 6.94 (ddd, J = 8.0, 7.5, 1.1 Hz, 1H, H^{2}), 6.82 (dd, J = 8.0, 1.2 Hz, 1H, H^{4}), 6.57 (ddd, J = 8.0, 7.5, 1.1 Hz, 1H, H^{3}), 5.38 (s, 2H, H^{5}), 4.21 (t, J = 6.6 Hz, 1H, H^{12}), 3.70 (tt, J = 10.2, 3.8 Hz, 1H, H^{8}), 2.84 – 2.78 (m, 2H, H^{10}), 2.70 (t, J = 6.6 Hz, 2H, H^{11}), 2.17 – 2.05 (m, 2H, H^{10}), 1.93 – 1.85 (m, 2H, H^{9}), 1.55 – 1.41

(m, 2H, H[9]). ^{13}C NMR (101 MHz, DMSO-d_6) δ 154.49, 143.49, 143.33, 138.76, 134.73, 132.97 (2C), 130.42 (2C), 128.11, 121.15, 118.96, 115.63, 112.43, 110.57, 108.13, 105.22, 57.93, 52.67 (2C), 50.37, 49.59, 44.61, 32.34 (2C). LC-MS (APCI+/ESI): found m/z = 426 [M+H]$^+$ (cal. For $C_{25}H_{27}N_7$, 425.23). Purity: 98%, t_R = 2.122 min.

4-((2-((1-(2-(292yrrolid-2-yl)ethyl)piperidin-4-yl)amino)-1-benzimidazyl) methyl) benzonitrile (50)

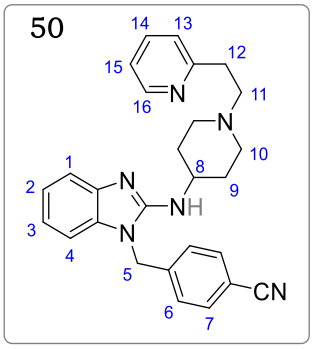

Obtained from **14d** (0.100 g, 0.30 mmol) and **1b** (0.067 g, 0.36 mmol) as an off-white solid (0.101 g, 75%). M.p.: 138 – 140 ˚C; R_f(10% MeOH/DCM) 0.27. ^{1}H NMR (400 MHz, Methanol-d_4) δ 8.45 (dd, J = 5.0, 1.9 Hz, 1H, H[16]), 7.76 (dd, J = 7.7, 1.8 Hz, 1H, H[14]), 7.67 (d, J = 8.5 Hz, 2H, H[7]), 7.37 – 7.32 (m, 2H, H[1,15]), 7.29 – 7.23 (m, 3H, H[6,13]), 7.06 (ddd, J = 7.9, 7.1, 1.5 Hz, 1H, H[2]), 7.00 (dd, J = 8.0, 1.4, 1H, H[4]), 6.95 (ddd, J = 8.1, 7.1, 1.1 Hz, 1H, H[3]), 5.38 (s, 2H, H[5]), 3.86 (tt, J = 10.9, 4.1 Hz, 1H, H[8]), 3.11 – 3.06 (m, 2H, H[10]), 3.05 – 3.00 (m, 2H, H[11]), 2.88 – 2.82 (m, 2H, H[12]), 2.45 – 2.36 (m, 2H, H[10]), 2.15 – 2.08 (m, 2H, H[9]), 1.70 – 1.59 (m, 2H, H[9]). ^{13}C NMR (101 MHz, Methanol-d_4) δ 159.50, 153.95, 148.38, 142.32, 141.61, 137.33, 133.90, 132.27 (2C), 127.15 (2C), 123.58, 121.67, 121.33, 119.62, 118.04, 114.88, 111.05, 107.56, 57.71, 52.02 (2C), 49.73, 44.27, 34.19, 31.22 (2C). LC-MS (APCI+/ESI): found m/z = 437.2 [M+H]$^+$ (cal. For $C_{27}H_{28}N_6$, 436.24). Purity: 99%, t_R = 2.134 min.

4-((2-((1-(2-(piperidin-1-yl)ethyl)piperidin-4-yl)amino)-1H-benzo[d]imidazol-1-yl) methyl) benzonitrile (51)

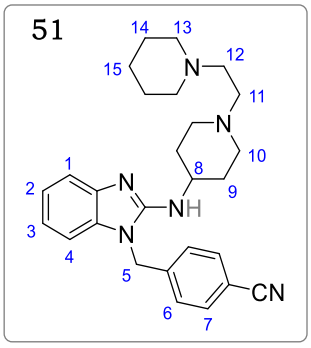

Obtained from **14d** (0.060 g, 0.18 mmol) and 1-(2-bromoethyl)piperidine (0.040 g, 0.22 mmol) as a white solid (0.036 g, 45%). M.p.: 105 – 107 °C; R_f(10% MeOH/DCM) 0.18. ^{1}H NMR (400 MHz, Methanol-d_4) δ 7.67 (d, J = 8.4 Hz, 2H, H[7]), 7.33 (dd, J = 7.4, 0.9 Hz, 1H, H[1]), 7.25 (d, J = 8.4, 2H, H[6]), 7.05 (ddd, J = 8.2, 7.4, 1.1 Hz, 1H, H[2]), 7.00 (dd, J = 8.1, 1.2 Hz, 1H, H[4]), 6.94 (ddd, J = 8.1, 7.4, 1.1 Hz, 1H, H[3]), 5.37 (s, 2H, H[5]), 3.81 (tt, J = 10.9, 5.3 Hz, 1H, H[8]), 2.94 (t, J = 3.1 Hz, 2H, H[12]), 2.60 – 2.52 (m, 4H, H[10e,11]), 2.51 – 2.48 (m, 4H, H[10a,13e]), 2.25 (dtd, J = 12.3, 11.8, 2.6 Hz, 2H, H[13a]), 2.05 – 1.88 (m, 2H, H[9e]), 1.65 – 1.52 (m, 6H, H[9a,14]), 1.49 – 1.41 (m, 2H, H[15]). ^{13}C NMR (101 MHz, Methanol-d_4) δ 154.01, 142.35, 141.71, 133.91, 132.25 (2C),

127.15 (2C), 121.28, 119.54, 118.04, 114.86, 111.04, 107.49, 55.83, 54.81, 54.51 (2C), 52.63 (2C), 49.91, 44.24, 31.45 (2C), 25.09 (2C), 23.68. LC-MS (APCI+/ESI): found m/z = 443.2 $[M+H]^+$ (cal. For $C_{27}H_{34}N_6$, 442.28). Purity: 98%, t_R = 2.236 min.

4-((2-((1-(2-morpholinoethyl)piperidin-4-yl)amino)-1H-benzo[d]imidazol-1-yl) methyl) benzonitrile (52)

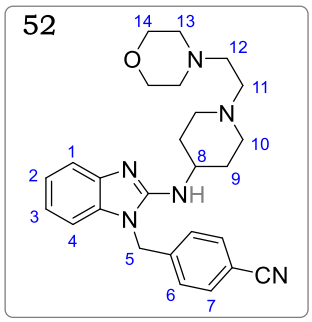

Obtained from **14d** (0.070 g, 0.21 mmol) and 4-(2-bromoethyl)morpholine (0.047 g, 0.25 mmol) as a pale-yellow solid (0.039 g, 42%). M.p.: 111 – 112 °C; R_f(10% MeOH/DCM) 0.19. ^{1}H NMR (400 MHz, Methanol-d_4) δ 7.69 (d, J = 8.3 Hz, 2H, H^7), 7.34 (dd, J = 7.8, 1.0 Hz, 1H, H^1), 7.26 (d, J = 8.3 Hz, 2H, H^6), 7.07 (ddd, J = 8.0, 7.1, 1.0 Hz, 1H, H^2), 7.02 (dd, J = 8.0, 0.9 Hz, 1H, H^4), 6.97 (ddd, J = 8.0, 7.2, 1.1 Hz, 1H, H^3), 5.40 (s, 2H, H^5), 3.90 (tt, J = 10.6, 5.2 Hz, 1H, H^8), 3.73 – 3.69 (m, 4H, H^{14}), 3.27 (t, J = 6.9 Hz, 2H, H^{12}), 2.89 (t, J = 7.0 Hz, 2H, H^{11}), 2.67 (m, 4H, $H^{10e,13e}$), 2.59 – 2.52 (m, 4H, $H^{10a,13a}$), 2.22 – 2.15 (m, 2H, H^{9e}), 1.78 – 1.72 (m, 2H, H^{9a}). ^{13}C NMR (101 MHz, Methanol-d_4) δ 142.22, 133.85, 132.28 (2C), 127.13 (2C), 121.44, 119.83, 118.02, 114.91, 112.34, 111.09, 107.71, 66.22, 54.28, 54.01 (2C), 53.44 (2C), 52.22 (2C), 48.89, 44.34, 30.18 (2C). LC-MS (APCI+/ESI): found m/z = 445.2 $[M+H]^+$ (cal. For $C_{26}H_{32}N_6O$, 444.26). Purity: 99%, t_R = 2.025 min.

(R)-4-((2-((1-(4-(3-methyl-1,2,4-oxadiazol-5-yl)phenethyl) pyrrolidine-3-yl) amino)-1H-benzo[*d*]imidazol-1-yl) methyl) benzonitrile (58)

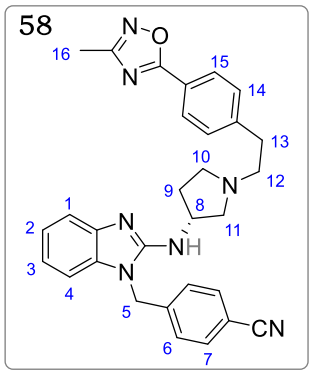

Obtained from **57a** (0.070 g, 0.22 mmol) and **7a** (0.075 g, 0.26 mmol) as a pale-yellow solid (0.087 g, 78%); m.p.: 74 – 76 °C; R_f(10% MeOH/DCM), 0.37. ^{1}H NMR (600 MHz, Methanol-d_4) δ 8.02 (d, J = 8.3 Hz, 2H, H^{15}), 7.66 (d, J = 8.4 Hz, 2H, H^7), 7.45 (d, J = 8.3 Hz, 2H, H^{14}), 7.33 (dd, J = 7.7, 1.1 Hz, 1H, H^1), 7.25 (d, J = 8.4 Hz, 2H, H^6), 7.06 (ddd, J = 7.7, 7.3, 1.0 Hz, 1H, H^2), 7.01 (dd, J = 8.0, 1.3 Hz, 1H, H^4), 6.96 (ddd, J = 8.0, 7.3, 1.1 Hz, 1H, H^3), 5.36 (s, 2H, H^5), 4.49 (tt, J = 6.8, 4.3 Hz, 1H, H^8), 2.99 – 2.89 (m, 4H, $H^{10,11,12}$), 2.86 – 2.74 (m, 3H, $H^{10,13}$), 2.59 (d, J = 6.8 Hz, 1H, H^{11}), 2.46 – 2.34 (m, 4H, $H^{9,16}$), 1.85 – 1.79 (m, 1H, H^9). ^{13}C NMR (151 MHz, Methanol-d_4) δ 175.43, 167.62, 154.06, 145.66, 142.19, 141.48, 133.92, 132.27

(2C), 129.32 (2C), 127.73 (2C), 127.13 (2C), 121.90, 121.34, 119.79, 118.01, 115.07, 111.06, 107.63, 60.32, 56.79, 52.70, 52.04, 44.32, 34.41, 31.40, 10.00. LC-MS (APCI$^+$/ESI): found m/z = 504.2 [M+H] $^+$ (cal. For $C_{30}H_{29}N_7O$, 503.24). Purity: 98%, t_R = 2.917 min. Specific rotation, $[\alpha]^{25}_D$ = -4.59°.

(S)-4-((2-((1-(4-(3-methyl-1,2,4-oxadiazol-5-yl)phenethyl)294yrrolidine-3-yl) amino)-1H-benzo[*d*]imidazol-1-yl)methyl)benzonitrile (59)

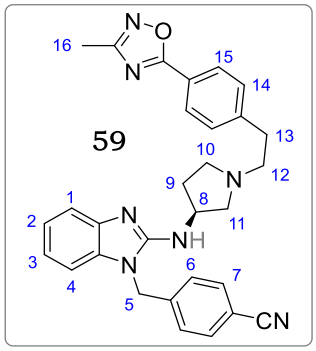

Obtained from **57b** (0.070 g, 0.22 mmol) and **7a** (0.075 g, 0.26 mmol) as a pale-yellow solid (0.089 g, 80%); m.p.: 75 – 77 °C; R_f(10% MeOH/DCM), 0.36. ^{1}H NMR (600 MHz, Methanol-d_4) δ 8.00 (d, J = 8.1 Hz, 2H, H^{15}), 7.65 (d, J = 8.2 Hz, 2H, H^7), 7.45 (d, J = 8.1 Hz, 1H, H^{14}), 7.32 (dd, J = 7.9, 1.2 Hz, 1H, H^1), 7.25 (d, J = 8.2 Hz, 2H, H^6), 7.05 (ddd, J = 7.9, 7.0, 1.1 Hz, 1H, H^2), 7.01 (dd, J = 8.0, 1.0 Hz, 1H, H^4), 6.96 (ddd, J = 8.0, 7.0, 1.0 Hz, 1H, H^3), 5.36 (s, 2H, H^5), 4.49 (tt, J = 7.0, 4.1 Hz, 1H, H^8), 3.09 – 2.98 (m, 2H, H^{10,11}), 2.98 – 2.80 (m, 5H, H^{11,12,13}), 2.69 – 2.61 (m, 1H, H^{10}), 2.48 – 2.38 (m, 4H, H^{9,16}), 1.91 – 1.80 (m, 1H, H^9). ^{13}C NMR (151 MHz, Methanol-d_4) δ 176.27, 168.51, 154.80, 146.19, 143.02, 142.19, 134.78, 133.17 (2C), 130.22 (2C), 128.67 (2C), 128.01 (2C), 122.89, 122.26, 120.75, 118.90, 115.98, 111.96, 108.56, 61.02, 57.44, 53.68, 52.84, 45.24, 35.04, 32.09, 10.90. LC-MS (APCI$^+$/ESI): found m/z = 504.2 [M+H] $^+$ (cal. For $C_{30}H_{29}N_7O$, 503.24). Purity: 97%, t_R = 2.745 min. Specific rotation, $[\alpha]^{25}_D$ = +4.58°.

4-((2-(2-(4-(3-methyl-1,2,4-oxadiazol-5-yl)phenethyl)-2,6-diazaspiro[3.4]octan-6-yl)-1H-benzo[*d*]imidazol-1-yl)methyl)benzonitrile (60)

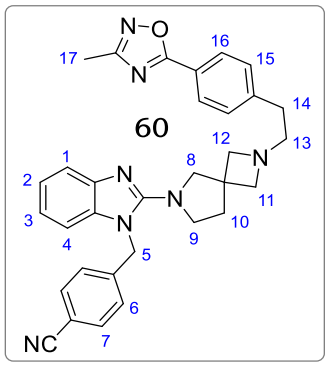

Obtained from **57c** (0.055 g, 0.16 mmol) and **7a** (0.055 g, 0.19 mmol) as a pale-yellow solid (0.065 g, 77%); m.p.: 113 – 115 °C; R_f(10% MeOH/DCM), 0.40. ^{1}H NMR (600 MHz, Methanol-d_4) δ 8.02 (d, J = 8.2 Hz, 2H, H^{15}), 7.68 (d, J = 8.3 Hz, 2H, H^7), 7.43 (d, J = 8.2 Hz, 2H, H^{14}), 7.39 (dd, J = 7.9, 1.2 Hz, 1H, H^1), 7.27 (d, J = 8.3 Hz, 2H, H^6), 7.12 (ddd, J = 7.9, 7.5, 1.0 Hz, 1H, H^2), 7.06 (dd, J = 8.1, 1.2 Hz, 1H, H^4), 7.02 (ddd, J = 8.1, 7.5, 1.0 Hz, 1H, H^3), 5.47 (s, 2H, H^5), 3.64 (s, 2H, H^8), 3.54 (t, J = 6.9 Hz, 2H, H^9), 3.26 (m, 4H, H^{11,12}), 2.82 – 2.77 (m, 2H, H^{13}), 2.77 – 2.73 (m, 2H, H^{14}), 2.42 (s, 3H, H^{17}), 2.12 (t, J = 6.9 Hz, 2H, H^{10}). ^{13}C NMR (151 MHz, Methanol-d_4) δ 175.43, 167.62, 155.97, 145.30, 142.84, 141.26, 135.41, 132.41 (2C), 129.40 (2C), 127.73 (2C),

126.70 (2C), 121.93, 120.37, 118.01, 115.53, 111.11, 108.32, 63.00, 59.92, 59.05, 48.58, 46.77, 40.63, 35.33, 33.53, 29.33, 10.00. LC-MS (APCI$^+$/ESI): found m/z = 530.2 [M+H]$^+$ (cal. For $C_{32}H_{31}N_7O$, 529.26). Purity: 97%, t_R = 2.340 min.

4-((2-(4-(4-(3-methyl-1,2,4-oxadiazol-5-yl)phenethyl)piperazin-1-yl)-1H-benzo[*d*]imidazol-1-yl)methyl)benzonitrile (61)

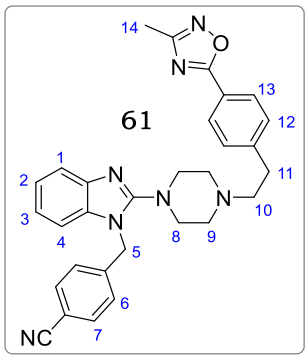

Obtained from **57d** (0.078 g, 0.25 mmol) and **7a** (0.084 g, 0.29 mmol) as a pale-yellow solid (0.094 g, 76%); m.p.: 141 – 143 °C; R_f(10% MeOH/DCM), 0.43. ^{1}H NMR (600 MHz, Methanol-d_4) δ 8.02 (d, J = 8.0 Hz, 2H, H^{13}), 7.70 (d, J = 8.2 Hz, 2H, H^7), 7.52 (dd, J = 8.2, 1.1 Hz, 1H, H^1), 7.46 (d, J = 8.0 Hz, 2H, H^{12}), 7.32 (d, J = 8.2 Hz, 2H, H^6), 7.19 (ddd, J = 8.2, 5.6, 1.6 Hz, 1H, H^2), 7.14 – 7.10 (m, 2H, H^{3,4}), 5.42 (s, 2H, H^5), 3.30 – 3.27 (br-t, 4H, H^8), 2.95 – 2.91 (m, 2H, H^{10}), 2.73 – 2.71 (m, 2H, H^{11}), 2.71 – 2.67 (m, 4H, H^9), 2.42 (s, 3H, H^{14}). ^{13}C NMR (151 MHz, Methanol-d_4) δ 176.38, 168.49, 158.60, 146.88, 143.14, 141.54, 135.53, 133.33 (2C), 130.30 (2C), 128.56 (2C), 128.00 (2C), 123.00, 122.69, 118.84, 117.96, 112.12, 110.28, 60.04, 53.13 (2C), 51.03 (2C), 49.05, 47.64, 33.53, 10.88. LC-MS (APCI$^+$/ESI): found m/z = 504.2 [M+H]$^+$ (cal. For $C_{30}H_{29}N_7O$, 503.24). Purity: 99%, t_R = 2.512 min.

(S)-4-((2-(3-methyl-4-(4-(3-methyl-1,2,4-oxadiazol-5-yl) phenethyl) piperazin-1-yl)-1H-benzo[*d*]imidazol-1-yl) methyl) benzonitrile (62)

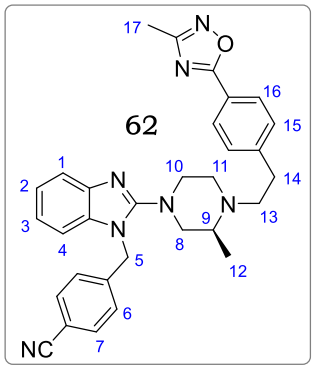

Obtained from **57e** (0.110 g, 0.33 mmol) and **7a** (0.114 g, 0.40 mmol) as a pale-yellow solid (0.115 g, 67%); m.p.: 77 – 80 °C; R_f(10% MeOH/DCM), 0.49. ^{1}H NMR (600 MHz, Methanol-d_4) δ 8.01 (d, J = 8.4 Hz, 2H, H^{16}), 7.69 (d, J = 8.6 Hz, 2H, H^7), 7.52 (dd, J = 8.0, 0.9 Hz, 1H, H^1), 7.44 (d, J = 8.4 Hz, 2H, H^{15}), 7.31 (d, J = 8.6 Hz, 2H, H^6), 7.18 (ddd, J = 8.0, 6.1, 1.7 Hz, 1H, H^2), 7.13 – 7.10 (m, 2H, H^{3,4}), 5.42 (s, 2H, H^5), 3.40 – 3.34 (m, 1H, H^{11}), 3.30 – 3.26 (m, 1H, H^9), 3.21 (ddd, J = 12.3, 9.9, 2.8 Hz, 1H, H^{11}), 3.03 – 2.96 (m, 2H, H^{8,10}), 2.95 – 2.82 (m, 3H, H^{8,13}), 2.76 – 2.68 (m, 2H, H^{14}), 2.67 – 2.62 (m, 1H, H^{10}), 2.41 (s, 3H, H^{17}), 1.05 (d, J = 6.3 Hz, 3H, H^{12}). ^{13}C NMR (151 MHz, Methanol-d_4) δ 176.88, 169.00, 158.98, 147.63, 143.73, 142.06, 136.12, 133.86 (2C), 130.84 (2C), 129.09 (2C), 128.48 (2C), 123.51, 123.18, 119.35, 118.44, 112.64, 110.72, 58.12, 55.79, 55.30, 51.71, 51.21, 48.18, 33.06, 30.73, 15.59, 11.41. LC-MS

(APCI$^+$/ESI): found m/z = 518.2 [M+H] $^+$ (cal. For $C_{31}H_{31}N_7O$, 517.26). Purity: 99%, t_R = 2.531 min. Specific rotation, $[\alpha]^{25}_D$ = +7.74°.

4-((2-(1-(4-(3-methyl-1,2,4-oxadiazol-5-yl)phenethyl)piperidin-4-yl)-1H-benzo[d]imidazol-1-yl)methyl)benzonitrile (65)

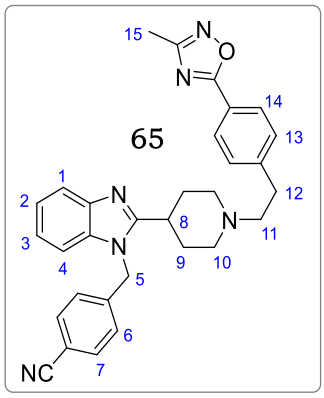

Obtained from **64** (0.100 g, 0.32 mmol) and **7a** (0.109 g, 0.38 mmol) as a yellow solid (0.137 g, 85%. M.p.: 158 – 160 °C; R_f (10% MeOH/DCM), 0.45. ^{1}H NMR (400 MHz, Methanol-d_4) δ 8.04 (d, J = 8.2 Hz, 2H, H^{14}), 7.74 – 7.62 (m, 3H, H^{1,7}), 7.47 (d, J = 8.2 Hz, 2H, H^{13}), 7.33 (ddd, J = 7.8, 7.0, 2.0 Hz, 1H, H^2), 7.30 – 7.19 (m, 4H, H^{3,4,6}), 5.67 (s, 2H, H^5), 3.21 – 3.12 (m, 2H, H^{10e}), 3.07 – 2.91 (m, 3H, H^{8,11}), 2.77 – 2.69 (m, 2H, H^{12}), 2.43 (s, 3H, H^{15}), 2.32 – 2.21 (m, 2H, H^{10a}), 2.09 (dtd, J = 13.8, 12.0, 6.9 Hz, 2H, H^{9a}), 1.91 – 1.82 (m, 2H, H^{9e}). ^{13}C NMR (101 MHz, Methanol-d_4) δ 175.50, 167.63, 157.88, 145.93, 142.46, 141.78, 134.81, 132.52 (2C), 129.42 (2C), 127.72 (2C), 126.91 (2C), 122.73, 122.33, 121.84, 118.18, 117.90, 111.37, 109.80, 59.31, 52.84 (2C), 45.76, 34.15, 32.60, 30.25 (2C), 9.99. LC-MS (APCI$^+$/ESI): found m/z = 503.2 [M+H] $^+$ (cal. For $C_{31}H_{30}N_6O$, 502.25). Purity: 99%, t_R = 2.558 min.

N-(1-(4-(3-Methyl-1,2,4-oxadiazol-5-yl)phenethyl)piperidin-4-yl)-1H-benzo[*d*]imidazol-2-amine (66)

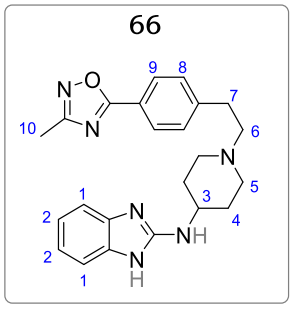

Obtained from **14a** (0.85 g, 3.93 mmol) and **7a** (1.35 g, 4.72 mmol) as a pale-yellow solid (1.18 g, 75%); m.p.: 171 – 173 °C; R_f (10% MeOH/DCM), 0.20. ^{1}H NMR (400 MHz, Methanol-d_4) δ 8.04 (d, J = 8.3 Hz, 2H, H^9), 7.46 (d, J = 8.3 Hz, 2H, H^8), 7.20 (dd, J = 5.8, 3.2 Hz, 2H, H^2), 6.98 (dd, J = 5.8, 3.2 Hz, 2H, H^1), 3.69 (tt, J = 10.9, 4.3 Hz, 1H, H^3), 3.10 – 3.03 (m, 2H, H^5), 2.97 – 2.91 (m, 2H, H^6), 2.75 – 2.68 (m, 2H, H^7), 2.42 (s, 3H, H^{10}), 2.40 – 2.31 (m, 2H, H^5), 2.15 – 2.08 (m, 2H, H^4), 1.71 – 1.59 (m, 2H, H^4). ^{13}C NMR (101 MHz, Methanol-d_4) δ 176.08, 167.11, 154.29, 145.78, 137.16, 129.36 (2C), 127.75 (2C), 121.89, 120.10, 111.31, 59.21, 51.95 (2C), 49.33, 43.55, 32.72, 31.63 (2C), 9.99. LC-MS (APCI$^+$/ESI): found m/z = 403.2 [M+H] $^+$ (cal. For $C_{23}H_{26}N_6O$, 402.22). Purity: 98%, t_R = 2.469 min.

N-(1-(4-(3-(Trifluoromethyl)-1,2,4-oxadiazol-5-yl) phenethyl) piperidin-4-yl)-1H-benzo[d]imidazol-2-amine (67)

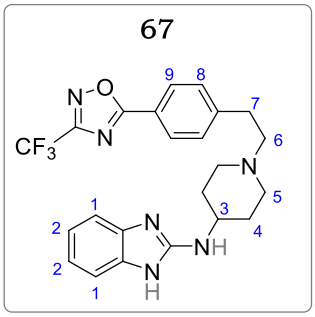

Obtained from **14a** (0.250 g, 1.16 mmol) and **7b** (0.474 g, 1.39 mmol) as a white crystalline solid (0.290 g, 55%). M.p.: 102 – 104 °C; R_f (10% MeOH/DCM), 0.38. ^{1}H NMR (400 MHz, Methanol-d_4) δ 8.02 (d, J = 8.4 Hz, 2H, H^9), 7.43 (d, J = 8.4 Hz, 2H, H^8), 7.22 – 7.17 (m, 2H, H^2), 7.02 – 6.98 (m, 2H, H^1), 3.68 (tt, J = 10.8, 4.2 Hz, 1H, H^3), 3.11 – 3.00 (m, 2H, H^5), 2.99 – 2.90 (m, 2H, H^6), 2.75 – 2.66 (m, 2H, H^7), 2.41 – 2.29 (m, 2H, H^5), 2.14 – 2.08 (m, 2H, H^4), 1.71 – 1.60 (m, 2H, H^4). ^{13}C NMR (101 MHz, Methanol-d_4) δ 175.88, 167.09, 154.23, 146.99, 137.35, 129.44 (2C), 127.15 (2C), 121.78, 120.00, 119.8 (q, J = 32.9 Hz), 110.11, 59.33, 50.05 (2C), 49.76, 43.67, 33.02, 30.33 (2C). LC-MS (APCI$^+$/ESI): found m/z = 457.2 [M+H] $^+$ (cal. For $C_{23}H_{23}F_3N_6O$, 456.19). Purity: 98%, t_R = 2.533 min.

1-Methyl-N-(1-(4-(3-methyl-1,2,4-oxadiazol-5-yl) phenethyl) piperidin-4-yl)-1H-benzo[*d*]imidazol-2-amine (68)

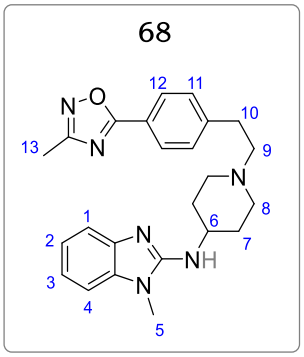

Obtained from **14b** (0.150 g, 0.65 mmol) and **7a** (0.223 g, 0.78 mmol) as a pale-yellow solid (0.203 g, 75%); m.p.: 134 – 136 °C; R_f(10% MeOH/DCM), 0.34. ^{1}H NMR (600 MHz, Methanol-d_4) δ 8.04 (d, J = 8.1 Hz, 2H, H^{12}), 7.47 (d, J = 8.1 Hz, 2H, H^{11}), 7.28 (dd, J = 7.9, 1.1 Hz, 1H, H^1), 7.12 (dd, J = 8.3, 1.2 Hz, 1H, H^4), 7.03 (ddd, J = 8.3, 7.1, 1.0 Hz, 1H, H^3), 7.00 (ddd, J = 7.9, 7.1, 1.0 Hz, 1H, H^2), 3.79 (tt, J = 11.1, 4.2 Hz, 1H, H^6), 3.52 (s, 3H, H^5), 3.14 – 3.07 (m, 2H, H^8), 2.98 – 2.92 (m, 2H, H^9), 2.75 – 2.70 (m, 2H, H^{10}), 2.42 (s, 3H, H^{13}), 2.37 – 2.30 (m, 2H, H^8), 2.17 – 2.10 (m, 2H, H^7), 1.74 – 1.65 (m, 2H, H^7). ^{13}C NMR (151 MHz, Methanol-d_4) δ 175.47, 167.62, 154.22, 145.84, 141.16, 134.55, 129.38 (2C), 127.75 (2C), 121.87, 120.72, 119.28, 114.37, 106.95, 59.27, 52.30 (2C), 49.86, 32.76, 31.57 (2C), 27.18, 10.00. LC-MS (APCI$^+$/ESI): found m/z = 417.2 [M+H] $^+$ (cal. For $C_{24}H_{28}N_6O$, 416.23). Purity: 99%, t_R = 2.530 min.

1-Methyl-N-(1-(4-(3-(trifluoromethyl)-1,2,4-oxadiazol-5-yl) phenethyl) piperidin-4-yl)-1H-benzo[d]imidazol-2-amine (69)

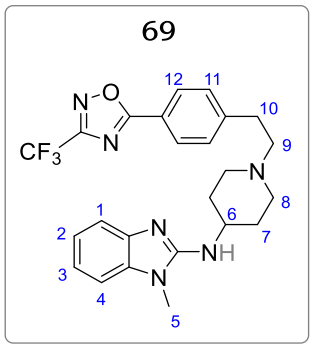

Obtained from **14b** (0.150 g, 0.65 mmol) and **7b** (0.266 g, 0.78 mmol) as a white solid (0.202 g, 66%). M.p.: 90 – 92 °C; R_f(10% MeOH/DCM), 0.35. ^{1}H NMR (400 MHz, Methanol-d_4) δ 8.08 (d, J = 8.2 Hz, 2H, H^{12}), 7.50 (d, J = 8.2 Hz, 2H, H^{11}), 7.29 (dd, J = 7.7, 1.1 Hz, 1H, H^1), 7.12 (dd, J = 8.1, 1.2 Hz, 1H, H^4), 7.03 (ddd, J = 8.1, 7.3, 1.0 Hz, 1H, H^3), 7.00 (ddd, J = 7.7, 7.3, 1.0 Hz, 1H, H^2), 3.80 (tt, J = 11.0, 4.3 Hz, 1H, H^6), 3.53 (s, 3H, H^5), 3.14 – 3.09 (m, 2H, H^8), 2.99 – 2.90 (m, 2H, H^9), 2.77 – 2.71 (m, 2H, H^{10}), 2.36 – 2.29 (m, 2H, H^8), 2.16 – 2.09 (m, 2H, H^7), 1.73 – 1.65 (m, 2H, H^7). ^{13}C NMR (151 MHz, Methanol-d_4) δ 175.77, 167.02, 155.12, 146.04, 140.96, 134.63, 130.01 (2C), 127.65 (2C), 121.66, 120.98, 120.08, 119.07 (q, J = 33.0 Hz), 114.45, 106.99, 59.78, 52.31 (2C), 49.97, 32.77, 31.54 (2C), 27.11. LC-MS (APCI$^+$/ESI): found m/z = 471.2 [M+H]$^+$ (cal. For $C_{24}H_{25}F_3N_6O$, 470.20). Purity: 99%, t_R = 2.606 min.

1-Isopropyl-*N*-(1-(4-(3-methyl-1,2,4-oxadiazol-5-yl) phenethyl) piperidin-4-yl)-1H-benzo[*d*]imidazol-2-amine (70)

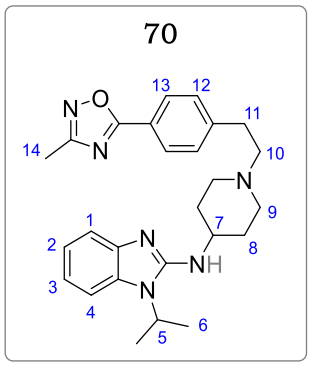

Obtained from **14c** (0.030 g, 0.12 mmol) and **7a** (0.040 g, 0.14 mmol) as a pale-yellow solid (0.047 g, 91%); m.p.: 183 – 185 °C; R_f(10% MeOH/DCM), 0.37. ^{1}H NMR (600 MHz, Methanol-d_4) δ 8.05 (d, J = 8.6 Hz, 2H, H^{13}), 7.48 (d, J = 8.6 Hz, 2H, H^{12}), 7.35 (dd, J = 7.9, 1.2 Hz, 1H, H^1), 7.29 (dd, J = 7.6, 1.1 Hz, 1H, H^4), 7.02 (ddd, J = 7.6, 7.1, 1.1 Hz, 1H, H^3), 6.96 (ddd, J = 7.9, 7.1, 1.2 Hz, 1H, H^2), 4.61 (hept, J = 6.9 Hz, 1H, H^5), 3.80 (tt, J = 11.1, 4.2 Hz, 1H, H^7), 3.16 – 3.09 (m, 2H, H^9), 3.00 – 2.93 (m, 2H, H^{10}), 2.77 – 2.73 (m, 2H, H^{11}), 2.43 (s, 3H, H^{14}), 2.39 – 2.32 (m, 2H, H^9), 2.17 – 2.10 (m, 2H, H^8), 1.73 – 1.66 (m, 2H, H^8), 1.57 (d, J = 6.9 Hz, 6H, H^6). ^{13}C NMR (151 MHz, Methanol-d_4) δ 175.48, 167.63, 153.03, 145.79, 141.73, 132.06, 129.39 (2C), 127.77 (2C), 121.91, 120.49, 118.98, 114.76, 109.88, 59.25, 52.33 (2C), 50.00, 45.94, 32.73, 31.51 (2C), 19.40 (2C), 9.99. LC-MS (APCI$^+$/ESI): found m/z = 445.2 [M+H]$^+$ (cal. For $C_{26}H_{32}N_6O$, 444.26). Purity: 97%, t_R = 2.581 min.

Methyl 4-(2-(4-((1-methyl-1H-benzo[d]imidazol-2-yl) amino) piperidin-1-yl) ethyl) benzoate (79)

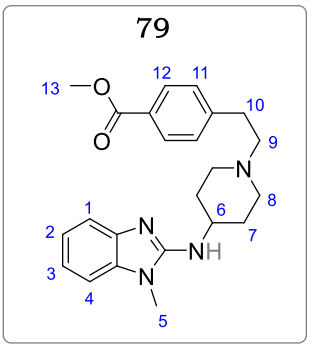

Obtained from **14b** (5.00 g, 21.7 mmol) and **9** (0.096 g, 6.37 mmol) as a cream white solid (5.78 g, 68%). M.p.: 148 – 149 °C; R_f(10% MeOH/DCM), 0.46. ^{1}H NMR (400 MHz, Methanol-d_4) δ 7.95 (d, J = 8.3 Hz, 2H, H^{12}), 7.37 (d, J = 8.3 Hz, 2H, H^{11}), 7.27 (dd, J = 7.4, 1.3 Hz, 1H, H^1), 7.13 (dd, J = 7.5, 1.6 Hz, 1H, H^4), 7.07 – 6.97 (m, 2H, H^{2,3}), 3.89 (s, 3H, H^{13}), 3.78 (tt, J = 11.2, 4.2 Hz, 1H, H^6), 3.52 (s, 3H, H^5), 3.15 – 3.06 (m, 2H, H^{8e}), 2.96 – 2.88 (m, 2H, H^9), 2.72 – 2.65 (m, 2H, H^{10}), 2.32 (td, J = 12.1, 2.5 Hz, 2H, H^{8a}), 2.17 – 2.09 (m, 2H, H^{7e}), 1.69 (dtd, J = 12.2, 10.2, 3.8 Hz, 2H, H^{7a}). ^{13}C NMR (101 MHz, Methanol-d_4) δ 167.16, 154.29, 145.88, 141.29, 134.58, 129.35 (2C), 128.57 (2C), 127.95, 120.69, 119.23, 114.39, 106.92, 59.43, 52.31 (2C), 51.11, 49.87, 32.76, 31.59 (2C), 27.16. LC-MS (APCI$^+$/ESI): found m/z = 393.2 [M+H]$^+$ (cal. For $C_{23}H_{28}N_4O_2$, 392.22). Purity: 98%, t_R = 0.422 min.

Ethyl 4-(2-(4-((1-methyl-1H-benzo[d]imidazol-2-yl)amino)piperidin-1-yl) ethyl) benzoate (80)

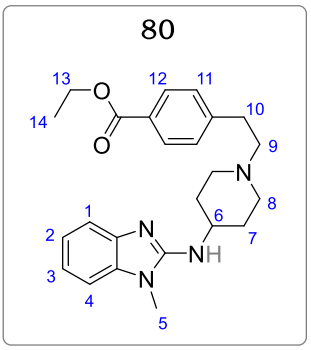

Obtained from **14b** (0.100 g, 0.43 mmol) and **8** (0.134 g, 0.52 mmol) as a pale-yellow solid (0.134 g, 77%); m.p.: 75 – 76 °C; R_f(10% MeOH/DCM) 0.48. ^{1}H NMR (400 MHz, Methanol-d_4) δ 7.49 (d, J = 8.0 Hz, 2H, H^{12}), 7.35 (d, J = 8.0 Hz, 2H, H^{11}), 7.29 (dd, J = 7.8, 1.2 Hz, 1H, H^1), 7.09 (dd, J = 7.9, 1.0 Hz, 1H, H^4), 6.98 (ddd, J = 7.8, 7.1, 0.9 Hz, 1H, H^2), 6.81 (ddd, J = 7.9, 7.1, 1.1 Hz, 1H, H^3), 4.45 (q, J = 6.9 Hz, 2H, H^{13}), 3.82 (tt, J = 11.1, 4.0 Hz, 1H, H^6), 3.50 (s, 2H, H^5), 3.11 – 3.05 (m, 2H, H^{8e}), 2.91 – 2.83 (m, 2H, H^9), 2.72 – 2.65 (m, 2H, H^{10}), 2.39 – 2.31 (m, 2H, H^{8a}), 2.09 – 1.98 (m, 2H, H^{7e}), 1.48 – 1.39 (m, 2H, H^{7a}), 1.33 (t, J = 6.9 Hz, 3H, H^{14}). ^{13}C NMR (151 MHz, Methanol-d_4) δ 165.23, 153.28, 144.58, 141.35, 133.65, 129.98 (2C), 129.48 (2C), 128.65, 121.21, 120.78, 116.58, 109.58, 62.58, 59.54, 52.54 (2C), 50.66, 32.44, 31.56 (2C), 23.56, 14.53. LC-MS (APCI$^+$/ESI): found m/z = 407.2 [M+H] $^+$ (cal. For $C_{24}H_{30}N_4O_2$, 406.24). Purity: 99%, t_R = 2.046 min.

1-methyl-2-((1-(4-(3-methyl-1,2,4-oxadiazol-5-yl) phenethyl) piperidin-4-yl) amino)-1H-benzo[d]imidazole-5-carbonitrile (132)

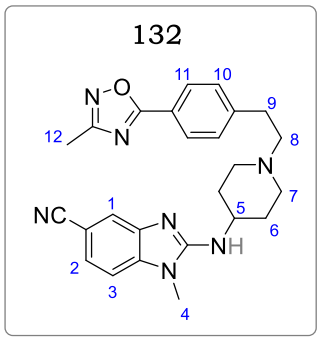

Obtained from **131a** (0.080 g, 0.32 mmol) and **7a** (0.108 g, 0.38 mmol) as a cream white solid (0.095 g, 69%). m.p.: 97 – 99 °C; R_f(10% MeOH/DCM), 0.21. ^{1}H NMR (400 MHz, Methanol-d_4) δ 8.04 (d, J = 8.1 Hz, 2H, H^{11}), 7.92 (d, J = 1.4 Hz, 1H, H^1), 7.75 (d, J = 7.5 Hz, 1H, H^3), 7.49 (dd, J = 7.5, 1.4 Hz, 1H, H^2), 7.29 (d, J = 8.1 Hz, 2H, H^{10}), 3.85 (tt, J = 10.8, 4.0 Hz, 1H, H^5), 3.51 (s, 3H, H^4), 3.21 – 3.13 (m, 2H, H^{7e}), 3.01 – 2.93 (m, 2H, H^8), 2.74 – 2.69 (m, 2H, H^9), 2.41 (s, 3H, H^{12}), 2.38 – 2.29 (m, 2H, H^{7a}), 2.17 – 2.09 (m, 2H, H^{6e}), 1.74 – 1.64 (m, 2H, H^{6a}). ^{13}C NMR (151 MHz, Methanol-d_4) δ 175.38, 159.17, 141.45, 139.33, 137.69, 133.76, 128.62 (2C), 127.91 (2C), 125.89, 121.34, 119.77, 118.32, 115.05, 106.31, 59.49, 56.675, 52.03 (2C), 34.63, 32.29, 31.64 (2C), 16.79. LC-MS (APCI$^+$/ESI): found m/z = 442.2 [M+H]$^+$ (cal. for $C_{25}H_{27}N_7O$, 441.23). Purity: 98%, t_R = 2.201 min.

1-methyl-N-(1-(4-(3-methyl-1,2,4-oxadiazol-5-yl) phenethyl) piperidin-4-yl)-5-(trifluoromethyl)-1H-benzo[d]imidazol-2-amine (133)

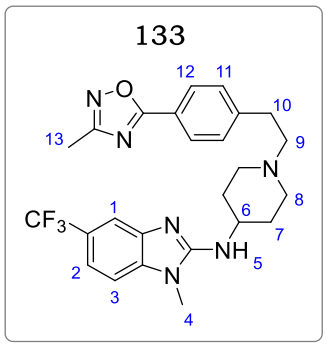

Obtained from **131b** (0.080 g, 0.27 mmol) and **7a** (0.092 g, 0.32 mmol) as an off white solid (0.081 g, 62%). m.p.: 156 – 157 °C; R_f (10% MeOH/DCM), 0.29. ^{1}H NMR (400 MHz, DMSO-d_6) δ 8.01 (d, J = 7.8 Hz, 2H, H^{12}), 7.50 (d, J = 7.8 Hz, 1H, H^{11}), 7.47 (s, 1H, H^1), 7.31 (d, J = 8.2 Hz, 1H, H^3), 7.23 (d, J = 8.2 Hz, 1H, H^2), 6.81 (s, 1H, H^5), 3.81 (m, 1H, H^6), 3.55 (s, 3H, H^4), 3.11 – 3.04 (m, 2H, H^{8e}), 2.96 – 2.88 (m, 2H, H^9), 2.77 – 2.68 (m, 2H, H^{8a}), 2.44- 2.38 (m, 2H, H^{10}), 2.08 (s, 3H, H^{13}), 2.04 – 2.00 (m, 2H, H^{7e}), 1.68 – 1.59 (m, 2H, H^{7a}). ^{13}C NMR (151 MHz, DMSO-d_6) δ 175.87, 162.17, 141.65, 139.23, 137.69, 133.76, 128.62 (2C), 127.91 (2C), 125.56, 124.22 (q, J = 27.3 Hz), 122.18, 119.23, 112.15, 107.35, 59.55, 56.68, 52.32 (2C), 34.87, 32.88, 29.35 (2C), 11.95. LC-MS (APCI$^+$/ESI): found m/z = 485.2 [M+H]$^+$ (cal. for $C_{25}H_{27}F_3N_6O$, 484.22). Purity: 99%, t_R = 2.382 min.

5-methoxy-1-methyl-N-(1-(4-(3-methyl-1,2,4-oxadiazol-5-yl) phenethyl) piperidin-4-yl)-1H-benzo[d]imidazol-2-amine (134)

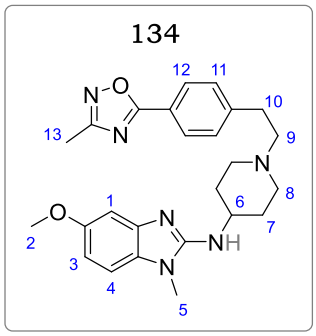

Obtained from **131c** (0.080 g, 0.31 mmol) and **7a** (0.106 g, 0.37 mmol) as a light brown solid (0.074 g, 54%). m.p.: 109 – 111 °C; R_f(10% MeOH/DCM), 0.22. ^{1}H NMR (400 MHz, Methanol-d_4) δ 8.01 (d, J = 8.0 Hz, 2H, H^{12}), 7.44 (d, J = 1.4 Hz, 1H, H^1), 7.30 (dd, J = 7.5, 1.4 Hz, 1H, H^3), 7.21 (d, J = 7.5 Hz, 1H, H^4), 7.10 (d, J = 8.0 Hz, 2H, H^{11}), 3.86 (tt, J = 10.7, 3.9 Hz, 1H, H^6), 3.86 (s, 3H, H^2), 3.51 (s, 3H, H^5), 3.20 – 3.12 (m, 2H, H^{8e}), 2.96 – 2.88 (m, 2H, H^9), 2.74 – 2.68 (m, 2H, H^{10}), 2.41 (s, 3H, H^{13}), 2.37 – 2.29 (m, 2H, H^{8a}), 2.09 – 1.99 (m, 2H, H^{7e}), 1.71 – 1.63 (m, 2H, H^{7a}). ^{13}C NMR (151 MHz, Methanol-d_4) δ 175.30, 162.37, 156.97, 142.04, 139.43, 137.71, 133.85, 128.88 (2C), 127.97 (2C), 126.32, 113.23, 112.42, 100.22, 59.64, 56.79, 52.37 (2C), 34.56, 32.19, 31.11 (2C), 56.81, 16.90. LC-MS (APCI$^+$/ESI): found m/z = 447.2 [M+H]$^+$ (cal. For $C_{25}H_{30}N_6O_2$, 446.24). Purity: 97%, t_R = 2.214 min.

1-methyl-N-(1-(4-(3-methyl-1,2,4-oxadiazol-5-yl) phenethyl) piperidin-4-yl)-5-(methylsulfonyl)-1H-benzo[d]imidazol-2-amine (135)

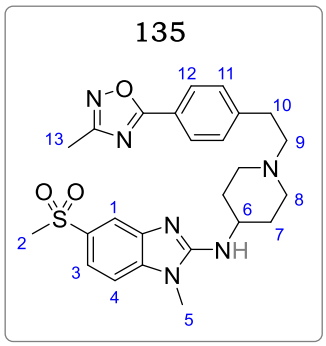

Obtained from **131d** (0.080 g, 0.26 mmol) and **7a** (0.089 g, 0.31 mmol) as an off white solid (0.082 g, 64%). m.p.: 202 – 204 °C; R_f(10% MeOH/DCM), 0.19. ^{1}H NMR (400 MHz, Methanol-d_4) δ 8.01 (d, J = 8.2 Hz, 2H, H^{12}), 7.83 (d, J = 1.3 Hz, 1H, H^1), 7.77 (d, J = 7.8 Hz, 1H, H^4), 7.35 (dd, J = 7.8, 1.3 Hz, 1H, H^3), 7.21 (d, J = 8.2 Hz, 2H, H^{11}), 3.88 (tt, J = 10.9, 4.0 Hz, 1H, H^6), 3.53 (s, 3H, H^2), 3.39 (s, 3H, H^5), 3.19 – 3.12 (m, 2H, H^{8e}), 2.98 – 2.92 (m, 2H, H^9), 2.75 – 2.70 (m, 2H, H^{10}), 2.42 (s, 3H, H^{13}), 2.37 – 2.99 (m, 2H, H^{8a}), 2.15 – 2.07 (m, 2H, H^{7e}), 1.69 – 1.60 (m, 2H, H^{7a}). ^{13}C NMR (151 MHz, Methanol-d_4) δ 175.82, 161.11, 141.58, 139.44, 138.09, 133.86, 132.03, 128.54 (2C), 127.85 (2C), 120.11, 119.35, 116.19, 112.38, 59.63, 56.74, 52.38 (2C), 47.09, 34.85, 32.71, 31.70 (2C), 16.96. LC-MS (APCI$^+$/ESI): found m/z = 495.2 [M+H]$^+$ (cal. for $C_{25}H_{30}N_6O_3S$, 494.21). Purity: 99%, t_R = 2.043 min.

Methyl 1-methyl-2-((1-(4-(3-methyl-1,2,4-oxadiazol-5-yl) phenethyl) piperidin-4-yl) amino)-1H-benzo[d]imidazole-5-carboxylate (136)

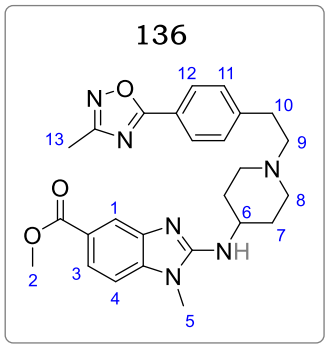

Obtained from **131e** (0.200 g, 0.69 mmol) and **7a** (0.238 g, 0.83 mmol) as a white solid (0.255 g, 78%). m.p.: 98 – 99 °C; R_f(10% MeOH/DCM), 0.20. ^{1}H NMR (400 MHz, Methanol-d_4) δ 8.16 (d, J = 0.9 Hz, 1H, H^1), 8.02 (d, J = 7.9 Hz, 2H, H^{12}), 7.89 (dd, J = 7.8, 1.0 Hz, 1H, H^3), 7.58 (d, J = 7.8 Hz, 1H, H^4), 7.36 (d, J = 7.9 Hz, 2H, H^{11}), 3.89 (tt, J = 11.2, 4.5 Hz, 1H, H^6), 3.80 (s, 3H, H^2), 3.52 (s, 3H, H^5), 3.20 – 3.13 (m, 2H, H^{8e}), 2.97 – 2.89 (m, 2H, H^9), 2.77 – 2.69 (m, 2H, H^{10}), 2.41 (s, 3H, H^{13}), 2.35 – 2.27 (m, 2H, H^{8a}), 2.17 – 2.09 (m, 2H, H^{7e}), 1.71 – 1.63 (m, 2H, H^{7a}). ^{13}C NMR (151 MHz, Methanol-d_4) δ 175.90, 167.32, 162.30, 141.55, 139.12, 137.87, 133.64, 128.36 (2C), 127.96 (2C), 125.68, 124.34, 119.35, 116.64, 112.44, 59.51, 56.72, 52.95 (2C), 52.22, 34.72, 32.99, 31.77 (2C), 16.85. LC-MS (APCI$^+$/ESI): found m/z = 475.2 [M+H]$^+$ (cal. For $C_{26}H_{30}N_6O_3$, 474.24). Purity: 98%, t_R = 2.245 min.

5-fluoro-1-methyl-N-(1-(4-(3-methyl-1,2,4-oxadiazol-5-yl) phenethyl) piperidin-4-yl)-1H-benzo[d]imidazol-2-amine (137)

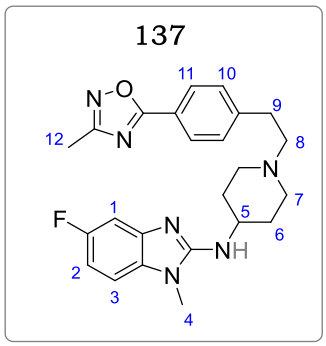

Obtained from **131f** (0.080 g, 0.32 mmol) and **7a** (0.109 g, 0.38 mmol) as a light brown solid (0.091 g, 65%). m.p.: 72 – 74 °C; R_f(10% MeOH/DCM), 0.25. ^{1}H NMR (400 MHz, Methanol-d_4) δ 8.03 (d, J = 8.1 Hz, 2H, H^{11}), 7.54 (dd, J = 8.3, 1.2 Hz, 1H, H^1), 7.41 (dd, J = 7.6, 1.5 Hz, 1H, H^3), 7.32 (d, J = 8.1 Hz, 2H, H^{10}), 6.88 (ddd, J = 8.0, 7.6, 1.3 Hz, 1H, H^2), 3.91 (tt, J = 11.2, 4.1 Hz, 1H, H^5), 3.52 (s, 3H, H^4), 3.19 – 3.10 (m, 2H, H^{7e}), 2.99 – 2.91 (m, 2H, H^8), 2.76 – 2.69 (m, 2H, H^9), 2.41 (s, 3H, H^{12}), 2.35 – 2.29 (m, 2H, H^{7a}), 2.16 – 2.09 (m, 2H, H^{6e}), 1.70 – 1.61 (m, 2H, H^{6a}). ^{13}C NMR (151 MHz, Methanol-d_4) δ 176.66, 160.23, 156.85 (d, J = 23.1 Hz), 141.45, 140.87, 138.23, 134.15, 128.54 (2C), 127.20 (2C), 120.08, 116.75, 110.55, 102.92, 59.33, 56.28, 52.26 (2C), 34.75, 32.29, 31.54 (2C), 16.98. LC-MS (APCI$^+$/ESI): found m/z = 435.2 [M+H]$^+$ (cal. for $C_{24}H_{27}FN_6O$, 434.22). Purity: 98%, t_R = 2.028 min.

5-bromo-1-methyl-N-(1-(4-(3-methyl-1,2,4-oxadiazol-5-yl) phenethyl) piperidin-4-yl)-1H-benzo[d]imidazol-2-amine (138)

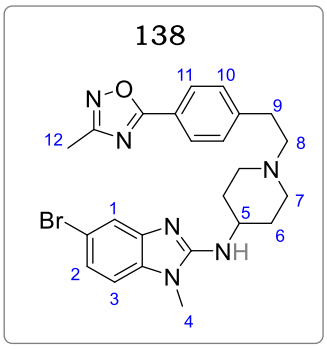

Obtained from **131g** (0.080 g, 0.26 mmol) and **7a** (0.089 g, 0.31 mmol) as a light brown solid (0.099 g, 77%). M.p.: 75 – 76 °C; R_f(10% MeOH/DCM), 0.30. ^{1}H NMR (400 MHz, Methanol-d_4) δ 8.03 (d, J = 8.1 Hz, 2H, H^{11}), 7.83 (d, J = 1.3 Hz, 1H, H^1), 7.54 (d, J = 7.8 Hz, 1H, H^3), 7.43 (dd, J = 7.8, 1.3 Hz, 1H, H^2), 7.35 (d, J = 8.1 Hz, 2H, H^{10}), 3.86 (tt, J = 10.9, 4.0 Hz, 1H, H^5), 3.52 (s, 3H, H^4), 3.20 – 3.12 (m, 2H, H^{7e}), 3.01 – 2.93 (m, 2H, H^8), 2.75 – 2.70 (m, 2H, H^9), 2.42 (s, 3H, H^{12}), 2.32 – 2.23 (m, 2H, H^{7a}), 2.14 – 2.09 (m, 2H, H^{6e}), 1.71 – 1.63 (m, 2H, H^{6a}). ^{13}C NMR (151 MHz, Methanol-d_4) δ 175.94, 160.08, 141.28, 141.10, 138.36, 134.05, 128.77 (2C), 127.86 (2C), 126.44, 119.06, 118.29, 116.11, 112.49, 59.67, 56.71, 52.28 (2C), 34.76, 32.90, 31.63 (2C), 16.88. LC-MS (APCI$^+$/ESI): found m/z = 495.2, 457.2 [M+H]$^+$ (cal. For $C_{24}H_{27}BrN_6O$, 494.14, 496.14). Purity: 98%, t_R = 2.285 min.

5,6-difluoro-1-methyl-N-(1-(4-(3-methyl-1,2,4-oxadiazol-5-yl) phenethyl) piperidin-4-yl)-1H-benzo[d]imidazol-2-amine (140)

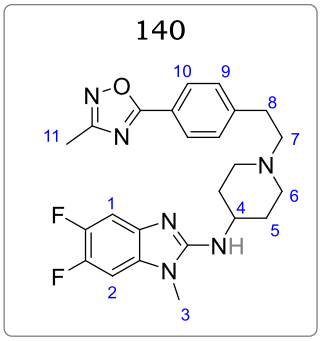

Obtained from **131h** (0.080 g, 0.30 mmol) and **7a** (0.103 g, 0.36 mmol) as a pale yellow solid (0.072 g, 53%). M.p.: 175 – 177 °C; R_f(10% MeOH/DCM), 0.38. ^{1}H NMR (400 MHz, Methanol-d_4) δ 7.99 (d, J = 8.0 Hz, 2H, H^{10}), 7.45 (dd, J = 7.4, 5.3 Hz, 1H, H^1), 7.36 (dd, J = 7.5, 5.5 Hz, 1H, H^2), 7.28 (d, J = 8.0 Hz, 2H, H^9), 3.85 (tt, J = 11.1, 4.2 Hz, 1H, H^4), 3.51 (s, 3H, H^3), 3.20 – 3.12 (m, 2H, H^{6e}), 2.97 – 2.91 (m, 2H, H^7), 2.75 – 2.69 (m, 2H, H^8), 2.41 (s, 3H, H^{11}), 2.35 – 2.28 (m, 2H, H^{6a}), 2.18 – 2.01 (m, 2H, H^{5e}), 1.73 – 1.65 (m, 2H, H^{5a}). ^{13}C NMR (151 MHz, Methanol-d_4) δ 176.22, 163.45, 144.04, 143.89, 141.92, 139.34, 138.04, 133.87, 128.75 (2C), 127.86 (2C), 119.29, 108.23, 107.93, 59.45, 56.51, 52.33 (2C), 34.98, 32.74, 31.77 (2C), 16.86. LC-MS (APCI$^+$/ESI): found m/z = 453.2 [M+H]$^+$ (cal. For $C_{24}H_{26}F_2N_6O$, 452.21). Purity: 99%, t_R = 2.223 min.

5,6-dichloro-1-methyl-N-(1-(4-(3-methyl-1,2,4-oxadiazol-5-yl) phenethyl) piperidin-4-yl)-1H-benzo[d]imidazol-2-amine (141)

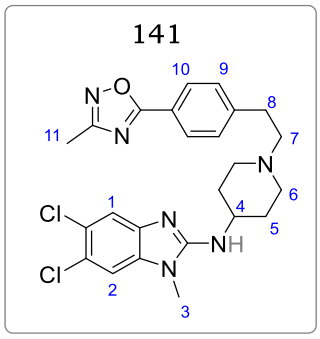

Obtained from **131i** (0.080 g, 0.27 mmol) and **7a** (0.089 g, 0.32 mmol) as a cream white solid (0.060 g, 46%). m.p.: 188 – 190 °C; R_f (10% MeOH/DCM), 0.39. ^{1}H NMR (400 MHz, Methanol-d_4) δ 8.19 (s, 1H, H^1), 8.15 (s, 1H, H^2), 8.04 (d, J = 8.1 Hz, 2H, H^{10}), 7.43 (d, J = 8.1 Hz, 2H, H^9), 3.86 (tt, J = 11.2, 4.4 Hz, 1H, H^4), 3.51 (s, 3H, H^3), 3.20 – 3.12 (m, 2H, H^{6e}), 2.97 – 2.90 (m, 2H, H^7), 2.75 – 2.69 (m, 2H, H^8), 2.41 (s, 3H, H^{11}), 2.35 – 2.29 (m, 2H, H^{6a}), 2.15 – 2.09 (m, 2H, H^{5e}), 1.71 – 1.64 (m, 2H, H^{5e}). ^{13}C NMR (151 MHz, Methanol-d_4) δ 175.45, 162.66, 141.86, 139.11, 137.87, 133.98, 130.03, 129.93, 128.83 (2C), 127.71 (2C), 119.22, 117.43, 116.99, 59.38, 56.44, 52.23 (2C), 34.90, 32.69, 31.62 (2C), 16.93. LC-MS (APCI$^+$/ESI): found m/z = 485.2, 487.2 [M+H]$^+$ (cal. for $C_{24}H_{26}Cl_2N_6O$, 484.15, 486.15). Purity: 99%, t_R = 2.400 min.

1,5,6-trimethyl-N-(1-(4-(3-methyl-1,2,4-oxadiazol-5-yl) phenethyl) piperidin-4-yl)-1H-benzo[d]imidazol-2-amine (139)

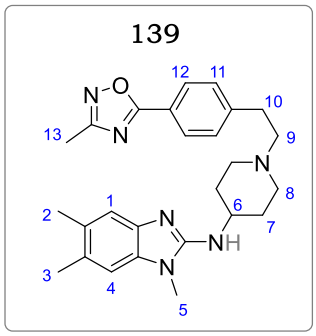

Obtained from **131j** (0.080 g, 0.31 mmol) and **7a** (0.108 g, 0.37 mmol) as a light brown solid (0.066 g, 48%). m.p.: 120 – 122 °C; R_f (10% MeOH/DCM), 0.33. ^{1}H NMR (400 MHz, Methanol-d_4) δ 8.01 (d, J = 7.8 Hz, 2H, H^{12}), 7.39 (s, 1H, H^1), 7.31 – 7.18 (m, 3H, H^{4,11}), 3.85 (tt, J = 11.0, 4.2 Hz, 1H, H^6), 3.51 (s, 3H, H^5), 3.19 – 3.12 (m, 2H, H^{8e}), 2.99 – 2.93 (m, 2H, H^9), 2.76 – 2.69 (m, 2H, H^{10}), 2.43 (s, 3H, H^{13}), 2.37 – 2.30 (m, 2H, H^{8a}), 2.25 (s, 3H, H^2), 2.19 (s, 3H, H^3), 2.06 – 1.92 (m, 2H, H^{7e}), 1.69 – 1.62 (m, 2H, H^{7a}). ^{13}C NMR (151 MHz, Methanol-d_4) δ 176.22, 162.48, 141.73, 139.19, 137.65, 133.83, 132.01, 129.27, 128.76 (2C), 127.88 (2C), 119.19, 116.21, 108.54, 59.44, 56.56, 52.29 (2C), 34.92, 32.73, 31.66 (2C), 19.86, 19.72, 16.80. LC-MS (APCI$^+$/ESI): found m/z = 445.3 [M+H]$^+$ (cal. for $C_{26}H_{32}N_6O$, 444.26). Purity: 98%, t_R = 2.301 min.

N-(1-(4-(3-(trifluoromethyl)-1,2,4-oxadiazol-5-yl)phenethyl)piperidin-4-yl)benzo[d]oxazol-2-amine (146)

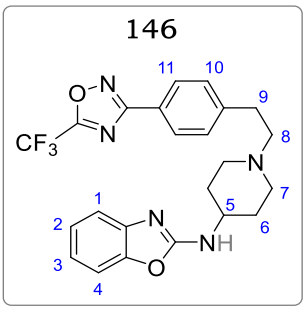

Obtained from **145a** (0.050 g, 0.23 mmol) and **3c** (0.089 g, 0.28 mmol) as a white solid (0.066 g, 63%). m.p.: 97 – 99 °C; R_f(10% MeOH/DCM), 0.42. ^{1}H NMR (400 MHz, Methanol-d_4) δ 8.04 (d, J = 7.8 Hz, 2H, H^{11}), 7.56 (dd, J = 8.1, 1.4 Hz, 1H, H^4), 7.33 – 7.18 (m, 3H, H^{1,10}), 6.95 (ddd, J = 7.8, 7.1, 1.1 Hz, 1H, H^3), 6.85 (ddd, J = 8.0, 7.1, 1.2, 1H, H^2), 3.95 (tt, J = 11.5, 4.2 Hz, 1H, H^5), 3.08 – 2.99 (m, 2H, H^{7e}), 2.96 – 2.87 (m, 2H, H^8), 2.73 – 2.64 (m, 2H, H^9), 2.40 – 2.29 (m, 2H, H^{7a}), 2.12 – 2.04 (m, 2H, H^{6e}), 1.68 – 1.55 (m, 2H, H^{6a}). ^{13}C NMR (101 MHz, Methanol-d_4) δ 174.23, 166.23, 155.24, 148.23, 137.54, 129.32 (2C), 127.95 (2C), 121.01, 119.25, 118.12 (q, J = 29.5 Hz), 111.23, 61.25, 51.24 (2C), 50.28, 43.65, 33.30, 30.85 (2C). LC-MS (APCI$^+$/ESI): found m/z = 458.2 [M+H] $^+$ (cal. For $C_{23}H_{22}F_3N_5O_2$, 457.17). Purity: 98%, t_R = 2.261 min.

***N*-(1-(4-(3-(trifluoromethyl)-1,2,4-oxadiazol-5-yl)phenethyl)piperidin-4-yl)-1H-imidazo[4,5-b]pyridin-2-amine (147)**

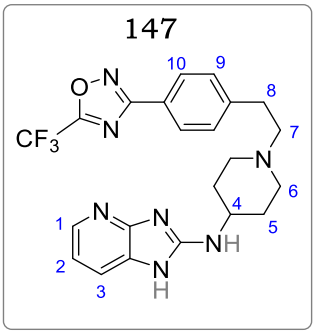

Obtained from **145b** (0.050 g, 0.23 mmol) and **3c** (0.089 g, 0.28 mmol) as a pale yellow solid (0.079 g, 75%). m.p.: 88 – 90 °C; R_f(10% MeOH/DCM), 0.22. ^{1}H NMR (400 MHz, Methanol-d_4) δ 8.33 (dd, J = 5.4, 1.4 Hz, 1H, H^1), 7.90 (d, J = 8.1 Hz, 2H, H^{10}), 7.45 – 7.32 (m, 3H, H^{3,9}), 7.19 (dd, J = 7.8, 5.4 Hz, 1H, H^2), 3.96 (tt, J = 10.2, 4.0 Hz, 1H, H^4), 3.12 – 3.01 (m, 2H, H^{6e}), 2.95 – 2.86 (m, 2H, H^7), 2.73 – 2.66 (m, 2H, H^8), 2.38 – 2.27 (m, 2H, H^{6a}), 2.10 – 2.01 (m, 2H, H^{5e}), 1.69 – 1.58 (m, 2H, H^{4a}). ^{13}C NMR (101 MHz, Methanol-d_4) δ 171.15, 158.65, 152.24, 148.89, 140.53, 138.65, 130.25 (2C), 128.33 (2C), 124.58, 122.30, 118.69, 116.58 (q, J = 32.9 Hz), 60.32, 51.62, 49.58 (2C), 34.55, 31.57 (2C). LC-MS (APCI$^+$/ESI): found m/z = 458.2 [M+H] $^+$ (cal. for $C_{22}H_{22}F_3N_7O$, 457.18). Purity: 98%, t_R = 2.106 min.

5-methyl-*N*-(1-(4-(3-(trifluoromethyl)-1,2,4-oxadiazol-5-yl)phenethyl)piperidin-4-yl)-1H-imidazo[4,5-b]pyridin-2-amine (148)

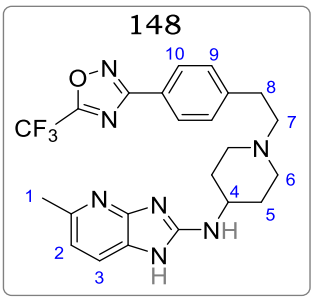

Obtained from **145c** (0.100 g, 0.43 mmol) and **3c** (0.166 g, 0.52 mmol) as a pale-yellow solid (0.158 g, 78%). m.p.: 105 – 107 °C; R_f(10% MeOH/DCM), 0.32. ^{1}H NMR (400 MHz, Methanol-d_4) δ 7.95 (d, J = 8.2 Hz, 2H, H^{10}), 7.61 (d, J = 8.3 Hz, 1H, H^3), 7.38 (d, J = 8.2 Hz, 2H, H^9), 6.86 (d, J = 8.3 Hz, 1H, H^2), 3.98 (tt, J = 10.2, 4.0 Hz, 1H, H^4), 3.13 – 3.08 (m, 2H, H^{6e}), 3.01 – 2.91 (m, 2H, H^7), 2.79 – 2.67 (m, 2H, H^8), 2.45 – 2.31 (m, 2H, H^{6a}), 2.18 – 2.08 (m, 2H, H^{5e}), 1.99 (s, 3H, H^1), 1.69 – 1.58 (m, 2H, H^{5a}). ^{13}C NMR (101 MHz, Methanol-d_4) δ 172.23, 165.23, 155.32, 145.30, 136.95, 130.01 (2C), 128.32 (2C), 121.88, 119.52, 118.52 (q, J = 29.3 Hz), 111.02, 61.32, 51.25 (2C), 50.20, 43.65, 34.08, 31.29 (2C), 24.19. LC-MS (APCI$^+$/ESI): found m/z = 472.2 [M+H] $^+$ (cal. For $C_{23}H_{24}F_3N_7O$, 471.20). Purity: 98%, t_R = 2.324 min.

***N*-(1-(4-(3-(trifluoromethyl)-1,2,4-oxadiazol-5-yl)phenethyl)piperidin-4-yl)-1H-imidazo[4,5-c]pyridin-2-amine (149)**

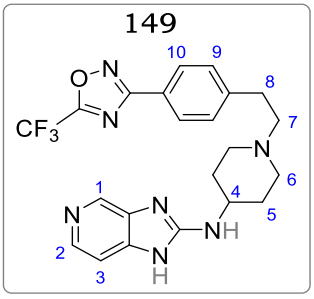

Obtained from **145d** (0.100 g, 0.46 mmol) and **3c** (0.178 g, 0.55 mmol) as a pale-yellow solid (0.158 g, 75%). m.p.: 145 – 147 °C; R_f(10% MeOH/DCM), 0.23. ^{1}H NMR (600 MHz, Methanol-d_4) δ 8.44 (d, J = 0.8 Hz, 1H, H^1), 8.23 – 8.14 (m, 3H, H^{2,10}), 7.61 (d, J = 7.9 Hz, 2H, H^9), 7.52 (d, J = 6.3 Hz, 1H, H^3), 4.07 (tt, J = 10.3, 4.4 Hz, 1H, H^4), 3.66 – 3.50 (m, 2H, H^{6e}), 3.34 – 3.26 (m, 2H, H^7), 3.22 – 3.17 (m, 2H, H^8), 3.09 (td, J = 13.3, 3.2 Hz, 2H, H^{6a}), 2.35 – 2.27 (m, 2H, H^{5e}), 1.97 (dtd, J = 13.2, 10.8, 3.9 Hz, 2H, H^{5a}). ^{13}C NMR (101 MHz, Methanol-d_4) δ 179.32, 166.53, 148.5, 147.50, 140.58, 138.96, 137.56, 133.56, 129.39 (2C), 127.45 (2C), 123.56, 116.08 (q, J = 28.5 Hz), 111.32, 62.98, 52.89, 49.32 (2C), 33.58, 32.08 (2C). LC-MS (APCI$^+$/ESI): found m/z = 458.2 [M+H] $^+$ (cal. for $C_{22}H_{22}F_3N_7O$, 457.18). Purity: 98%, t_R = 2.196 min.

6-chloro-*N*-(1-(4-(3-(trifluoromethyl)-1,2,4-oxadiazol-5-yl)phenethyl)piperidin-4-yl)-1H-imidazo[4,5-c]pyridin-2-amine (150)

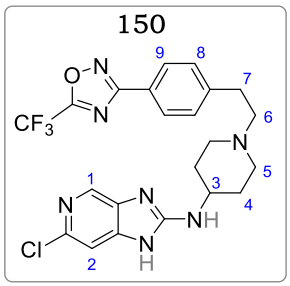

Obtained from **145e** (0.100 g, 0.40 mmol) and **3c** (0.152 g, 0.47 mmol) as a pale-yellow solid (0.155 g, 79%). m.p.: 113 – 114 °C; R_f (10% MeOH/DCM), 0.33. ^{1}H NMR (600 MHz, Methanol-d_4) δ 8.51 (s, 1H, H^1), 8.06 (d, J = 7.9 Hz, 2H, H^9), 7.48 (d, J = 7.9 Hz, 2H, H^8), 7.29 (s, 1H, H^2), 4.02 (tt, J = 11.0, 4.2 Hz, 1H, H^3), 3.55 (dt, J = 12.8, 3.9 Hz, 2H, H^{5e}), 3.33 – 3.27 (m, 2H, H^6), 3.20 – 3.13 (m, 2H, H^7), 3.05 (td, J = 12.5, 4.0 Hz, 2H, H^{5a}), 2.31 – 2.23 (m, 2H, H^{4e}), 1.92 (dtd, J = 14.0, 11.9, 4.1 Hz, 2H, H^{4a}). ^{13}C NMR (101 MHz, Methanol-d_4) δ 177.23, 167.23, 162.35, 147.56, 139.56, 138.85, 137.33, 132.41, 129.09 (2C), 128.02 (2C), 122.30, 115.95 (q, J = 29.6 Hz), 110.25, 63.25, 51.62, 50.25 (2C), 34.65, 31.24 (2C). LC-MS (APCI$^+$/ESI): found m/z = 492.1 [M+H] $^+$ (cal. For $C_{22}H_{21}ClF_3N_7O$, 491.14). Purity: 98%, t_R = 2.454 min.

***N*-(3-fluoro-1-(4-(3-(trifluoromethyl)-1,2,4-oxadiazol-5-yl)phenethyl)piperidin-4-yl)-1H-benzo[d]imidazol-2-amine (151)**

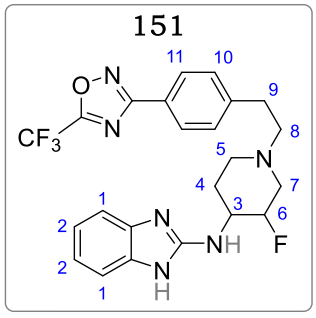

Obtained from **145f** (0.200 g, 0.85 mmol) and **3c** (0.329 g, 1.03 mmol) as a pale yellow solid (0.286 g, 71%). m.p.: 84 – 86 ˚C; R_f (10% MeOH/DCM) 0.45. ^{1}H NMR (600 MHz, Methanol-d_4) δ 8.03 (d, J = 7.8 Hz, 2H, H^{11}), 7.44 (d, J = 7.8 Hz, 2H, H^{10}), 7.21 (dd, J = 6.2, 3.1 Hz, 2H, H^1), 6.99 (dd, J = 6.2, 3.1 Hz, 2H, H^2), 4.49 (dtd, J = 49.6, 9.1, 4.5 Hz, 1H, H^6), 3.83 (qd, J = 10.3, 4.7 Hz, 1H, H^3), 3.30 – 3.22 (m, 1H, H^{7e}), 3.00 – 2.85 (m, 3H, H^{5e,8}), 2.79 – 2.69 (m, 2H, H^9), 2.39 – 2.26 (m, 2H, H^{5a,7a}), 2.19 (dt, J = 14.3, 4.4 Hz, 1H, H^{4e}), 1.61 (dtd, J = 11.6, 9.2, 3.9 Hz, 1H, H^{4a}). ^{13}C NMR (101 MHz, Methanol-d_4) δ ^{13}C NMR (101 MHz, Methanol-d_4) δ 169.10, 154.51, 145.13, 136.93, 129.39 (2C), 127.37 (2C), 122.80 (2C), 120.25 (2C), 111.38 (q, J = 28.5 Hz), 91.08, 89.31, 58.73, 55.70 (d, J = 19.5 Hz), 54.28 (d, J = 36.3), 51.05, 32.82, 29.57. LC-MS (APCI$^+$/ESI): found m/z = 475.2 [M+H]$^+$ (cal. for $C_{23}H_{22}F_4N_6O$, 474.18). Purity: 99%, t_R = 2.597 min.

_N_-(3,3-difluoro-1-(4-(3-(trifluoromethyl)-1,2,4-oxadiazol-5-yl) phenethyl) piperidin-4-yl)-1H-benzo[d]imidazol-2-amine (152)

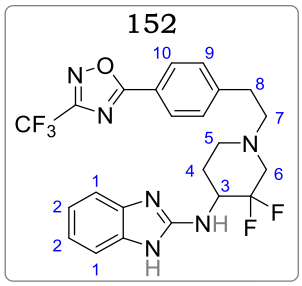

Obtained from **145g** (0.050 g, 0.20 mmol) and **3c** (0.076 g, 0.24 mmol) as a yellow solid (0.042 g, 43%). m.p.: 87 – 89 °C; R_f (10% MeOH/DCM) 0.46. ^{1}H NMR (400 MHz, Methanol-d_4) δ 7.95 (d, J = 8.1 Hz, 2H, H^{10}), 7.52 (d, J = 8.1 Hz, 2H, H^{9}), 7.26 (dd, J = 6.0, 2.9 Hz, 2H, H^{1}), 6.92 (dd, J = 6.0, 2.9 Hz, 2H, H^{2}), 4.08 (m, 1H, H^{3}), 3.35 – 3.23 (m, 1H, H^{6e}), 3.05 – 2.85 (m, 3H, H^{5e,7}), 2.80 – 2.69 (m, 2H, H^{8}), 2.37 – 2.24 (m, 2H, H^{5a,6a}), 2.19 (td, J = 13.5, 3.9 Hz, 1H, H^{4e}), 1.61 (dtd, J = 12.0, 9.3, 4.0 Hz, 1H, H^{4a}). ^{13}C NMR (101 MHz, Methanol-d_4) δ ^{13}C NMR (101 MHz, Methanol-d_4) δ 171.23, 155.23, 146.32, 135.62, 129.85 (2C), 128.05 (2C), 123.56, 123.01, 121.53 (2C), 119.65 (2C), 113.53 (q, J = 29.0 Hz), 96.32, 88.56, 59.08, 56.32 (t, J = 23.2 Hz), 53.21 (t, J = 28.3), 50.32, 33.32, 28.95. LC-MS (APCI$^+$/ESI): found m/z = 493.2 [M+H]$^+$ (cal. For $C_{23}H_{21}F_5N_6O$, 492.17). Purity: 99%, t_R = 2.499 min.

4-(2-(4-((1H-benzo[d]imidazol-2-yl)amino)piperidin-1-yl)acetyl)benzonitrile (158)

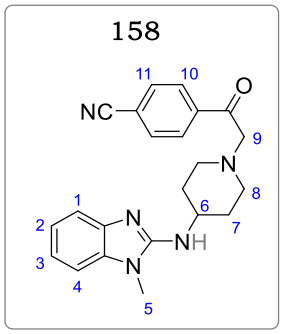

Obtained from **14b** (0.300 g, 1.30 mmol) and 4-(2-bromoacetyl)benzonitrile (0.350 g, 1.57 mmol) as a yellow solid (0.358 g, 74%); R_f (10% MeOH/DCM) 0.38. ^{1}H NMR (300 MHz, Methanol-d_4) δ 7.39 (d, J = 7.9 Hz, 2H, H^{11}), 7.22 (d, J = 7.9 Hz, 2H, H^{10}), 7.02 (dd, J = 8.0, 1.1 Hz, 1H, H^{1}), 6.89 (dd, J = 7.7, 1.5 Hz, 1H, H^{4}), 6.81 – 6.69 (m, 2H, H^{2,3}), 3.91 (tt, J = 11.0, 4.1 Hz, 1H, H^{6}), 3.42 (s, 3H, H^{5}), 2.66 (s, 2H, H^{9}), 2.48 – 2.32 (m, 2H, H^{8e}), 2.06 (td, J = 13.1, 3.0 Hz, 1H, H^{8a}), 1.96 – 1.85 (m, 2H, H^{7e}), 1.49 (dtd, J = 14.1, 11.0, 3.0 Hz, 2H, H^{7a}). ^{13}C NMR (101 MHz, Methanol-d_4) δ 185.32, 154.22, 145.32, 138.65, 132.32 (2C), 131.24, 128.57 (2C), 123.65, 122.35, 119.32, 117.25, 112.29, 110.95, 55.58, 53.39, 50.25 (2C), 33.59 (2C), 29.50. LC-MS (APCI$^+$/ESI): found m/z = 374.2 [M+H] $^+$ (cal. for $C_{22}H_{23}N_5O$, 373.19). Purity: 99%, t_R= 2.123 min.

4-(1-hydroxy-2-(4-((1-methyl-1H-benzo[d]imidazol-2-yl)amino)piperidin-1-yl) ethyl) benzonitrile (159)

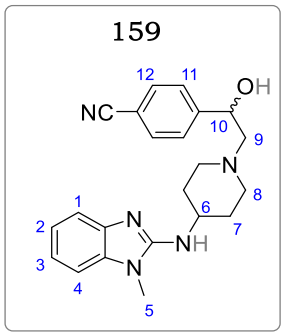

Following general procedure 5, obtained from **158** (0.320 g, 0.86 mmol) as a yellow solid (0.321 g, 93%); R_f (10% MeOH/DCM) 0.29. ^{1}H NMR (300 MHz, Methanol-d_4) δ 7.79 (d, J = 8.0 Hz, 2H, H^{12}), 7.60 (d, J = 8.0 Hz, 2H, H^{11}), 7.36 (dd, J = 7.8, 1.3 Hz, 1H, H^1), 6.95 (dd, J = 8.1, 1.2 Hz, 1H, H^4), 6.78 – 6.61 (m, 2H, H^{2,3}), 4.83 (t, J = 6.5 Hz, 1H, H^{10}), 3.91 (tt, J = 10.5, 3.9 Hz, 1H, H^6), 3.41 (s, 3H, H^5), 2.65 – 2.52 (m, 2H, H^{8e}), 2.41 (d, J = 6.5 Hz, 2H, H^9), 2.09 (td, J = 12.9, 4.1 Hz, 1H, H^{8a}), 1.95 – 1.83 (m, 2H, H^{7e}), 1.50 (m, 2H, H^{7a}). ^{13}C NMR (101 MHz, Methanol-d_4) δ 153.24, 143.20, 139.55, 133.78 (2C), 130.65, 129.54 (2C), 124.08, 123.25, 119.85, 116.32, 112.99, 110.21, 69.33, 54.52, 52.32, 50.45 (2C), 34.52 (2C), 28.01. LC-MS (APCI$^+$/ESI): found m/z = 376.2 [M+H] $^+$ (cal. for $C_{22}H_{25}N_5O$, 375.21). Purity: 98%, t_R= 2.352 min.

4-(1-fluoro-2-(4-((1-methyl-1H-benzo[d]imidazol-2-yl)amino)piperidin-1-yl) ethyl) benzonitrile (160)

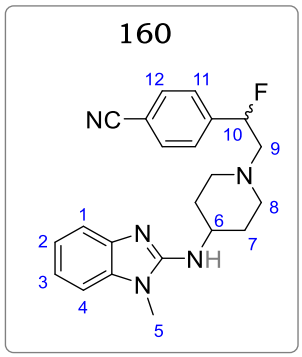

To a stirring solution of **159** (0.300 g, 0.80 mmol) in dry DCM (10 ml) at -70 °C, diethylaminosulfur trifluoride, DAST (117 µl, 0.88 mmol) was added dropwise. The resulting mixture was then stirred at that temperature for 2 hr. Upon completion the temperature was allowed to reach 0 °C, after which the reaction was quenched by adding 10% $NaHCO_3$ (5 ml). The mixture was extracted with DCM (3 × 20 ml), and combined organic phase washed with brine and dried over anhydrous Na_2SO_4. Removal of solvent followed by purification *via* flash column chromatography afforded the product as a yellow solid (0.289 g, 96%); R_f (10% MeOH/DCM) 0.45. ^{1}H NMR (400 MHz, Methanol-d_4) δ 7.79 (d, J = 8.1 Hz, 2H, H^{12}), 7.43 (d, J = 8.1 Hz, 2H, H^{11}), 7.10 (dd, J = 8.0, 1.3 Hz, 1H, H^1), 6.95 (dd, J = 7.7, 1.3 Hz, 1H, H^4), 6.83 – 6.70 (m, 2H, H^{2,3}), 5.43 (dt, J = 45.2, 6.5 Hz, 1H, H^{10}), 3.92 (tt, J = 10.5, 4.1 Hz, 1H, H^6), 3.38 (s, 3H, H^5), 2.95 – 2.83 (m, 2H, H^{8e}), 2.79 – 2.68 (m, 2H, H^9), 2.33 – 2.21 (m, 2H, H^{8a}), 1.98 – 1.86 (m, 2H, H^{7e}), 1.49 (dtd, J = 13.0, 10.5, 4.1 Hz, 2H, H^{7a}). ^{13}C NMR (101 MHz, Methanol-d_4) δ 153.25, 144.25, 140.25, 134.85 (2C), 130.25 (2C), 128.20, 121.45, 120.08, 117.98, 114.62, 110.25, 106.32, 98.25

(d, J = 19.2 Hz), 53.25 (2C), 49.65, 33.25, 30.30 (2C), 28.25. LC-MS (APCI$^+$/ESI): found m/z = 378.2 [M+H] $^+$ (cal. for $C_{22}H_{24}FN_5$, 377.20). Purity: 99%, t_R= 2.415.

N-(1-(2-fluoro-2-(4-(5-(trifluoromethyl)-1,2,4-oxadiazol-3-yl) phenyl) ethyl) piperidin-4-yl)-1-methyl-1H-benzo[d]imidazol-2-amine (161)

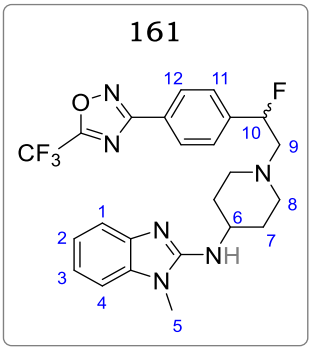

Following general procedure 2, followed by cyclocondensation as in **3c**, obtained from **160** (0.200 g, 0.53 mmol) as a yellow solid (0.139 g, 54%); m.p.: 103 – 104 °C; R_f (10% MeOH/DCM) 0.50. ^{1}H NMR (400 MHz, Methanol-d_4) δ 7.81 (d, J = 8.0 Hz, 2H, H^{12}), 7.45 (d, J = 8.0 Hz, 2H, H^{11}), 7.08 (dd, J = 8.0, 1.3 Hz, 1H, H^1), 6.92 (dd, J = 7.8, 1.3 Hz, 1H, H^4), 6.80 – 6.68 (m, 2H, H^{2,3}), 5.42 (dt, J = 49.5, 6.8 Hz, 1H, H^{10}), 3.95 (tt, J = 10.2, 4.0 Hz, 1H, H^6), 3.51 (s, 3H, H^5), 3.02 – 2.89 (m, 2H, H^{8e}), 2.82 – 2.69 (m, 2H, H^9), 2.27 (td, J = 12.0, 3.1 Hz, 2H, H^{8a}), 2.02 – 1.91 (m, 2H, H^{7e}), 1.60 – 1.48 (m, 2H, H^{7a}). ^{13}C NMR (101 MHz, Methanol-d_4) δ 168.52, 162.52, 147.37, 143.21, 139.45, 133.20 (2C), 129.58 (2C), 127.62, 121.54, 120.31, 119.07, 113.55, 110.86, 106.80, 93.85 (d, J = 19.2 Hz), 52.32 (2C), 48.25, 33.45, 29.56 (2C), 27.41. LC-MS (APCI$^+$/ESI): found m/z = 489.2 [M+H] $^+$ (cal. for $C_{24}H_{24}F_4N_6O$, 488.19). Purity: 99%, t_R= 2.498 min.

6-(2-(4-((1-methyl-1H-benzo[d]imidazol-2-yl) amino) piperidin-1-yl) ethyl) nicotinonitrile (154)

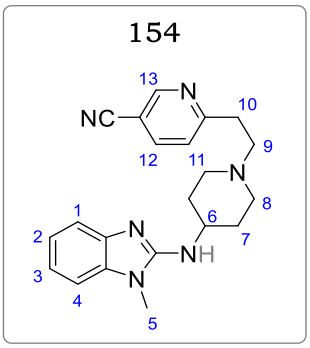

A mixture of **14b** (0.150 g, 0.65 mmol) and **153** (0.089 g, 0.68 mmol) in 10 ml MeCN was purged and degassed with N_2 for 15 minutes. Zinc chloride, $ZnCl_2$ (0.003 g, 2.5 mol%) was then added, the resulting reaction mixture sealed off and stirred at 50 °C for 4 hr. After completion, the solvent was taken off *in vacuo*, and water (5 ml) was added to the residue. The mixture was extracted with EtOAc (3 × 15 ml), combined organic extracts washed with brine, and dried over anhydrous Na_2SO_4. Following column chromatography, the product was isolated as a pale yellow solid (0.142 g, 61%). R_f (10% MeOH/DCM), 0.25. ^{1}H NMR (300 MHz, Methanol-d_4) δ 8.67 (d, J = 0.9 Hz, 1H, H^{13}), 8.11 (dd, J = 8.1, 0.9 Hz, 1H, H^{12}), 7.59 – 7.40 (m, 2H, H^{1,11}), 7.26 (dd, J = 7.8, 1.3 Hz, 1H, H^4), 6.98 (ddd, J = 8.0, 6.9, 1.2 Hz, 1H, H^2), 6.82 (ddd, J = 7.8, 6.9, 1.2 Hz, 1H, H^3), 3.91 (tt, J = 10.4, 4.1 Hz, 1H, H^6), 3.52 (s, 3H, H^5), 3.19 – 3.08 (m, 2H, H^{8e}), 2.95 – 2.84 (m, 2H, H^9), 2.73 – 2.57 (m, 4H, H^{8a,10}), 2.09 – 1.87 (m, 2H, H^{7e}), 1.69 – 1.55

(m, 2H, H^{7a}). ^{13}C NMR (151 MHz, Methanol-d_4) δ 170.54, 151.32, 145.20, 142.84, 139.25, 133.62, 124.54, 123.99, 123.21, 116.98, 114.25, 109.32, 105.65, 56.35, 49.55, 49.01 (2C), 33.54, 31.54 (2C), 28.79. LC-MS (APCI$^+$/ESI): found m/z = 361.2 $[M+H]^+$ (cal. for $C_{21}H_{24}N_6$, 360.21). Purity: 96%, t_R = 2.301 min.

6-(2-(4-((1H-benzo[d]imidazol-2-yl) amino)-3-fluoropiperidin-1-yl) ethyl) nicotinonitrile (155)

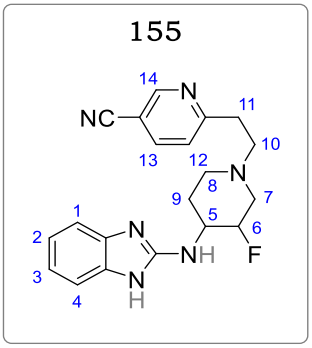

Following the procedure for **154**, obtained from **145g** (0.150 g, 0.64 mmol) and **153** (0.088 g, 0.67 mmol) as a yellow solid (0.079 g, 34%). R_f (10% MeOH/DCM) 0.31. ^{1}H NMR (400 MHz, Methanol-d_4) δ 8.55 (d, J = 1.0 Hz, 1H, H^{14}), 8.20 (dd, J = 8.1, 1.0 Hz, 1H, H^{13}), 8.03 (d, J = 8.1 Hz, 1H, H^{12}), 7.26 – 7.22 (m, 2H^{1,4}), 6.98 – 6.93 (m, 2H^{2,3}), 4.51 (dtd, J = 48.5, 9.5, 4.1 Hz, 1H, H^6), 3.89 (qd, J = 10.8, 4.4 Hz, 1H, H^5), 3.23 – 3.12 (m, 1H, H^{7e}), 2.96 – 2.84 (m, 3H, H^{8e,10}), 2.77 – 2.65 (m, 2H, H^{11}), 2.34 – 2.20 (m, 2H, H^{7a,8a}), 2.11 (dt, J = 13.1, 4.2 Hz, 1H, H^{9e}), 1.59 (dtd, J = 12.0, 9.3, 4.2 Hz, 1H, H^{9a}). ^{13}C NMR (101 MHz, Methanol-d_4) δ ^{13}C NMR (101 MHz, Methanol-d_4) δ 160.09, 152.58, 149.28, 139.66, 135.47, 128.45, 123.78 (2C), 123.07, 118.65, 112.97 (2C), 110.32, 109.74, 88.57, 53.21, 50.87, 35.86, 33.97, 30.57. LC-MS (APCI$^+$/ESI): found m/z = 365.2 $[M+H]^+$ (cal. for $C_{20}H_{21}FN_6$, 364.18). Purity: 99%, t_R = 2.298 min.

1-methyl-N-(1-(2-(5-(5-(trifluoromethyl)-1,2,4-oxadiazol-3-yl)pyridin-2-yl)ethyl) piperidin-4-yl)-1H-benzo[d]imidazol-2-amine (156)

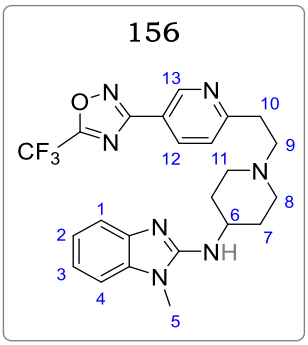

Following general procedure 2, followed by cyclocondensation as in **3c**, obtained from **154** (0.120 g, 0.33 mmol) as a pale yellow solid (0.075 g, 48%). m.p.: 131 – 133 °C; R_f (10% MeOH/DCM), 0.14. ^{1}H NMR (400 MHz, Methanol-d_4) δ 8.52 (d, J = 1.1 Hz, 1H, H^{13}), 8.11 (dd, J = 8.0, 1.1 Hz, 1H, H^{12}), 7.61 – 7.45 (m, 2H, H^{1,11}), 7.29 (dd, J = 8.0, 1.2 Hz, 1H, H^4), 7.01 (ddd, J = 7.8, 6.5, 1.1 Hz, 1H, H^2), 6.80 (ddd, J = 8.0, 6.5, 1.2 Hz, 1H, H^3), 3.95 (tt, J = 11.0, 4.2 Hz, 1H, H^6), 3.51 (s, 3H, H^5), 3.12 (td, J = 12.2, 4.1 Hz, 2H, H^{8e}), 2.92 – 2.81 (m, 2H, H^9), 2.73 – 2.58 (m, 4H, H^{8a,10}), 2.12 – 1.90 (m, 2H, H^{7e}), 1.67 – 1.52 (m, 2H, H^{7a}). ^{13}C NMR (151 MHz, Methanol-d_4) δ 173.87, 169.54, 152.24, 149.25, 144.52, 141.56, 139.65, 134.65, 124.98, 123.54, 123.04, 116.51 (q, J = 28.9 Hz), 113.25, 108.98, 105.65, 58.62, 49.97, 49.06 (2C), 33.68, 30.85

(2C), 28.10. LC-MS (APCI$^+$/ESI): found m/z = 472.2 $[M+H]^+$ (cal. for $C_{23}H_{24}F_3N_7O$, 471.20). Purity: 98%, t_R = 2.019 min.

N-(3-fluoro-1-(2-(5-(5-(trifluoromethyl)-1,2,4-oxadiazol-3-yl)pyridin-2-yl) ethyl) piperidin-4-yl)-1H-benzo[d]imidazol-2-amine (157)

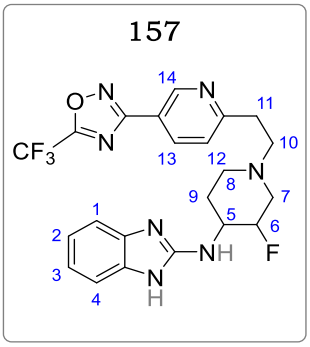

Following general procedure 2, followed by cyclocondensation as in **3c**, obtained from **155** (0.060 g, 0.16 mmol) as a pale yellow solid (0.038 g, 48%). m.p.: 109 – 111 °C; R_f (10% MeOH/DCM) 0.43. ^{1}H NMR (400 MHz, Methanol-d_4) δ 8.43 (d, J = 0.9 Hz, 1H, H^{14}), 8.22 (dd, J = 7.9, 0.9 Hz, 1H, H^{13}), 7.60 – 7.45 (m, 3H, $H^{1,4,12}$), 6.98 (dd, J = 6.1, 3.2 Hz, 2H, $H^{2,3}$), 4.51 (dtd, J = 47.8, 10.2, 3.9 Hz, 1H, H^6), 3.85 (qd, J = 11.2, 4.5 Hz, 1H, H^5), 3.28 – 3.19 (m, 1H, H^{7e}), 2.98 – 2.83 (m, 3H, $H^{8e,10}$), 2.76 – 2.65 (m, 2H, H^{11}), 2.33 – 2.19 (m, 2H, $H^{7a,8a}$), 2.15 (dt, J = 13.9, 4.0 Hz, 1H, H^{9e}), 1.59 (dtd, J = 13.2, 9.0, 4.0 Hz, 1H, H^{9a}). ^{13}C NMR (101 MHz, Methanol-d_4) δ ^{13}C NMR (101 MHz, Methanol-d_4) δ 167.96, 152.56, 144.36, 138.87, 129.39 (2C), 128.59 (2C), 124.65 (2C), 119.63 (2C), 112.34 (q, J = 28.5 Hz), 89.32, 87.98, 60.58, 56.95 (d, J = 19.5 Hz), 55.63 (d, J = 36.3), 50.82, 32.66, 28.65. LC-MS (APCI$^+$/ESI): found m/z = 476.2 $[M+H]^+$ (cal. for $C_{22}H_{21}F_4N_7O$, 475.17). Purity: 99%, t_R = 2.157 min.

1-methyl-2-((1-(4-(3-methyl-1,2,4-oxadiazol-5-yl) phenethyl) piperidin-4-yl) amino)-1H-benzo[d]imidazole-5-carboxylic acid (142)

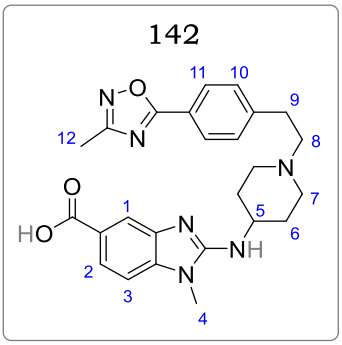

To a solution of **136** (0.200 g, 0.42 mmol) in 10 ml methanol, 2M aqueous KOH (1.1 ml, 2.1 mmol) was added, and the resulting mixture stirred at 79 °C for 2 hr. Following completion, the reaction mixture was cooled to 0 °C, and acidified to pH 2 while stirring. The product was filtered and obtained after recrystallization in methanol and drying, as an off white solid (0.181 g, 94%). m.p.: 134 – 136 °C; R_f (10% MeOH/DCM), 0.08. ^{1}H NMR (400 MHz, Methanol-d_4) δ 8.11 (d, J = 1.3 Hz, 1H, H^1), 8.01 (d, J = 8.0 Hz, 2H, H^{11}), 7.89 (dd, J = 7.8, 1.3 Hz, 1H, H^2), 7.58 (d, J = 7.8 Hz, 1H, H^3), 7.36 (d, J = 8.0 Hz, 2H, H^{10}), 3.87 (tt, J = 10.7, 4.0 Hz, 1H, H^5), 3.52 (s, 3H, H^4), 3.20 – 3.12 (m, 2H, H^{7e}), 2.97 – 2.90 (m, 2H, H^8), 2.78 – 2.69 (m, 2H, H^9), 2.44 (s, 3H, H^{12}), 2.36 – 2.27 (m, 2H, H^{7a}), 2.18 – 2.09 (m, 2H, H^{6e}), 1.71 – 1.64 (m, 2H, H^{6a}). ^{13}C NMR (151 MHz, Methanol-d_4) δ 175.87, 167.22, 161.89, 141.49, 139.19,

137.77, 133.78, 128.44 (2C), 127.10 (2C), 125.86, 124.13, 119.45, 116.48, 112.58, 56.98, 52.88 (2C), 52.29, 34.69, 33.01, 31.65 (2C), 16.98. LC-MS (APCI$^+$/ESI): found m/z = 461.2 $[M+H]^+$ (cal. for $C_{25}H_{28}N_6O_3$, 460.22). Purity: 96%, t_R = 0.135 min.

N-cyclopropyl-1-methyl-2-((1-(4-(3-methyl-1,2,4-oxadiazol-5-yl) phenethyl) piperidin-4-yl) amino)-1H-benzo[d]imidazole-5-carboxamide (143)

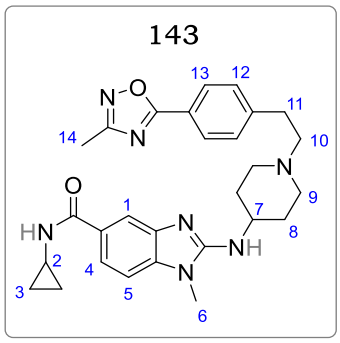

Following general procedure 2, obtained from **142** (0.080 g, 0.17 mmol) and cyclopropylamine (0.012 g, 0.21 mmol) as a white solid (0.045 g, 81%). m.p.: 85 – 87 °C; R_f (10% MeOH/DCM), 0.12. ^{1}H NMR (400 MHz, Methanol-d_4) δ 8.10 (d, J = 1.3 Hz, 1H, H^1), 7.99 (d, J = 8.0 Hz, 2H, H^{13}), 7.87 (dd, J = 7.7, 1.3 Hz, 1H, H^4), 7.58 (d, J = 7.7 Hz, 1H, H^5), 7.36 (d, J = 8.0 Hz, 2H, H^{12}), 3.86 (tt, J = 10.7, 4.0 Hz, 1H, H^7), 3.51 (s, 3H, H^6), 3.37 (tt, 9.1, 7.8 Hz, 1H, H^2), 3.20 – 3.11 (m, 2H, H^{9e}), 2.97 – 2.89 (m, 2H, H^{10}), 2.78 – 2.68 (m, 2H, H^1), 2.43 (s, 3H, H^{14}), 2.35 – 2.27 (m, 2H, H^{9a}), 2.17 – 2.09 (m, 2H, H^{8e}), 1.71 – 1.64 (m, 2H, H^{8a}), 1.22 – 1.16 (br-d, 4H, H^3). ^{13}C NMR (151 MHz, Methanol-d_4) δ 175.55, 167.22, 159.98, 141.58, 139.22, 137.64, 133.63, 128.28 (2C), 127.04 (2C), 125.65, 124.08, 119.33, 116.56, 112.59, 57.02, 52.75 (2C), 52.33, 34.73, 33.05, 31.44 (2C), 26.77, 16.56, 8.08 (2C). LC-MS (APCI$^+$/ESI): found m/z = 500.2 $[M+H]^+$ (cal. for $C_{28}H_{33}N_7O_2$, 499.27). Purity: 95%, t_R = 0.159 min.

General Procedure 16: S_N2 reaction using mesylates

A solution of an appropriate alcohol (1.2 equiv) and TEA (3.0 equiv) in 5 ml anhydrous DCM was cooled to 0 °C, after which mesyl chloride, MsCl (1.0 or 2.0 eq) in 2 ml DCM was added and the reaction mixture stirred at that temperature for 30 min. Amine **14d** (1.0 equiv) and TEA (1.0 equiv) in 4 ml anhydrous DCM was added to the cold mesylate reaction mixture, and the resulting solution stirred at room temperature (23 °C) for 4 hr. At completion, reaction mixture was cooled and diluted with 10 ml DCM, washed with saturated $NaHCO_3$ (3 × 10 ml), followed by brine, and dried over anhydrous Na_2SO_4. Products isolated after purification *via* by column chromatography using 4 – 7% MeOH/DCM as the eluent.

4-((2-((1-(2-(4-(methylsulfonyl)piperazin-1-yl)ethyl)piperidin-4-yl)amino)-1H-benzo[d]imidazol-1-yl)methyl)benzonitrile (53)

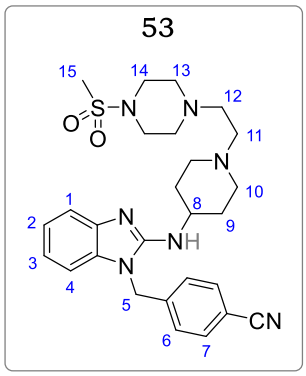

Obtained from **14d** (0.080 g, 0.24 mmol), 2-(piperazinyl)ethanol (0.038 g, 0.29 mmol) and MsCl (44.9 µl, 0.58 mmol) as a yellow crystalline solid (0.081 g, 65%). m.p.: 164 – 167 °C; R_f (10% MeOH/DCM) 0.22. ^{1}H NMR (400 MHz, Methanol-d_4) δ 7.69 (d, J = 8.5 Hz, 2H, H^7), 7.41 (dd, J = 7.8, 0.9 Hz, 1H, H^1), 7.30 (d, J = 8.5 Hz, 2H, H^6), 7.16 (ddd, J = 7.8, 7.2, 1.5 Hz, 1H, H^2), 7.12 (dd, J = 8.0, 1.4 Hz, 1H, H^4), 7.08 (ddd, 8.0, 7.2, 1.3 Hz, 1H, H^3), 5.46 (s, 2H, H^5), 4.03 (tt, J = 10.7, 4.0 Hz, 1H, H^8), 3.64 (m, 2H, H^{14e}), 3.45 – 3.31 (m, 6H, H^{11,12,14a}), 3.24 – 3.18 (m, 2H, H^{13e}), 2.86 (s, 3H, H^{15}), 2.82 – 2.77 (m, 2H, H^{10e}), 2.66 – 2.48 (m, 4H, H^{10a,13a}), 2.32 – 2.27 (m, 2H, H^{9e}), 2.06 – 1.93 (m, 2H, H^{9a}). ^{13}C NMR (101 MHz, Methanol-d_4) δ 147.22, 135.54, 132.98 (2C), 128.54 (2C), 121.32, 119.09, 117.78, 115.66, 113.76, 110.87, 107.21, 66.34, 54.58, 53.99, 53.05 (2C), 52.01 (2C), 48.33, 44.56 (2C), 35.23, 31.78 (2C). LC-MS (APCI+/ESI): found m/z = 522.1 [M+H]$^+$ (cal. for $C_{27}H_{35}N_7O_2S$, 521.2). Purity: 95%, t_R = 0.523 min.

4-N-Boc-(2-(4-((1-(4-cyanobenzyl)-1H-benzo[d]imidazol-2-yl)amino)piperidin-1-yl)ethyl)piperazine (54)

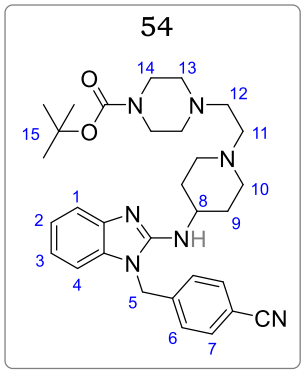

Obtained from **14d** (0.160 g, 0.42 mmol), **10** (0.132 g, 0.58 mmol) and MsCl (44.4 µl, 0.58 mmol) as a pale yellow crystalline solid (0.119 g, 46%). m.p.: 121 – 123 °C; R_f (10% MeOH/DCM) 0.28. ^{1}H NMR (600 MHz, Methanol-d_4) δ 7.67 (d, J = 8.4 Hz, 2H, H^7), 7.35 (dd, J = 7.6, 1.2 Hz, 1H, H^1), 7.25 (d, J = 8.4 Hz, 2H, H^6), 7.08 (ddd, J = 7.6, 1.3 Hz, 1H, H^2), 7.03 (dd, J = 7.9 Hz, 1.3 Hz, 1H, H^4), 6.98 (ddd, 7.9, 7.6, 1.3 Hz, 1H, H^3), 5.40 (s, 2H, H^5), 3.94 (tt, J = 10.6, 4.0 Hz, 1H, H^8), 3.46 (m, 4H, H^{14}), 3.35 (t, J = 6.8 Hz, 2H, H^{12}), 2.98 (t, J = 6.8 Hz, 2H, H^{11}), 2.81 (m, 2H, H^{13e}), 2.69 (m, 2H, H^{10e}), 2.49 (m, 4H, H^{10a,13a}), 2.21 (m, 2H, H^{9e}), 1.80 (m, 2H, H^{9a}), 1.46 (s, 9H, H^{15}). ^{13}C NMR (151 MHz, Methanol-d_4) δ 156.37, 155.04, 143.60, 142.65, 135.21, 133.68 (2C), 128.52 (2C), 122.87, 121.27, 119.42, 116.29, 112.45, 111.23, 109.15, 81.34, 66.87, 54.85 (2C), 54.04 (2C), 53.49 (2C), 50.00, 45.72, 31.21 (2C), 28.64 (3C). LC-MS (APCI+/ESI): found m/z = 544.2 [M+H] $^+$ (cal. for $C_{31}H_{41}N_7O_2$, 543.33). Purity: 97%, t_R = 2.103 min.

4-((2-((1-(2-(piperazin-1-yl)ethyl)piperidin-4-yl)amino)-1H-benzo[d]imidazol-1-yl)methyl)benzonitrile (55)

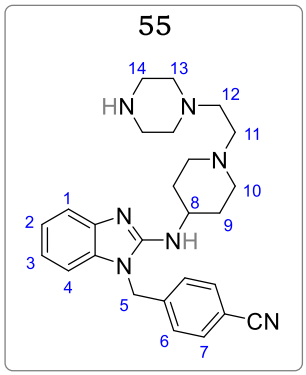

Following general procedure 16, obtained from **54** (0.070 g, 0.13 mmol) as a pale-yellow solid (0.054 g, 95%). m.p.: 104 – 106 °C; R_f (10% MeOH/DCM) 0.17. ^{1}H NMR (400 MHz, Methanol-d_4) δ 7.70 (d, J = 8.5 Hz, 2H, H^7), 7.33 (dd, J = 7.6, 1.0 Hz, 1H, H^1), 7.28 (d, J = 8.5 Hz, 2H, H^6), 7.09 (ddd, J = 8.1, 7.6, 1.0 Hz, 1H, H^2), 7.06 (dd, J = 8.1, 1.1 Hz, 1H, H^4), 6.99 (ddd, J = 8.1, 7.5, 1.0 Hz, 1H, H^3), 5.39 (s, 2H, H^5), 3.88 (tt, J = 10.4, 4.9 Hz, 1H, H^8), 3.75 – 3.68 (m, 4H, H^{14}), 3.27 (t, J = 6.6 Hz, 2H, H^{12}), 2.89 (t, J = 6.6 Hz, 2H, H^{11}), 2.65 (m, 4H, H^{10e,13e}), 2.53 (m, 4H, H^{10a,13a}), 2.17 (m, 2H, H^{9e}), 1.79 (m, 2H, H^{9a}). ^{13}C NMR (101 MHz, Methanol-d_4) δ 145.67, 134.56, 133.21 (2C), 127.55 (2C), 120.94, 119.50, 117.98, 114.84, 112.54, 111.22, 107.85, 66.87, 54.30, 53.98 (2C), 53.24 (2C), 52.08 (2C), 48.76, 44.47, 30.23 (2C). LC-MS (APCI+/ESI): found m/z = 444.2 $[M+H]^+$ (cal. for $C_{26}H_{33}N_7$, 443.28). Purity: 99%, t_R = 0.435 min.

General Procedure 17: Benzimidazole N-1 Alkylation, Synthesis of Target Compounds

A mixture of **15** or **66** (1.0 equiv), alkyl bromide (1.2 equiv) and K_2CO_3 (1.5 equiv) in 5 ml DMF was stirred under nitrogen at 70 °C for 12 hours. After cooling to ambient temperature (23 °C), the mixture was diluted with EtOAc (25 ml). The resulting mixture was washed with water (3 × 30 ml), combined aqueous layers were then extracted with EtOAc (2 × 20 ml). Thereafter, combined EtOAc layers where further washed with 5% LiCl (2 × 10 ml), brine (15 ml), then dried over anhydrous Na_2SO_4 and concentrated under reduced pressure. The crude product was triturated with Et_2O to obtain products. Further purification was performed by flash chromatography if required (based on LCMS-purity check).

4-((2-((1-(4-cyanophenethyl)piperidin-4-yl)amino)-1H-benzo[d]imidazol-1-yl) methyl)-2-fluorobenzonitrile (18)

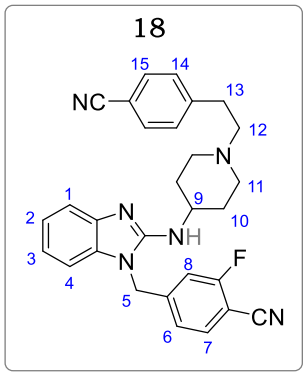

Obtained from **15** (0.070 g, 0.20 mmol) and 4-(bromomethyl)-2-fluorobenzonitrile (0.054 g, 0.24 mmol) as a white solid (0.077 g, 81%). m.p.: 79 – 81 °C; R_f(10% MeOH/DCM) 0.44. ^{1}H NMR (400 MHz, Methanol-d_4) δ 7.68 – 7.58 (m, 3H, H^{1,15}), 7.46 – 7.40 (m, 3H, H^{7,14}), 7.33 (ddd, J = 7.8, 7.2, 1.1 Hz, 1H, H^2), 7.06 (dd, J = 7.9, 1.4 Hz, 1H, H^4), 7.00 (d, J = 7.6 Hz, 1H H^6), 6.98 – 6.93 (m, 1H, H^3), 6.89 (d, J = 6.7 Hz, 1H, H^8), 5.42 (s, 2H, H^5), 3.84 (tt, J = 11.2, 5.4 Hz, 1H, H^9), 3.04 – 2.98 (m, 2H, H^{11}), 2.91 – 2.90 (m, 2H, H^{12}), 2.71 – 2.63 (m, 2H, H^{13}), 2.31 – 2.27 (m, 2H, H^{10}), 2.10 – 2.01 (m, 2H, H^{10}). ^{13}C NMR (101 MHz, Methanol-d_4) δ 161.26, 158.78, 154.01, 146.14, 141.66, 133.71, 131.96, 129.93, 129.79, 129.48, 128.64, 128.42, 121.45 (d, J = 22.3 Hz), 119.65, 118.73, 114.89, 112.63, 109.64, 107.40, 59.07, 52.18, 50.45 (2C), 39.12, 32.80, 31.46 (2C). LC-MS (APCI/ESI): found m/z = 479.1 [M+H]$^+$ (cal. for $C_{29}H_{27}FN_6$, 478.23). Purity: 99%, t_R = 2.325 min.

2-((2-((1-(4-cyanophenethyl)piperidin-4-yl)amino)-1H-benzo[d]imidazol-1-yl) methyl)-5-fluorobenzonitrile (19)

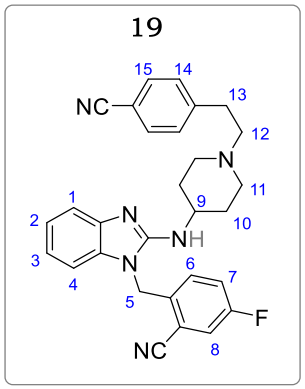

Obtained from **15** (0.070 g, 0.20 mmol) and 2-(bromomethyl)-5-fluorobenzonitrile (0.054 g, 0.24 mmol) as a white solid (0.076 g, 79%). m.p.: 82 – 84 °C; R_f(10% MeOH/DCM) 0.43. ^{1}H NMR (400 MHz, DMSO-d_6) δ 7.93 (dd, J = 8.5, 2.7 Hz, 1H, H^8), 7.72 (d, J = 8.2 Hz, 2H, H^{15}), 7.49 – 7.40 (m, 3H, H^{1,14}), 7.25 (d, J = 7.7 Hz, 1H, H^6), 6.97 (dd, J = 7.7, 5.3 Hz, 1H, H^7), 6.83 (ddd, J = 7.9, 7.2, 1.1 Hz, 1H, H^2), 6.63 – 6.57 (m, 2H, H^{3,4}), 5.49 (s, 2H, H^5), 3.82 (tt, J = 10.4, 3.9 Hz, 1H, H^9), 2.93 – 2.87 (m, 2H, H^{11e}), 2.83 (m, 2H, H^{12}), 2.61 – 2.53 (m, 2H, H^{13}), 2.16 – 2.02 (m, 2H, H^{11a}), 1.95 (m, 2H, H^{10e}), 1.47 (m, 2H, H^{10a}). ^{13}C NMR (101 MHz, Methanol-d_4) δ 164.45, 157.55, 154.23, 145.24, 141.03, 134.88, 130.45, 129.35, 128.88, 128.75, 128.60, 128.32, 121.33, 119.45, 118.21, 115.75 (d, J = 19.5 Hz), 112.87, 109.53, 107.37, 59.33, 52.21, 51.65 (2C), 39.33, 32.65, 31.08 (2C). LC-MS (APCI/ESI): found m/z = 479.1 [M+H] $^+$ (cal. for $C_{29}H_{27}FN_6$, 478.23). Purity: 99%, t_R = 2.330 min.

4-((2-((1-(4-cyanophenethyl)piperidin-4-yl)amino)-1H-benzo[d]imidazol-1-yl)methyl)-3-fluorobenzonitrile (20)

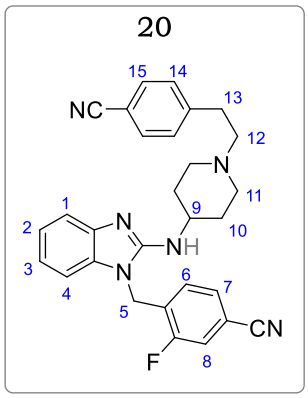

Obtained from **15** (0.070 g, 0.20 mmol) and 4-(bromomethyl)-3-fluorobenzonitrile (0.054 g, 0.24 mmol) as a pale yellow solid (0.070 g, 73%). m.p.: 87 – 89 °C; R_f(10% MeOH/DCM) 0.40. ^{1}H NMR (600 MHz, Methanol-d_4) δ 7.69 (dd, J = 3.9, 0.6 Hz, 1H, H^8), 7.65 (d, J = 8.0 Hz, 2H, H^{15}), 7.43 (d, J = 8.0 Hz, 2H, H^{14}), 7.34 (dd, J = 8.0, 0.8 Hz, 1H, H^7), 7.10 – 7.05 (m, 2H, H^{1,6}), 7.05 – 7.01 (m, 2H, H^{2,4}), 7.00 – 6.95 (m, 1H, H^3), 5.39 (s, 2H, H^5), 3.84 (tt, J = 11.1, 4.2 Hz, 1H, H^9), 3.08 – 2.99 (m, 2H, H^{11e}), 2.95 – 2.92 – 2.84 (m, 2H, H^{12}), 2.70 – 2.61 (m, 2H, H^{13}), 2.34 – 2.27 (m, 2H, H^{11a}), 2.12 – 2.05 (m, 2H, H^{10e}), 1.64 – 1.58 (m, 2H, H^{10a}). ^{13}C NMR (151 MHz, Methanol-d_4) δ 164.06, 162.35, 153.87, 145.98, 141.56, 133.85, 131.98 (2C), 128.94 (2C), 128.19, 122.88, 121.50, 119.74, 118.44, 114.92, 114.06 (d, J = 21.6 Hz), 113.10, 109.69, 107.62, 99.84, 58.99, 52.13 (2C), 49.89, 43.97, 32.70, 31.36 (2C). LC-MS (APCI+/ESI): found m/z = 479.1 [M+H]$^+$ (cal. for $C_{29}H_{27}FN_6$, 478.23). Purity: 99%, t_R = 2.325 min.

4-(2-(4-((1-(4-methoxybenzyl)-1H-benzo[d]imidazol-2-yl)amino)piperidin-1-yl) ethyl) benzonitrile (21)

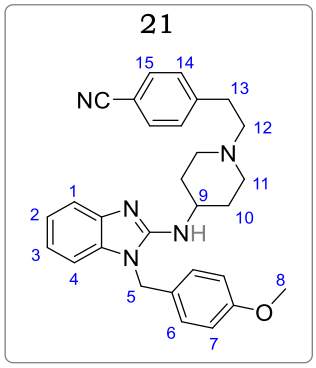

Obtained from **15** (0.070 g, 0.20 mmol) and 1-(bromomethyl)-4-methoxybenzene (0.040 g, 0.24 mmol) as a pale yellow solid (0.082 g, 88%). m.p.: 93 – 94 °C; R_f(10% MeOH/DCM) 0.45. ^{1}H NMR (600 MHz, Methanol-d_4) δ 7.64 (d, J = 8.2 Hz, 2H, H^7), 7.42 (d, J = 8.0 Hz, 2H, H^{15}), 7.30 (dd, J = 7.8, 1.5 Hz, 1H, H^1), 7.12 – 7.01 (m, 4H, H^{2,3,6}), 6.94 (ddd, J = 7.8, 7.2, 1.1 Hz, 1H, H^3), 6.85 (d, J = 8.0 Hz, 2H, H^{14}), 5.19 (s, 2H, H^5), 3.83 (tt, J = 10.6, 4.0 Hz, 1H, H^9), 3.73 (s, 3H, H^8), 3.01 – 2.95 (m, 2H, H^{11e}), 2.94 – 2.87 (m, 2H, H^{12}), 2.69 – 2.63 (m, 2H, H^{13}), 2.35 – 2.29 (m, 2H, H^{11a}), 2.11 – 2.06 (m, 2H, H^{10e}), 1.64 (dtd, J = 12.9, 10.1, 3.7 Hz, 2H, H^{10a}). ^{13}C NMR (151 MHz, Methanol-d_4) δ 159.26, 153.86, 146.07, 141.40, 134.04, 131.93 (2C), 129.46 (2C), 128.22 (2C), 127.65 (2C), 120.91, 119.34, 118.42, 114.54, 113.76, 109.62, 107.77, 59.05, 54.28 (2C), 51.95, 49.66, 44.08, 32.72, 31.35 (2C). LC-MS (APCI+/ESI): found m/z = 466.2 [M+H]$^+$ (cal. for $C_{29}H_{31}N_6O$, 465.25). Purity: 98%, t_R = 2.312 min.

4-(2-(4-((1-(4-(methylsulfonyl)benzyl)-1H-benzo[d]imidazol-2-yl) amino) piperidin-1-yl) ethyl) benzonitrile (22)

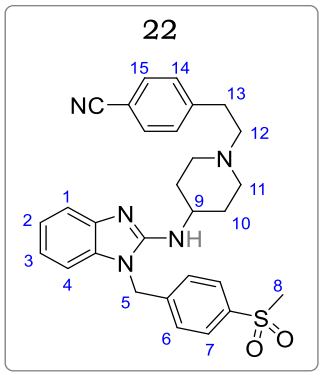

Obtained from **15** (0.070 g, 0.20 mmol) and 1-(bromomethyl)-4-(methylsulfonyl)benzene (0.060 g, 0.24 mmol) as a pale-yellow solid (0.095 g, 93%); m.p.: 115 – 116 °C; R_f (10% MeOH/DCM) 0.41. ^{1}H NMR (600 MHz, Methanol-d_4) δ 7.88 (d, J = 8.5 Hz, 2H, H^7), 7.64 (d, J = 8.2 Hz, 2H, H^{15}), 7.42 (d, J = 8.2 Hz, 2H, H^{14}), 7.38 – 7.29 (m, 3H, H^{1,6}), 7.06 (ddd, J = 7.8, 7.3, 1.3 Hz, 1H, H^2), 7.01 (dd, J = 8.1, 1.5 Hz, 1H, H^4), 6.95 (ddd, J = 8.1, 7.3, 1.1 Hz, 1H, H^3), 5.41 (s, 2H, H^5), 3.84 (tt, J = 10.9, 4.1 Hz, 1H, H^9), 3.07 (s, 3H, H^8), 3.05 – 3.00 (m, 2H, H^{11e}), 2.94 – 2.86 (m, 2H, H^{12}), 2.70 – 2.64 (m, 2H, H^{13}), 2.33 (td, J = 11.9, 2.5 Hz, 2H, H^{11a}), 2.13 – 2.06 (m, 2H, H^{10e}), 1.68 – 1.58 (m, 2H, H^{10a}). ^{13}C NMR (151 MHz, Methanol-d_4) δ 153.93, 146.00, 143.01, 141.56, 139.92, 133.84 (2C), 131.94 (2C), 129.47 (2C), 127.47 (2C), 127.15, 121.31, 119.58, 118.43, 114.79, 109.63, 107.56, 58.98, 52.09 (2C), 49.85, 44.12, 42.87, 32.69 (2C), 31.35. LC-MS (APCI$^+$/ESI): found m/z = 514.2 [M+H]$^+$ (cal. for $C_{29}H_{31}N_5O_2S$, 513.22). Purity: 99%, t_R = 2.093 min.

4-(2-(4-((1-(4-nitrobenzyl)-1H-benzo[d]imidazol-2-yl) amino) piperidin-1-yl) ethyl) benzonitrile (23)

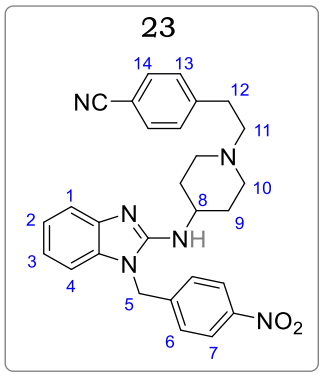

Obtained from **15** (0.070 g, 0.20 mmol) and 1-(bromomethyl)-4-nitrobenzene (0.052 g, 0.24 mmol) as an orange solid (0.096 g, 96%); m.p.: 95 – 96 °C; R_f(10% MeOH/DCM) 0.48. ^{1}H NMR (600 MHz, Methanol-d_4) δ 8.17 (d, J = 8.7 Hz, 2H, H^7), 7.64 (d, J = 8.1 Hz, 2H, H^{14}), 7.42 (d, J = 8.7 Hz, 2H, H^6), 7.34 (dd, J = 8.0, 1.2 Hz, 1H, H^1), 7.31 (d, J = 8.1 Hz, 2H, H^{13}), 7.06 (ddd, J = 7.8, 7.2, 1.2 Hz, 1H, H^2), 7.02 (dd, J = 8.1, 1.3 Hz, 1H, H^4), 6.96 (ddd, J = 8.1, 7.2, 1.1 Hz, 1H, H^3), 5.42 (s, 2H, H^5), 3.85 (tt, J = 10.4, 5.0 Hz, 1H, H^8), 3.10 – 3.02 (m, 2H, H^{10e}), 2.96 – 2.89 (m, 2H, H^{11}), 2.73 – 2.65 (m, 2H, H^{12}), 2.39 – 2.31 (m, 2H, H^{10a}), 2.14 – 2.07 (m, 2H, H^{9e}), 1.64 (dtd, J = 12.4, 11.6, 3.6 Hz, 2H, H^{9a}). ^{13}C NMR (151 MHz, Methanol-d_4) δ 153.87, 147.39, 145.87, 144.10, 141.51, 133.81, 131.96 (2C), 129.45 (2C), 126.84 (2C), 123.43 (2C), 121.36, 119.64, 118.41, 114.81, 109.67, 107.54, 58.91, 52.06 (2C), 49.79, 44.05,

32.61, 31.27 (2C). LC-MS (APCI$^+$/ESI): found m/z = 481.2 [M+H] $^+$ (cal. for $C_{28}H_{28}N_6O_2$, 480.23). Purity: 99%, t_R = 2.322 min.

Methyl 4-((2-((1-(4-cyanophenethyl) piperidin-4-yl) amino)-1H-benzo[d]imidazol-1-yl) methyl) benzoate (24)

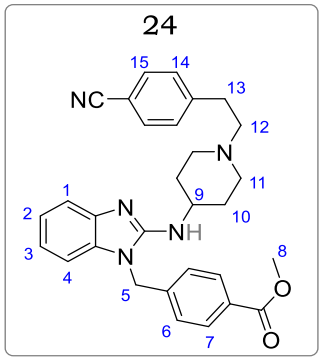

Obtained from **15** (0.070 g, 0.20 mmol) and methyl 4-(bromomethyl)benzoate (0.055 g, 0.24 mmol) as a pale-yellow solid (0.092 g, 93%); m.p.: 99 – 101 °C; R_f(10% MeOH/DCM) 0.48. ^{1}H NMR (600 MHz, Methanol-d_4) δ 7.95 (d, J = 8.4 Hz, 2H, H^7), 7.64 (d, J = 8.0 Hz, 2H, H^{15}), 7.42 (d, J = 8.0 Hz, 2H, H^{14}), 7.33 (dd, J = 7.7, 1.3 Hz, 1H, H^1), 7.20 (d, J = 8.4 Hz, 2H, H^6), 7.05 (ddd, J = 7.9, 7.2, 1.2 Hz, 1H, H^2), 7.02 (dd, J = 8.1, 1.3 Hz, 1H, H^4), 6.95 (ddd, J = 8.1, 7.2, 1.1 Hz, 1H, H^3), 5.36 (s, 2H, H^5), 3.88 – 3.81 (m, 4H, H^{8,9}), 3.04 – 2.98 (m, 2H, H^{11e}), 2.93 – 2.87 (m, 2H, H^{12}), 2.71 – 2.62 (m, 2H, H^{13}), 2.36 – 2.29 (m, 2H, H^{11a}), 2.12 – 2.07 (m, 2H, H^{10e}), 1.63 (dtd, J = 11.6, 9.5, 3.7 Hz, 2H, H^{10a}). ^{13}C NMR (151 MHz, Methanol-d_4) δ 166.69, 153.93, 146.01, 141.99, 141.48, 133.95 (2C), 131.94 (2C), 129.51 (2C), 129.45 (2C), 129.23, 126.30, 121.18, 119.52, 118.41, 114.71, 109.63, 107.58, 58.99, 52.00 (2C), 51.17, 49.75, 44.29, 32.67 (2C), 31.31. LC-MS (APCI$^+$/ESI): found m/z = 494.2 [M+H] $^+$ (cal. for $C_{30}H_{31}N_5O_2$, 493.25). Purity: 98%, t_R = 2.347 min.

4-((2-((1-(4-cyanophenethyl)piperidin-4-yl)amino)-1H-benzo[d]imidazol-1-yl) methyl) benzoic acid (25)

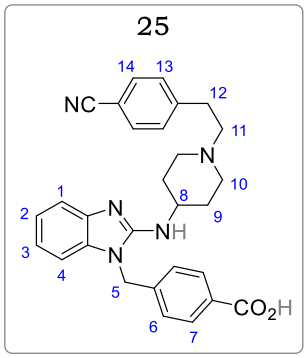

To a solution of **24** (0.050 g, 0.10 mmol) in 5 ml methanol, 2M aqueous KOH (253 µl, 0.51 mmol) was added, and the resulting mixture stirred at 79 °C for 2 hr. Following completion, the reaction mixture was cooled to 0 °C, and acidified to pH 2 while stirring. The product was filtered and obtained after recrystallization in methanol and drying, as a pale-yellow solid (0.044 g, 90%); m.p.: 138 – 140 °C; R_f(10% MeOH/DCM) 0.12. ^{1}H NMR (600 MHz, Methanol-d_4) δ 7.85 (d, J = 8.4 Hz, 2H, H^7), 7.63 (d, J = 8.1 Hz, 2H, H^{14}), 7.38 (d, J = 8.4 Hz, 2H, H^6), 7.25 (dd, J = 7.9, 1.2 Hz, 1H, H^1), 7.08 (d, J = 8.1 Hz, 2H, H^{13}), 6.97 (ddd, J = 7.9, 7.0, 1.2 Hz, 1H, H^2), 6.46 (dd, J = 7.8, 1.2 Hz, 1H, H^4), 6.28 (ddd, J = 7.8, 7.0, 1.2 Hz, 1H, H^3), 5.39 (s, 2H, H^5), 3.89 (tt, J = 10.8, 4.0 Hz, 1H, H^8), 3.04 (td, J = 13.2, 3.9 Hz, 2H, H^{10e}), 2.90 – 2.83 (m, 2H, H^{11}), 2.68 – 2.59

(m, 2H, H^{12}), 2.29 (td, J = 12.3, 3.1 Hz, 2H, H^{10a}), 2.10 – 1.97 (m, 2H, H^{9e}), 1.66 – 1.52 (m, 2H, H^{9a}). ^{13}C NMR (151 MHz, Methanol-d_4) δ 171.56, 149.58, 145.65, 142.20, 141.33, 135.78, 130.98 (2C), 129.28 (2C), 126.56 (2C), 125.80 (2C), 125.32, 121.03, 119.32, 117.26, 114.09, 109.64, 106.57, 60.87, 51.68 (2C), 50.44, 44.39, 32.36, 30.68 (2C). LC-MS (APCI$^+$/ESI): found m/z = 480.2 $[M+H]^+$ (cal. for $C_{29}H_{29}N_5O_2$, 479.23). Purity: 98%, t_R = 2.135 min.

4-(2-(4-((1-(4-(trifluoromethyl) benzyl)-1H-benzo[d]imidazol-2-yl) amino) piperidin-1-yl) ethyl) benzonitrile (26)

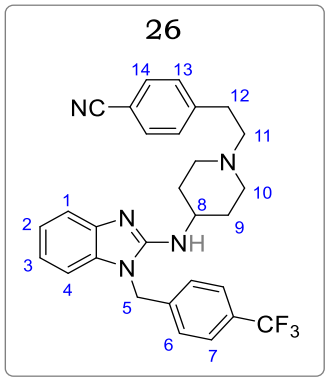

Obtained from **15** (0.070 g, 0.20 mmol) and 1-(bromomethyl)-4-(trifluoromethyl)benzene (0.057 g, 0.24 mmol) as a pale-yellow solid (0.091 g, 90%); m.p.: 86 – 88 °C; R_f (10% MeOH/DCM) 0.57. ^{1}H NMR (600 MHz, Methanol-d_4) δ 7.64 (d, J = 8.2 Hz, 2H, H^{14}), 7.60 (d, J = 8.1 Hz, 2H, H^7), 7.42 (d, J = 8.2 Hz, 2H, H^{13}), 7.33 (dd, J = 7.8, 1.3 Hz, 1H, H^1), 7.27 (d, J = 8.1 Hz, 2H, H^6), 7.06 (ddd, J = 7.9, 7.2, 1.3 Hz, 1H, H^2), 7.01 (dd, J = 7.7, 1.2 Hz, 1H, H^4), 6.95 (ddd, J = 7.7, 7.2, 1.3 Hz, 1H, H^3), 5.38 (s, 2H, H^5), 3.84 (tt, J = 10.9, 4.1 Hz, 1H, H^8), 3.06 – 3.00 (m, 2H, H^{10e}), 2.94 – 2.88 (m, 2H, H^{11}), 2.71 – 2.64 (m, 2H, H^{12}), 2.32 (td, J = 12.0, 2.5 Hz, 2H, H^{10a}), 2.13 – 2.07 (m, 2H, H^{9e}), 1.67 – 1.58 (m, 2H, H^{9a}). ^{13}C NMR (151 MHz, Methanol-d_4) δ 153.95, 146.02, 141.53, 141.06, 133.91, 131.93 (2C), 129.45 (2C), 126.75 (2C), 125.25 (2C), 125.22, 121.23, 119.55, 118.42, 114.74, 109.63, 107.57, 59.01, 52.09 (2C), 49.83, 44.10, 32.71, 31.36 (2C). LC-MS (APCI$^+$/ESI): found m/z = 504.2 $[M+H]^+$ (cal. For $C_{29}H_{28}F_3N_5$, 503.23). Purity: 98%, t_R = 2.463 min.

4-(2-(4-((1-(4-methylbenzyl)-1H-benzo[d]imidazol-2-yl)amino)piperidin-1-yl) ethyl) benzonitrile (27)

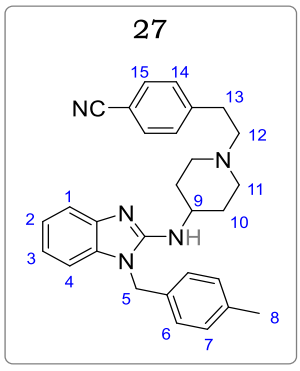

Obtained from **15** (0.070 g, 0.20 mmol) and 1-(bromomethyl)-4-methylbenzene (0.044 g, 0.24 mmol) as a pale-yellow solid (0.079 g, 88%); m.p.: 96 – 97 °C; R_f(10% MeOH/DCM) 0.51. ^{1}H NMR (600 MHz, Methanol-d_4) δ 7.64 (d, J = 8.3 Hz, 2H, H^{15}), 7.42 (d, J = 8.1 Hz, 2H, H^6), 7.30 (dd, J = 7.5, 1.2 Hz, 1H, H^1), 7.10 (d, J = 8.3 Hz, 2H, H^{14}), 7.07 – 6.97 (m, 4H, $H^{2,4,7}$), 6.93 (ddd, J = 8.0, 7.2, 1.5 Hz, 1H, H^3), 5.21 (s, 2H, H^5), 3.83 (tt, J = 10.8, 4.2 Hz, 1H, H^9), 3.03 – 2.95 (m, 2H, H^{11e}), 2.93 – 2.86 (m, 2H, H^{12}), 2.68 – 2.61 (m, 2H, H^{13}), 2.31 (td, J = 11.9, 2.6 Hz, 2H, H^{11a}), 2.27 (s, 3H,

H[8]), 2.12 – 2.04 (m, 2H, H[10e]), 1.63 (dtd, *J* = 12.6, 11.0, 3.7 Hz, 2H, H[10a]). ^{13}C NMR (151 MHz, Methanol-*d*$_4$) δ 155.65, 147.39, 144.68, 140.52, 138.69, 132.40 (2C), 130.48 (2C), 129.06 (2C), 128.57 (2C), 128.03, 120.57, 119.28, 118.66, 114.35, 110.43, 108.26, 59.68, 51.62 (2C), 49.36, 43.82, 41.86, 33.68 (2C), 30.07. LC-MS (APCI$^+$/ESI): found *m/z* = 450.2 [M+H] $^+$ (cal. for $C_{29}H_{31}N_5$, 449.26). Purity: 99%, t_r = 2.383 min.

4-(1-(2-((1-(4-cyanophenethyl)piperidin-4-yl)amino)-1H-benzo[d]imidazol-1-yl)ethyl)benzonitrile (28)

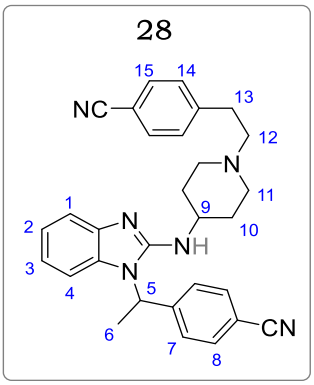

Obtained from **15** (0.070 g, 0.20 mmol) and **11b** (0.050 g, 0.24 mmol) as a white solid (0.074 g, 78%). m.p.: 121 – 123 °C; R$_f$ (10% MeOH/DCM) 0.76. ^{1}H NMR (600 MHz, Methanol-*d*$_4$) δ 7.72 (d, *J* = 8.5 Hz, 2H, H[15]), 7.65 (d, *J* = 8.3 Hz, 2H, H[8]), 7.47 – 7.42 (m, 4H, H[7,14]), 7.31 (dd, *J* = 7.8, 0.9 Hz, 1H, H[1]), 6.99 (ddd, *J* = 7.8, 7.4, 1.1 Hz, 1H, H[2]), 6.80 (dd, *J* = 8.3, 1.1 Hz, 1H, H[4]), 6.69 (ddd, *J* = 8.3, 7.4, 0.9 Hz, 1H, H[3]), 5.85 (q, *J* = 7.1 Hz, 1H, H[5]), 3.85 (tt, *J* = 11.0, 4.2 Hz, 1H, H[9]), 3.08 – 3.04 (m, 2H, H[11e]), 2.96 – 2.91 (m, 2H, H[12]), 2.73 – 2.68 (m, 2H, H[13]), 2.40 – 2.32 (m, 2H, H[11a]), 2.19 – 2.11 (m, 2H, H[10e]), 1.93 (d, *J* = 7.1 Hz, 3H, H[6]), 1.71 – 1.62 (m, 2H, H[10a]). ^{13}C NMR (151 MHz, Methanol-*d*$_4$) δ 153.70, 146.06, 145.45, 141.98, 132.25, 131.98 (2C), 129.50 (2C), 127.86 (2C), 127.03 (2C), 121.01, 119.17, 118.44, 118.00, 115.04, 111.15, 109.82, 109.68, 59.04, 52.17 (2C), 51.34, 50.04, 32.77, 31.48 (2C), 16.30. LC-MS (APCI+/ESI): found *m/z* = 474.9 [M+H] $^+$ (cal. for $C_{30}H_{30}N_6$, 474.25). Purity: 99%, t_R = 2.441min.

4-(2-(4-((1-((6-(trifluoromethyl)pyridin-3-yl)methyl)-1H-benzo[d]imidazol-2-yl)amino)piperidin-1-yl)ethyl)benzonitrile (29)

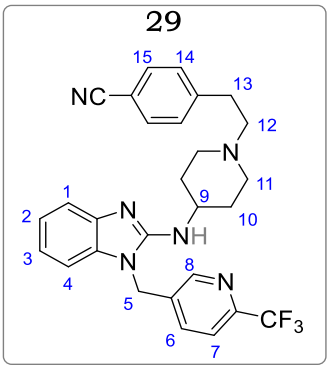

Obtained from **15** (0.070 g, 0.20 mmol) and 5-(bromomethyl)-2-(trifluoromethyl)pyridine (0.058 g, 0.24 mmol) as a white solid (0.075 g, 74%). m.p.: not determined; R$_f$ (10% MeOH/DCM) 0.44. ^{1}H NMR (600 MHz, Methanol-*d*$_4$) δ 8.54 (d, *J* = 2.1 Hz, 1H, H[8]), 7.75 (d, *J* = 8.2 Hz, 1H, H[7]), 7.67 – 7.62 (m, 3H, H[1,15]), 7.43 (d, *J* = 8.3 Hz, 2H, H[14]), 7.36 (dd, J = 8.2, 2.1 Hz, 1H, H[6]), 7.10 – 7.05 (m, 2H, H[2,4]), 6.99 (ddd, *J* = 8.0, 7.3, 1.3 Hz, 1H, H[3]), 5.45 (s, 2H, H[5]), 3.84 (tt, *J* = 11.0, 4.2 Hz, 1H, H[9]), 3.05 (m, 2H, H[11e]), 2.95 – 2.90 (m, 2H, H[12]), 2.71 – 2.68 (m, 2H, H[13]), 2.37 – 2.32 (m, 2H, H[11a]), 2.14 – 2.09 (m, 2H, H[10e]), 1.67 – 1.59 (m, 2H, H[10a]). ^{13}C NMR (151 MHz,

Methanol-d_4) δ 153.85, 148.25 (q, J = 33.1 Hz), 146.00, 141.61, 136.42, 135.99, 133.71, 131.98 (2C), 129.49 (2C), 128.87 (2C), 128.09 (2C), 121.52, 120.44, 119.78, 118.45, 114.96, 109.67, 107.47, 58.99, 52.13 (2C), 49.91, 42.02, 32.70, 31.37 (2C). LC-MS (APCI/ESI): found m/z = 505.1 $[M+H]^+$ (cal. for $C_{28}H_{27}F_3N_6$, 504.22). Purity: 99%, t_R = 2.356 min.

4-(2-(4-((1-((6-methylpyridin-3-yl)methyl)-1H-benzo[d]imidazol-2-yl) amino) piperidin-1-yl) ethyl) benzonitrile (30)

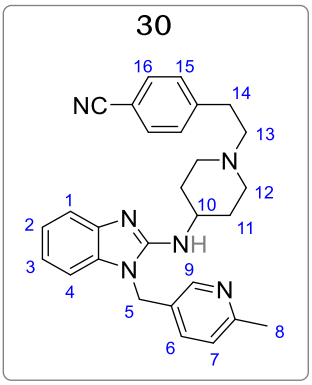

Obtained from **15** (0.070 g, 0.20 mmol) and 5-(bromomethyl)-4-methylpyridine (0.045 g, 0.24 mmol) as a pale-yellow solid (0.083 g, 92%); m.p.: 73 – 74 °C; R_f(10% MeOH/DCM) 0.35. ^{1}H NMR (600 MHz, Methanol-d_4) δ 8.28 (d, J = 1.2 Hz, 1H, H^9), 7.89 – 7.72 (m, 3H, $H^{6,16}$), 7.38 (d, J = 8.3 Hz, 2H, H^{15}), 7.29 – 7.11 (m, 2H, $H^{7,1}$), 6.98 (dd, J = 7.5, 1.2 Hz, 1H, H^4), 6.85 (ddd, J = 8.0, 7.2, 1.5 Hz, 1H, H^2), 6.79 (ddd, J = 8.1, 7.2, 1.3 Hz, 1H, H^2), 5.22 (s, 2H, H^5), 3.82 (tt, J = 10.5, 4.0 Hz, 1H, H^{10}), 2.98 – 2.85 (m, 2H, H^{12e}), 2.70 – 2.61 (m, 2H, H^{13}), 2.55 – 2.43 (m, 2H, H^{14}), 2.22 (td, J = 12.0, 2.9 Hz, 2H, H^{12a}), 2.18 (s, 3H, H^8), 2.03 – 1.91 (m, 2H, H^{11e}), 1.49 (dtd, J = 13.5, 10.2, 4.0 Hz, 2H, H^{11a}). ^{13}C NMR (151 MHz, Methanol-d_4) δ 157.55, 148.62, 145.33, 139.78, 138.07, 134.60, 133.89 (2C), 133.18, 131.45, 130.02 (2C), 128.87 (2C), 128.02, 121.21, 119.98, 118.20, 114.39, 110.58, 107.85, 60.87, 50.68 (2C), 49.68, 43.79, 30.55 (2C), 29.97. LC-MS (APCI$^+$/ESI): found m/z = 451.2 $[M+H]^+$ (cal. for $C_{28}H_{30}N_6$, 450.25). Purity: 99%, t_R = 2.436 min.

1-(Cyclohexylmethyl)-N-(1-(4-(3-methyl-1,2,4-oxadiazol-5-yl) phenethyl) piperidin-4-yl)-1H-benzo[*d*]imidazol-2-amine (71)

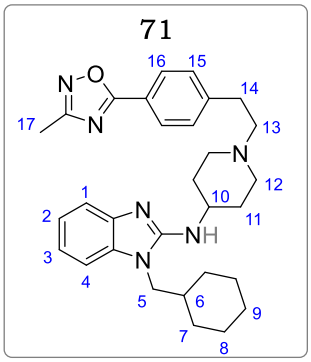

Obtained from **66** (0.080 g, 0.20 mmol) and (bromomethyl)cyclohexane (0.043 g, 0.24 mmol) as a pale yellow solid (0.080 g, 80%); m.p.: 78 – 80 °C; R_f (10% MeOH/DCM), 0.49. ^{1}H NMR (600 MHz, Methanol-d_4) δ 8.03 (d, J = 8.2 Hz, 2H, H^{16}), 7.46 (d, J = 8.2 Hz, 2H, H^{15}), 7.28 (dd, J = 7.7, 1.1 Hz, 1H, H^1), 7.11 (dd, J = 7.9, 1.3 Hz, 1H, H^4), 7.02 (ddd, J = 7.9, 7.2, 1.3 Hz, 1H, H^3), 6.98 (ddd, J = 7.7, 7.2, 1.3 Hz, 1H, H^2), 3.84 (d, J = 7.5 Hz, 2H, H^5), 3.81 (tt, J = 10.4, 4.0 Hz, 1H, H^{10}), 3.14 – 3.08 (m, 2H, H^{12}), 2.97 – 2.92 (m, 2H, H^{13}), 2.75 – 2.68 (m, 2H, H^{14}), 2.42 (s, 3H, H^{17}), 2.36 – 2.31 (m, 2H, H^{12}), 2.14 – 2.08 (m, 2H, H^{11}), 1.91 – 1.84 (m, 1H,

H[6]), 1.76 – 1.64 (m, 6H, H[8,9,11]), 1.63 – 1.57 (m, 2H, H[7]), 1.24 – 1.15 (m, 2H, H[8]), 1.11 – 1.03 (m, 2H, H[7]). ^{13}C NMR (151 MHz, Methanol-d_4) δ 176.35, 168.50, 154.86, 146.67, 141.92, 135.24, 130.27, 128.64, 125.33, 122.77, 121.54, 120.06, 115.27, 108.73, 60.14, 53.23 (2C), 50.89, 38.25, 33.62, 32.39 (2C), 31.14, 26.88 (2C), 26.36 (2C), 10.90. LC-MS (APCI$^+$/ESI): found m/z = 499.3 [M+H] $^+$ (cal. for $C_{30}H_{38}N_6O$, 498.31). Purity: 98%, t_R = 2.523 min.

1-((4,4-difluorocyclohexyl)methyl)-*N*-(1-(4-(3-methyl-1,2,4-oxadiazol-5-yl) phenethyl) piperidin-4-yl)-1H-benzo[*d*]imidazol-2-amine (72)

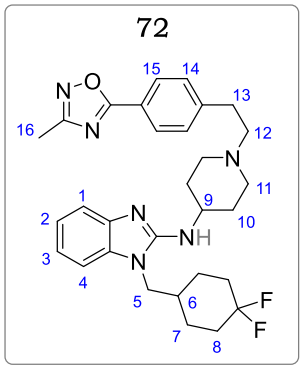

Obtained from **66** (0.080 g, 0.20 mmol) and 4-(bromomethyl)-1,1-difluorocyclohexane (0.051 g, 0.24 mmol) as a light brown solid (0.087 g, 68%); m.p.: 91 – 93 °C; R_f (10% MeOH/DCM), 0.66. ^{1}H NMR (600 MHz, Methanol-d_4) δ 8.11 (d, J = 8.0 Hz, 2H, H[15]), 7.81 (d, J = 8.0 Hz, 2H, H[14]), 7.30 (dd, J = 7.5, 1.1 Hz, 1H, H[1]), 7.09 (dd, J = 8.1, 1.1 Hz, 1H, H[4]), 7.01 (ddd, J = 8.1, 7.4, 1.1 Hz, 1H, H[3]), 6.92 (ddd, J = 7.5, 7.4, 1.1 Hz, 1H, H[2]), 4.01 (d, J = 7.6 Hz, 2H, H[5]), 3.77 (tt, J = 11.0, 4.1 Hz, 1H, H[9]), 3.11 – 3.04 (m, 2H, H[11]), 2.95 – 2.89 (m, 2H, H[12]), 2.76 – 2.67 (m, 2H, H[13]), 2.39 (s, 3H, H[16]), 2.37 – 2.31 (m, 2H, H[11]), 2.10 – 2.04 (m, 2H, H[10]), 1.88 – 1.80 (m, 1H, H[6]), 1.77 – 1.68 (m, 6H, H[8,10]), 1.65 – 1.59 (m, 2H, H[7]), 1.22 – 1.20 (m, 2H, H[7]). ^{13}C NMR (151 MHz, Methanol-d_4) δ 175.02, 167.48, 153.88, 147.87, 140.22, 134.00, 129.97 (2C), 128.09 (2C), 125.27, 121.70, 121.08, 119.96, 115.88, 107.98, 61.54, 53.11 (2C), 49.99, 38.76, 33.33, 32.01 (t, J = 24.5 Hz), 31.02, 25.91 (2C), 24.96 (2C), 11.01. LC-MS (APCI$^+$/ESI): found m/z = 537.3 [M+H] $^+$ (cal. For $C_{30}H_{36}F_2N_6O$, 534.29). Purity: 98%, t_R = 2.265 min.

N-(1-(4-(3-methyl-1,2,4-oxadiazol-5-yl)phenethyl)piperidin-4-yl)-1-(323yridine-3-ylmethyl)-1H-benzo[*d*]imidazol-2-amine (73)

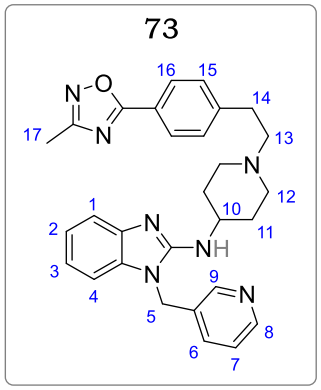

Obtained from **66** (0.080 g, 0.20 mmol) and 3-(bromomethyl)pyridine hydrochloride (0.061 g, 0.24 mmol) as a brown solid (0.066 g, 67%); m.p.: 217 – 219 °C; R_f (10% MeOH/DCM), 0.51. ^{1}H NMR (600 MHz, Methanol-d_4) δ 8.44 (dd, J = 4.9, 1.6 Hz, 1H, H[8]), 8.39 (d, J = 2.3 Hz, 1H, H[9]), 8.05 (d, J = 8.5 Hz, 2H, H[16]), 7.54 (ddd, J = 8.0, 2.3, 1.6 Hz, 1H, H[6]), 7.48 (d, J = 8.5 Hz, 2H, H[15]), 7.37 (dd, J = 8.0, 4.9 Hz, 1H, H[7]), 7.33 (dd, J = 8.0, 0.9 Hz, 1H, H[1]), 7.10 – 7.05 (m, 2H, H[2,4]), 6.98 (ddd, J = 8.0, 7.2, 1.1 Hz, 1H, H[3]), 5.37 (s, 2H, H[5]), 3.87

(tt, J = 11.0, 4.0 Hz, 1H, H^{10}), 3.16 – 3.09 (m, 2H, H^{12}), 2.99 – 2.94 (m, 2H, H^{13}), 2.81 – 2.76 (m, 2H, H^{14}), 2.43 (m, 5H, $H^{12,17}$), 2.17 – 2.11 (m, 2H, H^{11}), 1.73 – 1.64 (m, 2H, H^{11}). ^{13}C NMR (151 MHz, Methanol-d_4) δ 175.44, 167.63, 153.82, 147.91, 147.29, 145.44, 141.47, 135.19, 133.74, 133.10, 129.39 (2C), 127.79 (2C), 123.96, 121.99, 121.37, 119.69, 114.84, 107.58, 59.00, 52.12 (2C), 49.73, 42.19, 32.49, 31.21 (2C), 9.99. LC-MS (APCI$^+$/ESI): found m/z = 494.2 [M+H] $^+$ (cal. For $C_{29}H_{31}N_7O$, 493.26). Purity: 98%, t_R = 2.333 min.

N-(1-(4-(3-methyl-1,2,4-oxadiazol-5-yl) phenethyl) piperidin-4-yl)-1-((6-(trifluoromethyl) pyridin-3-yl)methyl)-1H-benzo[*d*]imidazol-2-amine (74)

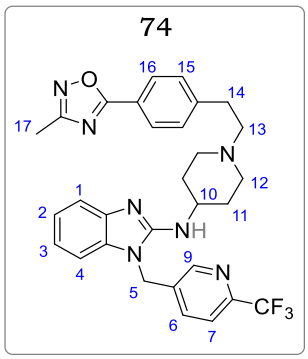

Obtained from **66** (0.080 g, 0.20 mmol) and 5-(bromomethyl)-2-(trifluoromethyl)pyridine (0.058 g, 0.24 mmol) as a white solid (0.065g, 58%); m.p.: 90 – 92 °C; R_f(10% MeOH/DCM), 0.45. ^{1}H NMR (600 MHz, Methanol-d_4) δ 8.54 (br-s, 1H, H^6), 7.75 (d, J = 8.2 Hz, 1H, H^8), 7.67 – 7.60 (m, 3H, $H^{7,15}$), 7.43 (d, J = 8.1 Hz, 2H, H^{14}), 7.35 (dd, J = 7.8, 1.1 Hz, 1H, H^1), 7.10 – 7.05 (m, 2H, $H^{2,4}$), 6.99 (ddd, J = 8.0, 7.3, 1.1 Hz, 1H, H^3), 5.45 (s, 2H, H^5), 3.84 (tt, J = 11.0, 4.1 Hz, 1H, H^9), 3.08 – 3.02 (m, 2H, H^{11}), 2.95 – 2.88 (m, 2H, H^{12}), 2.72 – 2.66 (m, 2H, H^{13}), 2.37 – 2.30 (m, 2H, H^{11}), 2.20 (s, 3H, H^{16}), 2.14 – 2.08 (m, 2H, H^{10}), 1.68 – 1.59 (m, 2H, H^{10}). ^{13}C NMR (151 MHz, Methanol-d_4) δ 177.09, 155.04, 149.13, 147.80 (q, J = 34.3 Hz), 144.89, 141.00, 137.49, 135.18, 133.10, 132.96 (2C), 128.44 (2C), 121.10, 120.23, 120.01, 119.77, 118.03, 115.95, 109.63, 107.44, 58.88, 51.12 (2C), 50.91, 41.11, 33.70, 31.47 (2C), 10.88. LC-MS (APCI$^+$/ESI): found m/z = 562.2 [M+H] $^+$ (cal. for $C_{30}H_{30}F_3N_7O$, 561.25). Purity: 97%, t_R = 2.708 min.

N-(1-(4-(3-methyl-1,2,4-oxadiazol-5-yl) phenethyl) piperidin-4-yl)-1-(4-(trifluoromethyl) benzyl)-1H-benzo[*d*]imidazol-2-amine (75)

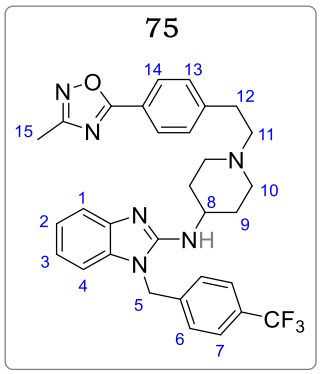

Obtained from **66** (0.080 g, 0.20 mmol) and 1-(bromomethyl)-4-(trifluoromethyl)benzene (0.057 g, 0.24 mmol) as a pale-yellow solid (0.090 g, 80%); m.p.: 171 – 173 °C; R_f (10% MeOH/DCM), 0.31. ^{1}H NMR (400 MHz, Methanol-d_4) δ 8.03 (d, J = 8.4 Hz, 2H, H^{14}), 7.70 (d, J = 8.4 Hz, 2H, H^{13}), 7.44 (d, J = 8.2 Hz, 2H, H^7), 7.34 (dd, J = 7.8, 1.1 Hz, 1H, H^1), 7.28 (d, J = 8.2 Hz, 2H, H^6), 7.19 (ddd, J = 7.8, 7.4, 1.2 Hz, 1H, H^2), 7.03 (dd, J = 8.1, 1.2 Hz, 1H, H^4), 6.89 (ddd, J = 8.1, 7.4, 1.1 Hz, 1H, H^3), 5.39 (s, 2H, H^5), 3.90 (tt, J = 10.9, 4.0 Hz, 1H, H^8),

3.11 – 3.03 (m, 2H, H^{10}), 2.95 – 2.82 (m, 2H, H^{11}), 2.71 – 2.66 (m, 2H, H^{12}), 2.43 (s, 3H, H^{15}), 2.34 – 2.26 (m, 2H, H^{10}), 2.11 – 2.01 (m, 2H, H^{9}), 1.64 – 1.56 (m, 2H, H^{9}). ^{13}C NMR (101 MHz, Methanol-d_4) δ 176.88, 164.40, 153.97, 144.61, 142.33, 141.62, 133.90 (q, J = 33.0 Hz), 132.27 (2C), 129.32 (2C), 127.15 (2C), 126.55 (2C), 121.32, 119.61, 118.04, 114.87, 111.05, 107.54, 59.27, 52.13, 49.88, 44.27, 35.22, 32.64, 31.38, 9.01. LC-MS (APCI$^+$/ESI): found m/z = 562.2 [M+H] $^+$ (cal. for $C_{31}H_{31}F_3N_6O$, 561.25). Purity: 97%, t_R = 2.803 min.

N-(1-(4-(3-methyl-1,2,4-oxadiazol-5-yl)phenethyl)piperidin-4-yl)-1-(3-methylbenzyl)-1H-benzo[*d*]imidazol-2-amine (76)

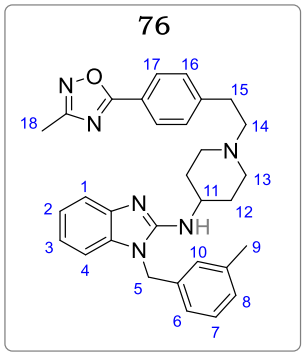

Obtained from **66** (0.080 g, 0.20 mmol) and 1-(bromomethyl)-3-methylbenzene (0.044 g, 0.24 mmol) as a brown solid (0.078 g, 77%); m.p.: 113 – 115 °C; R_f (10% MeOH/DCM), 0.60. ^{1}H NMR (600 MHz, Methanol-d_4) δ 8.03 (d, J = 8.3 Hz, 2H, H^{17}), 7.45 (d, J = 8.3 Hz, 2H, H^{16}), 7.32 (dd, J = 7.8, 1.3 Hz, 1H, H^{1}), 7.17 (ddd, J = 7.8, 7.2, 1.1 Hz, 1H, H^{2}), 7.05 (dd, J = 8.1, 1.2 Hz, 1H, H^{4}), 7.04 – 7.00 (m, 2H, $H^{3,7}$), 6.98 – 6.92 (m, 2H, $H^{6,10}$), 6.91 – 6.87 (br-d, 1H, H^{8}), 5.22 (s, 2H, H^{5}), 3.85 (tt, J = 10.6, 4.1 Hz, 1H, H^{11}), 3.03 – 2.96 (m, 2H, H^{13}), 2.95 – 2.89 (m, 2H, H^{14}), 2.71 – 2.63 (m, 2H, H^{15}), 2.42 (s, 3H, H^{18}), 2.37 – 2.29 (m, 2H, H^{13}), 2.26 (s, 3H, H^{9}), 2.13 – 2.05 (m, 2H, H^{12}), 1.69 – 1.59 (m, 2H, H^{12}). ^{13}C NMR (151 MHz, Methanol-d_4) δ 175.48, 167.62, 154.01, 145.86, 141.48, 138.24, 136.32, 134.13, 129.37 (2C), 128.30, 127.89, 127.75 (2C), 126.88, 123.36, 121.86, 120.96, 119.37, 114.60, 107.73, 59.30, 52.05 (2C), 49.75, 44.56, 32.74, 31.41 (2C), 20.05, 10.00. LC-MS (APCI$^+$/ESI): found m/z = 507.2 [M+H] $^+$ (cal. for $C_{31}H_{34}N_6O$, 506.28). Purity: 99%, t_R = 2.471 min.

2-Fluoro-4-((2-((1-(4-(3-methyl-1,2,4-oxadiazol-5-yl) phenethyl) piperidin-4-yl) amino)-1H-benzo[*d*]imidazol-1-yl) methyl) benzonitrile (77)

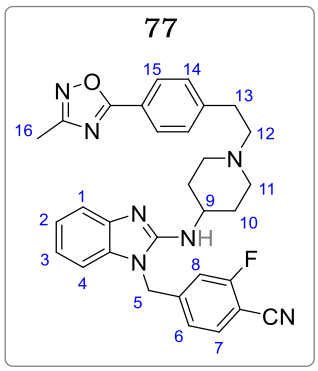

Obtained from **66** (0.080 g, 0.20 mmol) and 4-(bromomethyl)-2-fluorobenzonitrile (0.051 g, 0.24 mmol) as a pale-yellow solid (0.070 g, 65%); m.p.: 165 – 167 °C; R_f (10% MeOH/DCM), 0.51. ^{1}HNMR (400 MHz, Methanol-d_4) δ 7.99 – 7.78 (m, 3H, $H^{1,15}$), 7.46 – 7.40 (m, 3H, $H^{2,14}$), 7.38 (ddd, J = 8.0, 1.2 Hz, 1H, H^{4}), 7.11 (dd, J = 8.0, 7.3, 1.2 Hz, 1H, H^{3}), 7.05 (dd, J = 8.5, 2.4 Hz, 1H, H^{6}), 6.99 (d, J = 6.9 Hz, 1H H^{8}), 6.93 (dd, J = 6.9, 2.4, 1H,

H[7]), 5.42 (s, 2H, H[5]), 3.85 (tt, *J* = 11.2, 5.4 Hz, 1H, H[9]), 3.04 – 2.92 (m, 2H, H[11]), 2.89 – 2.80 (m, 2H, H[12]), 2.76 – 2.67 (m, 2H, H[13]), 2.44 (s, 3H, H[16]), 2.33 – 2.25 (m, 2H, H[11]), 2.10 – 2.02 (m, 2H, H[10]), 1.64 – 1.58 (m, 2H, H[10]). ^{13}C NMR (151 MHz, Methanol-d_4) δ 175.98, 164.04, 162.34, 153.85, 145.97, 141.55, 133.83, 133.73 (2C), 131.97, 129.48, 127.87 (2C), 121.49, 119.73, 118.42, 114.91, 114.12 (d, *J* = 20.6 Hz), 113.09, 109.68, 107.47, 99.78 (d, *J* = 15.1 Hz), 58.99, 52.13, 49.89, 43.97, 32.70, 31.35, 10.88. LC-MS (APCI$^+$/ESI): found *m/z* = 536.2 [M+H] $^+$ (cal. for $C_{31}H_{30}FN_7O$, 535.25). Purity: 97%, t_R = 2.667 min.

4-((2-((1-(4-(3-methyl-1,2,4-oxadiazol-5-yl) phenethyl)piperidin-4-yl) amino)-1H-benzo[d]imidazol-1-yl) methyl) benzoic acid (78)

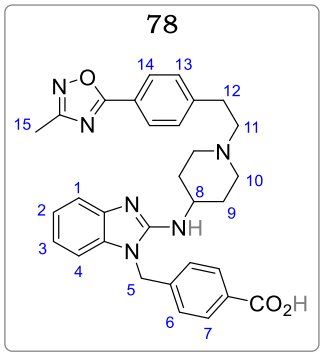

Obtained from **66** (0.080 g, 0.20 mmol) and **169p** (0.052 g, 0.24 mmol) as a white solid (0.074 g, 69%); m.p.: 153 – 155 °C; R_f(10% MeOH/DCM) 0.12. ^{1}H NMR (400 MHz, Methanol-d_4) δ 7.95 (d, *J* = 8.2 Hz, 2H, H[7]), 7.73 (d, *J* = 8.0 Hz, 2H, H[14]), 7.42 (d, *J* = 8.2 Hz, 2H, H[6]), 7.29 (dd, *J* = 8.0, 1.2 Hz, 1H, H[1]), 7.10 (d, *J* = 8.0 Hz, 2H, H[13]), 7.02 (ddd, *J* = 8.0, 7.1, 1.1 Hz, 1H, H[2]), 6.53 (dd, *J* = 7.8, 1.1 Hz, 1H, H[4]), 6.33 (ddd, *J* = 7.8, 7.1, 1.2 Hz, 1H, H[3]), 5.36 (s, 2H, H[5]), 3.88 (tt, *J* = 11.0, 4.1 Hz, 1H, H[8]), 3.06 – 2.95 (m, 2H, H[10e]), 2.89 – 2.79 (m, 2H, H[11]), 2.68 – 2.57 (m, 2H, H[12]), 2.31 (td, *J* = 11.8, 4.0 Hz, 2H, H[10a]), 2.08 – 1.93 (m, 2H, H[9e]), 1.65 – 1.50 (m, 2H, H[9a]). ^{13}C NMR (151 MHz, Methanol-d_4) δ 172.35, 159.33, 148.97, 143.68, 142.03, 139.00, 135.41, 130.45 (2C), 129.39 (2C), 126.52 (2C), 125.07 (2C), 124.30, 120.55, 119.06, 117.13, 114.30, 108.97, 105.95, 60.75, 50.93 (2C), 49.64, 44.23, 32.66, 30.54 (2C), 9.89. LC-MS (APCI$^+$/ESI): found *m/z* = 537.2 [M+H] $^+$ (cal. for $C_{31}H_{32}N_6O_3$, 536.25). Purity: 98%, t_R = 0.154 min.

4-(2-(4-((1-methyl-1H-benzo[d]imidazol-2-yl)amino)piperidin-1-yl) ethyl) benzoic acid (81)

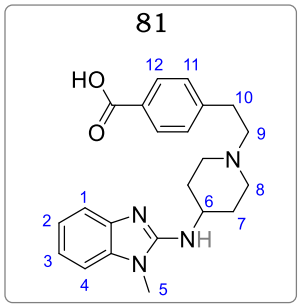

To a solution of **79** (4.00 g, 10.2 mmol) in MeOH (50 mol) was added 2M aqueous KOH (25 ml, 51 mmol). The reaction mixture was stirred at 79 °C temperature for 2 hr. After completion (monitored by TLC), MeOH was taken off *in vacuo* and the residue diluted with water. The solution was then acidified to pH 2 under ice with 3M HCl, and the precipitate was filtered and

recrystallized in MeOH to afford product as an off-white solid (3.77 g, 98%). m.p.: 159 – 161 °C; R_f(10% MeOH/DCM), 0.05. ^{1}H NMR (600 MHz, Methanol-d_4) δ 8.00 (d, J = 7.9 Hz, 2H, H^{12}), 7.42 (d, J = 7.9 Hz, 2H, H^{11}), 7.38 (dd, J = 5.9, 3.2 Hz, 1H, H^1), 7.32 (dd, J = 6.0, 2.9 Hz, 1H, H^4), 7.26 – 7.06 (m, 2H, $H^{2,3}$), 3.94 (tt, J = 11.0, 5.4 Hz, 1H, H^6), 3.65 – 3.58 (m, 5H, $H^{5,8e}$), 3.34 – 3.22 (m, 2H, H^9), 3.19 – 3.11 (m, 2H, H^{10}), 3.07 (td, J = 12.1, 4.0 Hz, 2H, H^{8a}), 2.46 – 2.24 (m, 2H, H^{7e}), 2.13 – 1.86 (m, 2H, H^{7a}). ^{13}C NMR (151 MHz, Methanol-d_4) δ 170.77, 166.88, 140.91, 138.24, 136.49, 130.13 (2C), 128.40 (2C), 122.80, 120.38, 119.89, 113.49, 105.66, 63.48, 60.24, 52.38 (2C), 51.55, 34.18, 30.19 (2C). LC-MS (APCI$^+$/ESI): found m/z = 379.2 $[M+H]^+$ (cal. for $C_{22}H_{26}N_4O_2$, 378.21). Purity: 95%, t_R = 0.140 min.

General Procedure 18: Synthesis of amides and 1,2,4-oxadiazoles *via* an acyl chloride

1. To a round bottomed flask containing carboxylic acid **81** (3.50 g, 9.26 mmol) thionyl chloride, $SOCl_2$ (15 ml) was added, and the resulting mixture refluxed at 80 °C for 2 hr. After completion (monitored *via* TLC), excess thionyl chloride was evaporated *in vacuo*, and the residue was taken up in 30 ml toluene and evaporated *in vacuo* three (3) times to give thionyl chloride **81'** in quantitative yield.
2. The appropriate amine or *N*-hydroxyl amidine (**112a** – **112h**, 1.2 equiv) was added to a stirring solution containing thionyl chloride **81'** (0.060 g, 0.151 mmol, 1.0 equiv) and TEA (43 µl, 0.303 mmol, 2.0 equiv) in 10 ml THF. The resulting mixture was stirred at room temperature (20 °C) for 6 – 10 h. After completion (monitored *via* TLC and LC–MS), THF was evaporated *in vacuo*, the residue purified *via* column chromatography to afford amides (**83** – **111**).
3. 1,2,4-oxadiazoles (**113** – **121**) where obtained after charging amidoximes obtained in step 2 with K_2CO_3 (0.042 g, 0.303 mmol, 2.0 equiv) and refluxing the resulting mixture at 85 °C for another 6 – 12 hr. Following completion (monitored by TLC and LC-MS), the solvent was taken off *in vacuo*. Products obtained *via* column chromatography using 7 – 12% MeOH/DCM gradient as eluent.

N,N-dimethyl-4-(2-(4-((1-methyl-1H-benzo[d]imidazol-2-yl) amino) piperidin-1-yl) ethyl) benzamide (83)

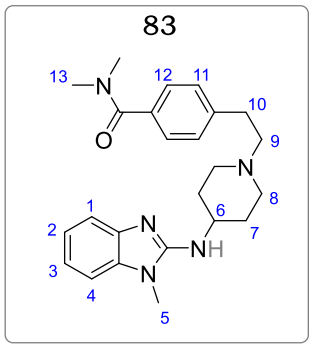

Obtained from dimethylamine hydrochloride (0.012 g, 0.18 mmol) as a pale yellow solid (0.054 g, 88%). m.p.: 133 – 135 °C; R_f(10% MeOH/DCM), 0.29. ^{1}H NMR (600 MHz, Methanol-d_4) δ 7.90 (d, J = 7.9 Hz, 2H, H^{12}), 7.44 (d, J = 7.9 Hz, 2H, H^{11}), 7.20 (dd, J = 7.8, 1.2 Hz, 1H, H^1), 7.08 (dd, J = 7.8, 1.2 Hz, 1H, H^4), 6.96 (ddd, J = 7.8, 7.5, 1.2 Hz, 1H, H^2), 6.85 (ddd, J = 7.8, 7.5, 1.2 Hz, 1H, H^3), 3.78 (s, 6H, H^{13}), 3.59 (tt, J = 10.9, 4.0 Hz, 1H, H^6), 3.53 (s, 3H, H^5), 3.15 – 3.07 (m, 2H, H^8), 2.97 – 2.90 (m, 2H, H^9), 2.75 – 2.69 (m, 2H, H^{10}), 2.38 – 2.30 (m, 2H, H^8), 2.19 – 2.10 (m, 2H, H^7), 1.73 – 1.64 (m, 2H, H^7). ^{13}C NMR (151 MHz, Methanol-d_4) δ 170.32, 142.04, 141.34, 138.53, 136.65, 130.04 (2C), 128.38 (2C), 122.84, 120.05, 119.81, 113.34, 105.87, 63.38, 60.17, 52.55 (2C), 51.42, 38.65 (2C), 34.03, 30.12 (2C). LC-MS (APCI$^+$/ESI): found m/z = 406.2 [M+H]$^+$ (cal. for $C_{24}H_{31}N_5O$, 405.25). Purity: 98%, t_R = 0.149 min.

N-cyclopropyl-4-(2-(4-((1-methyl-1H-benzo[d]imidazol-2-yl) amino) piperidin-1-yl) ethyl) benzamide (84)

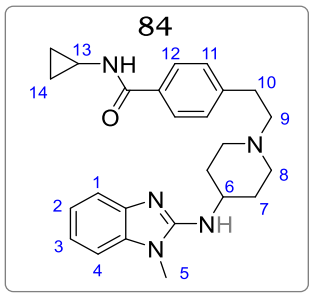

Obtained from cyclopropylamine (0.010 g, 0.18 mmol) as a light yellow solid (0.050 g, 79%). m.p.: 107 – 109 °C; R_f (10% MeOH/DCM), 0.34. ^{1}H NMR (600 MHz, Methanol-d_4) δ 7.89 (d, J = 8.1 Hz, 2H, H^{12}), 7.45 (d, J = 8.1 Hz, 2H, H^{11}), 7.29 (dd, J = 7.8, 1.3 Hz, 1H, H^1), 7.19 (dd, J = 7.8, 1.2 Hz, 1H, H^4), 7.09 (ddd, J = 7.8, 7.5, 1.2 Hz, 1H, H^2), 6.90 (ddd, J = 7.8, 7.5, 1.3 Hz, 1H, H^3), 3.71 (tt, J = 8.1, 7.3 Hz, 1H, H^{13}), 3.59 (tt, J = 10.8, 4.2 Hz, 1H, H^6), 3.53 (s, 3H, H^5), 3.14 – 3.06 (m, 2H, H^8), 2.96 – 2.88 (m, 2H, H^9), 2.75 – 2.68 (m, 2H, H^{10}), 2.37 – 2.29 (m, 2H, H^8), 2.18 – 2.09 (m, 2H, H^7), 1.75 – 1.65 (m, 2H, H^7), 0.88 – 0.60 (m, 4H, H^{14}). ^{13}C NMR (151 MHz, Methanol-d_4) δ 168.05, 142.99, 141.08, 139.03, 136.44, 130.29 (2C), 129.05 (2C), 122.38, 120.26, 119.05, 113.38, 105.75, 63.28, 60.81, 52.88 (2C), 51.37, 34.34, 30.17 (2C), 27.37, 8.02 (2C). LC-MS (APCI$^+$/ESI): found m/z = 418.2 [M+H]$^+$ (cal. For $C_{25}H_{31}N_5O$, 417.25). Purity: 98%, t_R = 0.169 min.

N-allyl-4-(2-(4-((1-methyl-1H-benzo[d]imidazol-2-yl) amino) piperidin-1-yl) ethyl) benzamide (85)

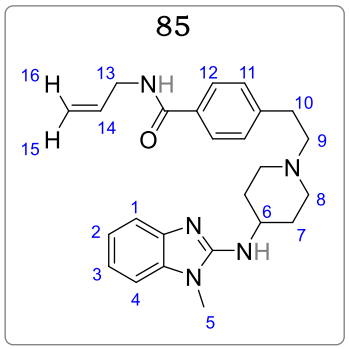

Obtained from prop-2-en-1-amine (0.010 g, 0.18 mmol) as an off white solid (0.042 g, 66%). m.p.: 128 – 129 °C; R_f(10% MeOH/DCM), 0.31. ^{1}H NMR (600 MHz, Methanol-d_4) δ 7.89 (d, J = 7.8 Hz, 2H, H^{12}), 7.42 (d, J = 7.8 Hz, 2H, H^{11}), 7.20 (dd, J = 8.0, 1.1 Hz, 1H, H^1), 7.09 (dd, J = 7.8, 1.3 Hz, 1H, H^4), 6.98 (ddd, J = 8.0, 7.5, 1.3 Hz, 1H, H^2), 6.87 (ddd, J = 7.8, 7.5, 1.1 Hz, 1H, H^3), 5.81 (dd, J = 15.2, 10.2 Hz, 1H, H^{15}), 5.33 (dd, J = 15.2, 3.2 Hz, 1H, H^{14}), 5.20 (dd, 10.2, 3.2 Hz, 1H, H^{16}), 3.57 (tt, J = 11.2, 4.2 Hz, 1H, H^6), 3.52 (s, 3H, H^5), 3.13 – 3.06 (m, 2H, H^8), 2.93 – 2.87 (m, 2H, H^9), 2.73 – 2.69 (m, 2H, H^{10}), 2.35 – 2.29 (m, 2H, H^8), 2.16 – 2.09 (m, 2H, H^7), 1.73 – 1.65 (m, 2H, H^7). ^{13}C NMR (151 MHz, Methanol-d_4) δ 167.55, 143.09, 140.88, 138.82, 136.77, 134.38, 130.19 (2C), 129.97 (2C), 122.22, 120.34, 119.28, 117.48, 113.48, 105.66, 63.38, 60.18, 52.86 (2C), 51.35, 43.02, 34.12, 30.24 (2C). LC-MS (APCI$^+$/ESI): found m/z = 418.2 [M+H]$^+$ (cal. for $C_{25}H_{31}N_5O$, 417.25). Purity: 99%, t_R = 0.175 min.

N-(2-hydroxyethyl)-4-(2-(4-((1-methyl-1H-benzo[d]imidazol-2-yl) amino) piperidin-1-yl) ethyl) benzamide (86)

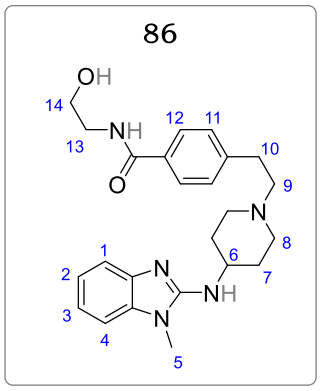

Obtained from 2-aminoethanol (0.011 g, 0.18 mmol) as an off white solid (0.052 g, 82%). m.p.: 214 – 216 °C; R_f (10% MeOH/DCM), 0.15. ^{1}H NMR (600 MHz, Methanol-d_4) δ 7.90 (d, J = 7.9 Hz, 2H, H^{12}), 7.43 (d, J = 7.9 Hz, 2H, H^{11}), 7.21 (dd, J = 8.0, 1.1 Hz, 1H, H^1), 7.10 (dd, J = 7.8, 1.3 Hz, 1H, H^4), 6.96 (ddd, J = 8.0, 7.5, 1.3 Hz, 1H, H^2), 6.88 (ddd, J = 7.8, 7.5, 1.1 Hz, 1H, H^3), 4.19 – 4.12 (dd, J = 13.8, 6.9 Hz, 2H, H^{14}), 4.08 – 4.01 (m, 2H, H^{13}), 3.58 (tt, J = 10.8, 4.1 Hz, 1H, H^6), 3.52 (s, 3H, H^5), 3.18 – 3.10 (m, 2H, H^8), 2.84 – 2.78 (m, 2H, H^9), 2.70 – 2.62 (m, 2H, H^{10}), 2.35 – 2.28 (m, 2H, H^8), 2.16 – 2.06 (m, 2H, H^7), 1.73 – 1.64 (m, 2H, H^7). ^{13}C NMR (151 MHz, Methanol-d_4) δ 168.03, 142.87, 140.48, 138.03, 136.44, 130.28 (2C), 128.92 (2C), 123.00, 120.38, 119.33, 113.74, 105.81, 63.28, 62.44, 60.24, 52.48 (2C), 51.22, 42.87, 34.34, 30.19 (2C). LC-MS (APCI$^+$/ESI): found m/z = 422.2 [M+H]$^+$ (cal. for $C_{24}H_{31}N_5O_2$, 421.25). Purity: 99%, t_R = 0.138 min.

Tert-butyl (2-(4-(2-(4-((1-methyl-1H-benzo[d]imidazol-2-yl)amino)piperidin-1-yl)ethyl)benzamido)ethyl)carbamate (87)

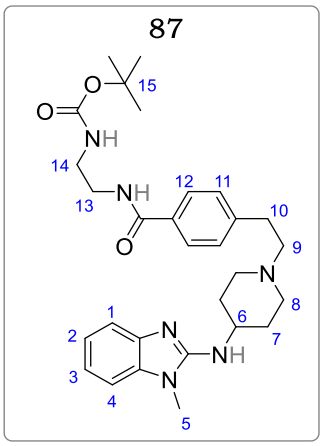

Obtained from tert-butyl (2-aminoethyl)carbamate (0.029 g, 0.18 mmol) as an off white solid (0.098 g, 85%). m.p.: 95 – 96 °C; R_f (10% MeOH/DCM), 0.45. ^{1}H NMR (600 MHz, Methanol-d_4) δ 7.98 (d, J = 7.9 Hz, 2H, H^{12}), 7.48 (d, J = 7.9 Hz, 2H, H^{11}), 7.19 (dd, J = 8.0, 1.2 Hz, 1H, H^1) 7.11 (dd, J = 7.8, 1.3 Hz, 1H, H^4), 7.01 (ddd, J = 8.0, 7.1, 1.3 Hz, 1H, H^2), 6.95 (ddd, J = 7.8, 7.1, 1.2 Hz, 2H, H^3), 4.19 – 4.15 (br-s, 4H, H^{13,14}), 3.95 (tt, J = 10.2, 4.0 Hz, 1H, H^6), 3.51 (s, 3H, H^5), 3.15 – 3.08 (m, 2H, H^{8e}), 2.83 – 2.72 (m, 2H, H^9), 2.69 – 2.58 (m, 2H, H^{10}), 2.30 – 2.21 (m, 2H, H^{8a}), 2.11 – 2.02 (m, 2H, H^{7e}), 1.69 – 1.52 (m, 2H, H^{7a}), 1.29 (s, 9H, H^{15}). ^{13}C NMR (151 MHz, Methanol-d_4) δ 178.95, 165.68, 145.30, 140.62, 138.11, 136.29, 130.89 (2C), 128.49 (2C), 123.33, 120.45, 119.31, 112.78, 104.79, 83.85, 63.32, 61.58, 59.96, 52.88 (2C), 50.50, 42.52, 33.97, 30.88 (2C), 15.59 (3C). LC-MS (APCI$^+$/ESI): found m/z = 521.3 [M+H]$^+$ (cal. for $C_{29}H_{40}N_6O_3$, 520.32). Purity: 99%, t_R = 2.144 min.

N-(2-aminoethyl)-4-(2-(4-((1-methyl-1H-benzo[d]imidazol-2-yl) amino) piperidin-1-yl) ethyl) benzamide (88)

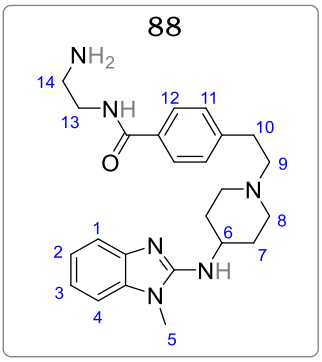

Following general procedure 2, obtained from **87** (0.050, 0.10 mmol) as a white solid (0.045 g, 98%). m.p.: 125 – 127 °C; R_f (10% MeOH/DCM), 0.28. ^{1}H NMR (600 MHz, Methanol-d_4) δ 7.88 (d, J = 8.0 Hz, 2H, H^{12}), 7.49 (d, J = 8.0 Hz, 2H, H^{11}), 7.21 (dd, J = 8.1, 1.2 Hz, 1H, H^1), 7.09 (dd, J = 7.8, 1.3 Hz, 1H, H^4), 6.99 (ddd, J = 8.1, 7.5, 1.3 Hz, 1H, H^2), 6.85 (ddd, J = 7.8, 7.5, 1.1 Hz, 1H, H^3), 4.15 – 4.06 (m, 2H, H^{13}), 3.86 – 3.61 (m, 3H, H^{6,14}), 3.53 (s, 3H, H^5), 3.15 – 3.08 (m, 2H, H^{8e}), 2.80 – 2.71 (m, 2H, H^9), 2.68 – 2.59 (m, 2H, H^{10}), 2.29 – 2.18 (m, 2H, H^{8a}), 2.09 – 2.01 (m, 2H, H^{7e}), 1.78 – 1.65 (m, 2H, H^{7a}). ^{13}C NMR (151 MHz, Methanol-d_4) δ 169.35, 144.69, 141.22, 139.39, 135.47, 129.39 (2C), 128.55 (2C), 123.30, 120.77, 119.20, 112.97, 105.35, 63.74, 62.08, 60.65, 52.23 (2C), 51.29, 42.55, 33.55 (2C), 27.35. LC-MS (APCI$^+$/ESI): found m/z = 421.2 [M+H]$^+$ (cal. for $C_{24}H_{32}N_6O$, 420.26). Purity: 99%, t_R = 0.120 min.

4-(2-(4-((1-methyl-1H-benzo[d]imidazol-2-yl) amino) piperidin-1-yl) ethyl)-N-(oxazol-4-ylmethyl) benzamide (89)

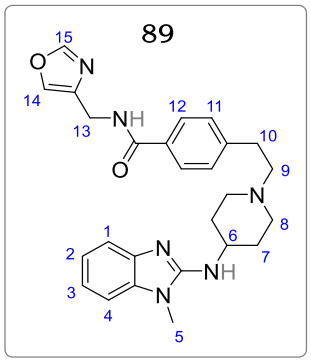

Obtained from oxazole-4-ylmethanamine (0.018 g, 0.18 mmol) as a white solid (0.053 g,76%). m.p.: 92 – 94 °C; R_f (10% MeOH/DCM), 0.34. ^{1}H NMR (600 MHz, Methanol-d_4) δ 8.10 (s, 1H, H^{15}), 8.02 (s, 1H, H^{14}), 7.87 (d, J = 8.1 Hz, 2H, H^{12}), 7.25 (d, J = 8.1 Hz, 2H, H^{11}), 7.12 (dd, J = 7.9, 1.2 Hz, 1H, H^1), 7.05 (dd, J = 8.1, 1.2 Hz, 1H, H^4), 6.83 (ddd, J = 7.9, 7.3, 1.2 Hz, 1H, H^2), 6.57 (ddd, J = 8.1, 7.3, 1.2 Hz, 1H, H^3), 4.98 (s, 2H, H^{13}), 3.63 (tt, J = 11.1, 4.4 Hz, 1H, H^6), 3.51 (s, 3H, H^5), 3.10 – 3.05 (m, 2H, H^8), 2.95 – 2.83 (m, 2H, H^9), 2.73 – 2.62 (m, 2H, H^{10}), 2.33 – 2.22 (m, 2H, H^8), 2.15 – 2.06 (m, 2H, H^7), 1.75 – 1.63 (m, 2H, H^7). ^{13}C NMR (151 MHz, Methanol-d_4) δ 167.33, 151.49, 146.87, 141.12, 137.03, 133.37, 130.72 (2C), 126.89 (2C), 125.39, 121.76, 121.03, 120.12, 114.50, 107.23, 60.11, 54.09 (2C), 43.99, 39.66, 32.53, 33.34, 31.77 (2C), 30.38 (2C). LC-MS (APCI$^+$/ESI): found m/z = 459.2 [M+H]$^+$ (cal. for $C_{26}H_{30}N_6O_2$, 458.24). Purity: 98%, t_R = 0.352 min.

N-(1-(hydroxymethyl) cyclopropyl)-4-(2-(4-((1-methyl-1H-benzo[d]imidazol-2-yl) amino) piperidin-1-yl) ethyl) benzamide (90)

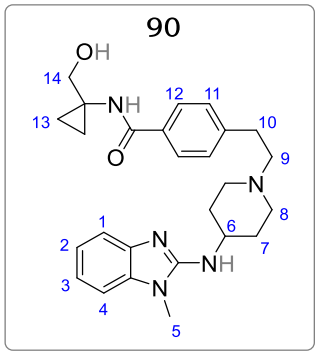

Obtained from 1-(aminomethyl)cyclopropanol (0.016 g, 0.18 mmol) as a cream white solid (0.048 g, 71%). m.p.: 221 – 223 °C; R_f (10% MeOH/DCM), 0.26. ^{1}H NMR (600 MHz, Methanol-d_4) δ 7.90 (d, J = 8.0 Hz, 2H, H^{12}), 7.44 (d, J = 8.0 Hz, 2H, H^{11}), 7.19 (dd, J = 7.8, 1.3 Hz, 1H, H^1), 7.08 (dd, J = 7.8, 1.2 Hz, 1H, H^4), 6.96 (ddd, J = 7.8, 7.5, 1.2 Hz, 1H, H^2), 6.86 (ddd, J = 7.8, 7.5, 1.3 Hz, 1H, H^3), 3.89 (s, 2H, H^{14}), 3.58 (tt, J = 11.1, 4.2 Hz, 1H, H^6), 3.52 (s, 3H, H^5), 3.15 – 3.07 (m, 2H, H^8), 2.92 – 2.84 (m, 2H, H^9), 2.73 – 2.65 (m, 2H, H^{10}), 2.38 – 2.31 (m, 2H, H^8), 2.18 – 2.10 (m, 2H, H^7), 1.74 – 1.65 (m, 2H, H^7), 1.18 – 1.02 (br-s, 4H, H^{13}). ^{13}C NMR (151 MHz, Methanol-d_4) δ 166.90, 143.32, 141.17, 138.23, 136.76, 130.55 (2C), 129.30 (2C), 122.87, 120.09, 119.10, 113.38, 105.49, 75.21, 63.03, 60.28, 52.78 (2C), 51.48, 37.08, 34.11, 30.30 (2C), 8.98 (2C). LC-MS (APCI$^+$/ESI): found m/z = 448.3 [M+H]$^+$ (cal. for $C_{26}H_{33}N_5O_2$, 447.26). Purity: 98%, t_R = 0.153 min.

(3-hydroxyazetidin-1-yl) (4-(2-(4-((1-methyl-1H-benzo[d]imidazol-2-yl) amino) piperidin-1-yl) ethyl) phenyl) methanone (91)

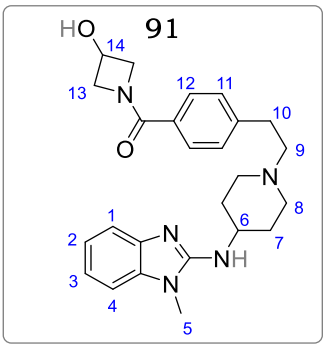

Obtained from azetidine-3-ol (0.012 g, 0.18 mmol) as a pale-yellow solid (0.057 g, 87%). m.p.: 185 – 187 °C; R_f (10% MeOH/DCM), 0.24. ^{1}H NMR (400 MHz, Methanol-d_4) δ 7.89 (d, J = 7.9 Hz, 2H, H^{12}), 7.42 (d, J = 7.9 Hz, 2H, H^{11}), 7.19 (dd, J = 8.0, 1.2 Hz, 1H, H^1), 7.09 (dd, J = 7.7, 1.3 Hz, 1H, H^4), 6.98 (ddd, J = 8.0, 7.5, 1.3 Hz, 1H, H^2), 6.87 (ddd, J = 7.7, 7.5, 1.2 Hz, 1H, H^3), 4.43 (tt, J = 7.5, 4.1 Hz, 1H, H^{14}), 4.30 (dd, J = 14.1, 7.5 Hz, 2H, H^{13e}), 4.24 (dd, J = 14.1, 4.1 Hz, 2H, H^{13a}), 3.5 9 (tt, J = 11.0, 4.1 Hz, 1H, H^6), 3.52 (s, 3H, H^5), 3.19 – 3.10 (m, 2H, H^{8e}), 2.88 – 2.79 (m, 2H, H^9), 2.72 – 2.64 (m, 2H, H^{10}), 2.38 – 2.30 (m, 2H, H^{8a}), 2.18 – 2.08 (m, 2H, H^{7e}), 1.72 – 1.63 (m, 2H, H^{7a}). ^{13}C NMR (151 MHz, Methanol-d_4) δ 172.22, 143.98, 140.70, 138.23, 136.76, 130.12 (2C), 128.43 (2C), 122.67, 120.38, 119.22, 113.48, 105.44, 63.19, 61.62, 60.03, 55.87 (2C), 52.83 (2C), 50.76, 34.13, 30.27 (2C). LC-MS (APCI$^+$/ESI): found m/z = 434.2 [M+H]$^+$ (cal. for $C_{25}H_{31}N_5O_2$, 433.25). Purity: 98%, t_R = 0.137 min.

1-(4-(2-(4-((1-methyl-1H-benzo[d]imidazol-2-yl) amino) piperidin-1-yl) ethyl) benzoyl) azetidine-3-carbonitrile (92)

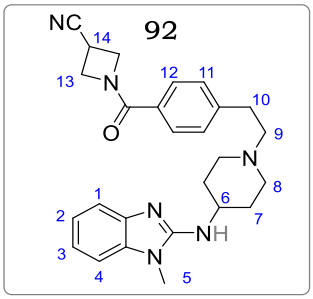

Obtained from azetidine-3-carbonitrile (0.015 g, 0.18 mmol) as a pale-yellow solid (0.053 g, 79%). m.p.: 198 – 200 °C; R_f(10% MeOH/DCM), 0.43. ^{1}H NMR (600 MHz, Methanol-d_4) δ 7.91 (d, J = 8.1 Hz, 2H, H^{12}), 7.43 (d, J = 8.1 Hz, 2H, H^{11}), 7.20 (dd, J = 8.0, 1.1 Hz, 1H, H^1), 7.09 (dd, J = 7.8, 1.3 Hz, 1H, H^4), 6.97 (ddd, J = 8.0, 7.5, 1.3 Hz, 1H, H^2), 6.86 (ddd, J = 7.8, 7.5, 1.1 Hz, 1H, H^3), 4.29 (dd, J = 13.8, 6.9 Hz, 2H, H^{13e}), 4.15 (dd, J = 13.8, 3.2 Hz, 2H, H^{13a}), 3.57 (tt, J = 11.1, 4.2 Hz, 1H, H^6), 3.52 (s, 3H, H^5), 3.26 (tt, J = 6.9, 3.2 Hz, 1H, H^{14}), 3.17 – 3.09 (m, 2H, H^{8e}), 2.86 – 2.79 (m, 2H, H^9), 2.73 – 2.63 (m, 2H, H^{10}), 2.37 – 2.29 (m, 2H, H^{8a}), 2.18 – 2.07 (m, 2H, H^{7e}), 1.74 – 1.64 (m, 2H, H^{7a}). ^{13}C NMR (151 MHz, Methanol-d_4) δ 172.51, 144.69, 141.02, 138.22, 136.75, 129.83 (2C), 128.01 (2C), 123.14, 120.76, 120.22, 119.36, 113.88, 105.82, 63.20, 60.22, 53.18 (2C), 51.81, 48.09 (2C), 34.18, 30.24 (2C), 17.82. LC-MS (APCI$^+$/ESI): found m/z = 443.2 [M+H]$^+$ (cal. for $C_{26}H_{30}N_6O$, 442.25). Purity: 98%, t_R = 0.145 min.

(3,3-difluoroazetidin-1-yl) (4-(2-(4-((1-methyl-1H-benzo[d]imidazol-2-yl) amino) piperidin-1-yl) ethyl) phenyl) methanone (93)

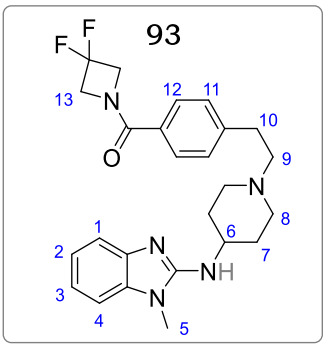

Obtained from 3,3-difluoroazetidine (0.017 g, 0.18 mmol) as a white solid (0.059 g, 86%). m.p.: 195 – 197 °C; R_f (10% MeOH/DCM), 0.49. ^{1}H NMR (400 MHz, Methanol-d_4) δ 7.90 (d, J = 8.0 Hz, 2H, H^{12}), 7.42 (d, J = 8.0 Hz, 2H, H^{11}), 7.22 (dd, J = 7.9, 1.2 Hz, 1H, H^1), 7.10 (dd, J = 7.8, 1.3 Hz, 1H, H^4), 6.99 (ddd, J = 7.9, 7.5, 1.3 Hz, 1H, H^2), 6.87 (ddd, J = 7.8, 7.5, 1.2 Hz, 1H, H^3), 4.19 – 4.02 (m, 4H, H^{13}), 3.58 (tt, J = 10.7, 4.1 Hz, 1H, H^6), 3.52 (s, 3H, H^5), 3.19 – 3.10 (m, 2H, H^{8e}), 2.87 – 2.80 (m, 2H, H^9), 2.73 – 2.64 (m, 2H, H^{10}), 2.38 – 2.30 (m, 2H, H^{8a}), 2.18 – 2.07 (m, 2H, H^{7e}), 1.74 – 1.65 (m, 2H, H^{7a}). ^{13}C NMR (151 MHz, Methanol-d_4) δ 172.77, 145.29, 141.29, 138.90, 137.01, 130.05 (2C), 128.99 (2C), 123.04, 120.18, 119.43, 113.87, 107.07, 105.45 (t, J = 24.1 Hz), 63.38, 60.22, 59.14 (2C), 53.24 (2C), 51.77, 33.86, 30.51 (2C). LC-MS (APCI$^+$/ESI): found m/z = 454.2 [M+H]$^+$ (cal. for $C_{25}H_{29}F_2N_5O$, 453.23). Purity: 98%, t_R = 0.205 min.

(3-hydroxy-3-methylpyrrolidin-1-yl) (4-(2-(4-((1-methyl-1H-benzo[d]imidazol-2-yl) amino) piperidin-1-yl) ethyl) phenyl) methanone (94)

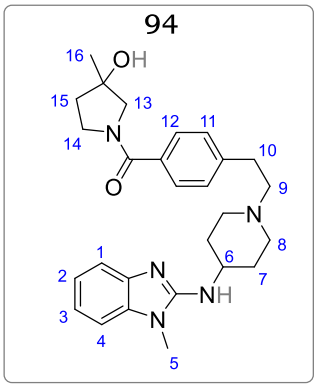

Obtained from 3-methylpyrrolidin-3-ol (0.012 g, 0.18 mmol) as a pale-yellow solid (0.054 g, 77%). m.p.: 119 – 121 °C; R_f(10% MeOH/DCM), 0.36. ^{1}H NMR (600 MHz, Methanol-d_4) δ 7.90 (d, J = 8.1 Hz, 2H, H^{12}), 7.41 (d, J = 8.1 Hz, 2H, H^{11}), 7.18 (dd, J = 7.8, 1.4 Hz, 1H, H^1), 7.09 (dd, J = 7.9, 1.3 Hz, 1H, H^4), 6.97 (ddd, J = 7.8, 7.4, 1.3 Hz, 1H, H^2), 6.84 (ddd, J = 7.9, 7.4, 1.4 Hz, 1H, H^3), 3.91 – 3.69 (m, 4H, H^{13,14}), 3.58 (tt, J = 11.2, 4.2 Hz, 1H, H^6), 3.52 (s, 3H, H^5), 3.24 – 3.11 (m, 2H, H^{8e}), 2.88 – 2.82 (m, 2H, H^9), 2.78 – 2.62 (m, 3H, H^{10,16}), 2.38 – 2.29 (m, 2H, H^{8a}), 2.23 (ddd, J = 14.0, 9.3, 7.2 Hz, H^{15e}), 2.18 – 2.06 (m, 3H, H^{7e,15a}), 1.70 – 1.62 (m, 2H, H^{7a}), 1.39 (s, 3H, H^{16}). ^{13}C NMR (151 MHz, Methanol-d_4) δ 172.58, 145.19, 141.02, 139.33, 136.12, 129.81 (2C), 128.78 (2C), 122.66, 120.43, 119.05, 113.73, 105.80, 77.24, 70.03, 63.11, 60.34, 52.97 (2C), 51.44, 48.10, 43.33, 34.17, 30.28 (2C), 25.09. LC-MS (APCI$^+$/ESI): found m/z = 462.3 [M+H]$^+$ (cal. for $C_{27}H_{35}N_5O_2$, 461.28). Purity: 98%, t_R = 0.173 min.

(S)-1-(4-(2-(4-((1-methyl-1H-benzo[d]imidazol-2-yl) amino) piperidin-1-yl) ethyl) benzoyl) pyrrolidine-3-carbonitrile (95)

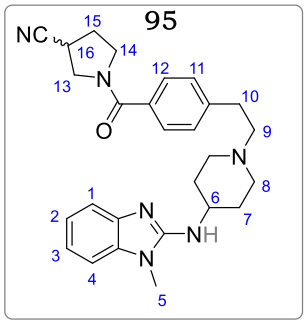

Obtained from (S)-pyrrolidin-3-carbonitrile (0.017 g, 0.18 mmol) as a pale-yellow solid (0.048 g, 69%). m.p.: 109 – 110 °C; R_f(10% MeOH/DCM), 0.38. ^{1}H NMR (600 MHz, Methanol-d_4) δ 7.89 (d, J = 8.1 Hz, 2H, H^{12}), 7.39 (d, J = 8.1 Hz, 2H, H^{11}), 7.18 (dd, J = 7.8, 1.4 Hz, 1H, H^1), 7.10 (dd, J = 7.9, 1.3 Hz, 1H, H^4), 7.01 (ddd, J = 7.8, 7.4, 1.3 Hz, 1H, H^2), 6.85 (ddd, J = 7.9, 7.4, 1.4 Hz, 1H, H^3), 3.84 – 3.66 (m, 4H, H^{13,14}), 3.58 (tt, J = 11.0, 4.1 Hz, 1H, H^6), 3.51 (s, 3H, H^5), 3.23 – 3.12 (m, 2H, H^{8e}), 2.87 – 2.82 (m, 2H, H^9), 2.78 – 2.63 (m, 3H, H^{10,16}), 2.39 – 2.30 (m, 2H, H^{8a}), 2.20 (ddd, J = 13.2, 9.1, 7.1 Hz, H^{15e}), 2.17 – 2.01 (m, 3H, H^{7e,15a}), 1.71 – 1.63 (m, 2H, H^{7a}). ^{13}C NMR (151 MHz, Methanol-d_4) δ 172.19, 144.83, 141.16, 138.77, 136.28, 129.85 (2C), 128.64 (2C), 122.84, 120.50, 119.66, 118.93, 113.48, 105.64, 63.11, 60.25, 53.39 (2C), 51.34, 49.05, 48.73, 34.16, 30.88 (2C), 23.56, 22.03. LC-MS (APCI$^+$/ESI): found m/z = 457.3 [M+H]$^+$ (cal. for $C_{27}H_{32}N_6O$, 456.26). Purity: 98%, t_R = 0.149 min.

(3-hydroxypyrrolidin-1-yl)(4-(2-(4-((1-methyl-1H-benzo[d]imidazol-2-yl)amino)piperidin-1-yl)ethyl)phenyl)methanone (96)

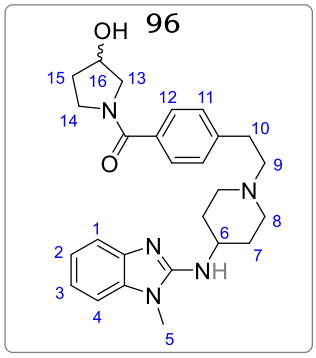

Obtained from pyrrolidin-3-ol (0.016 g, 0.18 mmol) as a yellow solid (0.035 g, 62%). m.p.: 130 – 132 °C; R_f(10% MeOH/DCM), 0.24. ^{1}H NMR (600 MHz, Methanol-d_4) δ 7.92 (d, J = 8.1 Hz, 2H, H^{12}), 7.41 (d, J = 8.1 Hz, 2H, H^{11}), 7.20 (dd, J = 7.8, 1.4 Hz, 1H, H^1), 7.08 (dd, J = 7.9, 1.3 Hz, 1H, H^4), 6.98 (ddd, J = 7.8, 7.4, 1.3 Hz, 1H, H^2), 6.83 (ddd, J = 7.9, 7.4, 1.4 Hz, 1H, H^3), 3.82 – 3.61 (m, 5H, H^{13,14,16}), 3.55 (tt, J = 11.0, 4.1 Hz, 1H, H^6), 3.49 (s, 3H, H^5), 3.19 – 3.08 (m, 2H, H^{8e}), 2.85 – 2.78 (m, 2H, H^9), 2.70 – 2.61 (m, 2H, H^{10}), 2.40 – 2.31 (m, 2H, H^{8a}), 2.18 (ddd, J = 14.0, 9.2, 6.8 Hz, H^{15e}), 2.16 – 2.00 (m, 3H, H^{7e,15a}), 1.66 – 1.58 (m, 2H, H^{7a}). ^{13}C NMR (151 MHz, Methanol-d_4) δ 175.35, 145.22, 139.58, 137.58, 129.20 (2C), 128.47 (2C), 122.23, 120.96, 119.02, 118.65, 113.79, 104.57, 64.08, 60.05, 53.32 (2C), 51.33, 49.25, 48.30, 34.49, 30.85 (2C), 23.69, 22.25. LC-MS (APCI$^+$/ESI): found m/z = 448.3 [M+H]$^+$ (cal. for $C_{26}H_{33}N_5O_2$, 447.26). Purity: 98%, t_R = 0.141 min.

(R)-(2-fluoropyrrolidin-1-yl) (4-(2-(4-((1-methyl-1H-benzo[d]imidazol-2-yl) amino) piperidin-1-yl) ethyl) phenyl) methanone (97)

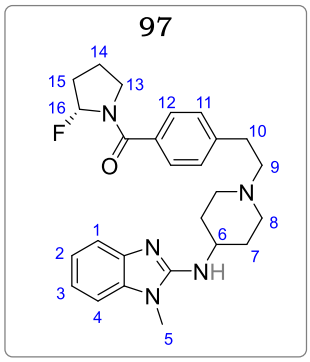

Obtained from (R)-2-fluoropyrrolidine (0.016 g, 0.18 mmol) as an off white solid (0.050 g, 74%). m.p.: 196 – 198 °C; R_f(10% MeOH/DCM), 0.59. ^{1}H NMR (600 MHz, Methanol-d_4) δ 7.90 (d, J = 8.0 Hz, 2H, H^{12}), 7.39 (d, J = 8.0 Hz, 2H, H^{11}), 7.20 (dd, J = 7.8, 1.1 Hz, 1H, H^1), 7.09 (dd, J = 7.7, 1.2 Hz, 1H, H^4), 6.97 (ddd, J = 7.8, 7.2, 1.2 Hz, 1H, H^2), 6.89 (ddd, J = 7.7, 7.2, 1.1 Hz, 1H, H^3), 5.66 (ddd, 36.8, 14.3, 4.5 Hz, 1H, H^{16}), 3.58 (tt, J = 10.9, 4.1 Hz, 1H, H^6), 3.55 – 3.40 (m, 5H, H^{5,13}), 3.18 – 3.10 (m, 2H, H^{8e}), 2.89 – 2.80 (m, 2H, H^9), 2.75 – 2.66 (m, 2H, H^{10}), 2.38 – 2.28 (m, 2H, H^{8a}), 2.20 – 2.05 (m, 5H, H^{7e,14,15}), 1.75 – 1.60 (m, 3H, H^{7a,14}). ^{13}C NMR (151 MHz, Methanol-d_4) δ 172.22, 144.64, 141.29, 139.00, 136.34, 130.55 (2C), 129.03 (2C), 122.44, 120.24, 119.22, 116.49 (d, J = 25.8 Hz), 113.64, 105.87, 63.29, 60.18, 52.72 (2C), 51.73, 45.78, 34.01, 30.43 (2C), 28.87, 19.23. LC-MS (APCI$^+$/ESI): found m/z = 450.2 [M+H]$^+$ (cal. for $C_{26}H_{32}FN_5O$, 449.26). Purity: 98%, t_R = 2.014 min.

(4-(2-(4-((1-methyl-1H-benzo[d]imidazol-2-yl) amino) piperidin-1-yl) ethyl) phenyl) (2-oxa-6-azaspiro [3.4] octan-6-yl) methanone (98)

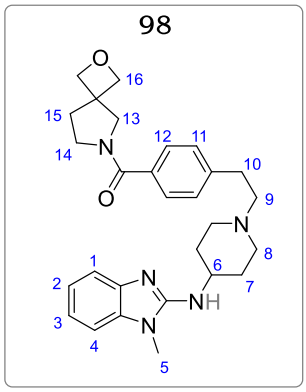

Obtained from 2-oxa-6-azaspiro[3.4]octane (0.020 g, 0.18 mmol) as a light-yellow solid (0.055 g, 77%). m.p.: 154 – 156 °C; R_f(10% MeOH/DCM), 0.48. ^{1}H NMR (600 MHz, Methanol-d_4) δ 7.89 (d, J = 8.2 Hz, 2H, H^{12}), 7.39 (d, J = 8.2 Hz, 2H, H^{11}), 7.20 (dd, J = 8.0, 1.3 Hz, 1H, H^1), 7.11 (dd, J = 7.8, 1.3 Hz, 1H, H^4), 6.97 (ddd, J = 8.0, 7.6, 1.3 Hz, 1H, H^2), 6.85 (ddd, J = 7.8, 7.6, 1.3 Hz, 1H, H^3), 4.39 (s, 4H, H^{16}), 3.87 – 3.71 (m, 4H, H^{13,14}), 3.60 (tt, J = 10.9, 4.3 Hz, 1H, H^6), 3.52 (s, 3H, H^5), 3.14 – 3.06 (m, 2H, H^8), 2.83 – 2.74 (m, 2H, H^9), 2.70 – 2.62 (m, 2H, H^{10}), 2.34 – 2.22 (m, 2H, H^8), 2.11 – 2.03 (m, 2H, H^7), 1.72 – 1.63 (m, 2H, H^7), 1.52 (t, J = 7.1 Hz, 2H, H^{15}). ^{13}C NMR (151 MHz, Methanol-d_4) δ 172.23, 143.67, 141.55, 138.32, 136.76, 130.34 (2C), 128.67 (2C), 122.53, 120.39, 119.11, 113.69, 105.77, 82.09 (2C), 60.43, 56.87, 55.03, 53.16 (2C), 51.20, 46.46, 43.28, 37.12, 34.04, 33.03, 30.21 (2C). LC-MS (APCI$^+$/ESI): found m/z = 474.3 [M+H]$^+$ (cal. for $C_{28}H_{35}N_5O_2$, 473.28). Purity: 99%, t_R = 0.179 min.

Tert-butyl 6-(4-(2-(4-((1-methyl-1H-benzo[d]imidazol-2-yl) amino) piperidin-1-yl) ethyl) benzoyl)-2,6-diazaspiro [3.4] octane-2-carboxylate (99)

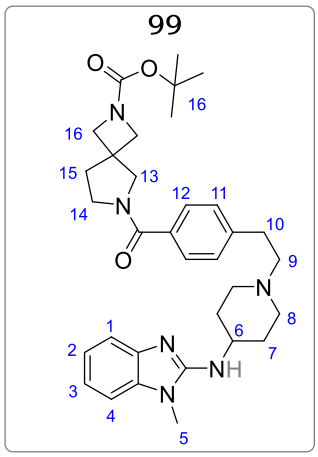

Obtained from tert-butyl 2,6-diazaspiro[3.4]octane-2-carboxylate (0.038 g, 0.18 mmol) as a pale yellow solid (0.073 g, 85%). m.p.: 197 – 199 °C; R_f (10% MeOH/DCM), 0.45. ^{1}H NMR (600 MHz, Methanol-d_4) δ 7.89 (d, J = 8.0 Hz, 2H, H^{12}), 7.40 (d, J = 8.0 Hz, 2H, H^{11}), 7.18 (dd, J = 8.0, 1.3 Hz, 1H, H^1), 7.10 (dd, J = 7.9, 1.3 Hz, 1H, H^4), 6.98 (ddd, J = 8.0, 7.8, 1.2 Hz, 1H, H^2), 6.86 (ddd, J = 7.9, 7.8, 1.2 Hz, 1H, H^3), 3.85 – 3.68 (m, 8H, H^{13,14,16}), 3.56 (tt, J = 10.8, 4.1 Hz, 1H, H^6), 3.51 (s, 3H, H^5), 3.21 – 3.11 (m, 2H, H^{8e}), 2.88 – 2.80 (m, 2H, H^9), 2.74 – 2.65 (m, 2H, H^{10}), 2.39 – 2.29 (m, 2H, H^{8a}), 2.18 – 2.07 (m, 2H, H^{7e}), 1.83 – 1.74 (m, 2H, H^{7a}), 1.67 (t, J = 6.8 Hz, 2H, H^{15}), 1.25 (s, 9H, H^{17}). ^{13}C NMR (151 MHz, Methanol-d_4) δ 172.51, 154.09, 142.97, 141.25, 139.08, 136.11, 130.33 (2C), 128.45 (2C), 122.40, 120.19, 119.02, 113.44, 105.75, 81.77, 60.30, 56.18, 55.02, 53.69 (2C), 53.36 (2C), 51.87, 46.71, 39.68, 37.15, 34.19, 30.35 (2C), 18.59 (3C). LC-MS (APCI$^+$/ESI): found m/z = 573.4 $[M+H]^+$ (cal. for $C_{33}H_{44}N_6O_3$, 572.35). Purity: 98%, t_R = 2.210 min.

(4-(2-(4-((1-methyl-1H-benzo[d]imidazol-2-yl) amino) piperidin-1-yl) ethyl) phenyl) (2,6-diazaspiro [3.4] octan-6-yl) methanone (100)

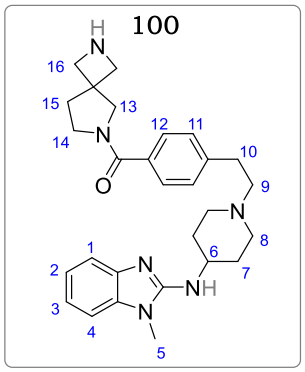

Following procedure 3, obtained from 99 (0.035 g, 0.06 mmol) as a pale-yellow solid (0.025 g, 89%). m.p.: 89 – 90 °C; R_f (10% MeOH/DCM), 0.28. ^{1}H NMR (600 MHz, Methanol-d_4) δ 7.91 (d, J = 8.1 Hz, 2H, H^{12}), 7.38 (d, J = 8.1 Hz, 2H, H^{11}), 7.20 (dd, J = 7.9, 1.3 Hz, 1H, H^1), 7.11 (dd, J = 7.9, 1.3 Hz, 1H, H^4), 6.98 (ddd, J = 7.9, 7.8, 1.3 Hz, 1H, H^2), 6.87 (ddd, J = 7.9, 7.8, 1.3 Hz, 1H, H^3), 3.81 – 3.69 (m, 8H, H^{13,14,16}), 3.59 (tt, J = 10.8, 4.1 Hz, 1H, H^6), 3.52 (s, 3H, H^5), 3.20 – 3.11 (m, 2H, H^{8e}), 2.88 – 2.79 (m, 2H, H^9), 2.73 – 2.64 (m, 2H, H^{10}), 2.39 – 2.30 (m, 2H, H^{8a}), 2.18 – 2.06 (m, 2H, H^{7e}), 1.74 – 1.64 (m, 2H, H^{7a}), 1.41 (t, J = 6.9 Hz, 2H, H^{15}). ^{13}C NMR (151 MHz, Methanol-d_4) δ 172.45, 143.34, 141.22, 138.88, 136.12, 130.29 (2C), 128.57 (2C), 122.49, 120.21, 119.98, 113.66, 105.81, 60.25, 56.12, 55.11, 53.67 (2C), 53.22 (2C), 51.36, 46.77, 39.59,

37.23, 34.10, 33.23, 30.30 (2C). LC-MS (APCI$^+$/ESI): found m/z = 473.3 $[M+H]^+$ (cal. for $C_{28}H_{36}N_6O$, 472.30). Purity: 98%, t_R = 0.120 min.

(4-(2-(4-((1-methyl-1H-benzo[d]imidazol-2-yl) amino) piperidin-1-yl) ethyl) phenyl) (morpholino) methanone (101)

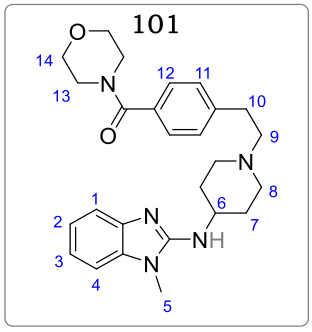

Obtained from morpholine (0.016 g, 0.18 mmol) as a pale-yellow solid (0.051 g, 76%). m.p.: 110 – 111 °C; R_f (10% MeOH/DCM), 0.39. ^{1}H NMR (600 MHz, Methanol-d_4) δ 7.93 (d, J = 8.2 Hz, 2H, H^{12}), 7.42 (d, J = 8.2 Hz, 2H, H^{11}), 7.19 (dd, J = 8.0, 1.3 Hz, 1H, H^1), 7.10 (dd, J = 7.9, 1.3 Hz, 1H, H^4), 7.04 (ddd, J = 8.0, 7.3, 1.3 Hz, 1H, H^2), 6.88 (ddd, J = 7.9, 7.3, 1.3 Hz, 1H, H^3), 3.83 – 3.78 (m, 4H, H^{13}), 3.75 – 3.71 (m, 4H, H^{14}), 3.61 (tt, J = 10.9, 4.3 Hz, 1H, H^6), 3.52 (s, 3H, H^5), 3.20 – 3.13 (m, 2H, H^8), 2.89 – 2.81 (m, 2H, H^9), 2.76 – 2.65 (m, 2H, H^{10}), 2.39 – 2.30 (m, 2H, H^8), 2.18 – 2.09 (m, 2H, H^7), 1.73 – 1.65 (m, 2H, H^7). ^{13}C NMR (151 MHz, Methanol-d_4) δ 168.87, 145.65, 141.11, 138.92, 135.48, 130.12 (2C), 128.23 (2C), 122.85, 120.33, 119.29, 113.61, 105.30, 63.82, 60.17, 53.24 (2C), 52.81 (2C), 51.24, 45.23 (2C), 34.01, 30.53 (2C). LC-MS (APCI$^+$/ESI): found m/z = 448.2 $[M+H]^+$ (cal. for $C_{26}H_{33}N_5O_2$, 447.26). Purity: 99%, t_R = 0.125 min.

Tert-butyl 4-(4-(2-(4-((1-methyl-1H-benzo[d]imidazol-2-yl) amino) piperidin-1-yl) ethyl) benzoyl) piperazine-1-carboxylate (102)

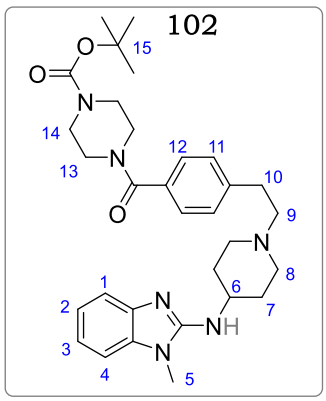

Obtained from *tert*-butyl piperazine-1-carboxylate (0.034 g, 0.18 mmol) as a pale off white solid (0.077 g, 93%). m.p.: 114 – 116 °C; R_f (10% MeOH/DCM), 0.52. ^{1}H NMR (600 MHz, Methanol-d_4) δ 7.90 (d, J = 8.1 Hz, 2H, H^{12}), 7.39 (d, J = 8.1 Hz, 2H, H^{11}), 7.19 (dd, J = 7.9, 1.3 Hz, 1H, H^1), 7.10 (dd, J = 8.0, 1.3 Hz, 1H, H^4), 6.98 (ddd, J = 7.9, 7.8, 1.3 Hz, 1H, H^2), 6.86 (ddd, J = 8.0, 7.8, 1.3 Hz, 1H, H^3), 3.80 – 3.69 (br-s, 8H, H^{13,14}), 3.60 (tt, J = 10.9, 4.3 Hz, 1H, H^6), 3.52 (s, 3H, H^5), 3.20 – 3.10 (m, 2H, H^{8e}), 2.89 – 2.81 (m, 2H, H^9), 2.76 – 2.65 (m, 2H, H^{10}), 2.38 – 2.30 (m, 2H, H^{8a}), 2.18 – 2.04 (m, 2H, H^{7e}), 1.73 – 1.65 (m, 2H, H^{7a}), 1.43 (s, 9H, H^{15}). ^{13}C NMR (151 MHz, Methanol-d_4) δ 169.88, 154.87, 145.39, 141.17, 138.87, 136.34, 130.25 (2C), 128.51 (2C), 122.26, 120.38, 119.38, 113.78, 105.88, 80.02, 63.23, 60.18, 53.39 (2C), 52.92 (2C), 51.34, 45.45 (2C), 34.03, 30.32 (2C), 19.58 (3C). LC-MS

(APCI$^+$/ESI): found m/z = 547.3 $[M+H]^+$ (cal. for $C_{31}H_{42}N_6O_3$, 546.33). Purity: 98%, t_R = 2.212 min.

(4-(2-(4-((1-methyl-1H-benzo[d]imidazol-2-yl) amino) piperidin-1-yl) ethyl) phenyl) (piperazin-1-yl) methanone (103)

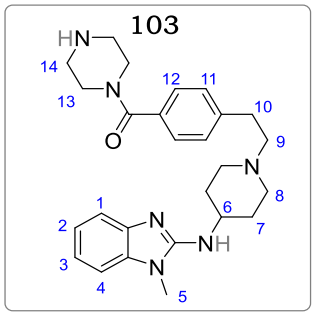

Following general procedure 2, obtained from **102** (0.040 g, 0.07 mmol) as an off white solid (0.030 g, 91%). m.p.: 108 – 109 °C; R_f (10% MeOH/DCM), 0.28. ^{1}H NMR (600 MHz, Methanol-d_4) δ 7.92 (d, J = 8.2 Hz, 2H, H^{12}), 7.40 (d, J = 8.2 Hz, 2H, H^{11}), 7.18 (dd, J = 7.9, 1.3 Hz, 1H, H^1), 7.09 (dd, J = 7.7, 1.3 Hz, 1H, H^4), 6.99 (ddd, J = 7.9, 7.4, 1.3 Hz, 1H, H^2), 6.86 (ddd, J = 7.7, 7.4, 1.3 Hz, 1H, H^3), 3.81 – 3.75 (m, 4H, H^{13}), 3.73 – 3.68 (m, 4H, H^{14}), 3.59 (tt, J = 10.9, 4.3 Hz, 1H, H^6), 3.52 (s, 3H, H^5), 3.20 – 3.11 (m, 2H, H^{8e}), 2.88 – 2.81 (m, 2H, H^9), 2.75 – 2.65 (m, 2H, H^{10}), 2.38 – 2.29 (m, 2H, H^{8a}), 2.18 – 2.05 (m, 2H, H^{7e}), 1.73 – 1.64 (m, 2H, H^{7a}). ^{13}C NMR (151 MHz, Methanol-d_4) δ 169.82, 145.44, 141.20, 138.98, 136.89, 130.33 (2C), 128.55 (2C), 122.98, 120.45, 119.30, 113.65, 105.76, 63.44, 60.20, 53.33 (2C), 52.88 (2C), 51.87, 45.77 (2C), 34.09, 30.44 (2C). LC-MS (APCI$^+$/ESI): found m/z = 447.3 $[M+H]^+$ (cal. for $C_{26}H_{34}N_6O$, 446.28). Purity: 98%, t_R = 0.122 min.

(4-(2-(4-((1-methyl-1H-benzo[d]imidazol-2-yl) amino) piperidin-1-yl) ethyl) phenyl) (4-methylpiperazin-1-yl) methanone (104)

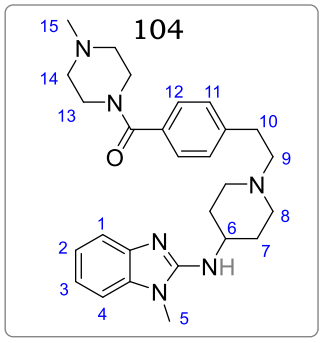

Obtained from 1-methylpiperazine (0.018 g, 0.18 mmol) as a pale-yellow solid (0.054 g, 77%). m.p.: 114 – 115 °C; R_f (10% MeOH/DCM), 0.36. ^{1}H NMR (600 MHz, Methanol-d_4) δ 7.93 (d, J = 8.3 Hz, 2H, H^{12}), 7.38 (d, J = 8.3 Hz, 2H, H^{11}), 7.16 (dd, J = 8.1, 1.3 Hz, 1H, H^1), 7.08 (dd, J = 7.9, 1.3 Hz, 1H, H^4), 6.97 (ddd, J = 8.1, 7.3, 1.3 Hz, 1H, H^2), 6.85 (ddd, J = 7.9, 7.3, 1.3 Hz, 1H, H^3), 3.60 (tt, J = 10.8, 4.1 Hz, 1H, H^6), 3.58 – 3.45 (m, 7H, H^{5,13}), 3.29 – 3.10 (m, 6H, H^{8e,14}), 2.89 – 2.80 (m, 2H, H^9), 2.72 – 2.64 (m, 2H, H^{10}), 2.37 – 2.30 (m, 2H, H^{8a}), 2.20 (s, 3H, H^{15}), 2.15 – 2.06 (m, 2H, H^{7e}), 1.73 – 1.67 (m, 2H, H^{7a}). ^{13}C NMR (151 MHz, Methanol-d_4) δ 169.11, 145.32, 142.01, 138.99, 135.29, 130.05 (2C), 128.87 (2C), 122.82, 120.53, 119.23, 113.54, 105.48, 63.79, 60.18, 53.28 (2C), 51.28 (2C), 51.18, 50.78 (2C), 47.03, 34.33, 30.59 (2C). LC-MS

(APCI$^+$/ESI): found m/z = 461.3 $[M+H]^+$ (cal. for $C_{27}H_{36}N_6O$, 460.30). Purity: 99%, t_R = 0.120 min.

(1,1-dioxidothiomorpholino) (4-(2-(4-((1-methyl-1H-benzo[d]imidazol-2-yl) amino) piperidin-1-yl) ethyl) phenyl) methanone (105)

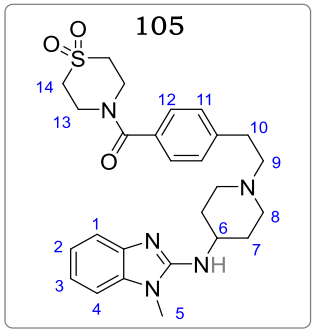

Obtained from thiomorpholine-1,1-dioxide (0.024 g, 0.18 mmol) as a pale white solid (0.055 g, 74%). m.p.: 239 – 241 °C; R_f(10% MeOH/DCM), 0.21. ^{1}H NMR (600 MHz, Methanol-d_4) δ 7.95 (d, J = 8.1 Hz, 2H, H^{12}), 7.42 (d, J = 8.1 Hz, 2H, H^{11}), 7.21 (dd, J = 7.7, 1.2 Hz, 1H, H^1), 7.11 (dd, J = 7.9, 1.2 Hz, 1H, H^4), 7.02 (ddd, J = 7.7, 7.2, 1.2 Hz, 1H, H^2), 6.87 (ddd, J = 7.9, 7.2, 1.2 Hz, 1H, H^3), 3.79 – 3.75 (m, 4H, H^{13}), 3.73 – 3.70 (m, 4H, H^{14}), 3.62 (tt, J = 11.0, 4.3 Hz, 1H, H^6), 3.52 (s, 3H, H^5), 3.19 – 3.11 (m, 2H, H^{8e}), 2.90 – 2.83 (m, 2H, H^9), 2.75 – 2.67 (m, 2H, H^{10}), 2.39 – 2.29 (m, 2H, H^{8a}), 2.18 – 2.10 (m, 2H, H^{7e}), 1.73 – 1.64 (m, 2H, H^{7a}). ^{13}C NMR (151 MHz, Methanol-d_4) δ 168.93, 145.51, 141.23, 138.95, 135.40, 130.08 (2C), 128.09 (2C), 122.66, 120.27, 119.21, 113.67, 105.29, 63.72, 60.11, 53.33 (2C), 52.87 (2C), 51.20, 45.51 (2C), 33.99, 30.52 (2C). LC-MS (APCI$^+$/ESI): found m/z = 496.2 $[M+H]^+$ (cal. for $C_{26}H_{33}N_5O_3S$, 495.23). Purity: 99%, t_R = 0.140 min.

((1R,4R)-2-oxa-5-azabicyclo [2.2.1] heptan-5-yl) (4-(2-(4-((1-methyl-1H-benzo[d]imidazol-2-yl) amino) piperidin-1-yl) ethyl) phenyl) methanone (106)

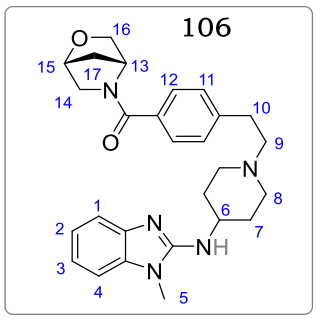

Obtained from (1R,4R)-2-oxa-5-azabicyclo[2.2.1] heptane (0.018 g, 0.18 mmol) as a pale-yellow solid (0.049 g, 71%). m.p.: 113 – 115 °C; R_f(10% MeOH/DCM), 0.44. ^{1}H NMR (600 MHz, Methanol-d_4) δ 7.94 (d, J = 8.0 Hz, 2H, H^{12}), 7.43 (d, J = 8.0 Hz, 2H, H^{11}), 7.21 (dd, J = 7.9, 1.3 Hz, 1H, H^1), 7.12 (dd, J = 7.9, 1.2 Hz, 1H, H^4), 7.06 (ddd, J = 7.9, 7.1, 1.2 Hz, 1H, H^2), 6.87 (ddd, J = 7.9, 7.1, 1.3 Hz, 1H, H^3), 4.41 – 4.22 (m, 2H, $H^{14e,15,16e}$), 3.89 – 3.82 (m, 2H, $H^{13,14a,16a}$), 3.62 (tt, J = 11.1, 4.4 Hz, 1H, H^6), 3.52 (s, 3H, H^5), 3.20 – 3.12 (m, 2H, H^{8e}), 2.90 – 2.82 (m, 2H, H^9), 2.77 – 2.68 (m, 2H, H^{10}), 2.40 – 2.31 (m, 2H, H^{8a}), 2.18 – 2.09 (m, 3H, $H^{7,17}$), 1.74 – 1.61 (m, 3H, $H^{7,17}$). ^{13}C NMR (151 MHz, Methanol-d_4) δ 160.86, 146.03, 141.34, 138.26, 135.38, 128.11 (2C), 127.23 (2C), 121.98, 120.34, 119.20, 113.71, 105.44, 82.11, 75.77, 63.88, 61.33, 60.15, 58.09, 52.93 (2C),

51.24, 39.54, 33.93, 30.48 (2C). LC-MS (APCI$^+$/ESI): found m/z = 460.2 $[M+H]^+$ (cal. for $C_{27}H_{33}N_5O_2$, 459.26). Purity: 98%, t_R = 0.148 min.

Tert-butyl (R)-2-methyl-4-(4-(2-(4-((1-methyl-1H-benzo[d]imidazol-2-yl) amino) piperidin-1-yl) ethyl) benzoyl) piperazine-1-carboxylate (107)

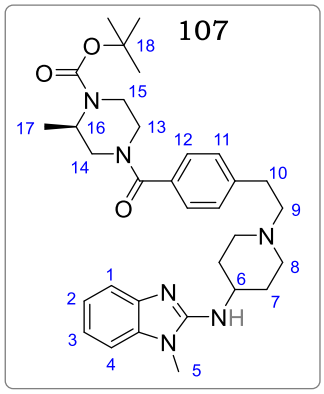

Obtained from tert-butyl (R)-2-methylpiperazine-1-carboxylate (0.036 g, 0.18 mmol) as a cream white solid (0.075 g, 88%). m.p.: 112 – 113 °C; R_f(10% MeOH/DCM), 0.51. ^{1}H NMR (600 MHz, Methanol-d_4) δ 7.90 (d, J = 8.2 Hz, 2H, H^{12}), 7.36 (d, J = 8.2 Hz, 2H, H^{11}), 7.19 (dd, J = 7.8, 1.3 Hz, 1H, H^1), 7.10 (dd, J = 8.0, 1.2 Hz, 1H, H^4), 6.96 (ddd, J = 7.8, 7.3, 1.2 Hz, 1H, H^2), 6.89 (ddd, J = 8.0, 7.3, 1.3 Hz, 1H, H^3), 4.59 (ddq, J = 14.2, 9.2, 6.9 Hz, 1H, H^{16}), 3.60 (tt, J = 11.0, 4.3 Hz, 1H, H^6), 3.52 (s, 3H, H^5), 3.44 – 3.37 (m, 2H, H^{15}), 3.27 – 3.18 (m, 4H, H^{13,14}), 3.12 – 3.05 (m, 2H, H^{8e}), 2.99 – 2.88 (m, 2H, H^9), 2.76 – 2.63 (m, 2H, H^{10}), 2.43 – 2.30 (m, 2H, H^{8a}), 2.19 – 2.10 (m, 2H, H^{7e}), 1.76 – 1.66 (m, 2H, H^{7a}), 1.48 (s, 9H, H^{18}), 1.22 (d, J = 6.9 Hz, 3H, H^{17}). ^{13}C NMR (151 MHz, Methanol-d_4) δ 168.95, 152.09, 146.08, 140.21, 138.64, 135.27, 130.18 (2C), 127.45 (2C), 122.31, 120.22, 119.25, 113.75, 105.23, 80.03, 58.71, 54.10, 53.25 (2C), 50.40, 49.01, 48.95, 42.88, 36.78, 34.59, 30.59 (2C), 23.55 (3C), 18.04. LC-MS (APCI$^+$/ESI): found m/z = 561.4 $[M+H]^+$ (cal. for $C_{32}H_{44}N_6O_3$, 560.35). Purity: 98%, t_R = 2.313 min.

(R)-(4-(2-(4-((1-methyl-1H-benzo[d]imidazol-2-yl) amino) piperidin-1-yl) ethyl) phenyl) (3-methylpiperazin-1-yl) methanone (108)

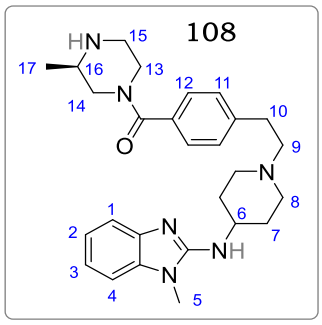

Following general procedure 2, obtained from **107** (0.035 g, 0.06 mmol) as an off white solid (0.025 g, 86%). m.p.: 98 – 99 °C; R_f(10% MeOH/DCM), 0.34. ^{1}H NMR (600 MHz, Methanol-d_4) δ 7.93 (d, J = 8.0 Hz, 2H, H^{12}), 7.41 (d, J = 8.0 Hz, 2H, H^{11}), 7.18 (dd, J = 7.8, 1.2 Hz, 1H, H^1), 7.11 (dd, J = 7.9, 1.2 Hz, 1H, H^4), 7.02 (ddd, J = 7.8, 7.3, 1.2 Hz, 1H, H^2), 6.87 (ddd, J = 7.9, 7.3, 1.2 Hz, 1H, H^3), 3.61 (tt, J = 10.8, 4.1 Hz, 1H, H^6), 3.51 (s, 3H, H^5), 3.40 – 3.31 (m, 1H, H^{16}), 3.25 – 3.19 (m, 4H, H^{13,14}), 3.11 – 3.05 (m, 2H, H^{8e}), 2.99 – 2.86 (m, 4H, H^{9,15}), 2.77 – 2.64 (m, 2H, H^{10}), 2.41 – 2.29 (m, 2H, H^{8a}), 2.19 – 2.11 (m, 2H, H^{7e}), 1.76 – 1.67 (m, 2H, H^{7a}), 1.08 (d, J = 6.8 Hz, 3H, H^{17}). ^{13}C NMR (151 MHz, Methanol-d_4) δ 169.55, 145.45, 140.23, 138.76, 135.33, 130.21 (2C), 127.39 (2C), 122.38,

120.25, 119.28, 113.71, 105.17, 60.66, 54.09, 53.22 (2C), 52.39, 51.53, 51.37, 43.97, 36.07, 34.46, 30.43 (2C), 14.98. LC-MS (APCI$^+$/ESI): found m/z = 461.3 $[M+H]^+$ (cal. for $C_{27}H_{36}N_6O$, 460.30). Purity: 99%, t_R = 0.212 min. Specific rotation, $[\alpha]^{25}_D$ = -8.24°.

(4-cyclopropylpiperazin-1-yl) (4-(2-(4-((1-methyl-1H-benzo[d]imidazol-2-yl) amino) piperidin-1-yl) ethyl) phenyl) methanone (109)

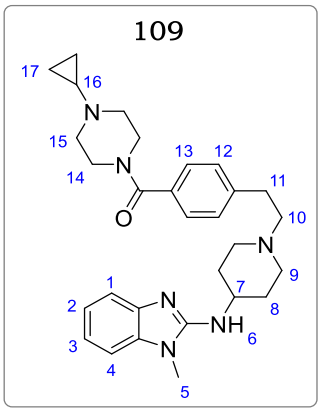

Obtained from 1-cyclopropylpiperazine (0.023 g, 0.18 mmol) as a pale-yellow solid (0.062 g, 85%). m.p.: 184 – 186 °C; R_f(10% MeOH/DCM), 0.50. ^{1}H NMR (300 MHz, DMSO-d_6) δ 7.32 (s, 4H, H^{12,13}), 7.19 (dd, J = 7.6, 1.2 Hz, 1H, H^1), 7.13 (dd, J = 7.4, 1.6 Hz, 1H, H^4), 7.02 – 6.94 (m, 2H, H^{3,4}), 6.49 (d, J = 7.3 Hz, 2H, H^6), 3.80 – 3.71 (m, 2H, H^{7,16}), 3.54 – 3.47 (m, 5H, H^{5,9e}), 2.88 – 2.81 (m, 4H, H^{10,11}), 2.79 – 2.71 (m, 2H, H^{9a}), 2.41 – 2.28 (br-s, 8H, H^{14,15}), 2.25 – 2.18 (m, 4H, H^{17}), 2.10 – 2.01 (m, 2H, H^{8e}), 1.70 – 1.62 (m, 2H, H^{7a}), 1.22 – 1.13 (dd, J = 13.9, 7.2 Hz, 2H, H^{16}). ^{13}C NMR (151 MHz, Methanol-d_4) δ 171.58, 153.28, 139.56, 134.01, 133.56, 128.54 (2C), 127.84 (2C), 122.38, 121.97, 113.85, 107.52, 58.08, 52.47, 48.95 (4C), 43.58 (2C), 37.56 (2C), 30.56, 29.35, 27.44, 15.18 (2C). LC-MS (APCI$^+$/ESI): found m/z = 487.3 $[M+H]^+$ (cal. for $C_{29}H_{38}N_6O$, 486.31). Purity: 98%, t_R = 0.181 min.

(hexahydropyrrolo [1,2-a] pyrazin-2(1H)-yl) (4-(2-(4-((1-methyl-1H-benzo[d]imidazol-2-yl) amino) piperidin-1-yl) ethyl) phenyl) methanone (110)

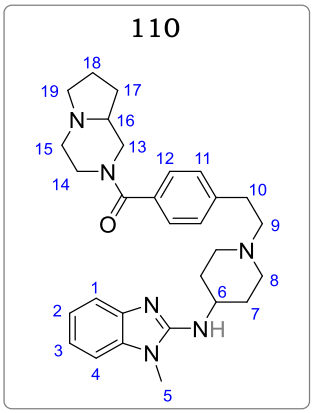

Obtained from octahydropyrrolo[1,2-a]pyrazine (0.023 g, 0.18 mmol) as an off white solid (0.054 g, 73%). m.p.: 85 – 87 °C; R_f (10% MeOH/DCM), 0.25. ^{1}H NMR (600 MHz, Methanol-d_4) δ 7.94 (d, J = 8.0 Hz, 2H, H^{12}), 7.47 (d, J = 8.0 Hz, 2H, H^{11}), 7.18 (dd, J = 7.8, 1.3 Hz, 1H, H^1), 7.09 (dd, J = 8.0, 1.2 Hz, 1H, H^4), 6.96 (ddd, J = 7.8, 7.3, 1.2 Hz, 1H, H^2), 6.87 (ddd, J = 8.0, 7.3, 1.3 Hz, 1H, H^3), 3.84 (tt, J = 10.9, 4.2 Hz, 1H, H^6), 3.52 (s, 3H, H^5), 3.31 – 3.20 (m, 4H, H^{13,14}), 3.12 – 3.05 (m, 2H, H^{8e}), 3.00 – 2.81 (m, 5H, H^{9,15,16}), 2.77 – 2.65 (m, 2H, H^{10}), 2.46 – 2.24 (m, 2H, H^{8a,19}), 2.18 – 2.11 (m, 2H, H^7), 1.77 – 1.61 (m, 4H, H^{7,18,17}), 1.54 – 1.41 (m, 2H, H^{17,18}). ^{13}C NMR (151 MHz, Methanol-d_4) δ 168.92, 145.22, 141.03, 138.53, 135.05, 130.10 (2C), 127.30 (2C), 122.38, 120.33, 119.27, 113.82, 105.31, 67.33, 60.08, 55.11, 53.12 (2C),

51.20, 50.17, 46.25, 47.05, 36.07, 34.34, 30.37 (2C), 27.01, 22.37. LC-MS (APCI$^+$/ESI): found m/z = 487.3 $[M+H]^+$ (cal. for $C_{29}H_{38}N_6O$, 486.31). Purity: 98%, t_R = 0.193 min.

(1,4-diazepan-1-yl)(4-(2-(4-((1-methyl-1H-benzo[d]imidazol-2-yl)amino)piperidin-1-yl)ethyl)phenyl)methanone (111)

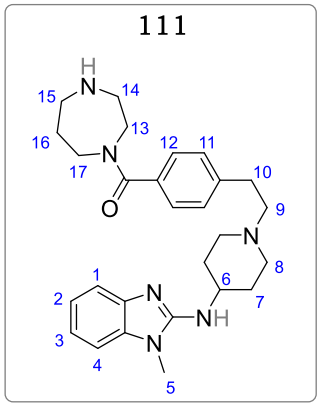

Obtained from azepane (0.018 g, 0.18 mmol) as a pale-yellow solid (0.035 g, 51%). m.p.: 185 – 186 °C; R_f(10% MeOH/DCM), 0.38. ^{1}H NMR (600 MHz, Methanol-d_4) δ 7.98 (d, J = 8.2 Hz, 2H, H^{12}), 7.46 (d, J = 8.2 Hz, 2H, H^{11}), 7.26 (dd, J = 7.8, 1.3 Hz, 1H, H^1), 7.11 (dd, J = 8.0, 1.2 Hz, 1H, H^4), 7.04 (ddd, J = 7.8, 7.2, 1.2 Hz, 1H, H^2), 6.89 (ddd, J = 8.0, 7.2, 1.3 Hz, 1H, H^3), 3.82 (tt, J = 10.8, 4.4 Hz, 1H, H^6), 3.58 – 3.31 (m, 7H, H^{5,13,17}), 3.20 – 3.07 (m, 4H, H^{8,14,15}), 2.91 – 2.88 (m, 2H, H^9), 2.78 – 2.67 (m, 2H, H^{10}), 2.40 – 2.26 (m, 4H, H^{8,14,15}), 2.19 – 2.12 (m, 2H, H^7), 1.77 – 1.68 (m, 4H, H^{7,16}). ^{13}C NMR (151 MHz, Methanol-d_4) δ 168.93, 145.34, 141.88, 139.25, 133.44, 130.11 (2C), 127.23 (2C), 122.27, 120.18, 119.13, 113.57, 105.78, 60.71, 53.20 (2C), 52.19, 51.60, 48.22, 48.08, 45.93, 36.08, 34.41, 30.51 (2C), 27.77. LC-MS (APCI$^+$/ESI): found m/z = 461.3 $[M+H]^+$ (cal. for $C_{27}H_{36}N_6O$, 460.30). Purity: 99%, t_R = 153 min.

(5-(4-(2-(4-((1-methyl-1H-benzo[d]imidazol-2-yl) amino) piperidin-1-yl) ethyl) phenyl)-1,2,4-oxadiazol-3-yl) methanol (115)

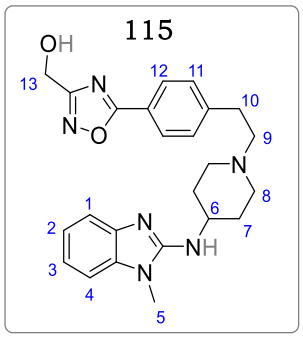

Obtained from **112c** (0.016 g, 0.18 mmol) as a cream white solid (0.029 g, 44% over two steps). m.p.: 105 – 107 °C; R_f (10% MeOH/DCM), 0.24. ^{1}H NMR (600 MHz, Methanol-d_4) δ 8.04 (d, J = 8.2 Hz, 2H, H^{12}), 7.49 (d, J = 8.2 Hz, 2H, H^{11}), 7.29 (dd, J = 7.8, 1.2 Hz, 1H, H^1), 7.10 (dd, J = 8.0, 1.2 Hz, 1H, H^4), 7.06 (ddd, J = 7.8, 7.2, 1.0 Hz, 1H, H^2), 6.96 (ddd, J = 8.0, 7.2, 1.0 Hz, 1H, H^3), 5.03 (d, J = 4.8 Hz, 2H, H^{13}), 3.80 (tt, J = 10.8, 4.3 Hz, 1H, H^6), 3.53 (s, 3H, H^5), 3.14 – 3.09 (m, 2H, H^8), 3.00 – 2.90 (m, 2H, H^9), 2.76 – 2.65 (m, 2H, H^{10}), 2.34 – 2.29 (m, 2H, H^8), 2.17 – 2.11 (m, 2H, H^7), 1.73 – 1.64 (m, 2H, H^7). ^{13}C NMR (151 MHz, Methanol-d_4) δ 176.87, 159.38, 148.55, 142.01, 139.82, 135.02, 130.33 (2C), 127.66 (2C), 121.92, 120.44, 119.02, 114.21, 105.65, 59.87, 52.87 (2C), 49.54, 35.12, 32.34, 30.49 (2C), 28.33. LC-MS (APCI$^+$/ESI): found m/z = 433.2 $[M+H]^+$ (cal. For $C_{24}H_{28}N_6O_2$, 432.23). Purity: 99%, t_R = 0.176 min.

1-methyl-N-(1-(4-(3-((methylthio)methyl)-1,2,4-oxadiazol-5-yl) phenethyl) piperidin-4-yl)-1H-benzo[d]imidazol-2-amine (116)

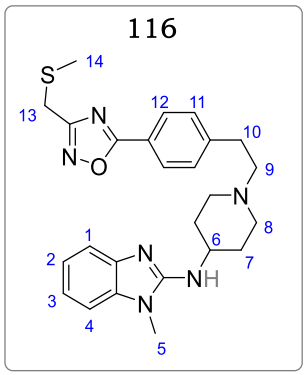

Obtained from **112d** (0.022 g, 0.18 mmol) as a pale yellow solid (0.036 g, 51% over two steps). m.p.: 66 – 68 °C; R_f (10% MeOH/DCM), 0.38. ^{1}H NMR (600 MHz, Methanol-d_4) δ 8.05 (d, J = 8.3 Hz, 2H, H^{12}), 7.50 (d, J = 8.3 Hz, 2H, H^{11}), 7.30 (dd, J = 7.8, 1.2 Hz, 1H, H^1), 7.11 (dd, J = 8.1, 1.2 Hz, 1H, H^4), 7.05 – 6.90 (m, 2H, H^{2,3}), 3.82 (tt, J = 10.9, 4.4 Hz, 1H, H^6), 3.68 (s, 2H, H^{13}), 3.52 (s, 3H, H^5), 3.14 – 3.10 (m, 2H, H^8), 3.00 – 2.92 (m, 2H, H^9), 2.77 – 2.69 (m, 2H, H^{10}), 2.35 – 2.30 (m, 2H, H^8), 2.16 – 2.03 (m, 5H, H^{7,14}), 1.72 – 1.66 (m, 2H, H^7). ^{13}C NMR (151 MHz, Methanol-d_4) δ 177.02, 159.32, 148.28, 142.54, 140.09, 134.33, 130.43 (2C), 127.79 (2C), 122.02, 120.88, 119.22, 114.27, 106.34, 59.99, 51.29 (2C), 49.99, 35.23, 32.83, 30.98 (2C), 27.87, 14.11. LC-MS (APCI$^+$/ESI): found m/z = 463.2 [M+H]$^+$ (cal. for $C_{25}H_{30}N_6OS$, 462.22). Purity: 98%, t_R = 2.034 min.

N-(1-(4-(3-((dimethylamino)methyl)-1,2,4-oxadiazol-5-yl) phenethyl) piperidin-4-yl)-1-methyl-1H-benzo[d]imidazol-2-amine (117)

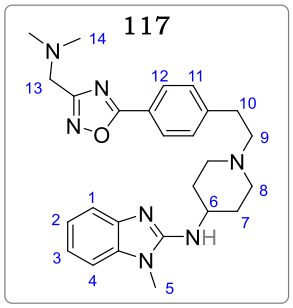

Obtained from **112e** (0.021 g, 0.18 mmol) as a pale yellow solid (0.037 g, 53% over two steps). m.p.: 119 – 120 °C; R_f (10% MeOH/DCM), 0.24. ^{1}H NMR (600 MHz, Methanol-d_4) δ 8.04 (d, J = 8.2 Hz, 2H, H^{12}), 7.57 (d, J = 8.2 Hz, 2H, H^{11}), 7.33 (dd, J = 7.8, 1.2 Hz, 1H, H^1), 7.13 (dd, J = 8.2, 1.2 Hz, 1H, H^4), 7.04 (ddd, J = 7.8, 7.1, 1.2 Hz, 1H, H^2), 6.96 (ddd, J = 8.2, 7.1, 1.2 Hz, 1H, H^3), 4.49 (s, 2H, H^{13}), 3.82 (tt, J = 10.9, 4.3 Hz, 1H, H^6), 3.53 (s, 3H, H^5), 3.09 – 3.00 (m, 2H, H^8), 2.98 – 2.89 (m, 2H, H^9), 2.75 – 2.65 (m, 2H, H^{10}), 2.37 – 2.26 (m, 3H, H^8), 2.20 – 2.09 (m, 8H, H^{7,14}), 1.71 – 1.59 (m, 2H, H^7). ^{13}C NMR (151 MHz, Methanol-d_4) δ 176.98, 169.06, 153.77, 145.12, 140.66, 133.08, 130.87 (2C), 127.88 (2C), 121.89, 120.02, 119.11, 114.83, 107.22, 61.03, 58.02, 54.33 (2C), 50.29, 46.76 (2C), 33.01, 31.37 (2C), 29.97. LC-MS (APCI$^+$/ESI): found m/z = 460.2 [M+H]$^+$ (cal. for $C_{26}H_{33}N_7O$, 459.27). Purity: 95%, t_R = 0.155 min.

N-(1-(4-(3-cyclopropyl-1,2,4-oxadiazol-5-yl) phenethyl) piperidin-4-yl)-1-methyl-1H-benzo[d]imidazol-2-amine (118)

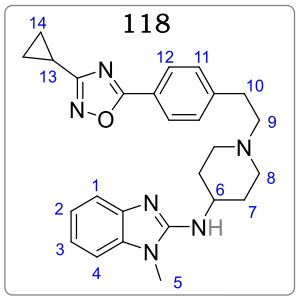

Obtained from **112f** (0.018 g, 0.18 mmol) as a pale-yellow solid (0.036 g, 56% over two steps). M.p.: 123 – 124 °C; R_f (10% MeOH/DCM), 0.39. ^{1}H NMR (600 MHz, Methanol-d_4) δ 8.05 (d, J = 8.3 Hz, 2H, H^{12}), 7.55 (d, J = 8.3 Hz, 2H, H^{11}), 7.34 (dd, J = 7.7, 1.2 Hz, 1H, H^1), 7.12 (dd, J = 8.2, 1.2 Hz, 1H, H^4), 7.05 (ddd, J = 7.7, 7.2, 1.2 Hz, 1H, H^2), 6.95 (ddd, J = 8.2, 7.2, 1.2 Hz, 1H, H^3), 3.81 (tt, J = 10.8, 4.4 Hz, 1H, H^6), 3.52 (s, 3H, H^5), 3.08 – 3.02 (m, 2H, H^8), 2.98 – 2.90 (m, 2H, H^9), 2.75 – 2.66 (m, 2H, H^{10}), 2.36 – 2.25 (m, 3H, H^{8,13}), 2.20 – 2.10 (m, 2H, H^7), 1.76 – 1.65 (m, 2H, H^7), 1.25 (dd, J = 11.3, 6.7 Hz, 2H, H^{14e}), 0.97 (dd, J = 11.3, 6.7, 2H, H^{14a}). ^{13}C NMR (151 MHz, Methanol-d_4) δ 177.04, 169.11, 153.87, 145.00, 140.43, 132.79, 130.55 (2C), 127.45 (2C), 121.65, 120.87, 119.68, 114.91, 107.33, 60.34, 54.18 (2C), 50.43, 32.09, 31.24 (2C), 30.57, 9.95 (2C), 8.78. LC-MS (APCI$^+$/ESI): found m/z = 443.2 [M+H]$^+$ (cal. For $C_{26}H_{30}N_6O$, 442.25). Purity: 98%, t_R = 2.122 min.

N-(1-(4-(3-isopropyl-1,2,4-oxadiazol-5-yl) phenethyl) piperidin-4-yl)-1-methyl-1H-benzo[d]imidazol-2-amine (119)

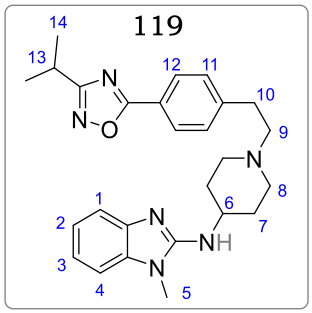

Obtained from **112g** (0.019 g, 0.18 mmol) as a light brown solid (0.041 g, 61% over two steps). M.p.: 135 – 137 °C; R_f (10% MeOH/DCM), 0.42. ^{1}H NMR (600 MHz, Methanol-d_4) δ 8.06 (d, J = 8.2 Hz, 2H, H^{12}), 7.53 (d, J = 8.2 Hz, 2H, H^{11}), 7.33 (dd, J = 7.6, 1.2 Hz, 1H, H^1), 7.11 (dd, J = 8.1, 1.2 Hz, 1H, H^4), 7.03 (ddd, J = 7.6, 7.2, 1.2 Hz, 1H, H^2), 6.97 (ddd, J = 8.1, 7.2, 1.2 Hz, 1H, H^3), 3.80 (tt, J = 10.9, 4.3 Hz, 1H, H^6), 3.52 (s, 3H, H^5), 3.21 (hept, J = 6.8 Hz, 1H, H^{13}), 3.09 – 3.02 (m, 2H, H^8), 2.99 – 2.89 (m, 2H, H^9), 2.75 – 2.67 (m, 2H, H^{10}), 2.36 – 2.24 (m, 2H, H^8), 2.19 – 2.08 (m, 2H, H^7), 1.76 – 1.62 (m, 2H, H^7), 1.22 (d, J = 6.8 Hz, 6H, H^{14}). ^{13}C NMR (151 MHz, Methanol-d_4) δ 175.44, 167.09, 155.33, 147.40, 141.09, 133.87, 130.69 (2C), 128.09 (2C), 121.88, 120.99, 120.08, 114.44, 107.28, 60.09, 54.11 (2C), 50.55, 39.85, 32.49, 31.89 (2C), 30.87, 28.76, 21.32 (2C). LC-MS (APCI$^+$/ESI): found m/z = 445.2 [M+H]$^+$ (cal. For $C_{26}H_{32}N_6O$, 444.26). Purity: 98%, t_R = 2.192 min.

N-(1-(4-(3-(tert-butyl)-1,2,4-oxadiazol-5-yl) phenethyl) piperidin-4-yl)-1-methyl-1H-benzo[d]imidazol-2-amine (120)

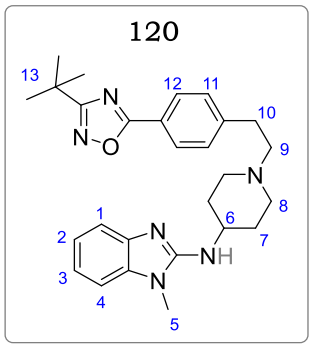

Obtained from **112h** (0.021 g, 0.18 mmol) as a light brown solid (0.046 g, 66% over two steps). M.p.: 164 – 166 °C; R_f (10% MeOH/DCM), 0.45. ^{1}H NMR (600 MHz, Methanol-d_4) δ 8.05 (d, J = 8.1 Hz, 2H, H^{12}), 7.51 (d, J = 8.1 Hz, 2H, H^{11}), 7.30 (dd, J = 7.6, 1.1 Hz, 1H, H^1), 7.11 (dd, J = 8.2, 1.2 Hz, 1H, H^4), 7.02 (ddd, J = 7.6, 7.2, 1.0 Hz, 1H, H^2), 6.98 (ddd, J = 8.2, 7.2, 1.1 Hz, 1H, H^3), 3.82 (tt, J = 10.9, 4.3 Hz, 1H, H^6), 3.53 (s, 3H, H^5), 3.12 – 3.08 (m, 2H, H^8), 2.99 – 2.91 (m, 2H, H^9), 2.75 – 2.69 (m, 2H, H^{10}), 2.35 – 2.28 (m, 2H, H^8), 2.17 – 2.10 (m, 2H, H^7), 1.74 – 1.64 (m, 2H, H^7), 1.29 (s, 9H, H^{13}). ^{13}C NMR (151 MHz, Methanol-d_4) δ 176.09, 166.66, 154.32, 147.44, 141.00, 133.93, 130.21 (2C), 127.66 (2C), 121.78, 120.93, 119.98, 114.40, 107.08, 59.73, 53.01 (2C), 50.03, 39.23, 32.45, 31.33 (2C), 30.94, 28.02 (3C). LC-MS (APCI$^+$/ESI): found m/z = 459.2 [M+H]$^+$ (cal. For $C_{27}H_{34}N_6O$, 458.28). Purity: 95%, t_R = 2.281 min.

5-(4-(2-(4-((1-methyl-1H-benzo[d]imidazol-2-yl) amino) piperidin-1-yl) ethyl) phenyl)-1,2,4-oxadiazole-3-carboxylic acid (122)

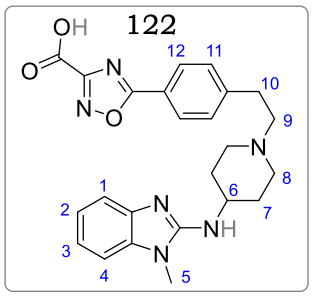

To a solution of **121** (0.040 g, 0.084 mmol) in EtOH was added 2M aqueous KOH (210 µl, 0.42 mmol). The reaction mixture was stirred at 79 °C temperature for 2 hr. After completion (monitored by TLC), EtOH was taken off *in vacuo* and the residue diluted with 1.0 ml water. The solution was then acidified to pH 2 under ice with 3N aq. HCl, and the precipitate was filtered. The product was collected after recrystallization in EtOH an off white crystalline solid (0.036 g, 96%). m.p.: 194 – 196 °C; R_f (10% MeOH/DCM), 0.05. ^{1}H NMR (600 MHz, Methanol-d_4) δ 8.03 (d, J = 8.1 Hz, 2H, H^{12}), 7.46 (d, J = 8.1 Hz, 2H, H^{11}), 7.24 (dd, J = 7.9, 1.3 Hz, 1H, H^1), 7.11 (dd, J = 8.0, 1.3 Hz, 1H, H^4), 6.97 – 6.83 (m, 2H, H^{2,3}), 3.82 (tt, J = 11.0, 4.4 Hz, 1H, H^6), 3.51 (s, 3H, H^5), 3.12 – 3.07 (m, 2H, H^8), 2.99 – 2.89 (m, 2H, H^9), 2.76 – 2.65 (m, 2H, H^{10}), 2.39 – 2.28 (m, 2H, H^8), 2.18 – 2.11 (m, 2H, H^7), 1.73 – 1.65 (m, 2H, H^7). ^{13}C NMR (151 MHz, Methanol-d_4) δ 176.09, 172.25, 169.36, 147.87, 140.33, 138.47, 134.98, 129.83 (2C), 127.22 (2C), 122.39, 120.19, 119.15, 113.88, 105.22, 60.29, 53.10 (2C), 51.51, 35.87, 34.12, 30.40

(2C). LC-MS (APCI$^+$/ESI): found m/z = 447.2 $[M+H]^+$ (cal. for $C_{24}H_{26}N_6O_3$, 446.21). Purity: 98%, t_R = 0.135 min.

N-(1-(1H-benzo[d]imidazol-2-yl)piperidin-4-yl)-7-chloroquinolin-4-amine (168)

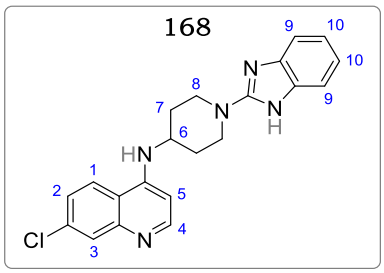

Following general procedure 12, obtained from **167** (0.080 g, 0.31 mmol) and 2-chlorobenzimidazole (0.056 g, 0.37 mmol) as a pale-yellow solid (0.087 g, 74%). m.p.: 165 – 167 °C. R_f (10% MeOH/DCM), 0.17. ^{1}H NMR (400 MHz, Methanol-d_4) δ 8.65 (d, J = 5.7 Hz, 1H, H^4), 8.11 (d, J = 8.5 Hz, 1H, H^1), 7.95 (d, J = 1.5 Hz, 1H, H^3), 7.56 – 7.49 (m, 3H, H^{2,9}), 7.20 – 7.16 (m, 2H, H^{10}), 6.92 (d, J = 5.7 Hz, 1H, H^5), 4.01 – 3.96 (m, 1H, H^6), 3.58 – 3.52 (m, 2H, H^{8e}), 3.18 – 3.11 (m, 2H, H^{8a}), 1.99 – 1.88 (m, 4H, H^7). ^{13}C NMR (151 MHz, Methanol-d_4) δ 155.85, 152.69, 148.65, 146.33, 138.77, 136.30, 132.89, 129.59, 128.94 (2C), 124.35, 116.87, 113.69, 112.08, 99.63, 53.64, 50.05 (2C), 33.39 (2C). LC-MS (APCI$^+$/ESI): found m/z = 378.1, 340.1 $[M+H]^+$ (cal. for $C_{21}H_{20}ClN_5$, 377.14, 379.13). Purity: 98%, t_R = 0.840 min.

7-chloro-N-(1-(1-methyl-1H-benzo[d]imidazol-2-yl)piperidin-4-yl)quinolin-4-amine (173)

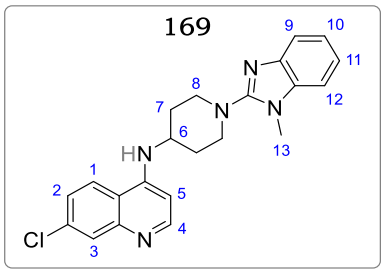

Following general procedure 12, obtained from **167** (0.080 g, 0.31 mmol) and **12b** (0.062 g, 0.37 mmol) as a pale-yellow solid (0.101 g, 83%). m.p.: 136 – 138 °C. R_f (10% MeOH/DCM), 0.19. ^{1}H NMR (400 MHz, Methanol-d_4) δ 8.59 (d, J = 5.5 Hz, 1H, H^4), 8.25 (d, J = 8.5 Hz, 1H, H^1), 7.98 (d, J = 1.2 Hz, 1H, H^3), 7.60 – 7.53 (m, 2H, H^{2,9}), 7.29 (dd, J = 7.8, 1.5 Hz, 1H, H^{12}), 6.95 – 6.88 (m, 3H, H^{5,10,11}), 4.05 – 3.97 (m, 1H, H^6), 3.83 (s, 3H, H^{13}), 3.55 (td, J = 12.5, 4.5 Hz, 2H, H^{8e}), 3.21 – 3.15 (m, 2H, H^{8a}), 1.99 – 1.90 (m, 4H, H^7). ^{13}C NMR (151 MHz, Methanol-d_4) δ 156.96, 153.64, 149.74, 145.30, 139.63, 135.05, 133.52, 131.38, 129.95, 128.33, 127.07, 119.96, 114.32, 112.54, 112.01, 98.58, 52.22, 49.63 (2C), 32.45 (2C), 26.68. LC-MS (APCI$^+$/ESI): found m/z = 392.1, 394.1 $[M+H]^+$ (cal. for $C_{22}H_{22}ClN_5$, 391.16, 393.15). Purity: 98%, t_R = 2.104 min.

7-chloro-N-(1-(1-isopropyl-1H-benzo[d]imidazol-2-yl)piperidin-4-yl)quinolin-4-amine (170)

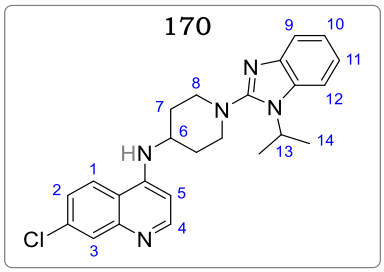

Following general procedure 12, obtained from **167** (0.080 g, 0.31 mmol) and **12c** (0.073 g, 0.37 mmol) as a pale yellow solid (0.116 g, 89%). m.p.: 119 – 121 °C. R_f (10% MeOH/DCM), 0.25. ^{1}H NMR (400 MHz, Methanol-d_4) δ 8.61 (d, J = 5.4 Hz, 1H, H^4), 8.29 (d, J = 8.2 Hz, 1H, H^1), 7.96 (d, J = 0.9 Hz, 1H, H^3), 7.58 – 7.50 (m, 2H, H^{2,9}), 7.25 (dd, J = 7.8, 1.5 Hz, 1H, H^{12}), 6.92 – 6.85 (m, 3H, H^{5,10,11}), 4.58 (hept, J = 6.5 Hz, 1H, H^{13}), 3.98 (tt, J = 10.8, 4.1 Hz, 1H, H^6), 3.85 (td, J = 13.0, 4.8 Hz, 2H, H^{8e}), 3.28 – 3.21 (m, 2H, H^{8a}), 1.97 – 1.91 (m, 4H, H^7), 1.49 (d, J = 6.5 Hz, 6H, H^{14}). ^{13}C NMR (151 MHz, Methanol-d_4) δ 155.32, 152.85, 148.88, 144.53, 140.56, 134.88, 132.23, 130.58, 129.08, 128.28, 127.70, 120.32, 115.84, 112.99, 112.03, 99.36, 53.30, 50.50 (2C), 32.85, 30.14 (2C), 18.16 (2C). LC-MS (APCI$^+$/ESI): found m/z = 420.2, 422.2 [M+H]$^+$ (cal. for $C_{24}H_{26}ClN_5$, 419.19, 421.18). Purity: 98%, t_R = 2.364 min.

7-chloro-N-(1-(1-(cyclopropylmethyl)-1H-benzo[d]imidazol-2-yl)piperidin-4-yl)quinolin-4-amine (171)

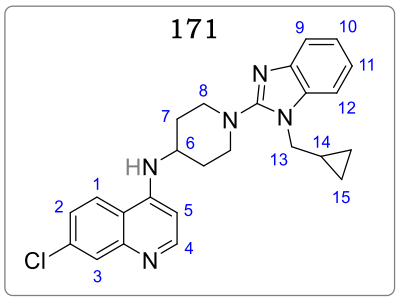

Following general procedure 12, obtained from **167** (0.080 g, 0.31 mmol) and **165a** (0.076 g, 0.37 mmol) as a light brown solid (0.113 g, 84%). m.p.: 101 – 103 °C. R_f (10% MeOH/DCM), 0.38. ^{1}H NMR (400 MHz, Methanol-d_4) δ 8.57 (d, J = 5.1 Hz, 1H, H^4), 8.16 (d, J = 8.0 Hz, 1H, H^1), 7.81 (d, J = 1.3 Hz, 1H, H^3), 7.60 – 7.51 (m, 2H, H^{2,9}), 7.16 – 7.09 (m, 2H, H^{5,12}), 6.86 – 6.79 (m, 2H, H^{10,11}), 4.88 (d, J = 5.9 Hz, 1H, H^{13}), 3.92 (tt, J = 11.1, 4.0 Hz, 1H, H^6), 3.82 (m, 2H, H^{8e}), 3.28 – 3.21 (m, 2H, H^{8a}), 1.98 – 1.89 (m, 5H, H^{7,14}), 1.42 (m, 4H, H^{15}). ^{13}C NMR (151 MHz, Methanol-d_4) δ 158.65, 151.98, 149.30, 145.25, 140.68, 135.02, 132.03, 129.98, 129.02, 128.32, 127.85, 119.86, 116.65, 112.32, 98.65, 52.46, 49.58 (2C), 47.24, 33.68, 30.07 (2C), 23.65, 10.24 (2C). LC-MS (APCI$^+$/ESI): found m/z = 432.2, 434.2 [M+H]$^+$ (cal. for $C_{25}H_{26}ClN_5$, 431.19, 433.18). Purity: 98%, t_R = 2.397 min.

7-chloro-N-(1-(1-(cyclobutyl methyl)-1H-benzo[d]imidazol-2-yl) piperidin-4-yl)quinolin-4-amine (172)

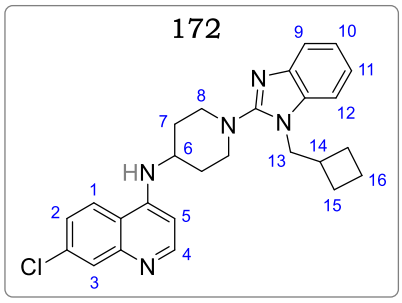

Following general procedure 12, obtained from **167** (0.080 g, 0.31 mmol) and **165b** (0.081 g, 0.37 mmol) as a light brown solid (0.121 g, 87%). m.p.: 111 – 113 °C. R_f (10% MeOH/DCM), 0.40. ^{1}H NMR (400 MHz, Methanol-d_4) δ 8.62 (d, J = 5.8 Hz, 1H, H^4), 8.25 (d, J = 7.8 Hz, 1H, H^1), 7.86 (d, J = 1.1 Hz, 1H, H^3), 7.58 – 7.52 (m, 2H, H^{2,9}), 7.16 – 7.10 (m, 2H, H^{5,12}), 6.89 – 6.81 (m, 2H, H^{10,11}), 4.85 (d, J = 6.1 Hz, 1H, H^{13}), 3.90 (tt, J = 10.8, 4.1 Hz, 1H, H^6), 3.82 (m, 2H, H^{8e}), 3.28 – 3.19 (m, 3H, H^{8a,14}), 2.35 – 2.28 (m, 4H, H^7), 1.89 – 1.74 (m, 4H, H^{15}), 1.23 – 1.19 (m, 2H, H^{16}). ^{13}C NMR (151 MHz, Methanol-d_4) δ 159.47, 151.58, 149.78, 147.56, 144.44, 141.21, 137.85, 136.00, 131.35, 129.86, 129.01, 128.32, 127.12, 120.01, 116.48, 111.17, 99.95, 52.58, 49.97 (2C), 41.68, 30.11 (2C), 23.58 (2C), 17.78. LC-MS (APCI$^+$/ESI): found m/z = 446.2, 448.2 [M+H]$^+$ (cal. for $C_{25}H_{26}ClN_5$, 445.20, 447.20). Purity: 98%, t_R = 2.469 min.

7-chloro-N-(1-(1-(cyclopentylmethyl)-1H-benzo[d]imidazol-2-yl)piperidin-4-yl) quinolin-4-amine (173)

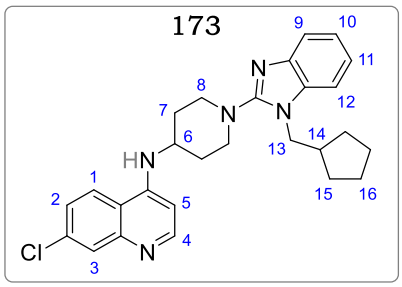

Following general procedure 12, obtained from **167** (0.080 g, 0.31 mmol) and **165c** (0.087 g, 0.37 mmol) as a pale-yellow solid (0.117 g, 82%). m.p.: 136 – 138 °C. R_f (10% MeOH/DCM), 0.44. ^{1}H NMR (400 MHz, Methanol-d_4) δ 8.59 (d, J = 4.9 Hz, 1H, H^4), 8.38 (d, J = 6.5 Hz, 1H, H^1), 7.83 (d, J = 0.8 Hz, 1H, H^3), 7.60 – 7.55 (m, 2H, H^{2,9}), 7.11 – 7.06 (m, 2H, H^{5,12}), 6.92 – 6.85 (m, 2H, H^{10,11}), 4.79 (d, J = 5.9 Hz, 1H, H^{13}), 3.90 (tt, J = 11.1, 4.0 Hz, 1H, H^6), 3.87 (m, 2H, H^{8e}), 3.22 – 3.15 (m, 3H, H^{8a}), 2.39 – 2.27 (m, 5H, H^{7,14}), 1.89 – 1.75 (m, 4H, H^{15}), 1.24 – 1.17 (m, 4H, H^{16}). ^{13}C NMR (151 MHz, Methanol-d_4) δ 158.89, 152.24, 148.65, 146.33, 143.28, 140.50, 139.07, 136.05, 131.52, 129.74, 128.87, 128.11, 127.08, 119.98, 116.36, 112.48, 98.63, 51.63, 49.38 (2C), 40.40, 31.07 (2C), 23.68 (2C), 17.58 (2C). LC-MS (APCI$^+$/ESI): found m/z = 460.2, 462.2 [M+H]$^+$ (cal. for $C_{27}H_{30}ClN_5$, 459.22, 461.22). Purity: 98%, t_R = 2.469 min.

7-chloro-N-(1-(1-(cyclohexylmethyl)-1H-benzo[d]imidazol-2-yl)piperidin-4-yl)quinolin-4-amine (174)

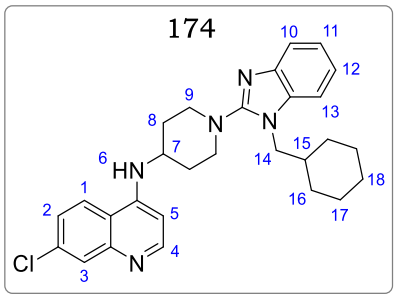

Following general procedure 12, obtained from **167** (0.080 g, 0.31 mmol) and **165d** (0.092 g, 0.37 mmol) as a light brown solid (0.116 g, 79%). m.p.: 120 – 122 °C. R_f (10% MeOH/DCM), 0.49. ^{1}H NMR (600 MHz, DMSO-d_6) δ 8.55 (d, J = 6.2 Hz, 1H, H^4), 8.50 (d, J = 8.2 Hz, 1H, H^1), 8.02 (dd, J = 7.8, 1.3 Hz, 1H, H^{10}), 7.90 (d, J = 2.2 Hz, 1H, H^3), 7.62 (dd, J = 8.2, 2.2 Hz, 1H, H^2), 7.46 – 7.38 (m, 2H, H^{5,13}), 7.14 – 7.06 (m, 2H, H^{11,12}), 6.87 (d, J = 6.3 Hz, 1H, H^6), 4.04 – 3.94 (m, 3H, H^{7,14}), 3.62 – 3.50 (m, 2H, H^{9e}), 3.12 (td, J = 12.6, 2.3 Hz, 2H, H^{9a}), 2.10 – 2.03 (m, 4H, H^{8e,16e}), 1.98 – 1.86 (m, 4H, H^{8a16a}), 1.68 – 1.58 (m, 2H, H^{17e}), 1.53 – 1.42 (m, 2H, H^{17a}), 1.26 – 1.15 (m, 2H, H^{18}). ^{13}C NMR (151 MHz, DMSO-d_6) δ 158.37, 152.21, 148.09, 144.64, 141.70, 136.10, 135.14, 125.73, 125.65, 123.87, 121.37, 121.11, 117.86, 116.98, 110.47, 99.56, 50.34, 50.08 (2C), 48.21, 39.19, 30.97 (2C), 30.05 (2C), 24.69 (3C). LC-MS (APCI$^+$/ESI): found m/z = 474.2, 476.2 [M+H]$^+$ (cal. for $C_{28}H_{32}ClN_5$, 473.23, 475.23). Purity: 98%, t_R = 2.571 min.

N-(1-(1-benzyl-1H-benzo[d]imidazol-2-yl)piperidin-4-yl)-7-chloroquinolin-4-amine (175)

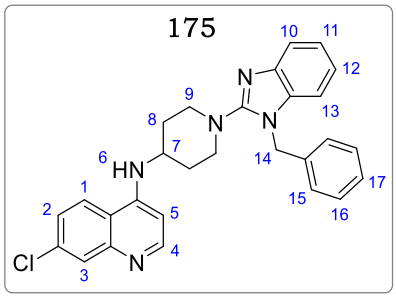

Following general procedure 12, obtained from **167** (0.080 g, 0.31 mmol) and **165e** (0.090 g, 0.37 mmol) as an off-white solid (0.129 g, 89%). m.p.: 99 – 100 °C. R_f (10% MeOH/DCM), 0.40. ^{1}H NMR (600 MHz, DMSO-d_6) δ 8.53 (d, J = 8.8 Hz, 1H, H^4), 8.45 (d, J = 7.9 Hz, 1H, H^1), 8.23 (d, J = 8.8 Hz, 1H, H^5), 7.98 (d, J = 1.9 Hz, 1H, H^3), 7.89 – 7.75 (m, 4H, H^{2,10,16}), 7.58 – 7.49 (m, 3H, H^{13,15}), 7.28 (dd, J = 8.3, 1.5 Hz, 1H, H^{13}), 7.10 (m, 2H, H^{11,17}), 7.03 (ddd, J = 8.3, 7.1, 1.2 Hz, 1H, H^{12}), 6.92 (d, J = 6.6 Hz, 1H, H^6), 5.45 (s, 2H, H^{14}), 3.98 (tt, J = 11.5, 4.2 Hz, 1H, H^7), 3.58 – 3.50 (m, 2H, H^{9e}), 3.19 – 3.12 (m, 2H, H^{9a}), 1.98 – 1.88 (m, 4H, H^8). ^{13}C NMR (151 MHz, DMSO-d_6) δ 159.32, 151.56, 146.35, 144.30, 138.56, 136.69, 132.85 (2C), 129.37, 128.48 (2C), 125.68, 122.85, 122.03, 120.54, 118.07, 116.29, 111.08, 110.23, 98.68, 52.04, 50.33, 48.97 (2C), 46.88, 46.03, 30.26 (2C). LC-MS (APCI$^+$/ESI): found m/z = 468.2, 470.2 [M+H]$^+$ (cal. for $C_{28}H_{26}ClN_5$, 467.19, 469.19). Purity: 98%, t_R = 2.468 min.

7-chloro-N-(1-(1-(2-fluorobenzyl)-1H-benzo[d]imidazol-2-yl) piperidin-4-yl) quinolin-4-amine (180)

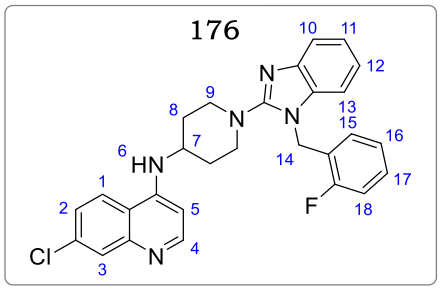

Following general procedure 12, obtained from **167** (0.080 g, 0.31 mmol) and **165f** (0.097 g, 0.37 mmol) as a pale-yellow solid (0.125 g, 83%). m.p.: 125 – 127 °C. R_f (10% MeOH/DCM), 0.40. ^{1}H NMR (600 MHz, DMSO-d_6) δ 8.53 (d, J = 8.3 Hz, 1H, H^4), 8.45 (d, J = 7.0 Hz, 1H, H^1), 8.27 (d, J = 8.3 Hz, 1H, H^5), 8.02 (d, J = 1.9 Hz, 1H, H^3), 7.79 – 7.65 (m, 3H, H^{2,10,15}), 7.47 – 7.42 (m, 2H, H^{16,17}), 7.29 (dd, J = 7.0, 1.2 Hz, 1H, H^{13}), 7.11 (ddd, J = 8.0, 7.1, 1.2 Hz, 1H, H^{11}), 7.02 – 6.97 (m, 2H, H^{12,18}), 6.89 (d, J = 6.6 Hz, 1H, H^6), 5.42 (s, 2H, H^{14}), 3.99 – 3.96 (m, 1H, H^7), 3.58 – 3.52 (m, 2H, H^{9e}), 3.21 – 3.15 (m, 2H, H^{9a}), 2.00 – 1.89 (m, 4H, H^8). ^{13}C NMR (151 MHz, DMSO-d_6) δ 159.57, 153.36, 147.68, 142.21, 140.04, 136.32, 134.78, 133.33, 131.58, 129.58, 127.40, 126.03, 123.51, 122.97, 122.08, 121.55, 117.80, 116.03, 111.17, 109.31, 98.98, 51.27, 50.45, 49.58 (2C), 48.23, 45.08, 30.08 (2C). LC-MS (APCI$^+$/ESI): found m/z = 486.2, 488.2 [M+H]$^+$ (cal. for $C_{28}H_{25}ClFN_5$, 485.18, 487.18). Purity: 98%, t_R = 2.491 min.

7-chloro-N-(1-(1-(3-fluorobenzyl)-1H-benzo[d]imidazol-2-yl) piperidin-4-yl) quinolin-4-amine (177)

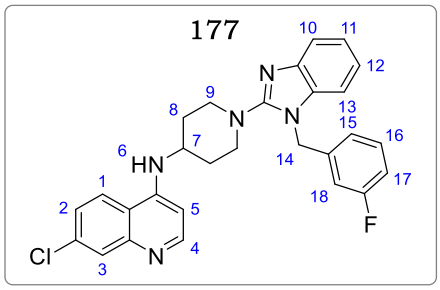

Following general procedure 12, obtained from **167** (0.080 g, 0.31 mmol) and **165g** (0.097 g, 0.37 mmol) as a pale-yellow solid (0.128 g, 85%). m.p.: 117 – 119 °C. R_f (10% MeOH/DCM), 0.45. ^{1}H NMR (600 MHz, DMSO-d_6) δ 8.55 (d, J = 8.6 Hz, 1H, H^4), 8.43 (d, J = 7.5 Hz, 1H, H^1), 8.26 (d, J = 8.6 Hz, 1H, H^5), 7.99 (d, J = 2.2 Hz, 1H, H^3), 7.80 – 7.68 (m, 3H, H^{2,10,15}), 7.43 (dd, J = 2.3, 1.8 Hz, 1H, H^{18}), 7.39 – 7.31 (m, 2H, H^{16,17}), 7.28 (dd, J = 8.2, 1.5 Hz, 1H, H^{13}), 7.09 (ddd, J = 8.3, 7.1, 1.2 Hz, 1H, H^{11}), 6.97 (ddd, J = 8.2, 7.1, 1.2, 1H, H^{12}), 6.90 (d, J = 6.6 Hz, 1H, H^6), 5.43 (s, 2H, H^{14}), 4.01 – 3.96 (m, 1H, H^7), 3.60 – 3.52 (m, 2H, H^{9e}), 3.23 – 3.16 (m, 2H, H^{9a}), 1.98 – 1.90 (m, 4H, H^8). ^{13}C NMR (151 MHz, DMSO-d_6) δ 158.32, 152.22, 146.96, 142.54, 139.98, 136.55, 134.21, 132.57, 130.69, 128.93, 127.21, 126.08, 124.06, 122.34, 122.04, 120.45, 118.07, 116.18, 110.75, 108.65, 99.04, 52.23, 50.89,

49.08 (2C), 48.65, 45.03, 30.11 (2C). LC-MS (APCI$^+$/ESI): found m/z = 486.2, 488.2 $[M+H]^+$ (cal. for $C_{28}H_{25}ClFN_5$, 485.18, 487.18). Purity: 99%, t_R = 2.488 min.

7-chloro-N-(1-(1-(4-fluorobenzyl)-1H-benzo[d]imidazol-2-yl) piperidin-4-yl) quinolin-4-amine (H-2)

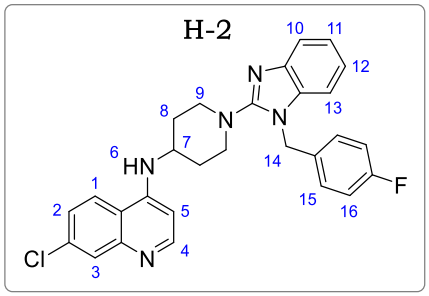

Following general procedure 12, obtained from **167** (0.080 g, 0.31 mmol) and **165h** (0.097 g, 0.37 mmol) as a pale-yellow solid (0.120 g, 79%). m.p.: 120 – 122 °C. R_f (10% MeOH/DCM), 0.43. ^{1}H NMR (600 MHz, DMSO-d_6) δ 8.59 (d, J = 8.5 Hz, 1H, H^4), 8.50 (d, J = 6.9 Hz, 1H, H^1), 8.22 (d, J = 8.5 Hz, 1H, H^5), 7.96 (d, J = 2.0 Hz, 1H, H^3), 7.85 (d, J = 8.0 Hz, 2H, H^{16}), 7.65 (dd, J = 6.9, 2.0 Hz, 1H, H^2), 7.50 (dd, J = 7.9, 1.3 Hz, 1H, H^{10}), 7.29 (d, J = 8.0 Hz, 2H, H^{15}), 7.18 (dd, J = 8.5, 1.5 Hz, 1H, H^{13}), 7.11 (ddd, J = 7.9, 6.8, 1.2 Hz, 1H, H^{11}), 7.01 (ddd, J = 8.5, 6.8, 1.5 Hz, 1H, H^{12}), 6.92 (d, J = 6.3 Hz, 1H, H^6), 5.42 (s, 2H, H^{14}), 3.98 (tt, J = 10.8, 3.9 Hz, 1H, H^7), 3.59 – 3.52 (m, 2H, H^{9e}), 3.15 (td, J = 13.1, 4.8 Hz, 2H, H^{9a}), 1.99 – 1.85 (m, 4H, H^8). ^{13}C NMR (151 MHz, DMSO-d_6) δ 158.33, 149.98, 146.33, 144.32, 140.08, 137.20, 134.07 (2C), 132.47, 128.54 (2C), 126.44, 123.08, 122.45, 121.51, 119.32, 116.75, 110.24, 110.02, 98.52, 51.58, 50.58, 49.47 (2C), 46.89, 46.080, 30.96 (2C). LC-MS (APCI$^+$/ESI): found m/z = 486.2, 488.2 $[M+H]^+$ (cal. for $C_{28}H_{25}ClFN_5$, 485.18, 487.18). Purity: 99%, t_R = 2.488 min.

4-((2-(4-((7-chloroquinolin-4-yl)amino)piperidin-1-yl)-1H-benzo[d]imidazol-1-yl)methyl)benzonitrile (178)

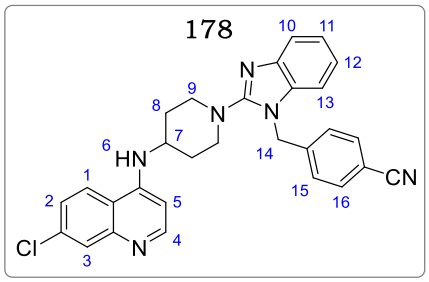

Following general procedure 12, obtained from **167** (0.080 g, 0.31 mmol) and **12d** (0.100 g, 0.37 mmol) as a pale-yellow solid (0.122 g, 80%). m.p.: 112 – 113 °C. R_f (10% MeOH/DCM), 0.39. ^{1}H NMR (600 MHz, DMSO-d_6) δ 8.58 (d, J = 9.3 Hz, 1H, H^4), 8.49 (d, J = 6.4 Hz, 1H, H^1), 8.25 (d, J = 9.3 Hz, 1H, H^5), 7.94 (d, J = 2.4 Hz, 1H, H^3), 7.81 (d, J = 8.3 Hz, 2H, H^{16}), 7.63 (dd, J = 6.4, 2.4 Hz, 1H, H^2), 7.47 (d, J = 7.8 Hz, 1H, H^{10}), 7.32 (d, J = 8.3 Hz, 2H, H^{15}), 7.20 (d, J = 7.2 Hz, 1H, H^{13}), 7.11 (ddd, J = 7.8, 6.5, 1.2 Hz, 1H, H^{11}), 7.05 (ddd, J = 7.2, 6.5, 1.2 Hz, 1H, H^{12}), 6.90 (d, J = 6.6 Hz, 1H, H^6), 5.43 (s, 2H, H^{14}), 4.05 – 3.96 (m, 1H, H^7), 3.60 – 3.54 (m, 2H, H^{9e}), 3.20 – 3.13 (m, 2H, H^{9a}), 2.03 – 1.89 (m, 4H, H^8). ^{13}C NMR

(151 MHz, DMSO-d_6) δ 158.02, 152.84, 146.92, 143.28, 141.82, 136.64, 135.43, 133.15 (2C), 132.68, 127.83 (2C), 126.07, 122.80, 122.00, 121.48, 117.88, 116.70, 110.71, 110.10, 99.55, 51.96, 50.39, 49.86 (2C), 47.11, 46.00, 30.45 (2C). LC-MS (APCI$^+$/ESI): found m/z = 493.2, 495.2 $[M+H]^+$ (cal. for $C_{29}H_{25}ClN_6$, 492.18, 494.18). Purity: 98%, t_R = 2.391 min.

7-chloro-N-(1-(1-(4-methoxybenzyl)-1H-benzo[d]imidazol-2-yl)piperidin-4-yl) quinolin-4-amine (179)

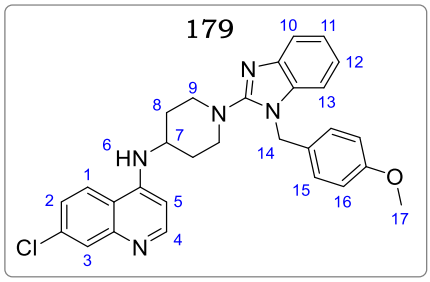

Following general procedure 12, obtained from **167** (0.080 g, 0.31 mmol) and **165i** (0.101 g, 0.37 mmol) as a pale-yellow solid (0.106 g, 69%). m.p.: 111 – 113 °C. R_f (10% MeOH/DCM), 0.38. ^{1}H NMR (600 MHz, DMSO-d_6) δ 8.53 (d, J = 6.9 Hz, 1H, H^4), 8.46 (d, J = 8.2 Hz, 1H, H^1), 8.29 (d, J = 6.9 Hz, 1H, H^5), 7.89 – 7.80 (m, 3H, $H^{3,16}$), 7.55 – 7.47 (m, 2H, $H^{2,10}$), 7.38 (d, J = 8.1 Hz, 2H, H^{15}), 7.22 (dd, J = 8.3, 1.3 Hz, 1H, H^{13}), 7.10 – 7.04 (m, 2H, $H^{11,12}$), 6.89 (d, J = 6.5 Hz, 1H, H^6), 5.42 (s, 2H, H^{14}), 3.98 – 3.91 (m, 4H, $H^{7,17}$), 3.59 – 3.54 (m, 2H, H^{9e}), 3.17 (td, J = 11.8, 2.9 Hz, 2H, H^{9a}), 2.02 – 1.90 (m, 4H, H^8). ^{13}C NMR (151 MHz, DMSO-d_6) δ 156.95, 153.20, 147.89, 143.08, 141.31, 135.36, 132.95 (2C), 131.42, 128.86 (2C), 126.30, 122.88, 122.35, 121.21, 118.86, 116.04, 111.58, 110.35, 98.23, 57.85, 53.62, 50.84, 50.06 (2C), 47.30, 46.09, 30.85 (2C). LC-MS (APCI$^+$/ESI): found m/z = 498.2, 500.2 $[M+H]^+$ (cal. for $C_{29}H_{28}ClN_5O$, 497.20, 499.20). Purity: 98%, t_R = 2.470 min.

7-chloro-N-(1-(1-(4-(trifluoromethyl)benzyl)-1H-benzo[d]imidazol-2-yl) piperidin-4-yl) quinolin-4-amine (180)

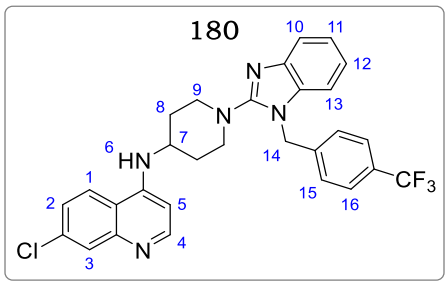

Following general procedure 12, obtained from **167** (0.080 g, 0.31 mmol) and **165j** (0.115 g, 0.37 mmol) as a pale yellow solid (0.170 g, 86%). m.p.: 121 – 123 °C. R*f* (10% MeOH/DCM), 0.42. ^{1}H NMR (600 MHz, DMSO) δ 8.75 – 8.64 (m, 2H, $H^{4,1}$), 8.52 (d, J = 6.7 Hz, 1H, H^5), 8.04 (d, J = 2.2 Hz, 1H, H^3), 7.75 – 7.64 (m, 3H, $H^{2,16}$), 7.47 (dd, J = 7.8, 1.5 Hz, 1H, H^{10}), 7.37 (d, J = 8.1 Hz, 2H, H^{15}), 7.20 (dd, J = 8.1, 1.2 Hz, 1H, H^{13}), 7.11 (ddd, J = 7.8, 6.5, 1.2 Hz, 1H, H^{11}), 7.05 (ddd, J = 8.1, 6.5, 1.2 Hz, 1H, H^{12}), 6.98 (d, J = 7.0 Hz, 1H, H^6), 5.44 (s, 2H, H^{14}), 4.08 (tt, J = 10.5, 4.0 Hz, 1H, H^7), 3.64 – 3.55 (m, 2H, H^{9e}), 3.24 – 3.13 (m, 2H, H^{9a}), 2.07 – 1.95 (m, 4H, H^8). ^{13}C NMR (151 MHz, DMSO) δ 158.00, 153.91, 145.06, 142.31,

141.81, 141.25, 137.51, 135.45, 127.64 (2C), 126.59, 126.20, 126.13 (2C), 126.08, 121.97, 121.47, 121.11, 117.84, 116.30, 110.13, 99.48, 50.74, 49.82 (2C), 47.02, 45.86, 30.33 (2C). LC-MS (APCI$^+$/ESI): found m/z = 536.2, 538.2 $[M+H]^+$ (cal. for $C_{29}H_{25}ClF_3N_5$, 535.18, 537.17). Purity: 99%, t_R = 2.547 min.

7-chloro-N-(1-(1-(4-(methylsulfonyl)benzyl)-1H-benzo[d]imidazol-2-yl) piperidin-4-yl) quinolin-4-amine (181)

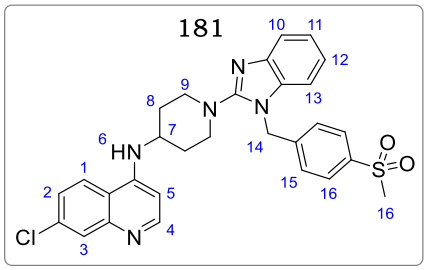

Following general procedure 12, obtained from **167** (0.080 g, 0.31 mmol) and **165k** (0.119 g, 0.37 mmol) as a pale-yellow solid (0.137 g, 81%). m.p.: 147 – 149 °C. R_f (10% MeOH/DCM), 0.37. ^{1}H NMR (600 MHz, DMSO-d_6) δ 8.62 (d, J = 8.0 Hz, 1H, H^4), 8.53 (d, J = 8.2 Hz, 1H, H^1), 8.19 (d, J = 8.0 Hz, 1H, H^5), 8.05 (d, J = 2.0 Hz, 1H, H^3), 7.79 – 7.66 (m, 3H, H^{2,16}), 7.42 (dd, J = 8.0, 1.5 Hz, 1H, H^{10}), 7.33 (d, J = 8.5 Hz, 2H, H^{15}), 7.19 (dd, J = 7.9, 1.2 Hz, 1H, H^{13}), 7.09 (ddd, J = 8.0, 6.7, 1.2 Hz, 1H, H^{11}), 7.01 (ddd, J = 7.9, 6.6, 1.2 Hz, 1H, H^{12}), 6.94 (d, J = 6.6 Hz, 1H, H^6), 5.40 (s, 2H, H^{14}), 4.01 (tt, J = 10.8, 4.3 Hz, 1H, H^7), 3.63 – 3.55 (m, 2H, H^{9e}), 3.22 – 3.15 (m, 2H, H^{9a}), 3.10 (s, 3H, H^{16}), 2.04 – 1.92 (m, 4H, H^8). ^{13}C NMR (151 MHz, DMSO-d_6) δ 157.55, 151.39, 145.83, 142.28, 140.28, 137.32, 132.98 (2C), 132.07, 127.68 (2C), 125.32, 122.86, 122.03, 120.27, 118.06, 116.75, 110.79, 110.03, 98.36, 52.06, 50.22, 49.63 (2C), 47.88, 46.03, 43.89, 31.08 (2C). LC-MS (APCI$^+$/ESI): found m/z = 546.2, 548.2 $[M+H]^+$ (cal. for $C_{29}H_{28}ClN_5O_2S$, 545.17, 547.16). Purity: 98%, t_R = 2.310 min.

4-((2-(4-((7-chloroquinolin-4-yl)amino)piperidin-1-yl)-1H-benzo[d]imidazol-1-yl) methyl) benzene sulfonamide (182)

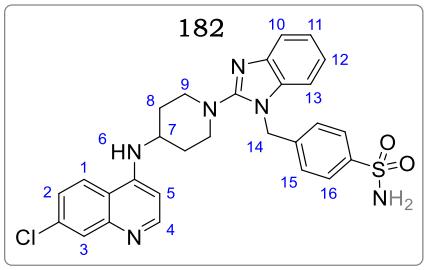

Following general procedure 12, obtained from **167** (0.080 g, 0.31 mmol) and **165l** (0.114 g, 0.37 mmol) as a pale-yellow solid (0.100 g, 59%). m.p.: 141 – 143 °C. R_f (10% MeOH/DCM), 0.19. ^{1}H NMR (600 MHz, DMSO-d_6) δ 8.65 (d, J = 7.6 Hz, 1H, H^4), 8.50 (d, J = 8.0 Hz, 1H, H^1), 8.17 (d, J = 7.6 Hz, 1H, H^5), 8.08 – 7.92 (m, 3H, H^{3,16}), 7.81 (dd, J = 8.0, 2.3 Hz, 1H, H^2), 7.48 (dd, J = 8.2, 1.5 Hz, 1H, H^{10}), 7.31 (d, J = 8.5 Hz, 2H, H^{15}), 7.20 (dd, J = 8.2, 1.2 Hz, 1H, H^{13}), 7.11 (ddd, J = 8.1, 7.0, 1.2 Hz, 1H, H^{11}), 7.05 (ddd, J = 8.1, 7.0, 1.2 Hz, 1H, H^{12}), 6.95 (d, J = 6.6 Hz, 1H, H^6), 5.41 (s, 2H, H^{14}), 4.08 (tt, J = 10.2, 4.1 Hz, 1H, H^7), 3.65 – 3.56 (m, 2H, H^{9e}), 3.19 – 3.12 (m,

2H, H^{9a}), 2.00 – 1.89 (m, 4H, H^{8}). ^{13}C NMR (151 MHz, DMSO-d_6) δ 160.32, 156.30, 146.38, 143.65, 139.96, 137.77, 133.65 (2C), 132.08, 128.85 (2C), 125.08, 123.08, 122.41, 120.36, 118.65, 116.70, 110.67, 109.85, 99.34, 53.54, 50.07, 49.55 (2C), 47.39, 44.47, 30.17 (2C). LC-MS (APCI$^+$/ESI): found m/z = 547.2, 549.2 [M+H]$^+$ (cal. for $C_{28}H_{27}ClN_6O_2S$, 546.16, 548.16). Purity: 98%, t_R = 2.264 min.

7-chloro-N-(1-(1-(4-nitrobenzyl)-1H-benzo[d]imidazol-2-yl)piperidin-4-yl) quinolin-4-amine (183)

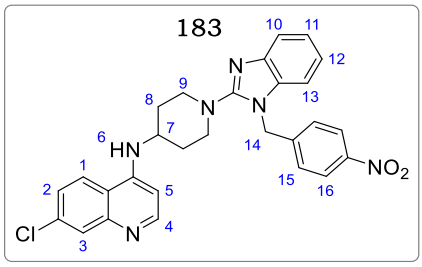

Following general procedure 12, obtained from **167** (0.080 g, 0.31 mmol) and **165m** (0.106 g, 0.37 mmol) as a yellow solid (0.115 g, 72%). m.p.: 117 – 119 °C. R_f (10% MeOH/DCM), 0.46. ^{1}H NMR (600 MHz, DMSO-d_6) δ 8.60 (d, J = 9.0 Hz, 1H, H^4), 8.44 (d, J = 8.0 Hz, 1H, H^1), 8.19 (d, J = 9.0 Hz, 1H, H^5), 7.96 – 7.80, 3H, H^{3,16}), 7.59 – 7.47 (m, 2H, H^{2,10}), 7.30 (d, J = 8.5 Hz, 2H, H^{15}), 7.19 (dd, J = 7.9, 1.6 Hz, 1H, H^{13}), 7.12 – 7.05 (m, 2H, H^{11,12}), 6.89 (d, J = 6.3 Hz, 1H, H^6), 5.41 (s, 2H, H^{14}), 3.99 (tt, J = 11.0, 4.2 Hz, 1H, H^7), 3.56 – 3.49 (m, 2H, H^{9e}), 3.20 – 3.12 (m, 2H, H^{9a}), 1.99 – 1.85 (m, 4H, H^8). ^{13}C NMR (151 MHz, DMSO-d_6) δ 162.34, 153.48, 149.35, 142.38, 141.33, 136.20, 132.58 (2C), 132.05, 128.56 (2C), 125.39, 123.55, 122.09, 120.47, 118.86, 116.66, 110.84, 110.11, 98.50, 52.34, 50.78, 50.06 (2C), 48.63, 45.79, 30.06 (2C). LC-MS (APCI$^+$/ESI): found m/z = 513.2, 515.2 [M+H]$^+$ (cal. for $C_{28}H_{25}ClN_6O_2$, 512.17, 514.17). Purity: 98%, t_R = 2.443 min.

N-(4-((2-(4-((7-chloroquinolin-4-yl)amino)piperidin-1-yl)-1H-benzo[d]imidazol-1-yl) methyl) phenyl) acetamide (184)

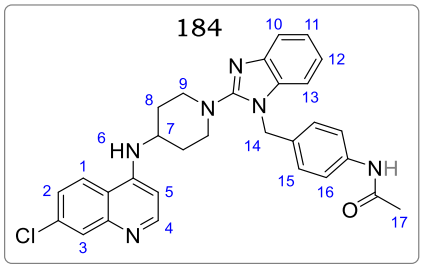

Following general procedure 12, obtained from **167** (0.080 g, 0.31 mmol) and **165n** (0.111 g, 0.37 mmol) as a pale-yellow solid (0.122 g, 75%). m.p.: 159 – 161 °C. R_f (10% MeOH/DCM), 0.10. ^{1}H NMR (600 MHz, DMSO-d_6) δ 8.60 (d, J = 8.5 Hz, 1H, H^4), 8.51 (d, J = 6.3 Hz, 1H, H^1), 8.20 (d, J = 8.5 Hz, 1H, H^5), 7.93 (d, J = 2.0 Hz, 1H, H^3), 7.83 (d, J = 8.5 Hz, 2H, H^{16}), 7.69 (dd, J = 6.3, 2.0 Hz, 1H, H^2), 7.51 (dd, J = 8.1, 1.5 Hz, 1H, H^{10}), 7.36 (d, J = 8.5 Hz, 2H, H^{15}), 7.19 (dd, J = 7.9, 1.2 Hz, 1H, H^{13}), 7.08 (ddd, J = 8.1, 6.5, 1.2 Hz, 1H, H^{11}), 7.01 (ddd, J = 7.9, 6.5, 1.2 Hz, 1H, H^{12}), 6.91 (d, J = 6.1 Hz, 1H, H^6), 5.41 (s, 2H, H^{14}), 4.05 (tt, J = 11.8, 4.6 Hz, 1H, H^7), 3.58 – 3.52 (m, 2H, H^{9e}), 3.24

– 3.17 (m, 2H, H^{9a}), 2.05 – 1.83 (m, 7H, H^{8,17}). ^{13}C NMR (151 MHz, DMSO-d_6) δ 166.34, 159.47, 153.54, 146.27, 142.28, 140.05, 135.68, 133.62 (2C), 133.02, 128.63 (2C), 126.37, 123.36, 122.54, 121.54, 118.65, 116.54, 111.17, 110.08, 98.35, 51.47, 50.78, 50.08 (2C), 47.34, 46.22, 30.98 (2C), 19.35. LC-MS (APCI$^+$/ESI): found m/z = 525.2, 527.2 [M+H]$^+$ (cal. for $C_{30}H_{29}ClN_6O$, 524.21, 526.21). Purity: 98%, t_R = 2.338 min.

Methyl 4-((2-(4-((7-chloroquinolin-4-yl) amino) piperidin-1-yl)-1H-benzo[d]imidazol-1-yl) methyl) benzoate (185)

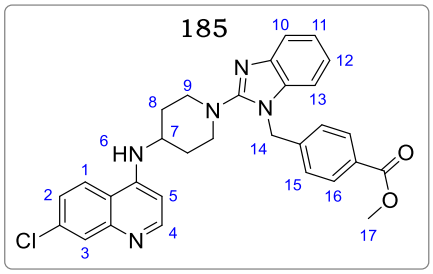

Following general procedure 12, obtained from **167** (0.080 g, 0.31 mmol) and **165o** (0.112 g, 0.37 mmol) as a pale yellow solid (0.131 g, 80%). m.p.: 132 – 134 °C. R_f (10% MeOH/DCM), 0.22. ^{1}H NMR (600 MHz, DMSO) δ 8.61 (d, *J* = 9.1 Hz, 1H, H^4), 8.48 (d, *J* = 6.5 Hz, 1H, H^1), 8.27 (d, *J* = 9.1 Hz, 1H, H^5), 7.97 (d, *J* = 2.2 Hz, 1H, H^3), 7.79 (d, *J* = 8.3 Hz, 2H, H^{16}), 7.62 (dd, *J* = 6.5, 2.2 Hz, 1H, H^2), 7.47 (dd, *J* = 7.7, 1.2 Hz, 1H, H^{10}), 7.37 – 7.28 (m, 3H, H^{13,15}), 7.11 (ddd, *J* = 7.7, 6.2, 1.2 Hz, 1H, H^{11}), 7.05 (ddd, *J* = 7.9, 6.2, 1.2 Hz, 1H, H^{12}), 6.89 (d, *J* = 6.5 Hz, 1H, H^6), 5.41 (s, 2H, H^{14}), 4.02 (tt, *J* = 11.5, 4.3 Hz, 1H, H^7), 3.85 (s, 3H, H^{17}), 3.65 – 3.51 (m, 2H, H^{9e}), 3.22 – 3.13 (m, 2H, H^{9a}), 2.08 – 1.88 (m, 4H, H^8). ^{13}C NMR (151 MHz, DMSO-d_6) δ 165.35, 157.35, 151.32, 146.30, 142.22, 141.08, 136.25, 132.75 (2C), 132.88, 128.80 (2C), 126.34, 122.82, 121.96, 120.23, 117.30, 116.83, 111.20, 110.63, 98.69, 54.36, 52.01, 51.07, 50.08 (2C), 47.32, 46.58, 31.07 (2C). LC-MS (APCI$^+$/ESI): found m/z = 526.2, 528.2 [M+H]$^+$ (cal. for $C_{30}H_{28}ClN_5O_2$, 525.19, 527.20). Purity: 98%, t_R = 2.269 min.

4-((2-(4-((7-chloroquinolin-4-yl)amino)piperidin-1-yl)-1H-benzo[d]imidazol-1-yl) methyl)-N-methyl benzamide (187)

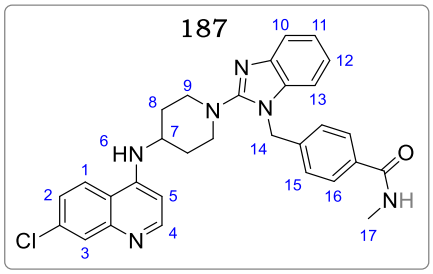

Following general procedure 12, obtained from **167** (0.080 g, 0.31 mmol) and **165q** (0.111 g, 0.37 mmol) as a pale-yellow solid (0.143 g, 88%). m.p.: 140 – 141 °C. R_f (10% MeOH/DCM), 0.08. ^{1}H NMR (600 MHz, DMSO) δ 8.58 (d, *J* = 8.5 Hz, 1H, H^4), 8.49 (d, *J* = 6.9 Hz, 1H, H^1), 8.25 (d, *J* = 8.5 Hz, 1H, H^5), 7.99 (d, *J* = 2.0 Hz, 1H, H^3), 7.81 (d, *J* = 8.2 Hz, 2H, H^{16}), 7.65 – 7.51 (m, 2H, H^{2,10}), 7.41 – 7.30 (m, 3H, H^{13,15}), 7.08 (ddd, *J* = 7.9, 6.6, 1.5 Hz, 1H, H^{11}), 7.05 (ddd, *J* = 8.0, 6.6, 1.3 Hz, 1H, H^{12}), 6.90 (d, *J* = 6.8 Hz, 1H, H^6), 5.42 (s, 2H, H^{14}), 4.00 – 3.95 (m, 4H, H^{7,17}), 3.64 – 3.52

(m, 2H, H^{9e}), 3.21 – 3.15 (m, 2H, H^{9a}), 2.05 – 1.89 (m, 4H, H^{8}). ^{13}C NMR (151 MHz, DMSO-d_6) δ 166.68, 158.38, 150.25, 147.36, 142.78, 140.30, 135.98, 132.62 (2C), 132.08, 128.31 (2C), 125.59, 122.38, 121.85, 120.03, 118.06, 116.58, 110.72, 110.05, 99.16, 54.58, 52.09, 51.22, 50.14 (2C), 47.63, 45.90, 31.12 (2C). LC-MS (APCI$^+$/ESI): found m/z = 525.2, 527.2 $[M+H]^+$ (cal. for $C_{30}H_{29}ClN_6O$, 524.21, 526.21). Purity: 98%, t_R = 2.329 min.

7-chloro-N-(1-(1-((6-methylpyridin-2-yl)methyl)-1H-benzo[d]imidazol-2-yl) piperidin-4-yl) quinolin-4-amine (188)

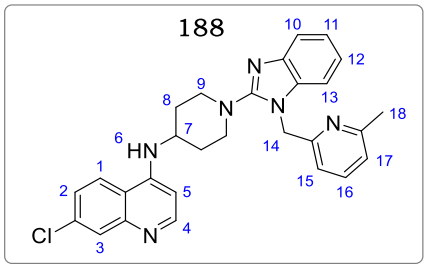

Following general procedure 12, obtained from **167** (0.080 g, 0.31 mmol) and **165r** (0.096 g, 0.37 mmol) as a light brown solid (0.125 g, 83%). m.p.: 158 – 160 °C. R_f (10% MeOH/DCM), 0.35. ^{1}H NMR (600 MHz, DMSO) δ 8.52 (d, J = 6.5 Hz, 1H, H^4), 8.46 (d, J = 8.2 Hz, 1H, H^1), 8.22 (d, J = 6.5 Hz, 1H, H^5), 8.01 (d, J = 2.2 Hz, 1H, H^3), 7.92 (t, J = 8.2 Hz, 1H, H^{16}), 7.69 – 7.50 (m, 4H, H^{2,10,15,17}), 7.39 (dd, J = 8.2, 1.5 Hz, 1H, H^{13}), 7.06 (ddd, J = 8.0, 6.7, 1.5 Hz, 1H, H^{11}), 6.98 (ddd, J = 8.2, 6.7, 1.3 Hz, 1H, H^{12}), 6.91 (d, J = 6.5 Hz, 1H, H^6), 5.41 (s, 2H, H^{14}), 3.98 (tt, J = 10.8, 3.9 Hz, 1H, H^7), 3.65 – 3.56 (m, 2H, H^{9e}), 3.22 – 3.18 (m, 2H, H^{9a}), 2.97 (s, 3H, H^{18}), 2.03 – 1.90 (m, 4H, H^8). ^{13}C NMR (151 MHz, DMSO-d_6) δ 159.35, 151.32, 148.35, 142.28, 141.35, 139.63, 135.62, 133.05, 132.86, 128.30, 125.68, 121.63, 120.15, 118.78, 116.49, 110.35, 109.32, 98.06, 54.29, 53.03, 51.78, 49.58 (2C), 48.06, 44.36, 30.56 (2C), 23.29. LC-MS (APCI$^+$/ESI): found m/z = 483.2, 485.2 $[M+H]^+$ (cal. for $C_{28}H_{27}ClN_6$, 482.20, 484.20). Purity: 98%, t_R = 2.416 min.

7-chloro-N-(1-(1-((6-methylpyridin-3-yl)methyl)-1H-benzo[d]imidazol-2-yl) piperidin-4-yl) quinolin-4-amine (189)

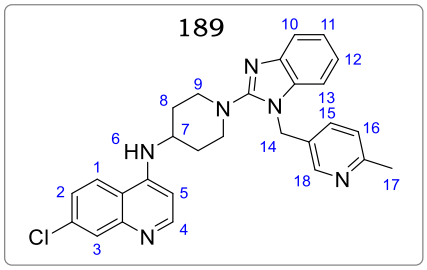

Following general procedure 12, obtained from **167** (0.080 g, 0.31 mmol) and **165s** (0.096 g, 0.37 mmol) as a pale-yellow solid (0.128 g, 85%). m.p.: 133 – 134 °C. R_f (10% MeOH/DCM), 0.21. ^{1}H NMR (600 MHz, DMSO) δ 8.73, (d, J = 1.9 Hz, 1H, H^{18}), 8.53 (d, J = 6.3 Hz, 1H, H^4), 8.43 (d, J = 8.2 Hz, 1H, H^1), 8.25 (d, J = 6.3 Hz, 1H, H^5), 8.05 – 7.93 (m, 1H, H^{3,15}), 7.68 – 7.60 (m, 2H, H^{2,10}), 7.51 (d, J = 8.2 Hz, 1H, H^{16}), 7.38 (dd, J = 8.0, 1.5 Hz, 1H, H^{13}), 7.09 (ddd, J = 8.2, 6.5, 1.2 Hz, 1H, H^{11}), 6.97 (ddd, J = 8.0, 6.5, 1.1 Hz, 1H, H^{12}), 6.92 (d, J = 6.5 Hz, 1H, H^6), 5.42 (s, 2H, H^{14}), 3.98 (tt,

J = 10.5, 3.8 Hz, 1H, H[7]), 3.62 – 3.56 (m, 2H, H[9e]), 3.23 – 3.18 (m, 2H, H[9a]), 2.95 (s, 3H, H[18]), 1.98 – 1.90 (m, 4H, H[8]). ^{13}C NMR (151 MHz, DMSO-d_6) δ 160.35, 152.86, 147.65, 142.86, 140.02, 139.36, 135.66, 133.65, 132.80, 129.68, 125.30, 121.68, 120.87, 118.60, 116.33, 110.37, 108.97, 98.20, 54.10, 53.27, 51.35, 49.57 (2C), 48.36, 44.60, 30.61 (2C), 22.68. LC-MS (APCI$^+$/ESI): found m/z = 483.2, 485.2 $[M+H]^+$ (cal. for $C_{28}H_{27}ClN_6$, 482.20, 484.20). Purity: 99%, t_R = 2.348 min.

7-chloro-N-(1-(1-((6-(trifluoromethyl) pyridin-3-yl) methyl)-1H-benzo[d]imidazol-2-yl) piperidin-4-yl) quinolin-4-amine (190)

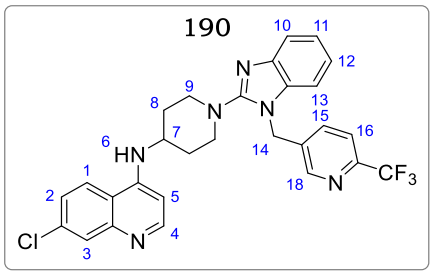

Following general procedure 12, obtained from **167** (0.080 g, 0.31 mmol) and **165t** (0.116 g, 0.37 mmol) as a pale-yellow solid (0.147 g, 88%). m.p.: 130 – 131 °C. R_f (10% MeOH/DCM), 0.29. ^{1}H NMR (600 MHz, DMSO) δ 8.75, (d, *J* = 2.1 Hz, 1H, H[18]), 8.51 (d, *J* = 6.5 Hz, 1H, H[4]), 8.40 (d, *J* = 8.5 Hz, 1H, H[1]), 8.20 (d, *J* = 6.5 Hz, 1H, H[5]), 8.02 – 7.90 (m, 1H, H[3,15]), 7.69 – 7.60 (m, 2H, H[2,10]), 7.52 (d, *J* = 8.5 Hz, 1H, H[16]), 7.36 (dd, *J* = 8.2, 1.5 Hz, 1H, H[13]), 7.10 (ddd, *J* = 8.5, 7.1, 1.2 Hz, 1H, H[11]), 6.98 (ddd, *J* = 8.2, 7.1, 1.1 Hz, 1H, H[12]), 6.90 (d, *J* = 6.5 Hz, 1H, H[6]), 5.40 (s, 2H, H[14]), 4.01 (tt, *J* = 11.5, 4.2 Hz, 1H, H[7]), 3.63 – 3.56 (m, 2H, H[9e]), 3.25 – 3.18 (m, 2H, H[9a]), 2.05 – 1.91 (m, 4H, H[8]). ^{13}C NMR (151 MHz, DMSO-d_6) δ 162.38, 152.62, 147.50, 142.03, 140.58, 138.30, 136.59, 133.62, 132.07, 129.38, 122.89, 120.98, 120.32, 118.68, 116.85 (q, *J* = 25.5 Hz), 110.33, 109.75, 99.63, 55.30, 52.37, 51.08, 49.59 (2C), 48.47, 44.10, 30.65 (2C). LC-MS (APCI$^+$/ESI): found m/z = 537.2, 539.2 $[M+H]^+$ (cal. for $C_{28}H_{24}ClF_3N_6$, 536.17, 538.17). Purity: 99%, t_R = 2.447 min.

2-(4-((7-chloroquinolin-4-yl)amino)piperidin-1-yl)-1-(4-fluorobenzyl)-1H-benzo[d]imidazole-5-carbonitrile (191)

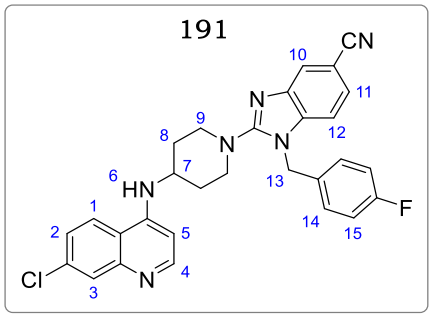

Following general procedure 12, obtained from **167** (0.080 g, 0.31 mmol) and **165u** (0.106 g, 0.37 mmol) as a pale-yellow solid (0.122 g, 77%). m.p.: 105 – 106 °C. R_f (10% MeOH/DCM), 0.25. ^{1}H NMR (600 MHz, DMSO-d_6) δ 8.58 (d, *J* = 7.5 Hz, 1H, H[4]), 8.43 (d, *J* = 7.9 Hz, 1H, H[1]), 8.19 (d, *J* = 7.5 Hz, 1H, H[5]), 7.92 (d, *J* = 2.0 Hz, 1H, H[3]), 7.89 (d, *J* = 8.5 Hz, 2H, H[15]), 7.65 – 7.58 (m, 2H, H[2,10]), 7.29 (d, *J* = 8.5 Hz, 2H, H[15]), 7.12 (dd, *J* = 8.1, 1.5 Hz, 1H, H[12]), 7.05

(dd, J = 8.1, 1.5 Hz, 1H, H^{11}), 6.95 (d, J = 6.5 Hz, 1H, H^{6}), 5.41 (s, 2H, H^{13}), 4.01 (tt, J = 11.3, 4.0 Hz, 1H, H^{7}), 3.58 – 3.51 (m, 2H, H^{9e}), 3.17 (td, J = 12.9, 4.1 Hz, 2H, H^{9a}), 1.95 – 1.82 (m, 4H, H^{8}). ^{13}C NMR (151 MHz, DMSO-d_6) δ 159.63, 150.30, 146.38, 144.09, 140.78, 137.60, 136.05, 133.22 (2C), 131.58, 128.59 (2C), 126.97, 123.74, 122.54, 120.39, 120.07, 116.13, 111.74, 110.32, 99.32, 51.49, 50.34, 49.18 (2C), 46.21, 46.09, 30.81 (2C). LC-MS (APCI$^+$/ESI): found m/z = 511.2, 513.2 $[M+H]^+$ (cal. for $C_{29}H_{24}ClFN_6$, 510.17, 512.17). Purity: 99%, t_R = 2.396 min.

7-chloro-N-(1-(1-(4-fluorobenzyl)-5-(methylsulfonyl)-1H-benzo[d]imidazol-2-yl) piperidin-4-yl) quinolin-4-amine (192)

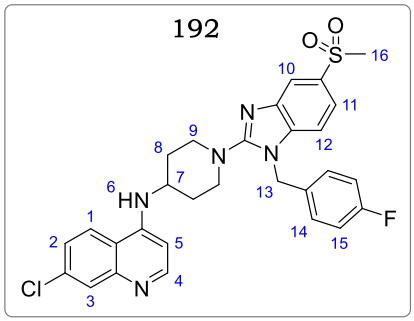

Following general procedure 12, obtained from **167** (0.080 g, 0.31 mmol) and **165v** (0.126 g, 0.37 mmol) as a pale-yellow solid (0.138 g, 79%). m.p.: 112 – 113 °C. R_f (10% MeOH/DCM), 0.19. ^{1}H NMR (600 MHz, DMSO-d_6) δ 8.60 (d, J = 7.9 Hz, 1H, H^4), 8.41 (d, J = 8.5 Hz, 1H, H^1), 8.22 (d, J = 7.9 Hz, 1H, H^5), 7.89 (d, J = 1.8 Hz, 1H, H^3), 7.83 (d, J = 8.5 Hz, 2H, H^{15}), 7.69 – 7.57 (m, 2H, $H^{2,10}$), 7.25 (d, J = 8.5 Hz, 2H, H^{15}), 7.10 (dd, J = 8.5, 1.5 Hz, 1H, H^{12}), 7.01 (dd, J = 8.5, 1.8 Hz, 1H, H^{11}), 6.92 (d, J = 6.1 Hz, 1H, H^6), 5.40 (s, 2H, H^{13}), 3.98 (tt, J = 10.9, 3.9 Hz, 1H, H^7), 3.55 – 3.48 (m, 2H, H^{9e}), 3.20 – 3.06 (m, 5H, $H^{9a,16}$), 1.92 – 1.79 (m, 4H, H^8). ^{13}C NMR (151 MHz, DMSO-d_6) δ 158.65, 149.38, 145.39, 142.05, 139.65, 137.56, 132.68 (2C), 132.01, 128.97 (2C), 126.64, 123.32, 122.07, 120.74, 119.38, 116.50, 111.27, 109.37, 98.95, 51.34, 50.07, 49.68 (2C), 46.30, 45.58, 44.86, 31.08 (2C). LC-MS (APCI$^+$/ESI): found m/z = 564.2, 566.2 $[M+H]^+$ (cal. for $C_{29}H_{27}ClFN_5O_2S$, 563.16, 565.15). Purity: 99%, t_R = 2.373 min.

Methyl 2-(4-((7-chloroquinolin-4-yl)amino)piperidin-1-yl)-1-(4-fluorobenzyl)-1H-benzo[d]imidazole-5-carboxylate (193)

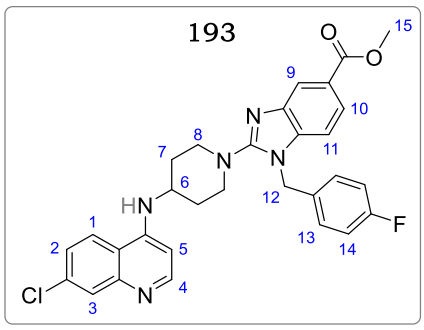

Following general procedure 12, obtained from **167** (0.080 g, 0.31 mmol) and **165w** (0.118 g, 0.37 mmol) as a pale-yellow solid (0.123 g, 73%). m.p.: 112 – 113 °C. R_f (10% MeOH/DCM), 0.19. ^{1}H NMR (400 MHz, Methanol-d_4) δ 8.41 – 8.34 (m, 2H, $H^{1,4}$), 8.06 (d, J = 1.7 Hz, 1H, H^9), 7.83 (d, J = 2.1 Hz, 1H, H^3), 7.70 (dd, J = 8.4, 1.7 Hz, 1H, H^{10}), 7.56 (dd, J = 9.1, 2.1 Hz, 1H,

H^{3}), 7.38 (d, J = 8.1 Hz, 1H, H^{5}), 7.23 (d, J = 8.5 Hz, 2H, H^{14}), 7.09 (d, J = 8.5 Hz, 2H, H^{13}), 6.88 (d, J = 8.4 Hz, 1H, H^{11}), 5.41 (s, 2H, H^{12}), 4.04 (tt, J = 11.1, 4.3 Hz, 1H, H^{6}), 3.79 – 3.68 (m, 2H, H^{8e}), 3.30 – 3.23 (m, 2H, H^{8a}), 3.12 (s, 3H, H^{15}), 2.24 – 2.14 (m, 2H, H^{7e}), 1.99 (dtd, J = 12.9, 9.3, 4.2 Hz, 1H, H^{7a}). ^{13}C NMR (101 MHz, Methanol-d_4) δ 163.64, 161.20, 160.06, 153.24, 146.16, 142.89, 140.86, 138.72, 137.72, 134.42, 131.74, 128.20 (d, J = 8.26 Hz), 126.17 (2C), 124.08, 122.01, 120.51 (2C), 116.33, 115.60, 115.38, 110.32, 98.86, 50.30, 49.34 (2C), 46.59, 43.64, 30.26 (2C). LC-MS (APCI$^+$/ESI): found m/z = 544.2, 546.2 $[M+H]^+$ (cal. for $C_{30}H_{27}ClFN_5O_2$, 543.18, 545.19). Purity: 98%, t_R = 2.497 min.

General Procedure 19: Microwave-assisted and solvent-free amination of 4-chloroquinolines (S_NAr)

Amine **200** (0.070g, 0.22 mmol, 1.0 equiv), an appropriately 7-substituted 4-chloroquinoline (1.0 equiv), and phenol (0.041 g, 0.44 mmol, 2.0 equiv) were charged into a 10 ml microwave tube containing a stirring bar. The reaction mixture was irradiated under microwave at 150 W for 5 min. The cooled crude reaction mixture was taken up in 10 ml of 10% MeOH/DCM and adsorbed on silica gel. The products were isolated after flash chromatography using 6 – 9% MeOH/DCM as eluent.

N-(1-(1-(4-fluorobenzyl)-1H-benzo[d]imidazol-2-yl)piperidin-4-yl)quinolin-4-amine (200)

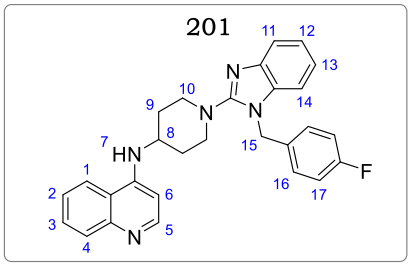

Obtained from 4-chloroquinoline (0.035 g, 0.22 mmol) as a pale-yellow solid (0.056 g, 58%). m.p.: 117 – 119 °C. R_f (10% MeOH/DCM), 0.28. ^{1}H NMR (400 MHz, DMSO-d_6) δ 8.53 (d, J = 8.9 Hz, 1H, H^{5}), 8.45 (d, J = 6.5 Hz, 1H, H^{1}), 8.22 (dd, J = 8.2, 1.4 Hz, 1H, H^{4}), 7.42 – 7.36 (m, 3H, $H^{4,11,14}$), 7.21 (d, J = 7.9 Hz, 2H, H^{17}), 7.10 – 7.01 (m, 5H, $H^{2,7,12,16}$), 6.89 – 6.80 (m, 2H, $H^{3,13}$), 5.35 (s, 2H, H^{15}), 4.05 (tt, J = 10.9, 4.1 Hz, 1H, H^{8}), 3.62 – 3.54 (m, 2H, H^{10e}), 3.19 – 3.09 (m, 2H, H^{10a}), 2.02 – 1.90 (m, 4H, H^{9}). ^{13}C NMR (101 MHz, DMSO) δ 165.28, 157.20, 152.56, 145.37, 142.74, 140.98, 135.29, 132.60, 129.71 (2C), 125.08, 122.58 (2C), 119.34 (d, J = 15.2 Hz), 118.02, 117.44, 116.68, 115.08, 111.85, 110.37, 102.45, 99.68, 56.30, 49.85 (2C), 46.64, 30.05 (2C). LC-MS (APCI$^+$/ESI): found m/z = 452.2 $[M+H]^+$ (cal. for $C_{28}H_{25}FN_5$, 451.22). Purity: 99%, t_R = 2.414 min.

7-fluoro-N-(1-(1-(4-fluorobenzyl)-1H-benzo[d]imidazol-2-yl)piperidin-4-yl) quinolin-4-amine (202)

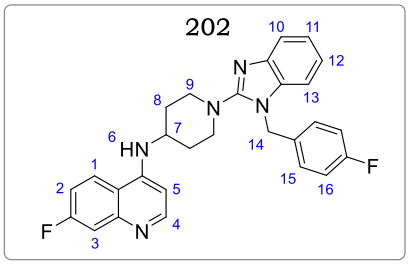

Obtained from **197a** (0.040 g, 0.22 mmol) as a pale-yellow solid (0.045 g, 44%). m.p.: 110 – 113 °C. R_f(10% MeOH/DCM), 0.26. ^{1}H NMR (400 MHz, DMSO-d_6) δ 8.52 (d, J = 8.2 Hz, 1H, H^4), 8.42 (d, J = 6.9 Hz, 1H, H^1), 7.98 (dd, J = 8.5, 1.2 Hz, 1H, H^3), 7.65 (d, J = 8.2 Hz, 1H, H^5), 7.45 (d, J = 8.0 Hz, 1H, H^{10}), 7.31 (d, J = 8.1 Hz, 2H, H^{16}), 7.26 – 7.08 (m, 4H, H^{6,13,15}), 6.99 – 6.92 (m, 2H, H^{11,12}), 6.78 (ddd, J = 8.5, 6.9, 1.2 Hz, 1H, H^2), 5.32 (s, 2H, H^{14}), 4.03 (tt, J = 10.8, 3.9 Hz, 1H, H^7), 3.60 – 3.53 (m, 2H, H^{9e}), 3.19 – 3.10 (m, 2H, H^{9a}), 2.02 – 1.95 (m, 2H, H^{8e}), 1.91 – 1.83 (m, 2H, H^{8a}). ^{13}C NMR (101 MHz, DMSO-d_6) δ 165.38, 158.36, 154.32, 151.30, 149.68, 146.37, 140.01, 136.72, 134.55, 129.36 (2C), 128.32, 126.48, 124.34, 122.09 (2C), 119.67, 118.32, 115.98, 114.38, 110.22, 99.52, 50.03 (2C), 49.38, 46.46, 30.28 (2C). LC-MS (APCI$^+$/ESI): found m/z = 470.2 [M+H]$^+$ (cal. for $C_{28}H_{25}F_2N_5$, 469.21). Purity: 98%, t_R = 2.443 min.

7-bromo-N-(1-(1-(4-fluorobenzyl)-1H-benzo[d]imidazol-2-yl)piperidin-4-yl) quinolin-4-amine (203)

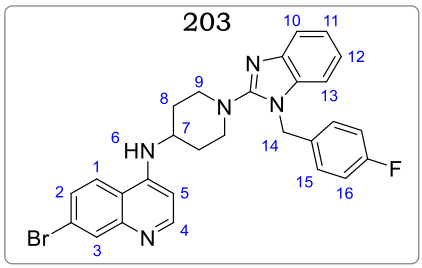

Obtained from **197b** (0.052 g, 0.22 mmol) as a pale-yellow solid (0.083 g, 72%). m.p.: 111 – 113 °C. R_f(10% MeOH/DCM), 0.42. ^{1}H NMR (400 MHz, DMSO-d_6) δ 8.55 (d, J = 9.1 Hz, 1H, H^4), 8.46 (d, J = 6.3 Hz, 1H, H^1), 8.10 (d, J = 1.9 Hz, 1H, H^3), 7.65 (d, J = 9.1 Hz, 1H, H^5), 7.48 (dd, J = 7.9, 1.5 Hz, 1H, H^{10}), 7.32 (d, J = 8.1 Hz, 2H, H^{16}), 7.27 – 7.13 (m, 4H, H^{6,13,15}), 7.12 – 7.05 (m, 2H, H^{11,12}), 6.74 (d, J = 6.3 Hz, 1H, H^2), 5.31 (s, 2H, H^{14}), 3.95 (tt, J = 10.5, 3.8 Hz, 1H, H^7), 3.59 – 3.51 (m, 2H, H^{9e}), 3.20 – 3.11 (m, 2H, H^{9a}), 2.05 – 2.00 (m, 2H, H^{8e}), 1.98 – 1.81 (m, 2H, H^{8a}). ^{13}C NMR (101 MHz, DMSO-d_6) δ 165.38, 159.04, 157.56, 150.33, 148.37, 146.32, 139.35, 134.20, 132.54, 129.68, 128.47 (2C), 126.58, 123.39, 121.08 (2C), 119.58 (d, J = 154 Hz), 118.34, 117.02, 116.52, 114.47 (2C), 110.68, 99.62, 49.85 (2C), 48.86, 46.33, 30.22 (2C). LC-MS (APCI$^+$/ESI): found m/z = 530.0, 532.0 [M+H]$^+$ (cal. for $C_{28}H_{25}BrFN_5$, 529.13, 531.13). Purity: 98%, t_R = 2.495 min.

N-(1-(1-(4-fluorobenzyl)-1H-benzo[d]imidazol-2-yl)piperidin-4-yl)-7-(trifluoromethyl) quinolin-4-amine (204)

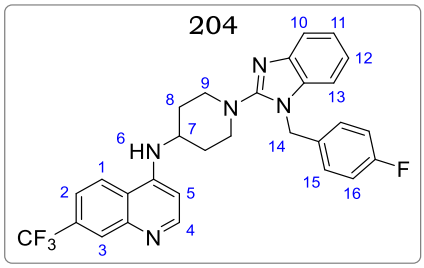

Obtained from **197c** (0.051 g, 0.22 mmol) as a pale-yellow solid (0.071 g, 63%). m.p.: 102 – 104 °C. R_f(10% MeOH/DCM), 0.47. ^{1}H NMR (400 MHz, DMSO-d_6) δ 8.58 (d, J = 8.9 Hz, 1H, H^4), 8.51 (d, J = 5.5 Hz, 1H, H^1), 8.08 (s, 1H, H^3), 7.68 (d, J = 8.9 Hz, 1H, H^5), 7.45 (d, J = 7.7 Hz, 1H, H^{10}), 7.29 – 7.13 (m, 6H, H^{6,13,15,16}), 7.12 – 7.01 (m, 2H, H^{11,12}), 6.76 (d, J = 5.5 Hz, 1H, H^2), 5.31 (s, 2H, H^{14}), 3.90 – 3.79 (m, 1H, H^7), 3.63 – 3.53 (m, 2H, H^{9e}), 3.20 – 3.09 (m, 2H, H^{9a}), 2.08 – 2.00 (m, 2H, H^{8e}), 1.94 – 1.81 (m, 2H, H^{8a}). ^{13}C NMR (101 MHz, DMSO-d_6) δ 163.08, 160.66, 158.19, 152.56, 149.56, 147.90, 141.90, 135.47, 133.68, 129.08 (d, J = 22 Hz, 2C), 128.99, 126.57, 124.77, 121.81, 121.32 (d, J = 154 Hz), 119.28, 117.81, 116.13, 115.91 (2C), 110.21, 100.79, 50.09 (2C), 49.59, 46.72, 30.79 (2C). LC-MS (APCI$^+$/ESI): found m/z = 520.2 [M+H]$^+$ (cal. for $C_{29}H_{25}F_4N_5$, 519.20). Purity: 98%, t_R = 2.526 min.

4-((1-(1-(4-fluorobenzyl)-1H-benzo[d]imidazol-2-yl)piperidin-4-yl) amino) quinoline-7-carbonitrile (205)

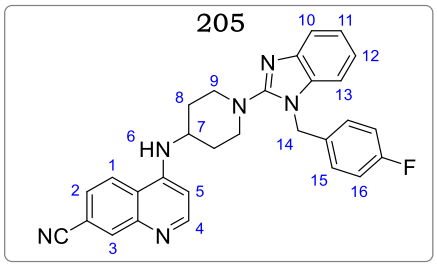

Obtained from **197d** (0.041 g, 0.22 mmol) as a pale-yellow solid (0.050 g, 49%). m.p.: 92 – 94 °C. R_f(10% MeOH/DCM), 0.31. ^{1}H NMR (400 MHz, DMSO-d_6) δ 8.55 – 8.47 (m, 2H, H^{1,4}), 8.27 (d, J = 1.5 Hz, 1H, H^3), 7.73 (d, J = 8.7 Hz, 1H, H^5), 7.45 (d, J = 7.7 Hz, 1H, H^{10}), 7.28 – 7.12 (m, 6H, H^{6,13,15,16}), 7.12 – 7.01 (m, 2H, H^{11,12}), 6.76 (dd, J = 5.6, 1.5 Hz, 1H, H^2), 5.30 (s, 2H, H^{14}), 3.91 – 3.74 (m, 1H, H^7), 3.64 – 3.51 (m, 2H, H^{9e}), 3.24 – 3.07 (m, 2H, H^{9a}), 2.09 – 1.98 (m, 2H, H^{8e}), 1.93 – 1.79 (m, 2H, H^{8a}). ^{13}C NMR (101 MHz, DMSO-d_6) δ 163.07, 160.65, 158.17, 152.78, 149.45, 147.90, 141.89, 135.47, 134.91, 133.68, 129.08 (d, J = 23 Hz, 2C)), 124.92, 121.81 (d, J = 15.3 Hz), 121.32, 119.18, 117.81, 116.13, 115.91 (2C), 111.92, 110.22, 101.12, 50.06 (2C), 49.59, 46.72, 30.75 (2C). LC-MS (APCI$^+$/ESI): found m/z = 477.2 [M+H]$^+$ (cal. for $C_{29}H_{25}FN_6$, 476.21). Purity: 99%, t_R = 2.441 min.

N-(1-(1-(4-fluorobenzyl)-1H-benzo[d]imidazol-2-yl)piperidin-4-yl)-7-(trifluoromethoxy)quinolin-4-amine (206)

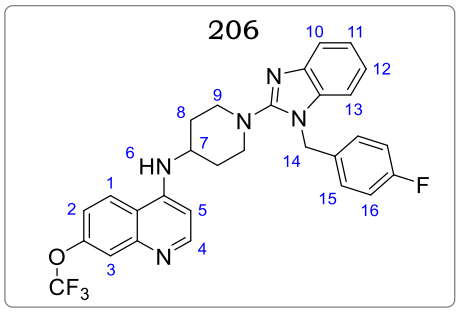

Obtained from **197e** (0.054 g, 0.22 mmol) as a pale-yellow solid (0.068 g, 59%). m.p.: 104 – 106 °C. R_f (10% MeOH/DCM), 0.45. ^{1}H NMR (400 MHz, DMSO-d_6) δ 8.63 (d, J = 8.5 Hz, 1H, H^4), 8.49 (d, J = 7.3 Hz, 1H, H^1), 7.98 (d, J = 2.1 Hz, 1H, H^3), 7.65 (d, J = 8.5 Hz, 1H, H^5), 7.46 – 7.38 (m, 3H, H^{10,16}), 7.30 – 7.15 (m, 4H, H^{6,13,15}), 7.09 – 6.98 (m, 2H, H^{11,12}), 6.72 (d, J = 7.3 Hz, 1H, H^2), 5.32 (s, 2H, H^{14}), 4.00 (tt, J = 10.5, 3.8 Hz, 1H, H^7), 3.60 – 3.53 (m, 2H, H^{9e}), 3.19 – 3.10 (m, 2H, H^{9a}), 2.08 – 2.01 (m, 2H, H^{8e}), 1.93 – 1.85 (m, 2H, H^{8a}). ^{13}C NMR (101 MHz, DMSO-d_6) δ 164.38, 159.32, 157.31, 151.32, 148.37, 146.85, 140.52, 136.30, 132.35, 129.68, 128.05 (2C), 125.38, 123.57, 121.22 (2C), 121.04 (q, J = 28.3 Hz), 119.35, 117.54, 116.96, 115.11, 109.34, 98.95, 50.02 (2C), 48.96, 45.68, 30.33 (2C). LC-MS (APCI$^+$/ESI): found m/z = 536.2 [M+H]$^+$ (cal. for $C_{29}H_{25}F_4N_5O$, 535.20). Purity: 98%, t_R = 2.521 min.

N-(1-(1-(4-fluorobenzyl)-1H-benzo[d]imidazol-2-yl)piperidin-4-yl)-7-methoxyquinolin-4-amine (207)

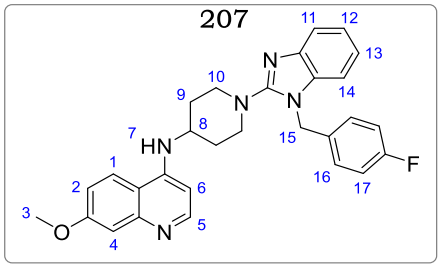

Obtained from **197f** (0.042 g, 0.22 mmol) as a pale-yellow solid (0.044 g, 42%). m.p.: 120 – 122 °C. R_f(10% MeOH/DCM), 0.22. ^{1}H NMR (400 MHz, DMSO-d_6) δ 8.49 (d, J = 9.4 Hz, 1H, H^5), 8.42 (d, J = 6.7 Hz, 1H, H^1), 8.30 (d, J = 9.4 Hz, 1H, H^6), 7.45 (d, J = 7.6 Hz, 1H, H^{11}), 7.30 (s, 1H, H^4), 7.28 – 7.12 (m, 6H, H^{7,14,16,17}), 7.12 – 7.01 (m, 2H, H^{12,13}), 6.85 (d, J = 6.7 Hz, 1H, H^2), 5.31 (s, 2H, H^{15}), 4.09 – 3.98 (m, 1H, H^8), 3.91 (s, 3H, H^3), 3.65 – 3.54 (m, 2H, H^{10e}), 3.22 – 3.09 (m, 2H, H^{10a}), 2.05 – 1.89 (m, 4H, H^9). ^{13}C NMR (101 MHz, DMSO) δ 162.47, 158.05, 153.56, 144.53, 143.05, 141.86, 135.45, 133.66, 129.00 (d, J = 23 Hz, 2C), 125.38, 121.84, 121.37 (d, J = 152 Hz), 117.82, 117.40, 116.14, 115.92, 111.91, 110.25, 102.31, 98.30, 56.23, 50.44, 49.92 (2C), 46.71, 30.64 (2C). LC-MS (APCI$^+$/ESI): found m/z = 482.2 [M+H]$^+$ (cal. for $C_{29}H_{28}FN_5O$, 481.23). Purity: 98%, t_R = 2.466 min.

N-(1-(1-(4-fluorobenzyl)-1H-benzo[d]imidazol-2-yl)piperidin-4-yl)-7-nitroquinolin-4-amine (208)

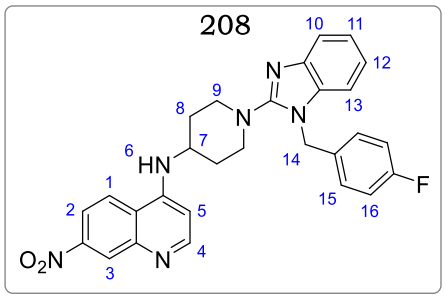

Obtained from **197g** (0.045 g, 0.22 mmol) as a yellow solid (0.042 g, 39%). m.p.: 97 – 99 °C. R_f (10% MeOH/DCM), 0.48. ^{1}H NMR (600 MHz, DMSO-d_6) δ 8.59 (d, J = 9.3 Hz, 1H, H^4), 8.56 (d, J = 5.5 Hz, 1H, H^1), 8.54 (d, J = 2.4 Hz, 1H, H^3), 8.13 (dd, J = 5.5, 2.4 Hz, 1H, H^2), 7.45 (d, J = 9.3 Hz, 1H, H^5), 7.29 (d, J = 7.6 Hz, 1H, H^{10}), 7.25 – 7.20 (m, 3H, H^{13,16}), 7.16 (d, J = 8.9 Hz, 2H, H^{15}), 7.10 (ddd, J = 8.0, 7.6, 1.2 Hz, 1H, H^{11}), 7.05 (ddd, J = 8.1, 7.2, 1.0 Hz, 1H, H^{12}), 6.81 (d, J = 5.5 Hz, 1H, H^6), 5.31 (s, 2H, H^{14}), 3.84 (tdt, J = 11.2, 5.5, 3.3 Hz, 1H, H^7), 3.61 – 3.55 (m, 2H, H^{9e}), 3.16 (td, J = 12.6, 2.4 Hz, 2H, H^{9a}), 2.07 – 2.02 (m, 2H, H^{8e}), 1.93 – 1.83 (m, 2H, H^{8a}). ^{13}C NMR (151 MHz, DMSO) δ 162.65, 161.04, 158.15, 153.52, 149.47, 148.22, 147.85, 141.88, 135.45, 133.65, 131.15, 129.03 (d, J = 25 Hz, 2C), 125.10, 123.08, 121.79 (d, J = 148 Hz), 117.79, 117.02, 116.07 (2C), 110.19, 101.48, 50.03 (2C), 49.61, 46.71, 30.72 (2C). LC-MS (APCI$^+$/ESI): found m/z = 497.2 $[M+H]^+$ (cal. for $C_{28}H_{25}FN_6O_2$, 496.20). Purity: 98%, t_R = 2.497 min.

6.3 Biological Evaluation

6.3.1 *In vitro* Antiplasmodium Activity Assay

6.3.1.1 Lactate Dehydrogenase (LDH) Assay

Compounds were tested using parasite lactate dehydrogenase assay as a marker for parasite survival. All parasite strains were acquired from MR4 (Malaria Research and Reference Reagent Resource Center, Manassas, VA). Briefly, the respective stock solutions of CQ diphosphate and test compounds were prepared to 2 mg.ml^{-1} in distilled water (for CQ) and 100% DMSO for test compounds and then stored at –20 °C, and further dilutions were prepared on the day of the experiment. The cultures were synchronized in the ring stage using 15 ml of 5% (w/v) D-sorbitol in water. Synchronous cultures of *Pf*NF54 (CQ-S) and *Pf*K1 (MDR) in the late trophozoite stage were prepared to 2% parasitemia & 2% hematocrit. Compounds were tested at starting concentrations of 10,000 ng.ml^{-1} (1000 ng.ml^{-1} for CQ), which were then serially diluted 2-fold in complete medium to give 10 concentrations with a final volume of 200 µl in each well. Parasites were incubated in the presence of the compounds at 37 °C under hypoxic conditions (4% CO_2 and 3% O_2 in N_2) for 48 h. After

incubation, 100 µl of MalStat reagent and 15 µl of resuspended culture were combined, followed by addition of 25 µl of nitro blue tetrazolium chloride (NBT). The plates were kept in the dark for 10 min in order to fully develop, after which absorbance was measured at 620 nm on a microplate reader. Raw data was processed using Microsoft Excel to analyze the dose-response.

6.3.1.2 Hypoxanthine Incorporation Assay

The modified [^{3}H]-hypoxanthine incorporation assay was used to test compounds against drug-sensitive (NF54) and resistant (K1) strains of *Plasmodium falciparum*. Parasites were cultivated in human erythrocytes (RBCs) following the procedure by Trager *et al.*,[1] however, medium variations included RPMI 1640, supplemented with 0.5% ALBUMAX® II, 25 mM HEPES, 25 mM NaHCO3 (pH 7.4), 0.36 mM hypoxanthine, and 100 µg/ml neomycin. The parasite cultures were maintained in an environment comprising 3% O_2, 4% CO_2, and 93% N_2, at 37 °C and in humid modular chambers. Test compounds were dissolved in DMSO (100%), to obtain 10 mg/ml stock solutions, which were diluted in culture medium without hypoxanthine. Infected RBCs (100 µl/well with 2.5% hematocrit, and 0.3% parasitemia) were added to each compound titrated in 100 µl duplicates over a 64-fold range, and incubated for 48 h. Afterwards, 0.5 microCi of [^{3}H] hypoxanthine in 50 µl media was added, and the culture plates were allowed to incubate further for 24 h. Radioactivity was then determined from the parasites harvested on glass fiber filters using a β-plate liquid scintillation counter (Wallac, Zurich). Radioactivity was recorded as counts/min/well at each concentration of test compound. This was presented as percentage relative to the untreated controls. IC_{50} values were determined by linear interpolation.

6.3.2 *In vitro* Gametocytocidal Activity Assay

Gametocytes were produced and prepared following the method reported by Reader *et al.*[2] A luciferase reporter assay was used to enable the quantification of the stage-specific activity of compounds for the early- and late-stage gametocyte marker cell line NF54-*Pf*S16-GFP-Luc. The assays were set up on days 5 and 10 to represent >90% of early-stage II/III or late-stage IV/V gametocytes, respectively. In both cases, the assays were set up using a 2 – 3% gametocytemia, 1.5% hematocrit culture, and 48 h drug pressure in a gas chamber containing 90% N_2, 5% O_2, and 5% CO_2 at 37 °C. Luciferase activity was determined in 30 µl parasite lysates by adding 30 µl of the luciferin substrate (Promega Luciferase Assay System) at 25 °C, followed by the detection of resulting bioluminescence at 10s integration

constant, with the GloMax® Explorer Detection System using the Instinct® Software. 5 µM methylene blue and internal standards were included as controls. The dual point screens were performed as technical triplicates for a single biological assay.

6.3.3 *In vitro* Cytotoxicity Assay

Compounds were screened against Chinese Hamster Ovarian (CHO) mammalian cell lines, using the 3-(4,5-dimethylthiazol-2-yl)-2,5-diphenyltetrazoliumbromide (MTT) assay.[3] Emetine was used as the reference standard. It was prepared to 2 mg/ml in distilled water, while the stock solutions of test compounds were prepared to 20 mg/ml in DMSO (100%), with the highest concentration of solvent to which the cells were exposed having no measurable effect on the cell viability. The initial concentration of the compounds and control was 100 µg/ml, which was serially diluted in complete medium with 10-fold dilutions to give 6 concentrations, the lowest being 0.001 µg/ml. Plates were incubated for 48 h with 100 µl of test compound and 100 µl of cell suspension in each well and developed afterward by adding 25 µl of sterile MTT (Thermo Fisher Scientific) to each well, followed by 4 h of incubation in the dark. The plates were then centrifuged, the medium aspirated, and 100 µl of DMSO was added to dissolve crystals before reading the absorbance at 540 nm. Data were analyzed, and the sigmoidal dose−response was derived using GraphPad Prism version 6.0 software (La Jolla, California, USA). All experiments were performed as three independent biological repeats, each with technical triplicates.

6.3.4 *In vitro* β-Hematin Inhibition Assay

Stock solutions of controls (CQ and Pyrimethamine) and test compounds were made to 20 mM in DMSO. A solution containing water/305.5 µM NP40/DMSO at a 70%/20%/10% (v/v) respectively, was added to every well in columns 1 – 11 on a 96–well plate, while 140 µl of water and 40 µl of 305.5 µM NP40 were added to column 12 to mediate the formation of β-hematin. 20 µl of control or test compound (20 mM) was added to column 12, and 100 µl of this solution was serially diluted to column 2, with column 1 left as a blank (no test compound). A 178.8 µl aliquot of hematin stock was suspended in 20 ml of a 1 M acetate buffer at pH 4.9, and 100 µl of this hematin suspension was added into each well. Plates were then incubated for 5 h at 37 °C, after which 32 µl of pyridine solution (20% water, 20% acetone, 10% 2 M HEPES buffer, pH 7.4, 50% pyridine) was added, followed by addition of 60 µl of acetone to all wells. The plates were read at 405 nm, and dose-response curves were plotted in GraphPad Prism version 6.01 (GraphPad Software Inc., La Jolla, California, USA) to obtain IC_{50} values.

6.3.5 *In vitro* hERG Inhibition Assay

These studies were carried out by Metrion Biosciences Ltd, Cambridge, UK.[4] A QPatch hERG assay in which a 4-point concentration response setup was used to assess hERG inhibition of the compounds. hERG was expressed in a CHO K1 cell line from the American Type Culture Collection (ATCC) which was grown and passaged under standard culture conditions. The external (e) and internal (i) recording solutions were of the following compositions (mM): NaCl – 140(e) : 0 (i); KCl – 2 (e): 70 (i); KF – 0 (e) : 60 (i); HEPES – 10 (e) : 10 (i); MgCl2 – 1 (e) : 0 (i); CaCl2 –2 (e) : 0 (i); Glucose – 5 (e) : 0 (i); EGTA - 0 (e) : 5 (i); Mg2ATP – 0 (e) : 5 (i) and pH – 7.4 (NaOH) (e) : 7.2 (KOH) (i). The external recording solution was regularly prepared and kept at 4 °C until required and was maintained at room temperature during recording. The internal recording solution was prepared and kept at –20 °C until required.

The QPatch is an automated chip-based planar patch clamp. Cells added to each well are drawn across a small aperture *via* suction, creating a Giga-ohm seal between the membrane surface and a treated silicon surface. A small volume of bathing solution containing the test compound or control bathing solution is added to a reservoir on the chip which perfuses across the cell through quartz-lined microfluidic channels. The solution is removed by capillary action before the next sample is added. Using the industry +40/–40 voltage protocol, currents were triggered from a holding potential of –90 mV at a stimulus frequency of 0.1 Hz.

Concentration response curves were established by cumulative addition of four increasing concentrations of the test compounds to an individual cell. This was achieved by allowing the whole-cell configuration to be attained, followed by addition of 0.1% DMSO (v/v) in external recording solution to each well in two bolus additions and allowing a two-minute recording time between each addition. Afterwards, four concentrations (0.3 – 10 μM) of test compound was added in two bolus additions at 2 min intervals. The effect on the hERG tail current amplitude was measured during the 4-minute recording time. The concentrations (0.3, 1, 3 and 10 μM) of the test samples were prepared to have a final concentration of 0.1% of DMSO (v/v) in the external recording solution. The experiments at each concentration were done in triplicate for each compound using a bioinformatics suite developed and running in Pipeline Pilot (Biovia, USA). The percent inhibition was calculated as a reduction in mean peak current relative to the value measured at the end of the vehicle control period. These data were used to construct the concentration-response curves which enabled

determination of the IC_{50} values. Compounds which could not achieve 50% inhibition at the highest tested concentration (10 μM), were extrapolated to obtain IC_{50} values. Therefore, all IC_{50} values above 10 μM reported in this thesis should be treated with caution.

6.4 Microsomal Metabolic Stability Assay

This assay was performed in duplicate using a 96-well microtiter plate. Test compounds (0.1 μM) were incubated at 37 °C in mouse and pooled human liver microsomes with a final protein concentration of 0.4 $mg.ml^{-1}$; XenoTech, Lenexa, KS suspended in 0.1 M phosphate buffer at pH 7.4 for predetermined time points. This was in the presence and absence of cofactor-reduced nicotinamide adenine dinucleotide phosphate (NADPH, 1.0 mM). The reactions were quenched by adding ice-cold MeCN containing an internal standard (Carbamazepine, 0.0236 μg/mL). The samples were centrifuged, and the supernatant was analyzed via liquid chromatography-tandem mass spectrometry (LC–MS/MS) (Agilent Rapid Resolution HPLC, AB SCIEX 4500 MS). The relative loss of the parent compound with time was monitored, and plots were prepared for each compound of Ln% remaining versus time to determine the first-order rate constant for compound depletion. This was used to calculate the degradation half-life and subsequently to predict the *in vitro* intrinsic clearance (CL_{int}) and *in vitro* hepatic extraction ratio (E_H).[5]

6.5 *In vivo* Efficacy Studies in *P. Berghei* Mice

For each compound, *In vivo* antimalarial activity was assessed for a group of five female Naval Medical Research Institute (NMRI) mice (20 – 22 g) intravenously infected on day 0 with *P. berghei* GFP ANKA malaria strain (2×10^7 parasitized erythrocytes, a donation from A.P Waters and C.J Janse, Leiden University). Untreated control mice die typically between day 6 and day 7 post-infection. Test compounds were formulated in 0.5% methyl cellulose/0.5% Tween 80 and administered orally as four consecutive doses of 50 mg/kg at 4, 24, 48 and 72 h post infection. Parasitemia was determined 72 h post infection using standard flow cytometry techniques. Activity was calculated as the difference between the mean percent parasitemia for the control and treated groups expressed as a percent relative to the control group. The survival time in days was recorded up to 30 days after infection. A compound was considered curative if the animal survived to day 30 after infection, with no detectable parasites by slide reading.

The Swiss TPH in Basel are approved for animal studies by the veterinary authorities of the Canton Basel-Stadt (Permit No. 1731 and 2303) based on Swiss Cantonal (Verordnung

Veterinäramt Basel-Stadt) and National Regulations (The Swiss Animal Protection Law, Tierschutzgesetz).

6.6 Pharmacokinetics Studies using Dried-Blood Spots (DBS)

Dried Blood spot samples of H3D-007251 (**67**) and H3D-007252 (**69**) were received from the Swiss Tropical Health Institute, following dosing of the compounds in a *P.berghei* mouse model. Dried blood spot samples were reproducibly punched out of the Munktell cards and extracted by protein precipitation using acetonitrile containing 10ng/ml MMV902 as internal standard, and subsequently centrifuged. Calibration standards and quality controls were extracted following the same procedure. Supernatants were injected onto the column for LC-MS/MS analysis. Data processing conducted using graph.

6.7 Solubility Assays

6.7.1 Kinetic Turbidimetric Method (pH 7.4)

Following the dissolution of test compound in DMSO to make a 10 mM stock solution, pre-dilution plate was prepared by taking from each stock solution and serially diluting in triplicate to yield concentrations from 0.25 mM to 10.0 mM on a 96 well plate. From each pre-dilution solution, secondary dilutions of the compounds in both DMSO and 0.01M pH 7.4 PBS where prepared in triplicate on a second 96-well plate. Wells in columns 1-6 would contain compound in DMSO, while those in columns 7-12 would contain samples in PBS at similar nominal concentrations as those in DMSO. The final volume of solvent in each assay plate was 200 µL, prepared by pipetting 4 µL each of solution from the pre-dilution plate to the corresponding well into both DMSO and PBS (both 196 µL). This ensures that the final concentration of DMSO in the PBS aqueous buffer does not exceed 2% v/v. Similarly, a second secondary plate containing compound concentrations of 60, 100 and 120 µM was prepared. Different concentrations in DMSO were prepared as controls to determine false turbimetric absorbance readings arising from the compounds in solution absorbing incident radiation at the test wavelength. Following preparation, the assay plate was covered and left to equilibrate for 2 h at 25 °C. Afterwards, UV-vis absorbance readings from the plate were measured at 620 nm using a SpectraMax 340PC^{384} microplate reader. Plots of corrected absorbance against compound concentration were computed for a graphical representation of the data using MS Excel. Reserpine and hydrocortisone were used as positive and negative controls, respectively.

6.7.2 Kinetic Solubility by HPLC (pH 6.5)

The shake flask method was used to carry out the kinetic solubility assay.[6] Calibration standards from 10 to 220 μM in DMSO were prepared using 10 mM stock solutions of the test compounds in DMSO. The stock solutions were used to spike in a ration of 1:50 duplicate aqueous samples in phosphate buffered saline at pH 6.5. The DMSO was dried off using a GeneVac (MiVac, 90 min, 37 °C), after which the samples were incubated for 20 hours at 25 °C while shaking. Following incubation, the solutions were filtered, and absorbance was measured using HPLC-DAD (Agilent 1200 Rapid Resolution HPLC with a diode array detector). The calibration standards prepared prior, were used to plot the calibration curves, which were used to determine the exact solubility of the aqueous samples.

6.8 References

(1) Trager, W.; Jensen, J. Human Malaria Parasites in Continuous Culture. *Science (80).* **1976**, *193* (4254), 673–675.

(2) Reader, J.; Botha, M.; Theron, A.; Lauterbach, S. B.; Rossouw, C.; Engelbrecht, D.; Wepener, M.; Smit, A.; Leroy, D.; Mancama, D.; et al. Nowhere to Hide: Interrogating Different Metabolic Parameters of Plasmodium Falciparum Gametocytes in a Transmission Blocking Drug Discovery Pipeline towards Malaria Elimination. *Malar. J.* **2015**, *14* (1), 213.

(3) Liu, Y.; Peterson, D. A.; Kimura, H.; Schubert, D. Mechanism of Cellular 3-(4,5-Dimethylthiazol-2-Yl)-2,5-Diphenyltetrazolium Bromide (MTT) Reduction. *J. Neurochem.* **2002**, *69* (2), 581–593.

(4) Ridder, B. J.; Leishman, D. J.; Bridgland-Taylor, M.; Samieegohar, M.; Han, X.; Wu, W. W.; Randolph, A.; Tran, P.; Sheng, J.; Danker, T.; et al. A Systematic Strategy for Estimating HERG Block Potency and Its Implications in a New Cardiac Safety Paradigm. *Toxicol. Appl. Pharmacol.* **2020**, *394*, 114961.

(5) Bertrand, M.; Jackson, P.; Walther, B. Rapid Assessment of Drug Metabolism in the Drug Discovery Process. *Eur. J. Pharm. Sci.* **2000**, *11*, S61–S72.

(6) Hill, A. P.; Young, R. J. Getting Physical in Drug Discovery: A Contemporary Perspective on Solubility and Hydrophobicity. *Drug Discov. Today* **2010**, *15* (15–16), 648–655.

6.9 Appendix

Table A1: Physicochemical properties of **phase I**, **SAR 1** analogues.

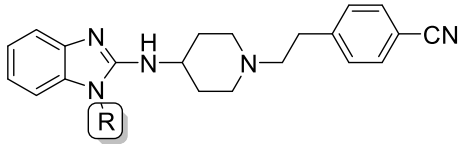

Code	R	R_1	MW (Da)	clog*P*	TPSA (Å²)	HBD	HBA	R_f[a]	t_R[b] (min)	m.p.[c] (°C)	Sol. (µM)
			Calculated properties‡					**Experimental properties**			
15	H	-	345.4	3.60	67.74	2	5	0.35	0.20	88.5	120
16	Me	-	359.5	3.80	56.88	1	5	0.39	0.21	111.5	100
17	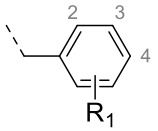	4-CN	460.6	4.70	80.67	1	6	0.40	2.38	123	90
18		3-F,4-CN	478.6	4.85	80.67	1	6	0.44	2.33	80	40
19		2-CN,4-F	478.6	4.85	80.67	1	6	0.43	2.33	83	80
20		2-F,4-CN	478.6	4.85	80.67	1	6	0.40	2.33	88	80
21		4-OMe	465.6	5.00	66.11	1	6	0.45	2.31	93.5	80
22		4-SO_2Me	513.7	4.07	91.02	1	7	0.41	2.09	115.5	40
23		4-NO_2	480.6	4.86	102.7	1	8	0.48	2.32	95.5	20
24		4-CO_2Me	493.6	4.86	83.18	1	7	0.48	2.35	100	100
25		4-CO_2H	479.6	4.45	94.18	2	7	0.12	2.14	139	140
26		4-CF_3	503.6	5.77	56.88	1	5	0.57	2.46	87	10
27		4-CH_3	449.6	5.49	56.11	1	5	0.51	2.38	96.5	40
28	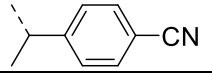	-	474.6	5.00	80.67	1	6	0.76	2.44	122	80
29	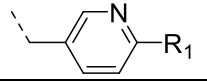	CF_3	504.6	4.83	69.77	1	6	0.44	2.36	ND	40
30		CH_3	450.6	4.45	69.77	1	6	0.35	2.44	73.5	60

MW = molecular weight in Daltons; clog*P* = calculated log value of the n-octanol/water partition coefficient; TPSA = topological polar surface area; HBD = hydrogen bond donors; HBA = hydrogen bond acceptors; R_f = retardation factor on thin layer chromatography (TLC); t_R = retention time in high power liquid chromatography (HPLC); m.p. = melting point; Sol = solubility at pH 7.4 using the turbidimetric method. ‡Predicted using StarDrop software, version 6.5.1-1. [a]TLC determined in 10% methanol in dichloromethane; [b]HPLC method described in chapter 6; [c]Avarage of two melting point runs (Tramadol hydrochloride used as the reference, m.p. = 178 – 180 °C).

Table A2: Physicochemical properties of **phase I**, **SARs 2** and **3** analogues

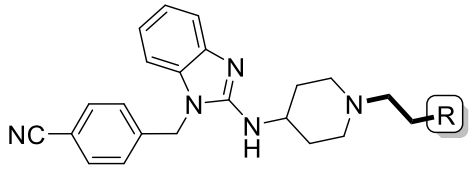

Code	R	R_1	MW (Da)	clog*P*	TPSA (Å²)	HBD	HBA	R_f[a]	t_R[b] (min)	m.p.[c] (°C)	Sol.[d] (μM)
31	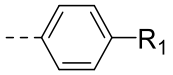	H	435.6	5.09	56.88	1	5	0.32	2.31	106	40
32		OH	451.6	4.62	77.11	2	6	0.29	2.13	ND	120
33		SO_2Me	513.7	4.07	91.02	1	7	0.31	2.16	232	80
34		CH_3	449.6	5.49	56.88	1	5	0.44	2.37	180	40
35		CF_3	503.6	5.71	56.88	1	5	0.51	2.63	92.5	20
36		NO_2	480.6	4.86	102.7	1	8	0.49	2.31	87	40
37		CO_2Me	493.6	4.86	83.18	1	7	0.34	2.33	166.5	80
38		CO_2Et	507.6	5.22	83.18	1	7	0.45	2.42	153	40
39		CO_2H	479.6	4.45	94.18	2	7	0.11	0.16	182	120
40			503.6	4.80	95.80	1	8	0.59	2.36	99	40
41		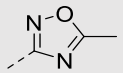	517.6	5.17	95.80	1	8	0.48	2.45	149	40
42		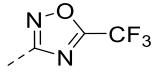	571.6	5.42	95.80	1	8	0.58	2.73	125	20
43		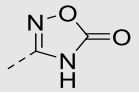	519.6	4.05	115.8	2	9	0.13	2.60	182	40
44		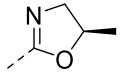	518.7	5.23	78.47	1	7	0.33	2.68	68	60
45		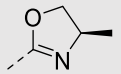	518.7	5.23	78.47	1	7	0.34	2.70	105	20

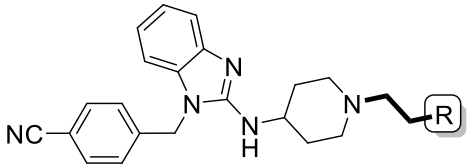

			Calculated properties‡					Experimental properties			
Code	**R**	**R_1**	**MW (Da)**	**clog*P***	**TPSA (Å²)**	**HBD**	**HBA**	**R_f[a]**	**t_R[b] (min)**	**m.p.[c] (°C)**	**Sol.[d] (μM)**
46	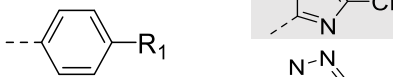	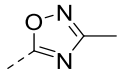	517.6	5.17	95.80	1	8	0.56	2.45	148	20
47		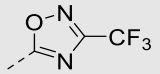	571.6	5.42	95.80	1	8	0.67	2.70	118	10
48		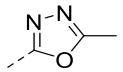	517.6	5.17	95.80	1	8	0.56	2.51	126	20
49	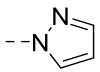	-	425.5	3.81	74.70	1	7	0.42	2.12	130	20
50	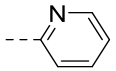	-	436.6	4.06	69.77	1	6	0.27	2.13	139	20
51	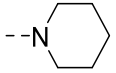	-	442.6	4.22	60.12	1	6	0.18	2.24	106	<5
52	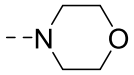	-	444.6	3.16	69.35	1	7	0.19	2.03	111.5	10
53	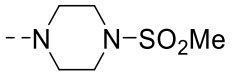	-	521.7	2.47	97.50	1	9	0.22	0.52	165	40
54	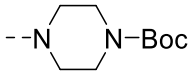	-	543.7	4.14	89.66	1	9	0.28	2.10	122	<10
55	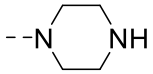	-	443.6	2.60	72.15	2	7	0.17	0.44	105	20

MW = molecular weight in Daltons; clog*P* = calculated log value of the n-octanol/water partition coefficient; TPSA = topological polar surface area; HBD = hydrogen bond donors; HBA = hydrogen bond acceptors; R_f = retardation factor on thin layer chromatography (TLC); t_R = retention time in high power liquid chromatography (HPLC); m.p. = melting point; Sol = solubility at pH 7.4 using the turbidimetric method. ‡Predicted using StarDrop software, version 6.5.1-1. [a]TLC determined in 10% methanol in dichloromethane; [b]HPLC method described in chapter 6; [c]Avarage of two melting point runs (Tramadol hydrochloride used as the reference, m.p. = 178 – 180 °C).

Table A3: Physicochemical properties of **phase I**, **SARs 4 and 1_B** analogues.

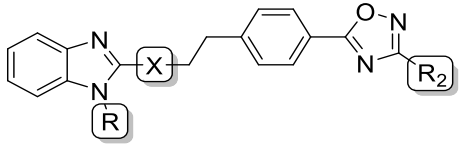

Code	R	R_1	X	R_2	MW (Da)	clog*P*	TPSA (Å²)	HBD	HBA	R_f[a]	t_R[b] (min)	m.p.[c] (°C)	Sol.[d] (µM)
58			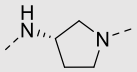	CH_3	503.6	5.02	95.80	1	8	0.37	2.92	75	80
59			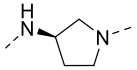		503.6	5.02	95.80	1	8	0.36	2.75	76	80
60			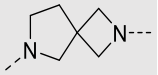		529.6	4.33	87.01	0	8	0.40	2.34	114	40
61			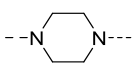		503.6	4.85	87.01	0	8	0.43	2.51	142	20
62			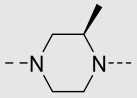		517.6	5.31	87.01	0	8	0.49	2.53	79	40
65			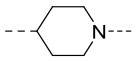		502.6	5.69	83.77	0	7	0.45	2.56	159	20
66	H			CH_3	402.5	4.08	82.87	2	7	0.20	2.47	172	80
67	H			CF_3	456.5	4.30	82.87	2	7	0.38	2.53	103	100
68	CH_3		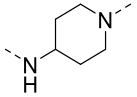	CH_3	416.5	4.28	72.01	1	7	0.34	2.53	135	160
69	CH_3			CF_3	470.5	4.51	72.01	1	7	0.35	2.61	91	160
70				CH_3	444.6	4.88	72.01	1	7	0.37	2.58	184	20

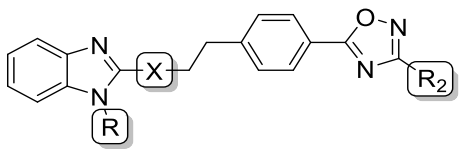

					Calculated properties‡					Experimental properties			
Code	**R**	**R_1**	**X**	**R_2**	**MW (Da)**	**clog*P***	**TPSA (Å²)**	**HBD**	**HBA**	**R_f[a]**	**t_R[b] (min)**	**m.p.[c] (°C)**	**Sol.[d] (µM)**
71	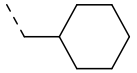	-	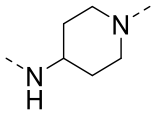	CH_3	498.8	5.88	72.01	1	7	0.49	2.52	79	80
72	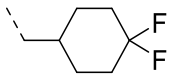	-			534.6	5.87	72.01	1	7	0.66	2.27	92	20
73	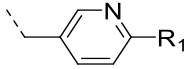	H		CH_3	493.6	4.52	84.90	1	8	0.51	2.33	218	ND
74		CF_3			561.6	5.08	84.90	1	8	0.45	2.71	91	40
75		4-CF_3	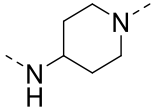		560.6	5.94	72.01	1	7	0.31	2.80	172	10
76	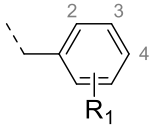	3-Me			506.6	5.80	72.01	1	7	0.60	2.47	114	20
77		3-F, 4-CN			535.6	5.29	95.80	1	8	0.51	2.67	166	<10
78		4-CO_2H			536.6	4.88	109.3	2	9	0.12	0.15	154	80

MW = molecular weight in Daltons; clog*P* = calculated log value of the n-octanol/water partition coefficient; TPSA = topological polar surface area; HBD = hydrogen bond donors; HBA = hydrogen bond acceptors; R_f = retardation factor on thin layer chromatography (TLC); t_R = retention time in high power liquid chromatography (HPLC); m.p. = melting point; Sol = solubility at pH 7.4 using the turbidimetric method. ‡Predicted using StarDrop software, version 6.5.1-1. [a]TLC determined in 10% methanol in dichloromethane; [b]HPLC method described in chapter 6; [c]Avarage of two melting point runs (Tramadol hydrochloride used as the reference, m.p. = 178 – 180 °C).

Table A4: Physicochemical properties of **phase II**, **SARs 1** and **2** analogues.

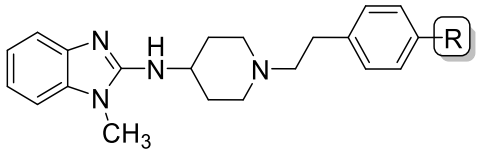

Code	R	Calculated properties‡					Experimental properties			
		MW (Da)	clog*P*	TPSA (Å²)	HBD	HBA	R_f[a]	t_R[b] (min)	m.p.[c] (°C)	Sol.[d] (µM)
79	CO_2Me	392.5	3.88	59.39	1	6	0.46	0.42	148.5	80
80	CO_2Et	406.5	4.25	59.39	1	6	0.48	2.05	75.5	120
81	CO_2H	378.5	3.41	70.39	2	6	0.05	0.14	153	160
83		405.5	3.02	53.40	1	6	0.29	0.15	134	80
84	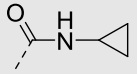	417.5	3.78	62.19	2	6	0.34	0.17	108	80
85	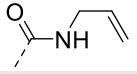	417.5	3.57	62.19	2	6	0.31	0.18	128.5	80
86	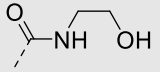	421.5	2.52	82.42	3	7	0.15	0.14	215	120
87	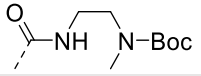	534.7	4.13	91.73	2	9	0.45	2.14	95.5	160
88	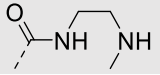	434.6	2.59	74.22	3	7	0.28	0.12	126	100
89	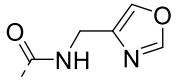	458.6	3.52	88.22	2	8	0.34	0.35	93	160
90	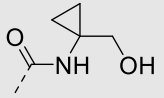	447.6	3.00	82.42	3	7	0.26	0.15	222	60

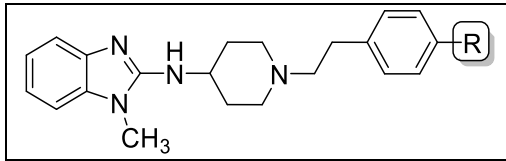

Code	R	MW (Da)	clog*P*	TPSA (Å²)	HBD	HBA	R_f[a]	t_R[b] (min)	m.p.[c] (°C)	Sol.[d] (µM)
		Calculated properties‡					**Experimental properties**			
91	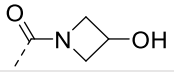	433.5	2.28	73.63	2	7	0.24	0.14	186	80
92	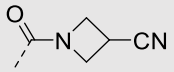	442.6	2.66	77.19	1	7	0.43	0.15	199	60
93	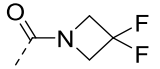	453.5	3.22	53.40	1	6	0.49	0.21	196	40
94	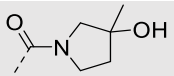	461.6	3.11	73.63	2	7	0.36	0.17	120	80
95	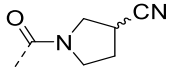	456.6	2.98	77.19	1	7	0.38	0.15	109.5	80
96	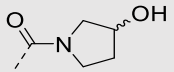	447.6	2.62	73.63	2	7	0.24	0.14	131	80
97	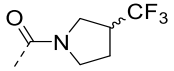	499.6	4.16	53.40	1	6	0.59	2.01	197	40
98	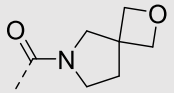	473.6	2.42	62.63	1	7	0.48	0.18	155	60
99	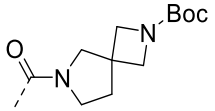	572.7	3.24	62.63	1	7	0.45	2.21	198	40
100	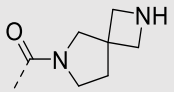	472.6	2.02	65.43	2	7	0.28	0.12	89.5	160
101	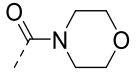	447.6	2.75	62.63	1	7	0.39	0.13	110.5	80
102	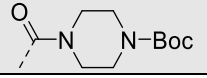	546.7	3.87	82.94	1	9	0.52	2.21	115	70

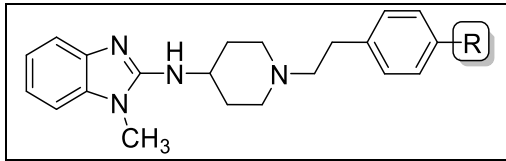

Code	R	MW (Da)	clog*P*	TPSA (Å²)	HBD	HBA	R_f[a]	t_R[b] (min)	m.p.[c] (°C)	Sol.[d] (µM)
		Calculated properties‡					**Experimental properties**			
103	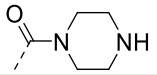	446.6	2.25	65.43	2	7	0.28	0.12	108.5	120
104	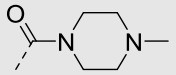	460.6	2.73	56.64	1	7	0.36	0.12	114.5	80
105	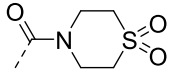	495.6	1.94	87.54	1	8	0.21	0.14	240	80
106	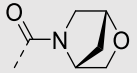	459.6	3.14	63.63	1	7	0.44	0.15	114	100
107	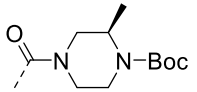	560.7	4.28	82.94	1	9	0.51	2.31	112.5	80
108	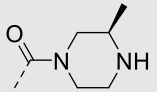	460.6	2.69	65.43	2	7	0.34	0.21	98.5	100
109	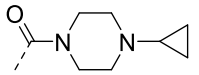	486.7	3.43	56.64	1	7	0.50	0.18	185	60
110	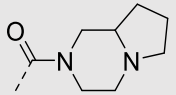	486.7	3.40	56.64	1	7	0.25	0.19	86	60
111	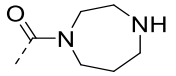	460.6	2.53	65.43	2	7	0.38	0.15	185.5	80
115	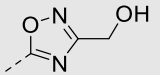	432.5	3.05	92.24	2	8	0.24	0.18	106	100
116	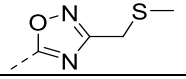	462.6	4.31	72.01	1	7	0.38	2.03	67	80

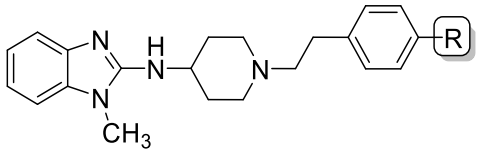

Code	R	Calculated properties‡ MW (Da)	clog*P*	TPSA (Å²)	HBD	HBA	Experimental properties R_f[a]	t_R[b] (min)	m.p.[c] (°C)	Sol.[d] (µM)
117	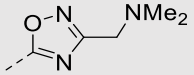	445.6	3.84	75.25	1	8	0.24	0.16	119.5	120
118	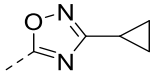	442.6	4.67	72.01	1	7	0.39	2.12	123	60
119	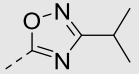	444.6	4.88	72.01	1	7	0.42	2.19	136	60
120	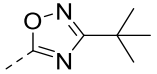	458.6	5.15	72.01	1	7	0.45	2.28	165	60
122	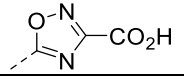	446.5	3.34	109.3	2	9	0.10	0.14	195	120

MW = molecular weight in Daltons; clog*P* = calculated log value of the n-octanol/water partition coefficient; TPSA = topological polar surface area; HBD = hydrogen bond donors; HBA = hydrogen bond acceptors; R_f = retardation factor on thin layer chromatography (TLC); t_R = retention time in high power liquid chromatography (HPLC); m.p. = melting point; Sol = solubility at pH 7.4 using the turbidimetric method. ‡Predicted using StarDrop software, version 6.5.1-1. [a]TLC determined in 10% methanol in dichloromethane; [b]HPLC method described in chapter 6; [c]Avarage of two melting point runs (Tramadol hydrochloride used as the reference, m.p. = 178 – 180 °C).

Table A5: Physicochemical properties of **phase II**, **SAR 3** analogues

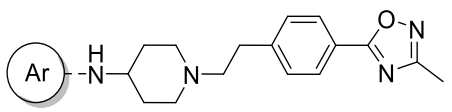

Code	Ar	R	MW (Da)	clog*P*	TPSA (Å²)	HBD	HBA	R_f[a]	t_R[b] (min)	m.p.[c] (°C)	Sol.[d] (µM)
			Calculated properties‡					**Experimental properties**			
132	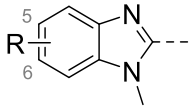	5-CN	441.5	4.02	95.80	1	8	0.21	2.20	98	80
133		5-CF_3	484.5	4.87	72.01	1	7	0.29	2.38	157	40
134		5-OCH_3	446.5	4.19	81.24	1	8	0.22	2.21	110	80
135		5-SO_2Me	494.6	3.53	106.2	1	9	0.19	2.04	203	60
136		5-CO_2Me	474.6	4.09	98.31	1	9	0.20	2.25	98.5	120
137		5-F	434.5	4.40	72.01	1	7	0.25	2.03	73	80
138		5-Br	495.4	4.75	72.01	1	7	0.30	2.29	75.5	80
139		5,6-CH_3	444.6	4.99	72.01	1	7	0.33	2.30	121	60
140		5,6-F	452.5	4.37	72.01	1	7	0.38	2.22	176	80
141		5,6-Cl	485.4	5.18	72.01	1	7	0.39	2.40	189	80
142		5-CO_2H	460.5	3.73	109.3	2	9	0.08	0.14	135	160
143		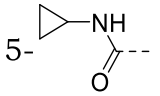	499.6	4.04	101.1	2	9	0.12	0.16	86	160

MW = molecular weight in Daltons; clog*P* = calculated log value of the n-octanol/water partition coefficient; TPSA = topological polar surface area; HBD = hydrogen bond donors; HBA = hydrogen bond acceptors; R_f = retardation factor on thin layer chromatography (TLC); t_R = retention time in high power liquid chromatography (HPLC); m.p. = melting point; Sol = solubility at pH 7.4 using the turbidimetric method. ‡Predicted using StarDrop software, version 6.5.1-1. [a]TLC determined in 10% methanol in dichloromethane; [b]HPLC method described in chapter 6; [c]Avarage of two melting point runs (Tramadol hydrochloride used as the reference, m.p. = 178 – 180 °C).

Table A6: Physicochemical properties of **phase II**, **SAR 4** analogues

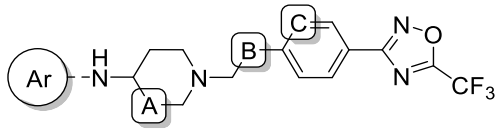

Code	Ar	A	B	C	MW (Da)	clog*P*	TPSA (Å²)	HBD	HBA	R_f[a]	t_R[b] (min)	m.p.[c] (°C)	Sol.[d] (µM)
					Calculated properties‡					**Experimental properties**			
146	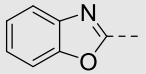	CH_2	CH_2	CH	457.5	4.40	80.22	1	7	0.42	2.26	98	100
147	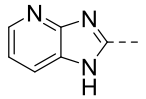				457.5	3.42	95.76	2	9	0.22	2.11	89	160
148	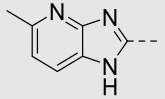				471.5	3.78	95.76	2	8	0.32	2.32	106	120
149	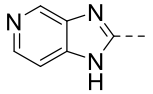				457.5	3.42	95.76	2	8	0.23	2.20	146	160
150	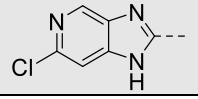				491.9	3.84	95.76	2	8	0.33	2.45	113.5	80
151	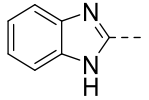		CH_2	CH	474.5	4.16	82.87	2	7	0.45	2.60	85	120
152					492.4	4.26	82.87	2	7	0.46	2.50	88	80
157			CH_2	N	475.4	3.31	95.76	2	8	0.43	2.16	110	120
156	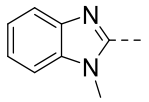	CH_2	CH_2	N	471.5	3.68	84.90	1	8	0.14	2.02	132	80
161				CH	488.5	4.32	72.01	1	7	0.50	2.50	103.5	80

Table A7: Physicochemical properties of **AST-CQ** hybrids, **SAR 1**.

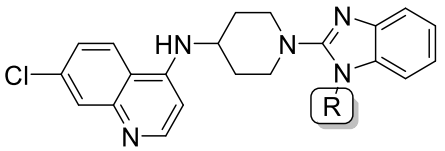

			Calculated properties‡					Experimental properties			
Code	**R**	**R_1**	**MW (Da)**	**cLog*P***	**TPSA (Å²)**	**HBD**	**HBA**	**R_f[a]**	**t_R[b] (min)**	**m.p.[c] (°C)**	**Sol.[d] (μM)**
168	H	-	377.9	4.32	56.84	2	5	0.17	0.84	166	80
169	CH_3	-	391.9	4.28	45.98	1	5	0.19	2.10	137	100
170		-	420.0	4.96	45.95	1	5	0.25	2.36	120	80
171	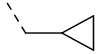	-	432.0	5.04	45.98	1	5	0.38	2.40	102	120
172	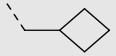	-	446.0	5.34	45.98	1	5	0.40	2.47	112	90
173	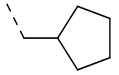	-	460.0	5.63	45.98	1	5	0.44	2.53	136	80
174	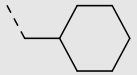	-	474.0	6.03	45.98	1	5	0.49	2.57	121	80
175		H	468.0	5.48	45.98	1	5	0.40	2.47	99.5	40
176		2-F	486.0	5.550	45.98	1	5	0.41	2.49	126	20
177		3-F	486.0	5.55	45.98	1	5	0.45	2.49	118	20
H-2		4-F	486.0	5.55	45.98	1	5	0.43	2.47	121	20
178	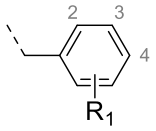	4-CN	493.0	5.23	69.77	1	6	0.39	2.39	113	60
179		4-Ome	498.0	5.38	55.21	1	6	0.38	2.47	112	60
180		4-CF_3	536.0	6.04	45.98	1	5	0.42	2.55	122	20
181		4-SO_2Me	546.1	4.37	80.12	1	7	0.37	2.31	148	80
182		4-$SONH_2$	531.1	4.61	89.07	2	7	0.19	2.26	142	100

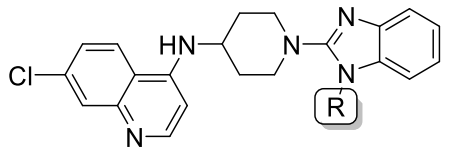			Calculated properties‡					Experimental properties			
Code	**R**	**R_1**	**MW (Da)**	**cLog*P***	**TPSA (Å²)**	**HBD**	**HBA**	**R_f[a]**	**t_R[b] (min)**	**m.p.[c] (°C)**	**Sol.[d] (µM)**
183	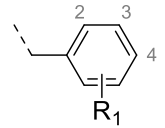	4-NO_2	513.0	5.25	91.80	1	8	0.46	2.44	118	80
184		4-NHCOMe	525.0	4.72	75.08	2	7	0.10	2.34	160	100
185		4-CO_2Me	526.0	5.28	72.28	1	7	0.22	2.27	133	80
187		4-CONHMe	525.0	4.61	75.08	2	7	0.08	2.33	140.5	80
188	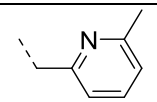	-	483.0	4.69	58.87	1	6	0.35	2.42	159	80
189	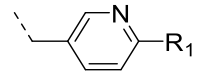	CH_3	483.0	4.69	58.87	1	6	0.21	2.35	133.5	80
190		CF_3	537.0	4.94	58.87	1	6	0.29	2.45	130.5	40

MW = molecular weight in Daltons; clog*P* = calculated log value of the n-octanol/water partition coefficient; TPSA = topological polar surface area; HBD = hydrogen bond donors; HBA = hydrogen bond acceptors; R_f = retardation factor on thin layer chromatography (TLC); t_R = retention time in high power liquid chromatography (HPLC); m.p. = melting point; Sol = solubility at pH 7.4 using the turbidimetric method. ‡Predicted using StarDrop software, version 6.5.1-1. [a]TLC determined in 10% methanol in dichloromethane; [b]HPLC method described in chapter 6; [c]Avarage of two melting point runs (Tramadol hydrochloride used as the reference, m.p. = 178 – 180 °C).

Table A8: Physicochemical properties of **AST-CQ** hybrids, **SARs 2** and **3**.

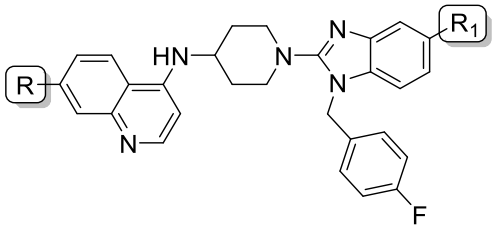

			Calculated Properties‡					Experimental Properties			
Code	**R**	**R_1**	**MW (Da)**	**cLog*P***	**TPSA (Å²)**	**HBD**	**HBA**	***R_f*** [a]	***t_R*** [b] **(min)**	**m.p.** [c] **(°C)**	**Sol.** [d] **(μM)**
191	Cl	CN	511.0	5.30	69.77	1	6	0.25	2.40	105.6	100
192		SO_2Me	564.1	4.49	80.12	1	7	0.19	2.37	112.5	120
193		CO_2Me	544.0	5.36	72.28	1	7	0.15	2.50	136.5	80
201	H	H	451.5	5.07	45.98	1	5	0.28	2.41	118	60
202	F		469.5	5.01	45.98	1	5	0.26	2.44	111	60
203	Br		530.4	5.57	45.98	1	5	0.42	2.50	112	40
204	CF_3		519.5	5.70	45.98	1	5	0.47	2.53	103	20
205	CN		476.5	4.83	69.77	1	6	0.31	2.44	93	120
206	OCF_3		535.5	5.50	55.21	1	6	0.45	2.52	105	40
207	OCH_3		481.6	4.98	55.21	1	6	0.22	2.47	121	80
208	NO_2		496.5	4.90	91.80	1	8	0.48	2.50	98	80

MW = molecular weight in Daltons; clog*P* = calculated log value of the n-octanol/water partition coefficient; TPSA = topological polar surface area; HBD = hydrogen bond donors; HBA = hydrogen bond acceptors; R_f = retardation factor on thin layer chromatography (TLC); t_R = retention time in high power liquid chromatography (HPLC); m.p. = melting point; Sol = solubility at pH 7.4 using the turbidimetric method. ‡Predicted using StarDrop software, version 6.5.1-1. [a]TLC eluted using 10% methanol in dichloromethane; [b]HPLC method described in chapter 6; [c]Avarage of two melting point runs (Tramadol hydrochloride used as the reference, m.p. = 178 – 180 °C.